# Crystallisation and layering of the Younger Giant Dyke Complex, SW Greenland

Susan C. Mingard

Thesis submitted for the degree of

Doctor of Philosophy

University of Edinburgh

1990

# DECLARATION

I declare that the work presented in this thesis is my own, unless otherwise stated.

"Jolly gees? Why, they're yon fellows who hammer little bits off the hills and then fancy they can tell the Lord himself how the earth was made," Morag replied.

*The Hills is Lonely* by Lillian Beckwith

# ABSTRACT

The Proterozoic Younger Giant Dyke Complex (YGDC) was emplaced during a period of widespread extensional continental magmatism in southwest Greenland and North America. The complex consists of a series of interconnected branching dyke segments up to 800m wide, which can be traced intermittently over 145km. The dykes were intruded into granitic basement and appear to have been halted at the unconformity between the basement and overlying supracrustal rocks. This project focusses on the Tugtutôq-Narsaq area of the complex.

The magmas producing the dykes were critically-undersaturated alkali olivine basalts to hawaiites with whole-rock MgO = c. 5wt%. They were carrying phenocrysts of olivine, stellate glomerocrysts of plagioclase + olivine, and anorthosite xenoliths up to 100m across. These xenoliths are found in the Narsaq area which represents a roof zone to the dykes. The magmas crystallised to form predominantly troctolitic cumulates. In western Tugtutôq these are olivine-plagioclase cumulates but in eastern Tugtutôq and Narsaq, magnetite and ilmenite (± apatite) joined the fractionating assemblage. Olivine and plagioclase core compositions range from $Fo_{68}$ to $Fo_{49}$ and $An_{65}$ to $An_{30}$. Salitic to ferrosalitic pyroxene is entirely intercumulus except in two evolved pods of syenogabbro and syenite enclosed by troctolite at the eastern end of Tugtutôq. These pods are ovoid in shape, elongated along the dyke, and up to 3km long. They are thought to have differentiated *in situ*. The distinction between syenogabbro and syenite is made on the presence or absence of plagioclase cores to alkali feldspar crystals. The order of appearance of fractionating minerals was: ol+pl at c. 5 wt% MgO, Fe-Ti oxides + apatite at c. 4 wt% MgO, cpx at c. 3.5 wt% MgO and alkali feldspar at 3 wt% MgO or less.

In ovoid pods at irregular intervals along the dyke segments, modal variation and/or plagioclase lamination define synformal layering. The modal variation takes the form of troctolite alternating with generally narrower layers of mafic cumulates. In the western YGDC these are olivine cumulates (gabbro picrites) but in the east they are olivine + magnetite + ilmenite ± apatite cumulates. Modal layering is best developed in the western YGDC where plagioclase lamination is absent. It may take the form of parallel mafic layers (1-30cm thick) or gabbro picrites filling channels (up to 8m wide and 4m deep) which plunge towards the synform axis. At two

localities breccias of gabbro picrite blocks within a troctolite matrix occupy the axial zone. They are inferred to have resulted from the breakup of thick picrite layers. The breccias and channels provide evidence that the synformal structure was primary.

During crystallisation, magma chambers along the dyke segments are inferred to have been tall and thin, with little interaction between laccolithic chambers at the top and V-shaped floors at the base. Crystals nucleated predominantly in the sidewall boundary layers and were carried to the floor by descending thermal convection currents. Crystallisation may also have taken place on the floor from descending crystal-free supercooled liquid. Periodic suppression of plagioclase nucleation, possibly due to fluctuations in volatile pressure or to repeated small influxes of magma, led to the crystallisation of olivine $\pm$ oxides alone. This may have taken place either at the base of the chamber, or in the sidewall boundary layers. Sidewall crystallisation produced high-density plumes which became density currents as they swept across the floor, eroding previously-formed cumulates.

Where olivine and plagioclase were the sole cumulus phases, the residual liquid was denser than the magma and ponded at the base of the chamber until the onset of postcumulus oxide crystallisation. In the eastern YGDC where oxides are primary minerals, compositional convection was more important. Plumes of light fluid moving up the walls may have reduced the efficiency of the crystal-laden currents, and convection from the crystal pile on the floor of the chamber resulted in the removal of a greater proportion of interstitial liquid, allowing rotation of the plagioclase crystals to form an igneous lamination. About half of the approximately 50% of initial intercumulus liquid was also expelled by compaction. A small amount of textural and compositional re-equilibration occurred during postcumulus crystallisation and subsolidus cooling, but the degree of re-equilibration was considerably less than in many other layered intrusions. It is hoped that this study of the YGDC will contribute towards the understanding of layering processes in other intrusions and of the genesis of some of the remarkable alkaline intrusions of the Gardar province.

# ACKNOWLEDGMENTS

I would like to thank Brian Upton and Cliff Ford for their supervision and numerous discussions. Brian's constant encouragement and enthusiam and Cliff's knowledge of computing and insights into the interpretation of my data were much appreciated. This project was undertaken during the tenure of a NERC studentship and I am particularly grateful for the opportunity of an unscheduled second field season.

Many people were of assistance during my fieldwork. Firstly I would like to thank the Grønlands Geologiske Undersøgelse for the provision of equipment and logistical backup. Ole Plesner and his family I cannot thank enough for their wonderful hospitality in Greenland. Anne Payne was an invaluable field assistant and Jørgen Lau of GGU, Ivan Bohm of Narsaq (the "big leader"), "Miss Piggy's father" who lent us the boat, and the staff of the Hotel Perlen, all gave us much-appreciated help.

Analytical work at Edinburgh was carried out with the help of Pete Hill and Stuart Kearns (electron microprobes), and Dodie James and Godfrey Fitton (XRF). Kenny Cameron, Eddie Clark and Jane Foster supplied me with thin sectins and probe slides. Yvonne Cooper is thanked for photographic work and Diana Baty for her great patience when showing me how to do it myself! Isotope work was undertaken at the Scottish Universities Research and Reactor centre at East Kilbride, where Graeme Rogers, Tony Fallick and Alison McDonald were particularly helpful. Mark Hallworth did a superb job of setting up experimental equipment in the Department of Applied Maths and Theoretical Physics at Cambridge.

I have benefitted from discussions with many people in addition to Brian and Cliff, including Becky Renner, Bob Hunter, Roy Gill, Herbert Huppert and Adrian Finch. Many of the computer programs I used were written by Andy Walker. Hugh Nicholson, Dave Latin, Mike Matthews, Martin Wilding and Björn Hardarson shared an office with me and are thanked for their friendship. Hugh Nicholson did a marvellous job of helping with the final stages of thesis preparation. Everyone else at the Grant Institute, especially Sue Wallis, Ed Follows, Pete Clift, Jóhanna Thorlacius, Adrian Finch and the secretaries (Heather Hooker, Helena Jack and Denise Wilson), helped to make my time there enjoyable.

The congregation of Central Hall Methodist Church and especially the East House Fellowship have provided loving support over the last few years, as have my family and the Mingard clan. But most of all, I could not have done it without Hugh, my husband, field assistant and proof-reader, who has been a constant source of love, patience and encouragement.

# CONTENTS


CHAPTER 1. INTRODUCTION 1

1.1 Aims of project 3
1.2 Regional geology 3
1.2.1 Previous work 3
1.2.2 Earlier Proterozoic basement 4
1.2.3 The Gardar Province 5

CHAPTER 2. FIELDWORK 8

2.1 Introduction 8
2.2 Terminology 11
2.2.1 Cumulus terminology 11
2.2.2 Troctolite 11
2.2.3 Gabbro picrite 12
2.2.4 Syenogabbro and syenite 12
2.2.5 Pyroxene 12
2.3 Contact relationships and lithologies 12
2.3.1 The western YGDC (localities A to E) 19
2.3.2 Southern branch of the eastern YGDC (localities F to I) 20
2.3.3 Northern branch of the eastern YGDC (localities J to L) 22
2.3.4 Narsaq (locality M) 25
2.4 Layering features 32
2.4.1 The western YGDC 32
2.4.1.1 Locality D (Itivdlip Sarqâ) 32
2.4.1.2 Locality C 42
2.4.1.3 Locality B 43
2.4.2 Southern branch of the eastern YGDC 44
2.4.2.1 Locality F 44
2.4.2.2 Locality G (Marrait) 44
2.4.2.3 Locality I (Sigssardlugtoq) 46
2.4.3 Northern branch of the eastern YGDC 47
2.4.3.1 Locality K (Krydssø) 47
2.4.3.2 Locality L (Assorutit) 59
2.4.4 Locality M (Narsaq) 59
2.5 Xenoliths 59
2.5.1 The western YGDC 59
2.5.2 Southern branch of the eastern YGDC 60
2.5.3 Northern branch of the eastern YGDC 60
2.5.4 Narsaq 61
2.6 The nunataq region 65
2.7 Summary and conclusions 65

CHAPTER 3. PETROGRAPHY AND MINERAL CHEMISTRY 68

3.1 Objectives 68
3.2 Petrography 69
3.2.1 Chilled margins 69
3.2.2 Troctolites 71
3.2.3 Mafic cumulates 76
3.2.4 Syenogabbros and syenites 80
3.2.5 Xenoliths 82

3.2.6 Late stage veins 83
3.2.7 The nunataq region 84
3.2.8 Summary 85
3.3 Textural analysis 85
3.3.1 Textural equilibration 85
3.3.2 Grain size analysis 97
3.4 Mineral Chemistry 105
3.4.1 Olivine 108
3.4.2 Feldspar 113
3.4.3 Pyroxene 119
3.4.4 Iron-titanium oxides 124
3.4.5 Apatite 127
3.4.6 Biotite 128
3.4.7 Amphibole 134
3.4.8 Summary 138

**CHAPTER 4. WHOLE ROCK CHEMISTRY 139**

4.1 Introduction 139
4.2 Nature of the YGDC magmas 139
4.2.1 Classification 139
4.2.2 Norms 141
4.3 Element variation with MgO 141
4.3.1 Major element variation 141
4.3.2 Trace element variation 148
4.3.3 Causes of MgO variation in chills 157
4.4 Fractional crystallisation 159
4.4.1 Mineral/whole-rock plots 159
4.4.2 CMAS plots 164
4.4.3 Numerical modelling 169
4.4.4 Fractionation within the dyke 171
4.5 Incompatible element variation 171
4.5.1 Chondrite-normalised plots 171
4.5.2 Rare earth elements 174
4.6 Relationship between chills and troctolites 178
4.7 Evolution of the YGDC magma 180
4.8 Summary 185

**CHAPTER 5. ISOTOPE GEOCHEMISTRY 186**

5.1 General comments 186
5.2 Strontium isotopes 186
5.3 Oxygen isotopes 191
5.3.1 Procedure and results 191
5.3.2 Origins of isotope ratios 198
5.3.3 Differences between layers 201
5.4 Summary and conclusions 201

**CHAPTER 6. REGIONAL PERSPECTIVES, AND YGDC EMPLACEMENT 204**

6.1 The Greenland-North American Proterozoic Rift 204
6.1.1 Description of rock types 204
6.1.2 Origin of the magmas 213

6.2 Genesis of the YGDC magmas 214
6.3 Emplacement and cooling of the YGDC 217
6.3.1 YGDC emplacement 217
6.3.2 An estimate of solidification time for the YGDC 220
6.4 Summary 221

CHAPTER 7. ORIGINS OF LAYERING 222

7.1 The YGDC in comparison with other layered intrusions 222
7.1.1 Archaean and Proterozoic examples 222
7.1.2 Phanerozoic examples 234
7.1.3 Comparison between the YGDC and other layered intrusions 239
7.2 Theories of Layering 241
7.2.1 Background 241
7.2.2 Proposed origins for layering 243
7.3 Magma crystallisation behaviour (and implications for the YGDC) 245
7.3.1 Crystal nucleation and growth 250
7.3.2 Movement of crystals and liquid 253
7.3.3 Postcumulus processes 266
7.4 Crystallisation experiments 269
7.5 Origin of the YGDC Layering 278
7.5.1 Summary 286

CHAPTER 8. SUMMARY AND CONCLUSIONS 287

References 295

Appendix I Sample Localities 313

Appendix II Analytical Techniques 323

Appendix III Representative mineral analyses 330

Appendix IV Representative whole-rock analyses 368

# CHAPTER 1: INTRODUCTION

Igneous layering is found in many large basic intrusions and also more rarely in syenitic or granitic bodies. The layering is defined by variations in modal mineralogy, grain-size, texture or mineral orientation, by appearance or disappearance of phases or by changes in mineral compositions. The examination of igneous layering provides important clues to some of the processes occurring during the crystallisation of magma chambers. Such processes involve both magma and crystals. They include magmatic convection (both thermal and compositional), stratification of the magma and replenishment of the chamber, together with crystal nucleation, growth and possible settling or floating, crystal redistribution by currents and the movement of unconsolidated crystal piles under gravity. In addition, information about the crystallisation of interstitial fluid and subsolidus re-equilibration can be obtained.

A great deal of early work on igneous layering was done by L. R. Wager and co-workers (e.g. Wager and Deer, 1939; Wager *et al.*, 1960; Wager and Brown, 1968). Their interpretation was that layering was produced as a result of crystal settling, but they recognised that certain structures in igneous rocks could be formed in other ways. More recently, the mechanism of crystal settling to produce layering has been questioned (e.g. Campbell, 1978) and the possibility put forward that all layering features could form *in situ* (McBirney and Noyes, 1979). Some workers, however, have remained convinced that crystal settling occurs (Irvine, 1980a, 1983; Cox and Mitchell, 1988; Martin and Nokes, 1989). New theories of layering have also arisen, such as crystallisation from a stratified magma column formed by double-diffusive convection (McBirney and Noyes, 1979, McBirney, 1985, Wilson *et al.*, 1987). In addition, recent work on layered intrusions has shown that large, slowly cooled bodies undergo considerable modification of textures (Hunter, 1987) and mineral compositions (Barnes, 1986; Chalokwu and Grant, 1987) both above and below the solidus. Many primary features may be obscured by this re-equilibration process.

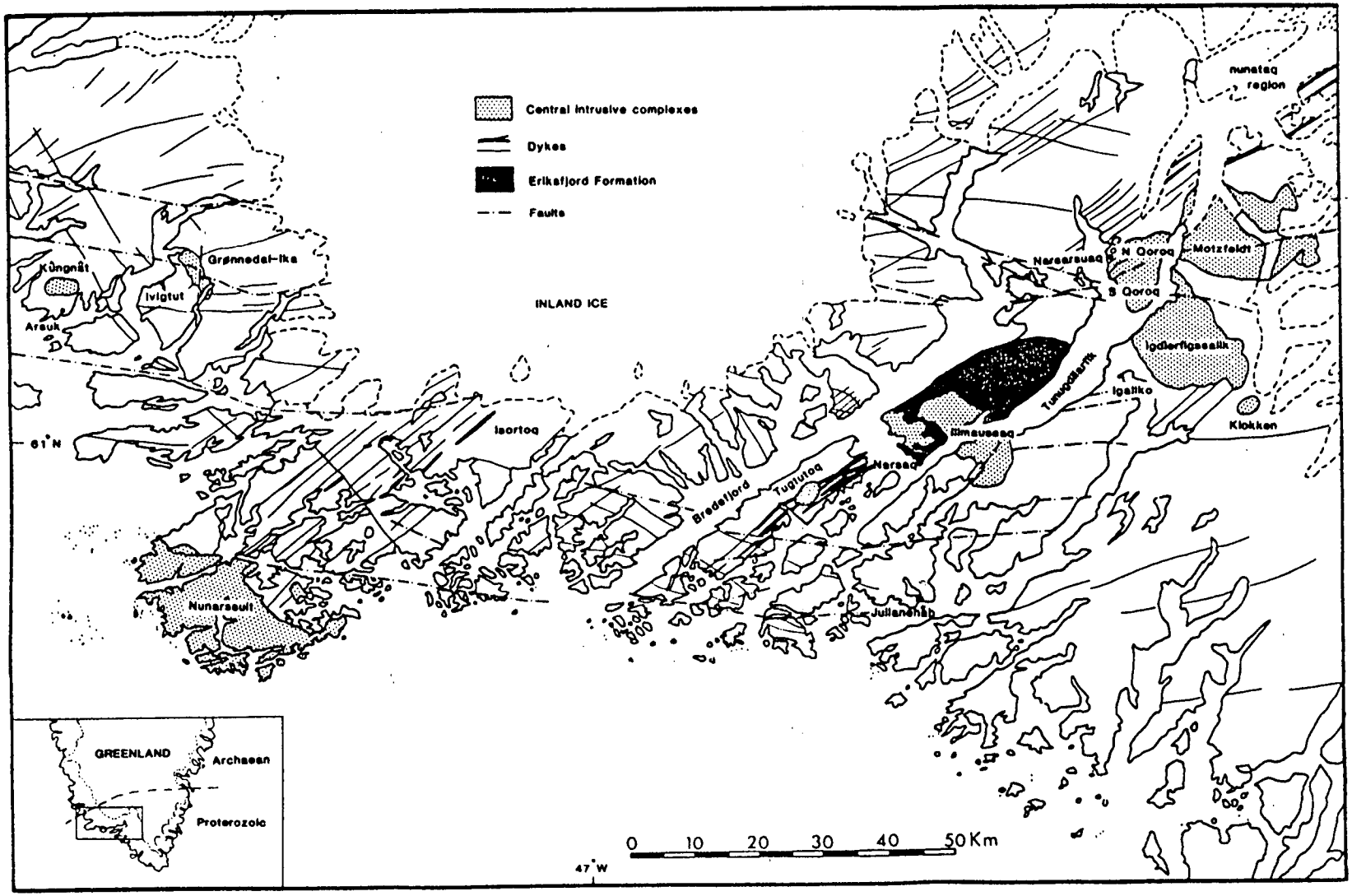


**Figure 1.1** Simplified geological map of south-west Greenland showing Gardar intrusions.

## 1.1 Aims of Project

The mid-Proterozoic Younger Giant Dyke Complex (YGDC) of southern Greenland, while showing very well-developed layering, is a tabular body with a relatively small minimum dimension and thus probably cooled at a faster rate than many intrusions of a roughly similar volume but different shape such as the Skaergaard intrusion of east Greenland.

The dyke complex displays good primary igneous textures and the rocks are typical orthocumulates. Since the layering is only developed intermittently at intervals along the branching dykes, the intrusion may have been of a critical size for the development of layering. This study was undertaken because, in the YGDC, a relatively early stage in the layering may have been "frozen in" due to the rapid cooling and it may thus provide insights into the history of other, more slowly-cooled, intrusions where re-equilibration has proceeded to a greater degree.

The YGDC has other unusual characteristics which make it worthy of study: unlike the majority of layered gabbroic rocks which are tholeiitic it is a large body of transitional alkali olivine-basaltic parentage and displays an unusual sequence of cumulus crystallisation. This sequence is documented and the implications considered. Finally, information on parental and derivative magmas of the YGDC will help in the understanding of the regional genesis and differentiation of the wide variety of magmas forming the rocks of the Gardar Province of south Greenland.

## 1.2 Regional Geology

### 1.2.1 Previous work

The Gardar Province is an area of Proterozoic alkaline continental magmatism found to the west of the southern tip of Greenland. It extends about 200km from W to E and 70km N to S (Fig. 1.1). The first geologist to study this area of south-west Greenland was Giesecke between 1806 and 1813 (Giesecke, 1910). He was followed by several others during the 19th and early 20th centuries who were either mineralogists (e.g. Steenstrup, 1881, Flink, 1898, Ussing, 1912) or geologists accompanying mapping expeditions (e.g. Jessen, 1896). Wegmann (1938) was the first worker to divide the rocks into an older basement, which he named the

Ketilidian after Ketils Fjord (now Tasermiut), and "younger formations". The latter he recognised as being the result of a single tectono-magmatic episode to which he gave the name Gardar, from the old Norse Bishopric now called Igaliko (Fig. 1.1). Wegmann also drew comparisons between these rocks and similar formations in Canada and Scandinavia.

Regional mapping by the Greenland Geological Survey (GGU) began in the mid 1950s and the first descriptions of the Tugtutôq area were published by Upton (1962, 1964a,b). The 1:100 000 map of the region (Sheet 60 V. 2 Nord Julianehåb) was published in 1967. Mapping of giant dykes in Johann Dahl Land and G.F. Holm nunataq, now thought to be continuations of the YGDC, was carried out by B.J. Walton and J.H. Allaart in the early 1960s. The 1:100 000 map (Sheet 61 V.3 Syd Narssarssuaq) was published in 1970. Since then several reviews of the regional geology have been published (Upton, 1974; Emeleus and Upton, 1976; Upton and Emeleus, 1987). The dykes of the Tugtutôq-Narsaq-nunataq region have been studied by several workers. Macdonald (1969), Macdonald and Edge (1970) and Martin (1985) have described the Tugtutôq dyke swarm, Upton *et al.* (1985) the Older Giant Dyke Complex, Upton and Thomas (1980) and Upton (1987) the YGDC and Upton and Fitton (1985) the dykes NE of Narsarsuaq.

### 1.2.2 Earlier Proterozoic basement

The basement rocks of SW Greenland are early Proterozoic granites and gneisses, which collectively constitute the Ketilidian Mobile Belt. The oldest gneisses have been dated by U-Pb at 1840±25 Ma and the younger granites at 1780±20 Ma (van Breemen *et al.*, 1974). Rb-Sr whole-rock ages (recalculated to a revised decay constant from Steiger and Jäger, 1977) are in good agreement with these dates. The youngest Rb-Sr mineral ages cluster around 1600 Ma. Initial Sr ratios obtained by van Breemen *et al.* suggested that the whole belt is of juvenile mantle material but later isotopic studies by Kalsbeek and Taylor (1985) using Pb-Pb, Rb-Sr and Sm-Nd indicated a significant amount of reworked crustal material in the zone of older granite gneisses adjacent to the Archaean craton to the north. Piper (1982) put the case for a Proterozoic Supercontinent existing during the period ca. 2600-1100 Ma, with Greenland probably joined to eastern Canada during both the Ketilidian and the subsequent Gardar activity.

### 1.2.3 The Gardar province

The age of the Gardar province is thought to be within the period 1320-1120 Ma (Upton and Emeleus, 1987, using dates recalculated from Blaxland et al., 1978). The rocks were the product of intra-plate alkaline magmatism. Similar activity was occurring in north-eastern Canada at around the same time (Baragar, 1977) but the rocks of Greenland tend to be more alkaline in nature. The Gardar province includes lavas, dykes and central complexes with magma compositions ranging from alkali olivine-basalt to trachyte, phonolite and rhyolite. Coarse-grained equivalents are troctolitic gabbros to silica over- and under-saturated syenites, with occasional extreme differentiation to highly alkaline rock types. Small volumes of silica-deficient rocks including ultramafic lamprophyres and carbonatites were also erupted intermittently throughout the period of magmatism.

The earliest manifestation of magmatism in the province gave rise to the Eriksfjord Formation (Poulsen, 1964, Larsen, 1977), now only preserved in downfaulted blocks but thought to have originally been much more extensive (Upton, 1974). The Formation comprises a thick sequence of lavas (greater than 1km on the Ilímaussaq peninsula) underlain by and interbedded with continental sandstones and occasional conglomerates derived from the underlying basement. The lavas are dominated by olivine-basalt and hawaiite with minor ultramafic flows composed predominantly of olivine and clinopyroxene but without a characteristic komatiite spinifex texture. The lavas become more evolved upwards with a trachytic and phonolitic succession forming roughly 20% by volume of the formation (Larsen, 1977). Dating has not yet been possible; the Formation is bracketed only by dates for cooling of the basement (1600 Ma) and intrusion of the Motzfeldt Complex by which it is cut (1282 Ma), but it is thought to have formed only shortly before the earliest Gardar intrusions. Jones (1980) proposed that the Motzfeldt Complex was in fact the source of the trachytes and phonolites. North American flood basalts, including the Seal Lake province in Labrador and the Keweenawan of Lake Superior, are younger than the Eriksfjord lavas (Baragar, 1977; Windley, 1989).

Upton and Emeleus (1987), following Blaxland et al. (1978), divided the Gardar into three cycles on the basis of field relations and Rb-Sr dates. Each cycle appears to have begun with widespread extrusion or intrusion of basic magmas and to have ended with the emplacement of syenitic central complexes. There are, however, some exceptions to this generalisation; for example, some of the late Gardar central complexes appear to have been emplaced near the beginning of the cycle. The Early

Gardar period encompasses the Eriksfjord Formation and the nepheline syenite complexes of Grønnedal-Ika, North Qôroq and Motzfeldt (see Fig. 1.1). The Middle Gardar commenced with the intrusion of doleritic "brown dykes" (BDs in Survey literature), initially with an E-W trend but with later trends swinging round to the ESE, S, SW and finally WSW. Subsequent dyke intrusion was almost entirely along the WSW-ENE trend. Only two small oversaturated complexes (Ivigtut and Kûngnât) were intruded during the Middle Gardar. The Late Gardar (1200-1120Ma) was the period of greatest activity during which the Tugtutôq-Narsaq-nunataq and probably the Nunarssuit-Isortoq dyke swarms were intruded, although the latter may possibly be older than this. Both of these swarms contain giant dykes (greater than 100m in width), one of which is the YGDC of Tugtutôq. Central complexes include the oversaturated Nunarssuit, Tugtutôq, Klokken and Dyrnaes-Narsaq intrusions and the undersaturated South Qôroq, and Igdlerfigssalik intrusions. The Ilímaussaq complex is predominantly agpaitic (peralkaline and undersaturated) but late-stage magmas were oversaturated.

Contemporaneous faulting took place along prominent WNW-ESE or W-E trending sinistral strike-slip faults (with movements of several kilometres) and less extensive dextral faults trending approximately N-S (with movements of tens to hundreds of metres). These appear to form a conjugate set of faults corresponding to tension in a NW-SE direction. Vertical movements are also demonstrable for some of the faults. Many, though not all, of the central complexes are sited where left-lateral faults intersect dyke swarms. Most of the dykes appear to have been emplaced as a result of crustal dilation but in the central complexes stoping becomes more important. The giant dykes, which are frequently composite with gabbroic margins and more differentiated central portions, may provide a link between the two methods of emplacement, with early gabbroic members filling tensional fissures but later syenitic magmas emplaced more permissively (Upton, 1974; Becker, 1984).

Anorthositic xenoliths and plagioclase megacrysts are abundant in many Gardar rocks and imply the presence of large bodies of anorthosite underlying the province (Bridgwater, 1967). In this we see another parallel to the activity in North America, where gabbroic and alkaline rocks are found intimately associated with (generally older) massif-type anorthosites. There is a relationship between the composition of the plagioclase crystals and that of their host, implying that the genesis of the anorthosites was closely linked to that of the other rocks of the province.

Studies of initial $^{87}Sr/^{86}Sr$ (Blaxland et al., 1978) indicate that the majority of Gardar rocks were probably mantle-derived; crustal contamination probably occurred in two members of the Nunarssuit complex (see Chapter 5). However, there is field evidence for considerable crustal stoping in most of the oversaturated intrusions (e.g. Upton *et al.*, 1990). Two complexes (Ivigtut and Ilímaussaq) possess high initial Sr ratios but this may be due to selective enrichment in $^{87}Sr$, possibly due to interaction between F-rich late stage fluids and country rocks. Patchett *et al* (1976) have shown that initial Sr ratios for the YGDC and included anorthosite xenoliths are identical, supporting the idea of a related genesis.

Most of the Gardar basaltic magmas are thought to have undergone high pressure fractionation to produce high Fe/Mg and Ca/Al ratios before intrusion (Upton and Emeleus, 1987; Chapter 6). Their diversity can be explained by low pressure crystal fractionation. For all of the rocks, high volatile contents (F, Cl and $CO_2$) are inferred from apatite, biotite and amphibole compositions and from the common occurrence of fluorite and calcite in late-stage veins. These high volatile contents suggest low magma viscosities which may have facilitated the development of layering and in-situ fractionation, both of which are common features in the province. The anorthosite xenoliths are thought to be fragments of large bodies at depth, possibly flotation cumulates from batches of hawaiitic magma which never rose to the surface.

The Gardar province has been largely unaffected by regional tectonics, since the Grenville-Fennoscandian metamorphic front of North America passes to the south of Greenland. The opening of the Davis Strait during the Cretaceous Period caused minor magmatic activity and was followed by major Tertiary uplift and erosion exposing the sub-volcanic central complexes at the surface.

# CHAPTER 2: FIELDWORK

## 2.1 Introduction

The country rocks in the area of study are granites and granodiorites, facies of the Julianehåb Granite, one of the younger members of the Ketilidian Mobile Belt. The overall colour of the rocks is generally pale pink although it may vary to white or grey. They contain variable proportions of quartz, two feldspars and mafic minerals including amphibole and biotite. Different facies can be distinguished; in places the country rocks are non-porphyritic while elsewhere they contain pink phenocrysts of potassium feldspar up to 3cm in length. Shear planes are common and frequently accompanied by considerable reddening of the rock; these areas were avoided when sampling.

On the island of Tugtutôq two episodes of giant dyke intrusion can be recognised (Fig. 2.1). The unlayered Older Giant Dyke Complex (OGDC) is about 500m wide, traceable for 20km and composed of undersaturated syenite with gabbroic margins. The predominantly troctolitic Younger Giant Dyke Complex (YGDC) is a system of branching dykes. On Tugtutôq, two separate branches are seen; because of their lithological similarity these are assumed to merge in the Narsaq area to the east of Tugtutôq, and probably also to connect at depth. The giant dykes of the nunataq region NE of Narsarsuaq (Fig 1.1) appear to be an offset continuation of this younger complex (Upton and Fitton, 1985). Thus the YGDC can be traced intermittently over a total length of about 145km. The dyke components vary from <100m to 800m in width and are commonly not parallel-sided but show pinch and swell structures. Some of the dyke branches end in blunt terminations against what are assumed to be old fractures in the basement (Upton, 1987).

It is thought that the region around the town of Narsaq (Fig. 2.1) represents an eastward broadening and merging of the two main dyke branches seen on Tugtutôq. A sub-horizontal contact between the troctolite and Eriksfjord sandstones near Narsaq, together with the lack of giant dykes cutting the outcrop of the Eriksfjord formation to the east, suggest that the YGDC magma was halted at the basement-Eriksfjord unconformity and ponded to form a lopolithic upper termination with only minor intrusions being emplaced at higher levels.

Intermittent layered "pods" up to 3km long occur within the dyke segments. The layering may be defined by modal variation or feldspar lamination or both, and is usually synformal in shape, with the synform axes parallel to the trend of the dyke. The synforms may plunge along the dyke, commonly to the east but occasionally to the west.

The giant dykes of Tugtutôq are displaced by sinistral wrench faults and partly obliterated by the later syenite intrusions of the Tugtutôq Central Complex. The Narsaq gabbro is similarly truncated by the Dymæs-Narsaq complex. There is an important swarm of smaller dykes in the region whose principal axis coincides approximately with that of the YGDC. Most are post-YGDC but some may be a result of contemporaneous activity. These smaller dykes have been studied in detail by Macdonald (1969) and Martin (1985), and their compositions may provide clues to the evolution of the giant dyke magma (Chapter 4).

In the YGDC, the plagioclase crystals are light to dark grey in colour when fresh but weather to white or beige, so in the field, the troctolites appear pale in colour. Mafic cumulates are dark greenish brown to black in colour and contrast sharply with the troctolite. The olivine ranges in colour from light yellow-brown to dark green-brown or black, and weathers to a rusty brown. Olivine crystals 2mm or more are always dark in colour due to their size. Clinopyroxene and Fe-Ti oxides are black and shiny with little tendency to weather much but can be distinguished in the field on the basis of their lustre and crystal shape.

The dykes have prominent sets of vertical joints perpendicular and parallel to their trend. The latter are rather obscured by the intrusion of numerous smaller dykes (which often weather out) along the giant dykes.

Fieldwork and sampling for this project took place during the summers of 1987 and 1988. However, a substantial collection of GGU (Greenland Geological Survey) samples exists in Edinburgh as a result of the visits of B.G.J. Upton and co-workers to this area, and some of these GGU samples have been analysed or re-analysed as part of this project. Localities of samples collected for this project, and of analysed GGU samples, are presented in Appendix I. Figure 2.1 indicates all localities from which samples have been analysed; those actually visited in 1987/88 were B, C, D, F, G, I, K, L and M. Many of these localities are the same as the numbered localities of Upton (1987) but relabelling was found necessary and in this project letters have been used to avoid confusion. Localities correspond as follows: A=1, B=2, D=3, F=4, G=5, H=6, I=7, J=8, K=9, L=10 and M=11.

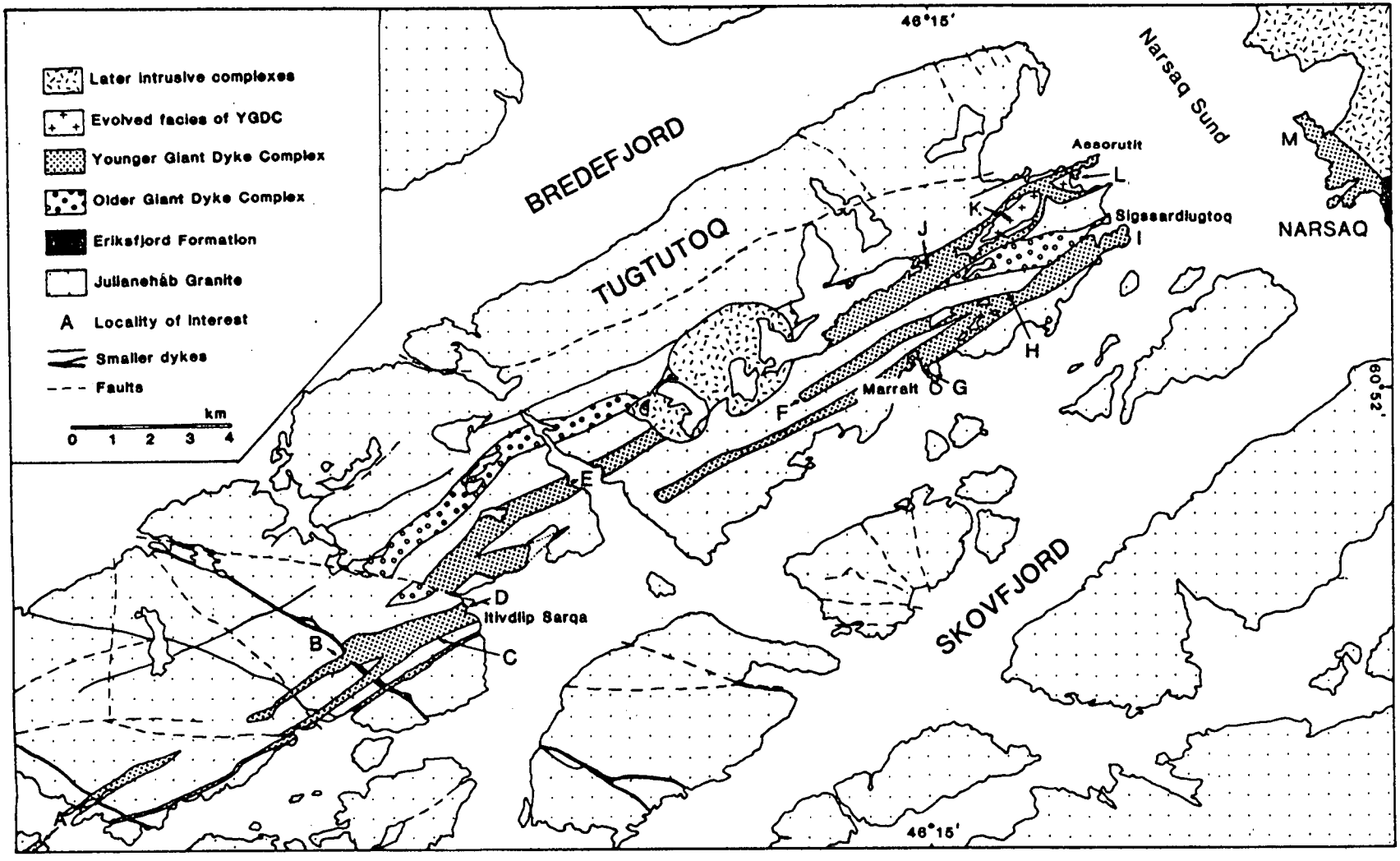


Figure 2.1 Principal geological features of the Tugtutôq-Narsaq region. Lettered localities are those from which samples have been analysed.

## 2.2 Terminology

### 2.2.1 Cumulus terminology

The original definition of the majority of *cumulate* rocks by Wager *et al.* (1960) implied an origin by crystal settling. The term cumulate was redefined by Irvine (1982) as "an igneous rock characterized by a framework of touching mineral crystals and grains that evidently were concentrated through fractional crystallisation of their parental magmatic liquids". This almost certainly applies to the modally layered rocks of the YGDC, since the bulk compositions of some layers match no known magma and thus concentration of minerals probably occurred. The unlayered portions of the dykes may also involve cumulates. The terms *orthocumulate*, *mesocumulate* and *adcumulate* were proposed by Wager and Brown (1968) for cumulates containing decreasing proportions of material crystallised in the interstices of the cumulate framework. The terms were quantified by Irvine (1982) who suggested that orthocumulates might contain 25-50% by volume *postcumulus* (or *intercumulus*) material, including overgrowths on cumulus crystals; mesocumulates 7-25% and adcumulates 0-7%. A suggestion of Wadsworth (1985) is followed here, namely that the term "postcumulus" should refer to events occurring after the primary or cumulus phase of crystallisation while "intercumulus" should refer to the products of such processes. The term *heteradcumulate*, for a rock containing poikilitic intercumulus material of the same composition as cumulus crystals in adjacent layers, has generally been replaced by *poikilitic adcumulate*. Wager *et al.* (1960) also introduced the term *crescumulate*, for a rock containing highly elongate crystals of a cumulus mineral, the crystals being usually perpendicular to the intrusion margins or to the layering. A useful summary of terms applicable to layered intrusions is given by Irvine (1987b).

### 2.2.2 Troctolite

Most of the YGDC exposure is composed of rocks with either plagioclase and olivine, or plagioclase, olivine, apatite, and oxides as primary phases. These rocks are generally referred to as troctolites rather than olivine gabbros, following the classification of Streckeisen (1976), since although clinopyroxene is present it is a late, interstitial phase.

### 2.2.3 Gabbro picrite

Minor but important mafic facies are found in the layered portions of the dyke, containing up to 70% cumulus olivine ± oxides ± apatite. The remaining material is intercumulus plagioclase, clinopyroxene, apatite and oxides. The olivine cumulates are referred to as gabbro picrites to imply that they are coarse-grained olivine-rich rocks. This term has been used to describe similar rocks from several layered intrusions including the Skaergaard intrusion of east Greenland, although the Skaergaard picrites are now thought to be xenoliths (Hoover, 1978; Kays and McBirney, 1982). An alternative term would be "feldspathic peridotite" as used by workers in the Rhum intrusion, but this has been avoided. The mafic cumulates containing oxides ± apatite as well as olivine are simply referred to as olivine-magnetite cumulates or olivine-magnetite-apatite cumulates.

### 2.2.4 Syenogabbro and syenite

At some localities more differentiated facies are found within the dyke complex, recognised by the appearance of clinopyroxene as a cumulus phase and alkali feldspar as a modally important phase. These rocks are referred to as syenogabbros. When plagioclase is lost the rocks are termed syenites. These two rock types are easily distinguishable from the troctolites in the field, but not always easily told apart. The syenogabbros, however, tend to be more mafic and to show rusty brown weathering.

### 2.2.5 Pyroxene

The term pyroxene when unqualified denotes clinopyroxene throughout. Low-Ca pyroxene has never been observed in YGDC rocks.

## 2.3 Contact relationships and lithologies.

A summary of lithologies at different localities can be found in Table 2.1, and maps of selected localities in Figs. 2.2 to 2.6.

Table 2.1 Summary of YGDC lithologies

| Locality | Description |
|---|---|
| B, C, D | Chilled margins may contain feldspar phenocrysts. Troctolite forming the dyke interior contains 60-70% plagioclase, 20-30% olivine and minor pyroxene, oxides, and biotite. Olivines tend to clump together. Subordinate gabbro picrite is 80-90% olivine, 10-20% plagioclase. Near N margin of loc B and N margin of dyke east of fault at loc D, troctolite has blockier feldspar, single olivines and higher oxide content. An elongate feldspar facies is developed at loc B. |
| F | The fine-grained chill often contains olivine and plagioclase phenocrysts and roughly spherical composite glomerocrysts (up to 3cm in diameter) of radiating plagioclase with olivine and interstitial pyroxene, oxides and biotite. Phenocrysts become more common away from the blunt termination and from the margins of the dyke until they merge to give coarse-grained troctolite. |
| G | A finer-grained pod showing synformal plagioclase lamination is surrounded by coarser-grained unlaminated troctolite. The central pod takes up roughly a third of the dyke width. The troctolite has plagioclase, olivine and oxides as major components and apatite crystals several cm in length can sometimes be seen. Subordinate mafic facies are olivine-oxide cumulates. Veins of alkali feldspar and blue-green amphibole are common and there is some epidotisation. |
| I | Troctolites of well-laminated plagioclase, olivine and oxides make up this part of dyke. Feldspar lamination begins 20m from N margin and 200m from S margin defining an elongate basin. A 10m x 10m pod near the S margin is composed of browner-weathering finer-grained troctolite. Subordinate olivine-oxide cumulates occur. |
| K, L | Chilled margins grade into 100-150m wide troctoltie sheaths surrounding pods of more evolved syenogabbro and syenite. Clinopyroxene is still interstital in the troctolite but becomes a primary phase in the syenogabbro and syenite. At locality L pyroxene crystals in the syenogabbro zone may become highly elongated (10-15cm x 2mm). The evolved rocks contain relatively small proportions of mafic minerals (10-20% ol+cpx+oxides), the rest being feldspar (predominantly alkali feldspar). Some more mafic facies occur but mafic minerals never form more than 70% of the rock. Pegmatitic patches are common in all rock types and veining is widespread. Anorthosite xenoliths are abundant in the northern part of the troctolite sheath at loc L. |
| M | A vertical chill against Julianehåb Granite is exposed on Narsaq Island and a low-angle contact with Eriksfjord sandstones is seen south of Narsaq. Alteration caused by the Dymæs-Narsaq Complex affects a large area including the latter chill. Anorthosite xenoliths are common, especially within the zone of alteration and are frequently disaggregated. Fresh troctolite is coarse-grained (feldspars may be several cms long) with plagioclase, olivine and oxides as major components. Minor olivine-oxide cumulates occur. |

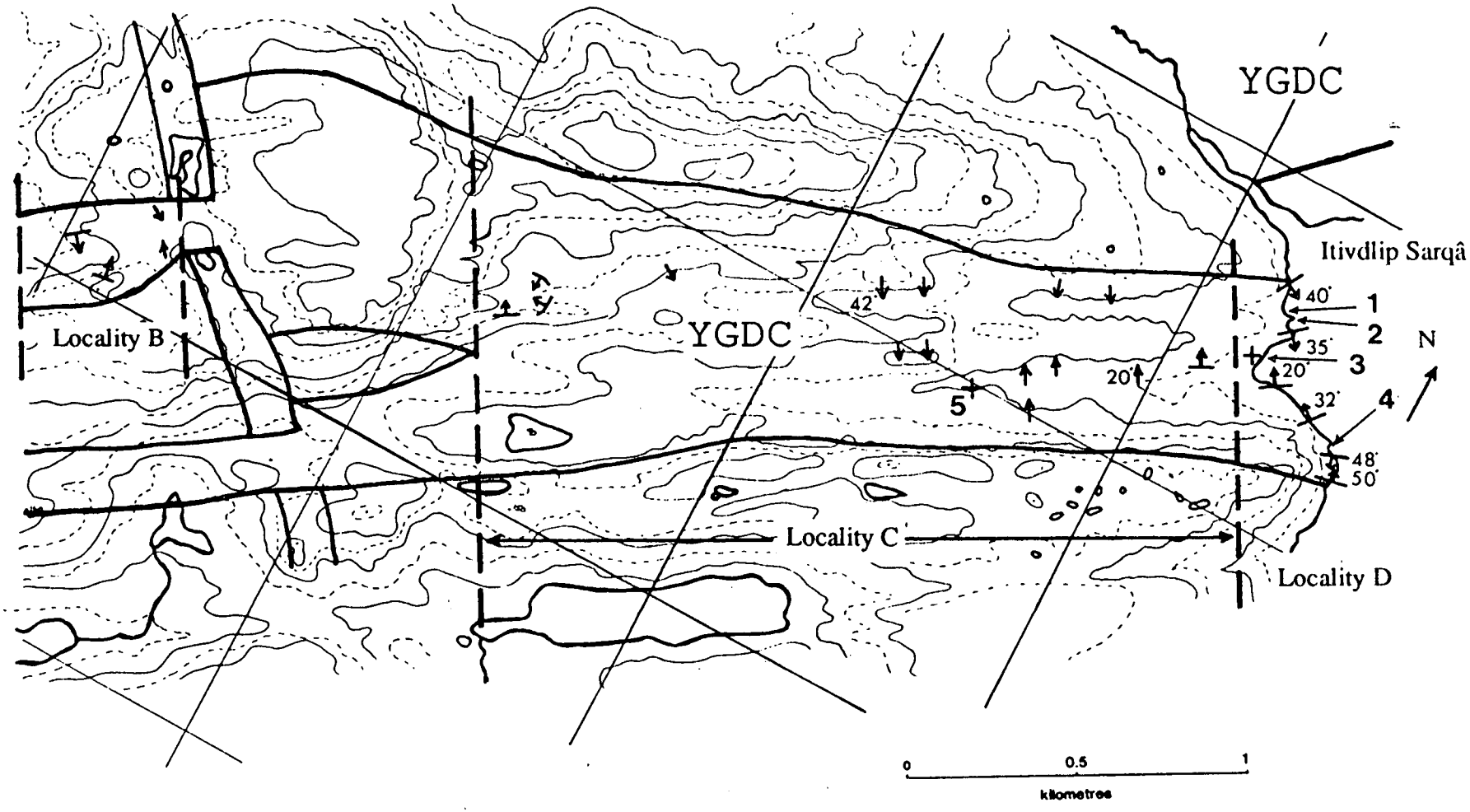


Figure 2.2 Map of localities B to D of Fig. 2.1 with some layer dips indicated. Localities 1 to 5 are mentioned in the text.

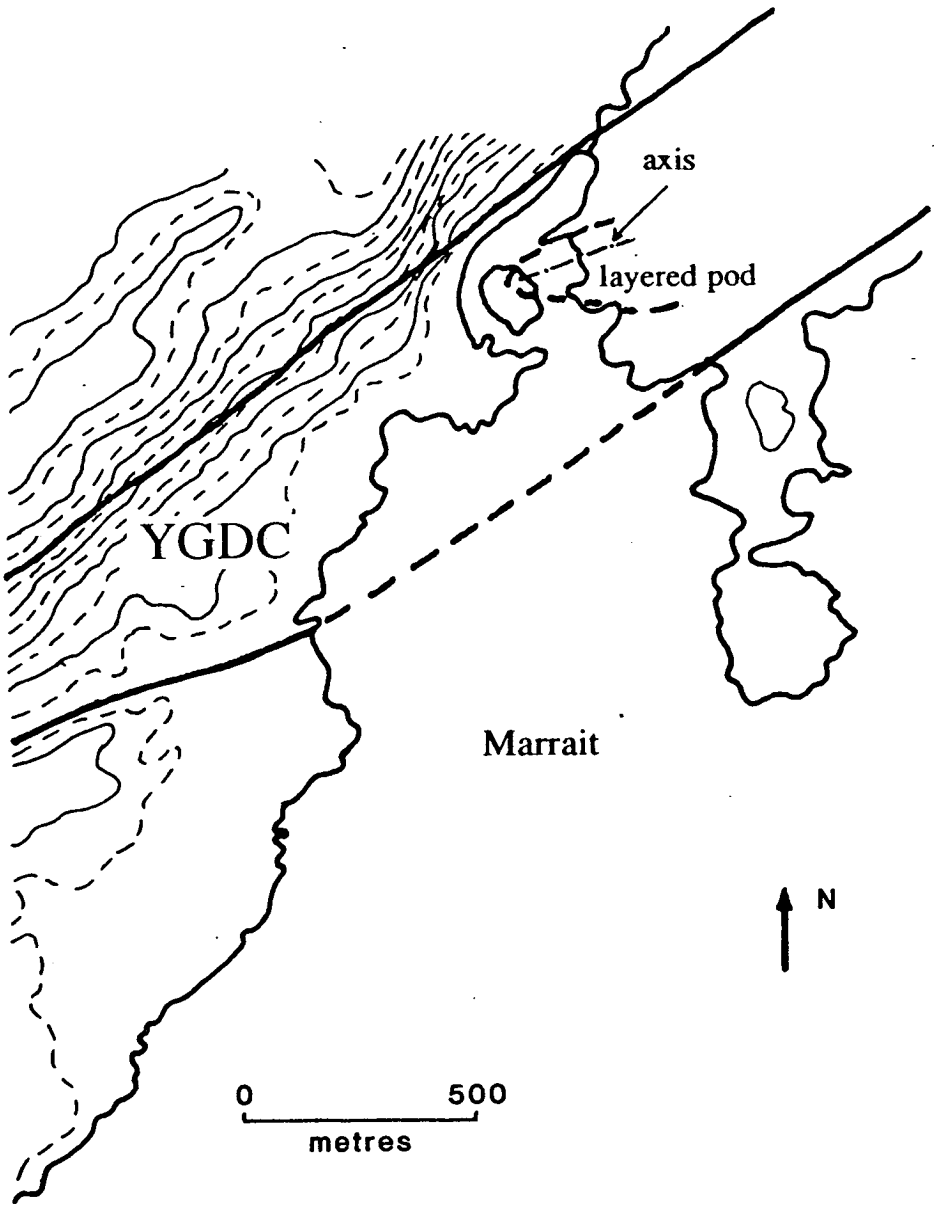


**Figure 2.3** Map of Marrait (locality G of Fig. 2.1) with extent of finer-grained, layered pod and axis of synform indicated.

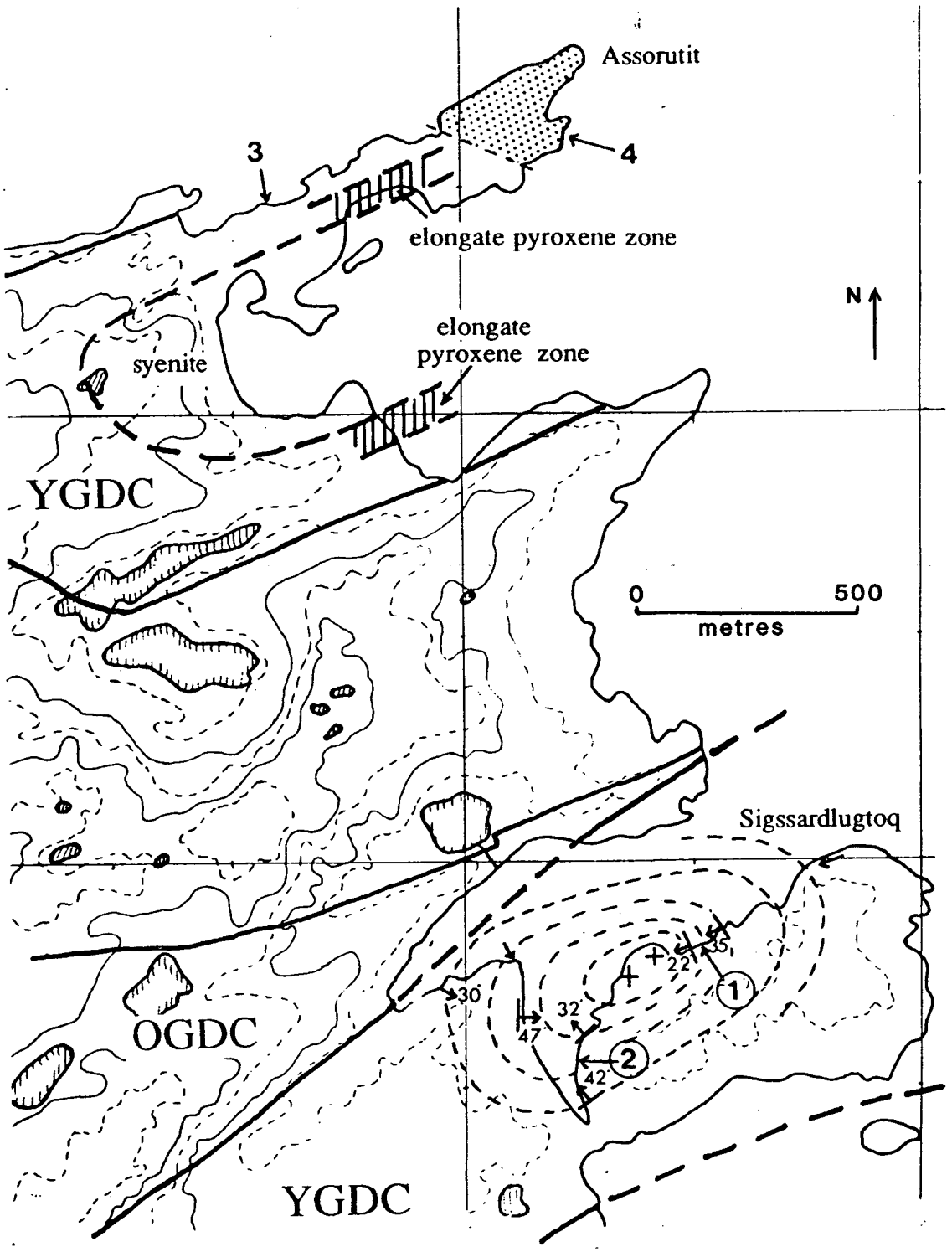


**Figure 2.4** Localities I (Sigssardlugtoq) and L (Assorutit) of Fig. 2.1. At locality I, feldspar lamination defines an elongate basin, and some lamination dips are shown. At locality L, a syenite pod is surrounded by syenogabbro characterised by elongate pyroxene crystals. Anorthosite xenoliths are common in the stippled area on Assorutit point; this area may have a faulted contact with the rest of the dyke segment at this locality. Localities 1-4 are mentioned in the text.

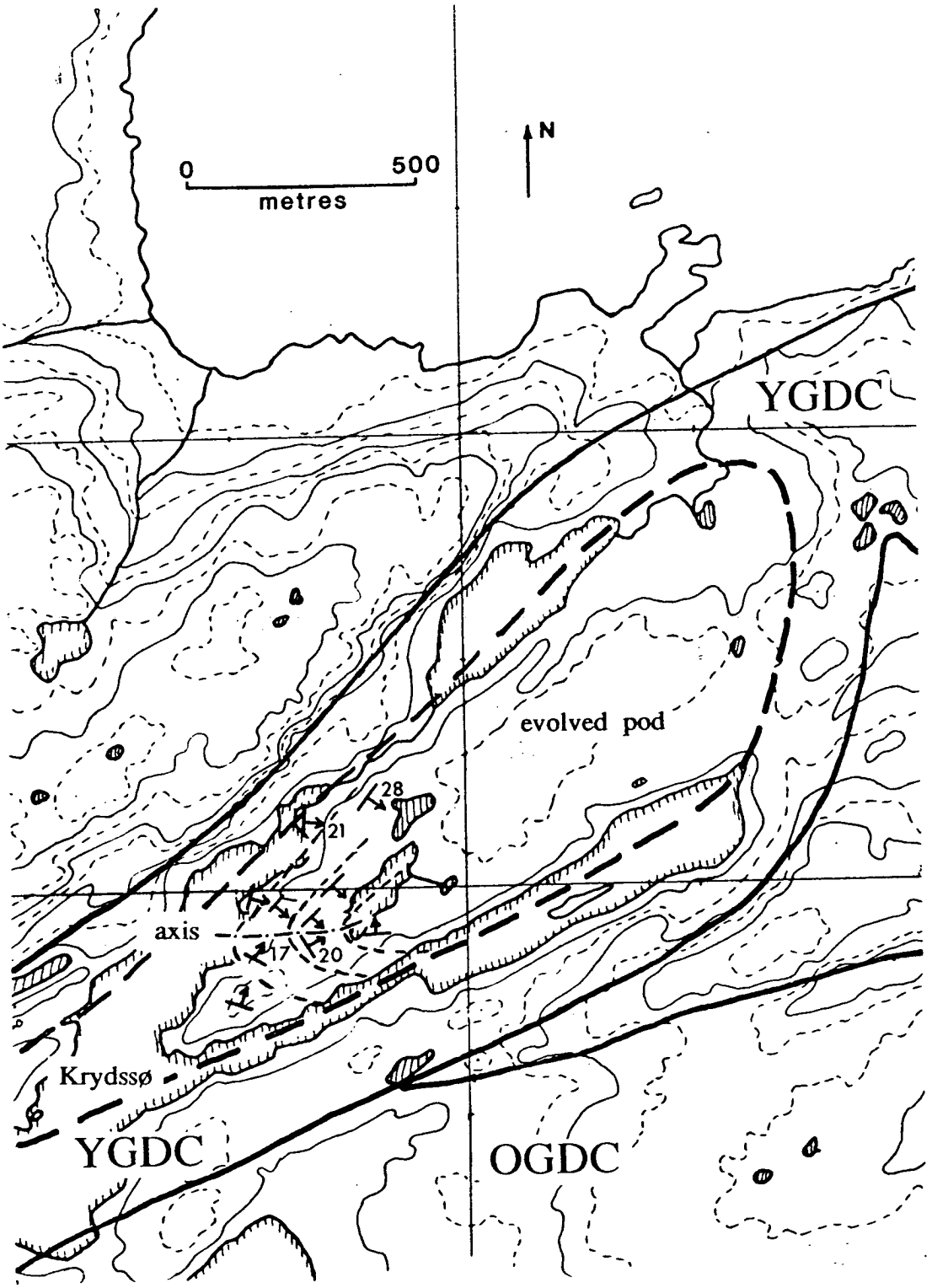


**Figure 2.5** Krydssø (Locality K of Fig. 2.1), showing the evolved pod surrounded by troctolite, with synformal layering at its western end.

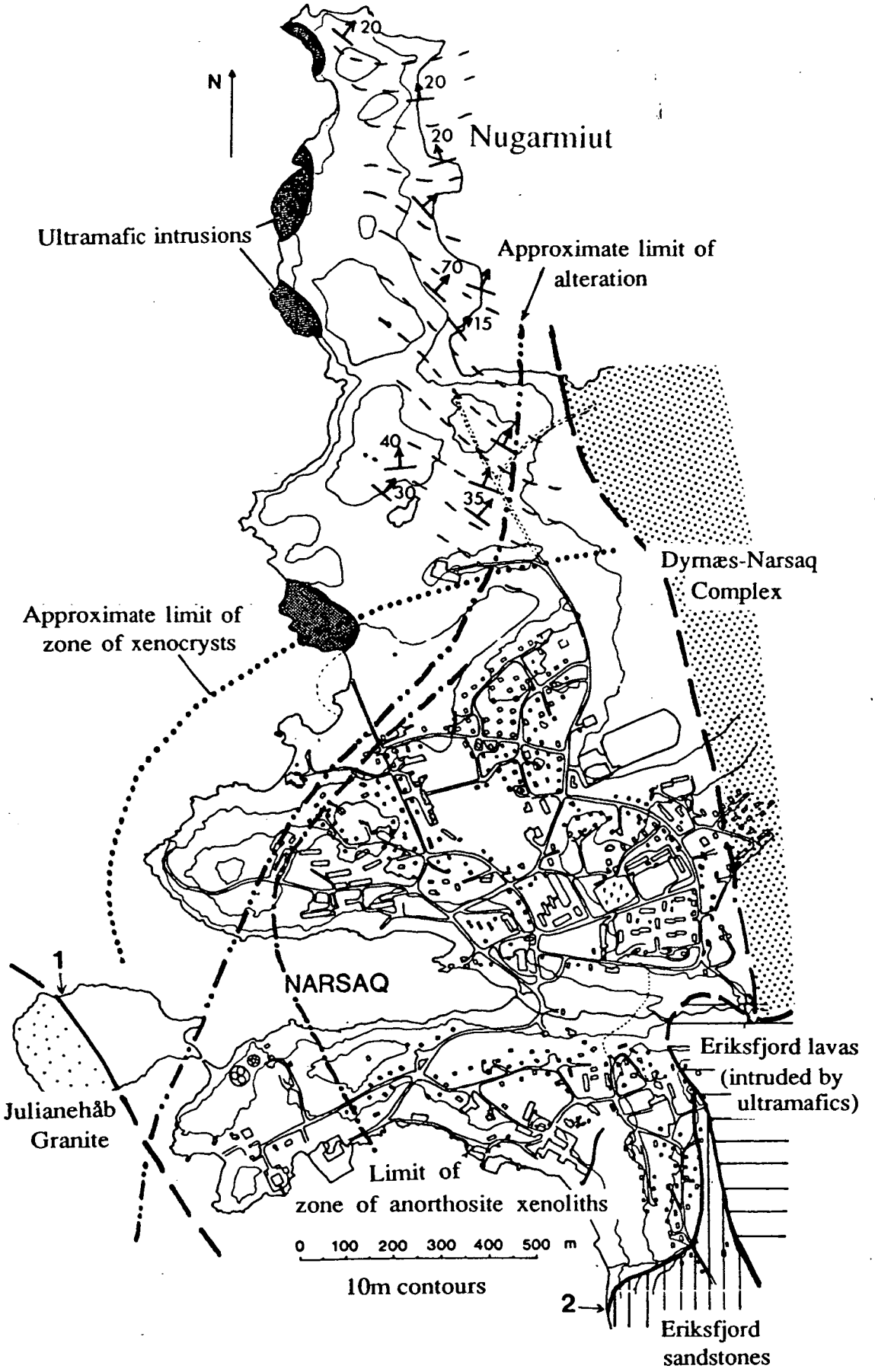


**Figure 2.6** Map of the Narsaq area (locality M of Fig. 2.1). Areas of anorthosite xenoliths, plagioclase xenocrysts and hydrothermal alteration due to the Dymæs-Narsaq complex are outlined. On the east side of the Nugarmiut peninsula, feldspar lamination dips approximately NE.

### 2.3.1 The western YGDC (localities A to E)

Dyke contacts are generally vertical, except for part of the northern margin at locality B, where the contact appears to dip inwards at about 80°. Chilled margins are 0.5-1m wide with some back-veining of the granite into the dyke, and at locality B some irregular coarser-grained patches within the chill. The northern margin at locality D is well-exposed and accessible and has been studied in detail; here there is a hybrid zone 0.5-1m wide where the granite contains irregular fine-grained dark patches up to 80cm in size (Plate 2.1a) and occasional large plagioclase crystals up to 1.5cm long, sometimes as radiating clusters. Between this zone and the inner troctolite there is a 1m zone of fine-grained gabbro (plagioclase 3-4mm, olivine 0.5-1mm) which has a sharp contact (within about 5mm) against the troctolite (Plate 2.1b). This rock appears to be compositionally very similar to the YGDC troctolite and may represent a late intrusion of the same magma.

The chilled margins (roughly 1-3m wide) have grain sizes of 0.5-1mm. The troctolites and subordinate gabbro picrites forming the dyke interior have plagioclase and olivine as major components; pyroxene, oxide and biotite are of minor importance. Feldspar forms roughly 70% of the troctolite and 5-20% of the gabbro picrite. Plagioclase is generally 0.5-1cm in length but noticeably larger crystals up to 2cm long, sometimes as stellate clusters, may form up to 30% of the rock in a few areas, most commonly near the margins of the dyke. Olivine crystals are 0.5-2mm, occasionally 3-4mm and tend to occur in irregular clusters, giving the impression of a larger grain size.

The above-described troctolite is very widespread in this western part of the dyke but exceptions are found. At locality B the troctolite of the northernmost 30m of the giant dyke, between the margin and a younger 20m wide dyke, is rather different from that seen elsewhere. The feldspar tablets are relatively thick and the mafic minerals form a smaller proportion of the rock than usual (about 20%). Oxide minerals are prominent and occur in roughly the same quantity as the olivines; both may be up to 1.5mm in size. The olivine crystals show little tendency to form aggregates and are often a lighter brown than is usual in this part of the dyke. Gabbro picrite slightly more feldspathic than that found in the most of the western YGDC, with 30-40% feldspathic material instead of 5-20%, also occurs in the northern limb of the synform at locality B. The gabbro of the northern part of the dyke east of the left-lateral fault at locality D (Fig. 2.2) also shows such features and contains grey

plagioclase megacrysts, probably xenocrysts, which are 2-4cm in length and often show dark rims of olivine 1-2mm wide. The alignment of these tabular xenocrysts defines a synformal structure. A hand specimen from locality E is rich in feldspar (70-80% of the mode) and contains anhedral olivine and oxide crystals scattered singly throughout the rock. The feldspars are 5mm long on average, and the mafic minerals 1-2mm in size. Clinopyroxene forms large, widely-spaced oikocrysts and makes up <5% of the rock.

Another feature of locality B is the development of elongated feldspars (a feldspar crescumulate rock) in areas within the outer 50m of the dyke. Feldspar crystals may be up to 6cm long but no more than 2mm wide, and are frequently curved, with their convex sides towards the dyke margins. Some radiate from a point while others grow perpendicular to the layering (Plate 2.1c & d). It usually appears as though these crystals are a relatively late phase growing across the layering and are often associated with, and sometimes grow inside, fine-grained leucocratic xenoliths (Plate 2.2).

Leucocratic veins up to 20cm wide composed of alkali feldspar up to 2cm in size with alkali pyroxene or amphibole are found occasionally in the western YGDC.

### 2.3.2 Southern branch of the eastern YGDC (localities F to I)

In this section of the giant dyke, rocks of locality F are similar to those seen further west, but at locality G and eastwards, Fe-Ti oxide minerals join plagioclase + olivine as major components of the troctolites. Feldspar still forms 60-70% of the rocks. Mafic facies are olivine + oxide cumulates, with roughly equal proportions of olivine and oxide, and feldspar forming 5-30% of the mode. Thus oxides are present modally at the expense of olivine.

Dyke contacts are again mainly vertical, but between localities H and I the contacts dip steeply outward, and the narrowing of the dyke in this region (Fig. 2.1) is a function of topography. Margins are often well-chilled but some back-veining of the granite occurs. At localities F and G hybrid zones up to 1.5m wide are seen, consisting either of granite with diffuse dark patches as at locality D, or of marginal giant dyke material containing rounded crystals of quartz and alkali feldspar with dark reaction rims. At locality I, two 30cm wall-rock xenoliths are found within the dyke.

A blunt termination of the dyke is seen at locality F (Fig. 2.1). The chilled facies at this locality consists of a homogeneous rock having a grain size of about 1mm and containing phenocrysts of olivine and plagioclase. The olivine may be up to 3mm in size while tabular plagioclase phenocrysts are commonly 1-2cm long and may reach 4cm. Roughly spherical stellate composite glomerocrysts consisting of plagioclase and olivine with interstitial oxides, pyroxene and biotite are common and may be up to 3cm in diameter (Plate 2.3a). There appears to be a complete range between a phenocryst-free chill (usually at the very margins of the dyke) to a coarse-grained rock composed of crystals and clusters of crystals identical to the phenocrysts, with none of the interstitial fine-grained material. There is a general decrease in the proportion of fine-grained groundmass away from the margins and the blunt termination of the dyke, but there may sometimes be abrupt transitions between rocks with a majority of groundmass and rocks with a majority of large crystals. About 200m east from the termination the dyke is composed entirely of coarse-grained troctolite (apart from 1m wide chilled margins). Minor gabbro picrites occur.

Localities G and I are notable for showing feldspar alignment which defines the synformal structure. At locality G a coarse-grained troctolite with plagioclase crystals up to 2cm surrounds a finer-grained layered pod (plagioclase 3-5mm) showing modal layering and feldspar lamination. The finer-grained pod takes up only about a third of the dyke width. The western end of the pod can be seen on the small island in Marrait bay (Fig. 2.3); to the west of this the troctolite is very coarse with numerous stellate clusters of plagioclase (Plate 2.3b). The rock also contains olivine and oxide crystals which are frequently 1-2mm in size and which show less tendency to clumping than do olivine crystals in the western part of the dyke complex. Interstitial pyroxene may reach 3mm and, on broken surfaces, slender needles of apatite up to 5mm long can be seen. A small amount of biotite is also present.

To the north and south of the layered pod the troctolite is less coarse-grained but there is still a noticeable transition between this and the finer-grained rock of the layered pod. The transition varies from fairly sharp (taking place over about 1cm) to more gradual. The boundary is irregular; in places it may be subvertical and in others subhorizontal, and some areas of the coarse-grained rock are found within the edges of the pod. The finer-grained troctolite contains plagioclase up to 1cm long and olivine and oxides of about 1mm. The plagioclase crystals show a marked alignment

and define a synformal shape. Large stellate clusters of plagioclase such as occur in the marginal troctolite are found occasionally in the layered pod (Plate 2.3c) and the lamination sometimes bends around them.

Veining is common in this part of the giant dyke complex; veins may contain blocky alkali feldspar, blue-green amphibole and biotite. Grain sizes vary from 1mm to 1cm but within a single vein all grains tend to be of a similar size. Epidotised veins are also found, as are occasional pegmatitic patches with crystals up to 5cm in size. The troctolite may be propylitised along shear planes, with the feldspars becoming chalky white and the olivine being replaced by fine-grained green-black material.

At locality I, the rocks are composed of 60% tabular plagioclase showing well-defined lamination, with interstitial olivine and oxides (Plate 2.3d). Feldspar lamination begins 20m from the northern margin and 200m from the southern margin of the dyke and defines a basin slightly elongated along the dyke (Fig. 2.4). A 10m x 10m pod near the south margin is composed of browner-weathering finer-grained troctolite. Within this pod, plagioclase crystals are generally 0.5cm in size, occasionally larger, with mafic minerals less than 1mm in size, showing a tendancy to cluster together. A little pyroxene, biotite and apatite are also present. The rock is very similar in appearance to the troctolite of localities B to D but shows much browner weathered surfaces. Outside the layered pod the plagioclases may be up to 1cm, and the weathered surfaces are not so brown. Subordinate olivine-oxide cumulates occur associated with both types of troctolite.

Locality H has been described by Upton (1987) as similar to locality I, showing synformal plagioclase lamination. Hand specimens from the GGU collection are similar to laminated rocks from localities G and I.

### 2.3.3 Northern branch of the eastern YGDC (localities J to L)

The geology of the eastern part of this dyke branch is dominated by the two pods of more evolved rock which occupy the central portion of the dyke (localities K and L of Fig. 2.1). These were originally thought by Upton (1964b, p.26) to be separate intrusions but were later ascribed to in-situ differentiation (Upton and Thomas, 1980, Upton, 1987). The latter possibility is thought more likely here, because the transitions between troctolite and evolved facies seem to be gradual

wherever they are exposed, and in-situ differentiation is common in other Gardar intrusives (e.g. Klokken, Parsons, 1979, 1981). However, the central syenitic portions of the giant dykes of Isortoq, to the north, do appear to be separate intrusions (Becker, 1984).

Anorthosite xenoliths, up to 100m in size, and plagioclase xenocrysts are common in the troctolite to the north of the evolved pod at locality L (Assorutit). They are described more fully in section 2.5.

Good chill samples were obtained from both localities; at locality L there has been some interaction with the granite to produce a hybrid rock but samples taken 1-2m into the dyke appear to be uncontaminated. At locality K about 15m of vertical contact between the giant dyke chill and the granite are exposed, and the outermost metre of the troctolite contains horizontal pegmatitic "strings" 1-2cm thick and up to 50cm long. Pegmatitic patches are also common in the troctolite at locality L and will be described in detail below.

At locality K (Krydssø), the troctolite sheath, which is about 100m wide, is composed of plagioclase crystals which are relatively thick in proportion to their length and up to 1.5cm long, with olivine crystals up to 3mm and oxides up to 5mm in size. The mafic minerals tend to be irregular in shape and the olivines do not clump together. Pyroxene is still interstitial and the rock is similar in appearance to the troctolite found near the northern margin at locality B and at locality D east of the fault. The rock in the central pod is here referred to as a syenogabbro. In the field, it can be seen to contain prismatic pyroxenes up to 2mm long with less olivine than the troctolite, and the olivines tend to be light brown to yellow-green rather than black. Feldspar crystals are blocky and 3-4mm long. Oxides of 1-2mm are evident, as is a relatively large amount of apatite (a few % of the mode), while biotite forms perhaps 10% of the mode, much more than in the troctolite. The rock is nearly always deeply weathered, brown, crumbly and difficult to sample, probably due to the hydration and oxidation of iron-rich olivines, and possibly to the relatively high proportion of micas.

The troctolite of locality L is similar to that at locality K but contains pegmatitic patches. The first pegmatites are seen within 1m of the margin and the proportion of pegmatite in the rock increases to about 20% near the syenogabbroic

facies. Pegmatitic areas may be up to 40cm in size but are frequently smaller (Plate 2.4a). They have a grain size which may be anything from slightly larger than the troctolite (about 1.5cm) to 3cm, and contain feldspar, pyroxene and olivine.

100-140m from the margins at locality L, a zone of syenogabbro characterised by highly elongated pyroxene crystals occurs. The zone is up to 80m wide, although some of this width is taken up by younger dykes. The pyroxene occurs as crystals 1-2mm wide and up to 10cm long, in bunches of about 5 to 15 sub-parallel crystals. The bunches show a slight tendency for a N-S orientation with inclinations from vertical to horizontal, but in general give the impression of being randomly orientated (Plate 2.4b & c). In places within this zone the pyroxene crystals lack the elongate habit and form 5mm prisms in an equigranular rock.

The syenogabbro passes transitionally into syenite composed of 80% stubby alkali feldspar with prismatic pyroxene and oxides, all up to 5mm in size. The rock is slightly coarser than the syenogabbro at locality K. Olivine is difficult to distinguish in the field but a little biotite, less than at locality K, is visible. The rock is a slightly greenish grey when fresh and weathers to a pinkish brown. Occasionally, more elongate feldspars up to 2mm long occur and very locally these appear to be aligned with one another to some extent.

A fine-grained grey aplite with a grain size of 1-3mm is found within the syenite (Plate 2.4d). This may occur as rounded to irregular patches up to 40cm across, with sharp to more diffuse margins, and as vein-like structures up to 30cm wide and several metres long. It contains pink feldspars with mafic minerals which occasionally show a streaky banding. Coarser patches a few centimetres in size within the aplite contain feldspar, pyroxene or amphibole and quartz.

Pegmatitic patches are common in the syenite as in the troctolite, containing feldspar crystals up to 15cm long, sometimes with dark rims (Plate 2.5a). Associated mafic minerals are probably predominantly amphibole, but depending upon composition and extent of hydration the colour and appearance may vary from dark (blue-black to green-black) and shiny to blue or green and fibrous. Interstitial quartz and calcite are also present.

Numerous veins up to 0.5m wide, showing no preferred orientation, cut the troctolites and syenites at both localities; the veins contain alkali feldspar, sometimes up to 10cm long, with pyroxene or amphibole and interstitial quartz and calcite. The feldspars sometimes show a schiller effect and may have dark rims. Some shear

zones also occur, and along these the troctolite has been substantially altered, with the mafic minerals being replaced by a very fine-grained greenish black alteration product. Vertical shear zones up to 0.5m wide also cut the syenite. No sense-of-shear criteria could be determined.

### 2.3.4 Narsaq (locality M)

The town of Narsaq is built on troctolite which is similar to that of the YGDC on Tugtutoq, especially the southern branch, except that it is often coarser-grained. As at locality L, plagioclase xenocrysts and anorthosite xenoliths are very common in a particular area within the troctolite. The later syenitic and granitic Dymæs-Narsaq complex cuts across the troctolite, obliterating most of its contacts with the country rock and causing considerable hydrothermal alteration and veining of the rocks. However, two intrusive contacts can be seen. One of these is between troctolite and granite on Narsaq Island (locality 1 of Fig. 2.6); this is vertical with a zone of altered country rock a few metres wide and horizontal pegmatitic "strings" in the gabbro chilled margin (Plate 2.5b,c & d). On the mainland to the south of Narsaq (locality 2 of Fig. 2.6) the troctolite has a contact against sandstones of the Eriksfjord Formation, the contact varying between low and high angle. The troctolite matrix here has a grain size of a few mm, slightly coarser than some of the chilled margins against granite, and is full of plagioclase xenocrysts. The contact is irregular, with plagioclase crystals up to 2cm long apparently at the very margins of the intrusion (Plate 2.6a & b).

The zone containing xenoliths usually shows considerable alteration (Fig. 2.6) and the troctolite is best studied on the Nugarmiut peninsula. Here, plagioclase crystals are 1-3cm in length and exceptionally up to 6cm, sometimes showing lamination (Plate 2.6c). Olivine, oxides and interstitial pyroxene are up to 3mm and do not tend to form aggregates. The best lamination and the coarsest grain size are found on the east of the peninsula; on the west most of the coastal exposure is of ultramafic pyroxenite intrusions but some troctolite with an average grain size and poor lamination is seen. Olivine-oxide cumulates are also found on the Nugarmiut peninsula and will be described in more detail below.

**Plate 2.1**

(a) Hybrid rocks at the northern margin of the giant dyke at locality D (Itivdlip Sarqâ). The country-rock granite (showing large orthoclase crystals) contains diffuse dark patches, up to 1m in size, of giant dyke material.

(b) Abrupt transition between fine-grained and coarser-grained marginal facies about 0.5m further into the dyke than (a). The coarser-grained rock contains some plagioclase phenocrysts. Lens cap (about 5cm across) for scale.

(c) Elongate feldspars near the south margin of the dyke at locality B, growing from the top of a discontinuous troctolite layer which runs from top left to bottom right of the photo. The feldspars appear to have grown across a gabbro picrite layer containing fine feldspathic streaks. Pocket knife is about 10cm long.

(d) Close-up of elongate feldspars, showing their slight curvature with convex sides towards the dyke margin.


a

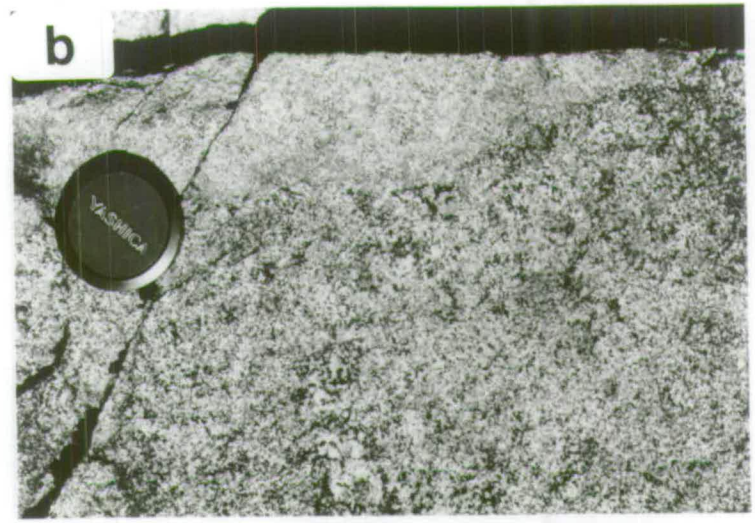
b

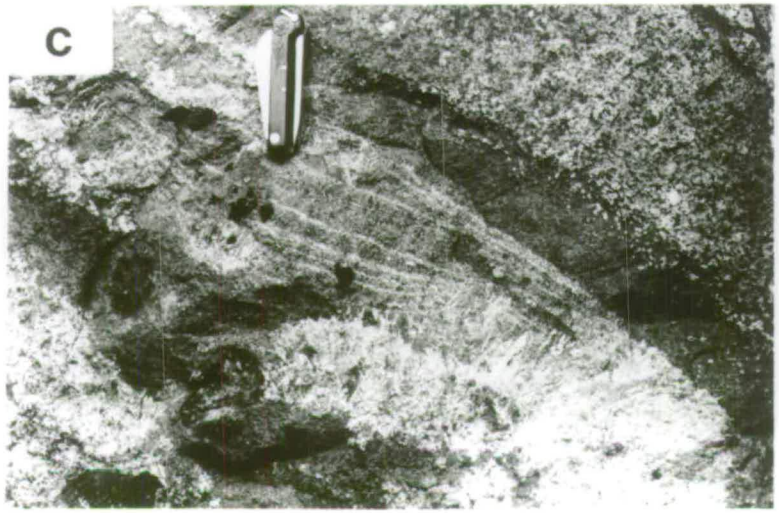
c

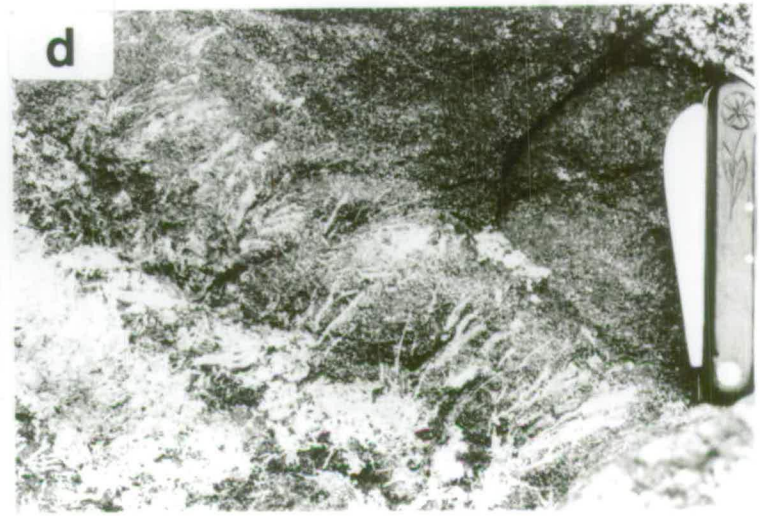
d

Plate 2.2

(a) Elongate feldspars at locality B apparently growing from fine-grained leucocratic xenoliths within a gabbro picrite layer. Lens cap for scale.

(b) Sketch of (a). Heavy stipple denotes gabbro picrite, light stipple troctolite.

(c) Elongate feldspars growing within a fine-grained leucocratic xenolith in a gabbro picrite layer at locality B. Scale bar has 5cm divisions.

(d) Sketch of (c). Shading as (b).


a

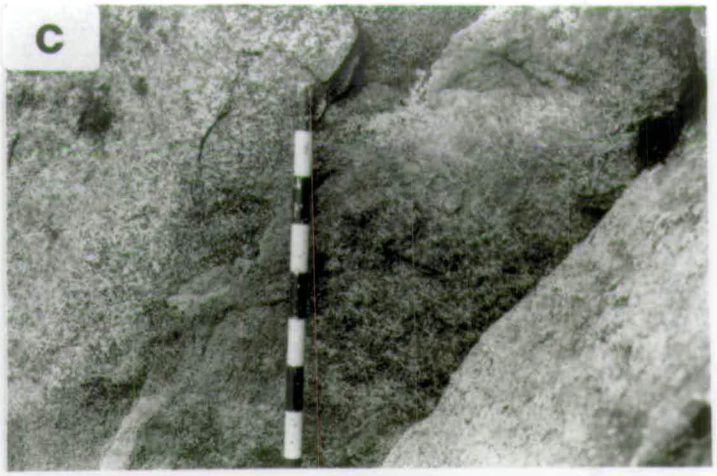
c

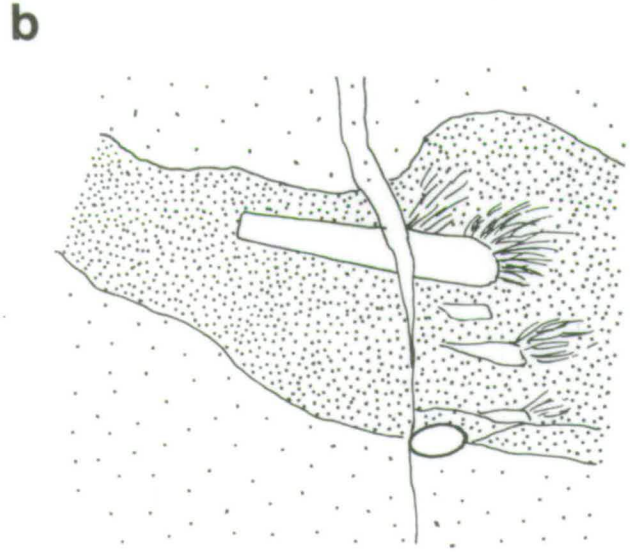
b


d

**Plate 2.3**

(a) Plagioclase and olivine phenocrysts, sometimes as composite glomerocrysts, in the chilled margin of locality F. Lens cap for scale.

(b) Coarse-grained troctolite on the west side of Marrait bay (locality G). Some of the plagioclase crystals form stellate aggregates. Lens cap for scale.

(c) Finer-grained laminated troctolite in the layered pod at locality G. Some coarser stellate aggregates of plagioclase + olivine can be seen. A faint mafic layer (running from left to upper right) is also visible. The dark crescent at the base of the photo is an area of damp rock. Coin c. 2cm in diameter.

(d) Laminated troctolite at locality I.

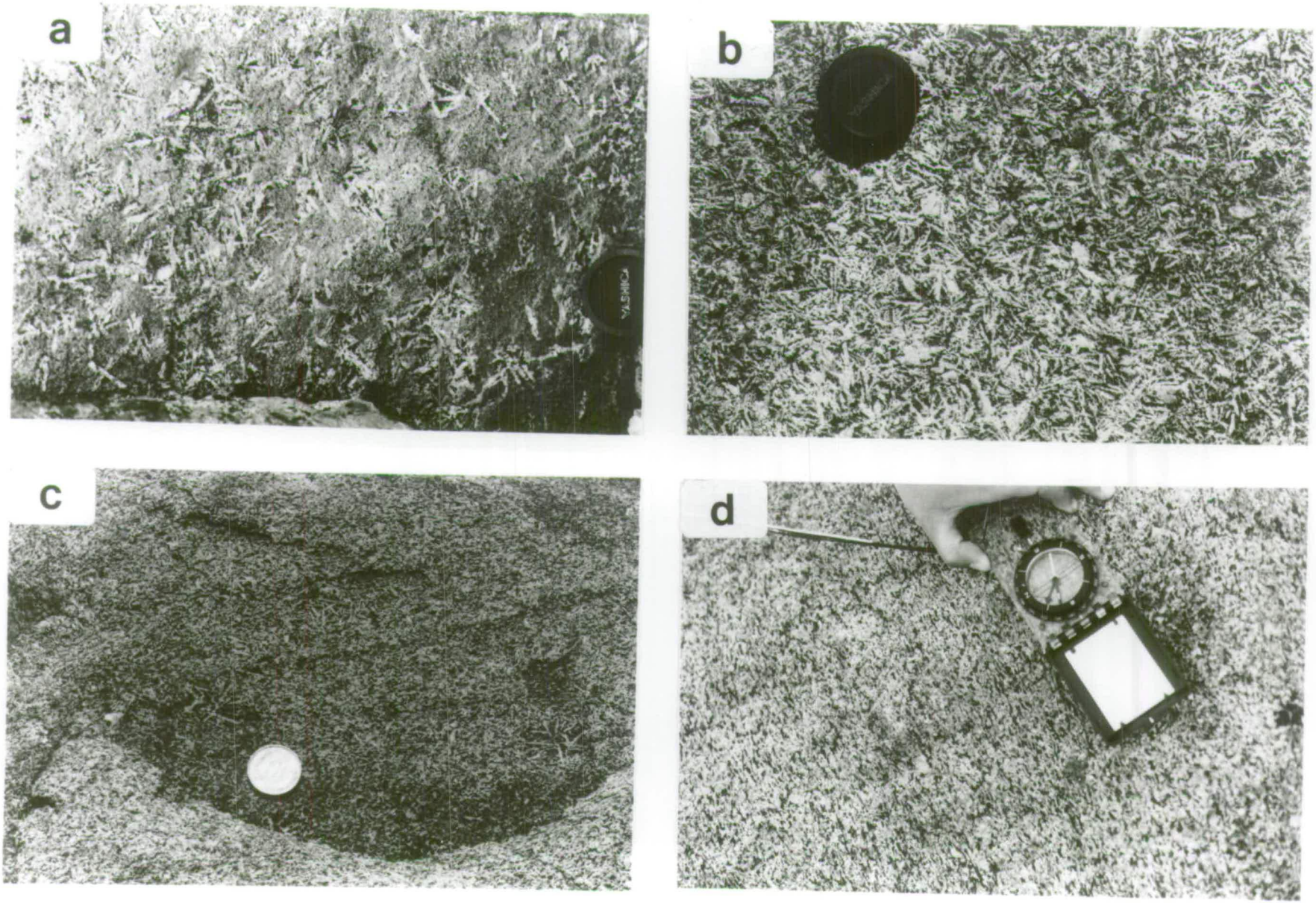
a
b
c
d

**Plate 2.4**

(a) Pegmatitic patch containing feldspar, olivine and clinopyroxene, in the troctolite sheath at locality L (Assorutit). Lens cap for scale.

(b) Elongate pyroxene facies in the syenogabbro zone of locality L. Lens cap for scale.

(c) Elongate pyroxene facies in the syenogabbro zone of locality L. Pocket knife c. 10cm long.

(d) Fine-grained grey aplite within the syenite of locality L. Hammer handle 50cm long.

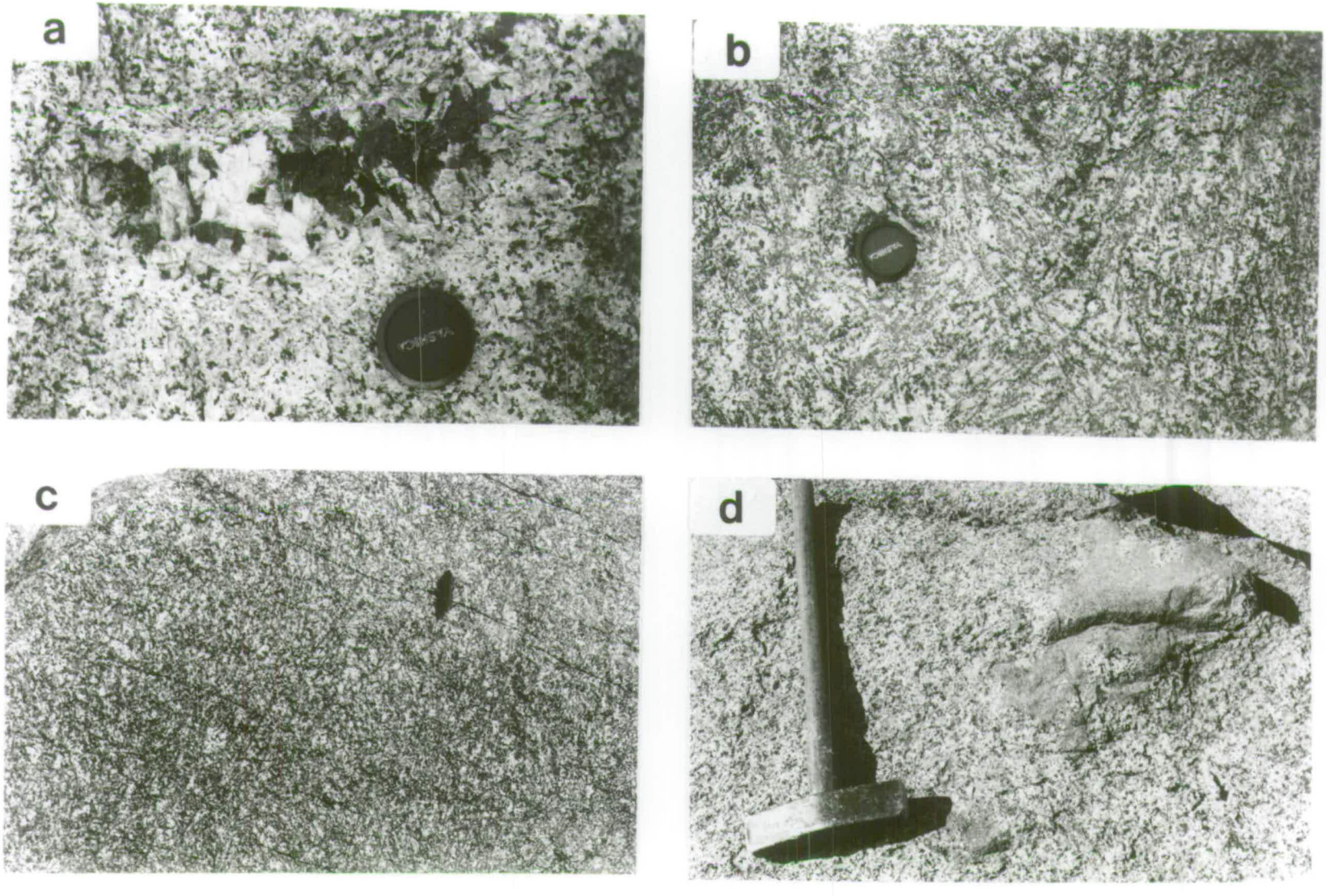
a
b
c
d

**Plate 2.5**

(a) Pegmatite within the syenite at locality L. Feldspars show dark reaction rims. Lens cap for scale.

(b) Vertical contact three-quarters of the way across photo from the left hand edge, between giant dyke and Julianehåb granite on Narsaq Island. The granite outcrops forming the right-hand quarter of the photograph are paler-weathering and more rounded than the troctolite. Total vertical height c. 30m.



(c) Contact between giant dyke (left) and granite (right) on Narsaq island. The dyke margin shows horizontal pegmatitic "strings" several metres long while the granite (appearing darker here) contains rounded patches of dyke material. Total width of rock face showing pegmatite strings is about 10m.

(d) Sketch of (c) with the contact shown as a dotted line, giant dyke chill as heavy stipple and country-rock granite as light stipple.

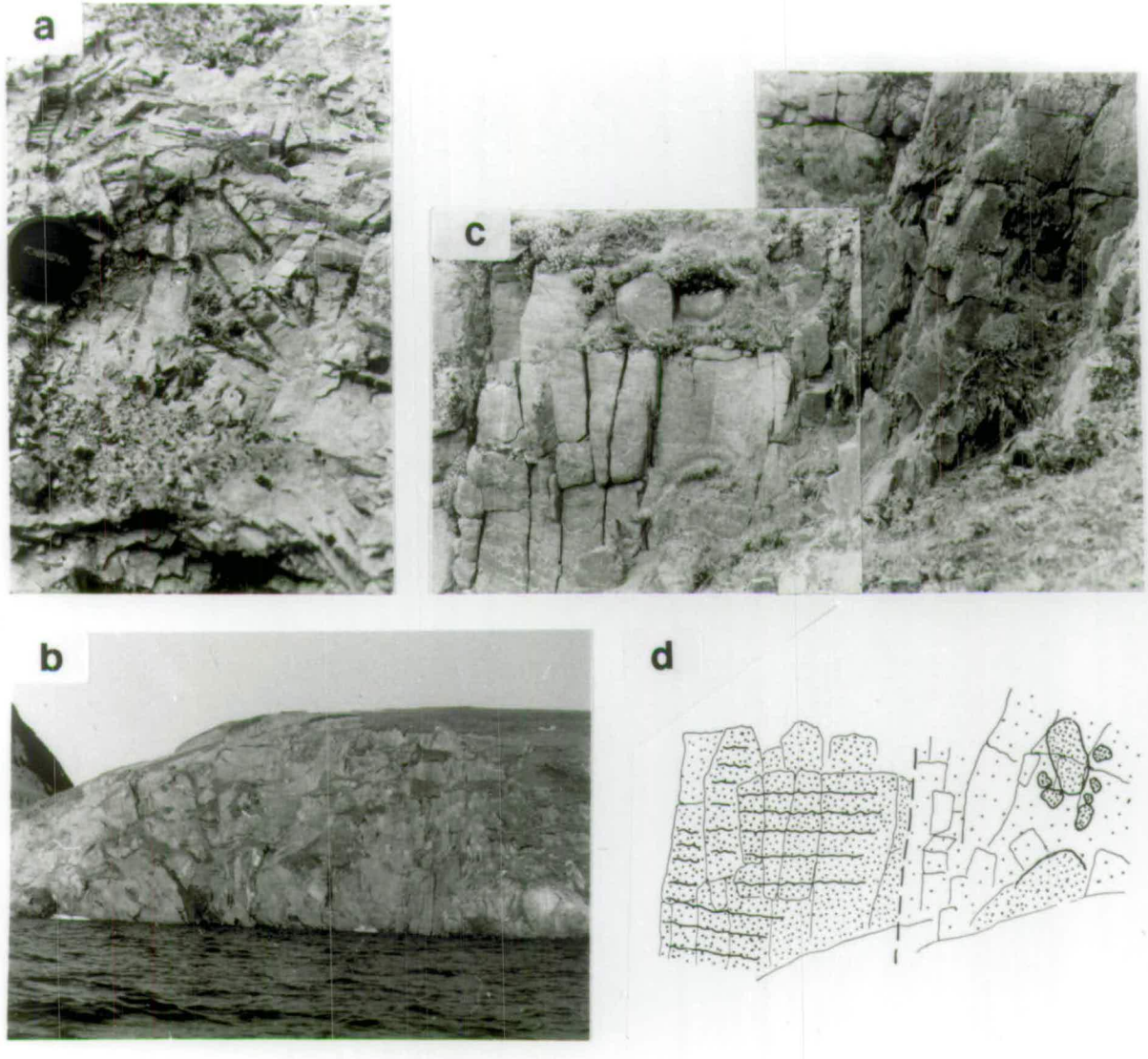
a
c
b
d

Plate 2.6

(a) Contact between YGDC and overlying Eriksfjord sandstone south of Narsaq. The uppermost YGDC is full of plagioclase xenocrysts (foreground) and the sandstone (top right) shows rather poorly defined bedding, roughly parallel with the contact. Both slope gently from left to right.

(b) Close-up of part of (a) showing plagioclase xenocrysts in the topmost YGDC protruding upwards into the sandstone, which may have experienced partial melting. Lens cap for scale.

(c) Coarse-grained troctolite on the east side of the Nugarmiut peninsula, showing feldspar alignment and faint mafic streaks parallel to the lamination. Lens cap for scale.


a


b

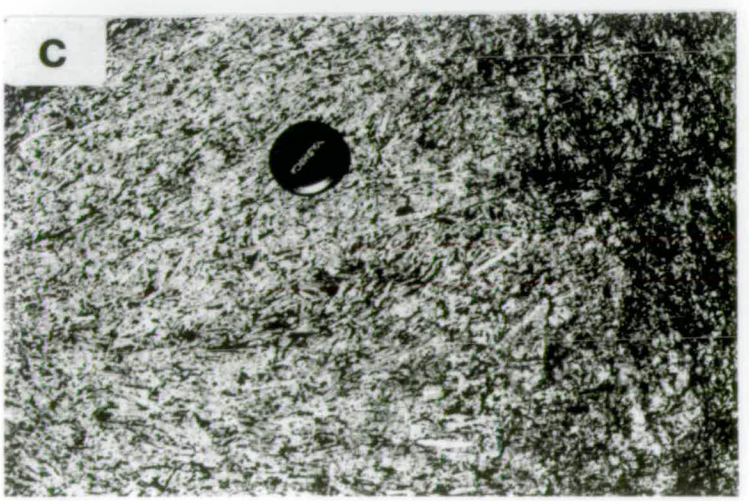
c

## 2.4 Layering features

A summary of layering features is given in Table 2.2, and schematic cross-sections of the dyke at different localities are presented in Figure 2.7.

### 2.4.1 The western YGDC

There is little or no plagioclase lamination in this portion of the dyke and the synformal structure is defined by modal layering. This is best exposed along the coast at Itivdlip Sarqâ (locality D) where both regular layering and occasional channel-like features or troughs occur. These are concave-upward lenses of gabbro picrite filling channels which eroded underlying layers. At locality B similar features are seen, whereas at locality C, gabbro picrites occur mainly as thick isolated troughs separated laterally and vertically by homogeneous troctolite. Gabbro picrite layers thicker than about 2cm almost invariably show prominent jointing perpendicular to, or at a high angle to, the edges of the layer or trough. This will be evident in many of the photographs.

Fine-grained leucocratic xenoliths are found in this area of the dyke and are often associated with mafic layers. They will be described more fully in section 2.5.

Several minor faults may be seen within the cumulates, some being ductile high temperature features while others are lower temperature, brittle failures. Faults showing ductile deformation are usually normal and parallel to the dyke margins with inward throws of up to 3m. Faults at high angles to the dyke trend tend to show brittle failure and may have normal, reverse and/or strike slip movements of up to 1m.

Locality A was not visited but is described by Upton (1987) as having a wide unlayered margin with synformal modal layering in the central portion of the dyke. Locality E is unlayered.

#### 2.4.1.1 Locality D (Itivdlip Sarqâ)

This locality is described first because it provides the best developed and best exposed layering. It is unique in having two synforms side by side, with a northern synform 550m wide and a narrower southern synform about 100m wide. The

Table 2.2 Summary of YGDC layering features (see also Fig. 2.7)

| Locality | Description |
|---|---|
| B | Synform defined by modal layering. Sharply bounded gabbro picrite layers (1cm-1m) separated by thicker troctolite layers are often laterally discontinuous and non-parallel. Gabbro picrite troughs up to 3.5m deep occur. |
| C | Layering is dominated by large troughs of gabbro picrite (several metres wide by 0.5-2m deep) within otherwise unlayered trocotlite. Some localised, often irregular, finer-scale modal layering also seen. Layering still synformal. |
| D | Unique double synform, with sharp contact between synforms. Shallow northern synform 550m broad defined by predominantly regular modal layering dipping 30-40$^{o}$ at margins. Gabbro picrite layers 1cm-1m, troctolite thicker. Small troughs of gabbro picrite also occur. Area of gabbro picrite blocks within troctolite matrix in synform axis. Southern synform 100m wide, with modal layering often less well-defined than in northern synform and more steeply dipping (40-50$^{o}$). Channelling, cross-bedding and ductile faulting seen. Massive gabbro picrite in centre of synform. East of the fault no modal layering, synform defined by sparse plagioclase megacrysts. |
| F | Slumped and brecciated near-vertical layers seen near S margin. Poorly-defined layers of relatively feldspathic gabbro picrite 1-40cm thick dip inward from margins. In axial zone, outcrops of massive gabbro picrite found, containing sparse synformally aligned plagioclase tablets. |
| G | Synformal modal layering found in central finer-grained laminated pod. Dips are 70$^{o}$ at edge of pod. Olivine-oxide layers are diffuse, 1-5cm thick and 3-15cm apart, showing some normal grading in the synform axis. |
| I | Plagioclase lamination defines an elongate basin, dipping 30-40$^{o}$ at edges. Occasional wispy concentrations of mafic minerals or of feldspar are seen parallel to the lamination. Irregular areas of olivine-oxide cumulates cut across the lamination in places. The pod of finer-grained troctolite near the S margin shows thin (1cm) synformal layers. |
| K | Poorly-defined modal variation within evolved pod defines an eastward plunging synform. Layers are 1-10cm in thickness and may be more felsic or more mafic than average rock. Some are graded from mafic bases to feldspathic tops. |
| L | No true layering, only wispy mafic schlieren. |
| M | Feldspar lamination (only seen to N of Narsaq) shows variable dip and dip direction but latter generally to NE. The lamination may be disrupted in places. Streaks and pods of olivine-oxide cumulates are seen, the largest several metres long and up to 1m wide. |

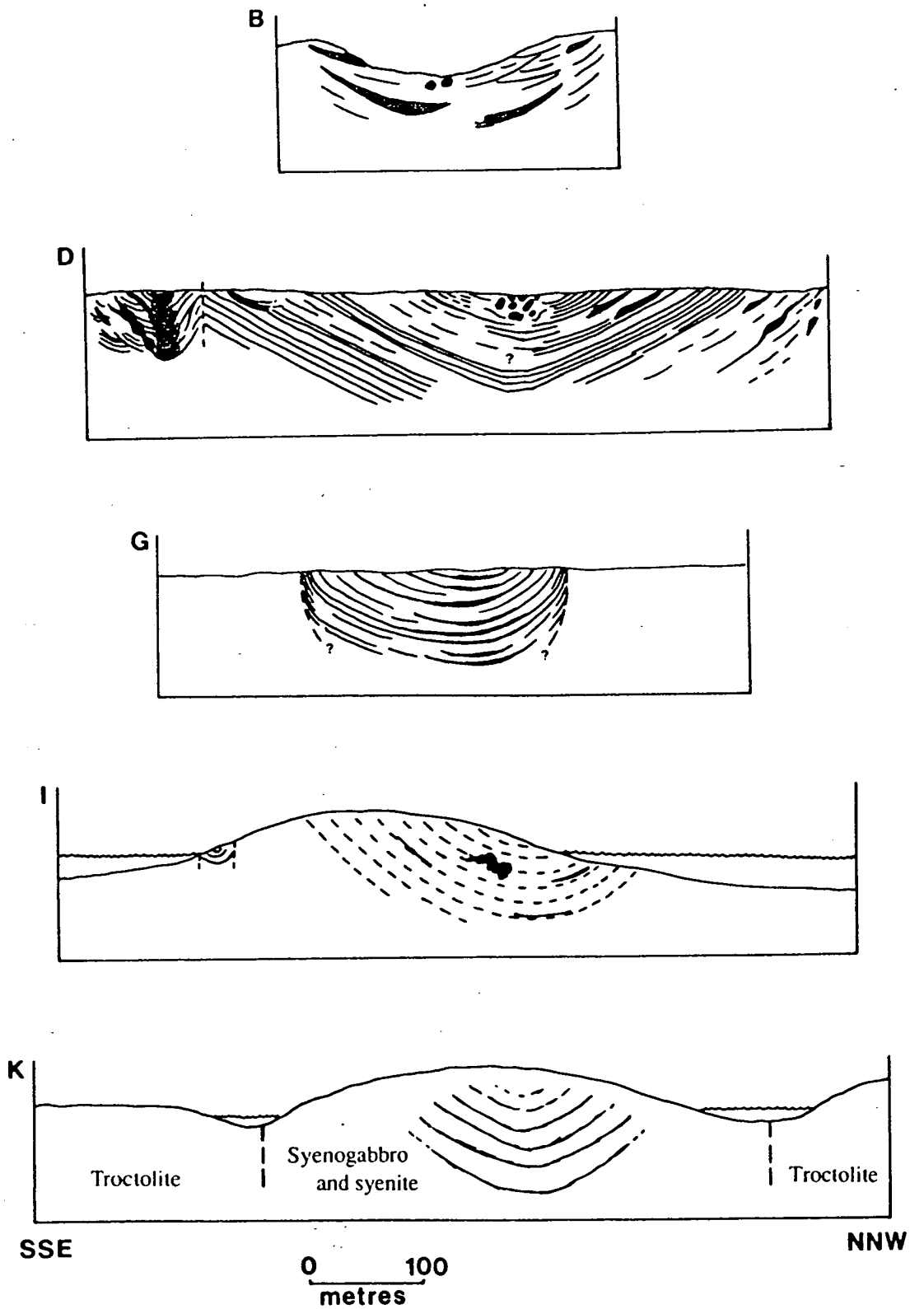


**Figure 2.7** Schematic cross sections of layering at localities B, D, G, I and K of Fig. 2.1. The relative widths of the dyke segments are indicated, but layer dips are not accurate. Dotted lines at locality I denote feldspar lamination without modal layering.

northern synform will be described first, from north to south. The northern contact has been described in the previous section; faint modal layering dipping 40°S and defined by concentration of olivine appears within 1m of the contact but the layering tends to be weak and disturbed for the first 80m into the dyke. Within this first section a gabbro picrite layer with a maximum thickness of 0.5m is offset by steep normal faults dipping 60-70°S (Fig. 2.8a). Two small channels are also seen plunging towards the synform axis (Fig. 2.8b). About 80m into the dyke fairly regular layering begins, dipping about 30°S and persisting for about 75m measured on the ground (40m perpendicular to the layering). The northernmost part of this regular layering is defined by layers of gabbro picrite 0.5-2cm in thickness separated by troctolite 10-40cm thick (Plate 2.7a). A stratigraphic section of Plate 2.7a (100m from the northern margin, locality 1 of Fig. 2.2) is shown in Fig. 2.9. Nearer the axis the gabbro picrite layers are generally thicker (1-5cm with channels up to 1m thick) and more closely spaced (troctolite 2-40cm) (Plate 2.7b). Two stratigraphic sections measured at this locality (150m from the margin, locality 2 of Fig. 2.2) are shown in Fig. 2.10.

Many of the gabbro picrite layers in this locality, while appearing approximately parallel, show changes in thickness and spacing and may divide or merge when followed along strike. It is thought that these features represent very low-angle unconformities.

Layer boundaries may be either sharp (within a few grain diameters) or more diffuse, and either flat or irregular. The most common type of gabbro picrite layer in the northern synform at locality D is one with a sharp but irregular base and a flatter, sometime more diffuse top (Plate 2.7c). The irregularities in the base may be loading features, since the gabbro picrite material will have been more dense than the troctolite, or may represent the shape of the underlying cumulates when the mafic layers formed. The layer tops can be sharp or more diffuse, with cumulus feldspar reappearing either as discrete crystals, or as aggregates of feldspar crystals. These aggregates are rounded in shape with no preferred orientation of the crystals and may be 0.5-3cm in size. They may also appear in the basal part of a layer, or especially of a channel (Plate 2.7d). Occasionally feldspar at the top of a gabbro picrite layer may be in the form of stellate clusters (Plate 2.8a).

This well-layered portion of the dyke is separated from another, nearer the synform axis, by about 30m (on the ground) of poorly layered troctolite containing one or two isolated channels (up to 30cm thick). The second section is about 40m

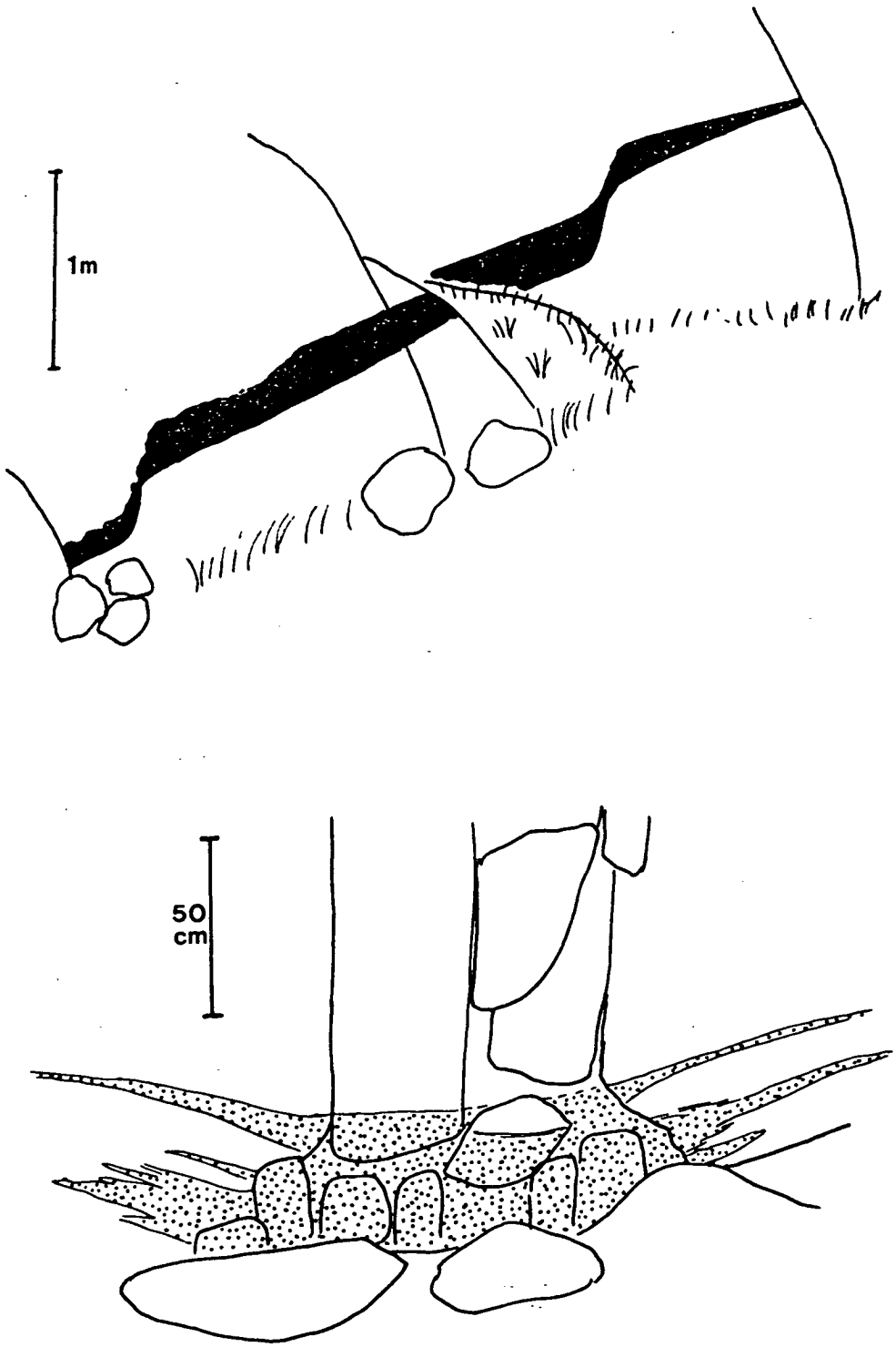


**Figure 2.8 (a)** Thick faulted gabbro picrite layer (black) a few metres from the northern margin at locality D, **(b)** Small channel plunging towards the synform axis, viewed looking S. Stipple indicates gabbro picrite.

wide and within it, layer dips change rapidly from 25-30° to horizontal, so that the overall shape defined by the layering is that of a flat-bottomed V rather than a U. On the coast the horizontal layers in the axis of the synform are relatively thin, consisting of gabbro picrite layers up to 1cm in thickness separated by 10-30cm troctolites (Plate 2.8b). In part of the axial zone (locality 3 of Fig. 2.2), an area of gabbro picrite blocks enclosed in a troctolitic matrix is found resting on undisturbed horizontal layering (Plate 2.8c & d and Plate 2.9).

Such blocks are found for about 10m perpendicular to the dyke axis and for about 30m inland; they appear to become less frequent inland but this may be due to the poorer exposure. The blocks range from a few cms to 3m in size and may be roughly square, rounded or irregular in shape. Some of the blocks are themselves layered and have been variously rotated. Where the gabbro picrite is slightly more feldspathic the margins of the blocks are less distinct (Plate 2.9b). Some are surrounded by mafic streaks and schlieren in the troctolitic matrix. These observations suggest that in this area, the gabbro picrite solidified earlier than the troctolite and was sufficiently coherent to break up into blocks while the troctolite was still unconsolidated. It is difficult to determine the direction of movement of the blocks; where indicators of movement, such as trailing mafic streaks, are present, they give different directions for different blocks. These blocks presumably result from the breakup of a thick gabbro picrite layer or layers, perhaps along the prominent jointing seen. They may have tumbled down into the synform axis under the influence of gravity or, alternatively, may have been transported along the axis as a debris flow. The underlying horizontally layered cumulates must have been essentially solidified at the time of deposition of the blocks, although there is evidence for one layer being broken and disrupted (Plate 2.9c). There must have been about 2m of unconsolidated troctolite above these horizontally-layered cumulates. The fact that the underlying layers are undisturbed indicates that the blocks were not derived from the disruption of these cumulates.

The southern limb of the synform is less well-exposed than the northern one, but shows a similar pattern of more and less strongly layered sections. About 450m from the northern margin, several gabbro picrite layers are seen, some of them channel-shaped, ranging from 5cm to 30cm in thickness.

Near the contact between the two synforms, but still within the northern synform, is a locality with regular layering of 2-5cm gabbro picrite layers separated by 3-30cm troctolite layers, which are truncated by an unconformity (Plate 2.10a).

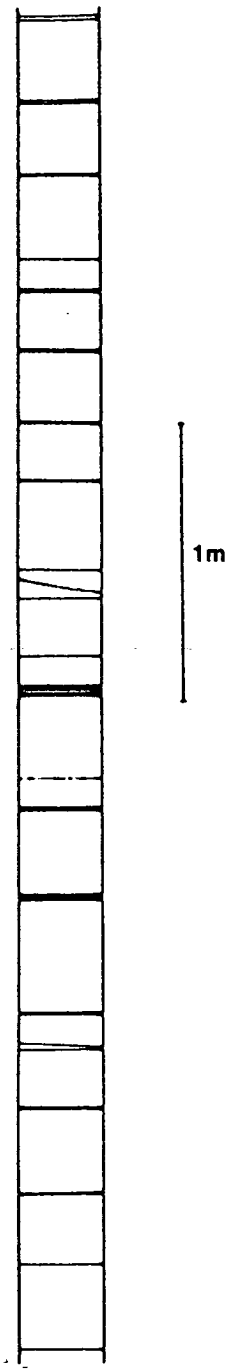


**Figure 2.9** Stratigraphic section 100 m from the N margin at locality D (see Plate 2.7a).

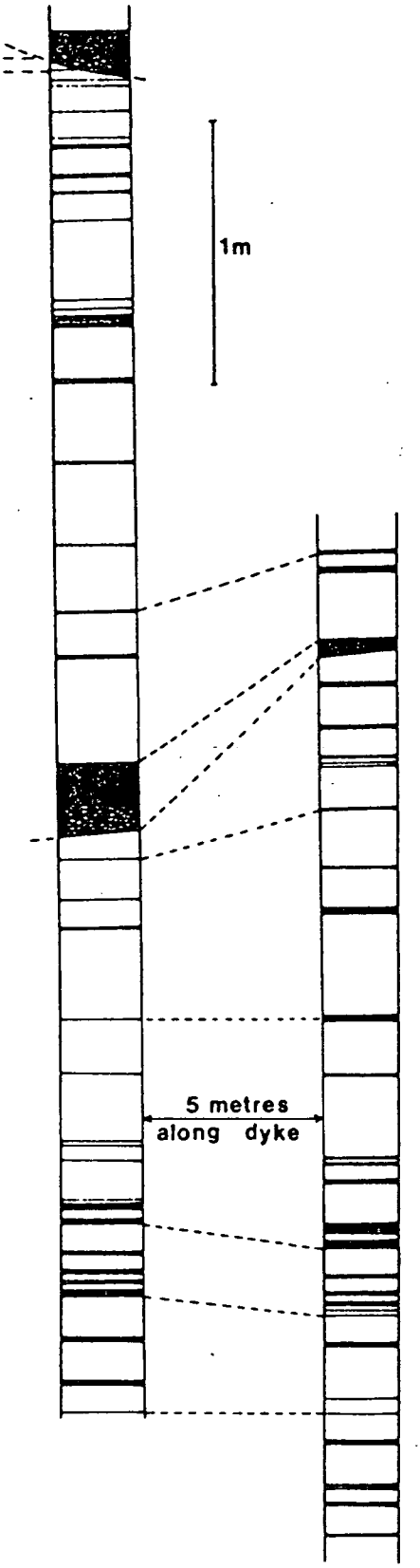


**Figure 2.10** Two stratigraphic sections, 5m apart parallel to the dyke trend, 150 m from the N margin at locality D (see Plate 2.7b). Note the two channels which erode underlying layers.

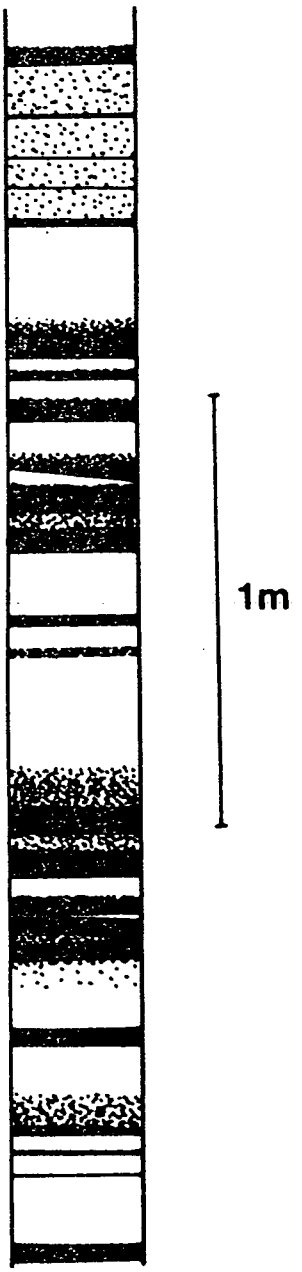


**Figure 2.11** Stratigraphic section of the outcrop shown in Plate 2.10d, within the N limb of the N synform at locality D. This section shows a greater proportion of gabbro picrite, and more diffuse layer contacts than those in Figs. 2.9 and 2.10.

This unconformity may have been caused by a channelling event, as the sketch in Plate 2.10b shows.

The contact between the two synforms (locality 4 of Fig. 2.2) is somewhat obscured by closely-spaced jointing, but as far as can be seen it is very sharp (within 2cm). The layering to the north of the contact is typical of that in the northern synform: northward dipping 1-2cm gabbro picrite layers are separated by 20-50cm troctolite layers. Some of the layers appear to be continuous across the contact, although with others it is unclear. The southward-dipping layers are less well-defined and less parallel than those to the north, with frequent changes in dip and apparent bifurcations which may be unconformities (Plate 2.10c). Average dips are about 40°, compared to 20-30° for the layers dipping northward. The contact between the synforms is only exposed on the coast.

Similar steep, relatively diffuse layering extends for perhaps 30m into the southern synform. The gabbro picrite layers are generally 1-10cm thick with poorly defined margins, especially at the layer tops; some could be described as normally graded (Plate 2.10d). Intervening troctolites are 5-50cm thick and frequently more mafic than the troctolites of the northern synform (ca. 40% mafic minerals instead of ca. 30%). There tends to be a higher ratio of picrite to troctolite; a stratigraphic section of Plate 2.10d is shown in Fig. 2.11, and can be compared with Figs. 2.9 and 2.10. 1-2cm aggregates of feldspar crystals are very common, especially at the tops of mafic layers. Dips are variable, from 30 to 50°S, and unconformities common (Plate 2.11a). Towards the axis, gabbro picrite layers thicken and the troctolite layers thin until they disappear altogether leaving a massive gabbro picrite unit at least 20m across and 20m thick occupying the axial portion of the synform. Occasional feldspar-rich streaks within this unit show the attitude of the layering.

To the south of the thick gabbro picrite, troctolite reappears and becomes the dominant rock type again, and a well-defined layered sequence forms the southern limb of the synform. Described from the dyke margin inwards, the layering begins with faint narrow (0.5-1cm) shallowly dipping gabbro picrite layers appearing about 5m from the margin. About 20m into the dyke the dips of the gabbro picrite layers become steeper and the layers thicken downwards, truncating earlier shallower ones (Plate 2.11b). A 2m gabbro picrite unit, dipping at 40-50° and offset by several normal faults with throws of up to 0.5m, is found within this layered sequence. It is made up of several layers which thicken and coalesce down dip, and may be a channel seen in dip section (Fig. 2.11c). Above this unit, fine (1cm) gabbro picrite

layers with 5-50cm intervening troctolites appear, some seeming to onlap onto the top of the thick layer, although this appearance may be due to the faulting. About 8m higher in the sequence another picrite unit thickens down dip to about 4m but is then faulted out. Another 10m (measured on the ground; 6-7m stratigraphically) of well-layered troctolite occurs before the gabbro picrite layers thicken and merge to form the axial picritic unit. Within this area of troctolite the layering is like that seen in the northern synform (well defined and parallel). Some striking high-temperature faults showing ductile deformation are seen here (Plate 2.11d & e).

To the east of the left-lateral strike slip fault which offsets this part of the giant dyke complex (east of the river in Fig. 2.2), no modal layering is seen. The only structure within the dyke is the synform defined by plagioclase megacrysts up to 5cm long, which show maximum dips of 30-40°. It is concluded that there has been vertical as well as lateral movement on the fault, so that the continuation of the layered pod is not seen at the surface.

#### 2.4.1.2 Locality C

The regular layering seen at the coast persists inland for 30-50m, with gabbro picrite layers gradually thinning and disappearing leaving unlayered troctolite. About 150m from the coast an area of isolated troughs and disturbed layering begins and extends for about 2km inland (Fig. 2.2).

The troughs or channels are similar to those seen on the coast (lenses of gabbro picrite thickening at the centre with concave sides upwards) but are generally larger. They plunge towards the synform axis and are best seen at the sides of valleys formed by the weathering of younger dykes parallel to the giant dyke. The width of the troughs may be 1-10m and the depth up to 2m, although many of them do not become thicker than 40cm (Plate 2.12a & b). Some of the troughs are multiple, composed of two or more vertically-stacked lenses of gabbro picrite separate at the edges but coalescing in the centre. In one place thin discontinuous concave-up layers are seen, which may be incipient channels that failed to develop a significant thickness (Plate 2.12c). At least ten large troughs were noted. The lower and upper contacts of these troughs are generally very sharp (within a few grain diameters), but the tops may be diffuse over a few centimetres with increasing proportions of feldspar aggregates (1-2cm in size) upwards.

Finer-scale layering is also found in this area; gabbro picrite layers between 1 and 10cm are seen, either singly or in groups forming a layered section of perhaps a metre, but never for tens of metres at a time as seen on the coast, These layers frequently have variable thickness, spacing and dip and sometimes show unconformities (Plate 2.12d).

About 800m west of the horizontal layering seen on the coast in the axis of the northern synform (locality 5 of Fig. 2.2), thick horizontal gabbro picrites are found. Over a vertical distance of about 2.5m, gabbro picrite is dominant over troctolite; the latter forms several layers 10cm thick (Plate 2.13a). It is possible that these thick gabbro picrites could have been a source for the blocks seen on the coast at locality 3, but there is no sign of disruption of the layers and in fact the prominent gabbro picrite jointing seen elsewhere is not so well developed here. The olivine crystals in these layers are noticeably coarser than those seen elsewhere and may reach 4mm.

Dips of the layers and plunges of the troughs are 10°-40°, except for two areas of discontinuous layering on the south side of the dyke which dip northward at 54°. These areas are thought to represent slipped blocks of layered material which came to rest lower down on the crystal pile. The dips and plunges are shown on Fig. 2.2; location of the various features is somewhat approximate due to the small scale of the original maps, but it can be seen that the pattern of dips differs from that on the coast. Either the thick horizontal gabbro picrites are equivalent to the picritic unit in the axial zone of the southern synform on the coast, in which case the southern synform widens considerably inland, or they correspond to the horizontal layers of the northern synform and the synform axis shows considerable lateral sinuosity.

The westernmost layering seen before locality B consists of a series of thin (1cm) layers which define a small westward-plunging synform that dies out to the west (Fig. 2.2).

#### 2.4.1.3 Locality B

At this locality the giant dyke cuts across a 100m wide mid-Gardar dolerite dyke (one of the BD0 suite (Emeleus and Upton, 1976)). To the east of the BD0, the giant dyke is considerably widened, to about 650m, while to the west it is only 200m

wide. The widened portion is unlayered, and it is only in the narrower western part that layering is again developed, for a distance of about 100m along the dyke.

The layering is again synformal with dips ranging from 14° to 38°. The shape of the synform cannot be determined as easily as at locality D because layer dips are variable and the synform axis has weathered out to form a valley, but here too it is thought to be a flat-bottomed V. Gabbro picrite layers up to 80cm thick appear within a few metres of the northern contact but were found no closer than 60m to the southern margin. The layering is generally much less parallel, regular and laterally continuous than that seen on the coast (locality D), though better developed than in the intervening dyke segment (locality C). Unconformities are common (Plate 2.13b). Gabbro picrite layers are 0.5cm-1m in thickness, with a few exceptions, and frequently thicken down-dip (Plate 2.13c); however some may thin down-dip. Most layers are discontinuous along strike, some thickening to form channels. On both limbs of the synform discontinuous curved concave-upward layers may have been incipient channels, as seen at locality C. On the south limb, but not on the north, the thickest gabbro picrite layers of the YGDC are found; these constitute a series of channels thickening to between 2 and 4m (Fig. 2.12). As at locality D, isolated blocks of gabbro picrite up to 2m long are found in the synform axis. These presumably resulted from the breakup of thick layers of gabbro picrite into blocks, which rolled down into the axis, as was inferred at locality D.

Layer contacts are frequently sharp but irregular at mafic layer bases, with layer tops being made more diffuse by increasing proportions of discrete or clustered feldspar crystals (the clusters ranging from 1-3cm in size) in the top 1-5cm of the layer (Plate 2.13d). Occasionally the lower boundaries of layers may also be more gradual.

### 2.4.2 Southern branch of the eastern YGDC

#### 2.4.2.1 Locality F

Near the south margin near-vertical layers are slumped and brecciated (Plate 2.14a). Relatively feldspathic gabbro picrite (about 40% feldspar) occurs within the dyke as layers 1-40cm thick and 2cm to 1m apart, with dips up to 20° towards the centre of the dyke. Outcrop is poor and the layers cannot be followed far. There is a small amount of channelling within the layered sections and a few isolated channels up to 2m wide and 30cm deep are also seen (Plate 2.14b). In the axial zone outcrops

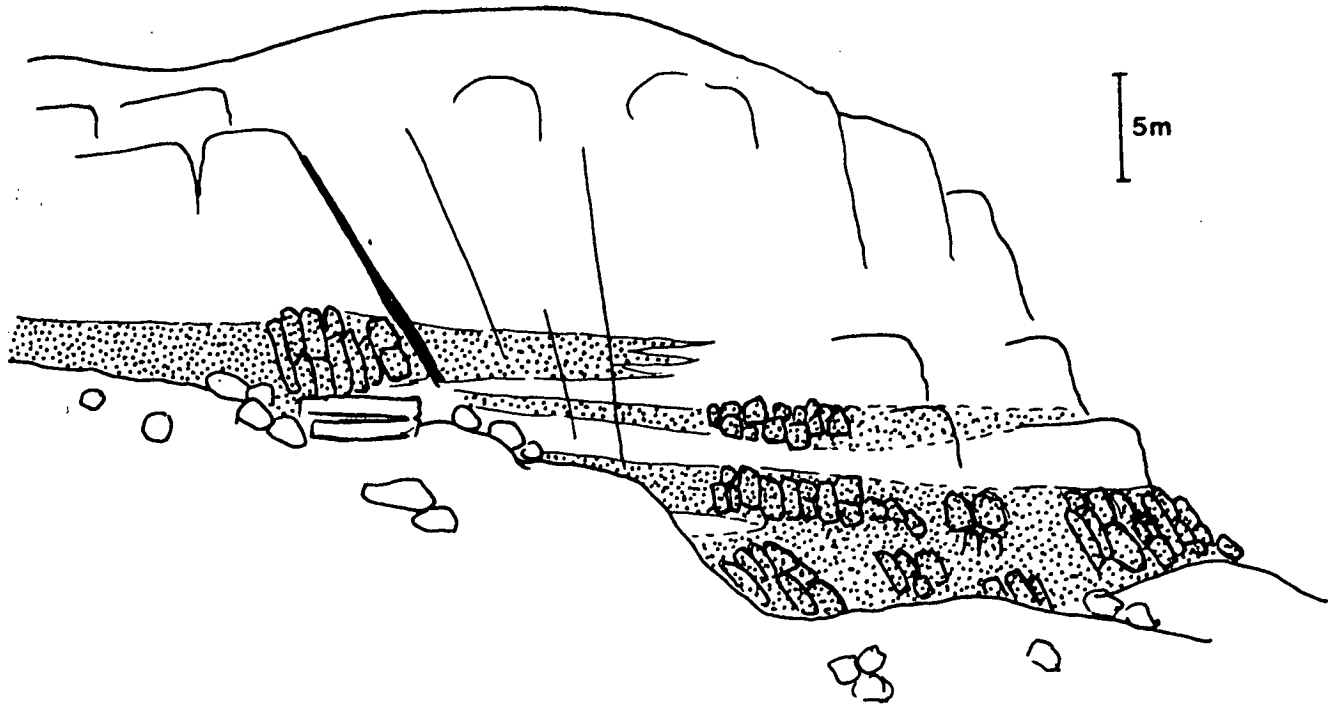


Figure 2.12 Sketch of thick gabbro picrite channels viewed looking S from the synform axis at locality B.

of massive gabbro picrite are found, very similar to the picrite of the western part of Tugtutôq. These picrites are at least 3.5m thick and sometimes contain isolated tablets of plagioclase which define a synform (Plate 2.14c).

### 2.4.2.2 Locality G (Marrait)

Modal layering is found only within the finer-grained central pod and is parallel to the synformal plagioclase lamination. It consists of olivine-oxide-apatite cumulate layers with intervening troctolite. The layering and lamination are steep (70°) at the edges of the pod but shallow rapidly over 1-2m to about 40° and then gradually to horizontal in the axis of the synform, which is towards the north side of the pod (Fig. 2.3). The mafic cumulate layers are diffuse, 1-5cm thick and 3-15cm apart (Plate 2.15a); as at locality D, layered and unlayered sections alternate but here the sections are a few metres rather than tens of metres wide. Layers may sometimes show normal modal grading, and this is particularly well shown in the axis of the synform where the layers thicken to about 15cm (Plate 2.15b). The troctolite here is slightly coarser than at the edges of the pod but still finer than that of the unlayered troctolite sheath. Layer dips are frequently variable and low-angle unconformities are common. Layers may also be discontinuous along strike. The layering appears to die out inland, to the east.

### 2.4.2.3 Locality I (Sigssardlugtoq)

As at locality G, a synformal structure is defined by plagioclase lamination, but here modal layering is not so well developed. Feldspar lamination begins about 200m from the southern margin but only 20m from the northern margin. The lamination defines a basin, slightly elongated along the dyke, dipping inward from all sides (Fig. 2.4). Dips are 30-40° at the edges shallowing to horizontal in the centre, but with a few undulations. On a surface parallel to the lamination the feldspar tablets are approximately equidimensional and so show no preferred alignment. Within this basin discontinuous concentrations of mafic minerals (olivine and oxides) are sometimes seen approximately parallel to the lamination (Plate 2.15c). In two localities larger areas of olivine-oxide cumulates are seen, forming irregular masses which may cut across the feldspar lamination. At locality 1 of Fig. 2.4, these cumulates have little or no visible feldspar (Plates 2.15d and 2.16a) but at locality 2 a

large but poorly exposed fine-grained mass at least 4m thick is seen, containing 20-30% feldspathic material. A few concentrations of feldspar forming blebs up to 4cm across and streaks parallel to the lamination are also seen (Plate 2.16b).

About 140m from the southern margin the small isolated pod characterised by browner weathering, shows synformal modal layering with mafic layers generally 1cm thick and 10-20cm apart (Plate 2.16c). The layering in the pod dips inwards from the north, south and east; to the west the layers die out and are somewhat disrupted. Within the layered sequence are two irregular masses of mafic material which could be thicker layers. However, they are discontinuous along strike with relatively sharp terminations and could perhaps be described as inclusions (Plate 2.16d). A little more layering of a similar type occurs to the east of the pod dipping east, but this dies out after a few metres.

### 2.4.3 Northern branch of the eastern YGDC

Locality J is characterised by "centimetre scale" layering (Upton, 1987). Locality K shows some rather diffuse layering but locality L is essentially unlayered.

#### 2.4.3.1 Locality K (Krydssø)

The troctolite sheath is unlayered, but an alignment of mafic minerals is often seen within the evolved pod here; due to the weathering and the small grain size it is not easy to determine whether this is due to alignment of prismatic minerals or of lines of small equant crystals of one or more minerals. Some poorly-defined modal variation is also seen at the better-exposed western end of the pod between the two arms of Krydssø. This layering defines an eastward-plunging synform (Fig. 2.5 and Plate 2.17a). The first modal variation is seen about 100m from the northern margin of the dyke, at the edge of the syenogabbro pod. The layers may be more mafic than the normal rock, more feldspathic, or graded from mafic bases to feldspathic tops. They can be 1-10cm in thickness and may or may not be separated by "normal" syenogabbro up to 0.5m thick (Plate 2.17b & c). One mafic layer thickens down-dip from 5cm to 50cm and may be a channel like those seen at localities B to D. One outcrop shows vertically alternating layered and unlayered sections, each about 1m thick, measured perpendicular to the layering (Plate 2.17d).

Plate 2.7

(a) Layered section 100m from northern margin at locality D (Itivdlip Sarqâ), taken looking south towards dyke axis. Hammer handle (centre right) is 50cm long.

(b) Layered section 150m from northern margin of locality D, looking SE. Gabbro picrite layers are generally thicker than those in (a). Hammer handle 30cm long.

(c) Close-up of mafic layers near (b), showing sharp tops and bases. The layer bases are much less regular than the tops. Scale bar has 5cm divisions.

(d) Feldspar blebs in a mafic channel which erodes two underlying layers, just to the left of the section shown in (b). Scale bar has 5cm divisions.

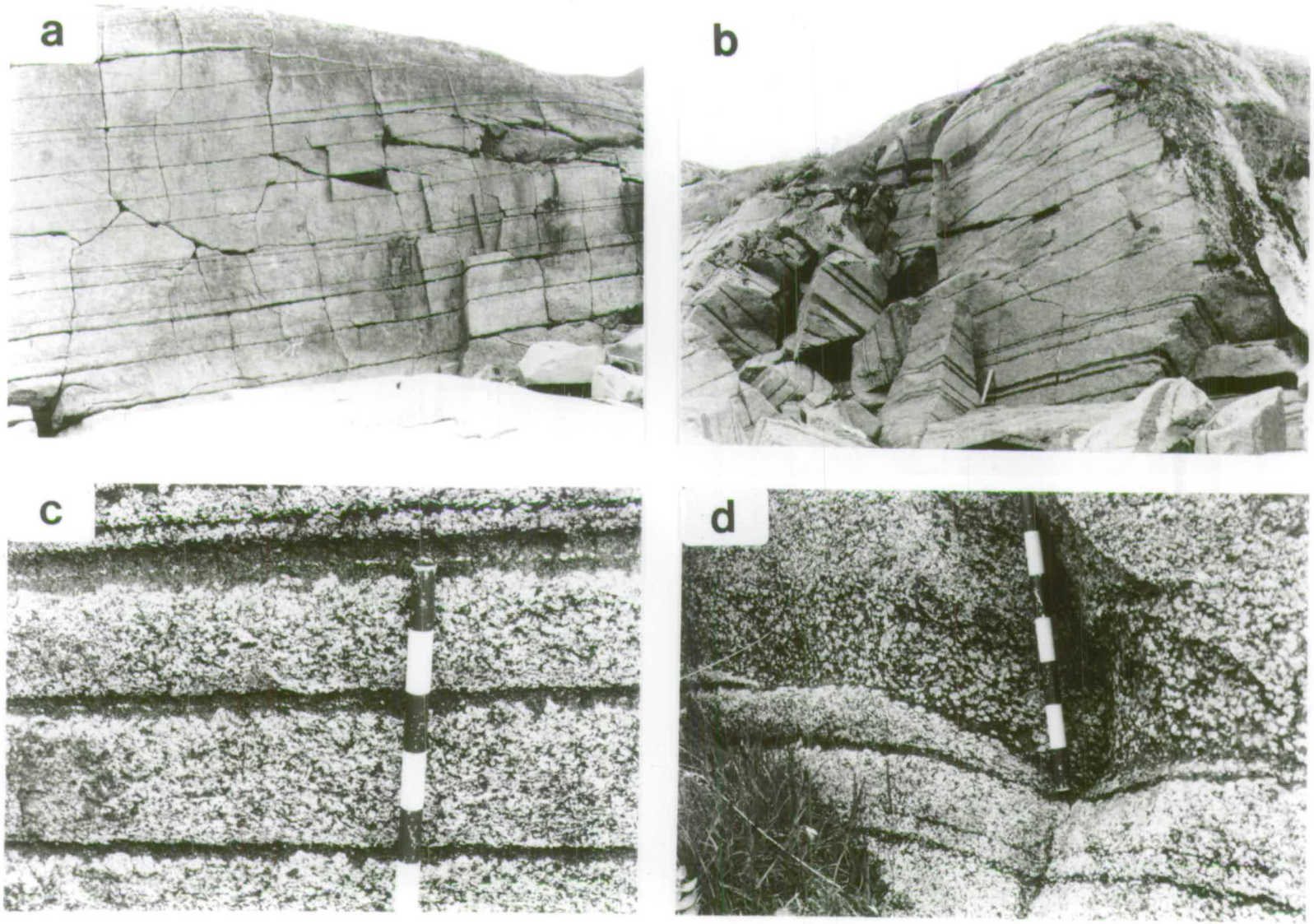
a
b
c
d

**Plate 2.8**

(a) Starry feldspar aggregates at the top of a mafic layer at locality D. Photo taken looking down onto the surface of a fallen block. Lens cap for scale.

(b) Thin horizontal mafic layers in the axis of the northern synform at locality D. Field assistant and hammer (handle 50cm long) for scale.

(c) Irregular to crudely rectilinear blocks of gabbro picrite within troctolite. The block to the right of the hammer shows traces of feldspathic layering within it. This photo and the following four were taken in the axis of the northern synform at locality D (Itivdlip Sarqâ). Hammer handle 30cm long.

(d) Irregular gabbro picrite blocks with trailing mafic schlieren. Note jointing in largest block. Scale bar has 5cm divisions.

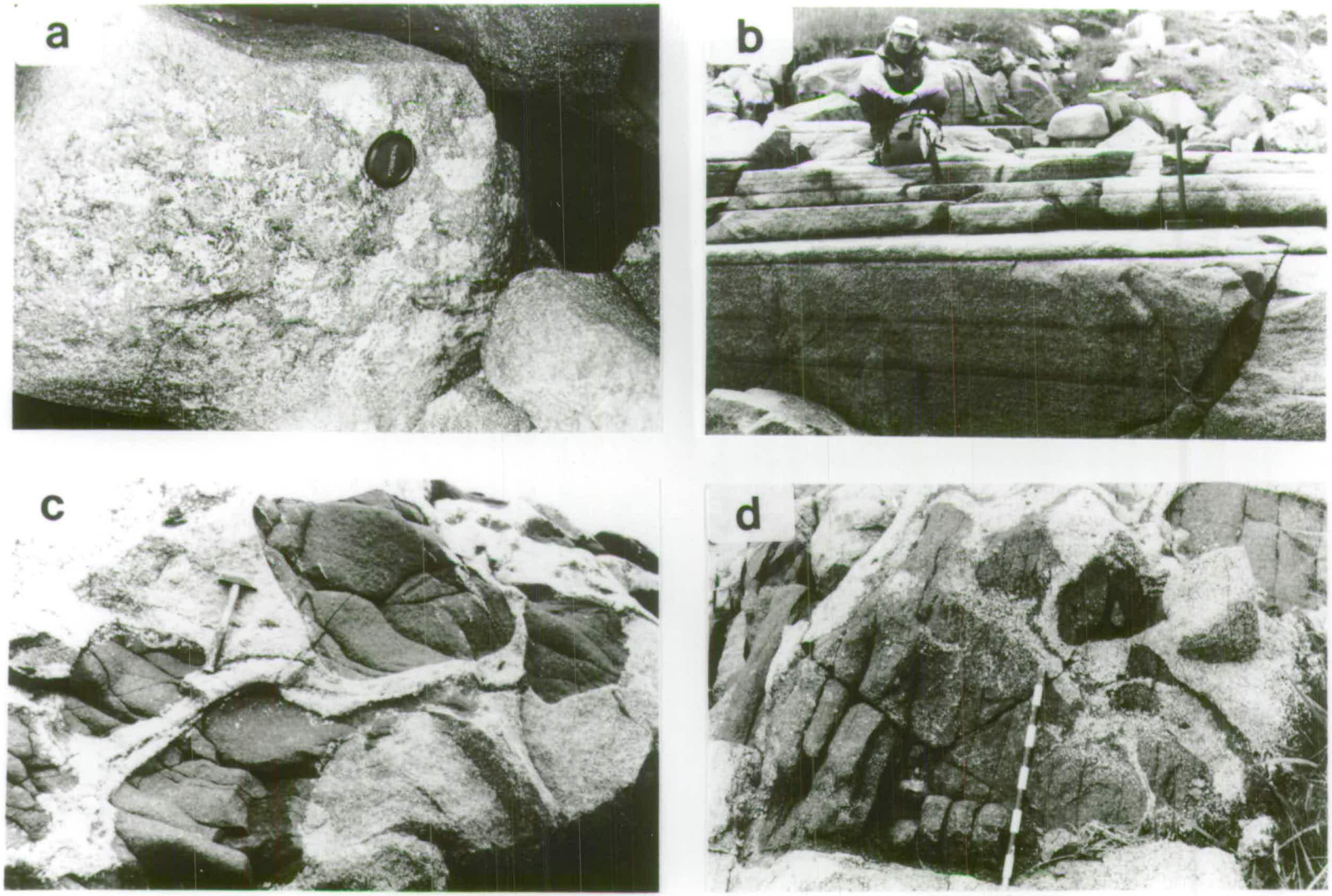
a
b
c
d

**Plate 2.9**

(a) Gabbro picrite blocks showing a variety of sizes and shapes. Some (on the right) appear to have been more consolidated at the time of brecciation, since they possess sharper margins and more regular shapes than blocks to the left. Scale bar has 5cm divisions.

(b) This block shows internal layering and has a less distinct edge on its feldspathic side. Hammer handle 50cm long.

(c) Gabbro picrite block showing well-developed jointing above a broken double picrite layer. At the base of this outcrop the horizontal layering is undisturbed. Scale bar has 5cm divisions.

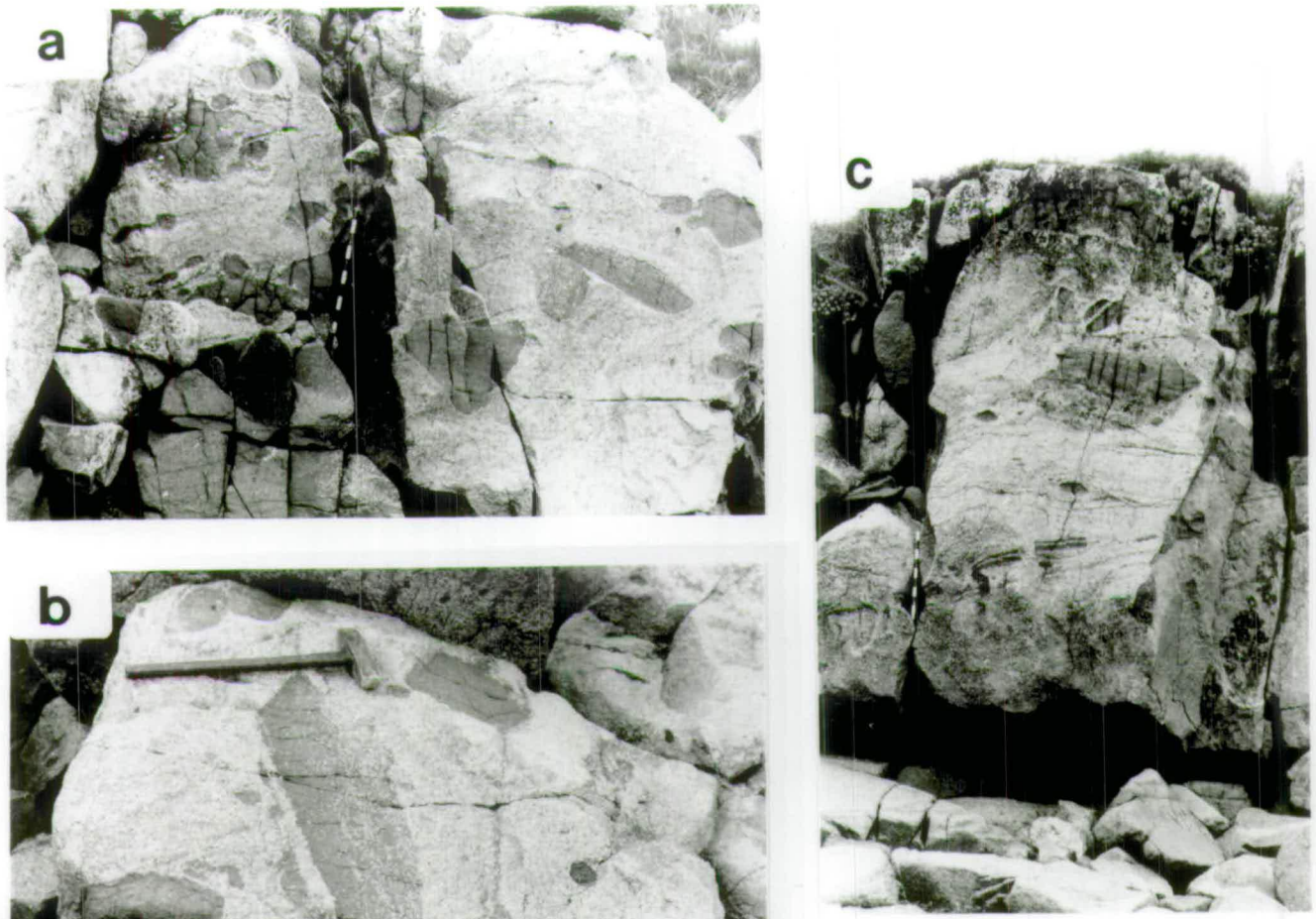
a
b
c

Plate 2.10

(a) Regular gabbro picrite layers dipping towards the centre of the northern synform at locality D (which is to the right of the picture), truncated by an unconformable layer. Hammer handle is 50cm long.

(b) Sketch of the area near (a). The location of photograph (a) is shown by a box at the bottom right. A gabbro picrite channel is seen to be causing the unconformity, although it has apparently died out down-dip before reaching the truncated layers. This may have been due to the picrite pushing a flow of troctolite ahead of it. Scale bar is 1m long.

(c) Junction between the two synforms at locality D, looking south. Layers of the northern synform dip shallowly to the right and are more parallel than those of the southern synform, which dip steeply to the left. Scale bar has 5cm divisions.

(d) Sequence of layered rock a few metres into the southern synform from the junction with the northern synform. The sequence contains a higher proportion of gabbro picrite than layered sections in the northern synform and the layers are less well-defined. Some show normal modal grading. Hammer handle is 50cm long.


a


c


b


d

**Plate 2.11**

(a) An unconformity in steeply-dipping layers of the northern limb of the southern synform of locality D. Viewed looking east, the synform axis is to the left of the photo. Hammer handle is 50cm long.

(b) Steeper layers truncating earlier shallower ones in the southern synform at locality D. A fine-grained leucocratic xenolith can just be seen below the steeper layers. Hammer handle is 50cm long.

(c) Southern limb of the southern synform at locality D, viewed looking east. The prominent gabbro picrite layer is about 2m thick and shows well-developed perpendicular jointing. The offsets in the layer are caused by extensional faults, downthrowing towards the synform axis. Below this layer are the cross-bedded layers seen in (b). Above it, thinner mafic layers appear to onlap onto the upper surface. A second thick layer occurs higher up in the cliff.

(d) Faulted layers just north of (c). The offset on this fault is about 2m and deformation appears to have been ductile. Two smaller offsets also occur in the lowermost group of layers to the right of the fault. Hammer handle is 50cm long.

(e) Another offset in the same group of layers a few metres north of (d). The layers have been bent but not broken, indicating that the cumulates were sufficiently consolidated to preserve their layering but still sufficiently plastic not to show brittle behaviour. Hammer head is 15cm across.


a


b


c


d

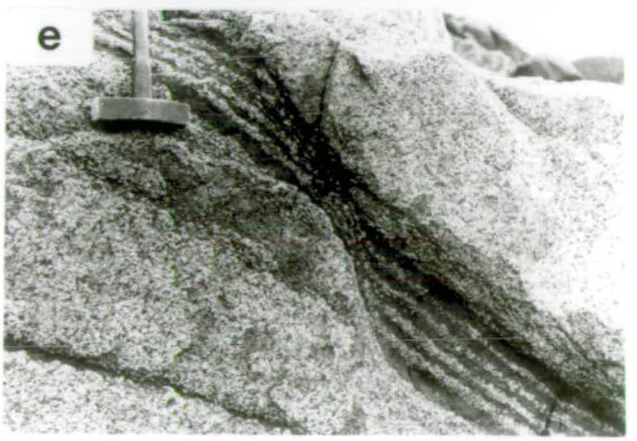
e

**Plate 2.12**

(a) Faulted gabbro picrite channel 2m thick in the centre, showing prominent vertical jointing. The photo is taken at locality C, looking south at a strike section. Scale bar in centre of channel.

(b) Several channels in strike section at locality C, broader and less deep than that shown in (a). Maximum thickness 1m.

(c) Thin, concave-up curved layers at locality C, possibly incipient channels. Height of rock face roughly 5m.

(d) Irregular fine-scale layers at locality C.

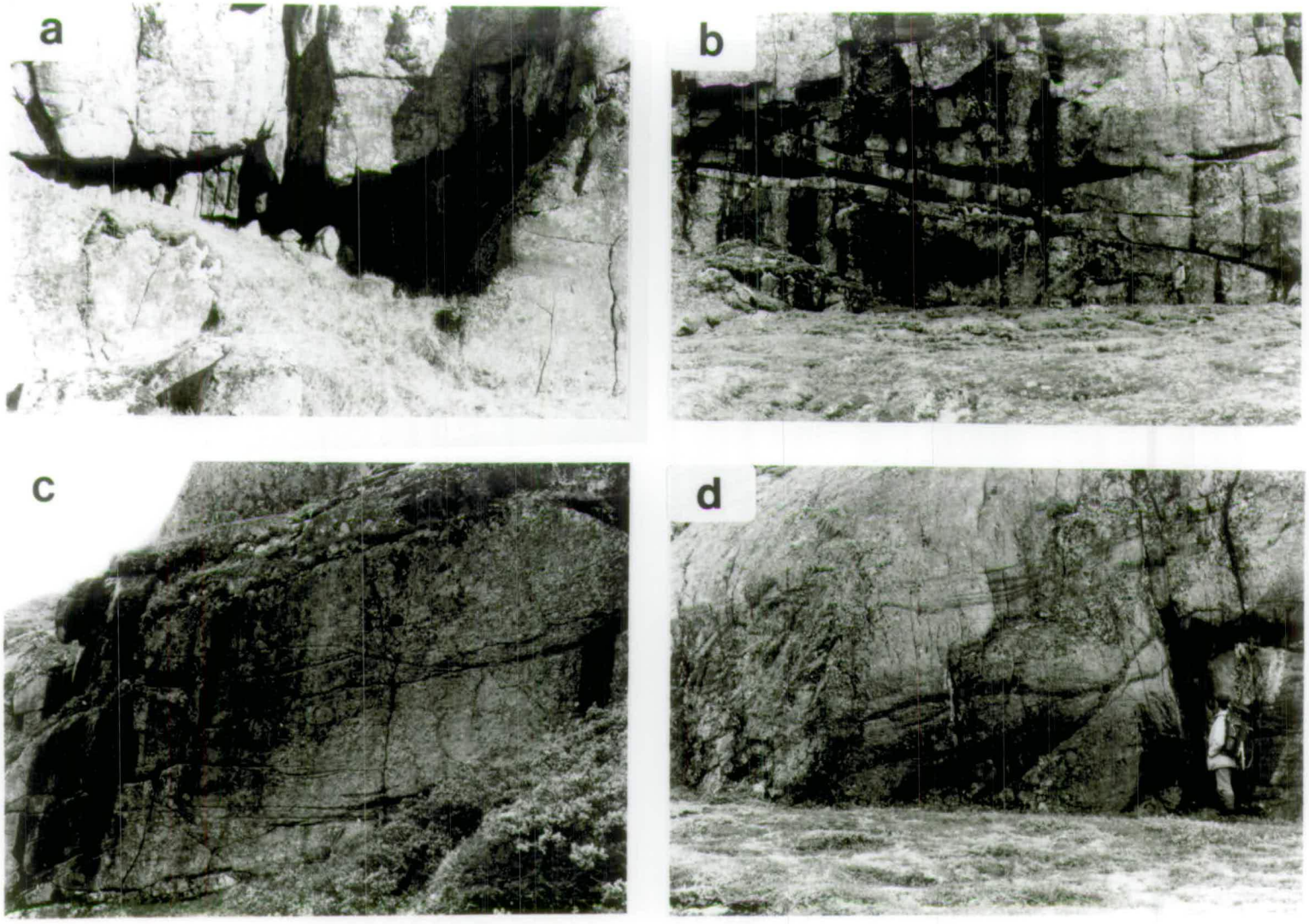
a
b
c
d

Plate 2.13

(a) Thick gabbro picrite layers in the axis of the synform at locality C. Thinner troctolite layers weather proud of the surface. Scale bar has 5cm divisions.

(b) Gabbro picrite layers truncated by an unconformity (possibly a shear zone) at locality B. The topmost layer is continuous so the disturbance was very localised. Scale bar as above.

(c) A downward-thickening gabbro picrite layer at locality B, viewed from the west. The synform axis is to the right. Hammer handle is c. 60cm long. Photo by B.G.J. Upton.

(d) Upper edge of a gabbro picrite layer at locality B. The feldspar of the overlying troctolite forms large aggregates up to 3cm in size. In some of these the crystals have a radial arrangement but in most they show no preferential alignment. Scale bar has 5cm divisions.

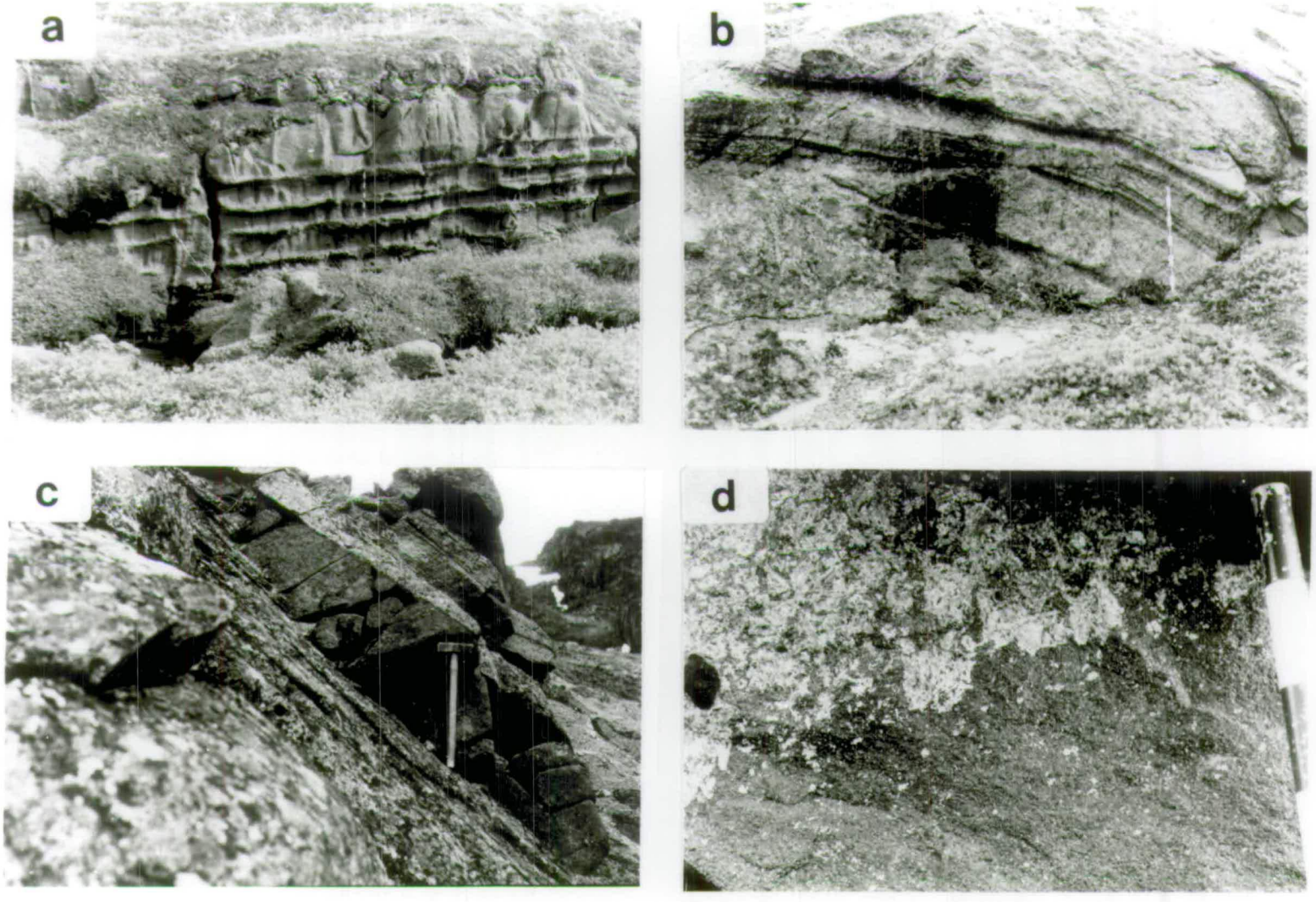
a
b
c
d

**Plate 2.14**

(a) Slumped cumulates near the northern margin at locality F. Gabbro picrites have weathered out. Hammer handle is 30cm long.

(b) Isolated trough of blocky gabbro picrite within evenly-weathering troctolite at locality F. Scale bar has 5cm divisions.

(c) Massive unit of gabbro picrite containing isolated large plagioclase crystals which stand out from the face and throw shadows in the sun. These plagioclases show a rough alignment and define a synform (axis to the left of this photo). Scale bar has 5cm divisions.

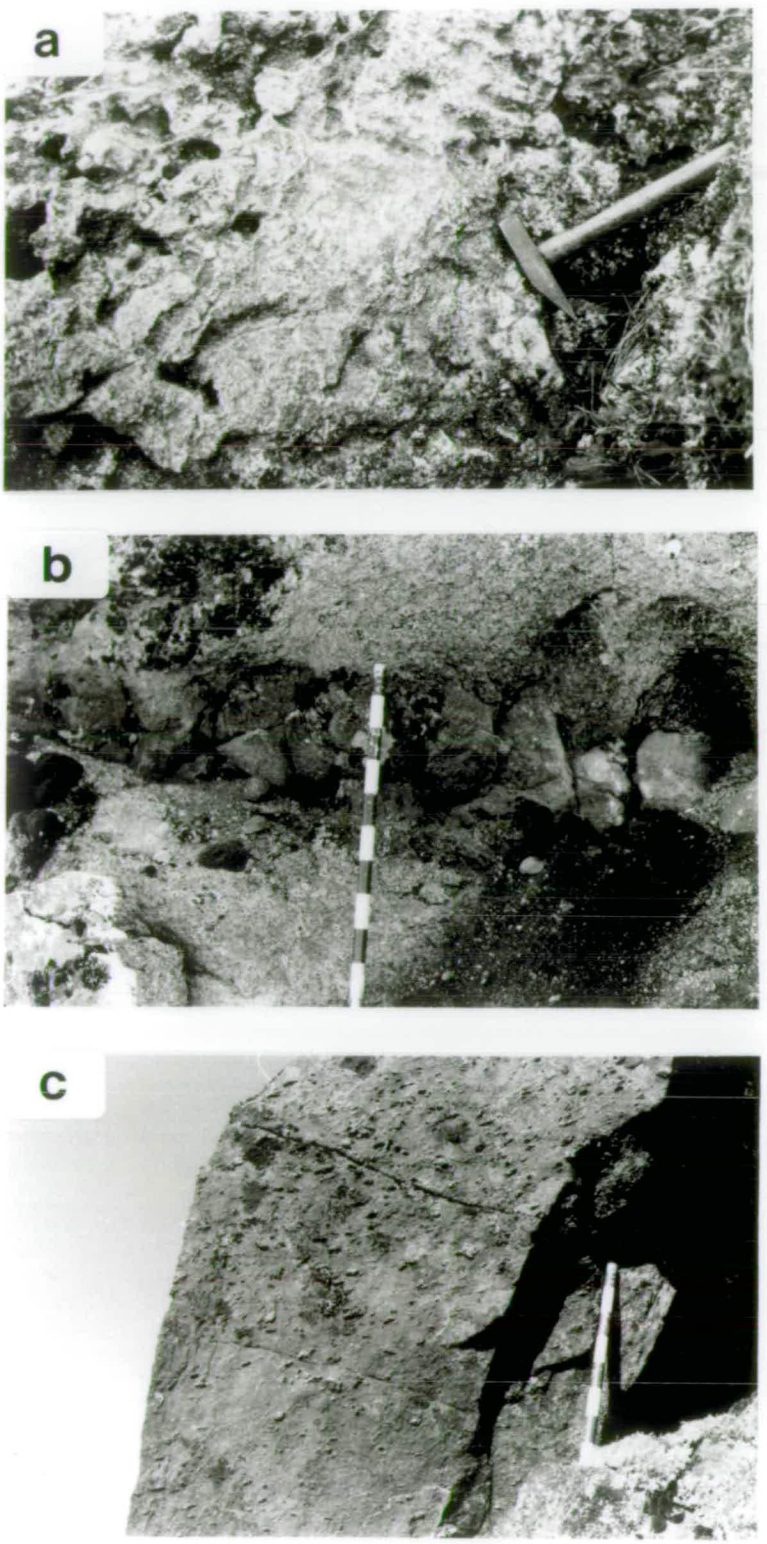
a
b
c

**Plate 2.15**

(a) Fine, steeply dipping layering at the edge of the layered pod at locality G. Hammer handle (lower centre) is 50cm long.

(b) Fallen block showing layering of the type seen in the synform axis at locality G. The layers of olivine-oxide-apatite cumulate are parallel to the feldspar lamination. They may reach 15cm in thickness and many show normal modal grading. The way up is to the top of the photo. Pencil for scale.

(c) Faint mafic layers parallel to the feldspar lamination at locality I. Hammer handle is 50cm long.

(d) Irregular areas of olivine-oxide cumulate at locality I, containing very little feldspar. Hammer head (centre left) is c. 15cm across.

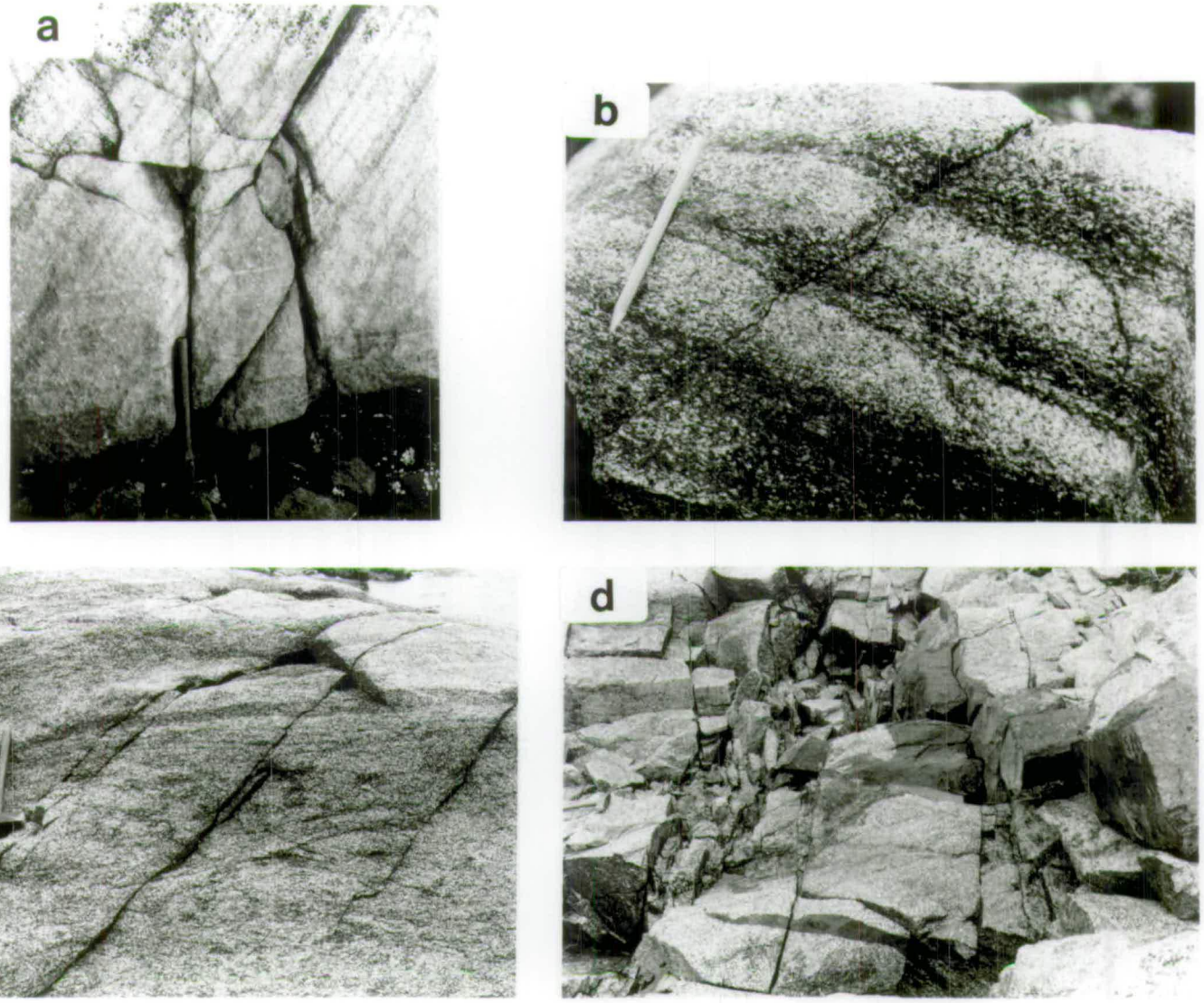
a
b
c
d

## Plate 2.16

(a) Close-up of the edge of one of the mafic areas shown in Plate 2.15d. The contact between the mafic cumulate (above) and the plagioclase-olivine-oxide cumulate is in places concordant and in places discordant with the feldspar lamination. Individual plagioclase crystals may be "caught up" in the edge of the mafic cumulate. Lens cap for scale.

(b) Feldspathic blebs and streaks parallel to the feldspar lamination at locality I. Concentrations of feldspar are rare in the YGDC, occurring locally here and at localities K and M. Hammer head is c. 15cm across.

(c) Faint mafic layering in a small modally layered pod near the southern margin of the dyke segment at locality I. The rocks have much browner weathered surfaces than in the rest of the dyke at this locality. Hammer handle is 50cm long.

(d) Mafic "layer" (olivine-oxide cumulate) with abrupt termination (to the left) in the modally layered pod shown in (c). This appears to be an inclusion rather than a layer. Hammer handle is 50cm long.

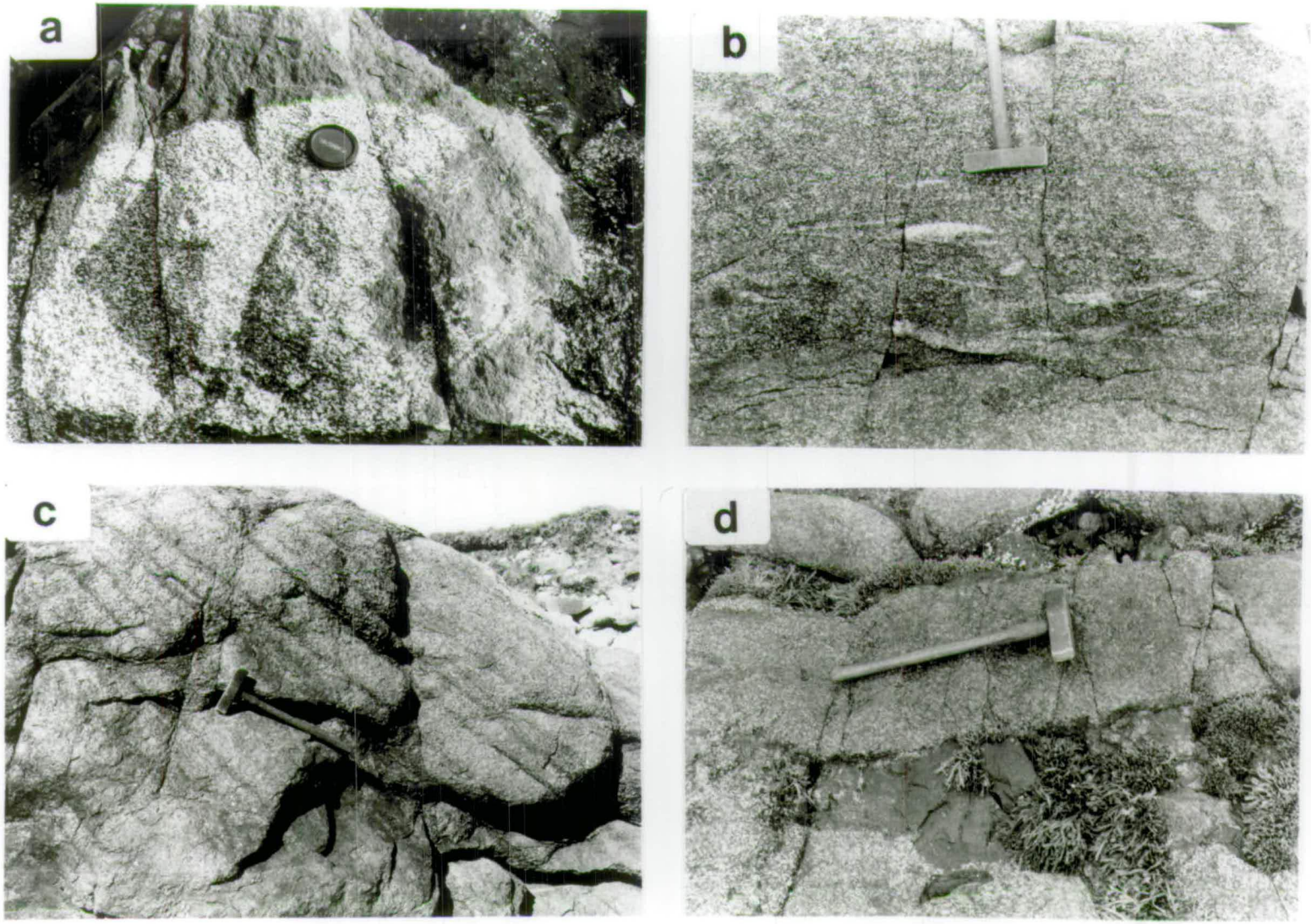
a
b
c
d

**Plate 2.17**

(a) Looking east along the synform axis at locality K (Krydssø). To the right of A the layers dip to the right, at B they are roughly horizontal and at C they dip to the left. Above and to the left of A, cliffs of Julianehåb Granite mark the edge of the dyke.

(b) Faint feldspathic layering separated by uniform rock at locality K. Scale bar has 5cm divisions.

(c) Layers showing grading from mafic bases to felsic tops at locality K. Scale bar has 5cm divisions.

(d) An outcrop with alternate layered and unlayered sections. The hammer rests on the base of one 1m layered section and the scale bar near the base of another, while the rock between is unlayered.

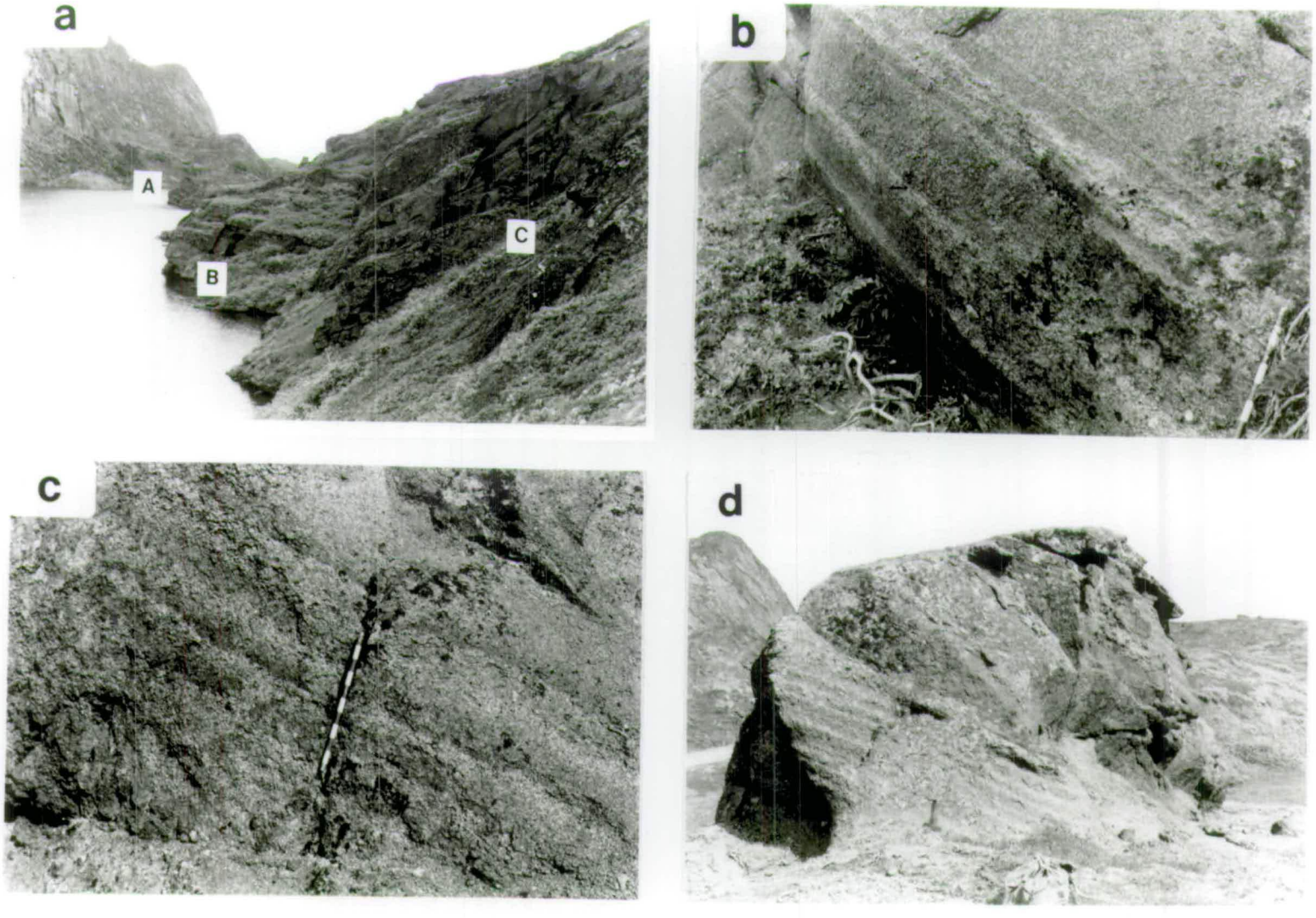
a
A
B
C
b
c
d

#### 2.4.3.2 Locality L (Assorutit)

There is very little layering at this locality, but a few thin mafic layers do occur in the syenite. Some mafic schlieren are also seen, which sometimes surround or partly surround pegmatitic patches.

### 2.4.4 Narsaq (locality M)

The feldspar lamination seen on the Nugarmiut peninsula generally dips NE. Approximate dips of the feldspar lamination are shown in Fig. 2.6 (some measurements taken by B.G.J. Upton). The dips tend to be variable and are sometimes disturbed by high-angle bands, which may have been caused by contemporaneous movement on a fault which runs through the bay to the east of the peninsula. Rare mafic pods and schlieren are seen in the laminated parts of the troctolite, usually parallel to the lamination. The largest of these pods, at the north-eastern point of the peninsula, is several metres long and 5cm-1m wide, composed of dense, slightly magnetic olivine-oxide cumulate with only 5-10% feldspar.

## 2.5 Xenoliths

### 2.5.1 The western YGDC

A number of fine-grained leucocratic xenoliths are seen, usually within the outer third of the dyke. They range from a few cms to about 1m by 0.5m in size and are usually associated with and surrounded by gabbro picrite material. They are often elongated parallel to the layering (Plate 2.18a). In the field these xenoliths appear to be made up of plagioclase with olivine and other mafic minerals, similar to the troctolites but with a grain size of 1mm or less and a higher proportion of plagioclase. They are frequently associated with the development of pegmatites containing alkali feldspar and idiomorphic pyroxene, which may have resulted from the crystallisation of fluids trapped beneath the xenoliths. At locality B such xenoliths are found associated with the development of slender elongate plagioclase crystals (Plate 2.2).

Near the northern margin of locality D, several relatively fine-grained mafic xenoliths are found, together with ~~apparently later~~ leucocratic xenoliths. The mafic

xenoliths are elongated parallel to the dyke margin both horizontally and vertically (Plates 2.18b & c). They may possibly represent a disrupted early layer and thus be autoliths.

Plagioclase xenocrysts are found occasionally in this area of the dyke, notably at locality D east of the fault, as mentioned above.

### 2.5.2 Southern part of the eastern YGDC

Some xenoliths are seen in this part of the dyke but they are less common than the fine-grained leucocratic xenoliths of the western part of the dyke. At localities G and I, fine-grained leucocratic xenoliths or autoliths up to 1.5m in size, often elongated parallel to the contact, are found near the southern margin of the dyke; these could be spalled pieces of the chilled margin.

### 2.5.3 Northern part of the eastern YGDC

Within the troctolite to the north of the syenite pod at locality L, anorthosite xenoliths join the plagioclase xenocrysts which are found in the troctolite sheaths at localities K and L. These xenocrysts are like those seen occasionally in the western YGDC, especially at locality D east of the fault. The westernmost xenolith is seen at locality 3 of Fig. 2.4 and a zone at the end of the promontory (locality 4) is crowded with them. The abrupt change from syenite to anorthosite on the south side of the promontory suggests a fault, although the actual contact is not exposed. On the north side there is less evidence for a fault but a zone of epidotisation containing numerous joint planes, some showing slickensides, suggests that the movement may have been taken up along a number of minor planes rather than one major one.

The matrix to the xenoliths appears identical to the troctolite seen elsewhere around the syenite pod, with occasional pegmatitic patches. Some mafic streaks are seen draping one of the anorthosite blocks (Plate 2.18d). The xenoliths range from a few centimetres to about 100m in size and are of many different types of anorthosite, distinguished by colour and size of the plagioclase crystals, the degree of lamination and the amount of interstitial material (mainly olivine) (Plate 2.19a). The plagioclase crystals vary from light to dark grey in colour (depending upon the concentration of inclusions) and from 1-15cm in length. Within any one xenolith the crystals may be

of a similar size or of a variety of sizes. The degree of lamination varies from good to non-existent and the proportion of interstitial material from c. 5-30%. Lithologies with more than 20% interstitial material are referred to as gabbroic anorthosites.

Some of the xenoliths have abrupt variations in grain size within them and may be composite, with a finer-grained facies enclosing a coarser (Plate 2.19b). A few contain very large poikilitic olivine crystals up to 20cm across (Plate 2.19c). The large xenoliths (10-100m in size) are usually of a type of anorthosite with some variation in crystal size and proportion of interstitial olivine. These two characteristics tend to be linked, with the smaller feldspars appearing to have less good lamination and packing and thus a higher proportion of interstitial olivine. This tends to give the rocks a patchy appearance, and sometimes layers 10-30cm thick are formed by this variation (Plate 2.19d, Plate 2.20a & b).

Most of the xenoliths have dark rims of olivine up to 0.5cm wide. Some finer-grained veins occur within the xenoliths; sometimes these are of troctolite, presumably infilling fractures, and sometimes they are of anorthositic material.

### 2.5.4 Narsaq

The zone where anorthosite xenoliths are common is shown in Fig. 2.6, and outside this is a zone where isolated xenocrysts are found. On the peninsula of Nugarmiut xenocrysts seem to be absent. The xenoliths are almost all found within the town. Outcrops are limited in area and may be smaller than the xenoliths which reach at least 10m across. The anorthosite is altered along with the host troctolite, but it can be seen that the plagioclase crystals are 2-5cm in length and that more than one type of anorthosite is present. Disaggregation of xenoliths is more common than at locality K. Xenocrysts and elongate xenoliths sometimes show a crude, approximately horizontal alignment (Plate 2.20c). Both xenoliths and xenocrysts frequently have dark reaction rims (Plate 2.20d), here probably of chlorite and/or serpentine after olivine.

Plate 2.18

(a) Fine-grained leucocratic xenolith partially enclosed within a mafic layer at locality D. The xenolith is elongated parallel to the layer. Scale bar has 5cm divisions.

(b) Mafic xenoliths near the northern margin of locality D, elongated parallel to the margin. Hammer handle is 30cm long.

(c) The lefthand xenolith in (b) seen on a vertical face, looking west parallel to the dyke margin. It encloses two small felsic xenoliths. Hammer handle is 50cm long.

(d) Dark grey anorthosite xenolith at locality L with faint mafic layers in the surrounding troctolite draped over the top. Xenolith is c. 50cm wide.

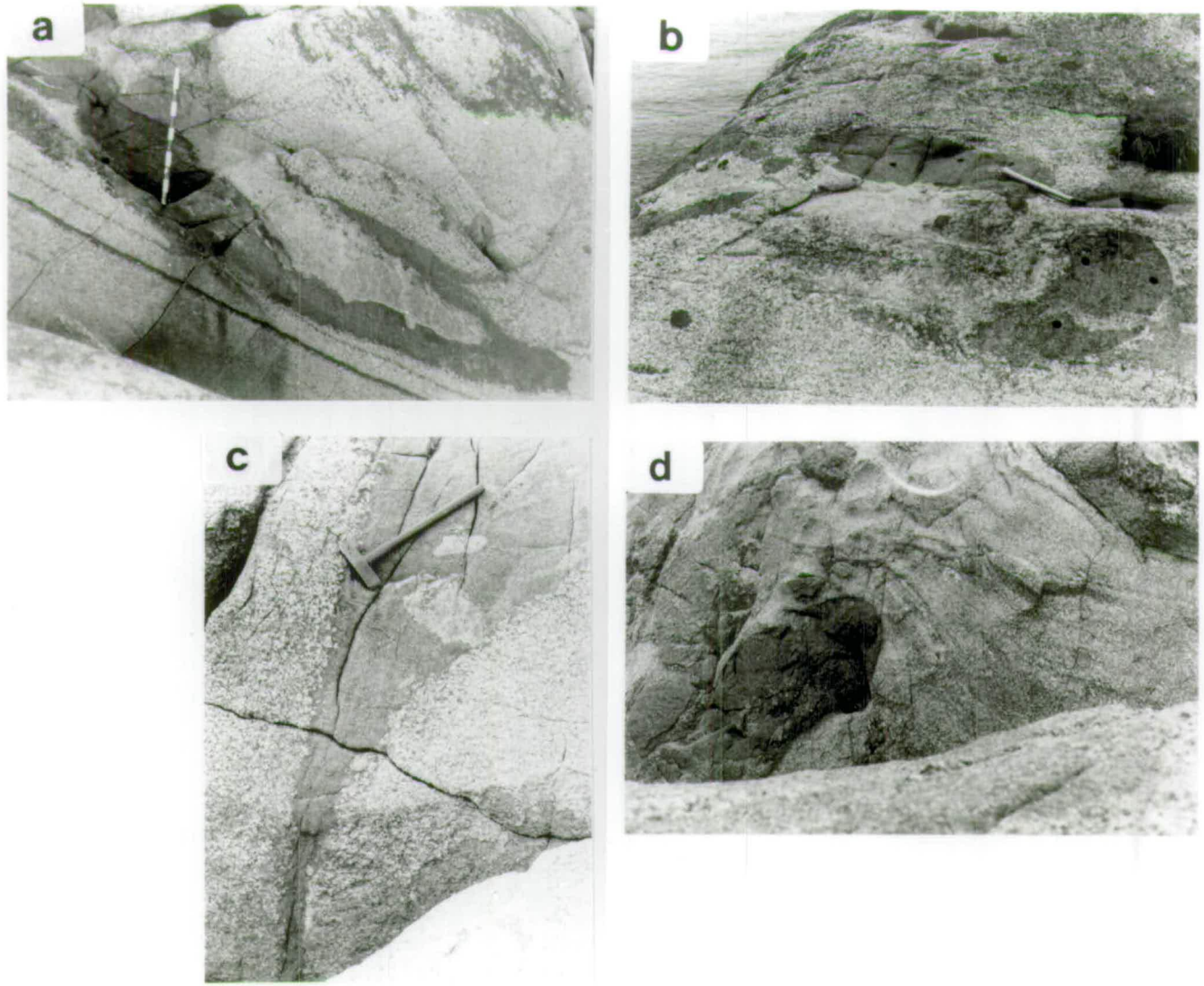
a
b
c
d

**Plate 2.19**

(a) Zone of small anorthosite xenoliths (up to 1m) between two large ones (foreground and background), locality L. Several different colours of anorthosite can be seen. Hammer handle (right of centre) is 50cm long.

(b) Fragment of coarse-grained anorthosite within a finer-grained xenolith, locality L. The plagioclase in the finer-grained rock shows a slight lamination around the inclusion. Lens cap for scale.

(c) The dark patch is a large single olivine crystal within a small anorthosite xenolith. The surrounding troctolite is darker in colour than the xenolith. Lens cap for scale.

(d) All visible outcrop in this photo is part of one very large anorthosite xenolith on the Assorutit peninsula (locality L). Varying amounts of intercumulus material give the rocks a banded appearance. When seen close to, the apparent layering is less obvious. Distance from sea-level to highest point is about 20m.

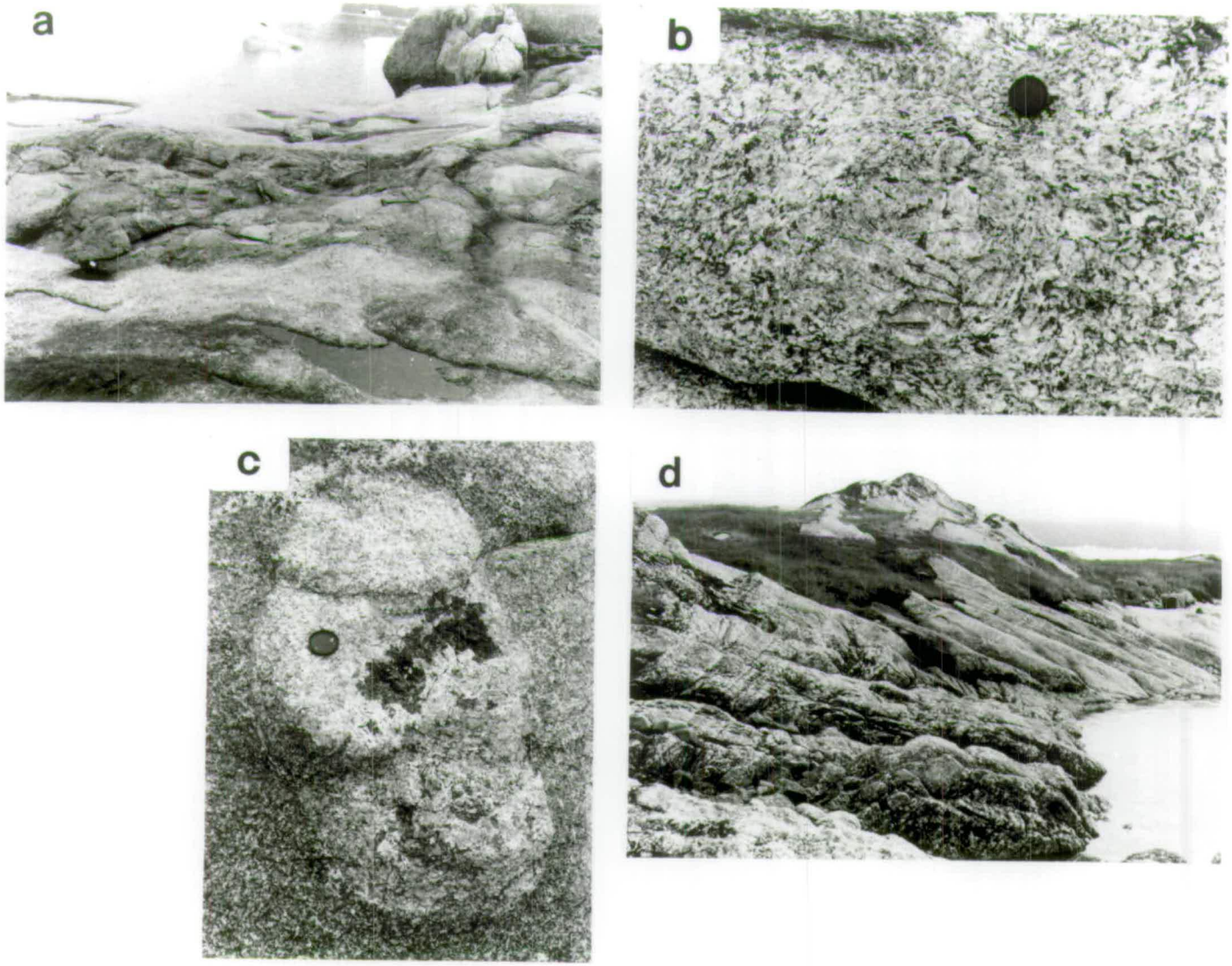
a
b
c
d

Plate 2.20

(a) Typical "patchy" appearance of anorthosite within some of the large xenoliths at locality L. The variation in colour appears to be due to variations in the amount of interstitial material, principally olivine. Hammer handle is 40cm long.

(b) A rare layer of gabbroic anorthosite with a greater proportion of interstitial olivine than the surrounding rock. Within a large xenolith, locality L. Lens cap for scale.

(c) Troctolite full of plagioclase xenocrysts in Narsaq harbour, near the upper contact of the dyke with the Eriksfjord formation (locality M). The grain size of the xenocrysts is only slightly greater than that of the troctolite, and they show a horizontal alignment. Coin for scale.

(d) Plagioclase xenocrysts at locality M, the largest showing a dark rim, probably of chlorite and/or serpentine. To the left of this a stellate aggregate of plagioclase can be seen within the troctolite matrix. Lens cap for scale.

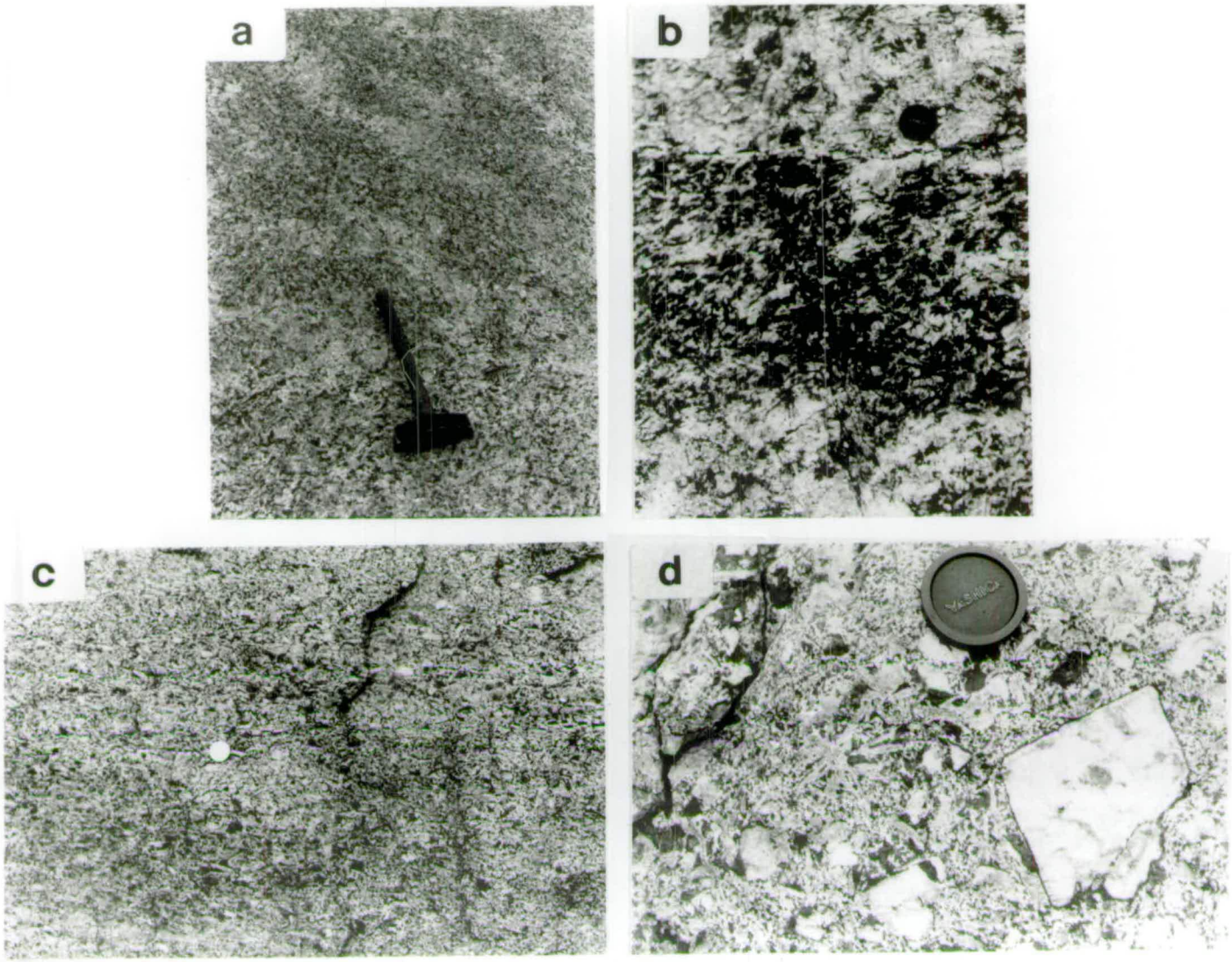
a
b
c
d

## 2.6 The nunataq region

The nunataq area was not visited as part of this project due to lack of time and to operational difficulties, but it has been described by Walton (1965), Upton and Fitton (1985) and Upton (1987). A dyke swarm with compositions ranging from basalt to trachyte and rhyolite with rarer phonolite, including up to three parallel gabbroic giant dykes, is thought to be an offset continuation of the "extraordinary" Tugtutoq swarm (Upton and Fitton, 1985). The giant dykes are of troctolitic gabbro and sometimes show plagioclase lamination and/or modal layering defining a synform. Hand specimens of some of these rocks show striking similarities to rocks from locality I. Others have high contents of apatite and are similar to rocks from locality G (though coarser-grained) or are like the pegmatitic troctolites of locality L. Marginal facies are also similar to those seen on Tugtutôq. Two differentiated pods occur, one of poorly exposed ferro-syenogabbro which is strongly layered and shows trough-like features, the other of syenite. As at locality L (Assorutit), this is surrounded by a sheath of syenogabbro; unlike locality L, the pod is of nepheline syenite and shows some synformal modal layering. Hand specimens from the nunataq region appear less altered than those from locality L. A large block of gabbro containing numerous plagioclase megacrysts is found within the nunataq syenite and is thought (by analogy with Narsaq) to be a detached block of roofing facies.

## 2.7 Summary and conclusions

The YGDC is composed of troctolite with subordinate gabbro picrite and olivine-oxide cumulates, the mafic facies often defining the layering. The primary phase assemblage changes from plagioclase + olivine in the west to plagioclase + olivine + oxides ± apatite in the east. At two localities (K and L) on Tugtutôq and also two localities in the nunataq region, elongate pods up to 3km long containing evolved facies are seen. These are thought to have differentiated in situ but may represent separate magma pulses. They contain the assemblage feldspar + olivine + apatite + oxides + clinopyroxene. The feldspar composition varies, becoming perthitic alkali feldspar in the most evolved rocks. These lithologies are referred to as syenogabbro and syenite and can be said to show phase layering, since they are defined by the entry of clinopyroxene and alkali feldspar respectively, into the fractionating assemblage.

The layering in the YGDC is discontinuous and only found in a few isolated portions of the dykes, ranging from a few hundred metres to 3km in length. Unlayered zones marginal to the layered pods, range from a few metres to two-thirds of the dyke width in total. Within the layered pods a synformal structure is defined, either by modal layering or by feldspar lamination or both. Inward dips may be steep (70° or more) at the margins but are more commonly 30-40°. Locality D of Fig. 2.1 is unique in having a double synform. Modal layering is defined by layers of gabbro picrite or other mafic lithologies and these range from 1cm to several m in thickness, with thinner layers being more common. Modal variation is best developed in the western part of Tugtutôq. Where oxide minerals are primary phases mafic cumulates are less commonly found and less well-defined. In the western YGDC, gabbro picrite layers are usually sharply bounded but may be more diffuse or occasionally modally graded. The layering is frequently parallel but may show annealed faults, slumps, unconformities, channelling, cross-bedding and detached blocks of gabbro picrite within a troctolite matrix.

Evidence that the synformal shape was primary comes from the troughs or channels which are invariably perpendicular to the trend of the dyke and plunge inwards. The gabbro picrite filling the channels would have been denser than the surrounding troctolite and would have moved down any slope that was present. The possible onlapping of layers onto a thick mafic unit at locality D provides further evidence. In addition, detached blocks of gabbro picrite, presumably formed from the break-up of thick layers, are only found in the axial portion of the synform and are also inferred to have reached their present position under the influence of gravity. The dips of the synform limbs may have been steepened from their original configuration by compaction of less well-solidified cumulates in the centre of the dyke so it is not possible to infer exactly the original shape of the magma chamber floor.

Feldspar lamination is totally absent in the western YGDC but the eastern part of the complex is characterised by layered pods in which feldspar lamination is frequently more important than modal variation. This may indicate a change of regime within the magma chamber. Concentrations of felsic minerals are only found at localities I and K of Fig. 2.1

Anorthosite xenoliths up to 100m in size and plagioclase xenocrysts occur abundantly in the Narsaq-Assorutit area; some xenocrysts are also found elsewhere in

the dyke complex. Several different types of anorthosite are present, distinguished by variations in plagioclase colour, grain size, packing and degree of lamination.

The overall change in composition and cumulus assemblage from west to east along the dyke complex may be a result of tilting along its axis. This would explain the occurrence of differentiated facies to the east since the more evolved liquids which produced these rocks would have been less dense than those crystallising the western troctolite (see Chapter 7). The anorthosite xenoliths and xenocrysts found in abundance in the Narsaq area would also have been lighter than the magma and would have floated, to become concentrated in the uppermost part of the complex. The coarser grain size in the Narsaq troctolite may be indicative of a thick, slowly-cooled lopolithic chamber which developed as the magma ponded at the basement-Eriksfjord Formation unconformity.

An alternative explanation of the compositional variation might be lateral propagation from a stratified magma chamber (Chapter 6). Unfortunately, the lack of structures in the basement makes it impossible to distinguish between these two hypotheses.

# CHAPTER 3: PETROGRAPHY AND MINERAL CHEMISTRY

## 3.1 Objectives

Thin sections and polished sections of representative lithologies from all localities marked in Fig. 2.1 have been studied to obtain information on mineral assemblages, textures and compositions. Such information is vital to a study of the possible processes operating during the genesis of these rocks, such as nucleation, growth and movement of primary crystals, and postcumulus crystallisation and re-equilibration. Compositions of cumulus crystals are used in Chapter 4 to constrain models of magmatic evolution.

Petrographic descriptions are given below, and include the results of point-counting representative samples to determine modes. During point-counting, the heterogeneity of the thin sections of coarse-grained rocks made repeatability poor (and each thin section is not always representative of the rock from which it was cut). In addition, the variable grain size made the selection of a suitable step size difficult. However, it was found that 500 counts per sample gave a reasonable accuracy; the error from three sets of counts on one sample was about 5% for minerals with modal proportions >5%. For chill samples, 300 points were counted as this was found to give a result indistinguishable from that obtained by counting 500 points.

Some secondary alteration products were identified using cathodo-luminescence. Minerals present in the YGDC which fluoresce are feldspar, apatite, calcite, zeolites and fluorite. Feldspar fluoresces blue when fresh and red when it has experienced fluid activity (Marshall, 1988). Apatite fluoresces in shades of yellow and grey and may show zoning. Calcite, zeolites and fluorite occur in very small quantities, usually as alteration products, although some primary calcite is found in the evolved rocks.

Petrographic details are followed by the results of textural studies, and mineral composition data obtained by electron microprobe analysis are presented in section 3.4. Sample localities will be found in Appendix I.

## 3.2 Petrography

### 3.2.1 Chilled margins

One sample (GGU 40454) taken across a very sharp contact between dyke rock and country-rock granite shows the outermost YGDC to be an extremely fine-grained dark rock, probably a devitrified glass (Plate 3.1a). There is some shearing along the contact and two generations of thin (0.1mm or less) hydrothermal veins are seen. The dyke rock has been extensively altered and is now made up of opaque oxides, biotite and alkali feldspar, the grain size increasing from <<0.1mm to about 0.2mm at a distance of 2cm from the contact. The minerals show a rather patchy distribution, possibly indicating a former spherulitic texture. Between the dyke chill and the country-rock is a zone of well-developed pyroxene crystals 0.1-0.5mm wide. Beyond this the country-rock granite shows widespread development of granophyric texture due to partial melting.

Hybrid rocks from areas where the contact is less sharp (taken at the north contact of locality D and the south contact of locality F) contain extremely altered feldspar, together with green amphibole and biotite totally replacing mafic minerals. At locality F, polycrystalline pods of quartz from the granite are enclosed within the hybrid rock. Such rocks indicate hydrothermal alteration at the margins of the intrusion but have not been studied in detail. The original mineralogy and textures of these rocks are obscured; this justifies the taking of "chilled margin" samples at least 1m into the dyke where all minerals appear to be fresh (see Chapter 4).

At the contact between the giant dyke complex and Eriksfjord sandstones there is again pervasive turbid alteration of feldspars and the mafic minerals are replaced by chlorite, epidote and green amphibole. Interstitial granophyric intergrowths, found at least 5cm into the dyke, indicate contamination of the giant dyke by the sandstone, which must have suffered some degree of melting. The contact is gradual over about 1cm and the sandstone consists of 0.5-1mm interlocking quartz grains with interstitial fine-grained material, possibly clays or mica.

The rocks designated "chilled margins" consist of plagioclase, olivine, opaque oxides, clinopyroxene, apatite and biotite (Plate 3.1b). The average grain size varies between samples from about 0.2 to 2mm. Rocks with a grain size at the upper end of this range are texturally dolerites rather than basalts but they show no evidence of

mineral accumulation and are still taken to represent a reasonable approximation to the magma compositions. In any one sample the plagioclase crystals form 50 to 65% of the rock. They are lath-shaped and usually randomly orientated, but in chills from locality F some lamination occurs, around large composite glomerocrysts of olivine and plagioclase (Plates 3.1c and 3.3a). This is considered to be due to flow alignment rather than compaction. Continuous normal zoning is seen in most of the plagioclases. Some larger plagioclase crystals (3-8mm) are found in most of the chill samples, particularly at locality D, and are probably phenocrysts. The margins of the groundmass plagioclase crystals are sometimes irregular, possibly indicating recrystallisation. A few percent of interstitial alkali feldspar are found, especially in chills from the eastern end of Tugtutôq.

Olivine occurs as euhedral to subhedral crystals which are generally smaller than the plagioclase laths. It forms 10 to 30% of the rocks and usually shows some variation in grain size within a single sample. Sections of some samples (from localities B, D and F) contain one or more olivines which are noticeably larger than the average (2-3mm in size) and which are probably phenocrysts. The olivine grains show a tendency to group in clusters. They are generally free from inclusions.

Opaque oxides compose 5 to 10% and are rather variable in size and shape. They may be of a similar size to the olivine crystals, or significantly larger. Euhedral crystals occur but are rare; subhedral to anhedral shapes are more common and the oxide crystals sometimes partially enclose olivine or plagioclase, indicating that they grew at a slightly later stage in the crystallisation of the rock. Studies in reflected light show that both magnetite and ilmenite are present as discrete grains. The magnetite usually shows ilmenite exsolution. Composite magnetite-ilmenite grains are also present, as are minute grains of sulphide minerals. The different mineral grains sometimes, but not always, show different shapes, the magnetites being more angular. The ratio of magnetite to ilmenite varies and either can be the dominant phase. Samples from the western half of Tugtutôq contain variable proportions of the two minerals, while in the east, magnetite tends to dominate and small sulphide grains (predominantly chalcopyrite and pyrrhotite) become more common.

Clinopyroxene, making up 2 to 10%, is invariably sub-ophitic, occurring as poikilitic crystals up to 3mm across. It is a slightly pinkish brown in colour. Apatite occurs as extremely elongate crystals (length:width = 20:1 to 30:1) within oxide and pyroxene and in interstices between plagioclase crystals, forming a few percent of the

rocks. Biotite forms fringes around oxide crystals and makes up 1-2%. The rocks are generally slightly altered, with some sericitisation of plagioclase and some marginal alteration of olivine to chlorite and occasionally opaque oxides.

The composite glomerocrysts found at locality F consist of radiating clusters of plagioclase 1-2cm long (frequently showing either normal or oscillatory zoning) with olivine, oxides and interstitial clinopyroxene. The mafic minerals may reach 4mm in size (Plate 3.2).

The presence of olivine, one high-Ca pyroxene, alkali feldspar and biotite shows that these rocks have alkaline rather than tholeiitic affinities. This is confirmed by whole-rock chemistry (Chapter 4).

### 3.2.2 Troctolites

Western Tugtutôq (Localities A to F)

From locality F of Fig. 2.1 westwards the troctolites of the YGDC interior are characterised by a cumulus assemblage of plagioclase + olivine only and will be described separately from the eastern troctolites. It is apparent in thin section that rocks from locality F are much more similar to those of localities A to D than to those of locality G eastwards and are here included in the section on western Tugtutôq. All cumulates from the YGDC are orthocumulates, showing zoning of cumulus minerals and distinct intercumulus phases.

One rock type forms the majority of the western troctolites (from localities A to D). In it, plagioclase is dominant, forming 60 to 70% of the mode (Plate 3.3b). The crystals have a length:width ratio of c. 5:1 and a seriate distribution of grain sizes ranging from 1mm to 1cm with occasional larger crystals up to 2cm. Zoning is common and usually continuous although a few large crystals show some oscillatory zoning. There is a population of strongly-zoned, rather squat crystals which tend to have little twinning and sometimes show rather patchy extinction. These rarely exceed 2-3mm in length and form only a few percent of the total plagioclase population (Plate 3.3c).

The crystals of plagioclase are euhedral to subhedral and, as in the chilled margins, often show irregular contacts with other crystals (irregularities are lobate and around 0.1mm in size) (Plate 3.3b). Overall, the orientation of plagioclase crystals is

random but locally they may show a slight alignment. In some areas clusters of plagioclase crystals form virtually monominerallic areas within the rock, up to about 8mm across (Plate 3.4a). Some crystals, although apparently unzoned, partially enclose olivine crystals and thus must possess overgrowths on the original cumulus crystals; there are also minor overgrowths of untwinned alkali feldspar on some grains. Small inclusions of opaque oxides and biotite (probably secondary) are found within the plagioclase. There is little quantifiable variation between samples except in the degree of sericitisation which may be from about 5-20%.

Olivine makes up 20 to 25% of these rocks and ranges from 0.1-5mm in size, with most crystals being between 0.1 and 2mm. There is also a range of shapes; some of the crystals are euhedral but most are subhedral, either rounded or irregular in shape. Some of the smaller crystals may be very rounded. Irregular twinning is common in the large crystals (Plate 3.3b & f). The tendency of the olivines to cluster which was noted in the field is obvious in thin section (Plate 3.4a). The clusters vary from 2 to 8mm in size and from roughly equidimensional to strongly elongate and chain-like in shape. Orientated sections show no obvious three-dimensional shape or preferred orientation of the clusters. Olivines within the clusters tend to show straight or gently curved grain boundaries and equiangular triple junctions, indicating a certain amount of textural equilibrium (see section 3.3.1). Outside the clusters, overgrowths on the olivines tend to fill plagioclase interstices, giving single crystals a less regular shape than those in clusters.

Olivine crystals within the clusters may be completely enclosed within poikilitic oxide or clinopyroxene grains (Plate 3.3d). Those within oxide crystals tend to be slightly smaller and more rounded on average than those outside, but the difference is slight. No differences were observed between olivine crystals within pyroxene oikocrysts and those outside. Minor alteration products of chlorite and fine-grained opaque minerals may rim some of the olivine grains and trails of fine-grained opaques are also found within crystals (Plate 3.3e).

Opaque oxides form poikilitic crystals 0.2-2mm across, making up 5% or less of the rocks. These crystals almost always occur within olivine clusters. Ilmenite usually forms slightly more than half of the oxide grains and most of the magnetite occurs as composite grains with ilmenite rather than as discrete crystals. Magnetite usually shows ilmenite exsolution. A few sulphide grains are found.

Clinopyroxene also occurs as poikilitic crystals; these are up to 6mm in size and may be roughly equidimensional or considerably elongated. They enclose either olivine or plagioclase but single crystals of pyroxene rarely enclose both olivine and plagioclase. Around the latter they tend to be made up of several irregular (often wedge-shaped) crystals which appear in thin section to be unconnected but which are in optical continuity. Where clinopyroxene and oxide crystals occur together, the pyroxene may partially enclose the oxide mineral, but not the other way round, indicating that the oxide began to crystallise first. Occasional irregular twinning may be seen within the pyroxene and it often contains small oxide crystals and well-formed prisms of apatite.

Apatite is seen as squat hexagonal prisms up to 1mm long, which are sometimes skeletal with central cavities, or as sub-poikilitic crystals between olivine grains. The prismatic crystals occur particularly in altered interstices between plagioclase crystals, possibly sites of the latest crystallisation products of the magma. Biotite forms orange-brown rims up to 0.2mm wide on opaque crystals. It may also occur as discrete crystals up to 0.5mm in size, sometimes with apatite in plagioclase interstices.

These troctolites and their associated gabbro picrites have been studied in greater detail than any other YGDC rocks because of their relatively simple cumulus assemblage. Textural studies on these rocks are presented in section 3.3.

Not all of the troctolites from this part of the YGDC conform to the above description. The troctolite from near the northern margin of locality B has a different appearance in thin section as well as in the field. Although the chills here look very similar to other chilled marginal samples, the troctolite has a mode which differs from that of the other troctolites. It is richer in oxides and pyroxene at the expense of olivine, consisting of about 65% feldspar, 15% olivine, 10% opaque oxides and 10% clinopyroxene.

The feldspar is mostly plagioclase, forming stubby crystals with strong normal zoning. About 30% of the feldspar is cryptoperthitic alkali feldspar, some of it possibly secondary (i.e. due to late stage fluid activity). Some degree of recrystallisation is suggested by irregular edges to many feldspar crystals and by areas of fine-grained interlocking alkali feldspar grains. Olivine occurs as subhedral to anhedral 1-3mm crystals, occurring singly rather than in clusters. The large numbers of small olivine crystals seen in the troctolites described above are not present. Inclusions of opaque oxides are relatively common in the olivine crystals. The

crystals of oxide minerals are generally subhedral, 1-2mm in size and appear, from their morphology and size, to have cumulus status. They are usually rimmed by biotite. Clinopyroxene occurs between, and partially surrounding, olivine as crystals up to 3mm (Plate 3.4b) and is probably a postcumulus phase, although the crystals are not as distinctly interstitial as those in the main troctolite. Relatively high apatite and biotite contents (about 10% together), with apatite forming crystals up to 2mm in length, are also untypical of troctolites from the western YGDC. The higher modal contents of Fe-Ti oxides, clinopyroxene, biotite and alkali feldspar, together with the cumulus status of the oxides, give the impression of a greater degree of differentiation than the troctolites forming the rest of the western segment of the dyke.

Samples from locality D east of the fault and from locality E are similar to those from the northern margin at locality B. The one available sample from locality E is more feldspathic than the rock described above, consisting of about 80% feldspar, 10% olivine, 5% oxides and 5% clinopyroxene. The feldspar is predominantly plagioclase but about 10% of it is probably alkali feldspar. Contacts between feldspar crystals are usually irregular. Olivines are anhedral and 1-3mm in size while opaque oxides and pyroxene are 0.5-2mm across and occur as anhedral crystals (Plate 3.4c).

Troctolites from locality F, away from the chilled margins, are similar to the main troctolite of the western YGDC but the olivines show less tendency to clump together.

Eastern Tugtutôq and Narsaq

At locality G (Marrait) and eastwards, the giant dyke troctolites contain opaque oxides and sometimes apatite as cumulus phases in addition to plagioclase and olivine. There is variation between different localities but some generalisations can be made. Plagioclase forms 50-60%, olivine 10-20%, opaque oxides 5-20%, clinopyroxene 5-15% and apatite and biotite 1-5% of the mode.

Olivine occurs as euhedral to subhedral crystals and is variable in size, but not to such a great extent as in the western troctolites. At locality G, the olivines tend to be 0.2-1mm in size (Plate 3.4d) but at locality I (Sigssardlugtoq) (Plate 3.5a) and in the marginal troctolites of localities K and L, they are 0.5-4mm. Some crystals may form clusters, but this is not very common. They may contain inclusions of opaque oxides, especially at locality M.

Plagioclase laths also show a variety of sizes; in the layered pod at locality G they are up to 5mm long but in the troctolites outside the pod, and at other localities in the eastern half of Tugtutôq, they can reach 1.5cm. In some samples there appears to be a bimodal plagioclase population with the 10-15% of larger crystals sometimes forming stellate clusters. Length:width ratios are commonly 4:1 or 5:1. There is some normal zoning of plagioclase but it is less pronounced than in the western troctolites. Occasional crystals may show oscillatory zoning or a more distinct break between core and rim. Interstitial alkali feldspar forms 5-20% of the total feldspar.

Opaque phases are frequently euhedral octahedra of magnetite. Less regular-shaped grains showing more rounded shapes are either ilmenite or composite grains. Both oxides have a grain size of up to 1mm. The proportion of magnetite to ilmenite is approximately 4:1 or 5:1. The magnetite is virtually always exsolved and sometimes two stages of exsolution can be seen, producing an earlier set of broad lamellae and a later set of much finer lamellae. Sulphides are slightly more common than in the western troctolites (Plates 3.5b & c).

Clinopyroxene is interstitial to other phases and may be sub-ophitic. Crystals are a few mm in size and often contain inclusions of apatite. The proportion of clinopyroxene tends to be variable. At locality G (Marrait) and localities K and L (Krydssø and Assorutit) it forms 10-15% of the rocks while at locality I (Sigssardlugtoq) the laminated gabbros contain only about 5% pyroxene and a single thin section may not contain any (Plate 3.5a). The small layered pod in the southern part of the dyke at locality I (section 2.3.2) contains 10-15% pyroxene and has a slightly smaller grain size. The latter may have allowed easier oxidation of ferrous minerals, producing the browner weathering observed.

Apatite is much more common in the rocks of locality G (5%) than those of locality I (about 1%) and may not be a cumulus phase in the latter. It generally occurs as stubby prisms up to 0.5mm long, but may be anhedral at locality I. Biotite forms a larger proportion of all these rocks than of the western troctolites (sometimes up to 10%) but still occurs as rims round oxide crystals.

In pegmatitic pods at locality L (Assorutit) minerals are coarser, with olivines reaching 7mm, oxide crystals 4mm and feldspars 15mm in size.

As seen in hand specimen, available samples from locality H are similar to rocks from the north margin of locality B.

At Narsaq (locality M), rock modes and textures are similar to those seen in the eastern half of Tugtutôq, but, as noted in the field, the grain size is coarser (Plate 3.5d). Plagioclase is commonly 0.5-1cm in length and sometimes larger, olivine crystals are up to 7mm and apatite prisms often 0.5mm thick and 3mm long. Poikilitic clinopyroxene is similar in size to other rocks from the area. One sample (GGU 30766) is extremely rich in feldspar and could be termed an anorthosite. The interstitial material, forming about 10% of the mode, is predominantly clinopyroxene with a few small crystals of oxide minerals. The feldspar crystals, which are 0.5-1cm in size and very well-aligned, have apparently been concentrated at the expense of olivine and oxides.

### 3.2.3 Mafic cumulates

Western Tugtutôq (Localities B to F)

The mafic cumulates found in the western part of Tugtutôq (localities B, C, D and F of Fig. 2.1) are all gabbro picrites and show very similar textures to associated troctolites, differing mainly in their modes. The olivine crystals exhibit a wide range of sizes (0.1-5mm) and the rocks tend to have a slightly higher proportion of large crystals (2-5mm) than do the troctolites (Plate 3.3f). The crystals are more often euhedral than those in the troctolite and are frequently in contact with one another. Separate clusters of crystals cannot be distinguished but the degree of "packing" is variable (Plate 3.6a). There is some alteration to chlorite and fine-grained opaques. No differences in texture can be seen in sections of different orientation.

The thick gabbro picrites from locality F (Plate 2.14c) contain the largest proportion (perhaps 10%) of large crystals. The olivines are partly altered to chlorite and serpentine so that it is difficult to deduce the original contiguity of the grains.

The distribution of plagioclase in the picrites is much more variable than is apparent in the field. Both single plagioclase crystals and clusters are found scattered throughout the rocks (Plate 3.6a). The plagioclase clusters are generally 2-5mm across but may be larger, especially at the tops of layers. This makes the rock very variable on a thin section scale, with the proportion of plagioclase in the rock apparently varying between 15 and 40% (commonly 15-20%). Plagioclase crystals

between olivine grains are rarely more than 2-3mm in size, strongly zoned and poikilitic. However, olivine crystals enclosed within plagioclase are sometimes further apart than those enclosed within oxide or pyroxene, and the space between them probably defines the shape of an original cumulus plagioclase crystal which has subsequently grown faster than the olivines (Plates 3.6b and 3.7a).

Crystals of opaque oxides, clinopyroxene, apatite and biotite are very similar in occurrence and modal proportions to those in the troctolites (Plate 3.6c). Ilmenite forms 60-90% of the total oxides, showing a greater tendency to dominate over magnetite. Clinopyroxene tends to form slightly larger (5mm) and more widely spaced crystals than in the troctolites and apatite crystals are usually interstitial to olivine rather than prismatic.

Two series of samples from the north limb of the northern synform at locality D (Itivdlip Sarqâ) have been studied in thin section. These represent two vertical "stratigraphic" sections, one of 50cm, the other about 1.5m. Apart from differences in mode, no significant variations were found with stratigraphic height. In one of the series a suggestion of normal grain-size grading was seen in a 13cm gabbro picrite layer. However, from the other series of samples it can be seen that a 60cm picrite layer shows no grading. The first of these series of thin sections was point-counted to determine modal proportions and results are shown in Fig. 3.1. These sections were also used for grain size analysis (section 3.3.2)

Eastern Tugtutôq and Narsaq

Mafic cumulates were found within troctolites at localities G, I and M, and within syenogabbros at locality K. The latter will be described in section 3.2.4.

At localities I and M olivine + oxide cumulates form lenses or irregular masses within troctolites (Chapter 2). Euhedral olivines 1-3mm in size, showing relatively little size variation but again having variable "packing", form c. 50% of the rock. At locality M the olivines are full of tiny elongated opaque inclusions (Plate 3.7b). Crystals of opaque oxide are 0.5-5mm in size and make up about 30% of the mode. They tend to vary in shape from equant in areas of low olivine concentration, to anhedral where olivine packing is closer (Plate 3.6d). Magnetite is the dominant oxide at locality I, with ilmenite forming overgrowths on magnetite crystals, sometimes having the effect of joining several together into a cluster. Magnetite

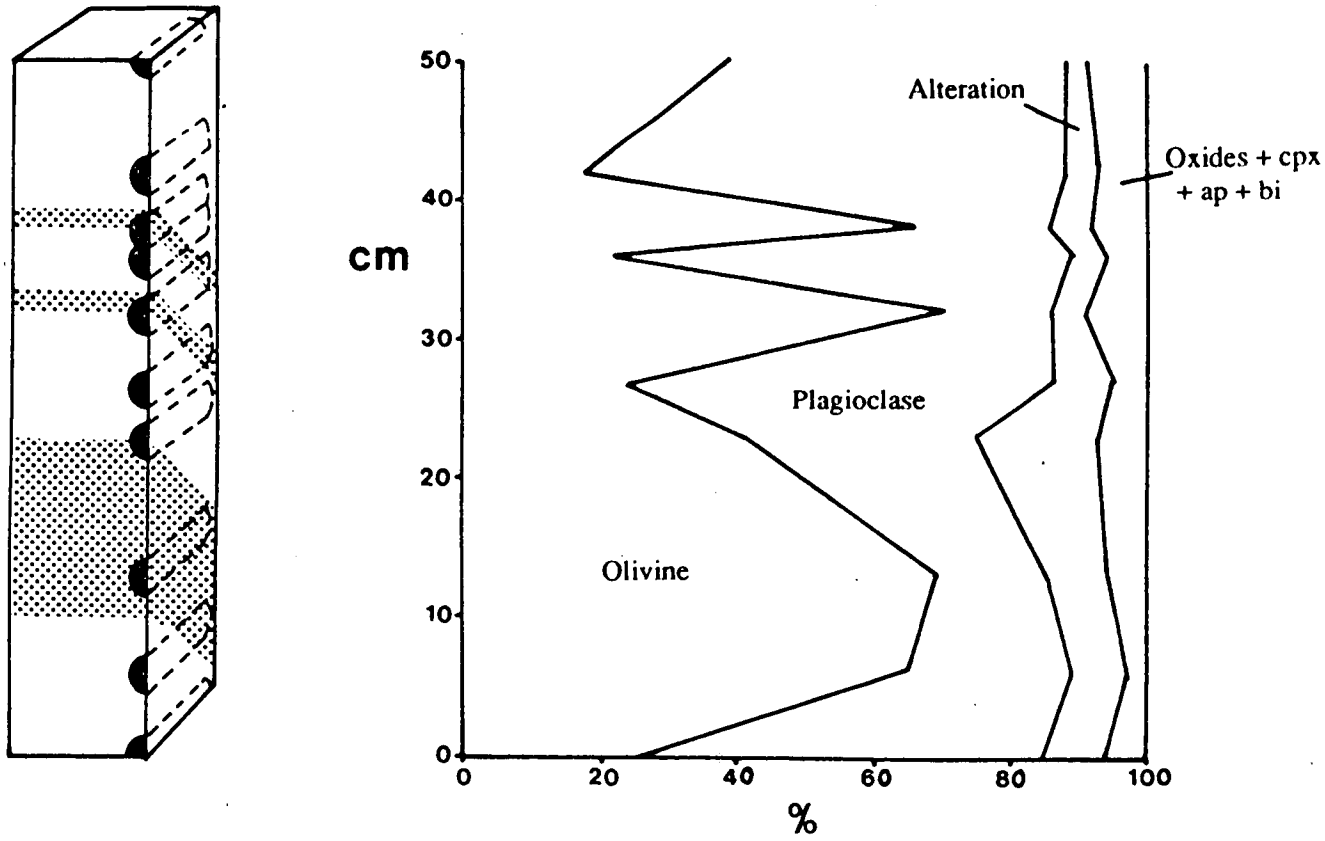


**Figure 3.1** Modal proportions of minerals in drill cores from a stratigraphic section from the north limb of the northern synform at locality D. The section is shown on the left and the black semicircles represent the localtions of the drill holes. The layers dipped away from the face drilled, so the horizontal cores sometimes intersected layers which were above them on the drilled face.

shows very fine exsolution, possibly of ulvöspinel. At locality M, discrete ilmenite crystals occur in slightly greater abundance than magnetite. As in the troctolites, sulphide grains are more common than in the western YGDC (Plate 3.8a).

Feldspar (predominantly plagioclase) fills interstices as poikilitic crystals up to 5mm across. Few of these seem to have cumulus cores. Feldspar makes up about 20% of the rock. Apatite is interstitial to other phases at both localities (unlike locality G). At locality I it forms only 1-2% of the rock but at locality M apatite may form up to 5% (Plate 3.7b). Dark red-brown biotite, composing only a few percent, forms narrow rims on the oxide crystals. Clinopyroxene has not been found in any thin section of these rocks.

At locality G layers of olivine + magnetite + apatite cumulate occur. These are a little finer-grained than the mafic cumulates to the east, as are the co-existing troctolites within the layered pod (see above). Olivine crystals are usually 0.1 to 0.5mm, but may occasionally be up to 3mm, oxide crystals occur up to 5mm but on average are 0.5 to 3 mm, and poikilitic plagioclase crystals are 1 to 5mm in size (Plate 3.8b).

Olivine forms about 30% of the rock. The crystals are often euhedral and show some tendency to cluster. They may contain tiny needles of apatite. Oxide crystals, also making up about 30%, vary from euhedral to anhedral and often contain abundant apatite inclusions in the outer parts. Magnetite and ilmenite occur in roughly equal proportions and composite grains are common. The magnetite is usually coarsely exsolved. Plagioclase may occur as clusters of crystals, usually well-twinned and with far less overgrowth material than in the olivine + magnetite cumulates described above. Apatite makes up nearly 10% of the assemblage and occurs as numerous small prisms about 0.2mm thick and 0.5mm long, enclosed within oxides, clinopyroxene and biotite. This shows that, unlike localities I and M, apatite and oxide crystallisation occurred roughly simultaneously. The existence of apatite inclusions within the outer rims of oxide crystals indicates that apatite nucleated slightly after the oxide crystals but while the latter were still growing. Poikilitic crystals of clinopyroxene up to 5mm in size enclose olivine, magnetite and apatite and make up between 5 and 20% of the rock, depending upon the thin section.

In cathodoluminescence, all of the troctolites, gabbro picrites and other mafic lithologies show no evidence of feldspar metasomatism (i.e. all of the feldspar luminesces blue) (Plate 3.7c). Apatite shows occasional zoning along fractures and in

overgrowths. Within cloudy patches between minerals, zeolites (Plate 3.7d) and occasionally calcite were found as alteration products.

### 3.2.4 Syenogabbros and syenites

The evolved pods at localities K and L of Fig. 2.1 are characterised by abundant prismatic clinopyroxene crystals, implying that pyroxene joined the fractionating assemblage. There appears to be a trend of increasing fractionation from the exposed base to the top of the synform at locality K, and inwards from the dyke margins at locality L, from syenogabbros containing plagioclase and alkali feldspar to syenites entirely lacking plagioclase. It seems likely that the syenites at locality L may overlie less fractionated cumulates in the same way as is seen at locality K. Rocks from these two localities are very similar in thin section, except that those from locality L tend to show a greater degree of alteration, especially of feldspar and olivine.

The syenogabbros from the lower part of locality K and the "elongate pyroxene zone" of locality L contain about 55% feldspar, 10% each of olivine, clinopyroxene, opaque oxides and biotite, together with 5% apatite. The feldspar is made up of 50-60% plagioclase with the remainder being cryptoperthitic alkali feldspar. Plagioclase crystals showing fine lamellar twinning are usually surrounded by wide margins of alkali feldspar, with a gradual transition between the two (Plate 3.7e). Discrete crystals of both plagioclase and alkali feldspar are also seen. The grains vary in size from 0.5 to 4mm and frequently possess very irregular grain boundaries. Some cloudy alteration affects both types of feldspar.

Olivines are modally less important than in the troctolites. They are generally anhedral and are scattered singly throughout the rock as 0.5-3mm crystals. Iddingsitisation and alteration to oxides at the margins of the crystals and along fractures is common, in contrast to the alteration to chlorite and serpentine shown by the more magnesian olivines. Some contain inclusions of apatite. Clinopyroxene crystals are prismatic in their overall shape (length:width = 2:1 to 3:1), but their outlines may be rather irregular. They are generally pinkish brown in colour, zoned to a more greenish brown at the rim, and are up to 4mm long at locality K. At locality L they are highly elongate (length:width = 5:1 to 10:1, see section 2.3.3). Inclusions of apatite prisms are common and small subhedral to anhedral oxide crystals may also form inclusions within pyroxene grains. Apatite inclusions are also

common within the 0.5-1.5mm anhedral crystals of opaque minerals. Opaque crystals are predominantly magnetite but ilmenite still makes up 10-30% of the total. Magnetite is not always exsolved; unexsolved grains sometimes show incipient bluish oxidation along fractures. Sulphides are more common than in the less evolved rocks but still form <1% of the mode. Pyrite, chalcopyrite and pyrrhotite occur, the latter sometimes altering to marcasite. Dark brown biotite rims the oxides but is not confined to such rims and may form poikilitic crystals up to 3mm across, enclosing any of the other minerals. Apatite composes several percent modally and occurs as numerous prisms about 0.3mm thick and up to 3mm long (Plate 3.8c). The mafic minerals and apatite tend to occur together in clumps.

Within the syenogabbro at locality K, more mafic cumulates are found, with concentrations of olivine, pyroxene and opaque oxides at the expense of feldspar. They do not become as mafic as those described in the previous section; feldspar still forms 30-40% of the rock.

With increasing fractionation the olivine content falls to 5% or less, with a concommitant increase in pyroxene. The amount of alkali feldspar increases at the expense of plagioclase until no plagioclase cores to the feldspar grains remain. The perthitic exsolution becomes coarser and it can be seen that much of the feldspar is antiperthite with an albite host. Turbidity of the feldspars is more intense. Apatite becomes less important modally and in the syenites of locality L, a dark brown hastingsitic amphibole appears as large crystals enclosing olivine, pyroxene and opaque minerals and forming up to 15% of the rock. Crystals of olivine, pyroxene and oxides become smaller (0.5-2mm) and form a smaller proportion of the rock (20-30%). A blue-green amphibole (riebeckite or arfvedsonite?) which often occurs as sheaves of small crystals is a secondary alteration product of the brown primary amphibole and of olivine (Plate 3.7f). Angular interstices between feldspar crystals are often rimmed by clear albite and contain quartz and calcite, the latter apparently primary in origin (Plate 3.9a). The albite rims to the feldspars may have resulted from unmixing of the sodic and potassic components of the feldspars, or may have grown from the siliceous, carbonated residual fluids which crystallised in the feldspar interstices.

In cathodoluminescence, syenogabbros and syenites from locality K (Krydssø) are very similar to the basic rocks from the YGDC, with all the feldspar luminescing blue and interstitial zeolites present. One sample (186221) is an exception and contains calcite and fluorite but no zeolites. In contrast, however,

evolved facies from locality L (Assorutit) do contain red-luminescing feldspar. The proportion of red feldspar varies from 10 to 50% in the syenogabbros and syenites (showing little correlation with locality) and rises to 95% in a late-stage vein (Plate 3.9b & c). Zeolites are absent but calcite is always present and may show modal abundances of a few percent (Plate 3.9d). The late-stage vein is most affected and the marginal troctolite not at all, and the distribution of the red feldspar has no spatial relationship with later intrusions that might have been the source of a metasomatising fluid. It is concluded that the metasomatism producing the red-luminescing feldspar is almost certainly caused by fluids associated with the late stages of syenite crystallisation, and is autometasomatism.

From the different degrees of metasomatism between localities K and L, it appears that the fluid phase associated with the crystallisation of the evolved pod at locality L was more important than that at locality K. This might be expected from the common occurrence of pegmatitic facies at locality L and the coarseness of the feldspar exsolution. It does not mean, however, that no fluid was involved at locality K; it is possible that a fluid at a different temperature or with a different chemistry was present.

### 3.2.5 Xenoliths

The elongate mafic xenolith from near the northern margin at locality D (Itivdlip Sarqâ) (section 2.5) appears to be extremely similar in all respects to picrites from this area. The only difference in texture is a slight tendency for the olivines to be more euhedral and less contiguous than those of the picrites, implying a slightly lower degree of textural equilibration. This "xenolith" is thus probably part of a disrupted layer.

Leucocratic xenoliths found in the area of localities B to D are rather different from the troctolites in that they are finer-grained and texturally more similar to chilled marginal samples. The mode is roughly 70-75% feldspar, 10-15% olivine, 10% opaque oxides and 10% clinopyroxene. Feldspar crystals are up to 2mm in length and range from stubby to slender, forming an interlocking framework. The olivines are frequently anhedral and do not occur in large clusters as in the troctolites. They are usually 0.5-1mm in size but larger grains up to 2mm may be found.

Scattered crystals of Fe-Ti oxides are 0.1-1mm in size and have not been examined in reflected light. Apatite occurs interstitially forming 1-2% of the rock and clinopyroxene occurs as sub-poikilitic crystals up to 4mm across.

Such leucocratic xenoliths are frequently associated with more evolved lithologies in which opaque oxides, apatite and occasionally pyroxene have cumulus status, and alkali feldspar is more prominent. These evolved facies may occur as small patches within xenoliths (on a thin section scale) but they are more common as a separate, often pegmatitic phase outside the xenoliths.

At locality B, the elongated plagioclase crystals which are often associated with fine-grained leucocratic xenoliths are seen in thin section to be rarely more than 1cm in length, but several crystals may give the appearance of one larger one. The crystals diverge from one another at angles ranging from 1-30° (Plate 3.10a).

Anorthosite xenoliths from locality L (Assorutit) are difficult to study in thin section due to the large grain size but the plagioclase crystals can be seen to be well-twinned and apparently unzoned. Interstitial phases are olivine and occasionally opaque oxides (both magnetite and ilmenite), augite and biotite.

### 3.2.6 Late-stage veins

Late-stage veins cut the YGDC in many places but become more common towards the eastern end of Tugtutôq. Most of the veins have a similar mineralogy, dominated by alkali feldspar with subordinate hastingsite to riebeckite or arfvedsonite, sometimes as an alteration product of pyroxene. Any of the following may also be present: fayalite pseudomorphs, magnetite, biotite, apatite, zircon, calcite and either quartz or possible pseudomorphs after nepheline. Alteration, especially of mafic minerals, is common.

A fairly typical vein sample (YGD86) from locality G comprises about 90% interlocking alkali feldspar crystals, up to 1.5mm in length, most of which show perthitic exsolution. (In other vein samples feldspar crystals may be coarser, occasionally over 1cm in length). Mafic minerals are predominantly brown clinopyroxene altering to an alkaline amphibole showing blue-green to brown pleochroism. Dark brown to dark green biotite is also present. A few crystals of opaque oxides are present but most occur as interlocking secondary growths, possibly replacing olivine. Apatite and calcite are present in small amounts but in this rock

neither quartz nor nepheline pseudomorphs appear to be present. Possible pseudomorphs after nepheline are found in vein samples from locality C and in the vicinity of localities K and L. In one sample from locality C they are interstitial to the feldspars, forming 5-10% of the rock and are partly isotropic and partly moderately birefringent (Plate 3.9e). Pseudomorphing minerals may include sodalite, zeolite minerals, clay, mica and carbonate.

Where quartz is present in veins it is usually found with calcite in interstices between feldpars. As in the syenites, these interstitial areas are often rimmed by albite.

### 3.2.7 The nunataq region

Most of the rocks from the nunataq region (Upton and Fitton, 1985; Upton, 1987) show great similarity in thin section to those from eastern Tugtutôq and Narsaq. There are no equivalents of the plagioclase + olivine cumulates or olivine cumulates from localities A to F. Both troctolites, some showing feldspar lamination, and mafic lithologies (olivine + oxide cumulates) are seen, and samples from the two evolved pods bear a striking resemblance to those from localities K and L on Tugtutôq, except that they do not contain quartz. One syenite sample (GGU 216627) shows sharply defined modal layering, unlike the syenites at localities K and L, and has been studied in detail as an example of a layered syenite (Plate 3.10b). In thin section it resembles rocks from locality K (Krydssø), with fresh olivines (10%), abundant prismatic clinopyroxene (20%), fairly finely exsolved perthitic feldspar (55%), small proportions of oxides, brown hastingsitic amphibole and biotite (5% each) and a few percent of apatite. The mafic layer is an olivine-oxide-pyroxene cumulate with 25% olivine, 15% oxides, 35% clinopyroxene, 5% biotite and apatite, and 15% feldspar.

In cathodoluminescence, this sample was found to contain about 10% red-luminescing feldspar. It also has late-stage fluorite rather than calcite (Plate 3.9f). Upton and Fitton (1985) reported late-stage veins from the nunataq region which contain both fluorite and calcite, so the lack of calcite in GGU 216627 is not representative of the whole region. However, fluorite has not been found in the YGDC on Tugtutôq.

### 3.2.8 Summary

Samples taken from the contact of the YGDC with its country rocks are generally very altered, but about 1m into the dyke the fine- to medium-grained chills are fresh. They consist of early-crystallised plagioclase and olivine with later opaque oxides, apatite and clinopyroxene. Minor biotite mantles the oxide crystals. Both magnetite and ilmenite are present as Fe-Ti oxides, with magnetite becoming dominant in the eastern part of Tugtutôq.

Troctolites from the dyke interior have plagioclase and olivine as primary phases in western Tugtutôq (locality F and westwards) but magnetite, ilmenite and sometimes apatite join the fractionating assemblage to the east. Apatite crystallised at roughly the same stage as the oxide minerals at locality G but was a later phase at localities I and M. Mafic lithologies are olivine cumulates (gabbro picrites) in the west, olivine-magnetite-ilmenite cumulates at localities I and M and olivine-magnetite-ilmenite-apatite cumulates at locality G. At locality I and in the mafic cumulates at locality M, clinopyroxene is rare or absent. No systematic differences in grain size, feldspar lamination, amount of postcumulus material or degree of alteration were observed between adjacent felsic and mafic layers.

At localities K and L, increasing fractionation inwards from the dyke margins gave rise to syenogabbros and syenites, both with clinopyroxene as a fractionating phase. Apatite and biotite are modally more important in the syenogabbros than in the troctolites or the syenites. The distinction between syenogabbro and syenite is made on the presence or absence of plagioclase cores to feldspar grains. Rocks from the nunataq region are very similar to those of eastern Tugtutôq and Narsaq and one syenite sample which shows a sharply defined layer of olivine-magnetite-ilmenite-clinopyroxene cumulate has been studied in detail since evolved facies at localities K and L are either poorly layered or unlayered.

## 3.3 Textural analysis

### 3.3.1 Textural equilibration

Grain sizes, shapes and configurations tend to change as rocks cool, in order to obtain a lower surface energy configuration (Hunter, 1987 and references therein). In slowly-cooled plutonic rocks this may lead to very different textures from those produced when crystals first come into contact.

**Plate 3.1**

(a) Thin section across a sharp contact between giant dyke (left) and Julianehåb granite (right). The dyke material is very fine-grained biotite, oxides and alkali feldspar while the granite shows widespread development of granophyric intergrowths. Sample GGU 40454, horizontal field of view 8mm, ppl.

(b) Typical chill sample composed of olivine (light grey), plagioclase (white, somewhat altered), oxides (black) and ophitic clinopyroxene (dark grey). The large olivine near the top edge of the photo may be a phenocryst. Sample GGU 101211 from the contact on Narsaq Island, field of view 8mm, ppl.

(c) Alignment of groundmass feldspar laths around part of a large composite phenocryst from locality F. Sample YGD126, field of view 2.4cm, crossed polars.

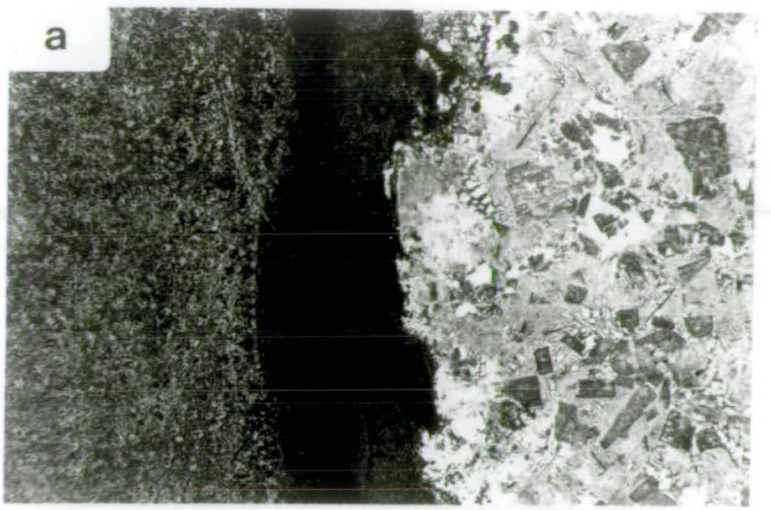
a

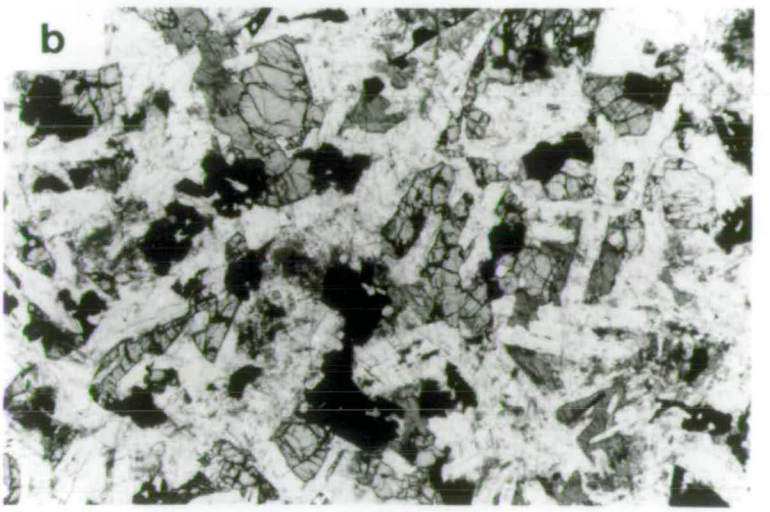
b

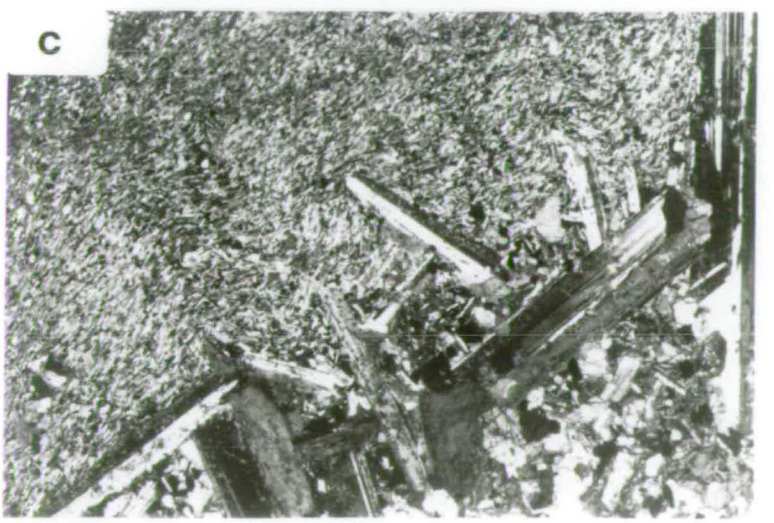
c

**Plate 3.2**

Composite phenocrysts in the chilled margin of locality L. Both phenocrysts and groundmass are composed of plagioclase, olivine, oxides and interstitial pyroxene and biotite. The large glomerocryst is 3cm across. Sample YGD126, ppl.

Plate 3.3

(a) Lamination of groundmass feldspars around part of a large composite phenocryst at locality F. A small olivine glomerocryst is also just visible at the top of the photo. The feldspar of the composite phenocryst has a zoned rim. Other groundmass minerals are olivine, oxides and ophitic clinopyroxene (the latter not visible in the photograph). Sample YGD126, field of view 9mm, crossed polars.

(b) Typical olivine-plagioclase troctolite from locality D. Variably-sized plagioclases show lamallar twinning, normal zoning and irregular margins. Several show a localised alignment. Olivines also display a range of sizes and the large olivine in the lower left shows irregular twinning. Sample YGD248, field of view 3.6mm, crossed polars.

(c) One of the occasional large, irregular (resorbed?), strongly-zoned plagioclase crystals found in troctolites from the western YGDC. Sample YGD248, field of view 3.6mm, crossed polars.

(d) Euhedral to rounded olivine crystals enclosed within intercumulus oxides and clinopyroxene in YGD404 from locality D. Olivines enclosed within oxide crystals tend to be smaller and more rounded (due to reaction) than those outside, but olivines within pyroxene show no such features. Field of view 3.6mm, ppl.

(e) Trails of fine-grained opaque oxides within a large olivine grain. Probably due to oxidation to magnetite along fractures. Sample YGD404, field of view 1.5mm, ppl.

(f) Gabbro picrite from locality D showing the variation in olivine sizes. The largest olivine (upper right) again shows irregular twinning. Sample GGU 186400, field of view 9mm, crossed polars.

a

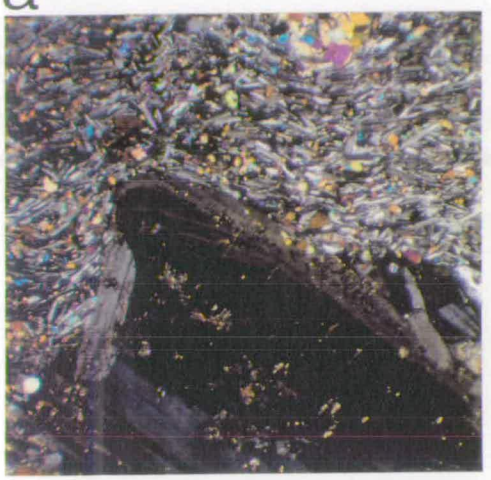

b

c

d

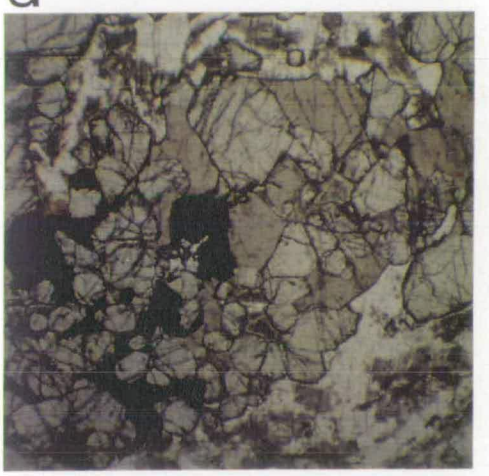

e

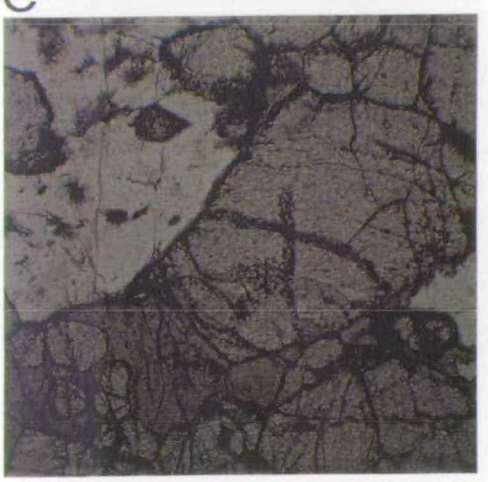

f

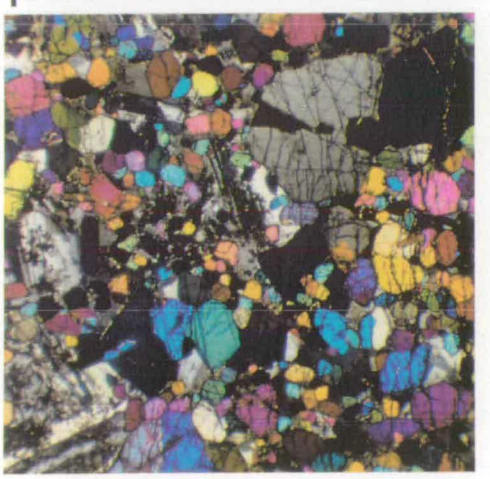

**Plate 3.4**

(a) Typical troctolite from the western YGDC, consisting of olivine (light grey), plagioclase (white), oxides (black) and clinopyroxene (dark grey). The olivine generally occurs in clusters, frequently with the intercumulus pyroxene. Plagioclase crystals tend to form clusters with little interstitial material. Sample YGD256, field of view 2.3cm, ppl.

(b) Troctolite from the northern margin of locality B, showing single olivines, stubby plagioclases, abundant oxides (probably cumulus) and less-poikilitic clinopyroxenes. Compare with (a). Sample YGD80, field of view 8mm, ppl.

(c) Feldspathic troctolite from locality E. Olivines are usually single and anhedral in shape. Oxides (top left) and pyroxene (lower left and lower centre) are intercumulus but less common than in (a). Sample GGU 40425, field of view 2.3cm, ppl.

(d) Plagioclase-olivine-oxide cumulate from locality G. The rock is finer-grained than most of the YGDC lithologies (compare with (a) and (c). A slight feldspar lamination runs from top right to lower left. Some intercumulus pyroxene can be seen in the top left hand corner. Sample YGD138, field of view 2.1cm, ppl.

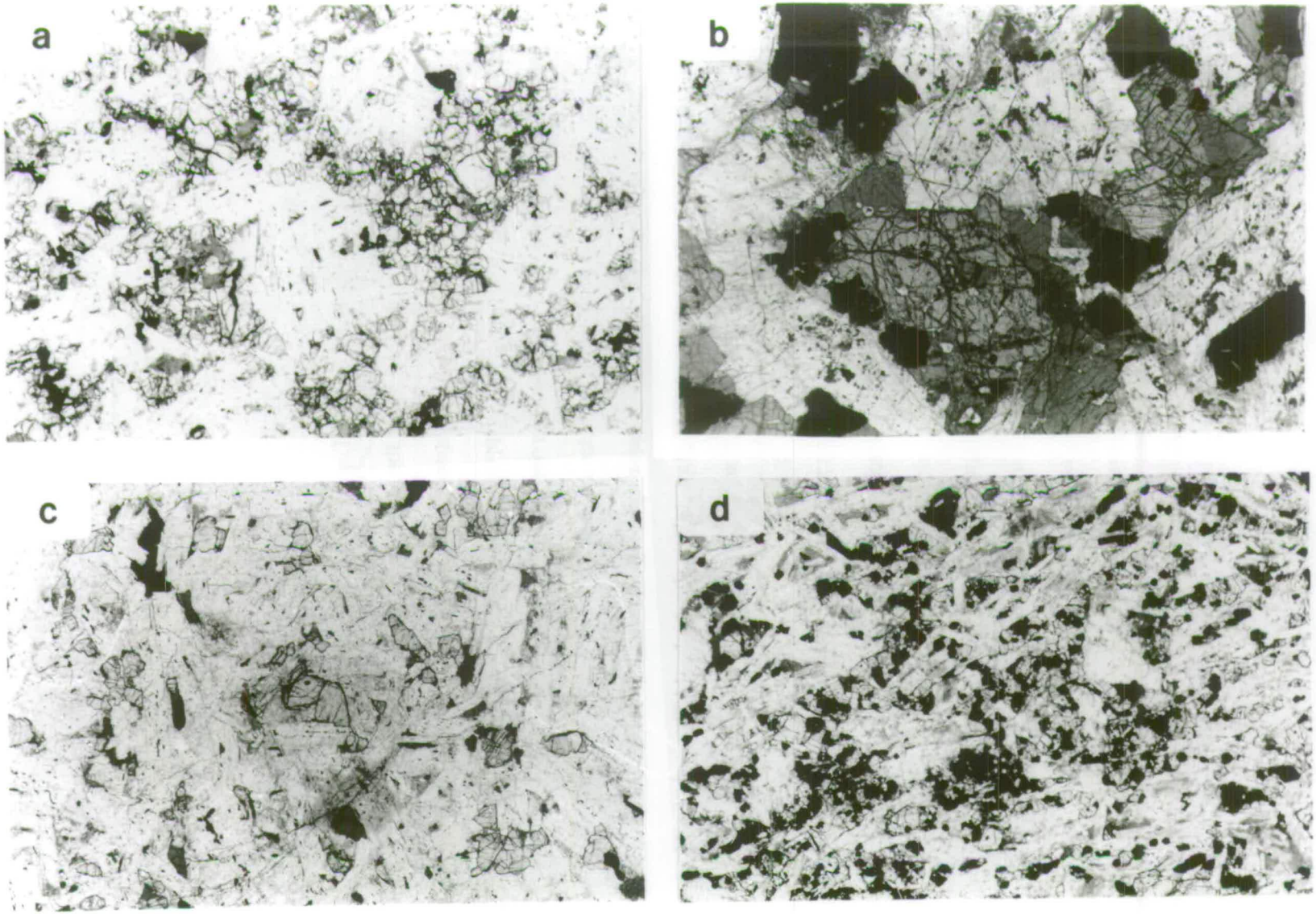
a
b
c
d

**Plate 3.5**

(a) Laminated troctolite from locality I (Sigssardlugtoq) made up of cumulus plagioclase, olivine and oxides with little intercumulus material. Some pyroxene is visible in the top right hand corner of the photo but it forms only a few percent of the rock. Note that the grain size is coarser than the laminated troctolite of locality G (Plate 3.4d). Sample GGU 86055, field of view 2.2cm, ppl.

(b) Reflected light photomicrograph of sample YGD364 (locality K) showing exsolved magnetite (mt) and a bright sulphide grain. The sulphide is predominantly chalcopyrite (ch) but a slightly darker area is pyrrhotite (py). Field of view 3mm.

(c) Magnetite showing much finer exsolution than (b) is adjoined by unexsolved ilmenite (ilm) enclosing a rounded grain of a sulphide mineral, probably pyrite or chalcopyrite. Sample YGD364, field of view 3mm, reflected light.

(d) Coarse-grained troctolite from locality M (Narsaq) composed of plagioclase, olivine (light grey), oxides and clinopyroxene (dark grey, near bottom of photo). The olivine and oxide crystals occur singly and tend to be anhedral in shape. Many plagioclase crystals contain numerous inclusions of opaque oxides. Sample YGD392, field of view 2.4cm, ppl.

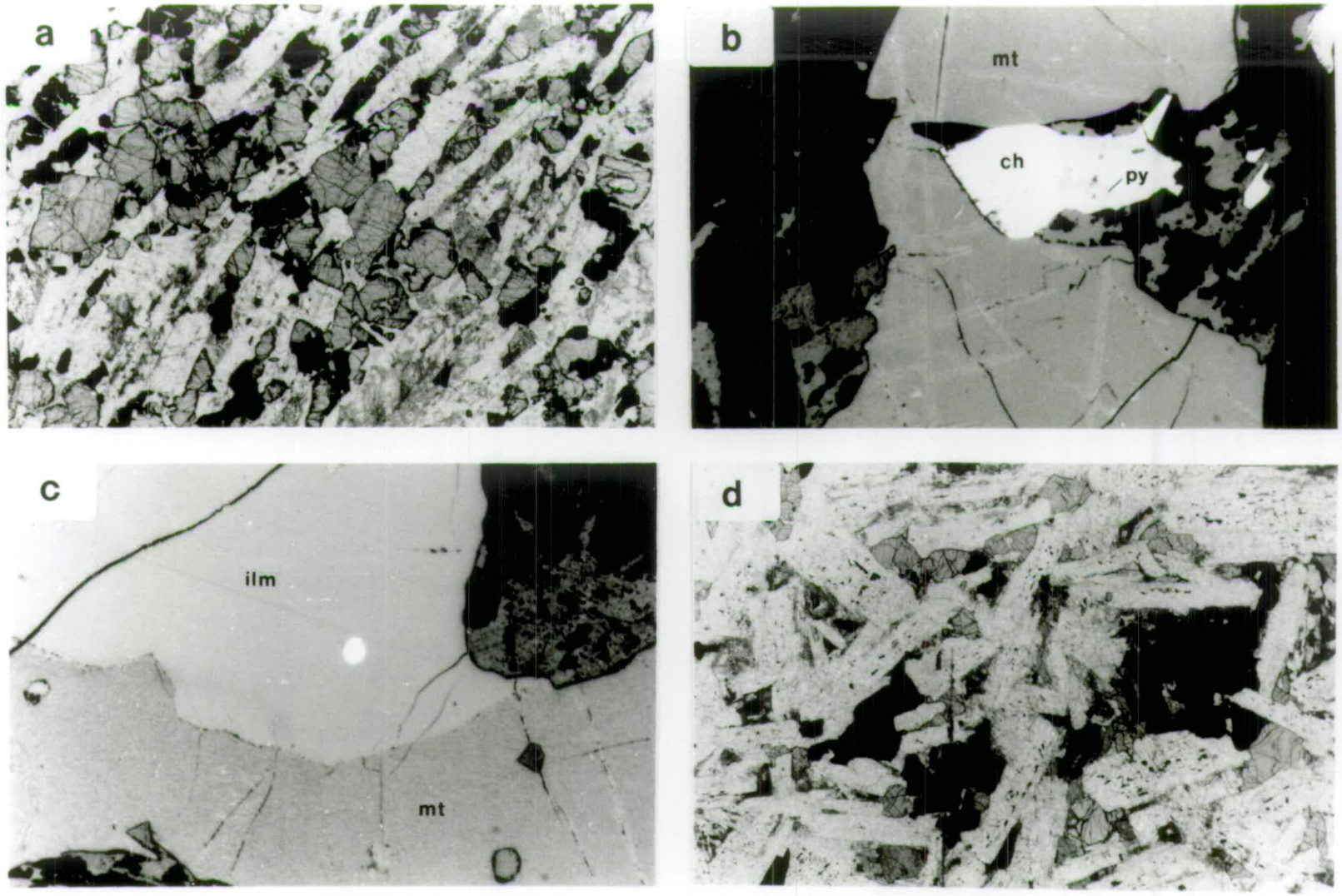
a
b
mt
ch
py
c
ilm
mt
d

Plate 3.6

(a) Gabbro picrite containing clusters of plagioclase. Most of the rock is made up of closely-packed olivines with interstitial plagioclase, oxides and clinopyroxene. However, rare cumulus plagioclase crystals occur throughout the rock and in places form near-adcumulate clusters, as seen here. The olivines display a wide range of sizes. See also Plate 3.3f. Sample YGD254, field of view 2.7cm, ppl.

(b) Olivines in a gabbro picrite surrounding an area of plagioclase that probably denotes an original cumulus crystal, although the crystal now surrounds several of the adjacent olivine grains. Note again the wide range of olivine sizes. GGU 186400, field of view 4.5mm, ppl.



(c) Intercumulus oxides and clinopyroxene in a gabbro picrite. As in the troctolite, olivines enclosed within oxide crystals tend to be slightly smaller and more rounded than those outside. Sample GGU 186400, field of view 4.5mm, ppl.

(d) An olivine-oxide cumulate from locality I (Sigssardlugtoq) with intercumulus plagioclase but no pyroxene. The cumulus crystals tend to be more euhedral in shape in areas where they are widely spaced (e.g. lower left of photograph) than in areas where they are more closely packed (upper right). Sample YGD196, field of view 1.5cm, ppl.

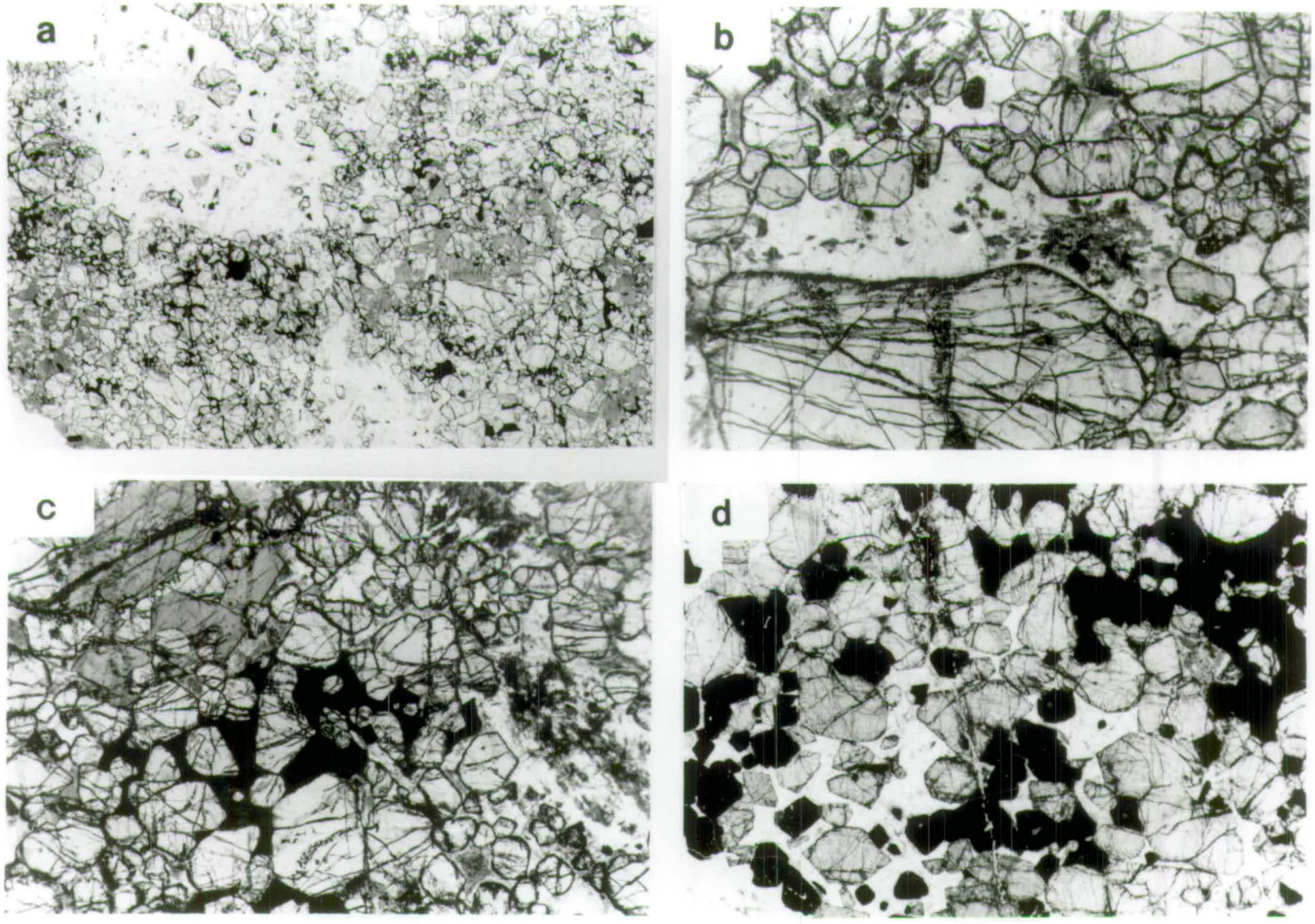
a
b
c
d

Plate 3.7

(a) A gabbro picrite containing a plagioclase crystal which probably had cumulus status but which now posses overgrowths enclosing surrounding olivines. Sample GGU 186400, field of view 3.6mm, crossed polars.

(b) An olivine-oxide(-apatite) cumulate from locality M (Narsaq). The olivines have a dusty appearance due to the presence of numerous elongate inclusions of oxide minerals, too small to be seen in this photo. The large white apatite evidently crystallised after olivine and oxides, as did the plagioclase (lower left). Brown biotite can be seen mantling oxide crystals. Sample YGD381, field of view 3.6mm, ppl.

(c) Cathodoluminescence photograph of YGD63 from locality D. Dark areas are non-luminescent ferromagnesian minerals, the blue is unaltered feldspar and the yellow crystals are mainly apatite. To the right of the largest apatite, a small area of zeolites is a slightly darker yellow. Field of view top to bottom is 2.6mm.

(d) Zeolite minerals fluorescing yellow under cathodoluminescence in a gabbro picrite from locality D. The blue-luminescing feldspar shows alteration to a dull-luminescing material near the top of the photo. Sample YGD5, field of view top to bottom is 2.6mm.

(e) Sodic plagioclase crystal mantled by alkali feldspar in a syenogabbro from locality K. Other minerals present are olivine (lower right), oxides, apatite (top centre) and pyroxene (upper left). Sample GGU 186224, field of view 1.8mm, crossed polars.

(f) Olivine pseudomorphs in GGU 50217, a syenite from locality L. Secondary oxides are mantled by blue-green amphibole and brown biotite. The two pseudomorphs are surrounded by alkali feldspar. Field of view 4.5mm, ppl.

a

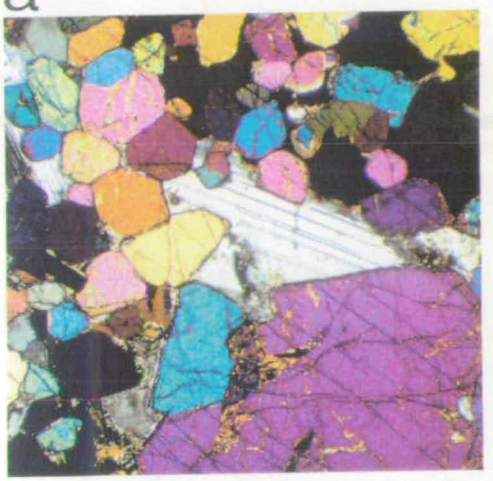

b

c

e

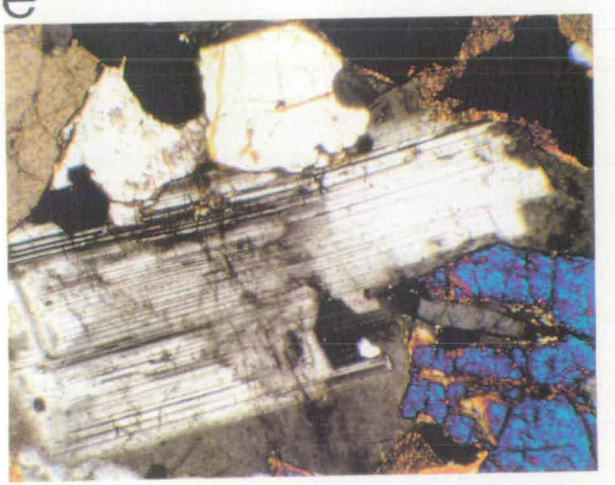

d

f

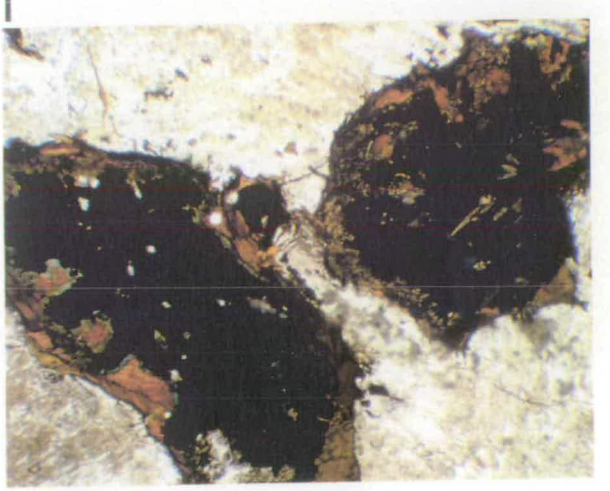

**Plate 3.8**

(a) Magnetite with ilmenite exsolution (left) and a complex sulphide grain in YGD392, a troctolite from locality M (Narsaq). Note the three exsolution planes within the magnetite. Horizontal field of view 3mm, reflected light.

(b) Olivine-oxide-apatite cumulate from locality G (Marrait). Some intercumulus feldspar (top left) and clinopyroxene (darker grey than the olivine) are also present. Sample GGU 30659 from the synform axis, field of view 7mm, ppl.

(c) Syenogabbro from locality K, showing cumulus pyroxene crystals (dark grey, lower centre and left) with olivine, plagioclase mantled by alkali feldspar (see Plate 3.7e), euhedral oxides, large apatites (right) and poikilitic biotites (right, dark grey crystal with horizontal cleavage). Sample GGU 186224, field of view 7mm, ppl.

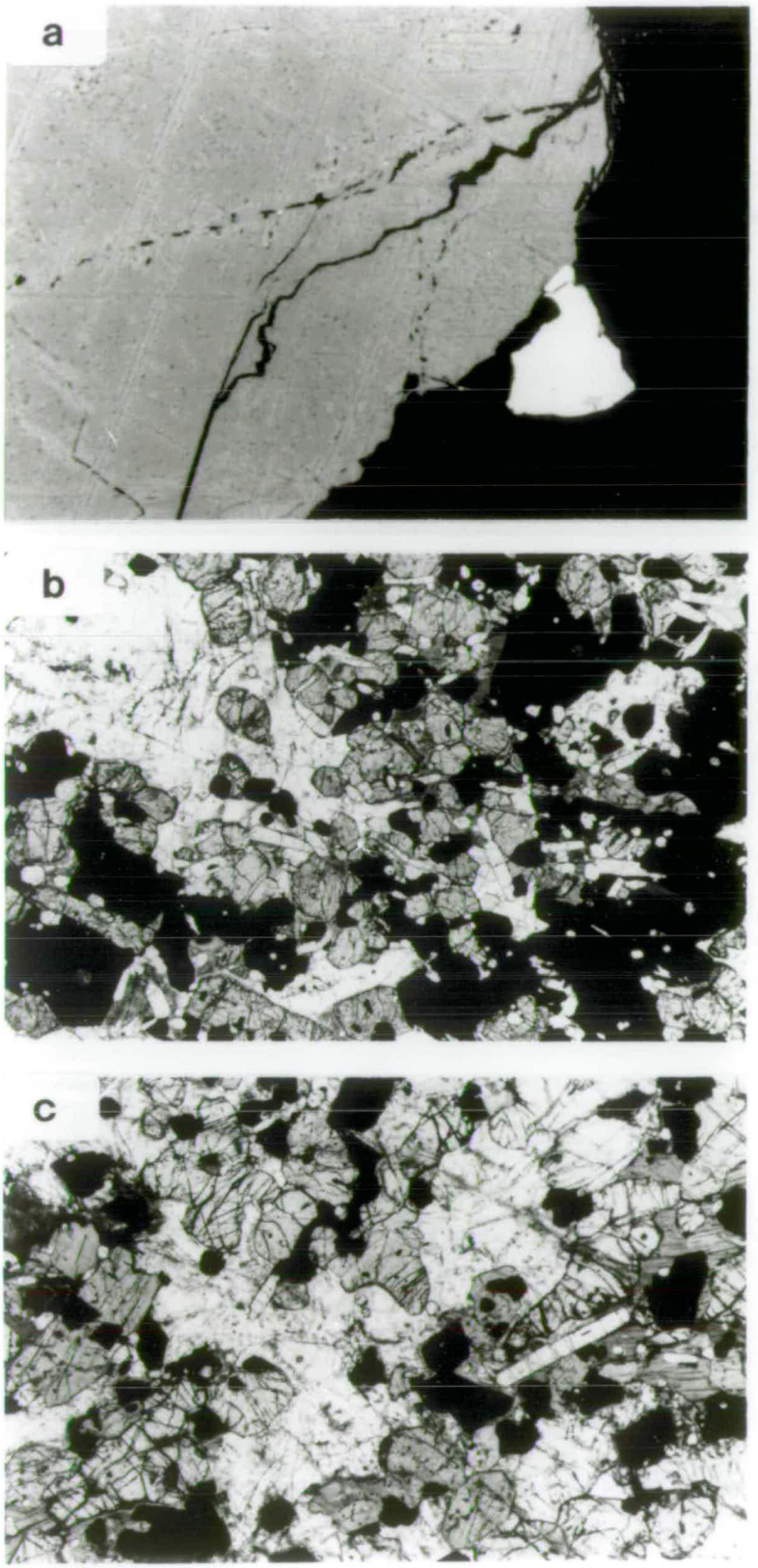
a
b
c

**Plate 3.9**

(a) Interstitial area between perthitic alkali feldspars in GGU 50217, a syenite from locality L (Assorutit). The interstice is rimmed by albite and filled by calcite (showing rhombohedral cleavage) and quartz (white). Field of view 1.5mm, crossed polars.

(b) A mafic syenite from locality L in cathodoluminescence. Dark areas are ferromagnesian minerals, the blue is the unaltered core of a feldspar, which is rimmed by red-luminescing metasomatised feldspar. Within the clear red area (left) some concentric zoning can be seen. The dull areas (between the red and blue parts of the feldspar and within the blue) can be seen under the electron microscope to be patch perthites while clear areas, both red and blue, are unexsolved. It seems that there are two types of alteration occurring (see Finch, 1990). Sample GGU 50218, field of view 2.6mm.

(c) A late-stage vein from locality L (YGD170) showing entirely red-luminescing feldspar. Two crystals can be seen; from the corner of the upper one a zoned protruberance extends into the area between the crystals. The orange rims to the black mafic minerals and bright orange patches within the feldspars are secondary calcite. Field of view 2.6mm, taken in cathodoluminescence.

(d) Cathodoluminescence photo showing secondary calcite (orange) within mafic minerals (black) and feldspar (blue- and dull-luminescing). Note how the calcite is concentrated in the dull (altered) parts of the feldspar. Pale yellow prisms are apatite crystals. Sample GGU 40548 (syenogabbro from locality L), field of view 3.6mm.

(e) Nepheline pseudomorph (centre of photo) in a late-stage vein from western Tugtutôq. The pseudomorph is predominantly isotropic (probably sodalite) with small amounts of birefringent material within it, possibly mica. Above it is perthitic feldspar, below it an amphibole showing brown absorption colours masking the birefringence. Sample GGU 186377, field of view 2.6mm, crossed polars.

(f) Sample GGU 216627, a syenite from the nunataq region, in cathodoluminescence. The feldspar is predominantly blue, but about 10% shows red luminescence. Within the red-luminescing area, a small amount of purple-blue fluorite can be seen. No calcite was found in this sample. Yellow apatite crystals can be seen with the non-luminescent mafic minerals. Field of view 2.6mm.

a

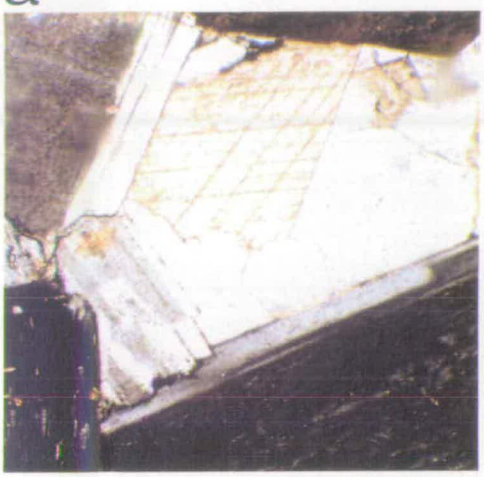

b

c

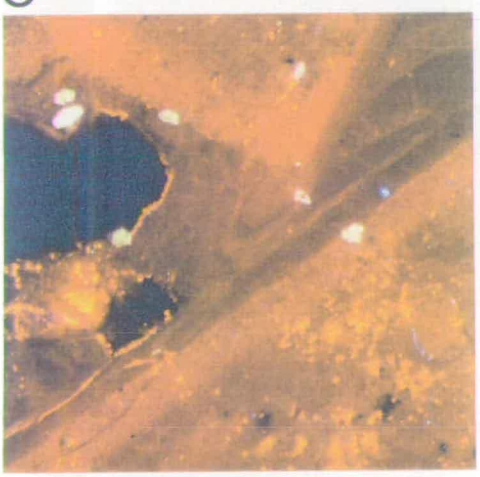

d

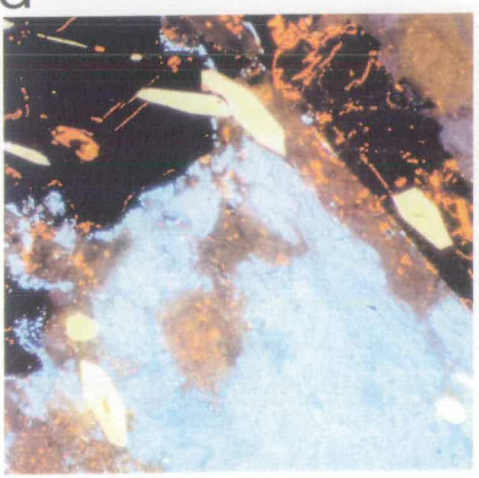

e

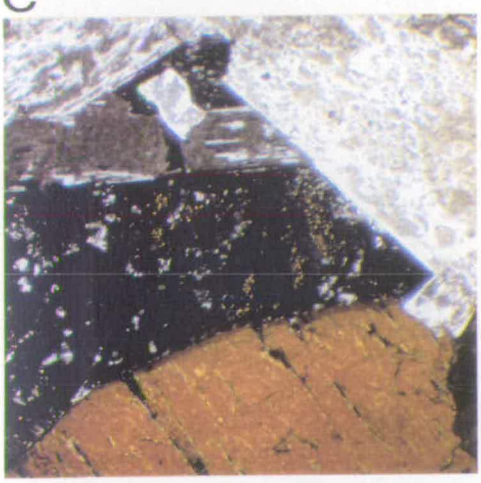

f

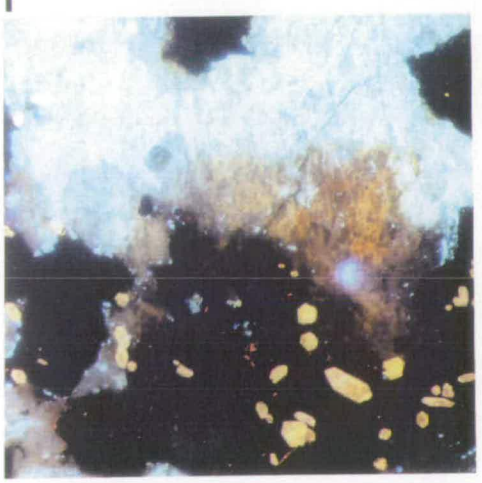

**Plate 3.10**

(a) At the bottom of the photo is a fine-grained felsic xenolith from locality B, consisting of plagioclase, olivine, oxides and clinopyroxene. From the upper surface of the xenolith, elongate plagioclase crystals grow into coarser-grained troctolite. At the right hand edge of the photo, one of the plagioclase crystals branches off another at a shallow angle. Olivine (light grey), oxides and clinopyroxene (dark grey) can be seen in the troctolite. Sample YGD262, field of view 3cm, ppl.

(b) The nunataq syenite sample studied, showing a mafic layer of olivine-oxide-pyroxene-apatite cumulate at the base. The dark-grey euhedral pyroxenes are a cumulus phase and tend to form clusters or chains with other mafic minerals in the syenite. The feldspar is generally perthitic. GGU 216627, field of view 2.5mm, ppl.

(c) A cluster of olivine grains in a troctolite from western Tugtutôq. Most of the triple junctions show angles approximating to 120° and are "dry". One, however (indicated by an arrow) contains a triangle of another phase, indicating that textural equilibrium was not complete before the rock solidified. Sample YGD404, field of view 1.8mm, ppl.

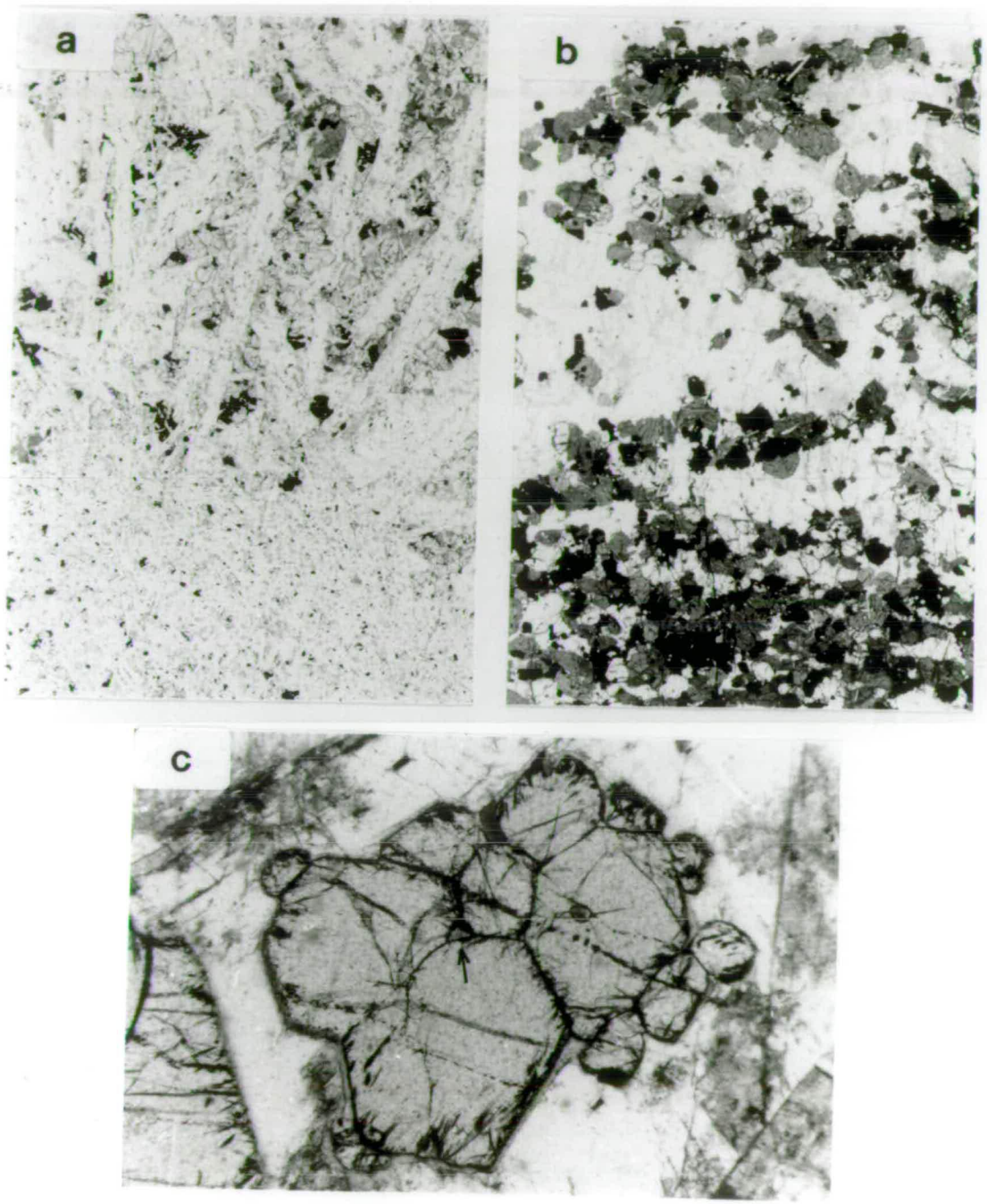
a
b
c

The dihedral angle is the angle between three crystals or between two crystals and melt. Each combination of phases has a specific equilibrium dihedral angle which is defined by the ratio of surface energies of the phases. Grains will have random dihedral angles the moment they first touch but will change shape as they cool to approach this equilibrium angle. At the same time, smaller grains with a high surface energy to volume ratio will tend to decrease in size and eventually disappear, while large grains grow larger (Boudreau, 1987). Above the solidus these changes in grain size and shape occur by solution and reprecipitation with diffusive transport through the melt (Cooper and Kohlstedt, 1986). Below the solidus, grain-boundary or volume diffusion (both much slower processes) are the only means of effecting such changes.

The equilibrium texture of a monominerallic rock will be a constant grain size (larger than the original grain size due to the growth of larger grains at the expense of smaller ones) with dihedral angles of 120°. Grains will have straight or gently curving boundaries. Where more than one phase is present, equilibrium dihedral angles will depend on the minerals involved. Some examples are: ol-ol-pl=40-60°, ol-ol-cpx=0-20°, pl-pl-ol=100-130°.

In a thin section, the angle measured between three crystals will not necesssarily be the true dihedral angle since a thin section gives a random slice through the three-dimensional angle. However, the true dihedral angle can be obtained from the median point on a cumulative frequency plot of measurements from a thin section. Around 100 measurements per section are needed to be statistically significant.

Troctolites and gabbro picrites from western Tugtutôq have been studied to try to assess the degree of textural equilibration attained in the YGDC. To the east the fractionating assemblage becomes more complex and textural study more difficult.

The fact that the rocks are orthocumulates is an indication that cooling was relatively rapid and thus it might be expected that there was insufficient time for textural equilibration to have occurred. The wide range of cumulus crystal sizes supports this theory, as does the fact that some junctions between three olivine grains show tiny triangles of other minerals, crystallised from an intercumulus liquid phase (Plate 3.10c). The olivine-olivine-melt dihedral angle is 40-60°, so the melt would have formed an interconnected network along all of the grain boundaries. If no textural equilibration had occurred, small triangles of crystallised melt would be

expected at all olivine triple junctions, but if the rock were in equilibrium all such melt pockets would have been eliminated, so it is possible to conclude that there has been partial equilibration.

Measurements were made of ol-ol-ol and ol-ol-pl angles for several samples from locality D. However, irregular edges to plagioclase crystals made measurement of pl-pl-pl angles difficult, and there was usually insufficient pyroxene within any one slide to obtain ol-ol-cpx or pl-pl-cpx angles. Olivine and ilmenite have a reaction relationship, which tends to cause rounding of olivine grains enclosed within ilmenite, obscuring the surface-energy related dihedral angle. Results for 4 samples are presented in Figs. 3.2 and 3.3 and compared to theoretical curves for different angles. It can be seen that ol-ol-ol triple junctions approximate to 120°, indicating that where olivine grains are in contact, in monominerallic domains, some textural equilibration has occurred. Ol-ol-pl angles are not in equilibrium. Junctions of the type A-A-B will always equilibrate more slowly than A-A-A junctions since diffusion of different chemical components is required for the two minerals; it is not possible to dissolve material from one grain and reprecipitate it on another. Thus textural equilibration has proceeded to some degree in the YGDC (where olivine grains are in contact) but cooling was too rapid to allow different phases in contact with one another to equilibrate. No significant differences were found between the sample from the edge of the dyke and one from the centre (Fig. 3.2) or between two pairs of mafic and felsic layers (one of which is shown in Fig. 3.3).

### 3.3.2 Grain Size Analysis

Grain size variation in igneous rocks may provide information on processes such as crystal nucleation, growth and accumulation. In recent years, with the advent of microcomputer-based image-analysis systems, grain size analysis has become comparatively easy, and published data using such systems include those of Cashman (1986), Naslund *et al.* (1986) and Cashman and Marsh (1988). These studies are concerned primarily with volcanic rocks, since plutonic rocks are much more likely to undergo modification of original textures, due to their greater cooling time. However, the large variation in grain size and the non-equilibrium dihedral angles observed between different mineral species, suggest that textural equilibration was only partially achieved in the YGDC. Grain size measurements of olivine in

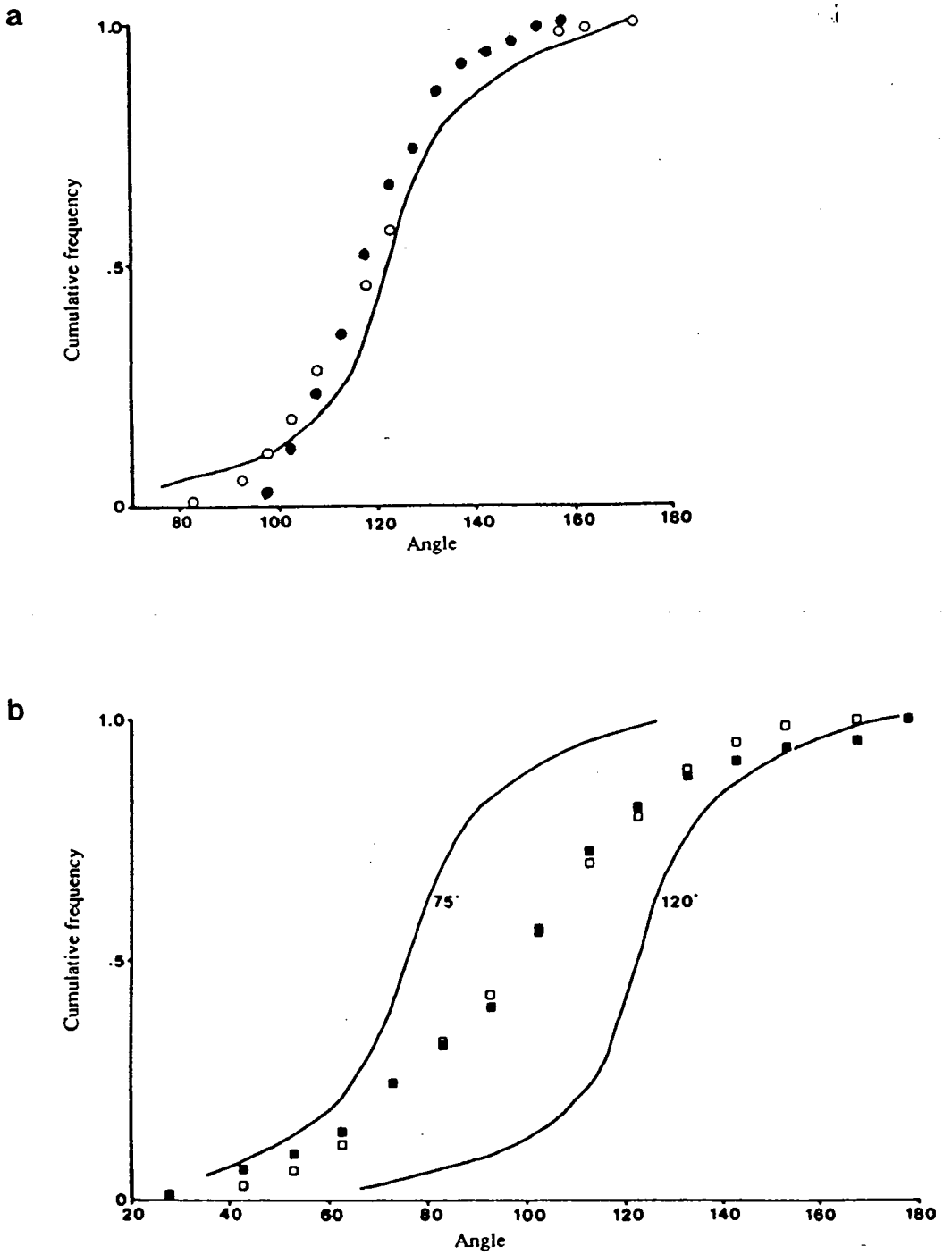


**Figure 3.2** Comparison of dihedral angles in YGD238 and YGD248 from locality D. YGD238 (open symbols) is from near the edge of the dyke and YGD248 (filled symbols) from the centre of the northern synform. (a) Ol-ol-ol angles, with theoretical curve for 120°; (b) Ol-ol-pl angles, with theoretical curves for 75° and 120°.

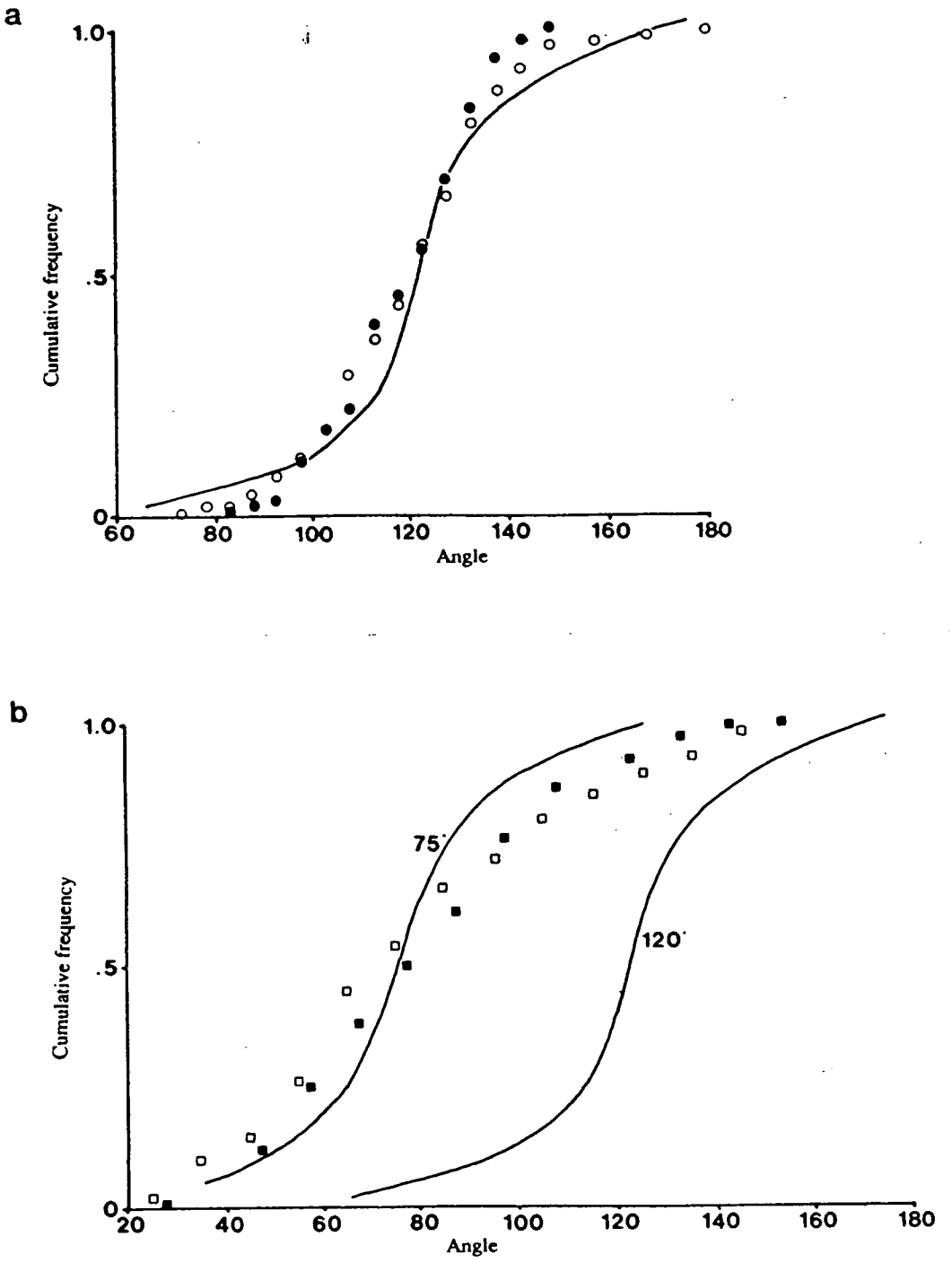


**Figure 3.3** Comparison of dihedral angles in adjacent mafic and felsic layers (sample GGU 186400). Open symbols = felsic layer, filled symbols = mafic layer. (a) Ol-ol-ol angles, with theoretical curve for 120°; (b) Ol-ol-pl angles, with theoretical curves for 75° and 120°.

cumulates from locality D were made to determine the mean grain size and grain size distribution in a series of samples. Relative differences between troctolitic and picritic layers were sought.

Measurements were made at Cambridge University using a VIDS IV system manufactured by Analytical Measuring Systems of Saffron Walden, UK. This system combines the output from a video camera with the graphics display of a microcomputer in such a way that measurement can be made directly from a TV image of a thin section using a digitiser tablet. The long and short axes of the olivine grains were measured, taking the long axis as the end-to-end distance parallel to the elongation of the grain, and the short axis perpendicular to it. Renner (1989) found in studies using this image analysis system, that to obtain reproducible results the number of grains counted per sample needed to be 500. The method of measurement used by Renner and in this study was to measure all grains within the area pictured on the TV screen and then to move to a different area. In this study it was found that for the troctolites, the whole area of a thin section (about six TV screens) had to be measured, while for the gabbro picrites, two areas at opposite ends of the thin section were chosen, to avoid any thin section-scale heterogeneities.

Several problems were encountered during this analysis. Normally the video camera would be mounted on a microscope, but this was unfortunately not possible at the time the analysis was carried out and photographs had to be used instead. These gave a rather poorer image than might otherwise have been obtained and also prevented the use of illumination using crossed polars. It was sometimes difficult to tell separate grains apart; on occasion several small ones may have been counted as one large fractured one, and vice versa. In addition, the smallest grains were at about the limit of resolution of the system and so measurements for these grains are likely to be less accurate than those for larger grains. Given these factors, the measurements presented here for different samples can probably only be used for comparison with one another and not with measurements obtained by other operators of the same or other systems, except in the general form of the distribution.

Renner (1989) calculated that the error on her measurements was roughly 2% of the mean grain size; repeat measurements of the same sample were not made as part of this project due to lack of time with the system, but it is assumed that the error is probably <5% of the mean grain size.

When interpreting the data, it must be remembered that the distribution of apparent grain sizes from a thin section is not the same as the distribution of true

grain diameters since the thin section intersects grains randomly. The problem may be approached by considering a random slice through a number of objects of identical size and shape. This is the same as taking an infinite number of random slices through a single three-dimensional object. Kellerhals *et al.* (1975) show the apparent grain size distribution for a randomly sectioned sphere and for various ellipsoids of rotation (Fig. 3.4). Naslund *et al.* (1986) chose a rectangular prism and used a computer program to generate a set of random planes through the solid and measure the longest dimension and longest side of the resulting cross sections. Renner (1989) presented graphs of the apparent grain size distribution using Naslund's program (Fig. 3.5). The olivine crystals in the YGDC rocks probably approximate to a shape between an ellipsoid and a rectangular prism, but the measured grain size distributions do not resemble any of the synthetic distributions. However, the olivine crystals are not all the same size and this introduces another factor. As well as altering the distribution, a bias is introduced because the probability of intersecting any grain is related to its size, so large grains will tend to be over-represented.

Generating a true grain size distribution mathematically from an apparent distribution is complex and has only been attempted for the simplest shapes. The approach used by Renner (1989) was to generate an apparent distribution from a measured one and to show that thin sectioning effects did not substantially alter the distribution. She took a positively skewed, approximately log-normal distribution (of olivine grains in a komatiite flow), assumed the grain shape to be a rectangular prism with axial ratios 1:0.67:0.54 and, to compensate for the size-dependant probability of intersection, increased the number of grains of a given size in proportion to their size. This gave a synthetic distribution closely resembling the original distribution, with a very similar mean but a larger standard deviation (Fig. 3.6). Renner concluded that the measured distribution is an inherent property of the sample and not an artifact of the thin sectioning process, and that the true distribution will have a similar mean to the measured distribution but a slightly smaller standard deviation.

These results are of significance for the present study since the apparent olivine grain size distributions from a layered sequence from locality D (Itivdlip Sarqâ) are very similar to those obtained by Renner and her conclusions are thus thought to hold true for the YGDC rocks. Histograms of measured long axis distribution and mean grain size are shown against stratigraphic height in Fig. 3.7. This is the same section as that shown in Fig. 3.1. It can be seen that two of the gabbro picrite layers have a larger mean grain size than the troctolite, but the third does not. Differences in cooling rate between adjacent layers do not seem plausible,

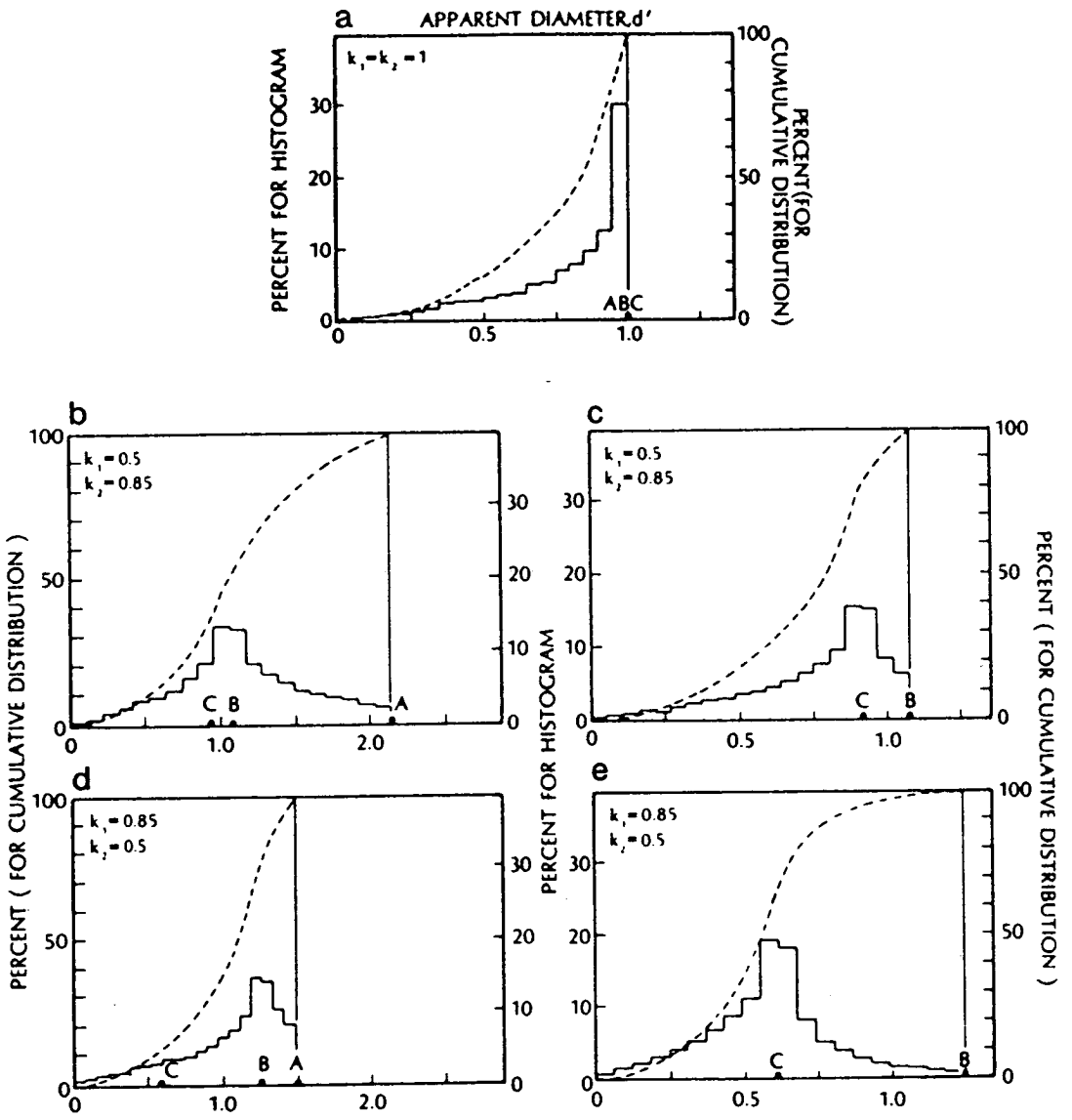


**Figure 3.4** Histograms of apparent major and minor axes for a sphere and ellipsoids of rotation, from Kellerhals *et al.* (1975). Dotted lines are cumulative frequency curves. A = shortest axis, B = intermediate axis and C = longest axis, $k_1$ = B/C, $k_2$ = A/B. (a) Distribution for a sphere; (b) long axes and (c) short axes of triaxial ellipsoids with $k_1 = 0.5$, $k_2 = 0.85$. This is the ellipsoid having the closest axial ratios to olivine crystals measured by Renner (1989). (d) long axes and (e) short axes for ellipsoids with $k_1 = 0.85$, $k_2 = 0.5$.

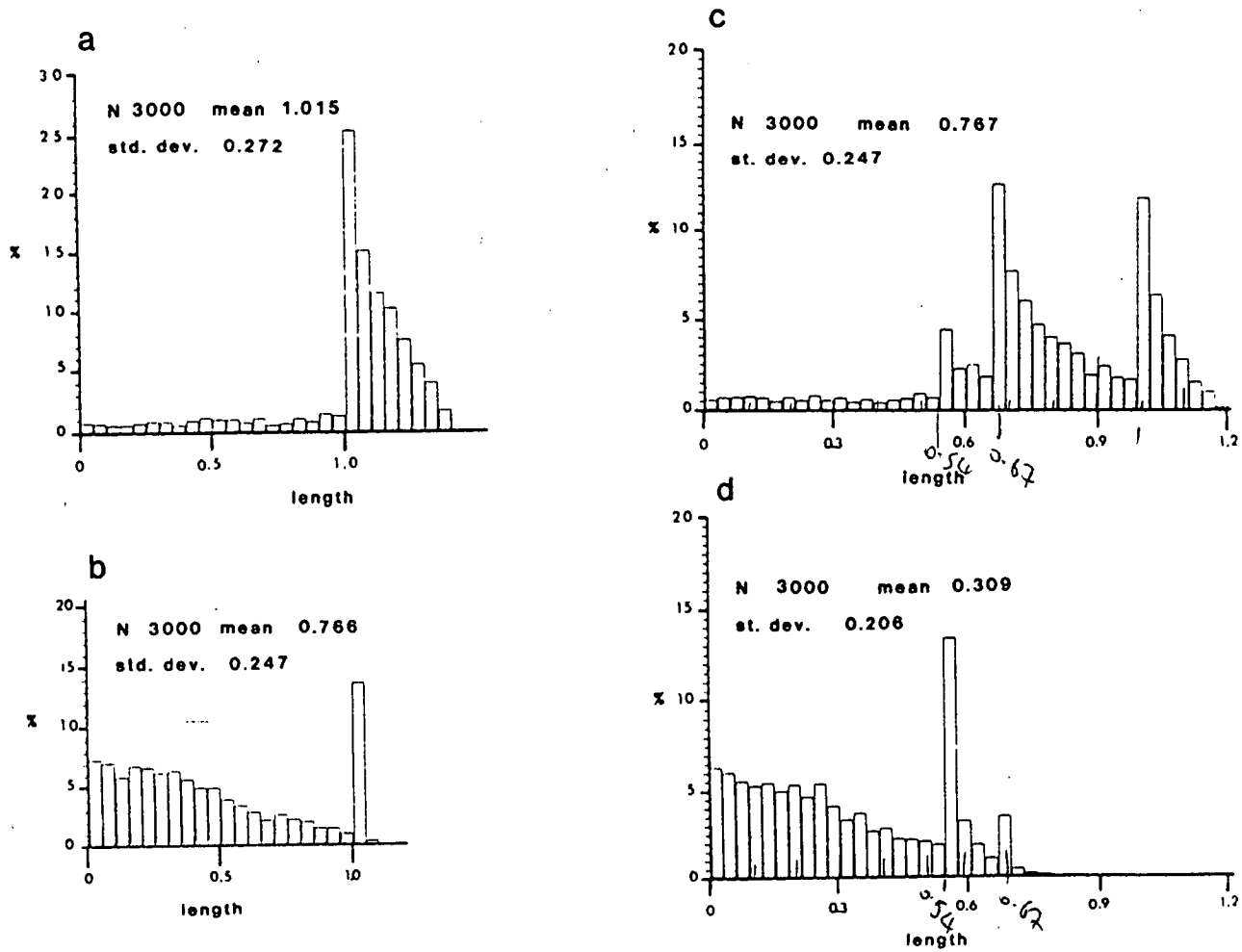


Figure 3.5 Apparent axes histograms generated by Naslund's program for (a) long axes and (b) short axes of a cube; (c) long axes and (d) short axes of a rectangular prism with A = 1, B = 0.67 and C = 0.54. N = number of sections measured. From Renner (1989).

Figure 3.6 Histograms to show how the shape and size-dependent probability of intersecting grains affect the apparent distribution of long axes. (a) The measured apparent long axis distribution of sample ZM5, from Renner (1989). This distribution was chosen to represent a hypothetical grain size distribution. (b) Synthetic histogram generated by numerically thin sectioning rectangular prisms with long dimensions distributed as in (a). This histogram incorporates both the effects of grain shape and the size-dependent probability of intersection, as described in the text. The mean is similar to that of (a). (c) Synthetic histogram generated as above but ignoring the size-dependent probability of intersection. The mean is significantly smaller than that of the original distribution.

**Figure 3.6** Histograms to show how the shape and size-dependent probability of intersecting grains affect the apparent distribution of long axes. (a) The measured apparent long axis distribution of sample ZM5, from Renner (1989). This distribution was chosen to represent a hypothetical grain size distribution. (b) Synthetic histogram generated by numerically thin sectioning rectangular prisms with long dimensions distributed as in (a). This histogram incorporates both the effects of grain shape and the size-dependent probability of intersection, as described in the text. The mean is similar to that of (a). (c) Synthetic histogram generated as above but ignoring the size-dependent probability of intersection. The mean is significantly smaller than that of the original distribution.

a

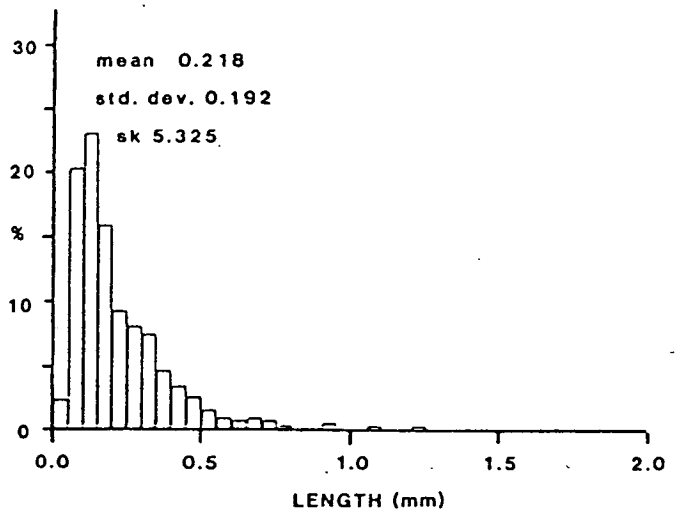
mean 0.218
std. dev. 0.192
sk 5.325
30
20
%
10
0
0.0
0.5
1.0
1.5
2.0
LENGTH (mm)

b

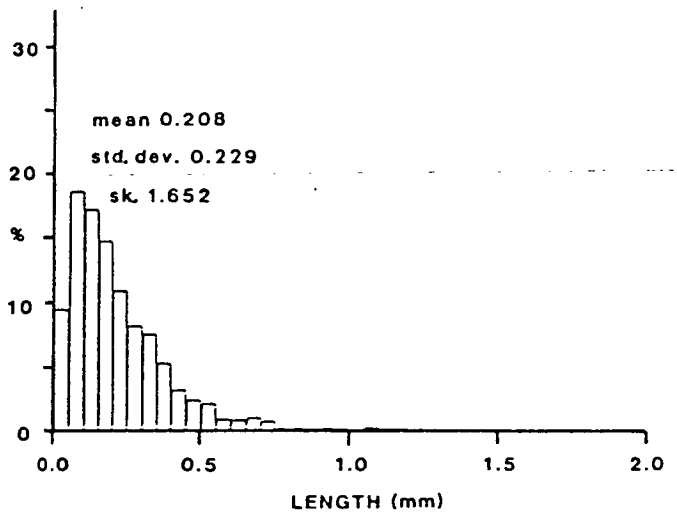
mean 0.208
std. dev. 0.229
sk. 1.652
30
20
%
10
0
0.0
0.5
1.0
1.5
2.0
LENGTH (mm)

c

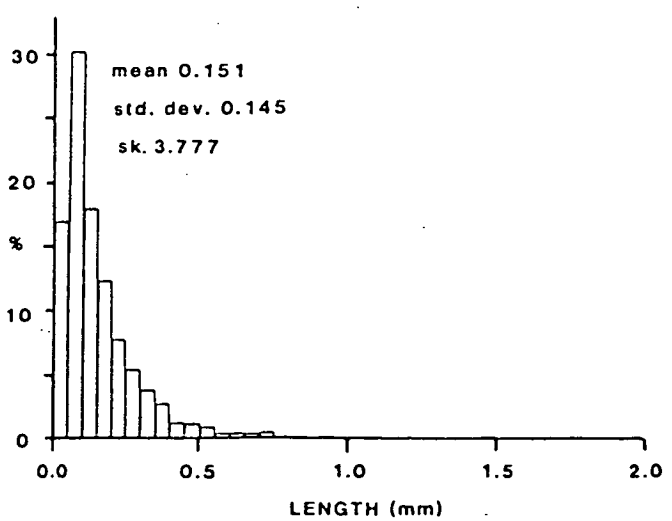
mean 0.151
std. dev. 0.145
sk. 3.777
30
20
%
10
0
0.0
0.5
1.0
1.5
2.0
LENGTH (mm)

so these variations could be primary and due to physical sorting of the olivine grains, or could be due to a greater degree of textural equilibration in the gabbro picrite layers. The difference in mean grain size is probably sufficiently small that an accompanying change in dihedral angle would not necessarily be expected.

It is concluded that the grain size distribution is an inherent property of the rock and not a product of thin-sectioning. Dowty (1980) has attempted to relate crystal size distributions to the nucleation and growth history of igneous rocks. He considered three thermal regimes: constant temperature, constant temperature decrease and constant rate of heat removal (Fig. 3.8). At a constant rate of heat removal (probably the most geologically realistic), no nucleation will occur until a certain degree of undercooling is attained, then a burst of nucleation will raise the temperature, inhibiting further nucleation. Any subsequent variation in growth rate will tend to affect all crystals equally so the crystal size distribution will show a peak. Although this may be the explanation for the olivine size distribution seen in the YGDC cumulates, it assumes homogeneous nucleation, which is probably not as likely as heterogeneous nucleation (see Chapter 7). Heterogeneous nucleation would produce a flatter distribution because a lower degree of undercooling would be required and nucleation would be more continuous. Textural equilibration will tend to shift any peak towards a coarser grain size and to itself produce a peak at the higher end of the range of grain sizes. Given the evidence for incomplete textural equilibration, it is inferred that the grain size distribution observed for olivine in YGDC cumulates is probably predominantly primary in origin but may have been slightly modified by textural equilibration.

## 3.4 Mineral Chemistry

Minerals from about 65 samples covering a range of lithologies from the YGDC, including a few of the anorthosite xenoliths from locality L of Fig. 2.1, were analysed by electron microprobe. One sample, a layered syenite (GGU 216627) came from the nunataq region. Analytical procedures and precision are given in Appendix II and representative mineral analyses in Appendix III.

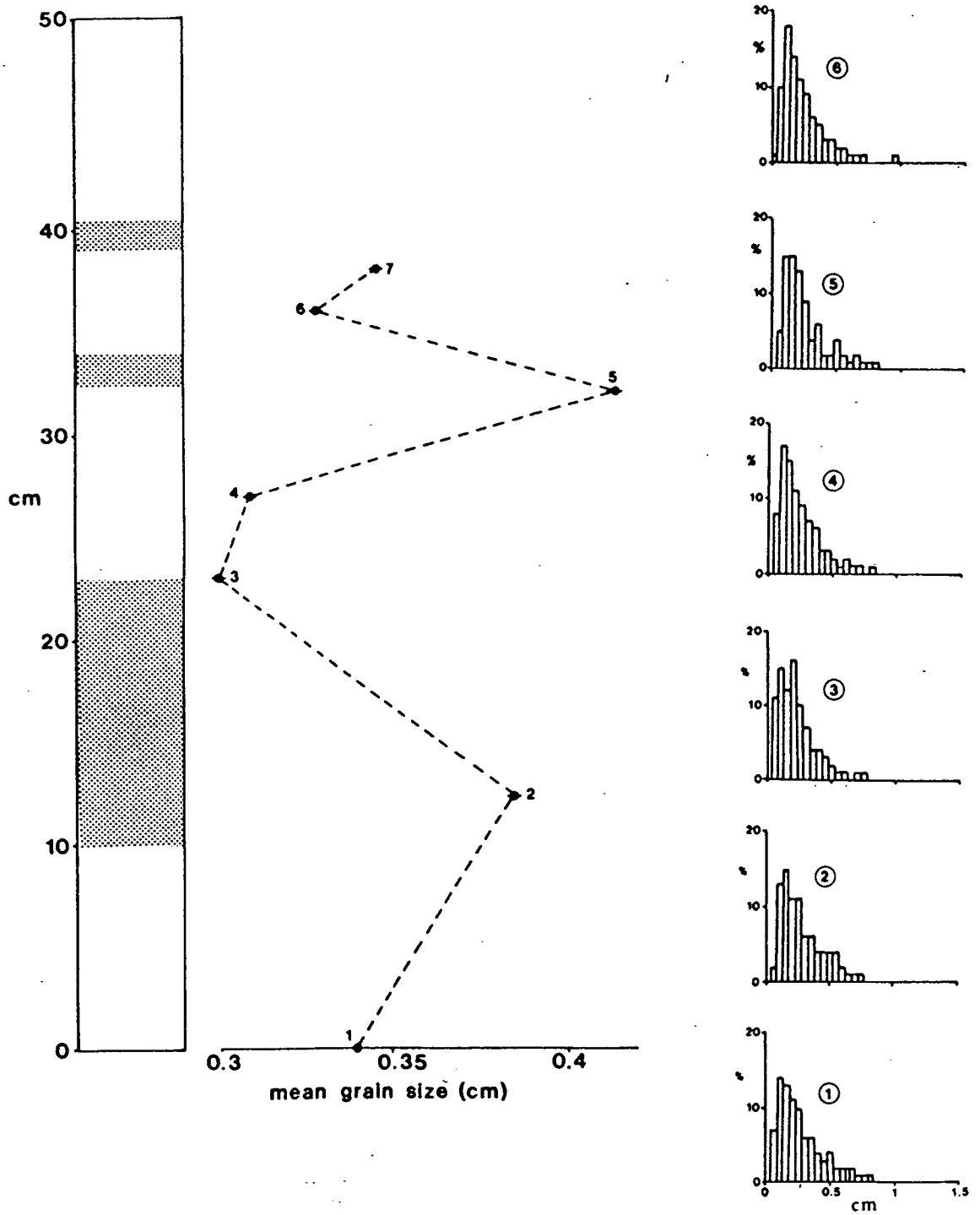


Figure 3.7 Mean grain size variation and grain size distribution measurements of samples from a stratigraphic section from the northern synform of locality D.

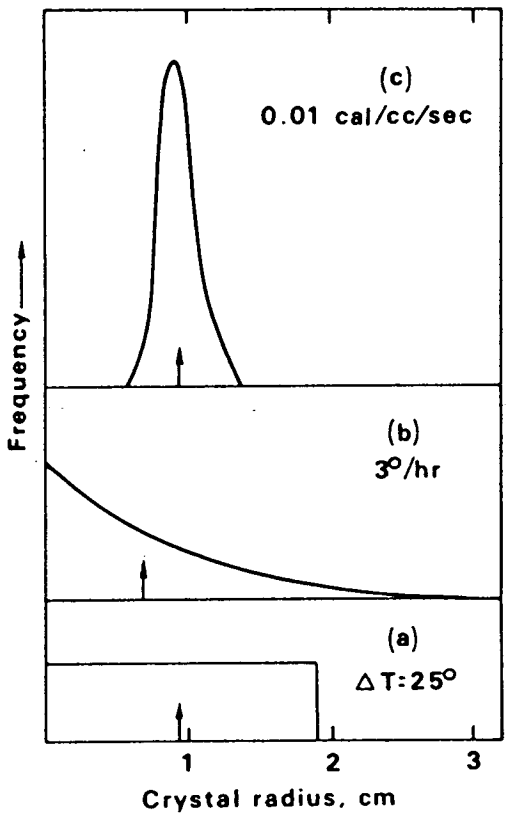


**Figure 3.8** Frequency distribution of grain sizes obtained numerically with three types of cooling history: (a) isothermal; (b) constant rate of temperature decrease and (c) constant rate of heat removal. Arrows indicate means. From Dowty (1980).

### 3.4.1 Olivine

Olivines or pseudomorphs after olivine are found in almost all YGDC rocks. In some of the syenogabbros and syenites subject to extensive alteration it may be difficult to tell whether olivine pseudomorphs are present or not. The total range of compositions, $Fo_{68}$-$Fo_3$ is shown on Fig. 3.9. The apparent gaps in the trend are thought to result from alteration making probing impossible in some of the more evolved rocks, rather than to reactions causing the loss of olivine. Olivines from the chilled marginal samples span the range $Fo_{68}$-$Fo_{42}$, those from mafic cumulates $Fo_{67}$-$Fo_{51}$ and those from troctolites $Fo_{64}$-$Fo_{41}$. One mafic syenogabbro contains olivines of $Fo_{55}$ and a more evolved one $Fo_{32}$-$Fo_{25}$; it is assumed that there is a continuous series from $Fo_{55}$-$Fo_{26}$ although some intermediate compositions have not been probed. Parsons (1979) and Upton *et al.* (1985) reported compositional gaps in the olivine trends from Klokken and the OGDC, which they attributed to a drop in temperature and an increase in water attendant upon a new intrusive pulse. However, since the compositional gap observed in the YGDC is smaller than that seen in either Klokken or the OGDC, and olivines of $Fo_{55}$ have been found in the syenogabbros, it is not thought that a similar gap exists between troctolite and syenogabbro olivines in the YGDC. The syenite from the nunataq region contains olivine of $Fo_{14}$-$Fo_9$ while syenites from Assorutit (locality L of Fig. 2.1) have olivines of $Fo_6$-$Fo_3$. Again it is assumed that there is a continuous sequence between the olivines of the syenogabbros and the Tugtutôq syenites. Olivines from the anorthosite xenoliths generally range from $Fo_{71}$-$Fo_{68}$ (except for one sample (YGD 340) which contains olivines of $Fo_{47}$-$Fo_{43}$) and are not shown on Fig. 3.9.

Within-sample variation for the chilled margins is between 2 and 9 mol% Fo and large olivines zoned by up to 9 mol% Fo are found in the chills of localities A, B, D, F and J (no chill samples were obtained for localities C and E). At locality D (in one of three samples), F and J, large, often zoned, olivines are found with plagioclase as glomerocrysts (e.g. Plates 2.3a and 3.2) and possess significantly higher Fo content than the groundmass olivines. The phenocrysts compositions are $Fo_{67}$-$Fo_{61}$ at localities B and F, and $Fo_{66}$-$Fo_{46}$ at locality J. Groundmass olivines are $Fo_{58}$-$Fo_{49}$ at localities B and F, $Fo_{46}$-$Fo_{42}$ at locality J (see Fig 3.10). In the troctolites, gabbro picrites and olivine-magnetite(-apatite) cumulates, within-sample variation is rarely more than 4 mol% Fo and commonly less, but in the syenogabbros and syenites it may be up to 7 mol%. Individual crystals are rarely zoned and then only up to 4 mol% Fo.

At some of the localities with well developed mafic cumulates (B to D, F, and the nunataq syenite), olivines in the mafic layers are slightly more magnesian than those in adjacent feldspathic layers. Differences are around 3 mol% (Fig. 3.10). This is attributed to re-equilibration of different volumes of olivine with roughly the same proportion of intercumulus liquid, in the manner proposed by Barnes (1986).

Manganese in the YGDC olivines increases regularly with $Fe^{2+}$ from 0.35 to 2.36 wt% MnO (0.4 to 3.5 mol% tephroite), and zoned olivines show an increase in Mn with increasing Fe content. This range is similar to that obtained by Simkin and Smith (1970) and to other Gardar intrusions such as Klokken (Parsons, 1979), Kûngnât (Stephenson and Upton, 1982) and the giant dykes of Isortoq (Becker, 1984). Mn enrichment is, however, less pronounced than in Igdlerfigssalik (Powell, 1978) and South Qôroq (Stephenson, 1974).

A plot of Ca against Fo content is shown in Fig. 3.11. Olivines from the chills show little variation in Ca but in troctolite and gabbro picrite olivines, Ca increases slightly with decreasing Fo. Mafic cumulates containing low-Ca olivines are those from locality M of Fig. 2.1. It can be seen that there is considerable scatter in the fayalitic olivines. Most of the high-Ca olivines are from the nunataq sample but two are from a syenite from locality L. The cluster of low-Ca samples are all from locality L; zoning in one grain is indicated by an arrow pointing towards the rim. In the zoned olivines of the chilled margins, Ca usually decreases but may increase towards the rims.

The Ca contents are 0.20 to 1.04 wt% CaO, which is equivalent to 0.14 to 0.74 wt% Ca. This means that the samples scatter across the plutonic and hypabyssal fields of Simkin and Smith (1970). The data of Becker (1984) show that the Ca contents of olivines in the Isortoq giant dykes are very similar to those of the YGDC but low-Ca fayalitic olivines seem to be absent. The Ca contents of Fe-rich olivines from Klokken are closely similar to those from the YGDC (Parsons, 1979).

Simkin and Smith (1970) suggested that pressure and silica activity probably play a part in determining the Ca content of olivines, while according to Jurewicz and Watson (1988), melt composition and iron activity are important factors. The higher Ca content of some syenitic olivines cannot be due to different depths of emplacement. Simkin and Smith (1970) found that increasing silica activity led to

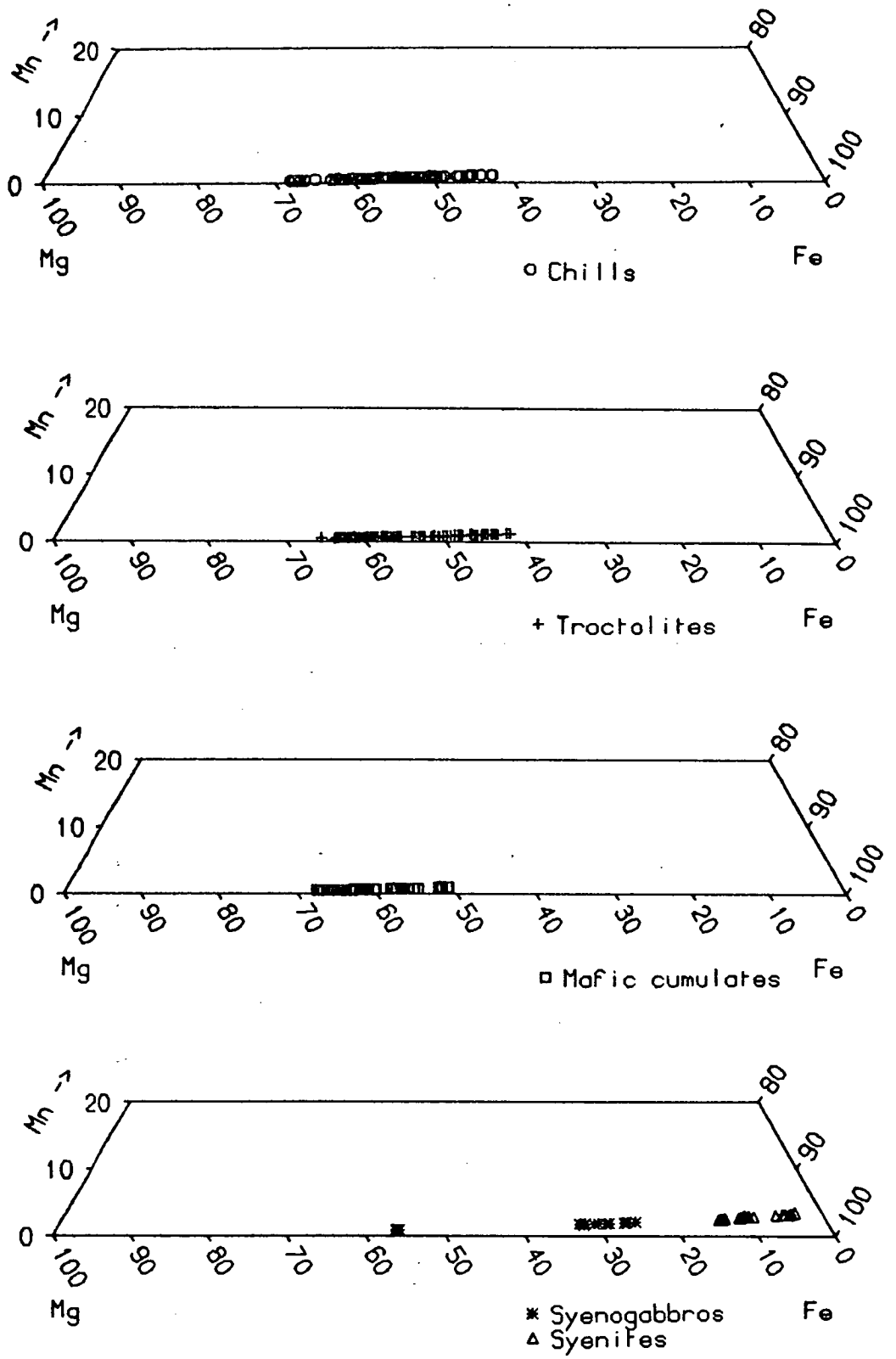


Figure 3.9 Olivine compositions for different lithologies of the YGDC.

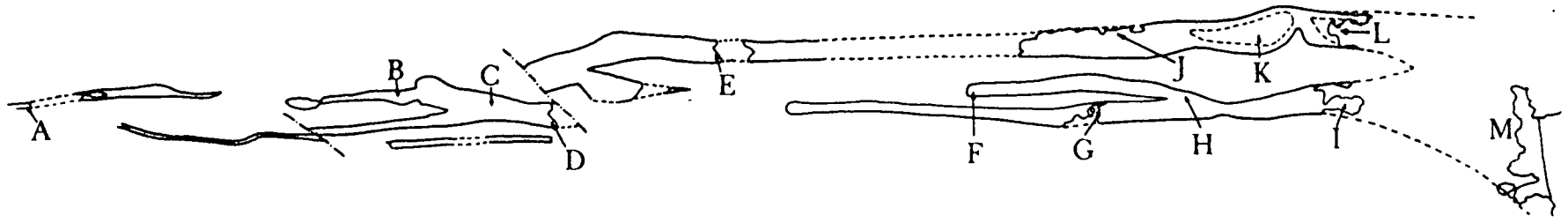


| | A | B | C | D | E | | J | K | L | M |
|---|---|---|---|---|---|---|---|---|---|---|
| FELSIC | $Fo_{62}$-$Fo_{59}$ | $Fo_{68}$-$Fo_{56}$ | $Fo_{63}$-$Fo_{61}$ | $Fo_{67}$-$Fo_{49}$ | $Fo_{50}$-$Fo_{45}$ | Olivine | $Fo_{66}$-$Fo_{42}$ | $Fo_{56}$-$Fo_{25}$ | $Fo_{60}$-$Fo_{3}$ | $Fo_{54}$-$Fo_{46}$ |
| | $An_{62}$ | $An_{64}$-$An_{61}$ | | $An_{63}$-$An_{56}$ | $An_{63}$ | Max. An in Plagioclase | | $An_{60}$-$An_{5}$ | $An_{61}$-$An_{0}$ | $An_{64}$-$An_{57}$ |
| MAFIC | | $Fo_{65}$-$Fo_{60}$ | | | | Olivine | | | | $Fo_{58}$-$Fo_{51}$ |
| | | $An_{63}$-$An_{56}$ | | | | Max. An in Plagioclase | | | | $An_{54}$-$An_{52}$ |

| | | F | G | H | I |
|---|---|---|---|---|---|
| FELSIC | Olivine | $Fo_{65}$-$Fo_{59}$ | $Fo_{57}$-$Fo_{55}$ | $Fo_{45}$-$Fo_{42}$ | $Fo_{60}$-$Fo_{59}$ |
| | Max. An in Plagioclase | $An_{58}$ | $An_{56}$ | $An_{50}$ | $An_{60}$ |
| MAFIC | Olivine | $Fo_{67}$-$Fo_{61}$ | $Fo_{56}$-$Fo_{55}$ | | $Fo_{61}$-$Fo_{60}$ |
| | Max. An in Plagioclase | $An_{64}$ | $An_{56}$-$An_{54}$ | | $An_{50}$ |

**Figure 3.10** Summary of olivine and plagioclase compositions from different localities in the YGDC of Tugtutôq and Narsaq.

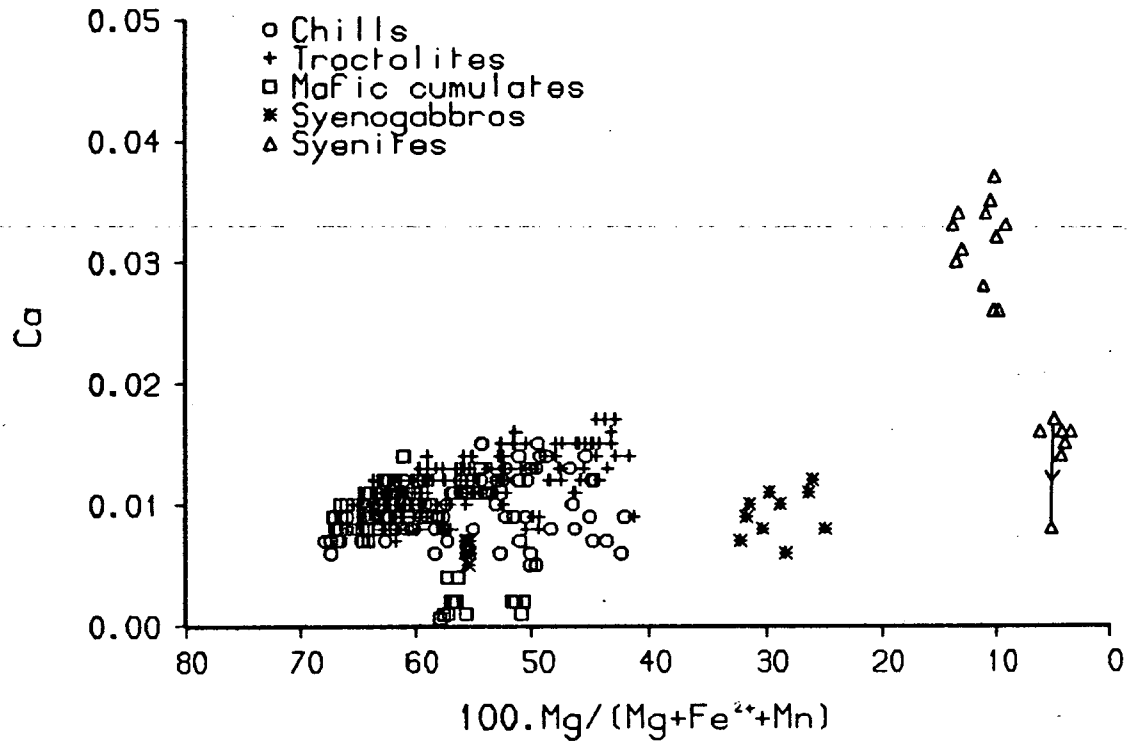


**Figure 3.11** Calcium (atoms to four oxygens) in olivines. Zoning in one olivine from a syenite is indicated by an arrow pointing towards the rim composition.

lower Ca contents in olivines and Becker (1984) noted that her low-Ca olivines all came from marginal rocks contaminated by granitic country rock. It is possible that the two evolved pods on Tugtutôq saw patchy assimilation of Julianehåb granite which raised the silica activity and lowered the Ca content of the olivines for some samples.

Nickel was only determined for grains analysed using the Cameca Camebax (see Appendix II). It reaches a maximum value of 0.06 wt% NiO and shows little correlation with Mg content. This may be because the Ni contents are low and thus the errors large. Chromium and titanium contents were also determined for these grains. Cr occurs in concentrations up to 0.05 wt% $Cr_2O_3$ and Ti up to 0.09 wt% $TiO_2$. Another minor element, aluminium, forms up to 0.08 oxide wt% of the YGDC olivines.

Zoning was investigated for a few crystals and zoning profiles are plotted in Fig. 3.12 and 3.13. Fo decreases steadily, or with slight undulations, from core to rim, while Mn (not shown on the diagrams) displays opposing behaviour. Nickel shows little relationship with Fo and has not been plotted, while calcium is generally lower in the core of the crystal than the margins. The results are probably less accurate than those of Kohn *et al.* (1989), obtained using an electron probe with double the normal accelerating voltage and beam current to improve detection limits, but show the general shape of the profiles.

One olivine separate from locality H (prepared several years ago so the preparation method is not known) was analysed by XRF, to investigate the contents of trace elements other than those determined by the probe. The analysis is presented in Appendix III and gives 281 ppm Ni, 185 ppm Zn, 24 ppm V, 16 ppm Ba and 12 ppm Cu, with minor amounts of Cr, Sc, Sr, Zr, La and Y. It is probably not a totally pure separate.

### 3.4.2 Feldspar

Feldspar compositions for the YGDC are plotted on Fig. 3.14 and show a compositional range from labradorite through andesine, oligoclase and intermediate alkali feldspar compositions to virtually pure albite and orthoclase. Chills, troctolites and picrites are dominated by plagioclase but small amounts of interstitial alkali

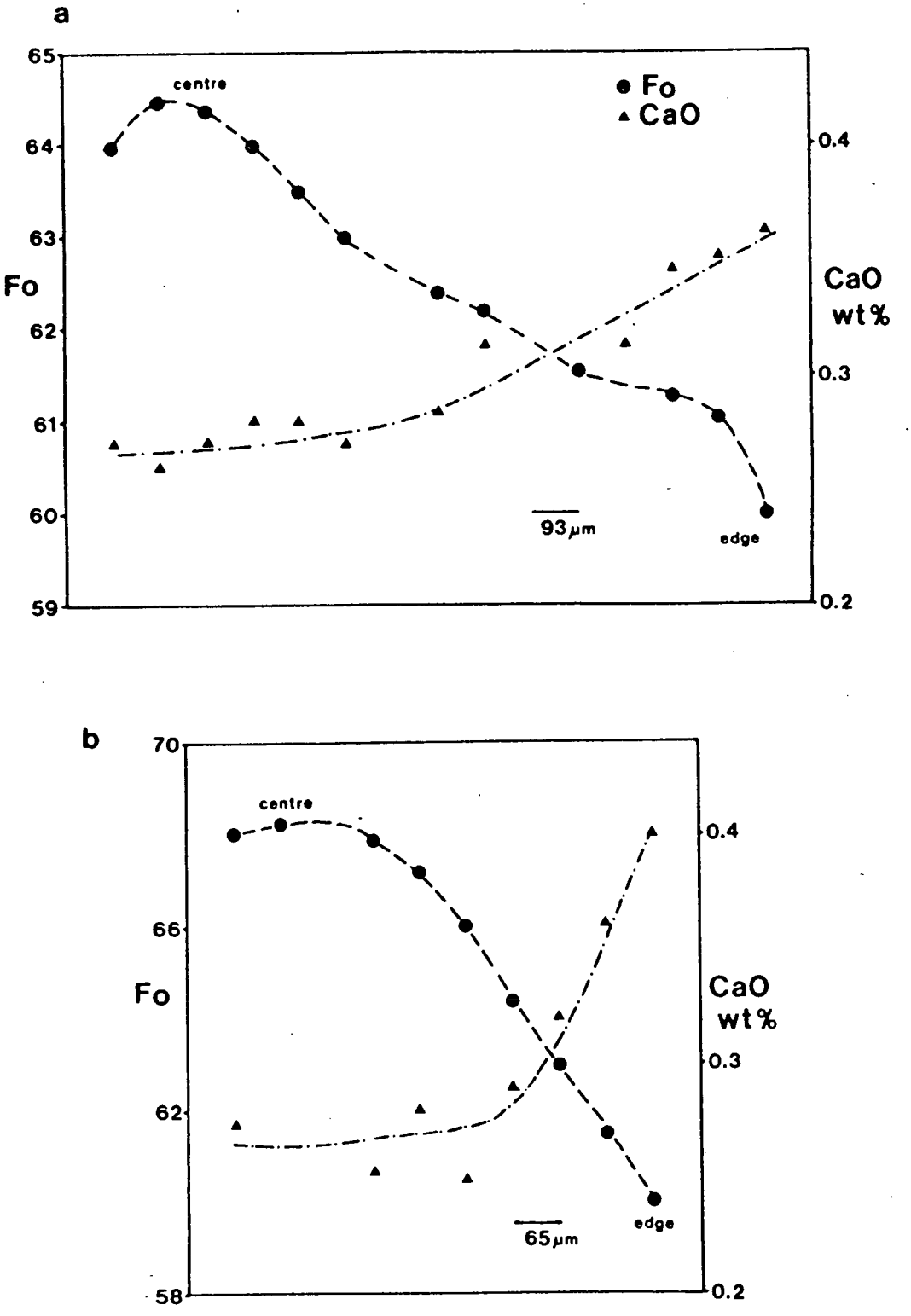


Figure 3.12 Zoning profiles from olivines in the chill samples (a) GGU 40559 and (b) YGD229.

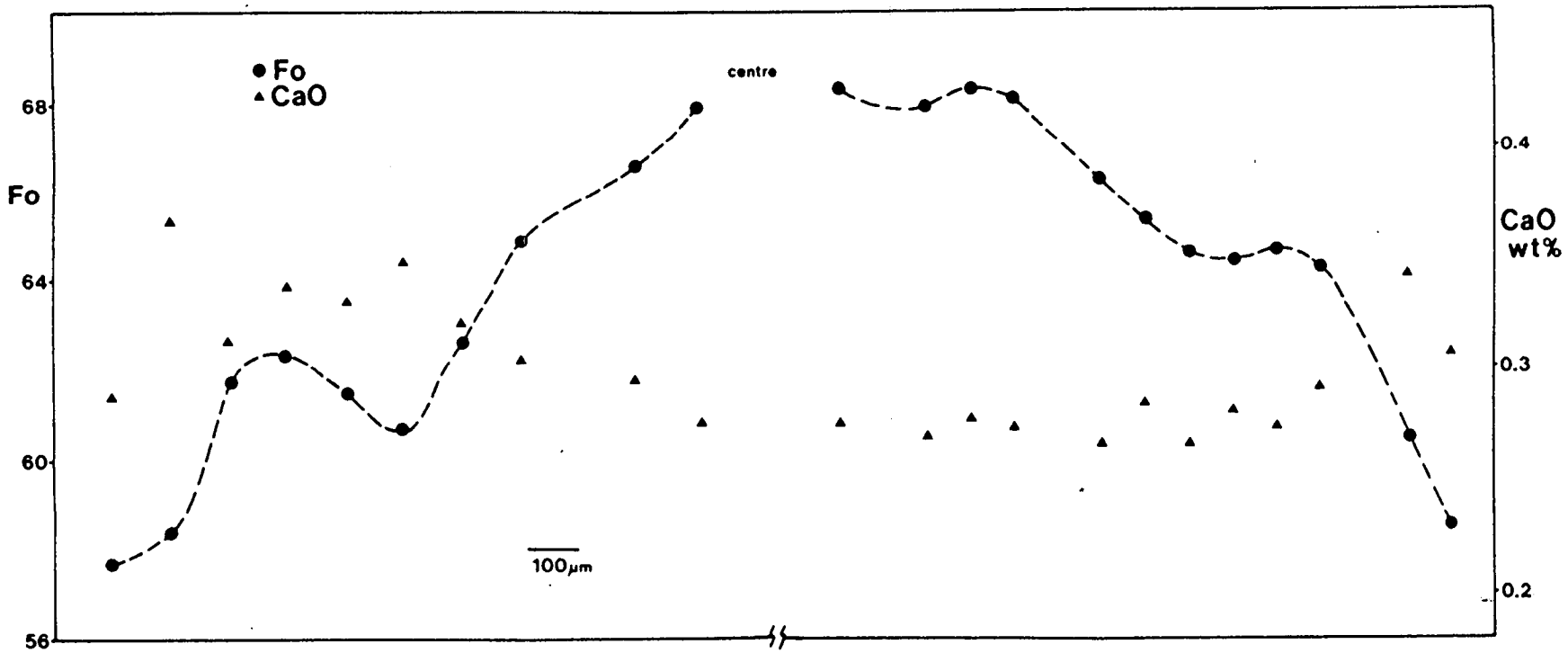


Figure 3.13 Zoning profile across the olivine showing maximum zoning in sample YGD229. Two traverses have been combined and the distance between them across the centre portion of the olivine (which was highly fractured) is only estimated. The inflection on the left is visible on backscattered electron images and probably indicates the location of a smaller grain which has been incorporated into the larger one.

feldspar occur. Plagioclase core compositions range from $An_{64}$-$An_{50}$ and rims from $An_{50}$-$An_{26}$ with zoning in a single crystal being 5-30 mol% An and frequently about 15 mol%. Within-sample variation for the cores is around 10% An, occasionally more. Interstitial alkali feldspar was encountered occasionally in the chills and troctolites, in cloudy interstitial patches between plagioclase crystals. This either had the composition of Ca-K anorthoclase, or gave endmember compositions, indicating exsolved perthite. A fine-grained leucocratic xenolith from locality D gives plagioclase compositions indistinguishable from those of the nearby troctolite.

In the syenogabbros, andesine to oligoclase cores are mantled by optically unexsolved alkali feldspar (K-anorthoclase). Two core-rim pairs are shown in Fig. 3.14. In the syenites, all the feldspar is alkali feldspar. Some cryptoperthitic crystals from Assorutit (locality L) and the nunataq region, have compositions slightly higher in K and lower in Ca than the syenogabbro alkali feldspars (K-anorthoclase to Na-sanidine). Most crystals show varying degrees of perthitic exsolution, some of which is probably deuterically coarsened. Coarse perthite may occur along grain boundaries and as irregular patches within crystals. One syenite from Assorutit (GGU 50218) which was viewed in cathodoluminescence has been examined with an electron microscope by F.D.L. Walker at Edinburgh University. This shows that the irregular turbid areas of the feldspar are in fact a coarse patch perthite while clear areas (whether red or blue-luminescing) appear to be entirely unexsolved.

In some of the syenites, and particularly the late-stage veins, the K-feldspar component of the perthite is preferentially altered and difficult to probe. Analyses near the albite and orthoclase corners of Fig. 3.14 are from perthites. It seems that there was only one, hypersolvus, feldspar throughout the crystallisation of the YGDC, as seen in other Gardar centres (e.g. Klokken, Parsons, 1979).

Iron contents (all Fe as $Fe^{2+}$) have been plotted against a fractionation index, K-Ca, in Fig. 3.15a. There is considerable scatter but maximum Fe contents can be seen to decrease with decreasing Ca and increasing K. Ba (Fig. 3.15b) is uniformly low in the labradorites, rises in the andesines and oligoclases and then falls again as K increases in the alkali feldspars. This is due to increasing Ba substitution for K as the feldspars become more potassic and consequent Ba depletion in the liquid.

Four feldspar separates were analysed by XRF and the analyses are given in Appendix III. These give average feldspar compositions for troctolites from localities

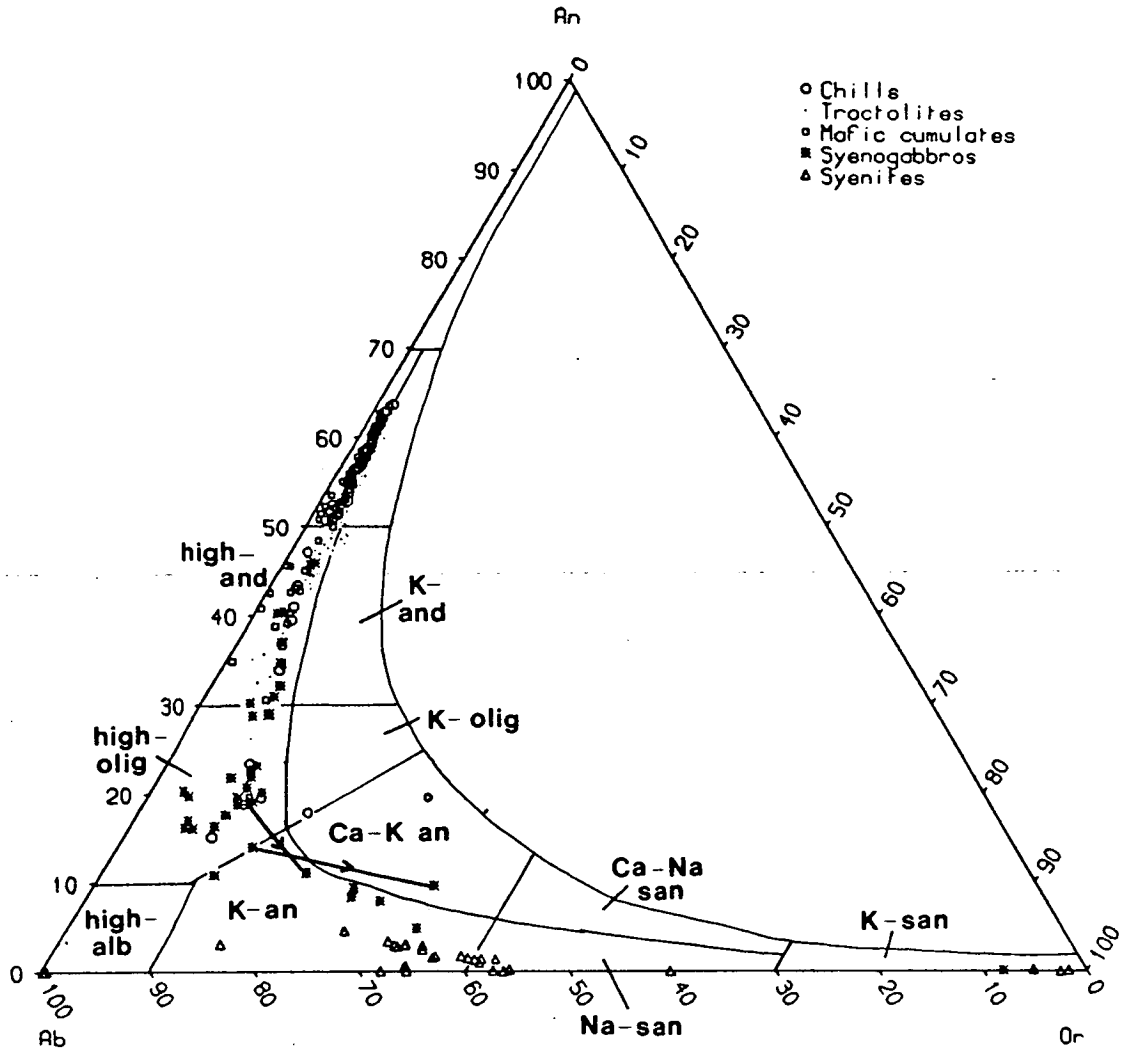


Feldspar compositions in the YGDC

**Figure 3.14** Feldspar compositions from the YGDC. Zoning in two syenogabbro feldspars is indicated by thick lines, with arrows pointing towards the rims. Compositional fields are slightly adapted from Smith (1974). Abbreviations are: and = andesine, olig = oligoclase, alb = albite, an = anorthoclase, san = sanidine.

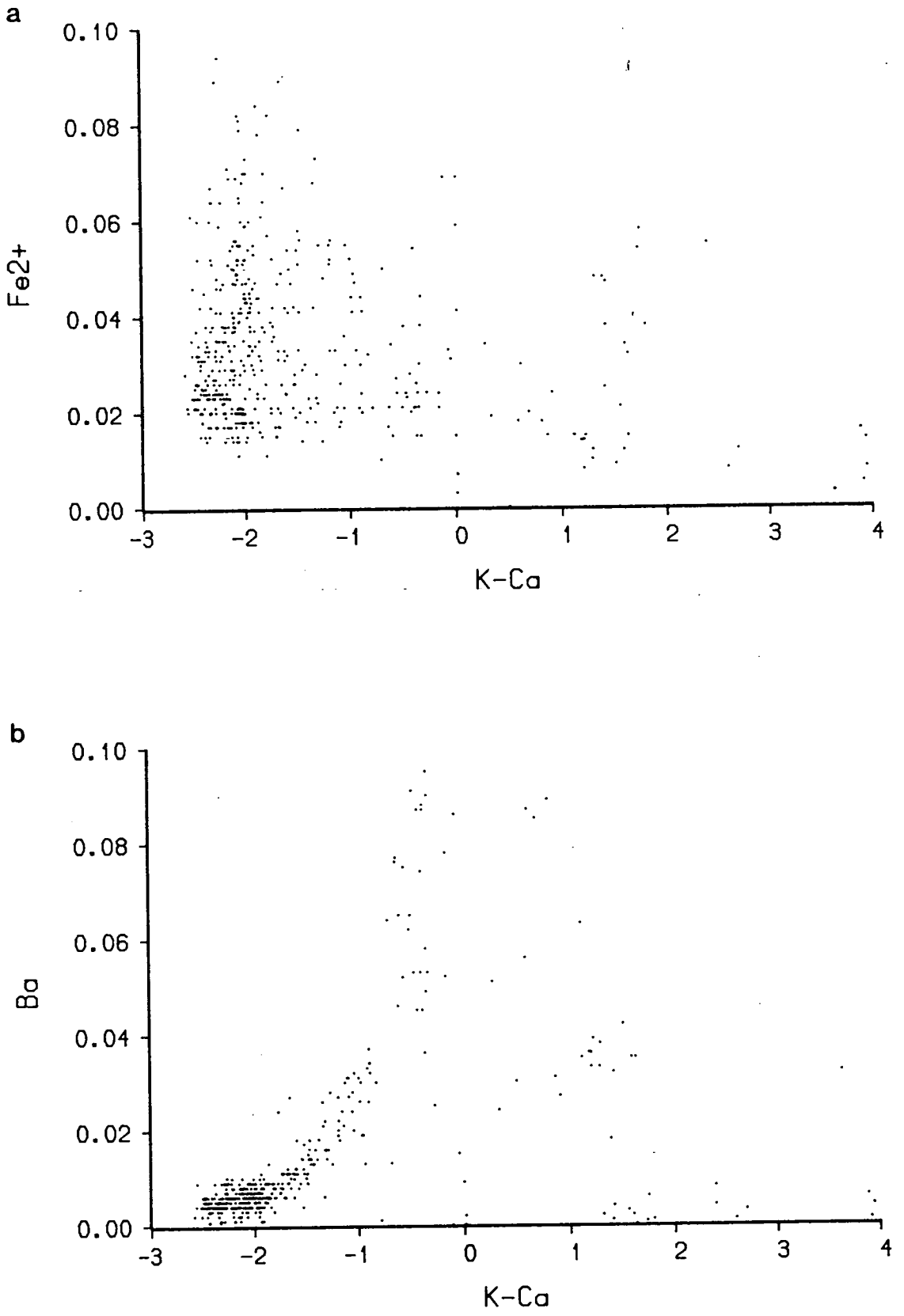


**Figure 3.15** (a) Total iron as $Fe^{2+}$ and (b) barium in YGDC feldspars plotted against a feldspar fractionation index, K-Ca.

D and G, a syenogabbro from locality K and a syenite from locality L. The Ba content of the feldspars increases from 1000 ppm in the troctolites to 4550 ppm in the syenogabbro, then decreases to 390 ppm in the syenite, as would be expected from Fig. 3.15b. Sr is high in the troctolites and the syenogabbro (1400-1700 ppm) but only 54 ppm in the syenite. La, Ce and Nd reach around 20 ppm in the syenogabbro (probably due to contamination of the sample by apatite) but are lower in the other lithologies. Rb and Zr reach their maximum levels, of 89 and 69 ppm respectively, in the alkali feldspars of the syenite.

### 3.4.3 Pyroxene

Pyroxenes in the YGDC are found as intercumulus or ophitic crystals in troctolitic and picritic rocks (except, apparently, some mafic cumulates from localities I and M). In the syenogabbros and syenites they become prismatic in habit and have cumulus status. All pyroxenes belong to a single high-Ca series. Electron microprobe analyses have been recast for $Fe^{2+}$ and $Fe^{3+}$ on the basis of stoichiometry (4 cations per 6 oxygens), following the procedure of Larsen (1976). From Fig. 3.16a it can be seen that the compositions lie in the salite and ferrosalite fields of Deer *et al.* (1966). The Na component is generally low, <1.0 wt% $Na_2O$ (Fig. 3.16b). Pyroxenes from the YGDC with higher Na and Fe contents were reported by Upton and Thomas (1980) but similar compositions were not encountered in this study. The fractionation trend in terms of Di-Hd-Ac resembles that of oversaturated complexes where considerable enrichment in Hd occurs before a significant Ac component develops (Fig 3.17).

Zoning is rare in the intercumulus crystals and when it does occur, Fe enrichments may be either in the direction of the rim or the core. Cumulus crystals are usually zoned to compositions richer in Fe and Mn, and poorer in Mg, Ti and Al at the rims. This variation is reflected optically in a colour change from brown to green-brown. The maximum zoning found in a single crystal was $Wo_{46}En_{41}Fs_{13}$ to $Wo_{46}En_{35}Fs_{19}$.

Aluminium and titanium show little correlation with Mg/(Mg + Fe) in the intercumulus crystals but fall with increasing Fe in the cumulus crystals (Fig. 3.18a,b). The maximum values are 3.7 wt% $TiO_2$ and 5.6 wt% $Al_2O_3$. This

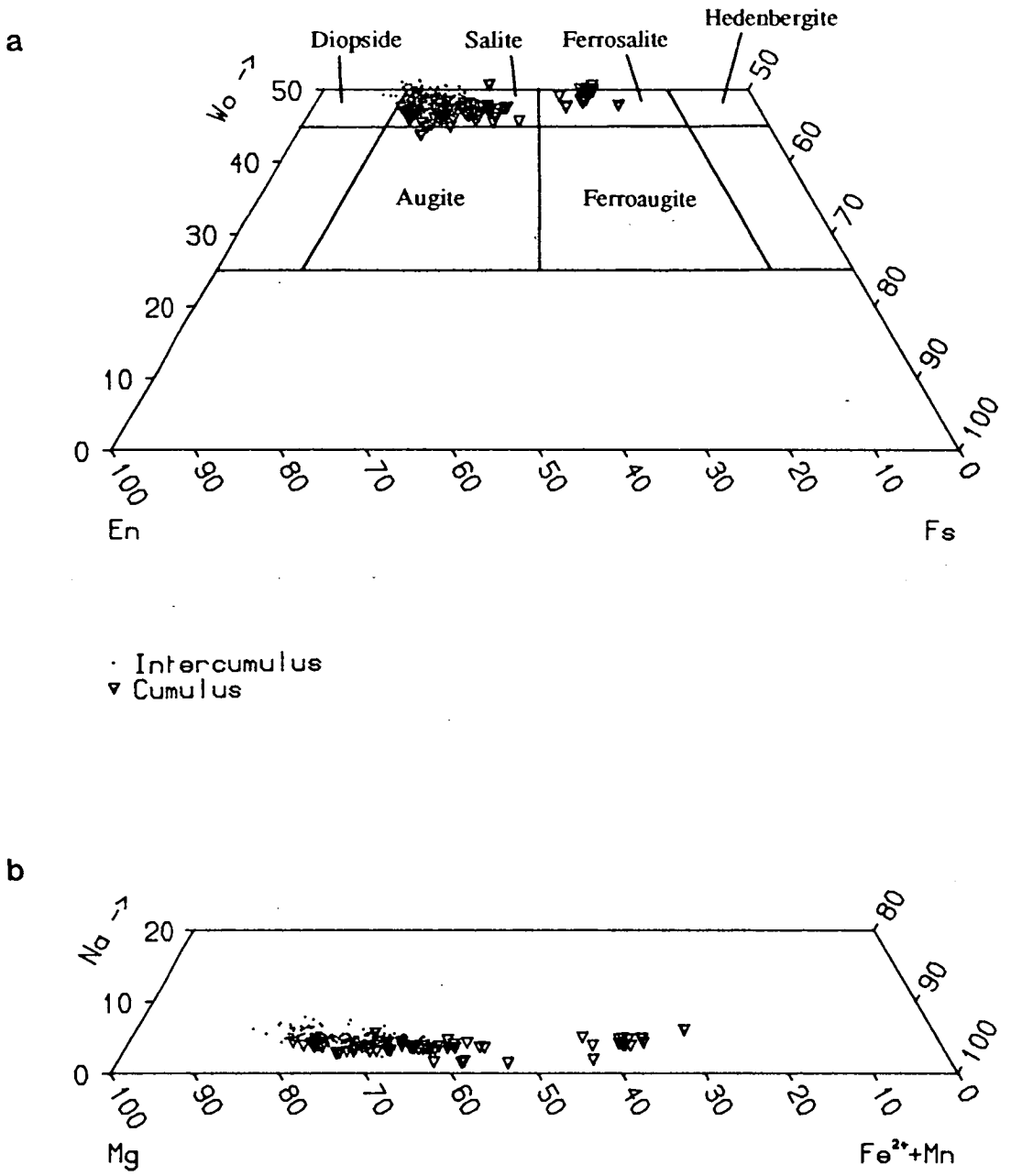


**Figure 3.16** (a) Pyroxene compositions with iron recalculated according to stoichiometry. Field boundaries are from Deer et al. (1966). (b) Pyroxenes plotted as Di(=Mg):Ac(=Na):Hd(=$Fe^{2+}$+Mn), after Larsen (1976).

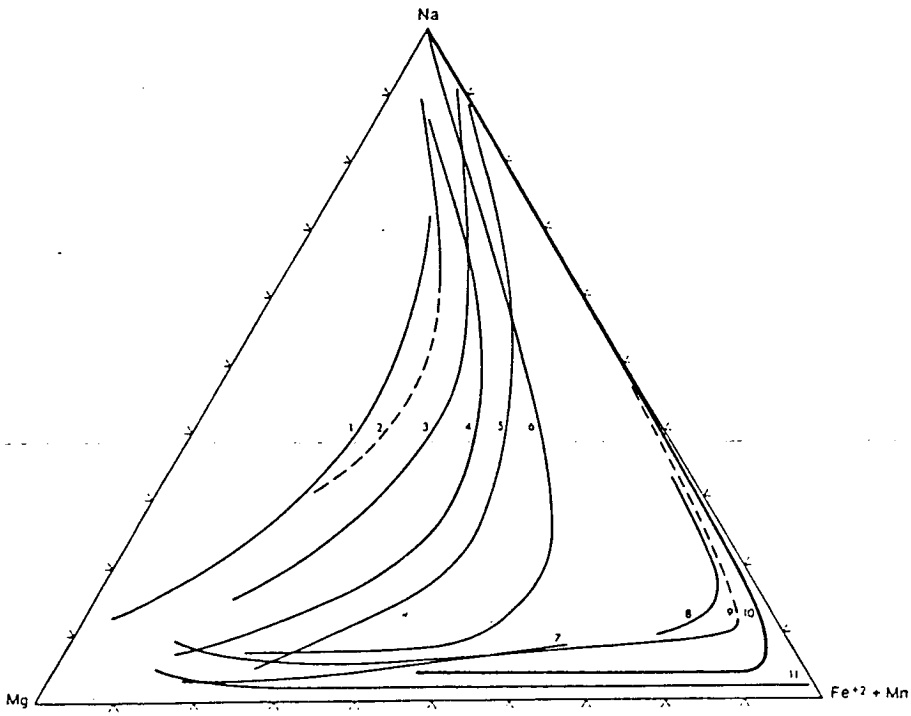


**Figure 3.17** A comparison of published pyroxene trends, from Larsen (1976). Undersaturated: (1) Auvergne, France (Varet, 1969), (2) Lovozero, USSR (Bussen and Sakharov, 1972), (3) Itapirapuã, Brazil (Gomes *et al.*, 1970), (4) Uganda (Tyler and King, 1967), (5) Morotu, Sakhalin (Yagi, 1966), (6) S Qôroq, S Greenland (Stephenson, 1974), (10) Ilímaussaq, S Greenland (Larsen, 1976).
Oversaturated: (7) Japanese alkali basalts (Aoki, 1964), (8) Pantellerite trend (Nicholls and Carmichael, 1969), (9) Nandewar volcano, Australia (Abbott, 1969), (11) Skaergaard intrusion, E Greenland (Brown and Vincent, 1963). Not alkaline but shown for comparison.

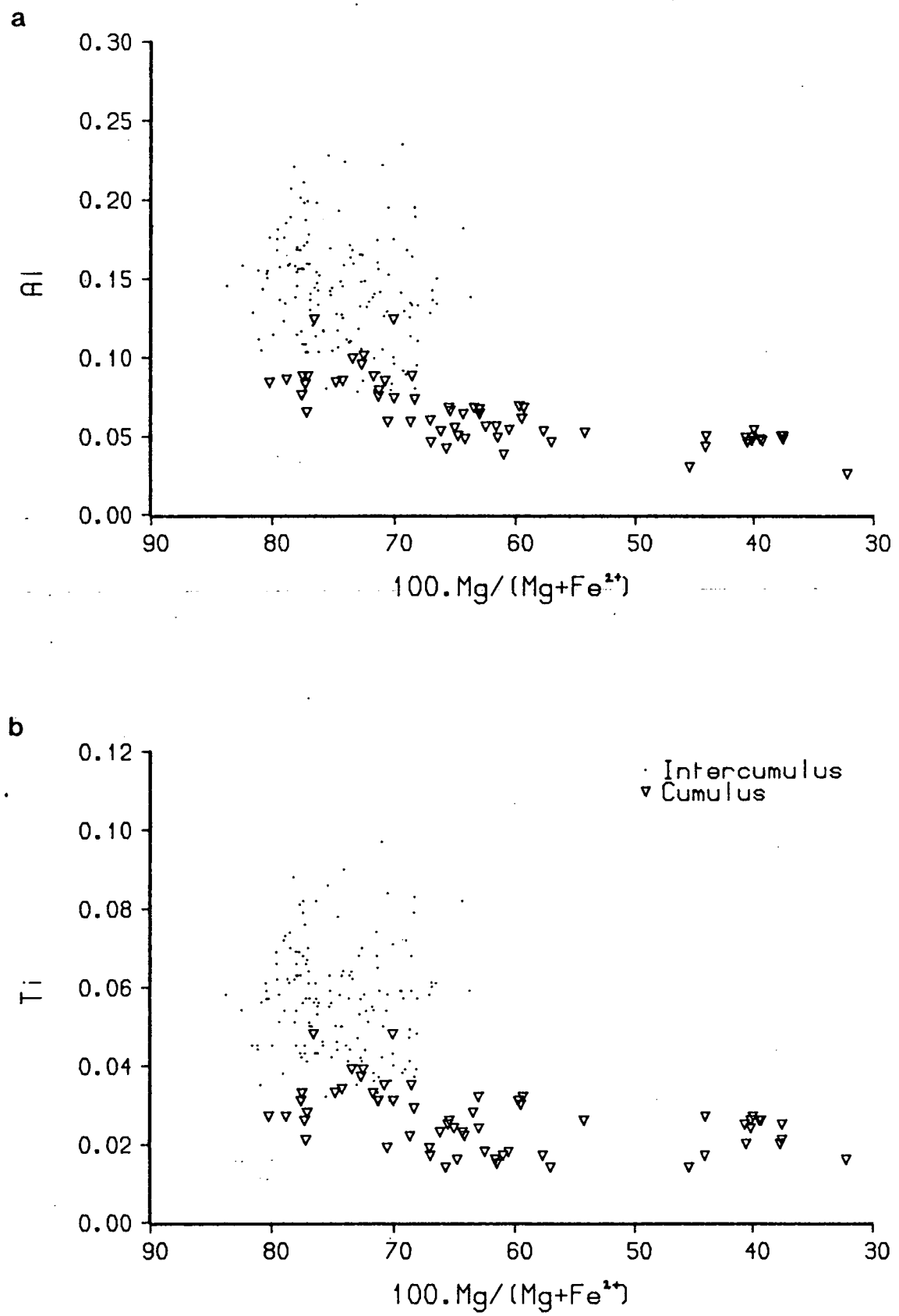


**Figure 3.18** (a) Al and (b) Ti variation in cumulus and intercumulus pyroxenes, plotted against 100.Mg/(Mg+$Fe^{2+}$).

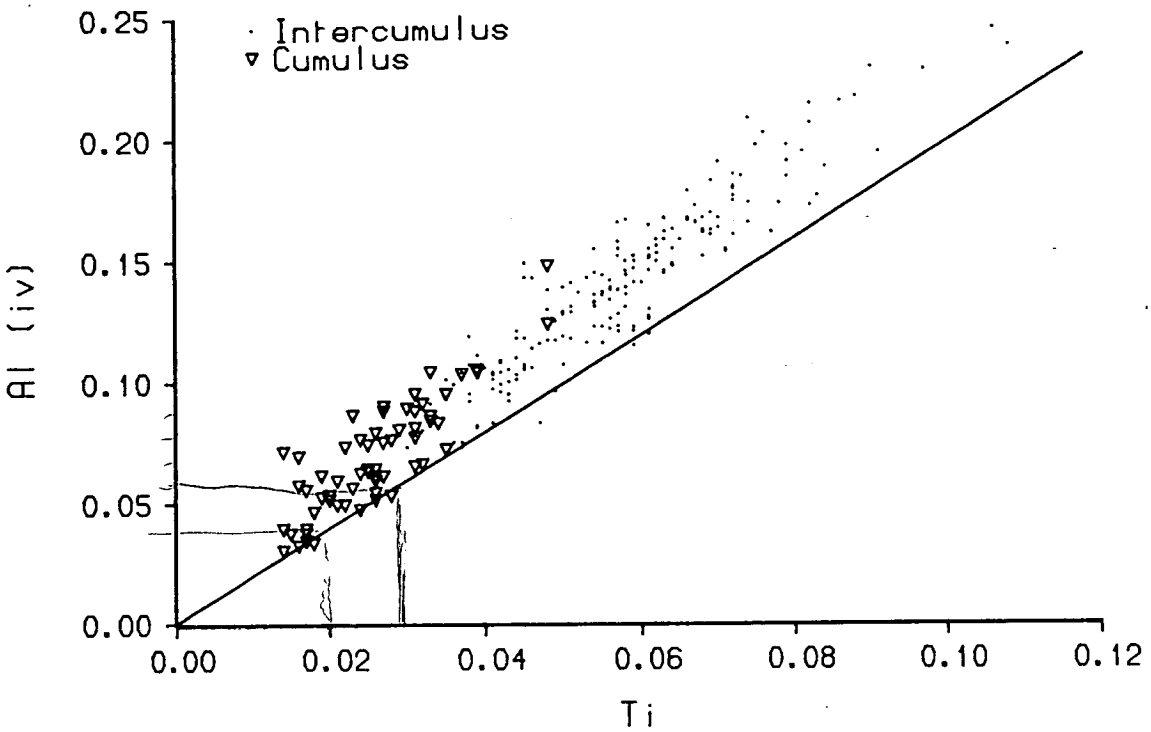


**Figure 3.19** $Al^{iv}$ (=2-Si) against Ti in the pyroxenes. Compositions lie near the line $Al^{iv}$=2Ti, indicating the presence of Ca-Ti-Tschermak's molecule. Most points lie above the line and may also contain Ca-Tschermak's molecule.

behaviour is similar to that observed in pyroxenes from Klokken (Parsons, 1979), Kûngnât (Stephenson and Upton, 1982) and the Tugtutôq Central Complex (Upton et al., 1990).

All the samples have sufficiently low $Al^{vi}$ to fall within the field of igneous rocks of Aoki and Kushiro (1968). When $Al^{iv}$ (2-Si) is plotted against Ti, the compositions lie along the line $Al^{iv} = 2Ti$ (Fig. 3.19). This indicates the presence of Ca-Ti-Tschermak's molecule and the operation of the coupled substitution: $M^{2+} + 2Si^{4+} = Ti^{4+} + 2Al^{3+}$ (Larsen, 1976). Points above the line may also contain Ca-Tschermak's molecule $CaAl_2SiO_6$, which is found in increasing concentration with increasing silica undersaturation.

### 3.4.4 Iron-titanium oxides

Discrete crystals of both titano-magnetite and ilmenite have been found in all YGDC rocks examined, with titano-magnetite becoming volumetrically more important as compositions become more evolved. Magnetite also occurs as a secondary alteration (oxidation) product of olivine and sulphides. Magnetite grains generally show varying degrees of exsolution, so the analyses obtained do not represent original magmatic compositions. The exsolution lamallae appear to be of ilmenite and not ulvöspinel since they occur along {111} planes. No haematite exsolution is visible in the ilmenite grains. Magnetite analyses have been recalculated on the basis of stoichiometry and magnetite and ilmenite compositions are plotted in terms of $FeO:TiO_2:Fe_2O_3$ in Fig. 3.20.

Minor elements are plotted in Fig. 3.21. Both magnetites and ilmenites become richer in Mn with increasing differentiation. Ilmenites have uniformly low Al contents while in magnetites, Al increases and then decreases again with differentiation. These compositions are similar to those given by Parsons (1979) for Klokken and Martin (1985) for the Tugtutôq dyke swarm. Vanadium has not been determined in the magnetites because the X-ray $K_\alpha$ peak is swamped by the $K_\beta$ peak for Ti, but V contents of magnetites can be estimated from whole-rock trace-element analysis. The highest whole-rock V (found in sample YGD196) is about 1200 ppm and the rock contains about 30 vol% Fe-Ti oxides. If two-thirds of the oxides are magnetite and no other phases contain V, then the magnetite contains roughly 0.6

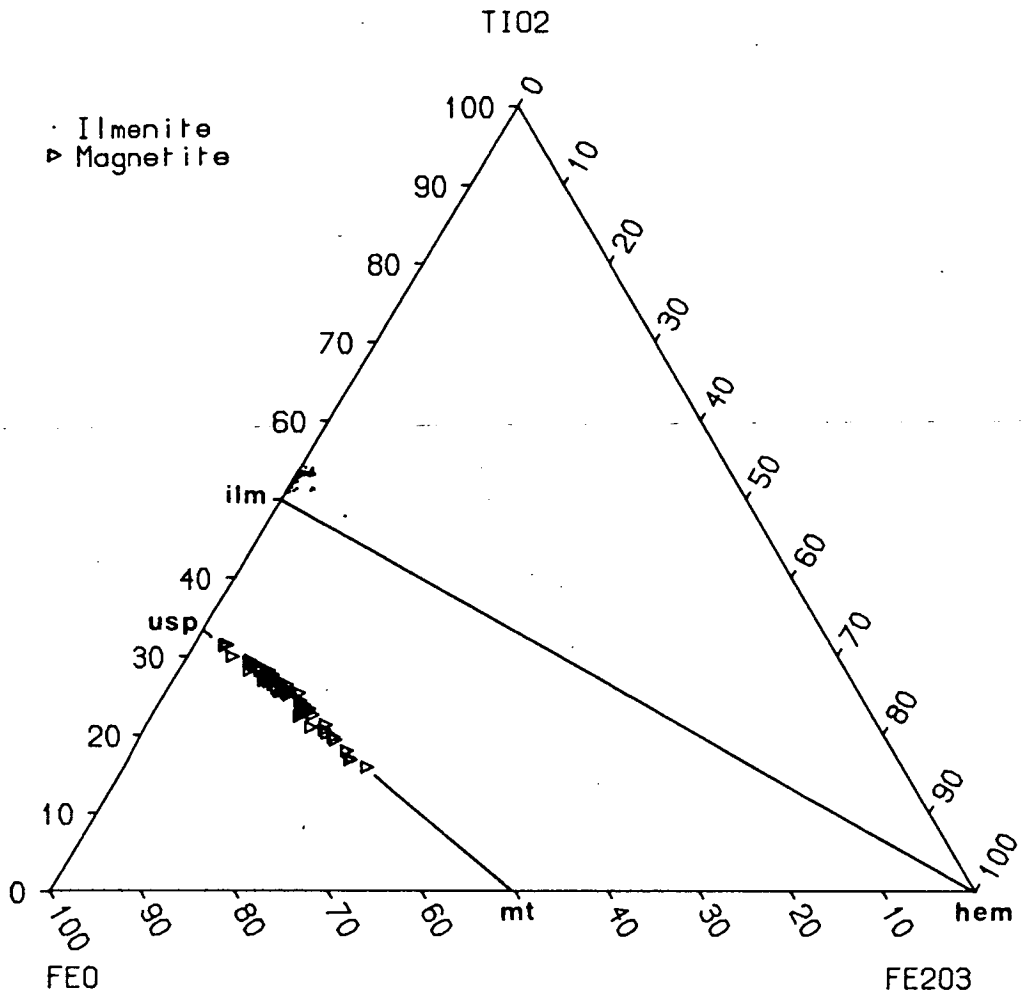


**Figure 3.20** Fe-Ti oxides plotted as molecular $FeO:TiO_2:Fe_2O_3$. Magnetites have almost all undergone ilmenite exsolution. Ilmenite compositions are displaced towards $TiO_2$ by the presence of MnO which is not included in the plotting parameters.

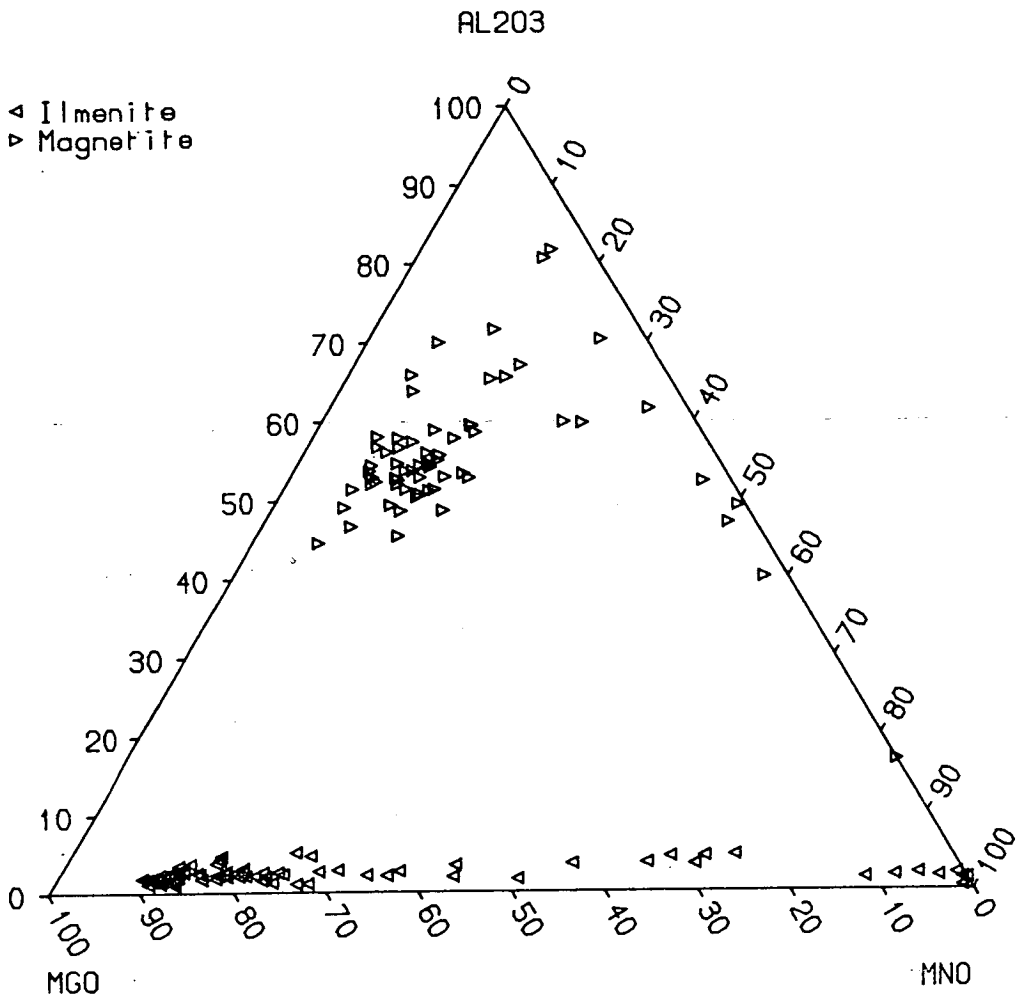


**Figure 3.21** Fe-Ti oxides plotted in terms of the minor elements MgO, MnO and $Al_2O_3$. Compositions move towards the MnO corner with increasing differentiation.

wt% V, or 2.1 wt% $V_2O_5$. This is similar to the $V_2O_5$ contents reported for Bushveld magnetites (Cawthorn and McCarthy, 1980).

Because most of the magnetite grains show exsolution they are unsuitable for geothermometry and oxygen barometry. A few apparently unexsolved grains were found, although these tend to show barely-visible oxidation to maghemite along cracks. When the sample is carbon-coated, such oxidation (and indeed the exsolution lamellae) are very difficult to see and thus avoid when probing, so even analyses of apparently unexsolved grains may be suspect. It was also found that in the rocks where a suitable magnetite analysis was obtained, the coexisting ilmenite contained no haematite and thus could not be used for geothermometry. However, Upton and Thomas (1980) reported temperatures in the range 845-590°C and log $fO_2$ values from -24.0 to -15.5 for coexisting magnetite-ilmenite pairs from the YGDC, using the method of Powell and Powell (1977). Martin (1985) obtained comparable values of T = 900-600°C and log $fO_2$ = -24 to -14 by the same method, for the Tugtutôq dyke swarm. These values lie between the QFM and IW buffers. They represent re-equilibration rather than original magmatic temperatures, but indicate that crystallisation occurred under highly reducing conditions. Parsons (1981) calculated approximate bulk compositions of exsolved magnetites from the Klokken intrusion by continuous scanning with the electron microprobe. Compositions obtained by this method, with those of coexisiting ilm-haem$_{ss}$ give temperatures of 750-850°C and and log $fO_2$ of -17 to -15 for the syenites, using the method of Buddington and Lindsley (1964). One sample of marginal gabbro gave T = 1015°C and log $fO_2$ = -11. Parsons reports that some ilmenites were too low in $Fe_2O_3$ to plot on T/log $fO_2$ diagrams, like some of the YGDC ilmenites. These data from Klokken, and data from other layered intrusions (Haggerty, 1976) also lie near the QFM buffer.

### 3.4.5 Apatite

Apatite is found in all YGDC rocks and becomes a cumulus phase at about the same time as magnetite and ilmenite. At locality G of Fig. 2.1 apatite appears to have preceded the Fe-Ti oxides but at localities I and M it postdated them. The apatite crystals are highly elongated in the chilled margins but more equant in the coarse-grained lithologies; this difference is attributed to faster cooling rates in the chilled margins. Greatest apatite abundances are found in the olivine-oxide-apatite cumulates of locality G and the syenogabbros of localities K and L.

Apatites were analysed for Ca, P, Si, Na, Ce, La, F and Cl. The major elements, Ca and P show little variation. Of the minor elements, $Na_2O$ varies from below detection limits to 0.1 wt% in chills and troctolites and from 0.03 to 0.19 wt% in syenogabbros and syenites. $SiO_2$ also increases slightly with increasing differentiation of the rocks, with a range from 0.12 to 0.68 wt%, but for both elements there is considerable within-sample variation. $La_2O_3$ and $Ce_2O_3$ reach maximum values of 0.26 and 0.54 wt% respectively in the syenites. Unpublished analyses of YGDC apatites by P.G. Hill (Edinburgh University) show that other minor elements (Al, Fe, Mg and Sr) generally occur in insignificant amounts (although FeO may reach 0.32 wt%) and that $Nd_2O_3$ contents are very similar to $La_2O_3$ contents. Mn, which may substitute for Ca in apatites, was not analysed for, but Becker (1984) found that Mn was absent from apatites of similar composition in the Isortoq giant dykes, and the good totals obtained for the YGDC apatites suggest low Mn contents.

Fluorine contents range from 3.3 to 6.8 wt% and within-sample variation is 2-3 wt%. No clearly-defined trends are seen between fluorine content and rock composition. Chlorine is uniformly low (0.03-0.3 wt%) except in sample GGU 85954 where it forms 0.5-1.3 wt% of the analysis. The reasons for this sample being different are not fully understood. Fluorine and chlorine do not seem to substitute for one another, so there is probably F-OH substitution, as seen in the biotites (section 3.4.6).

Apatites from the Isortoq giant dykes (Becker, 1984), Kûngnât and the OGDC (P.G. Hill, unpubl. data) are similar in composition to those of the YGDC. Isortoq apatites are slightly higher in Ca, Fe and sometimes Si and do not appear to contain much F or Cl, while those from the nepheline syenites of the OGDC are lower in Ca, higher in REE and probably higher in F, although since the fluorine standard has changed since the analyses were made, values cannot be directly compared.

### 3.4.6 Biotite

In the chills, troctolites and gabbro picrites, biotite forms fringes around Fe-Ti oxides, while in the syenogabbros and syenites, discrete, often poikilitic crystals of biotite may attain several centimetres in size. $Fe^{3+}$ and $H_2O$ were not determined

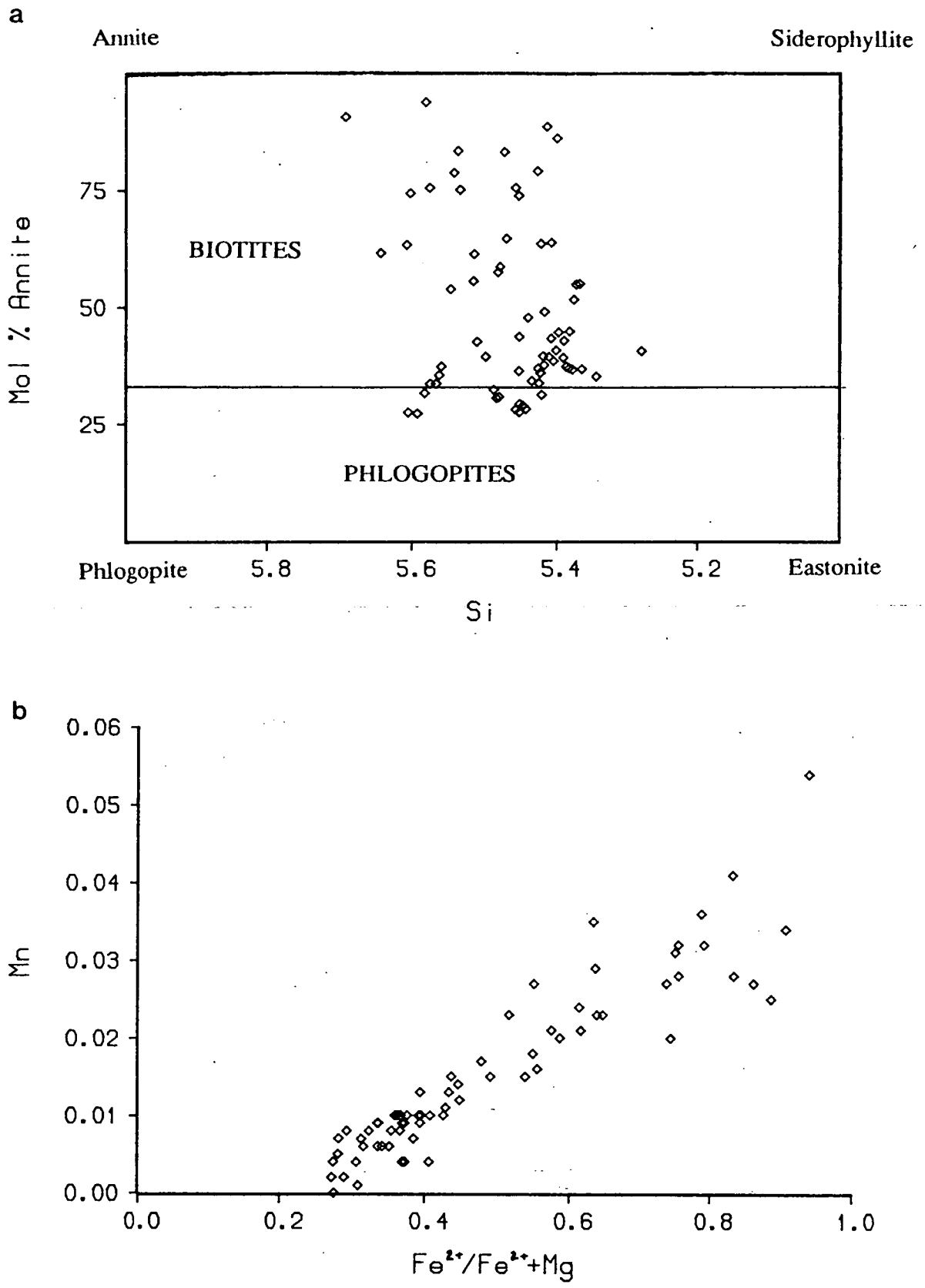


**Figure 3.22** (a) Biotite compositions in terms of the end members phlogopite, annite, siderophyllite and eastonite. Fields from Deer *et al.* (1966). (b) Mn in biotites (atoms per 22 oxygens) plotted against Fe/(Fe+Mg).

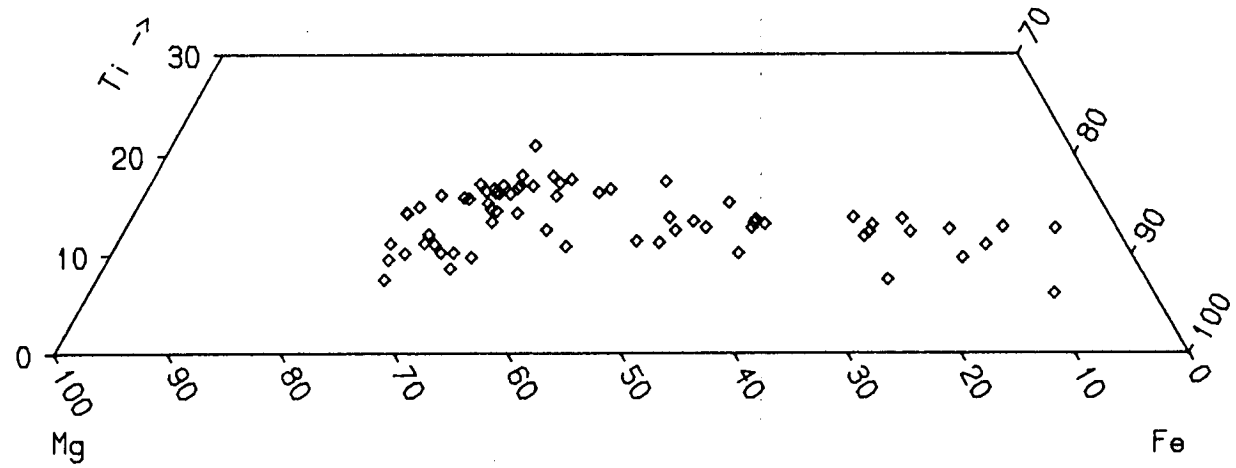


**Figure 3.23** Biotites plotted in terms of Mg:Ti:Fe.

during microprobe analyses so all iron was taken as $Fe^{2+}$ and cation proportions calculated on the basis of 22 oxygens. However, it is possible that there may be sufficient $Fe^{3+}$ in some of the analysed compositions for them to be termed lepidomelanes.

The annite component increases steadily from the troctolites through the syenogabbros to the syenites, ranging from 23 to 95 mol% with a gap between 65 and 73 mol%. Figure 3.22a gives the compositions in terms of the end members phlogopite, annite, siderophyllite and eastonite. The division between biotites and phlogopites was arbitrarily chosen by Deer *et al.* (1966) to be where Mg:Fe = 2:1. By this criterion, a few of the YGDC biotites (all from troctolites) should in fact be termed phlogopites.

The Mn content shows a steady increase with iron to a maximum value of 0.30 wt% MnO (Fig. 3.22b). The variation in Mg:Ti:Fe is plotted on Fig. 3.23 and shows a slight decrease of Ti with increasing Fe, although there is some scatter at the low-Fe end of the trend. $TiO_2$ contents range from 2.9 to 10.6 wt%.

Halogens can substitute for OH groups in micas and Gardar biotites tend to be rich in fluorine but poor in chlorine (Chambers, 1976; Rae, 1988; Parsons *et al.*, 1990), indicating an F-OH substitution. Fluorine contents were determined for many of the samples analysed, and further analyses were made by A.A. Finch. Wt% F is plotted against Fe/(Fe+Mg) for the combined data set in Fig. 3.24, and shows a fluorine-iron avoidance trend (Finch, 1990). The fluorine content of biotites can be used as an indicator of the fluorine content of late-stage fluids (Munoz, 1984). The YGDC biotites closely fit predicted trends for $f(H_2O)/f(HF) = 4$ at 1000 K (Finch, 1990), where $f(H_2O)$ is water fugacity. This indicates that the YGDC is essentially unmetasomatised. Other Garder complexes show higher fluorine contents of biotites due to metasomatism by late-stage magmatic fluids, originating either from the complex itself or from adjacent later complexes. The technique of Munoz (1984) does not apply so well to other Gardar complexes as to the YGDC, but comparison of maximum fluorine curves for the different intrusions reveals qualitative differences. Notably, silica-undersaturated magmatism is associated with higher fluorine contents in biotites (Fig. 3.25). This may simply be due to higher fluorine contents in the late-stage fluids, or to silicon in the oversaturated magmas binding to the fluorine as complexes (e.g. $SiF_6^{2-}$), reducing the amount of fluorine as HF or $F^-$ which is available to the biotites (Finch, 1990).

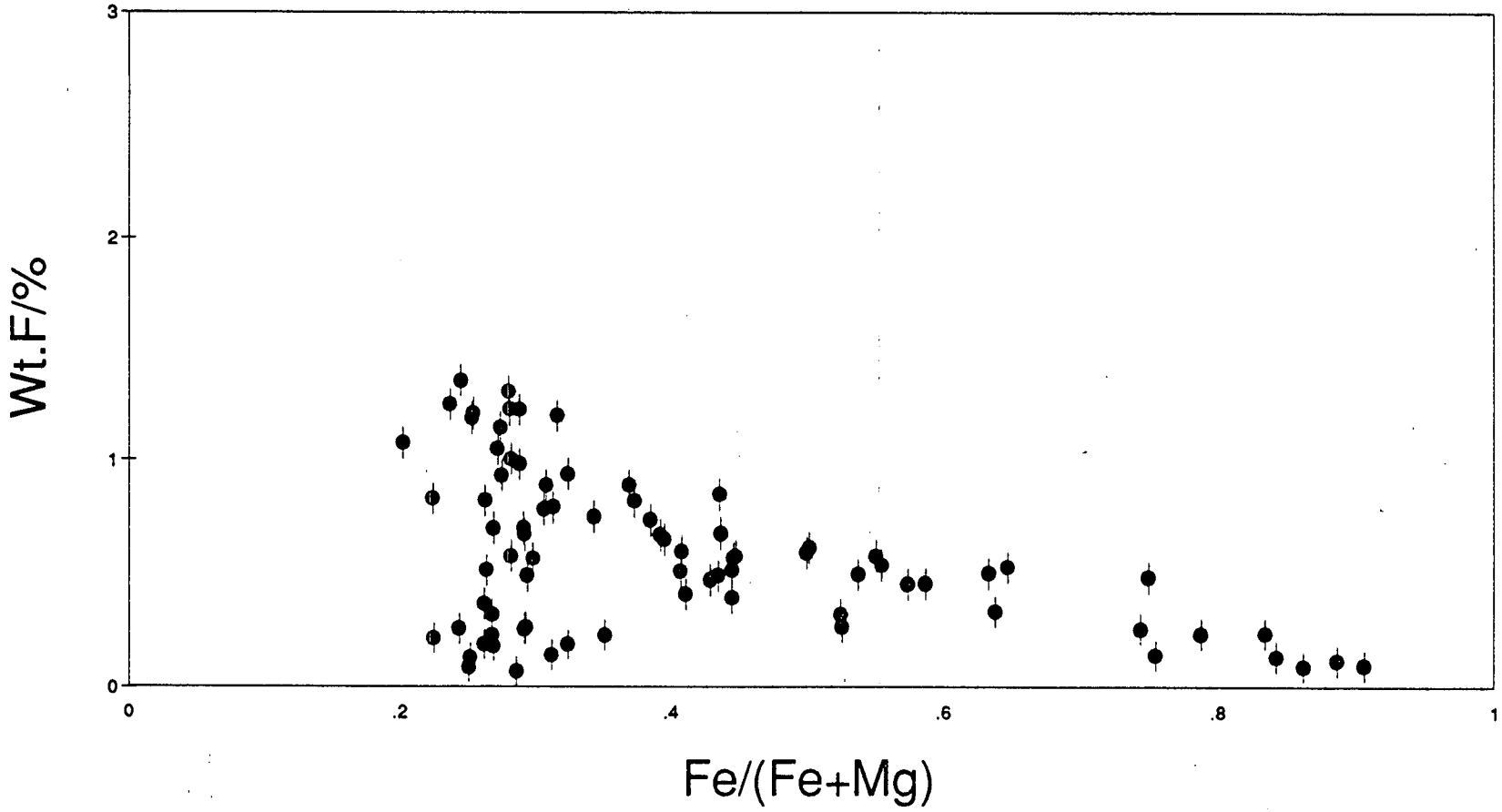


**Figure 3.24** Wt% fluorine against Fe/(Fe+Mg) in biotites with error bars indicated. Some analyses by A.A. Finch; diagram after Finch (1990).

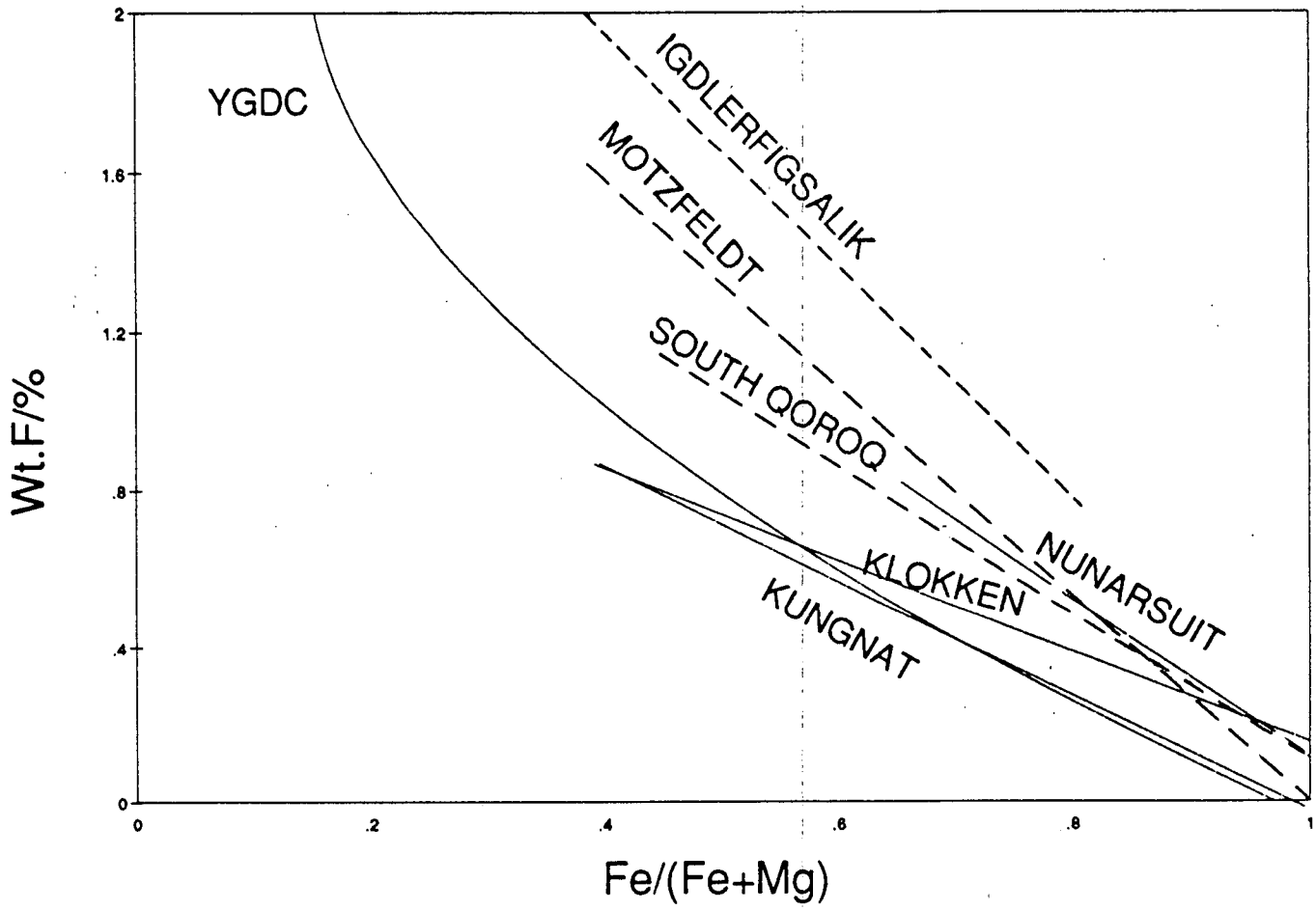


**Figure 3.25** A comparison of lines of maximum F in biotites for several Gardar centres. Oversaturated complexes are shown by solid lines, undersaturated complexes by dashed lines. After Finch (1990).

### 3.4.7 Amphibole

Amphiboles are considered to be primary (i.e. not formed by alteration) in the syenogabbros and the syenites of the YGDC. Compositions are plotted in terms of Mg:$Fe^{2+}$+Mn:Na+K (all iron as FeO) on Fig. 3.26. Trends for the undersaturated complexes of S Qôroq and Ilímaussaq, and the oversaturated complexes of Kûngnât and Nunarssuit are shown for comparison. Amphiboles from the Isortoq giant dykes (Becker, 1984) show a scatter and do not follow any one trend, possibly due to some of the Na enrichment being due to late stage fluids. It can be seen that analyses from the YGDC (as for the smaller dykes of Tugtutôq, Martin, 1985) tend to follow the trends for undersaturated rather than oversaturated complexes. Those reported for Klokken (Parsons, 1979) are similar to the YGDC analyses. It appears that there is not a simple silica activity control on amphibole compositions in the Gardar province. Stephenson and Upton (1982) suggest that the degree of peralkalinity of the residual liquid is the controlling factor.

YGDC amphiboles range from hastingsite ($NaCa_2Fe_4^{2+}Fe^{3+}Si_6Al_2O_{22}(OH)_2$ in the system of Leake (1978)) through katophorite ($NaCaNaFe_4^{2+}Fe^{3+}Si_7AlO_{22}(OH)_2$) to arfvedsonite ($Na_3Fe_4^{2+}Fe^{3+}Si_8O_{22}(OH)_2$) in a late-stage vein. They are fairly rich in titanium (up to 4.1wt% $TiO_2$) but not sufficiently so to be termed kaersutites. F probably substitutes for OH as it does in apatite and biotite, but has not been analysed for. Within-sample variation is generally small. Fig. 3.27a shows the compositions plotted on a diagram of $Al^{iv}$+Ca against Si+Na+K, combining the high-Ca and low-Ca plots of Giret *et al.* (1980), as suggested by Becker (1984). The main subsitution operating is CaAl→NaSi (Figs. 3.27b and 3.28a), together with Mg→$Fe^{2+}$ and possibly Ca(Mg,$Fe^{2+}$)→$NaFe^{3+}$ (Stephenson and Upton, 1982). Compositional change from ferro-richterite to arfvedsonite is achieved by $CaFe_{2+}$→$Na(Fe_{3+},Al)$. However, calculation of $Fe^{2+}/Fe^{3+}$ by the method of Leake (1978) shows that $Fe^{3+}$ enrichment is minor, even in the alkali amphiboles. Thus the amphiboles that appeared to be riebeckitic in thin section (section 3.2.4 and 3.2.6) are in fact arfvedsonites, as found in the Kûngnât Intrusion (Stephenson and Upton, 1982). Aluminium is predominantly tetrahedral (Fig. 3.28b). There are insufficient data to decide whether or not a compositional gap exists, as proposed by Giret *et al.* (1980), and reported by Stephenson and Upton (1982) for the YGDC.

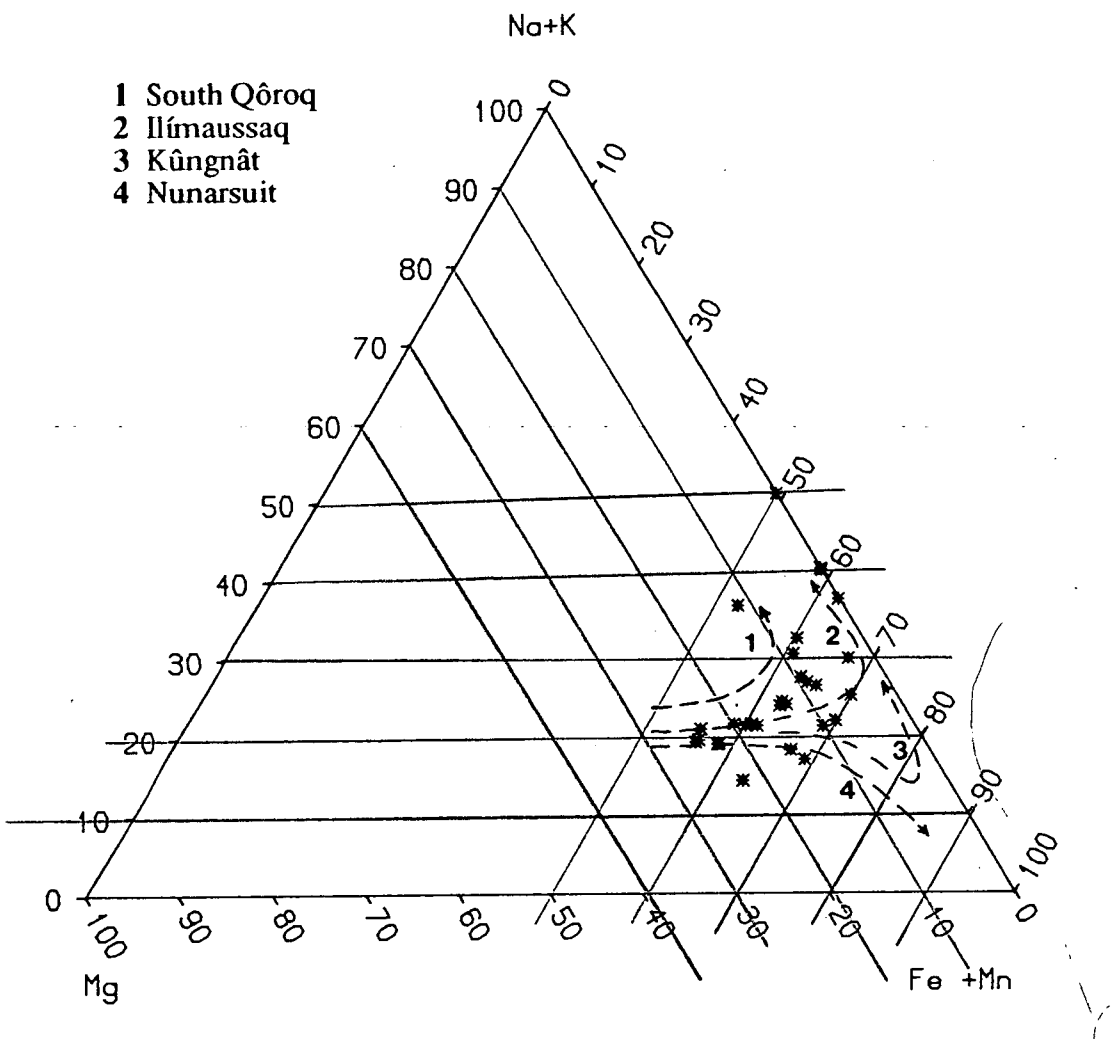


**Figure 3.26** Amphiboles in terms of Mg:$Fe^{2+}$+Mn:Na+K. Trends for other Gardar centres are from Stephenson and Upton (1982) for S Qôroq and Kûngnât, Larsen (1976) for Ilímaussaq and Butterfield (1980) for the Helene granite of Nunarsuit.

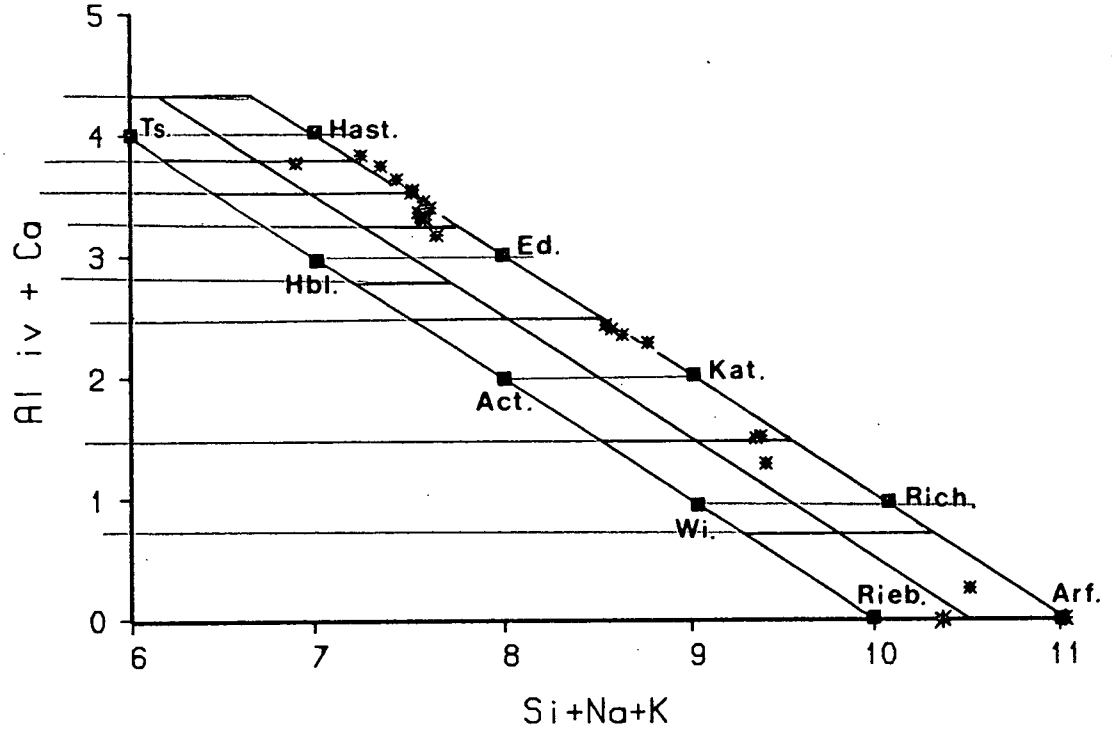


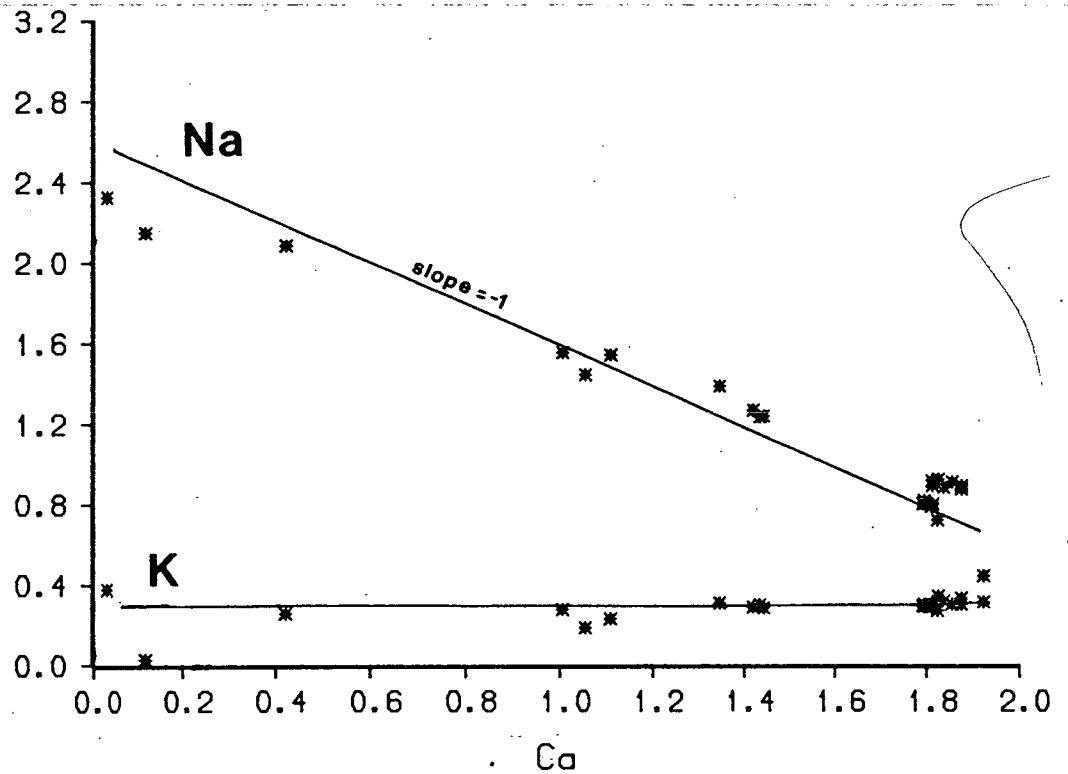


**Figure 3.27** (a) Plot of $Al^{iv}$+Ca against Si+Na+K (atoms to 13 cations) for amphiboles, after Giret *et al.* (1980). Their two plots for high-Ca and low-Ca amphiboles have been combined, following the method of Becker (1980). Amphibole endmembers are Ts = tschermakite, Hast = hastingsite, Hbl = hornblende, Ed = edenite/taramite, Act = actinolite/barroisite, Kat = katophorite, Wi = winchite, Rich = richterite, Rieb = riebeckite, Arf = arfvedsonite.
(b) Na and K plotted against Ca for amphiboles. Na-Ca substitution is clearly occurring.

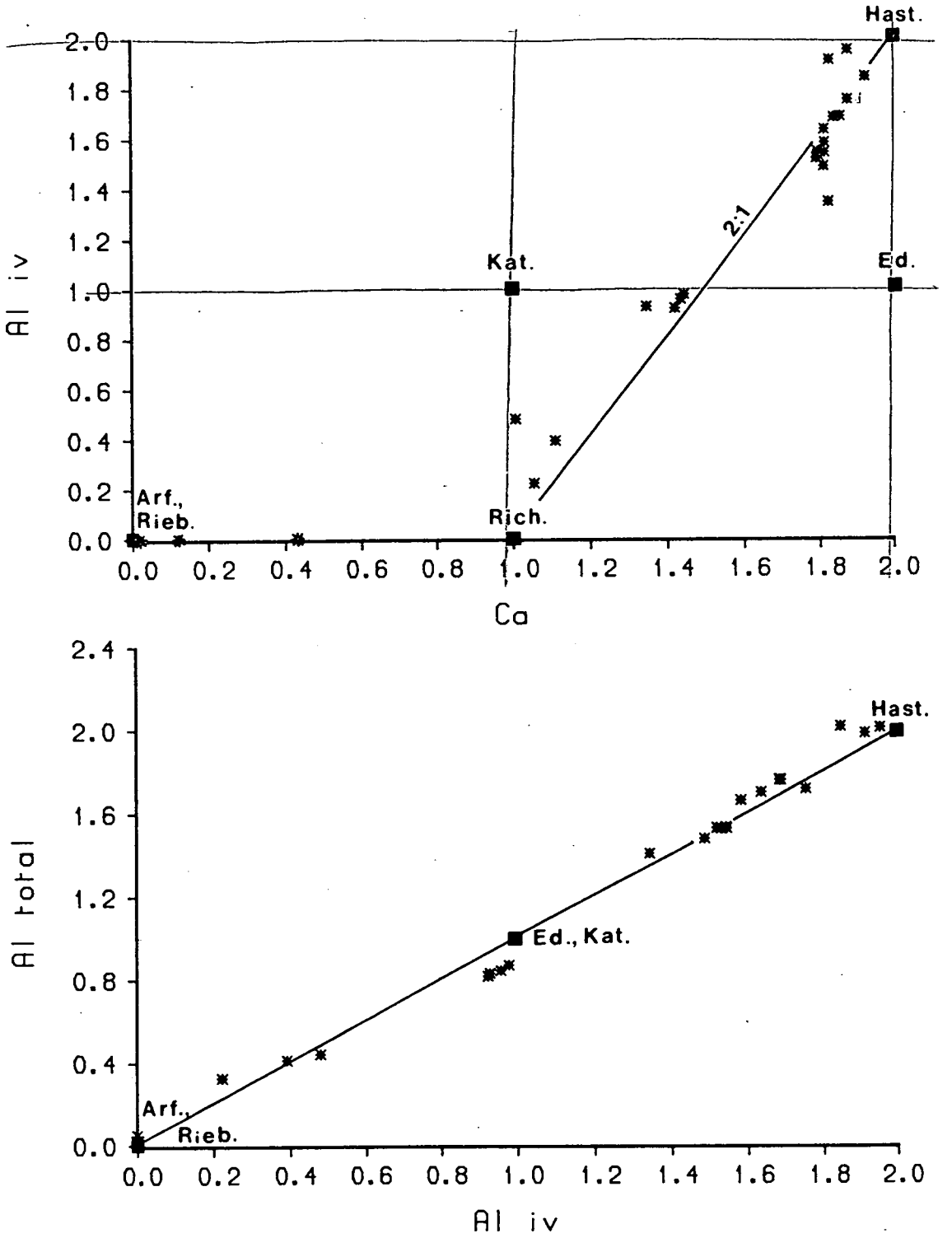


Figure 3.28 (a) $Al^{iv}$ against Ca for amphiboles indicates that the substitution is likely to be CaAl→NaSi. (b) Total Al against $Al^{iv}$, showing that virtually all Al is tetrahedral, as seen in the pyroxenes. Amphibole endmembers are Hast = hastingsite, Ed = edenite, Kat = katophorite, Rich = richterite, Rieb = riebeckite, Arf = arfvedsonite.

### 3.4.8 Summary

YGDC olivine compositions range from $Fo_{68}$-$Fo_3$ and show zoning of up to 9 mol% Fo in the chilled margins. At localities B to D, F and the nunataq region, olivines in mafic cumulates are slightly more magnesian ($Fo_3$) than those in adjacent felsic layers. Compositions of the feldspars range from labradorite through andesine and oligoclase to anorthoclase, sanidine and antiperthite. Normal zoning of up to $An_{20}$ is common. Ba contents are highest in the syenogabbros.

Intercumulus pyroxenes are salites, and cumulus pyroxenes salites to ferro-salites, with little enrichment in Na and $Fe^{3+}$. Co-existing magnetite and ilmenite were found unsuitable for geothermometry due to magnetite exsolution and to low haematite contents in the ilmenite. However, estimates of temperature and oxygen fugacity between the QFM and IW buffers were obtained by Upton and Thomas (1980) for the YGDC and Martin (1985) for the Tugtutôq dyke swarm.

Apatites and biotites are rich in F and the annite component of the biotites ranges from 23-95 mol%. Amphiboles are hastingsites, katophorites and arfvedsonites. The compositions of most minerals are similar to those from other Gardar intrusions and the YGDC shows one of the largest compositional ranges in the Gardar province.

# CHAPTER 4: WHOLE-ROCK CHEMISTRY

## 4.1 Introduction

X-Ray fluorescence spectrometry was used to analyse 105 whole-rock samples for major and trace elements. Analytical procedures are given in Appendix II and tables of analyses in Appendix IV. The samples analysed include a range of lithologies from the YGDC and its country-rocks, including fine-grained marginal facies ("chills"), troctolites, gabbro picrites and other mafic cumulates, syenogabbros, syenites and country-rock granites. Chills were taken about 1m into the dyke to avoid contamination (see Chapter 3) and are thus not glassy but are relatively fine-grained (grain size 0.2-2mm) compared to samples from the interior of the dyke. Troctolites were predominantly from the layered localities. Syenogabbros were from locality K of Fig. 2.1 and from the elongated pyroxene zone of locality L, while syenites were predominantly from locality L although two samples, one a mafic cumulate, came from the nunataq region of Fig. 1. The syenite samples analysed include two late-stage veins and an aplite. The rocks are fairly fresh and LOIs range from -1.87 to 3.47, with negative values usually occurring in the mafic cumulates due to oxidation of iron, and values >1.0 occurring in the syenites.

## 4.2 Nature of the YGDC magma

### 4.2.1 Classification

A plot of YGDC chill samples on a total alkalis versus silica diagram is shown in Fig. 4.1a. Data are from this study, from Upton and Thomas (1980) and B.G.J. Upton (unpublished data). The chills are mainly found in the basalt field of Cox *et al.* (1979), to the alkaline side of the alkaline/sub-alkaline divide. Three are in the hawaiite field and two in the basanite field, but the latter are unusually high in potassium and may be altered (section 4.3.1). Divisions suggested by Le Bas *et al.* (1986) would put a greater number of the samples in the basanite rather than the basalt field.

A second classification scheme is that suggested by Coombs and Wilkinson (1969) for undersaturated rocks where Differentiation Index (D.I.) is plotted against normative anorthite. D.I. = normative ne+ab+or+qz+lc+ks and normative anorthite = 100.An/(An+Ab) This classification is shown in Fig. 4.1b and the majority of the

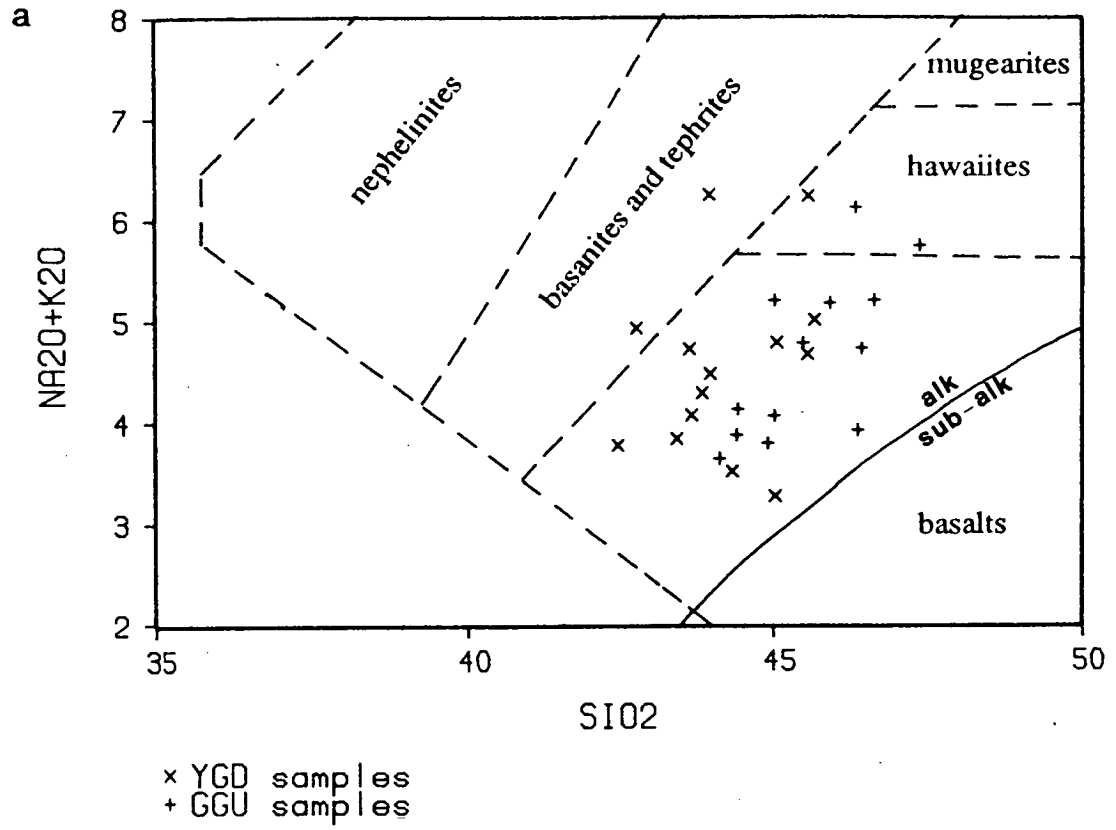


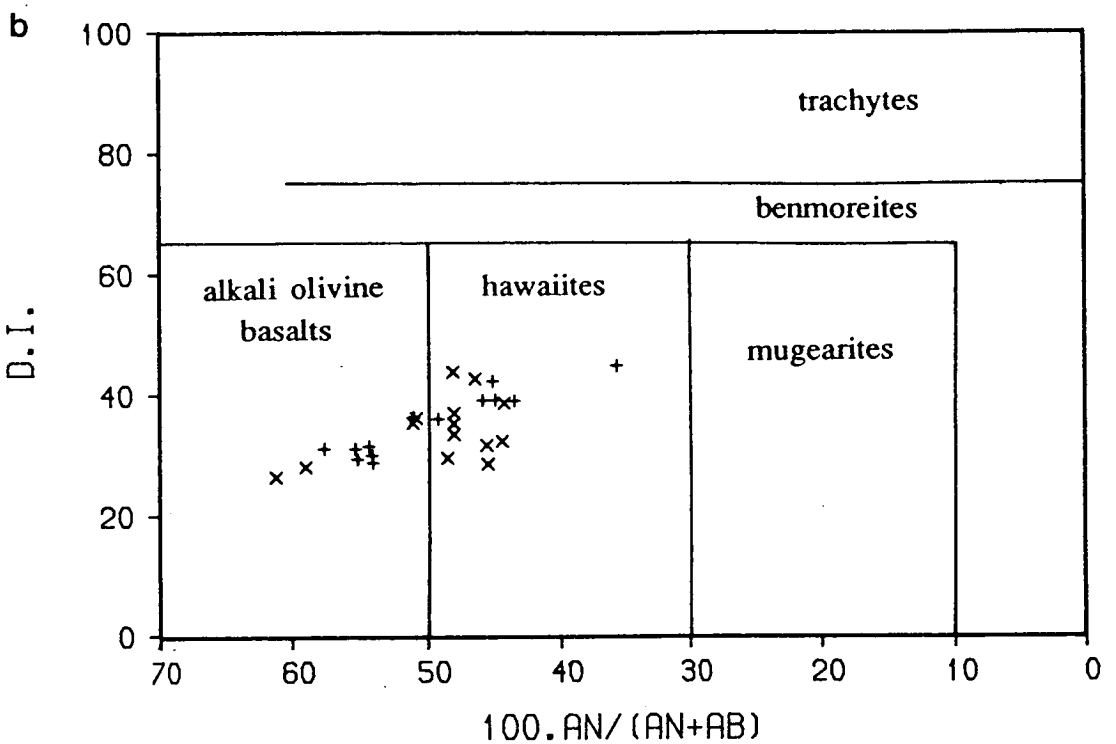


**Figure 4.1** Classification of YGDC chilled margins, (a) using total alkalis versus silica, with compositional fields from Cox *et al.* (1979) and alkaline-subalkaline divide from Irvine and Baragar (1971); (b) using the normative classification of Coombs and Wilkinson (1969).

YGDC chill samples fall in the hawaiite field with the remainder classed as basalts. It is concluded that in general the YGDC magmas ranged from basaltic to hawaiitic in composition, but different classifications divide them differently.

### 4.2.2 Norms

A large majority of the chills and troctolites are nepheline-normative, indicating the alkaline character of the magma, but some have orthopyroxene in the norm. Other normative minerals are diopside, olivine, anorthite, albite, orthoclase, magnetite, ilmenite and apatite; in other words, for most of the rocks the norm is very similar to the mode. The syenogabbros and syenites may be nepheline-, hypersthene- or hypersthene+quartz normative. Corundum appears in the norm of a few chills and troctolites and acmite in three syenites. Norms will be found with XRF analyses in Appendix IV.

## 4.3 Element variation with MgO

MgO is taken as a reasonable indicator of the degree of crystallisation since the YGDC remains relatively basic until the late stages of its crystallisation history. Wright (1974) recommended the use of MgO as an abscissa because basic rock suites generally display a wide range in MgO content, it falls continuously with falling temperature (cf. Thompson, 1973) and common fractionating minerals have distinct ranges of MgO content.

### 4.3.1 Major element variation

Major elements have been plotted against MgO in wt% for both chills and coarse-grained rocks on Figs. 4.2 to 4.6. The chilled marginal samples are thought to approximate to liquid compositions but the coarse-grained rocks may not, and compositional variations must be interpreted with more caution. There is generally a good correlation on the diagrams between major elements and MgO. Most of the analyses define a distinct linear trend; those samples lying off the trend are usually mafic cumulates which have accumulated more than one mineral (olivine + magnetite $\pm$ apatite $\pm$ clinopyroxene cumulates).

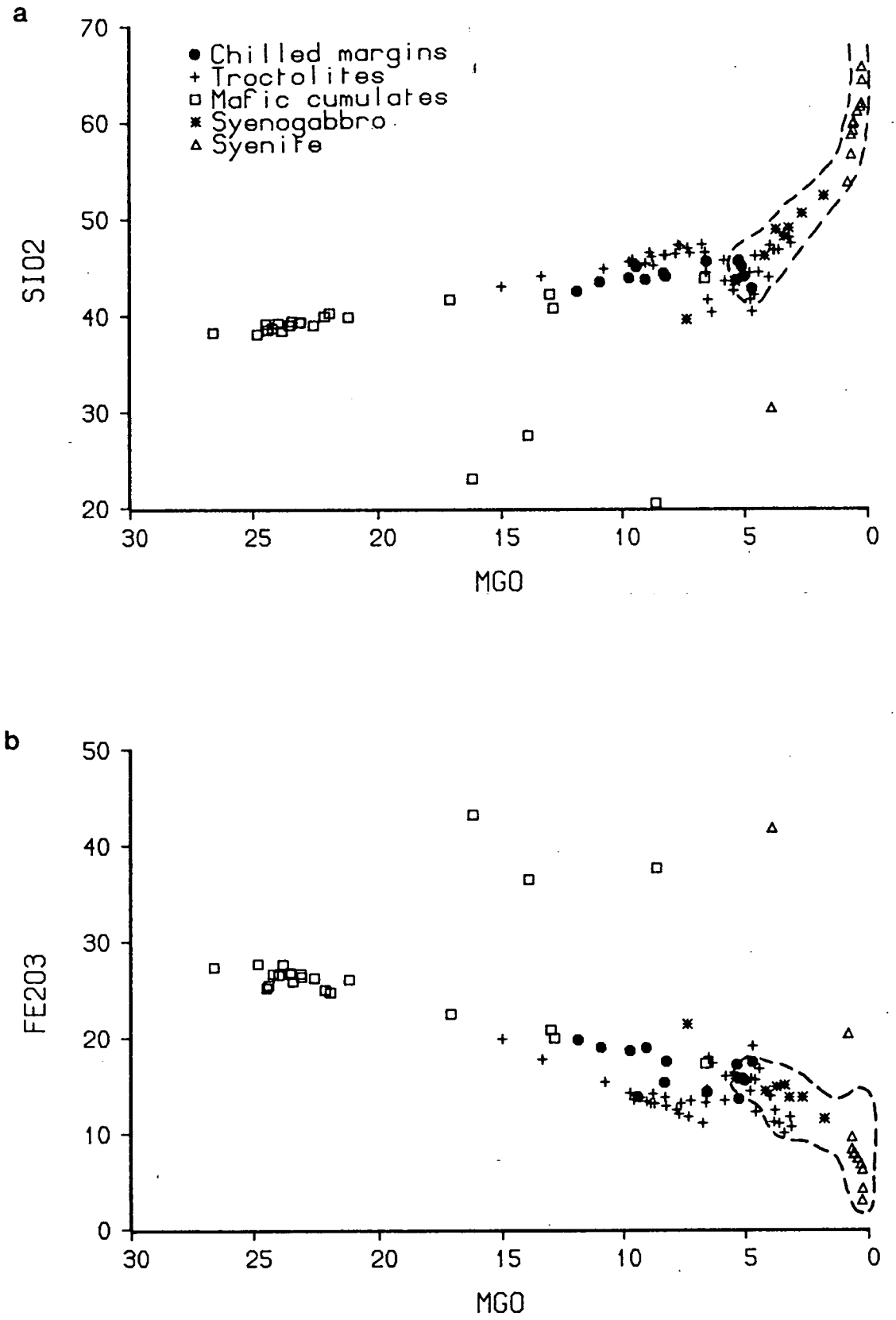


**Figure 4.2** (a) $SiO_2$ and (b) total iron as $Fe_2O_3$ plotted against MgO. Dashed lines indicate compositional field of smaller dykes, from Martin (1985).

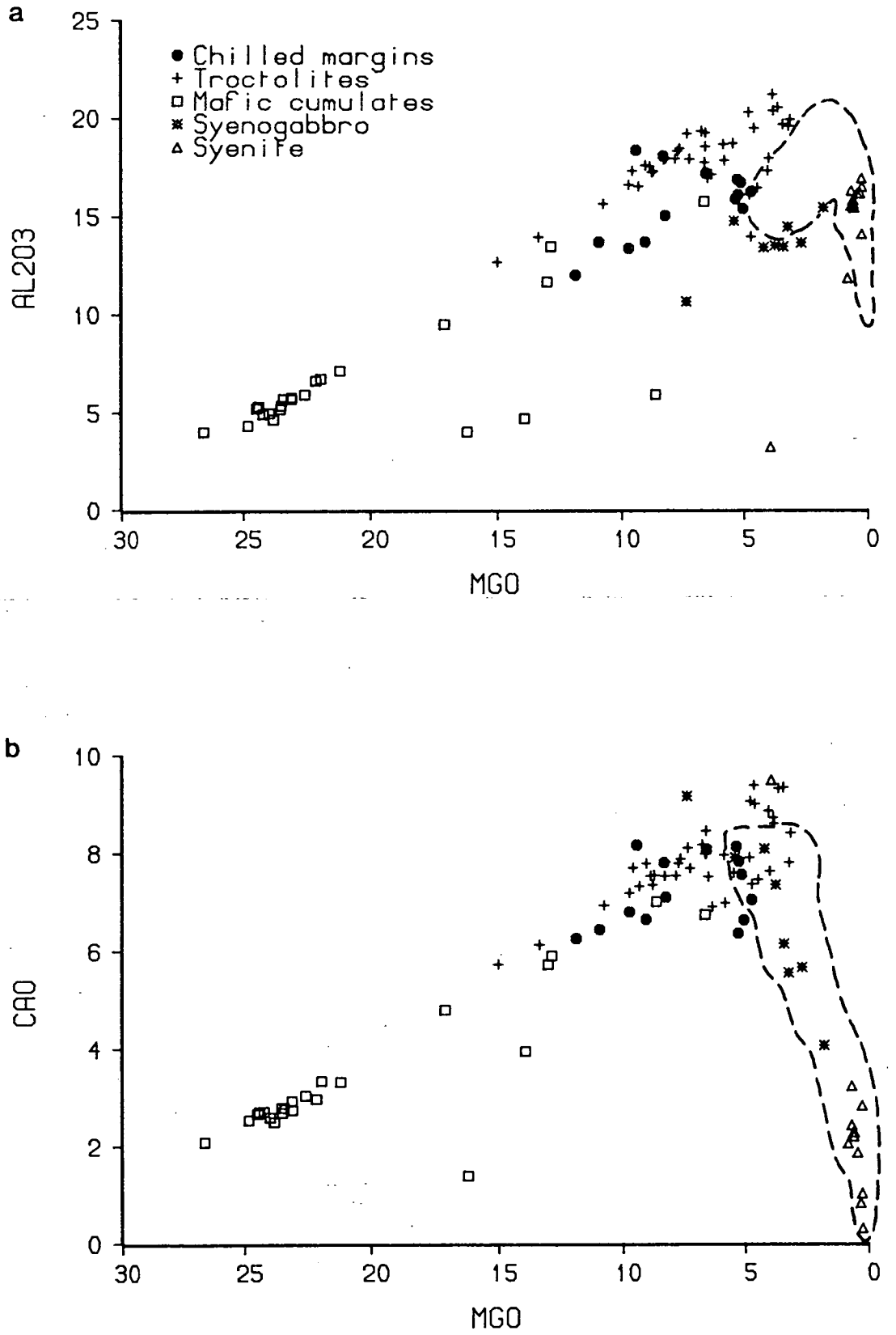


**Figure 4.3** (a) $Al_2O_3$ and (b) CaO plotted against MgO. Dashed lines indicate compositional field of smaller dykes, from Martin (1985).

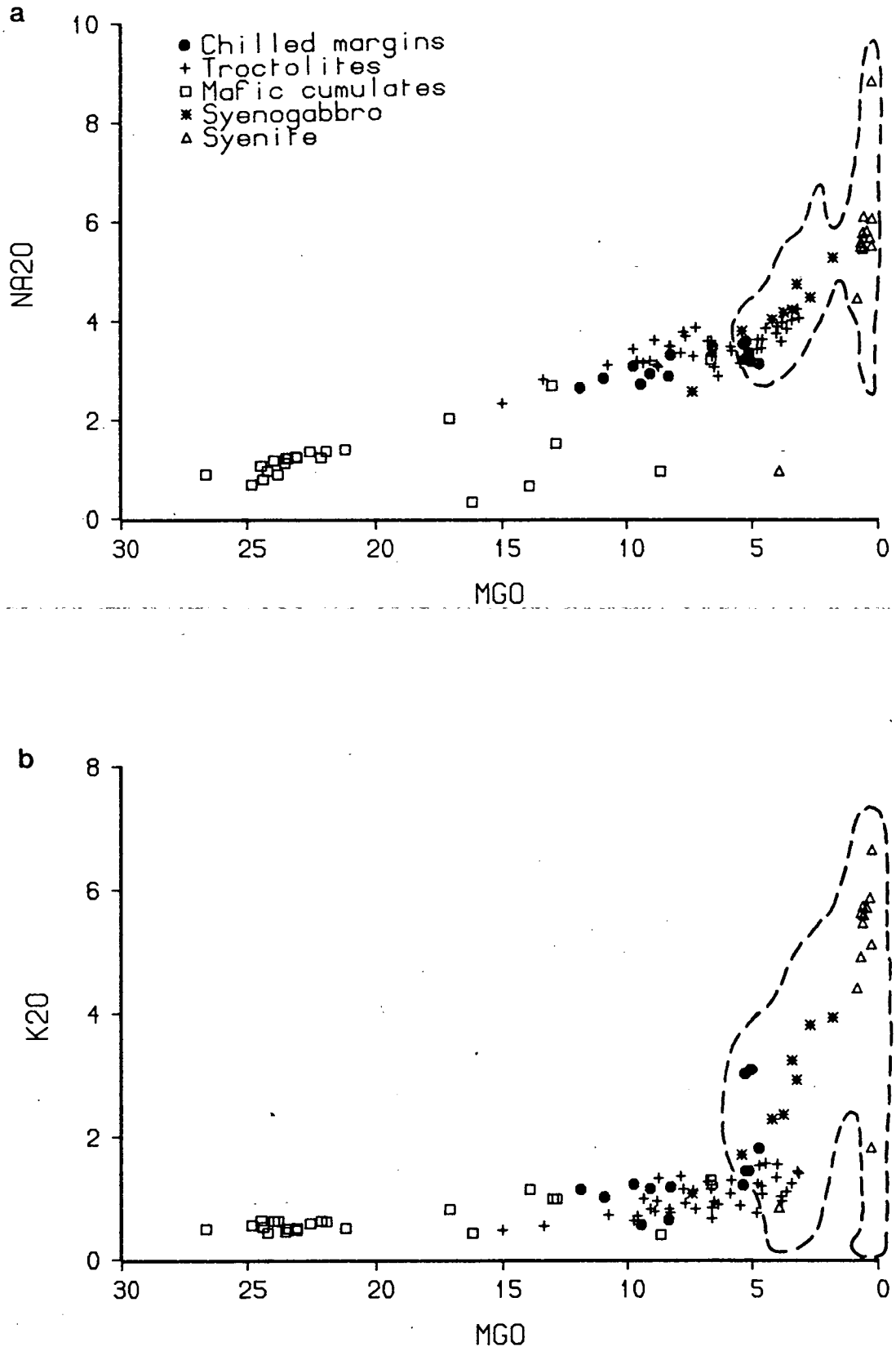


**Figure 4.4** (a) $Na_2O$ and (b) $K_2O$ plotted against MgO. Dashed lines indicate compositional field of smaller dykes, from Martin (1985).

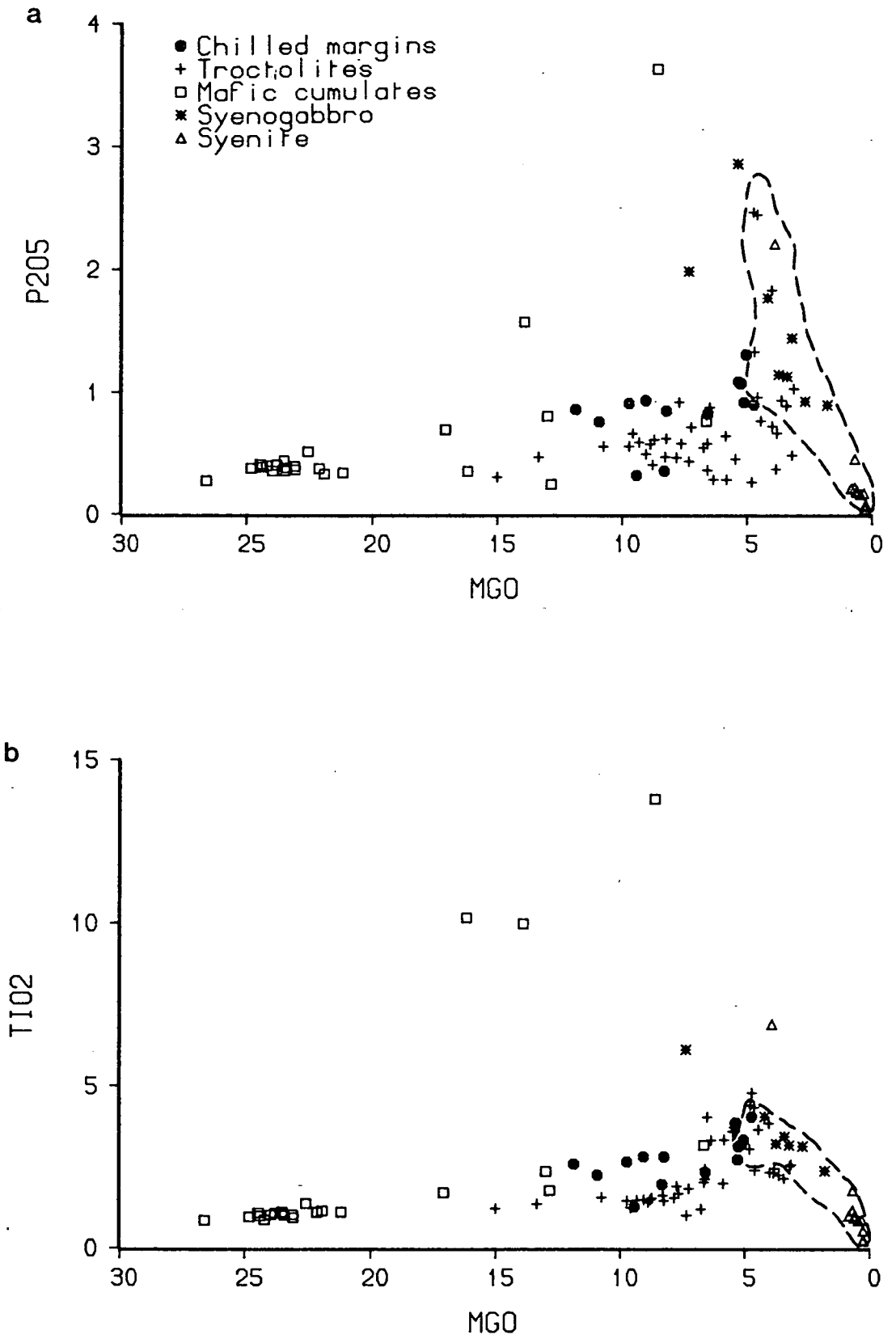


**Figure 4.5** (a) $P_2O_5$ and (b) $TiO_2$ plotted against MgO. Dashed lines indicate compositional field of smaller dykes, from Martin (1985).

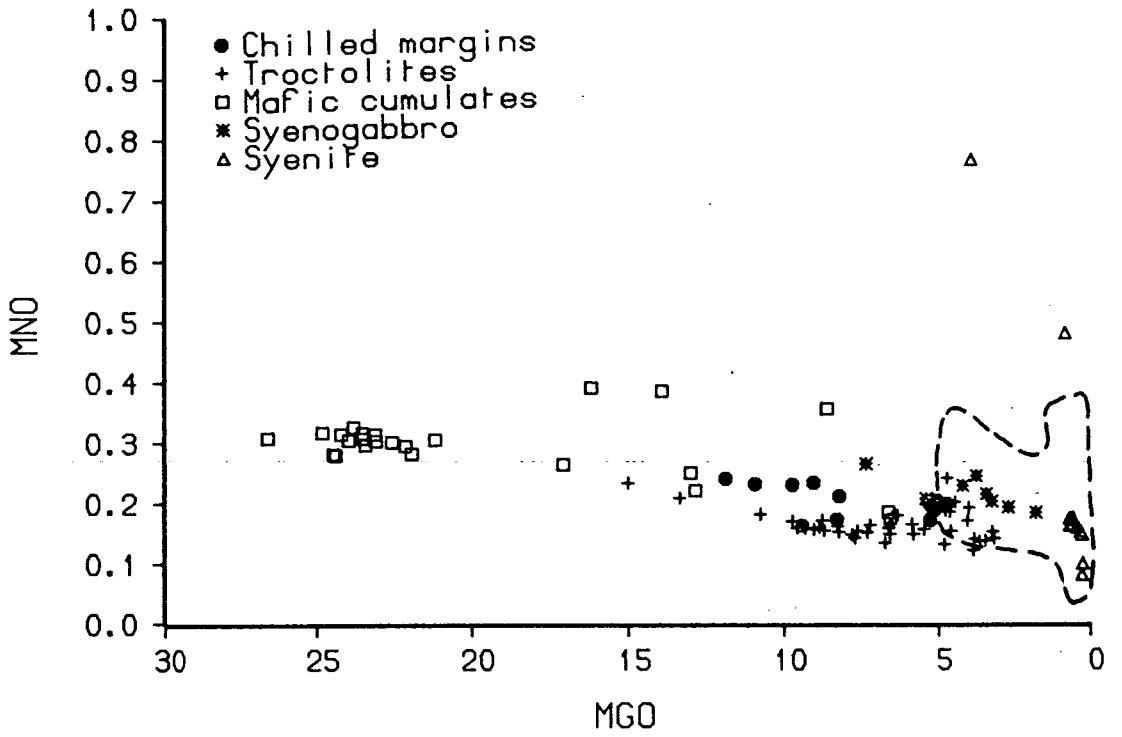


**Figure 4.6** MnO plotted against MgO. Dashed lines indicate compositional field of smaller dykes, from Martin (1985).

The regional swarm of smaller dykes, which may have had a similar magma source to the YGDC, has been studied by Macdonald (1969) and by Martin (1985). The compositional trend of this swarm, which has MgO contents from 6% to zero, is outlined on the plots of YGDC data.

Between about 15% and 5-6% MgO, $Fe_2O_{3(tot)}$ and MnO decrease in the chills and troctolites, whereas all other major elements increase. Two chills have unusually high $K_2O$, which may indicate alteration (Fig. 4.4b), although they show no field or petrographic evidence of contamination. From 5-6% MgO, $Al_2O_3$ and CaO begin to decrease in the evolved troctolites, syenogabbros and syenites, indicating the onset of plagioclase fractionation. $Fe_2O_3$ and MnO continue to decrease, but the decrease is more marked. $P_2O_5$ and $TiO_2$ begin to decrease when whole-rock MgO = 4-5%, suggesting apatite and Fe-Ti oxide fractionation. $SiO_2$, $Na_2O$ and $K_2O$ continue to increase. One syenite vein sample has unusually high $Na_2O$ (8.8%) and low $K_2O$ (1.8%).

The gabbro picrites are colinear with the chills and troctolites at higher MgO. The mafic cumulates which lie off the trend are high in $Fe_2O_3$, $TiO_2$, MgO and sometimes $P_2O_5$, indicating accumulation of magnetite and/or ilmenite and sometimes apatite. The mafic syenite cumulate, an olivine-oxide-clinopyroxene-apatite cumulate, contains about 4% MgO. It shows similar behaviour to the olivine + oxide $\pm$ apatite cumulates except that its CaO content is similar to that of the troctolites (Fig. 4.3b). This is because accumulation of clinopyroxene offsets the lowering of CaO due to magnetite accumulation.

Some troctolites and syenogabbros are rich in $P_2O_5$ (<1.2%) and have probably accumulated apatite. Some of the smaller dykes of Tugtutôq show similar high values and Martin (1985) suggested that they might have accumulated apatite phenocrysts. However, it is also possible that the magmas producing the smaller dykes were richer in $P_2O_5$ than those which gave rise to the YGDC.

A rather poor correlation is seen between $Al_2O_3$ in YGDC rocks and in the dyke swarm, with the troctolites being higher and the syenogabbros lower than the smaller dykes (Fig. 4.3a). Apart from this discrepancy, the more evolved rocks (MgO<5%) follow the trend of the smaller dykes quite closely and thus may themselves not be very different from liquid compositions (i.e. showing little cumulus character).

It can be seen that there is a distinct separation between chills and troctolites with MgO>6% on some of the major element variation diagrams. The troctolites are higher in $SiO_2$, CaO, $Na_2O$ and especially in $Al_2O_3$, but lower in $Fe_2O_3$, MnO, $K_2O$, $P_2O_5$ and $TiO_2$ than most of the chills. Two chills show the opposite behaviour; these are samples YGD78 and YGD298, both from the northern margin at locality B.

### 4.3.2 Trace element variation

Trace elements have also been plotted against MgO and are presented in Figs. 4.7 to 4.14. Thorium and lead have been omitted, since for most of the samples they are below detection limits. Thorium reaches a maximum value of 40ppm and lead of 51ppm in the syenites. As in the major element plots, a field for the smaller dykes is outlined on some diagrams.

There is a strong positive correlation between Ni and MgO, consistent with a dominant olivine control. Extrapolation to 35 wt% MgO (the composition of the most magnesian olivines) gives a Ni content of about 510 ppm. Cr and Zn generally decrease with decreasing MgO, although Zn remains constant or increases slightly when MgO<5%. One sample (YGD373) has an anomalously high Cr content of 210 ppm. V, Cu, Sc and Ba stay constant or increase slightly to about 5% MgO then decrease to low values in the syenites. Cu, Sc and Ba show a scatter of high values at around 3-5% MgO, probably indicating accumulation of sulphides, clinopyroxene and alkali feldspar respectively.

Sr shows a similar pattern to CaO, increasing until the onset of plagioclase fractionation at 5-6% MgO. Rb, Zr, Nb, La, Ce, Nd, and Y remain relatively constant or increase until MgO = 5 wt% then increase more rapidly in the evolved facies, showing incompatible behaviour. Three chills samples have unusually high Rb; two of these are from locality F and may possibly have been affected by fluids associated with the central complex. They also have high $K_2O$ (Fig. 4.4b). The third, with lower Rb, is from locality G. There is a distinct separation between the troctolites and the syenogabbros in the plots of rare earth elements (REE) and Y. The high values in the syenogabbros may be due to partitioning of the light REE and Y into the cumulus clinopyroxene; this possibility is reinforced by high values in the cpx-rich mafic syenite cumulate. Apatite accumulation is also important, as shown by high values in the olivine-oxide-apatite cumulate YGD158.

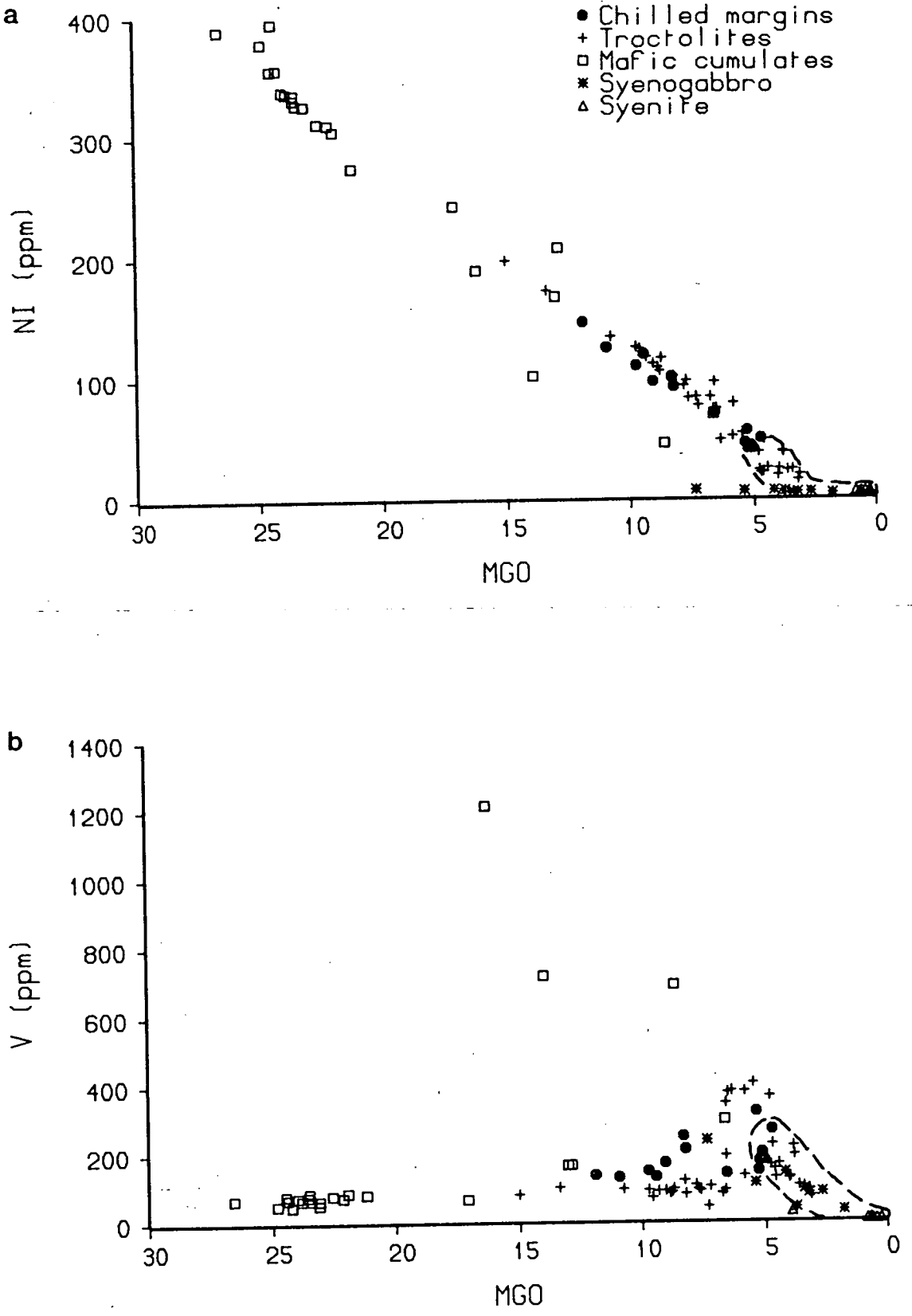


**Figure 4.7** (a) Ni and (b) V plotted against MgO. Dashed lines indicate compositional field of smaller dykes, from Martin (1985).

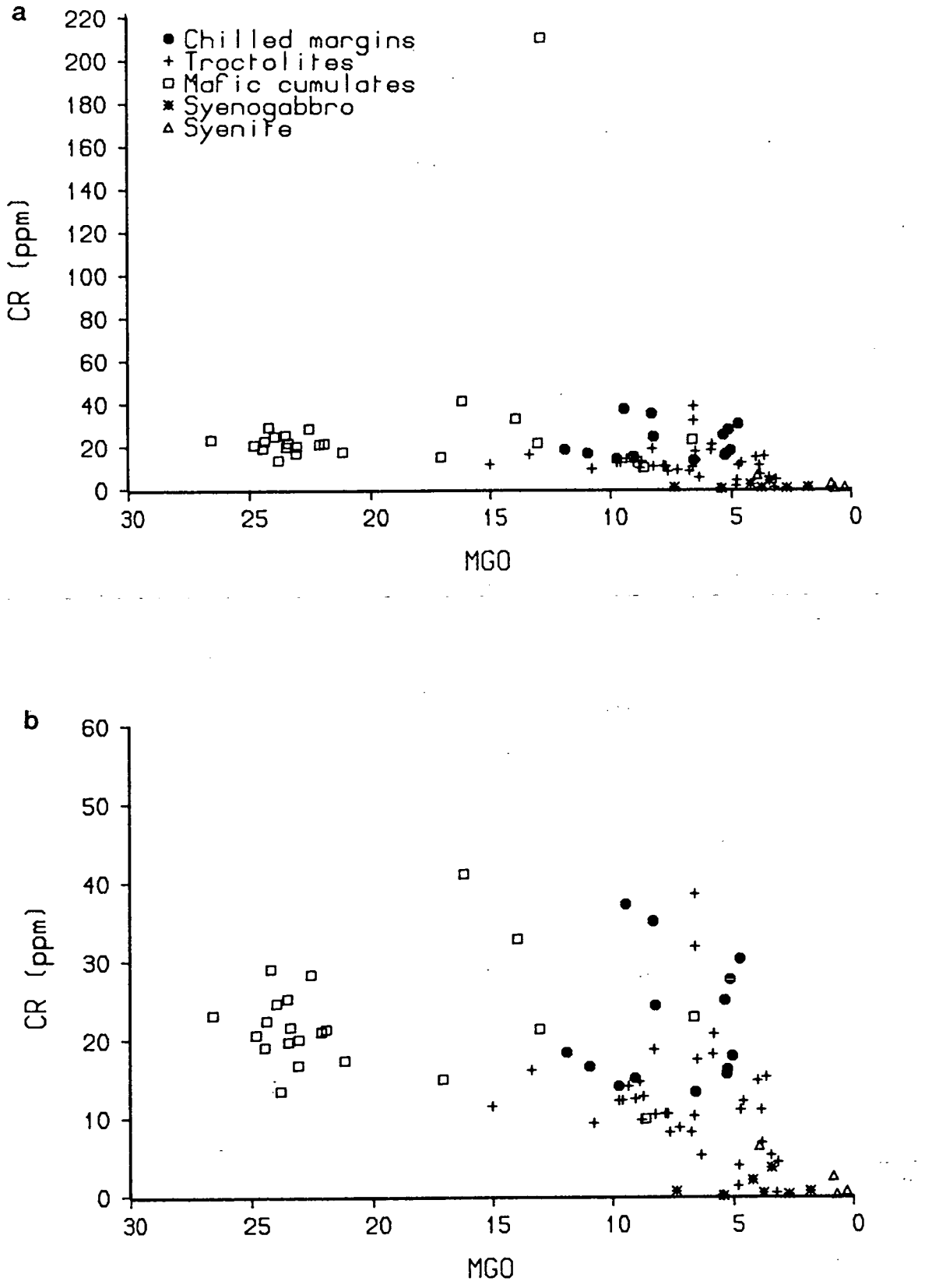


**Figure 4.8** Cr plotted against MgO. (a) and (b) show different scales.

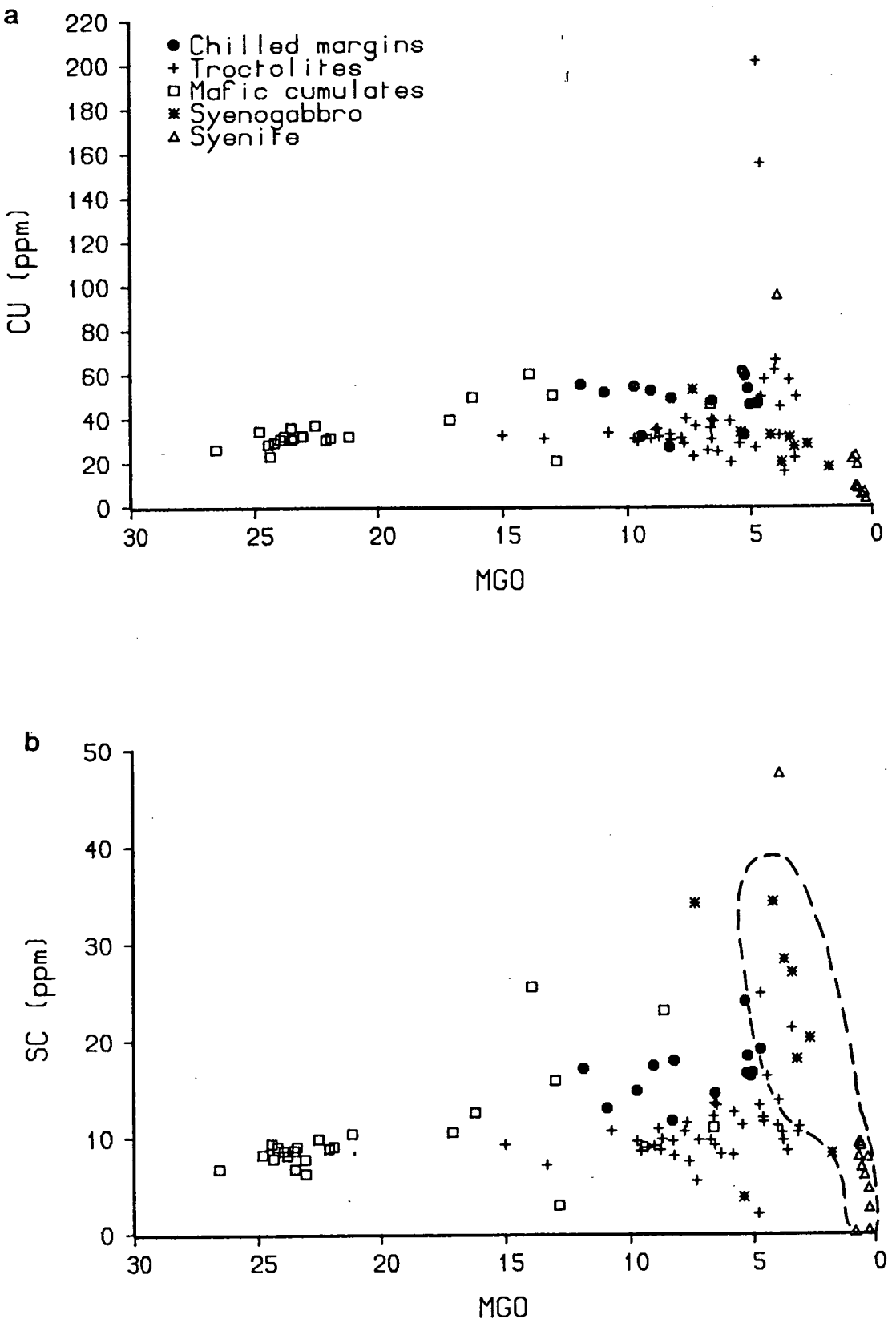


**Figure 4.9** (a) Cu and (b) Sc plotted against MgO. Dashed lines indicate compositional field of smaller dykes, from Martin (1985).

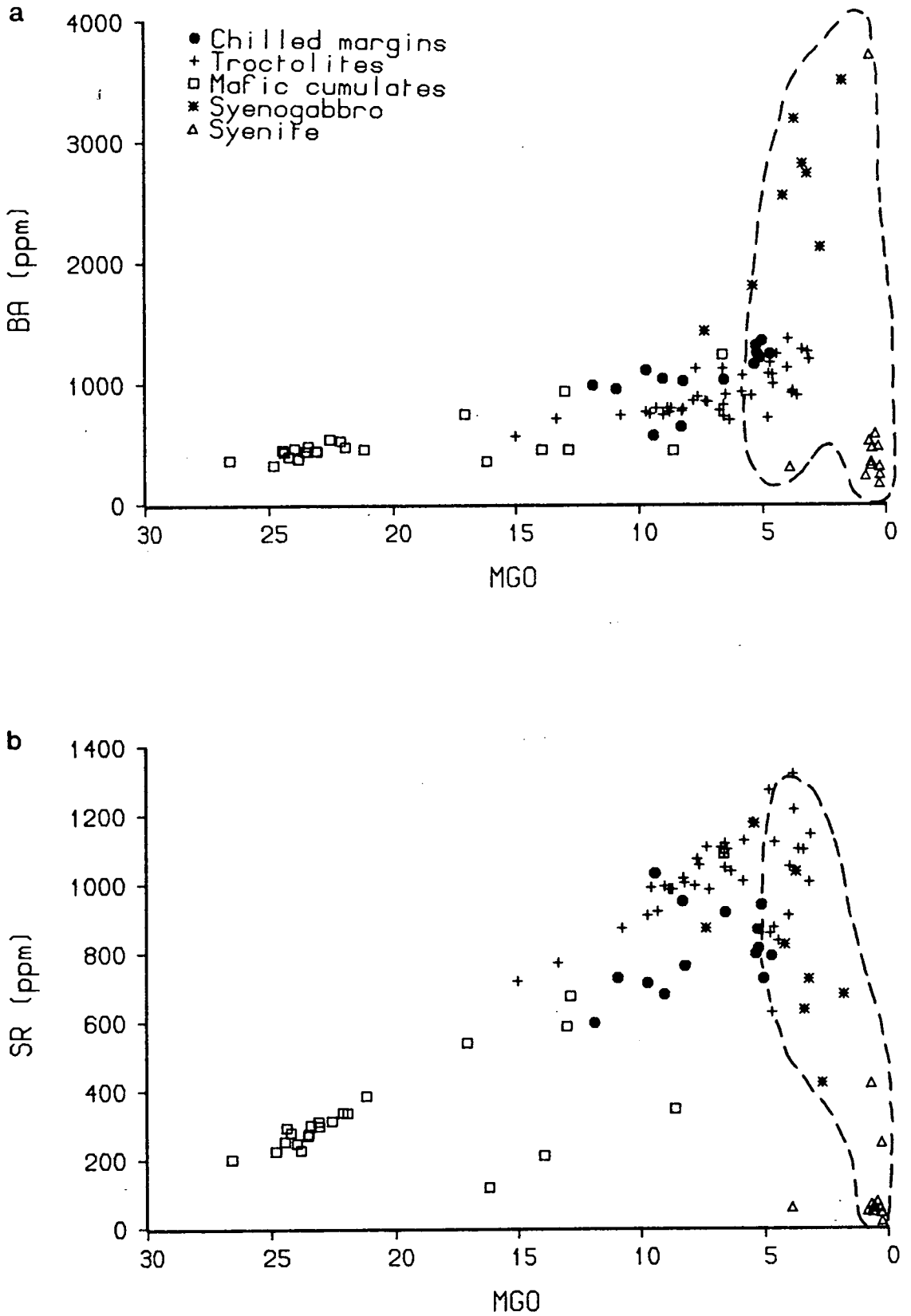


**Figure 4.10** (a) Ba and (b) Sr plotted against MgO. Dashed lines indicate compositional field of smaller dykes, from Martin (1985).

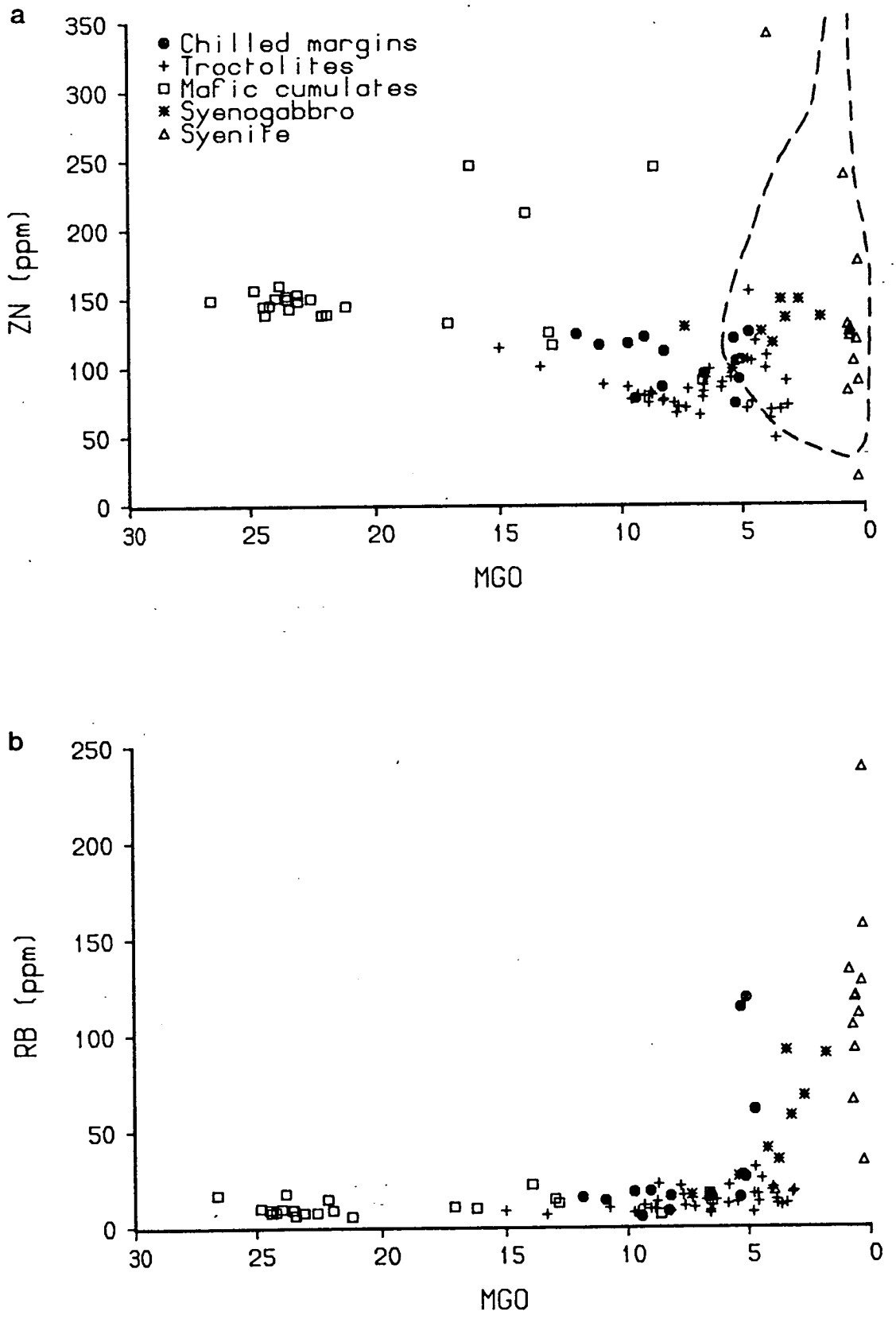


**Figure 4.11** (a) Zn and (b) Rb plotted against MgO. Dashed lines indicate compositional field of smaller dykes, from Martin (1985).

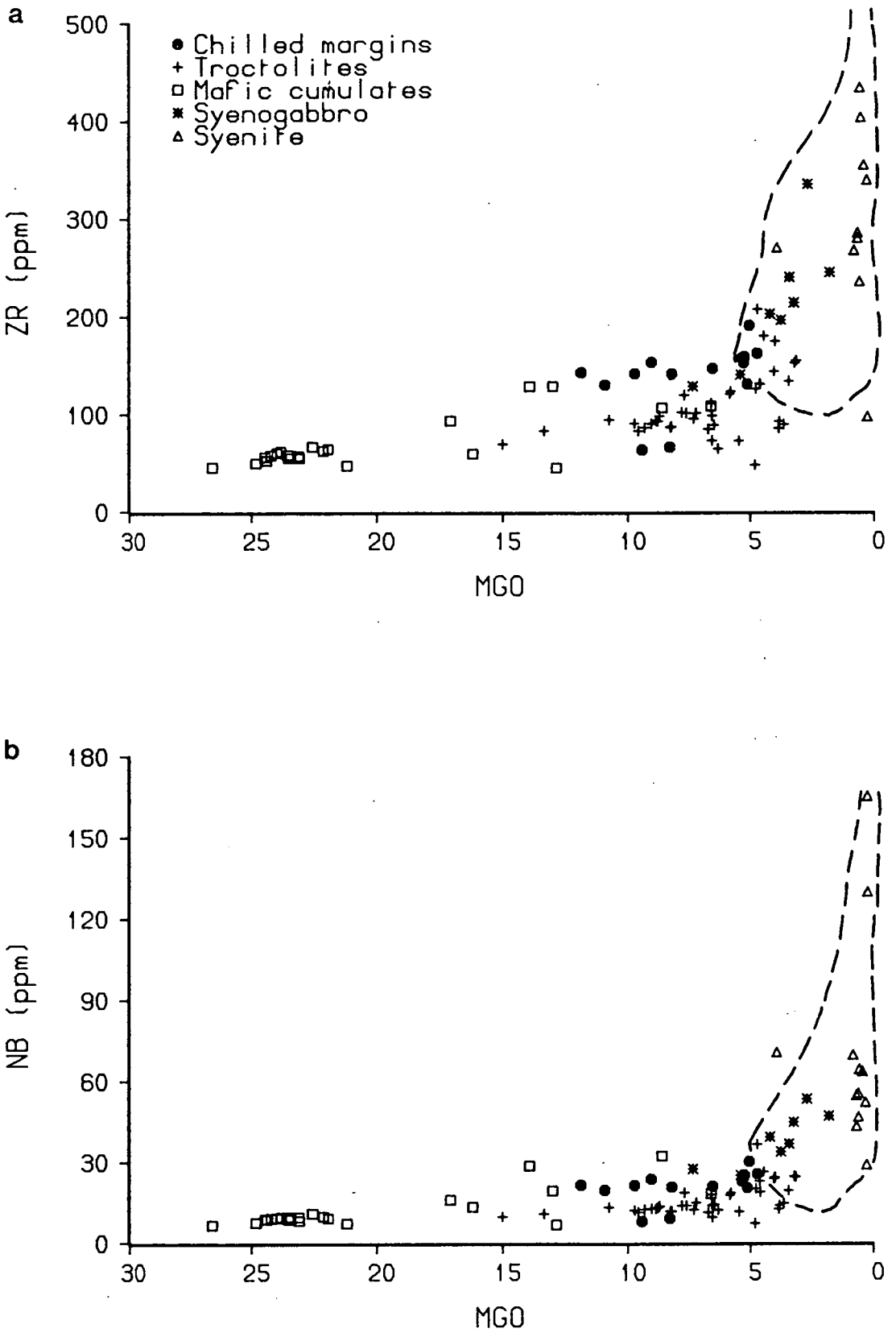


**Figure 4.12** (a) Zr and (b) Nb plotted against MgO. Dashed lines indicate compositional field of smaller dykes, from Martin (1985).

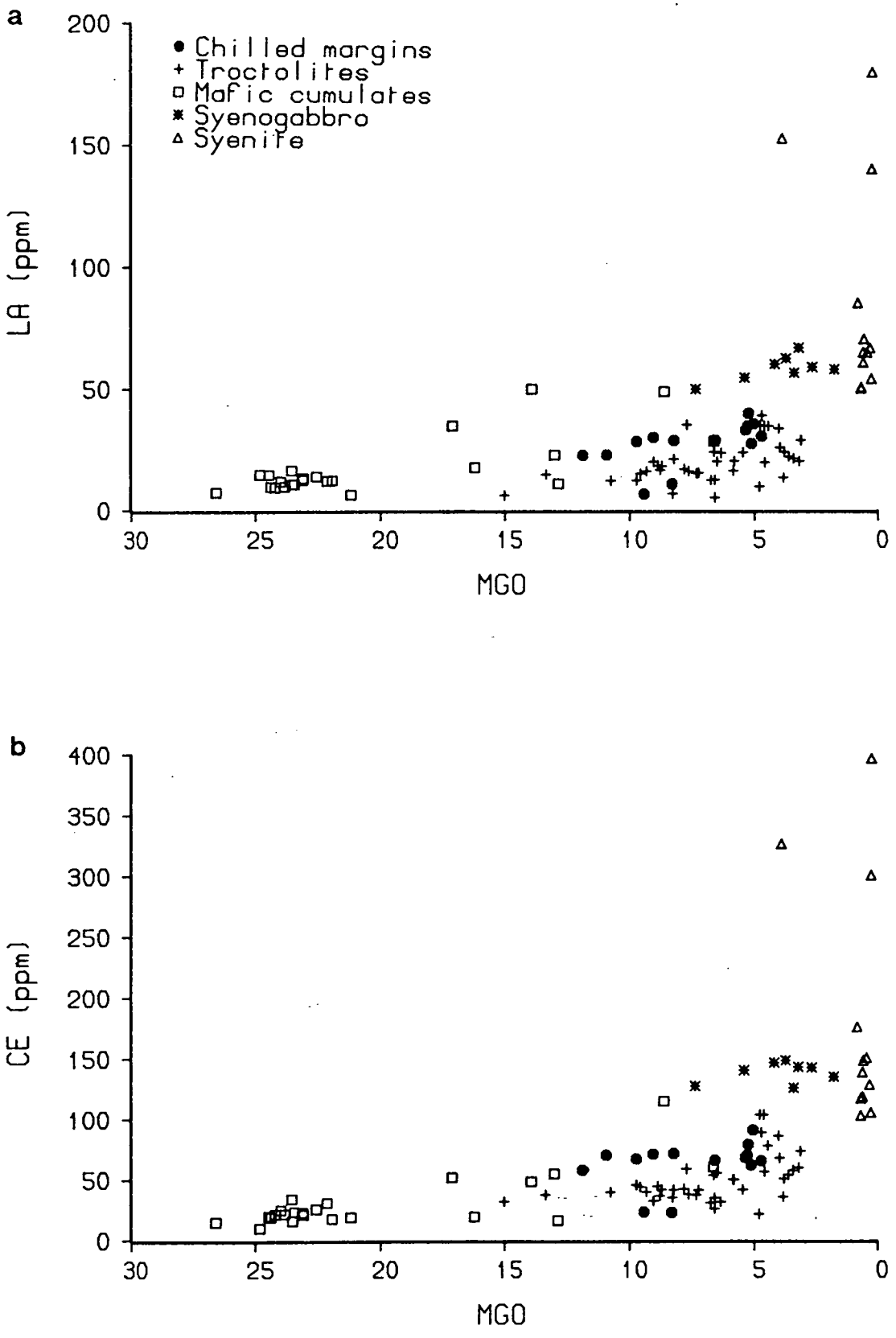


**Figure 4.13** (a) La and (b) Ce plotted against MgO.

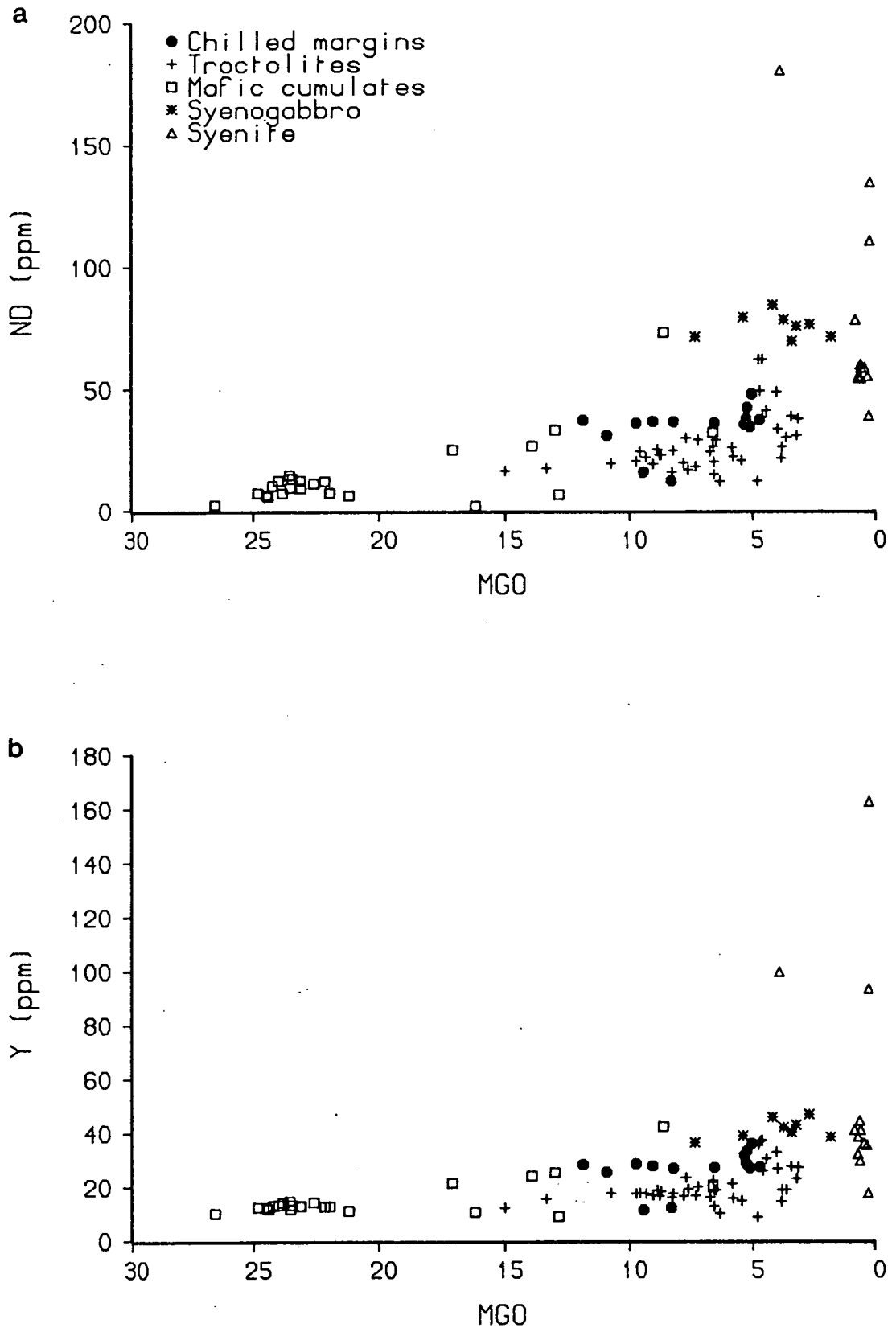


**Figure 4.14** (a) Nd and (b) Y plotted against MgO.

The gabbro picrites are again colinear with the chills and troctolites. The olivine + oxide ± apatite cumulates are high in V and Zn which partition into magnetite. Zn might be expected to decrease in the evolved rocks as a consequence of the fractionation of magnetite, but this is not observed. Zn also partitions into clinopyroxene (and to a small degree into alkali feldspar) (Henderson, 1982), so some accumulation of pyroxene and alkali feldspar in the evolved facies may have offset the expected decrease.

The mafic syenite is low in V, possibly indicating that it has accumulated ilmenite rather than magnetite. It is also low in Sr, despite being rich in Ca, probably because the liquid was depleted in Sr by the time the syenites crystallised.

In the same way as for the major elements, a marked separation is seen on some variation diagrams between the troctolites and most of the chills with MgO>6%. The chills are higher than the troctolites in all trace elements but Sr and, to a lesser extent, Ni. The two chills from the northern margin at locality B (YGD78 and YGD298) show the opposite behaviour.

### 4.3.3 Causes of MgO variation in the chills

The chilled margins show a range of MgO contents from about 12-5 wt%, but little correlation is seen between composition and locality. Two samples only a metre or less apart may sometimes differ by 5 wt% MgO. It is considered that contamination by country-rock granite was not a factor, since all samples were taken at least 1m from the dyke margins and appear fresh in hand specimen and thin section. (It was observed in Chapter 3 that samples close to the margins contain no olivine, but instead have abundant biotite, green amphibole, quartz and alkali feldspar.) In addition, it can be seen from Fig. 4.15 that the YGDC chill analyses do not lie on a mixing line between the most primitive chill composition and the country rock.

In thin section a population of olivine phenocrysts can be seen in the three most magnesian chills (>10% MgO) and in some other chill samples. These phenocrysts are only slightly larger than the groundmass olivines and are not obvious in hand specimen. However, it would take about 20% of olivine phenocrysts to account for all of the 7 wt% variation in MgO. The observed 5% or so phenocrysts

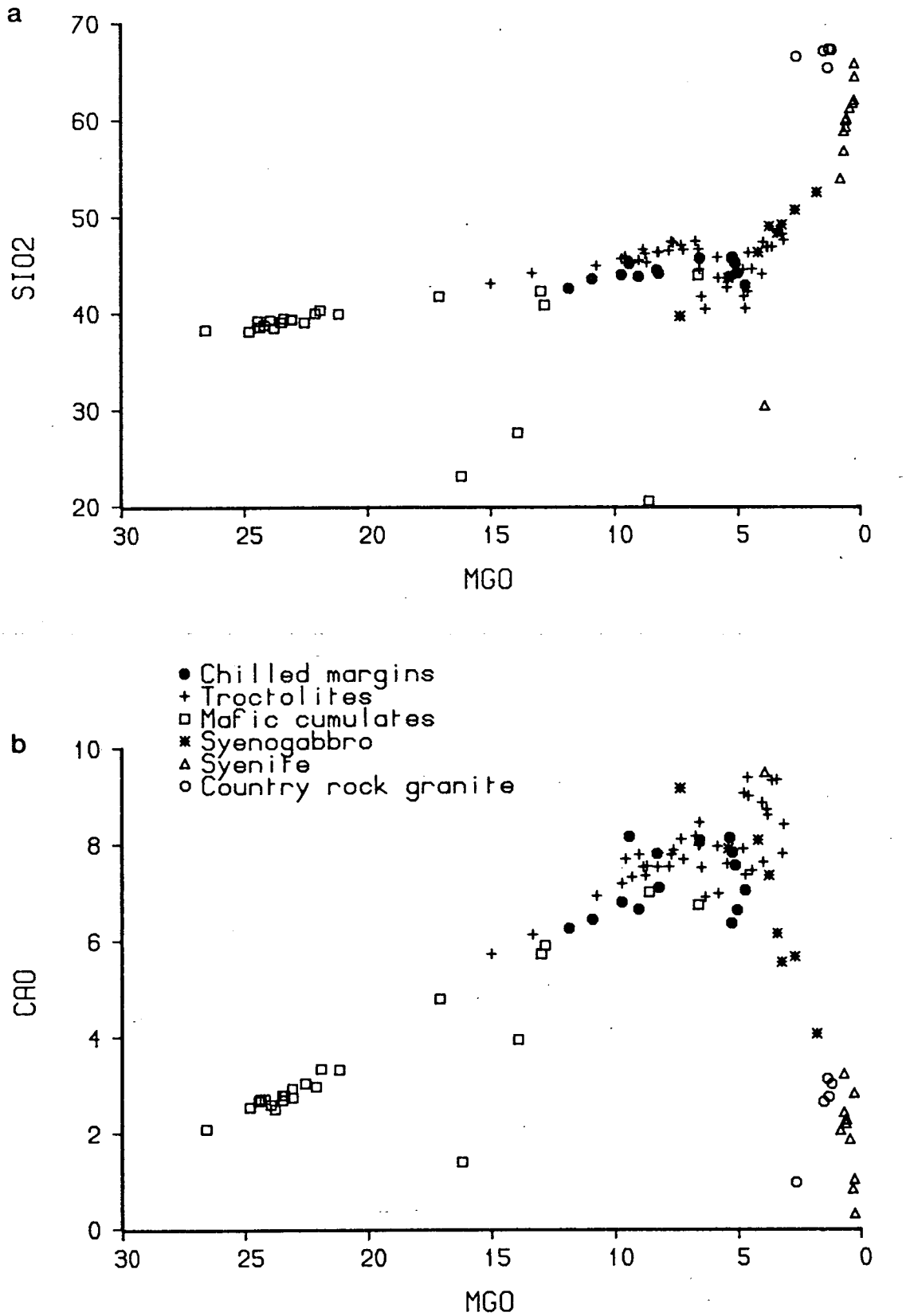


**Figure 4.15** (a) $SiO_2$ and (b) CaO plotted against MgO for both YGDC rocks and Julianehåb Granite.

could only account for up to 2% of the MgO variation, but it is possible that the liquids accumulated olivines which are of a similar size to other crystals in the rock and thus not readily identifiable.

Another possibility is that a heterogeneous (possibly stratified) magma chamber was present at depth and acted as a feeder to the YGDC. In this case, a range of magma compositions could have been available simultaneously at the time of intrusion. These possibilities will be explored further below.

The separation between most chills and troctolites with MgO>6% has been noted above. Two marginal samples from locality B show quite different behaviour from the other chills. Although these two chills themselves show no obvious differences in hand specimen or in thin section from other chill samples, it has already been noted (Chapters 2 and 3) that the troctolite slightly further into the dyke at this locality is distinctly different in character from the majority of troctolite exposed in the western YGDC. It is concluded that these two chills, and the rocks for about 20m into the dyke, crystallised from a rather different magma than the rest of the western YGDC. The relationships between the remaining chills and the troctolites are discussed in section 4.6.

## 4.4 Fractional crystallisation

### 4.4.1 Mineral/whole-rock plots

Mineral compositions obtained by electron microprobe analysis have been plotted with whole-rock trends on Figs. 4.16 and 4.17. For clarity, the number of mineral analyses has been reduced from those presented in Chapter 3, especially for olivine and feldspar. The olivine cumulates fall on a line between the chilled margin/troctolite compositions and olivine, although the line does not quite intersect the most magnesian olivines analysed ($Fo_{68}$). The intersected olivines have a composition of about $Fo_{66}$. The fact that a line through the whole-rock compositions does intersect the analysed olivines indicates that little re-equilibration of olivine with residual liquid has occurred. If it had done, the olivines would have become more iron-rich than when they crystallised. The field of olivine compositions would have shifted to lower MgO values and continuation of a line through the whole-rock analyses would no longer intersect the analysed olivines.

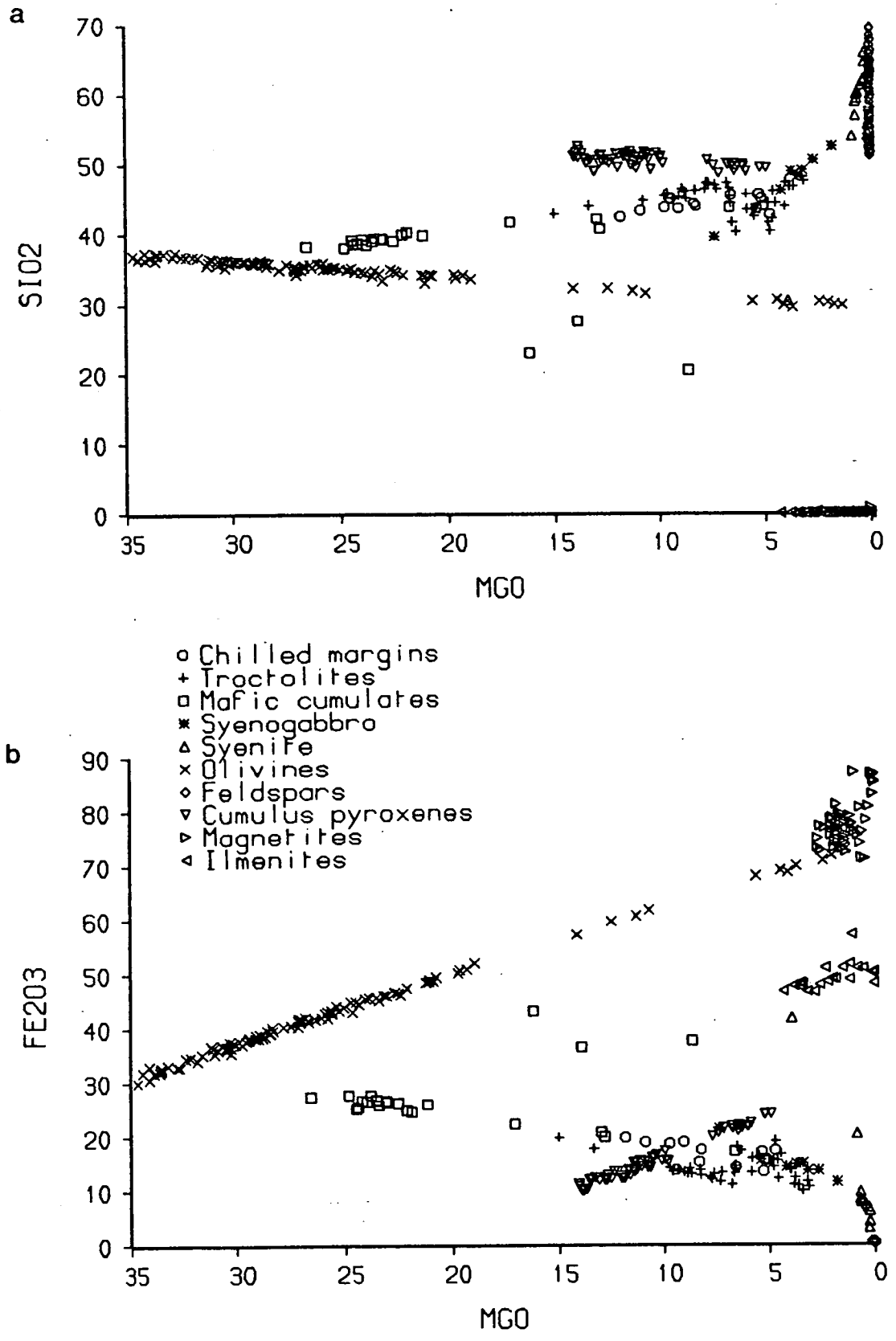


**Figure 4.16** (a) $SiO_2$ and (b) total iron as $Fe_2O_3$ plotted against MgO for whole-rock and mineral compositions. Figure continued over page.

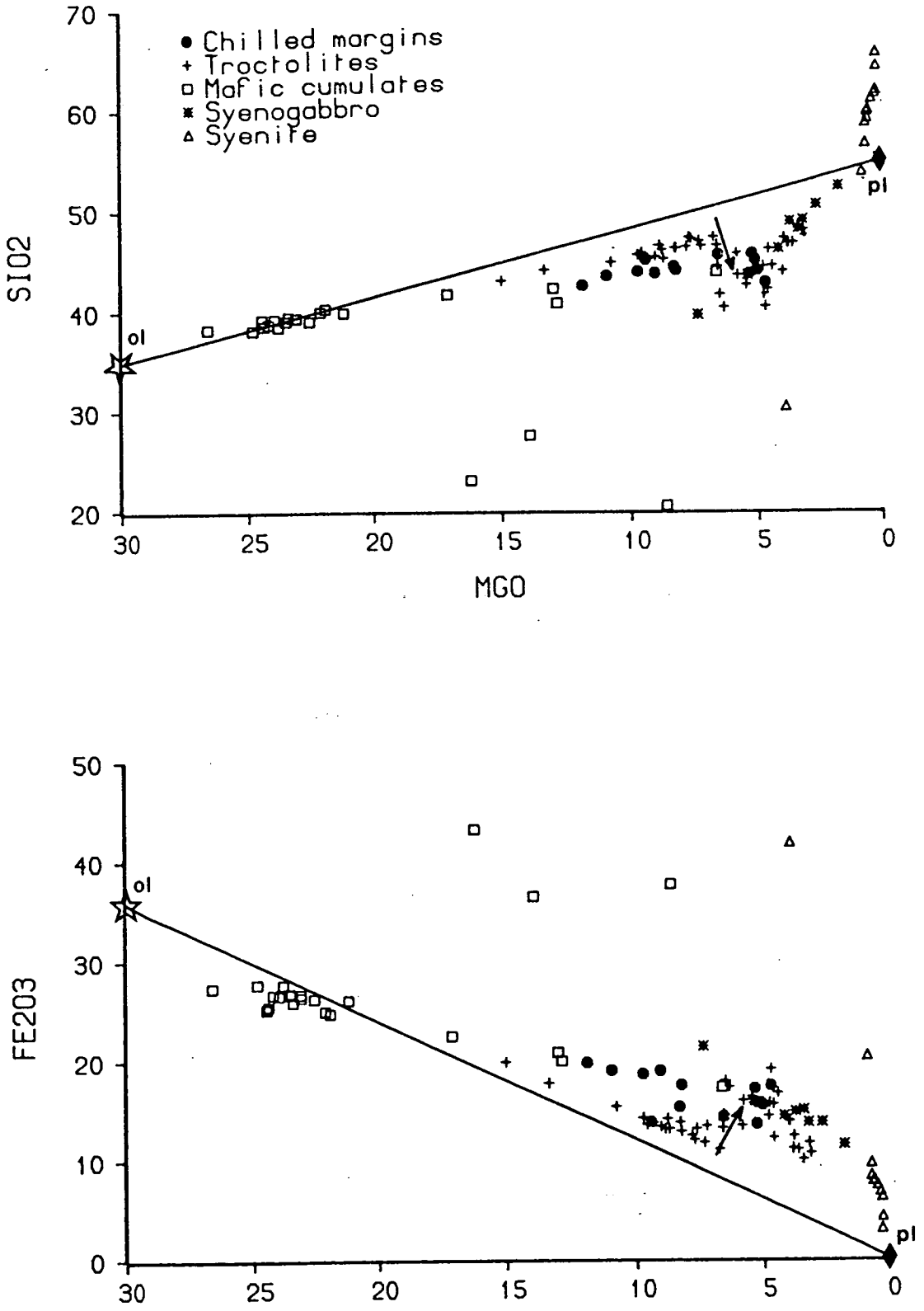


**Figure 4.16 (cont.)** (c) whole-rock $SiO_2$ and (d) $Fe_2O_3$ plotted against MgO. In both plots, the compositions of the olivine and plagioclase found in the chilled margins with 5-6 wt% MgO are indicated. Fractionation of these minerals produces the observed slight shift in whole-compositions in the direction of the arrows. The drop in $SiO_2$ and the rise in $Fe_2O_3$ are small because the compositions lie very close to the olivine-plagioclase tie-line.

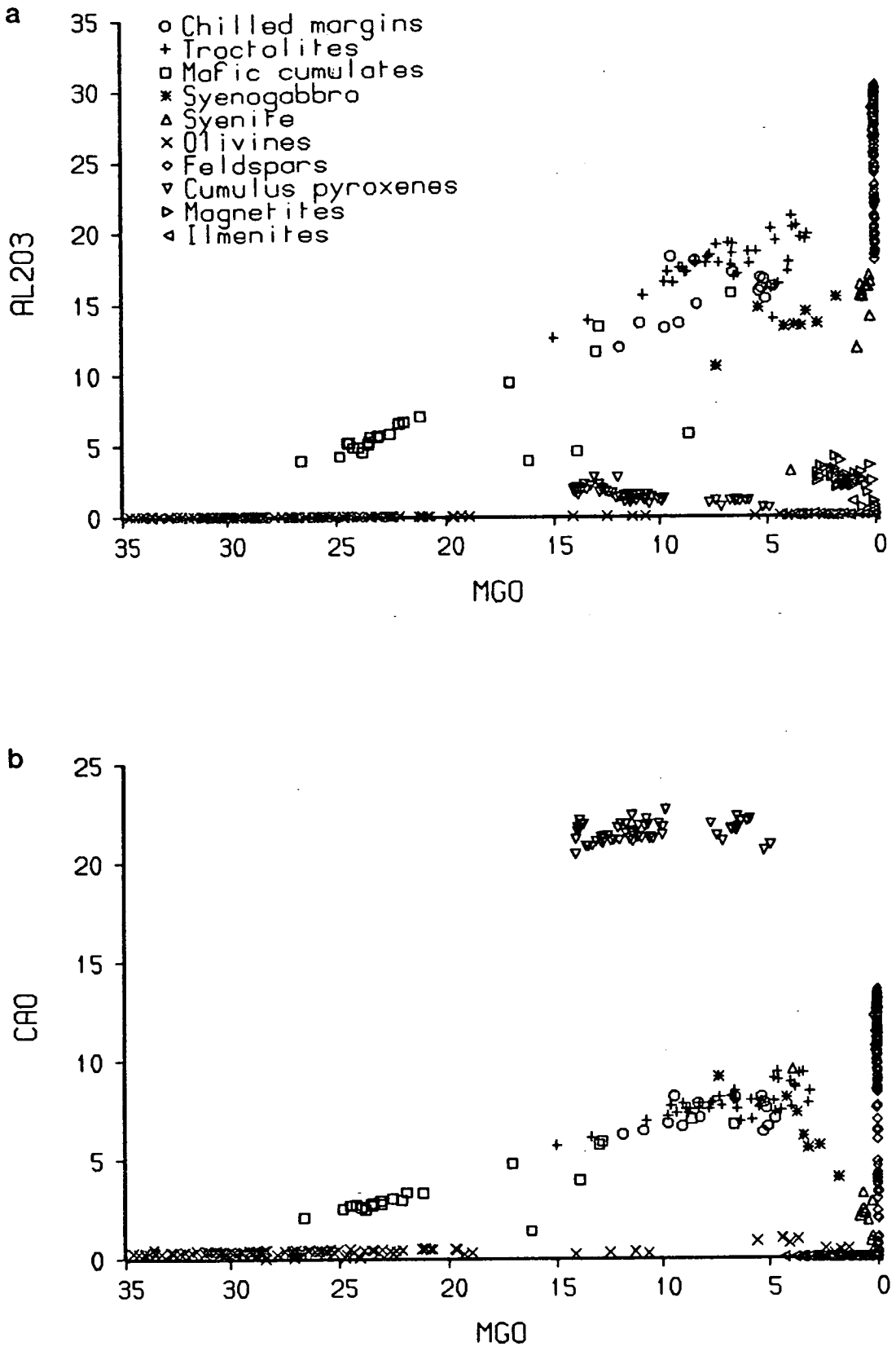


**Figure 4.17** (a) $Al_2O_3$ and (b) CaO plotted against MgO for whole-rock and mineral compositions.

In plots of $SiO_2$ and $Fe_2O_3$, fractionation of olivine could apparently account for the variation in the chilled margins and troctolites to about 6% MgO. However, the observed olivine compositions cover a much wider range than that expected from the linear trend defined by these compositions. The plots of $Al_2O_3$ and CaO against MgO (Figs. 4.17a and b) show a downturn at about 5% MgO, which is probably due to olivine + plagioclase fractionation in the rough proportions 1:3. These are also the observed phase proportions in the troctolites. Some fractionation of clinopyroxene could have contributed to this trend in the syenogabbros and syenites. A group of high-Al and high-Ca troctolites have probably accumulated plagioclase. Olivine and plagioclase fractionation should have led to a decrease in silica and an increase in iron, but only small shifts in whole-rock compositions occur at about 6-7 wt% MgO (Fig. 4.16c,d). However, this could be due to the fact that the compositions lie close to the olivine-plagioclase tie line, so relatively large amounts of fractional crystallisation would be needed for the compositions to move very far from the line. Alternatively, the trends may be explained by *in situ* crystallisation on the magma chamber floor where, although olivine + plagioclase were crystallising, they did not separate from the liquid. Residual liquid after crystallisation would have been denser than the bulk magma (see Chapter 7) and would have ponded at the floor until intercumulus oxides began to nucleate, producing a lighter liquid able to convect. Thus the signature of the residual liquids could reflect fractionation of non-liquidus phases (as suggested by Langmuir, 1989), in this case olivine + plagioclase + oxides.

The syenogabbros are relatively low in $Al_2O_3$ (Fig. 4.17a and Fig. 4.3a), possibly indicating slight accumulation of mafic minerals. The slight increase in $Al_2O_3$ from the syenogabbros to the syenites may indicate some fractionation of clinopyroxene. The plots of $TiO_2$ and $P_2O_5$ against MgO (Fig. 4.5 a and b) showed that Fe-Ti oxides and apatite began to fractionate at roughly the same time as each other (when the MgO content of the liquid was about 4%). Petrographic examination of mafic cumulates showed that in different areas, apatite could appear at the same time as, or after Fe-Ti oxides. Thus the order of appearance of fractionating phases appears to have been: olivine, plagioclase, magnetite + ilmenite + apatite, clinopyroxene, as predicted from the petrography. This agrees with other workers (Upton and Thomas, 1980; Upton, 1987) who suggested that oxides and apatite appeared when the liquid MgO content was 4.0-3.5 wt% and cpx at MgO = 3.5-3.0 wt%.

The trace element data presented in Figs. 4.7-4.14 agree qualitatively with the fractional crystallisation model developed from the major element data. Certain trace

elements are key indicators for the fractionation of particular minerals; nickel for olivine, strontium for plagioclase, vanadium for magnetite, scandium for clinopyroxene and barium for alkali feldspar. These elements indicate removal of these minerals in the order olivine, plagioclase, Fe-Ti oxides, clinopyroxene, alkali feldspar. Quantitative modelling has not been attempted because the coarse-grained rocks do not represent true liquid compositions.

The late entry of clinopyroxene into the fractionating assemblage is very unusual for basaltic magmas. Upton and Thomas (1980) suggested that this may have been due to low $fO_2$ conditions, resulting in turn from the relatively anhydrous nature of the magmas. The high Al/Ca ratio of the magmas must also have played a part in delaying pyroxene nucleation.

### 4.4.2 CMAS plots

The pseudoquaternary CMAS system of O'Hara (1968) is useful for studying fractional crystallisation since it avoids the problem of changing mineral compositions. In this scheme, all Fe-Mg-Mn-Ni olivines plot at $M_2S$, all Ca-Na-K feldspars at $CAS_2$, and clinopyroxenes between Di and Hd at $CMS_2$ (Fig 4.18). The system is suitable for basic and ultrabasic rocks but caution must be exercised in applying it to the YGDC rocks which are relatively rich in iron and alkalis. Nevertheless, the CMAS system plots shown in Figs. 4.19 to 4.21 reinforce the strong olivine control seen in the variation diagrams. Only olivine-oxide cumulates plot away from the trend. In particular, Fig. 4.20, which is projected from olivine, shows a tight cluster of points; fractionation of another phase would give a trend away from this cluster. However, these plots also show how close the compositions are to the olivine-plagioclase tie-line, indicating that about 50% olivine + plagioclase fractionation might be required to produce a trend away from the line. If less fractionation occurred it would probably not be distinguishable. The scatter in the syenites is probably due to feldspar fractionation.

For the purposes of these plots, all iron has been plotted as FeO, since the presence of any $Fe_2O_3$ gives a trend which does not intersect olivine and also laterally separates the mafic cumulate data from the troctolites and chills.

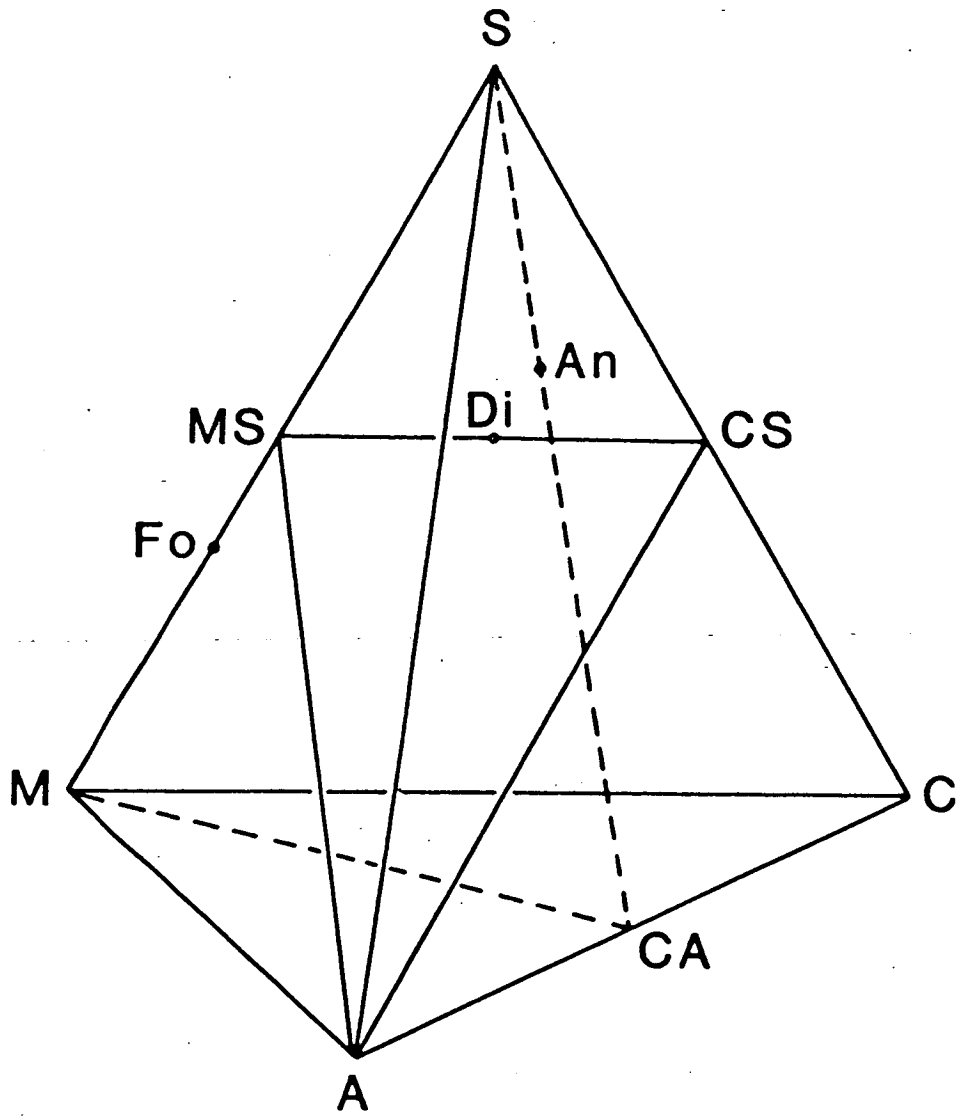


**Figure 4.18** The CMAS system of O'Hara (1968) with comers defined as follows:

C = (molar props. $CaO\text{-}3.33P_2O_5+2Na_2O+2K_2O$) x 56.08

M = (molar props. $MgO+FeO+MnO+NiO\text{-}TiO_2$) x 40.311

A = (molar props. $Al_2O_3+Cr_2O_3+Fe_2O_3+TiO_2+Na_2O+K_2O$) x 101.961

S = (molar props. $SiO_2\text{-}2Na_2O\text{-}2K_2O$) x 60.085

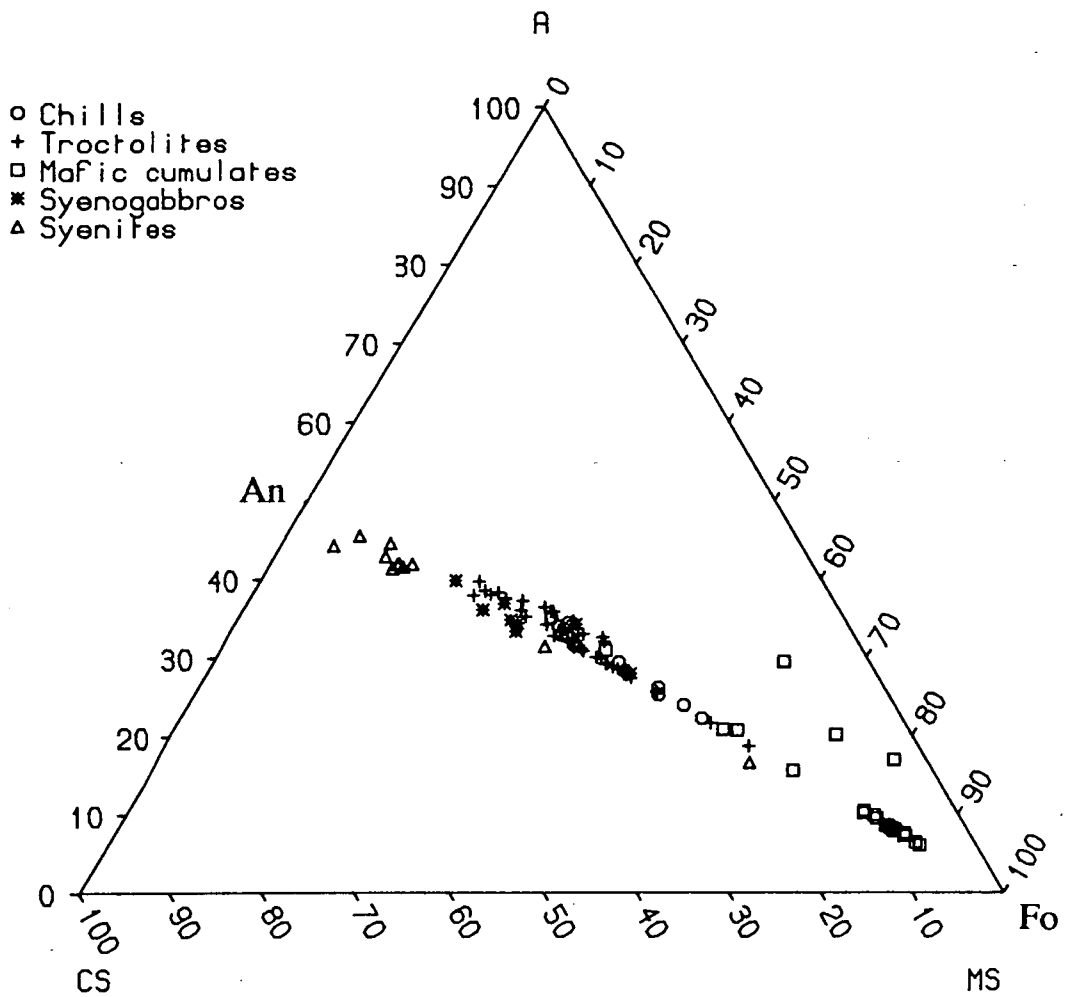


**Figure 4.19** Projection from S onto the plane CS-MS-A in the CMAS system.

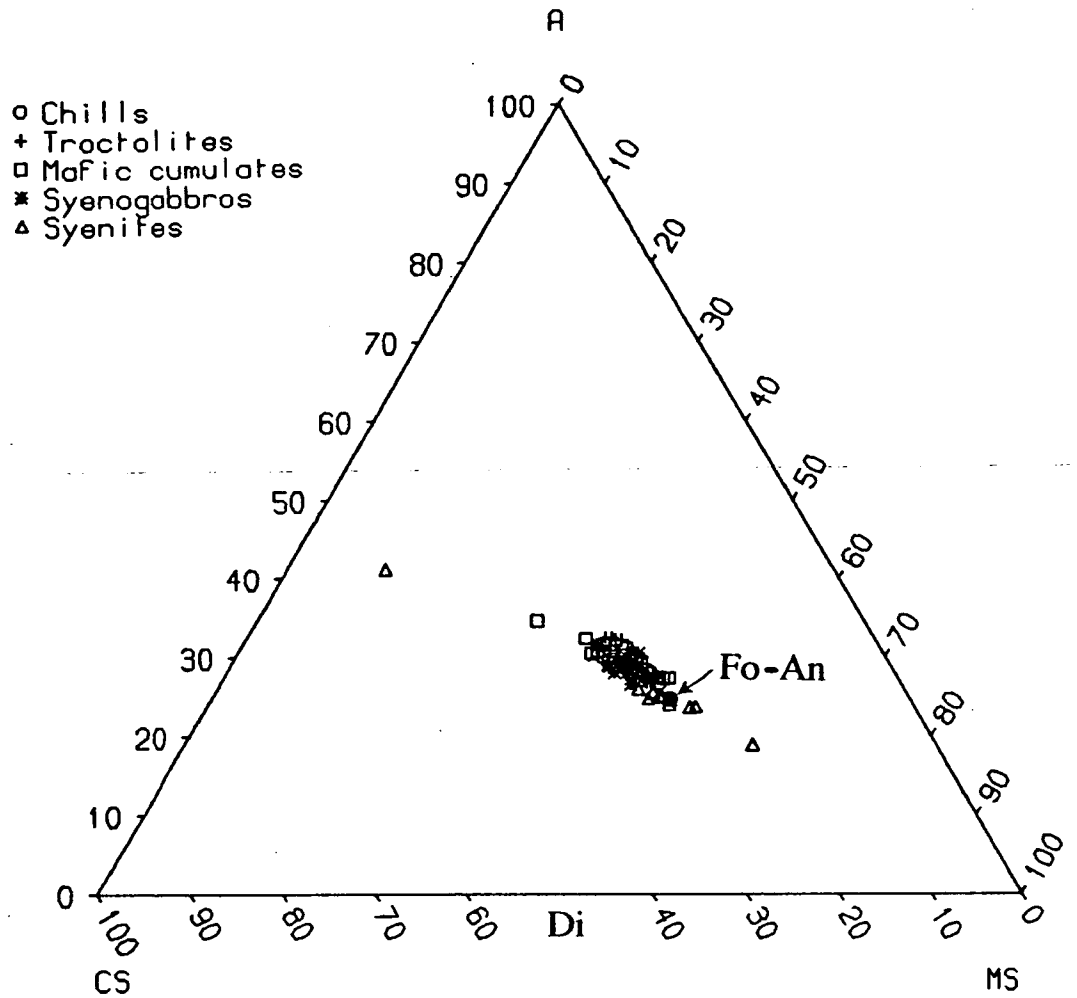


**Figure 4.20** Projection from $M_2S$ (olivine) onto the plane CS-MS-A in the CMAS system.

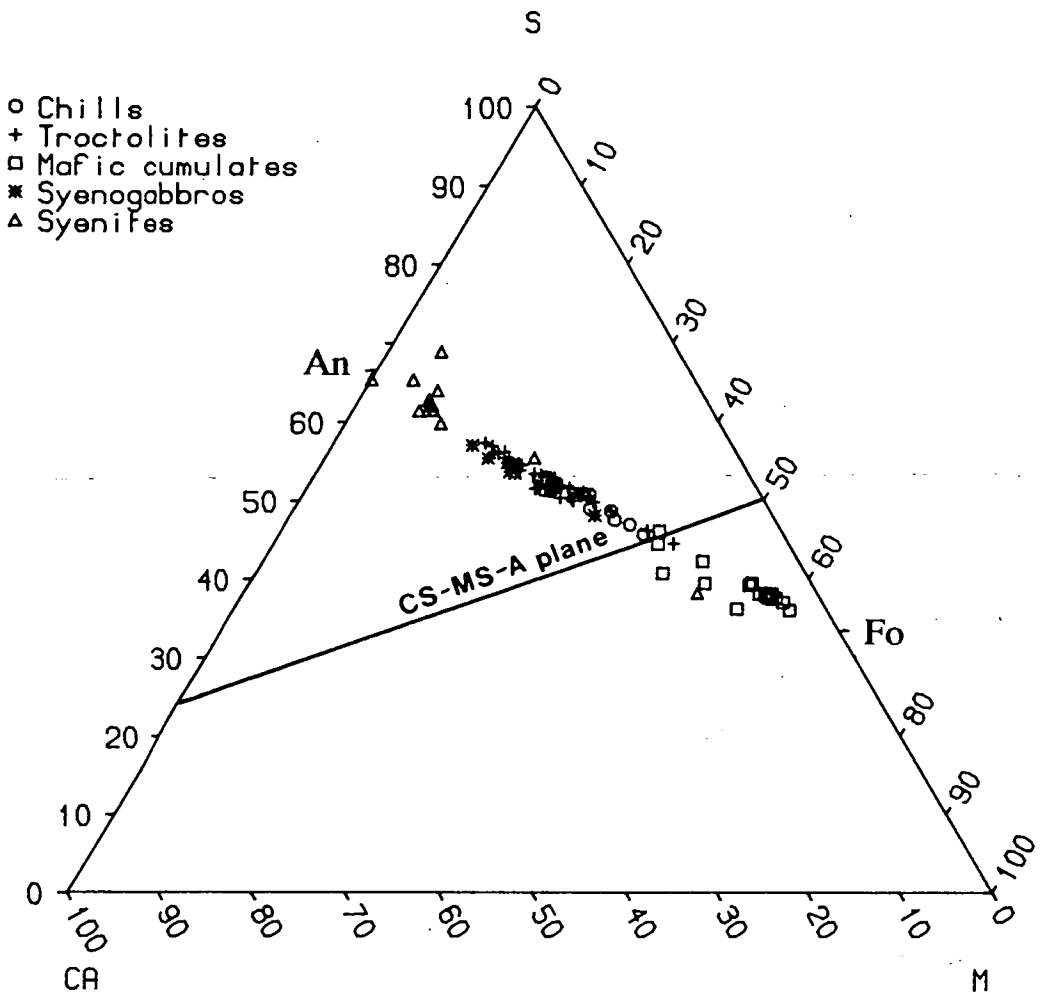


**Figure 4.21** Projection from $CMS_2$ (diopside) onto the plane CA-M-S in the CMAS system.

### 4.4.3 Numerical modelling

Liquidus temperatures and phase compositions can be predicted by means of computer programs (e.g. Nathan and Van Kirk, 1978). The method employed is to use theoretical equations with coefficients constrained by experimental data. The program used here was written by C.E. Ford and uses a large experimental data set of basic and ultrabasic rocks (see Ford, 1981). The effects of pressure have not been considered, since the YGDC is thought to have solidified at a pressure of <3kbar and in this range, pressure has little effect on the liquidus temperatures of olivine and plagioclase. The $Fe^{3+}/(Fe^{2+}+Fe^{3+})$ ratio was set at 0.15.

The program predicts all chill samples to have olivine on the liquidus, although those with low MgO (4-5 wt%) are only slightly above the temperature at which plagioclase begins to crystallise. Predicted liquidus temperatures are plotted against whole-rock MgO in Fig. 4.22, with predicted olivine and plagioclase compositions also indicated. The program correlates the data set to within 10-20°C, but a few compositions give larger errors than this (Ford, pers. comm., 1990). Samples YGD78 and YGD298 lie slightly off the trend, another indication that they do not represent the same magma as the other chills. For most samples with MgO<6 wt%, plagioclase was predicted to begin crystallising at between 1140 and 1160°C (one sample (YGD122) gave a temperature of 1105°C), with compositions of $An_{68}$-$An_{63}$. These plagioclase compositions are very similar to those found in the troctolites. Predicted co-existing olivine compositions are $Fo_{72}$-$Fo_{68}$ which are also close to the fractionating composition of about $Fo_{66}$. It appears that the predictions are realistic and indicate that the YGDC chills reached the ol-pl cotectic when whole-rock MgO was about 5 wt%. Samples more magnesian than MgO = 6% have predicted olivine compositions more magnesian than those of the analysed olivines, as found by Ford and Upton (1980). This might be explained by the fact that the olivines in the rocks are those which crystallised at the ol-pl cotectic and have re-equilibrated from liquidus compositions. However, it was shown in section 4.4.1 that the olivines which apparently *fractionated* to produce the variety of compositions seen in the chilled margins and troctolites had the compositions of some of the olivines found in the rocks (about $Fo_{66}$). Only the samples with around 5 wt% MgO crystallise olivine of near this composition. This suggests that these samples in fact represent the liquid compositions from which much of the YGDC crystallised, while other chill samples, and troctolites more magnesian than about 6 wt% MgO, accumulated olivine. The lines that can be drawn through the chills and gabbro

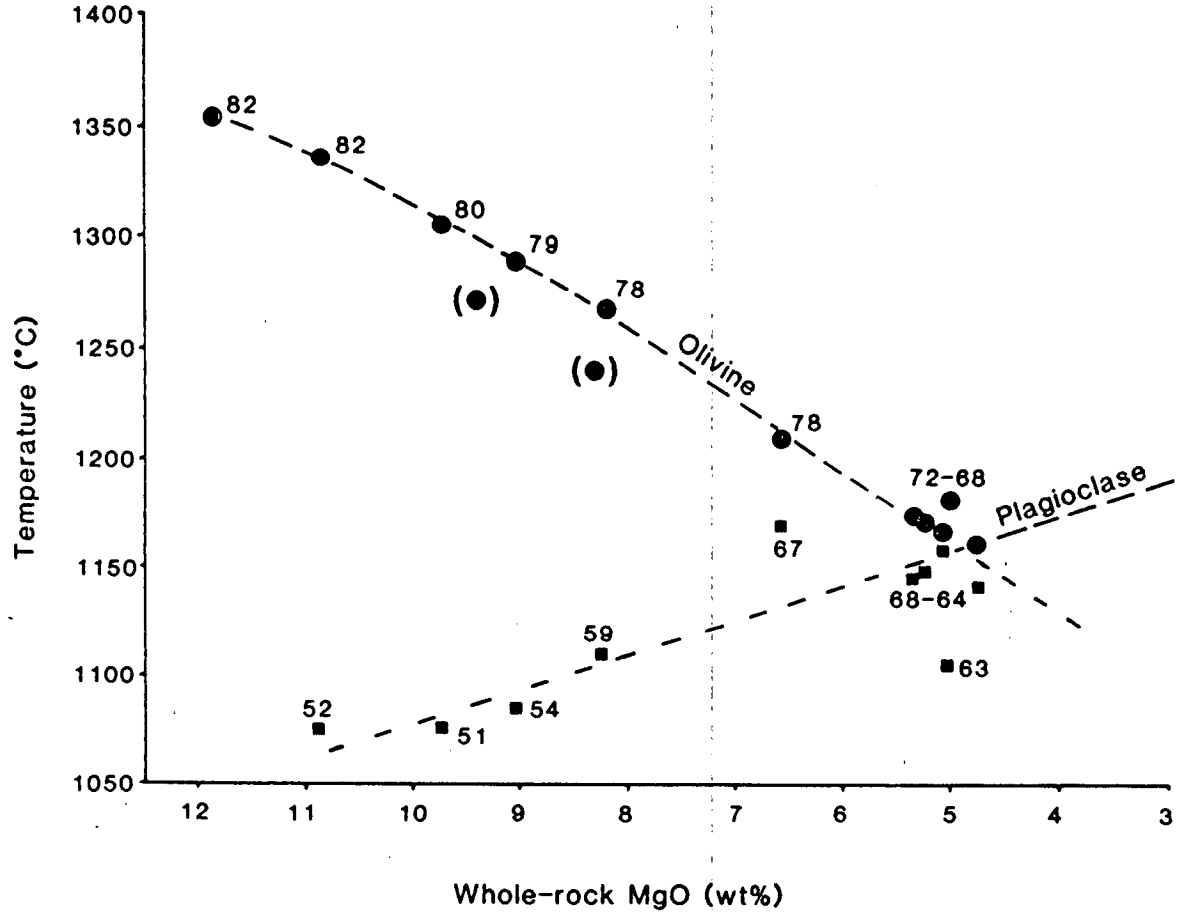


**Figure 4.22** Liquidus temperatures for olivine (circles) and plagioclase (squares) in the YGDC chilled marginal samples, predicted using the program SATURATE, plotted against whole-rock MgO. Numbers next to points are predicted compositions as forsterite contents for olivine and anorthite contents for plagioclase. The two points in brackets are YGD78 and YGD298, which do not fit the trend defined by the other samples.

picrites or the troctolites and picrites are straighter than would be expected for fractional crystallisation of olivine with changing composition, which should produce curved lines. This suggests "mixing" between liquid and olivine (accumulation).

### 4.4.4 Fractionation within the dyke

Suites of samples were collected across the dyke segments from margin to centre at localities D, G and L of Fig. 2.1. Selected trace elements have been plotted against distance in Figs. 4.23 and 4.24.

At locality D (Itivdlip Sarqâ) and locality G (Marrait) it can be seen that trace element abundances are fairly constant, except that, as seen in the variation diagrams (section 4.4.1) the chilled margins are richer than the troctolites in all trace elements except strontium and, at locality G, barium. There is no evidence for increased degrees of fractionation towards the centre of the dyke.

Locality L is characterised by a central syenite pod flanked by a zone of syenogabbro containing elongate pyroxene crystals (section 2.3.3). These lithologies are indicated on Fig. 4.24. Several trace elements show inconsistent variation in the syenogabbro zone, probably due to the fact that samples in this zone were drill cores and thus probably too small to be modally representative of such a coarse-grained rock. Incompatible elements (Rb, Zr and the REEs) together with Zn, increase through the syenogabbro to the syenite while Sr decreases, indicating fractionation of feldspar. Ba reaches maximum values in the syenogabbros, as seen in Fig. 4.18a. Ni has been omitted since it is highly variable in the troctolite (again probably due to modal variation) but it shows uniformly low values in the syenite. Again the chilled margin is seen to be poorer in Sr and richer in other trace elements than the troctolites.

## 4.5 Incompatible element variation

### 4.5.1 Chondrite-normalised plots

Chondrite-normalised incompatible element diagrams of the chilled margins are plotted in Fig. 4.25 (using factors from Sun, 1980). All chill samples except YGD78 and YGD298 fall within the shaded region. It can be seen that the patterns

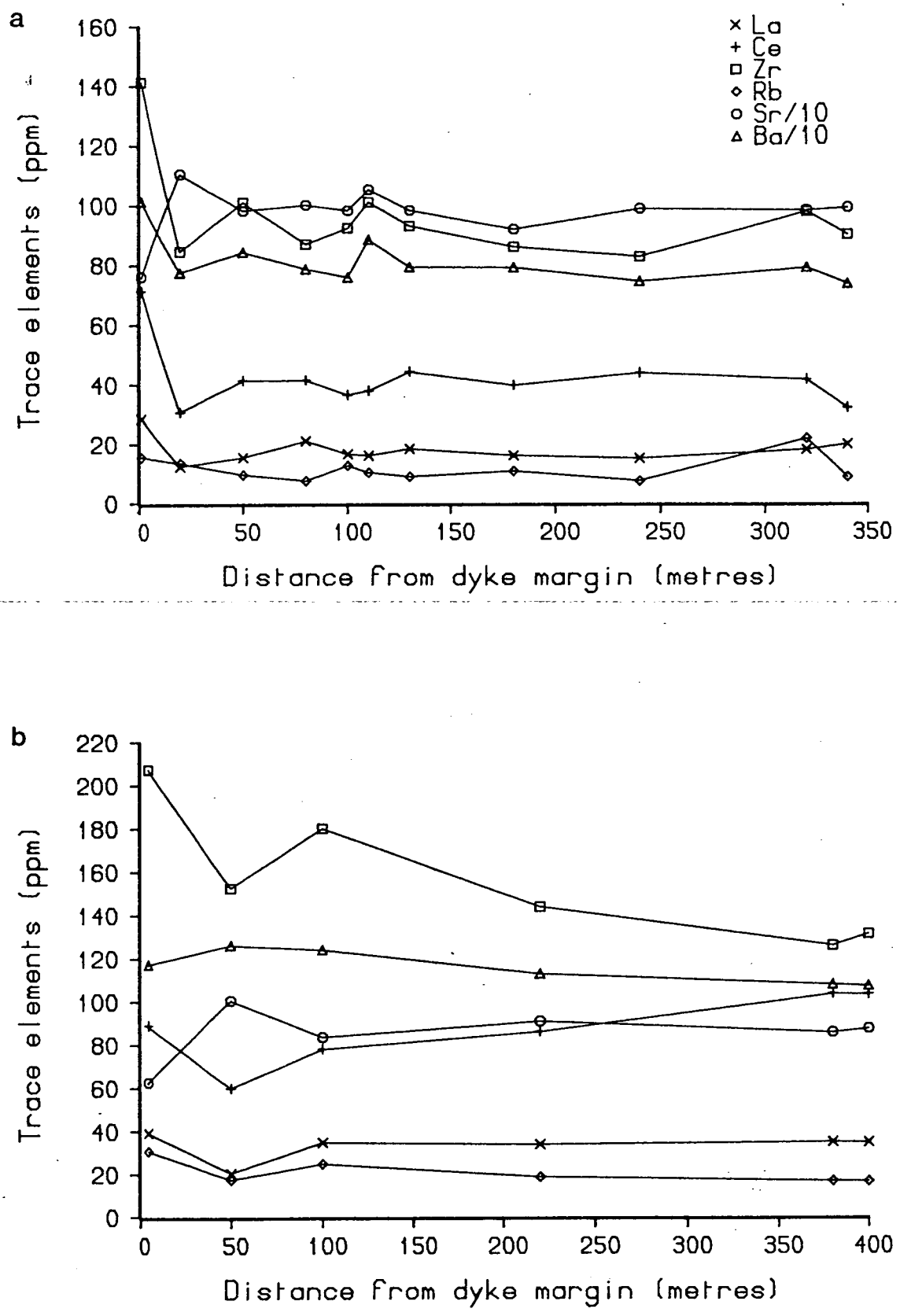


**Figure 4.23** Variation of selected trace elements from the edge to the centre of the dyke segments at (a) Itivdlip Sarqâ (locality D) and (b) Marrait (locality G).

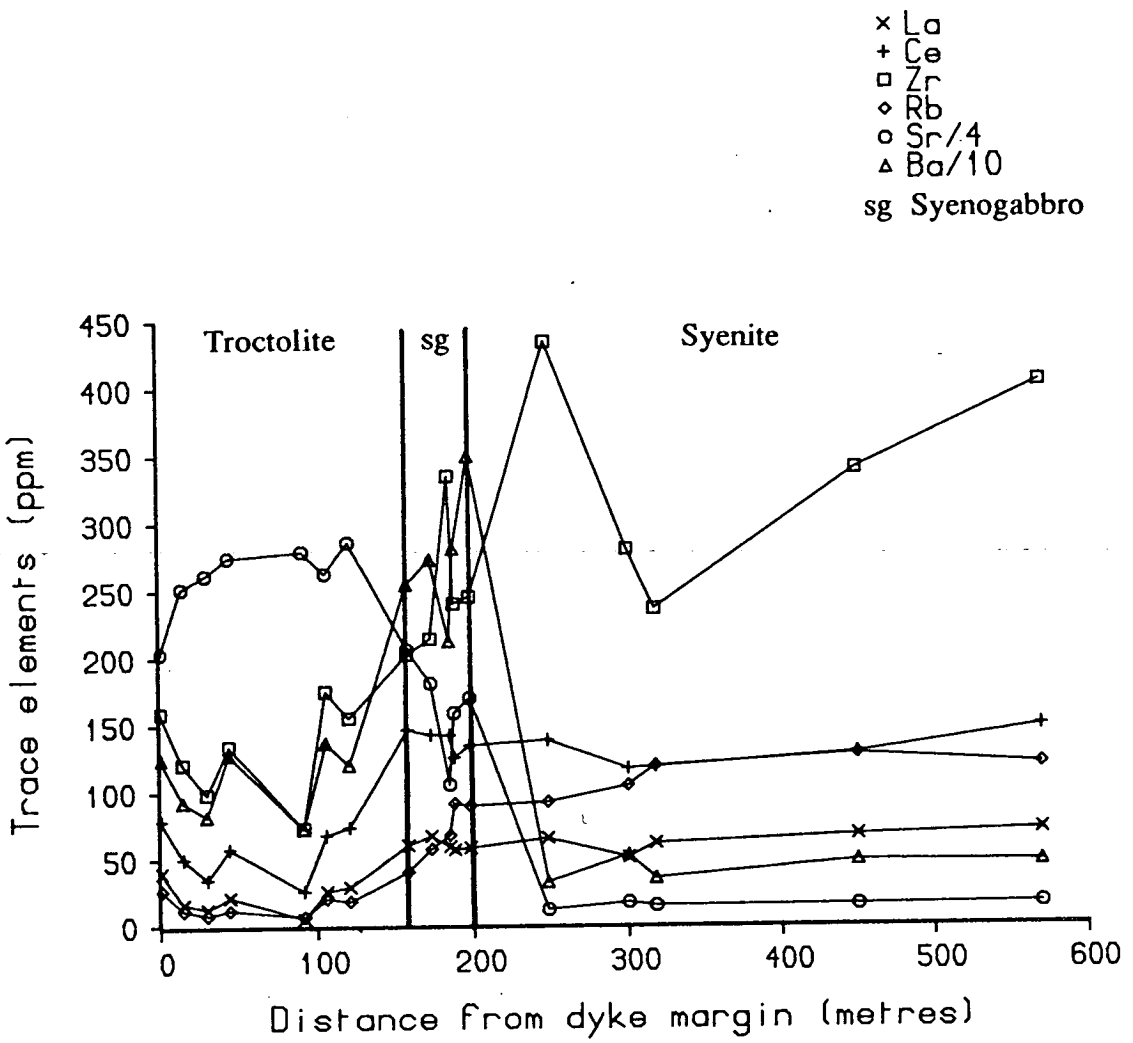


**Figure 4.24** Variation of selected trace elements from the edge to the centre of the dyke segments at Assorutit (locality L).

generally show a slight enrichment in the more incompatible elements (those at the left hand side of the plot). All the samples show peaks at Ba and P, which are thought to reflect source region characteristics (Upton and Emeleus, 1987; see also Chapter 6). The two chills which do not fit this pattern are also plotted, and show lower values for most elements but marked peaks at Sr, indicating plagioclase accumulation. Elements such as Nb, La, Ce, Nd and P have been diluted by about 60%, requiring about 60% accumulated plagioclase. Examination of the hand specimens shows that this is not in the form of plagioclase phenocrysts, so it is concluded that the magma must have accumulated a plagioclase component, possibly by melting plagioclase phenocrysts or xenocrysts.

Troctolite samples generally have slightly lower contents of incompatible elements than chills, probably due to the accumulation of cumulus minerals and the expulsion of some of the interstitial liquid containing incompatible elements which was frozen into the chills. Most of the troctolites show Sr peaks indicating accumulation of roughly 30% plagioclase, although those from locality G (Marrait) do not, and may show Sr troughs. Four troctolite samples spanning the range of observed incompatible element compositions are shown in Fig. 4.26. Syenite samples show troughs at Ba, Sr, P and Ti, indicating fractionation of feldspar, apatite and ilmenite.

### 4.5.2 Rare earth elements

REE determinations for YGDC rocks and anorthosite xenoliths have been made by Blaxland and Upton (1978) and were not determined as part of this project. Figure 2 of Blaxland and Upton is reproduced in Fig. 4.27. The findings of Blaxland and Upton were that:

1. All samples were LREE enriched.

2. Absolute REE concentrations increase by approximately an order of magnitude in the sequence: anorthosites-troctolites-chills-syenogabbros.

3. Striking positive Eu anomalies in the anorthosites, indicating plagioclase accumulation, decrease in the troctolites to zero in the chills. This suggests that there was no significant plagioclase fractionation of the YGDC magma prior to intrusion and is consistent with the observations of stellate plagioclase aggregates and feldspar crescumulates in some of the chills and troctolites, which probably indicate plagioclase supersaturation. The YGDC magma thus could not have been parental to the anorthosite xenoliths contained within it but the anorthosite may have crystallised

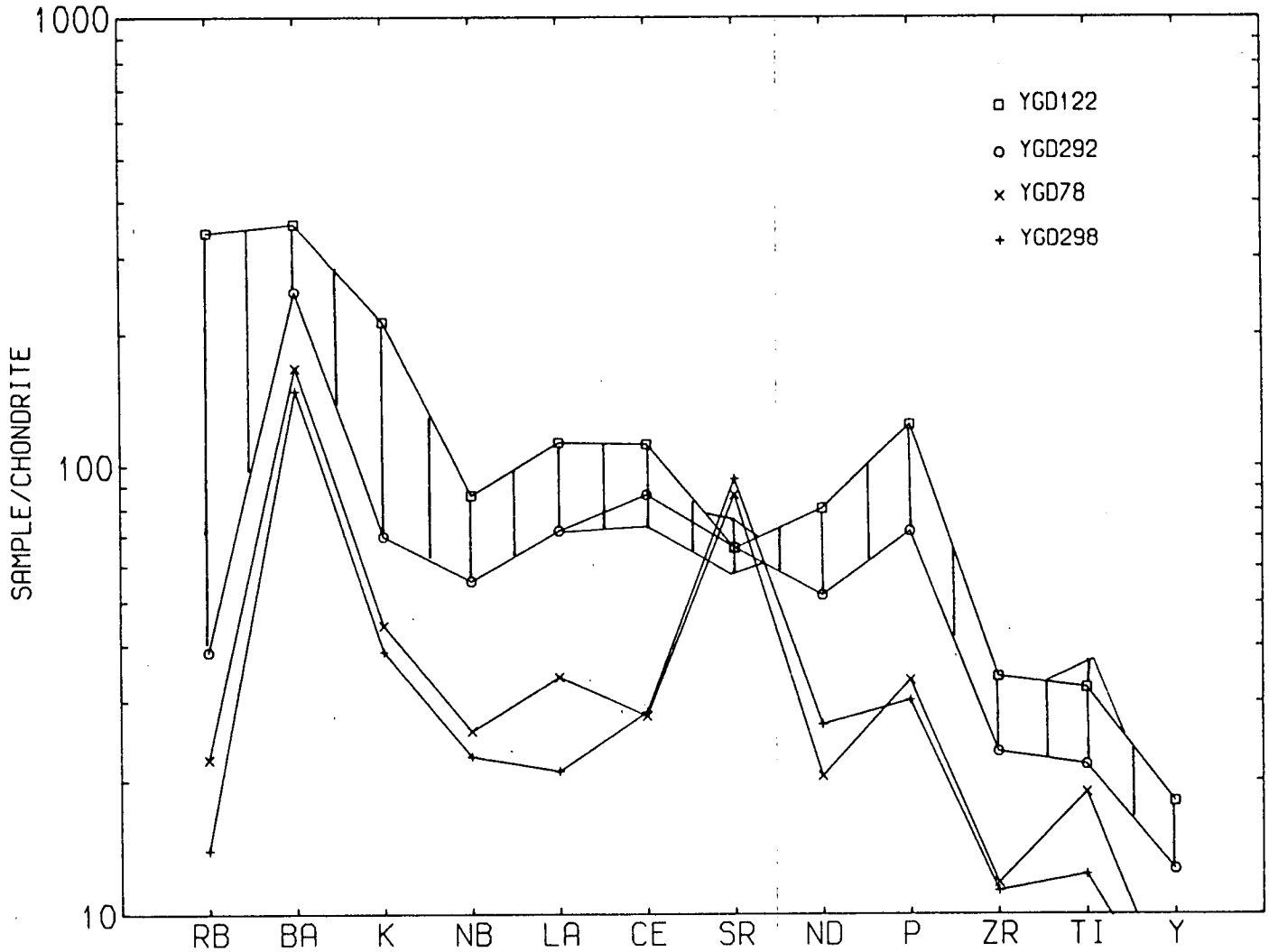


**Figure 4.25** Chondrite-normalised incompatible element plots for YGDC chilled margins. Twelve samples plot within the shaded region.

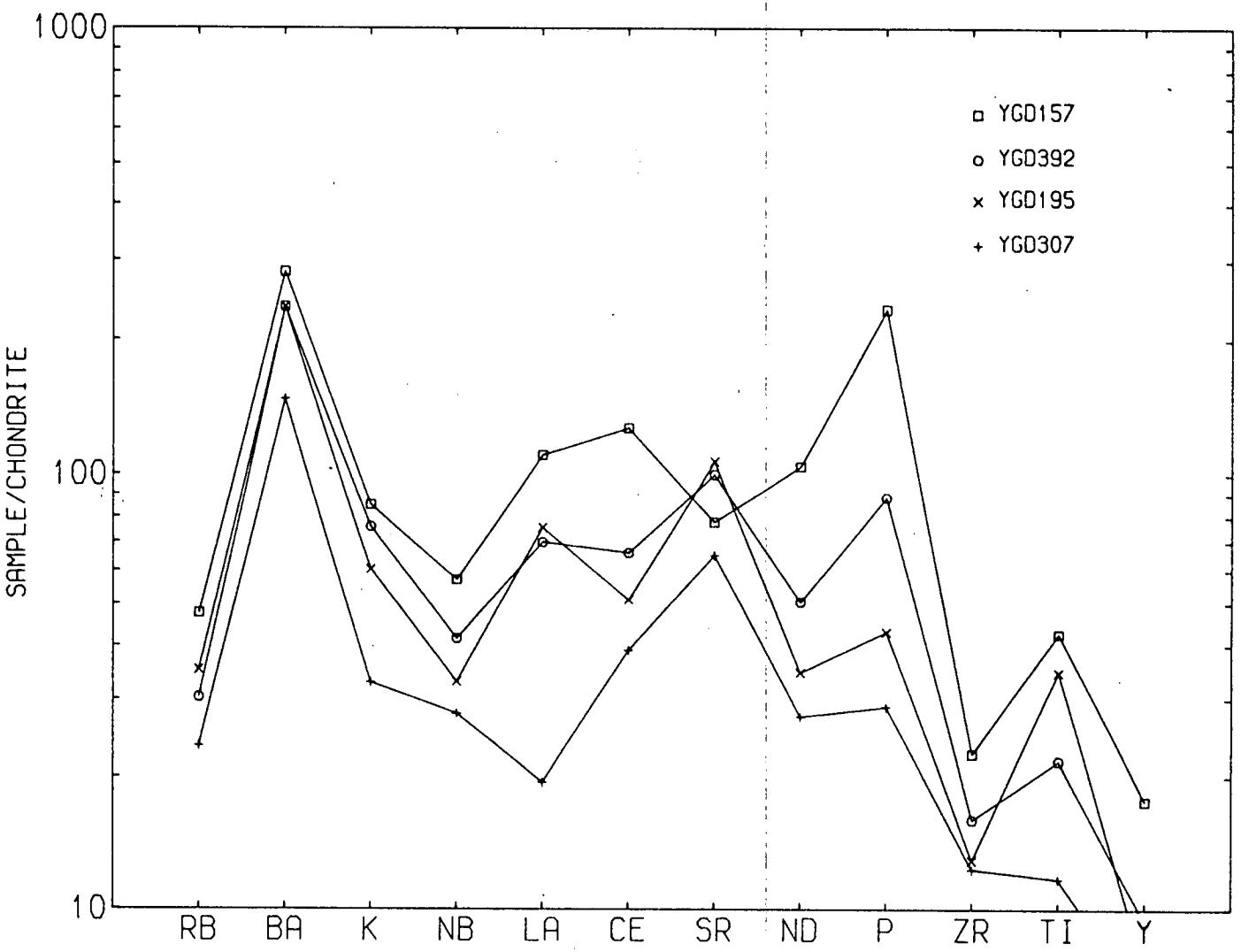


**Figure 4.26** Chondrite-normalised incompatible element plots for four troctolites showing the range of incompatible elements observed. Only samples from Marrait (locality G) do not show Sr peaks.

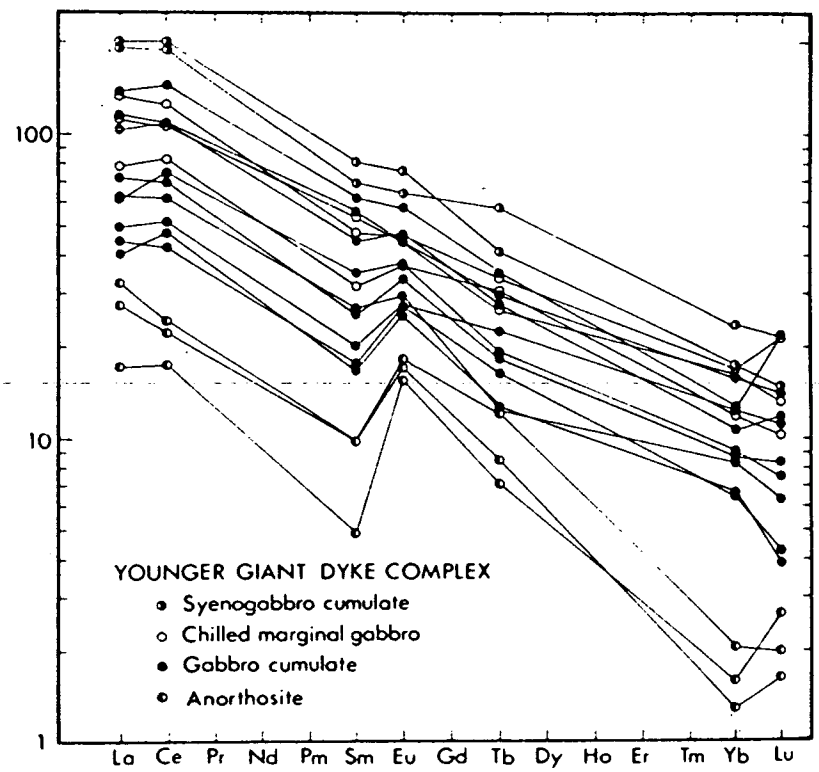


**Figure 4.27** Chondrite-normalised REE distribution in samples from the YGDC. From Blaxland and Upton (1978).

from a similar but earlier batch of magma which failed to reach the surface. The presence of positive Eu anomalies in the troctolites parallels the Sr peaks seen in Fig. 4.26 and suggests some degree of plagioclase accumulation.

## 4.6 Relationship between chills and troctolites

It can be seen from the variation diagrams in Figs. 4.2 to 4.14 that five of the more magnesian chills (MgO>6 wt%) are offset from the trend of the troctolites with similar MgO contents. The other two magnesian chills (YGD78 and YGD298) display different behaviour from the other chills and have been shown in Fig 4.25 to possess quite different incompatible element signatures. It has been concluded that they were the products of a magma which had accumulated about 60% plagioclase, and they are omitted from the following discussion.

It has already been suggested that samples with MgO greater than about 6 wt% formed by the accumulation of olivine of the composition that might be expected at the olivine-plagioclase cotectic. The troctolites are higher than the chills in $SiO_2$, $Al_2O_3$, CaO, $Na_2O$, and Sr, slightly higher in Ni, and lower in all other analysed elements. The troctolites are always displaced from the chills towards the olivine-plagioclase tie-line, and this would be consistent with the accumulation of varying amounts of olivine and plagioclase in the troctolites. Where samples lie almost on the tie line (e.g. for $Na_2O$ and Ni) there is very little separation. However, the proportions of olivine and plagioclase in most of the troctolites are fairly constant, about 25% olivine and 75% plagioclase.

A second possibility is that the troctolites crystallised from a liquid of a slightly different composition from that forming the chills and that each liquid underwent olivine accumulation (Fig. 4.28a). These two postulated liquids can be related to each other by olivine + plagioclase fractionation, probably occurring in a parental magma chamber at depth. The problem with this theory is the presence of Sr and Eu peaks in the troctolites and the absence of peaks in the chills. The two chills YGD78 and YGD298 provide evidence for the existence of liquids with Sr peaks. Such liquids must have arisen from melting of accumulated plagioclase and are probably caused by unusual circumstances. The rock crystallised from liquid of the composition of these two chill samples appears to be localised in outcrop. It seems unlikely for such a liquid to have been parental to the whole dyke complex and

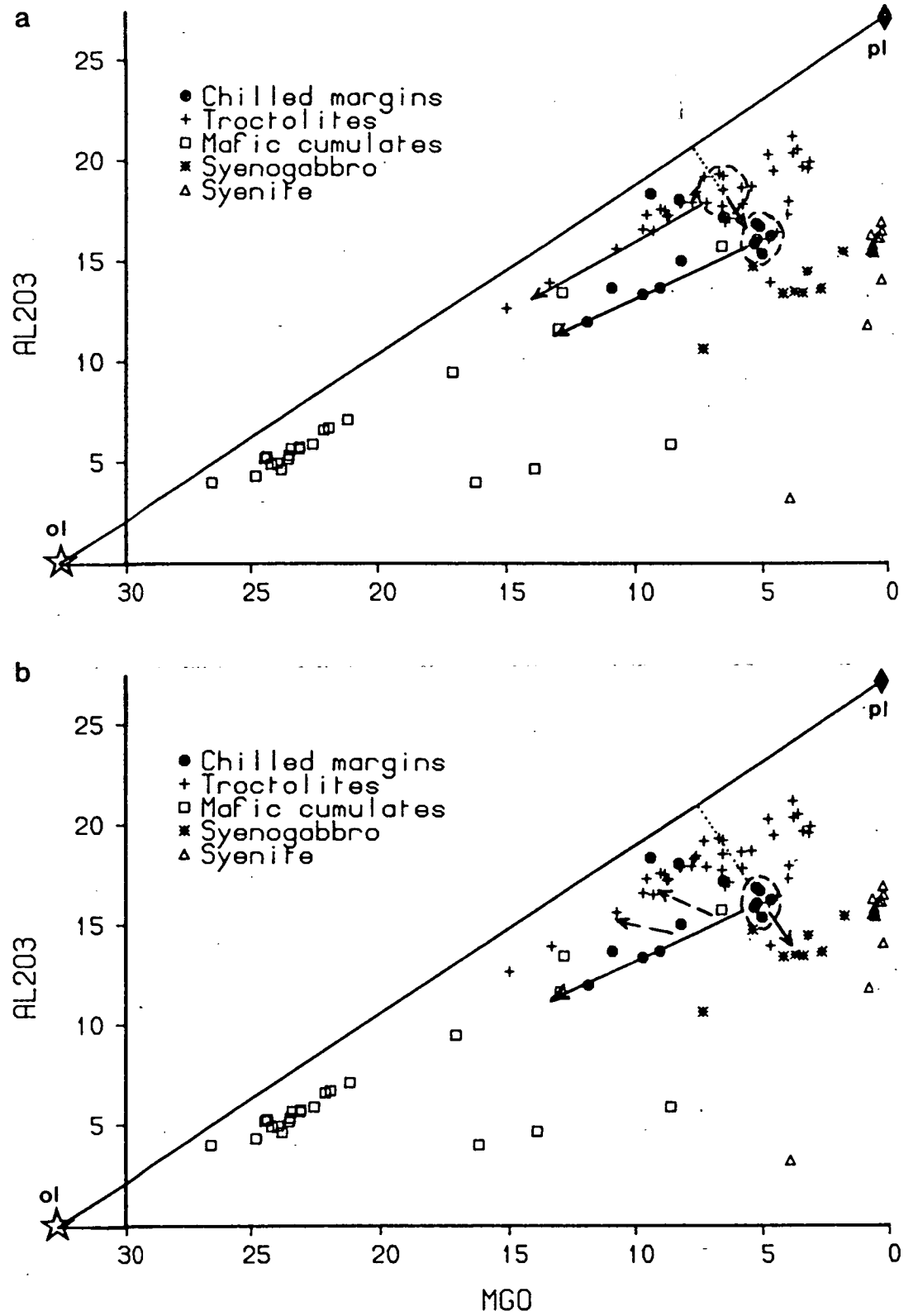


**Figure 4.28** (a) Two liquids (approximate compositions indicated by dashed lines) related by olivine + plagioclase fractionation (short arrow) could have produced the chills and troctolites by accumulation of olivine (long arrows). The problem with this theory is that the troctolites have positive Sr and Eu anomalies indicating accumulation of plagioclase whereas the chills do not (see text).
(b) An alternative explanation of the separation between chills and troctolites. An approximate initial liquid composition is circled by dashed lines, with the other chills generated by olivine accumulation (long arrow). The short arrow indicates the residual liquid resulting from olivine + plagioclase fractionation. Removal of this from the chills produces the troctolites (dashed arrows).

difficult for fractionation of plagioclase (with olivine) to occur in exactly the right degree to eliminate the Sr peak and produce a second liquid which was intruded as chilled margins to the complex.

It is concluded that the most likely cause of the chill-troctolite separation was the accumulation of olivine and plagioclase. Since the observed proportion of these minerals are relatively constant, the separation might have been achieved by the removal of elements excluded from olivine and plagioclase in a mobile interstitial melt phase. This would mean that the range of MgO contents in the troctolite compositions is, like the range in the chills, a function of accumulated olivine in the liquids, probably before intrusion. Magmas were intruded with about 5% MgO, carrying varying proportions of olivine of near-cotectic composition. The magmas may in fact have been at the cotectic but unable to crystallise plagioclase because it nucleates with more difficulty than olivine (Gibb, 1974; Donaldson, 1979; see also Chapter 7). Such inhibition of plagioclase nucleation would have led to supersaturation, which in turn gave rise to the stellate aggregates of plagioclase and olivine.

The chilled margins solidified while the magma in the dyke interior began to crystallise olivine and plagioclase. The crystals formed a touching framework with residual magma trapped in the interstices. During postcumulus crystallisation some of this residual magma was expelled, probably by compaction, thus removing elements excluded from olivine and plagioclase (Fig. 4.28b). Incompatible elements are 20-30% lower in the troctolites, indicating that this much residual liquid must have been expelled. Since olivine crystals and melt form an interconnected melt porosity (Hunter, 1987) this should have been possible. Many of the GGU chill samples plot with the troctolites; this can be explained if they were taken slightly further into the dyke than the chills for this study, and thus show cumulate characteristics.

## 4.7 Evolution of the YGDC magma

Major and trace element compositions of the YGDC rocks indicate that the magmas were transitional alkali olivine basalts to hawaiites which evolved by fractional crystallisation of the minerals they contain, the order of appearance being olivine, plagioclase, Fe-Ti oxides, clinopyroxene, alkali feldspar. All analysed YGDC samples are shown on plots of total alkalis versus silica and D.I. versus

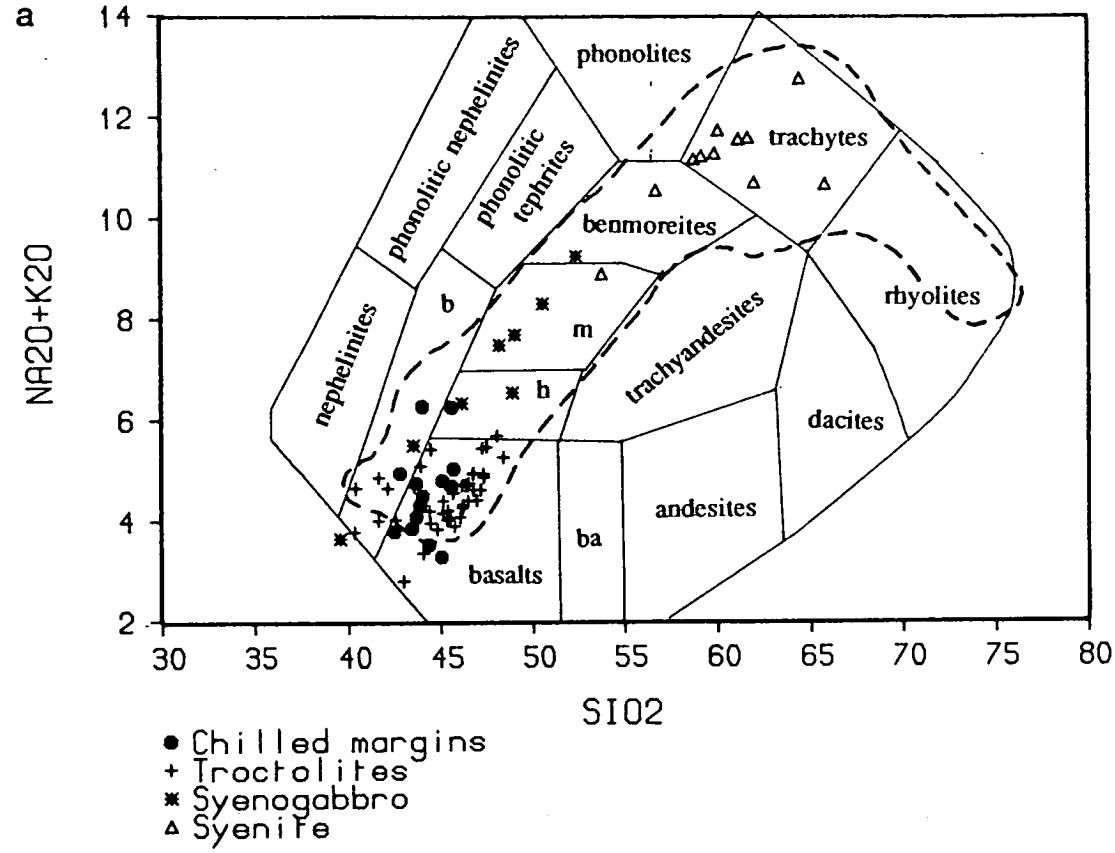


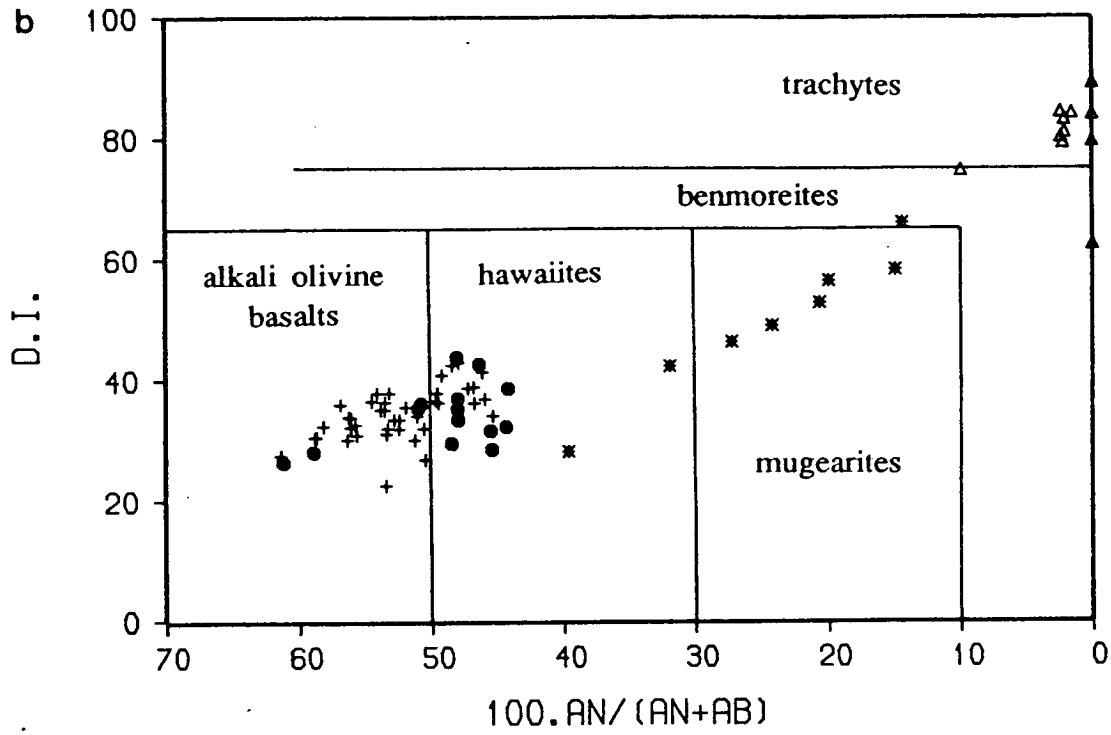


**Figure 4.29** All YGDC whole-rock analyses from this study plotted in terms of (a) total alkalis versus silica and (b) Differentiation Index versus normative plagioclase. In (a), field boundaries are from Cox *et al.* (1979) and b = basanites and tephrites, ba = basaltic andesites, h = hawaiites, m = mugearites. The rocks differentiated from alkali olivine basalts and hawaiites through mugearites and benmoreites to trachytes, closely following the compositional trend of the swarm of smaller dykes, shown with dashed outline on (a).

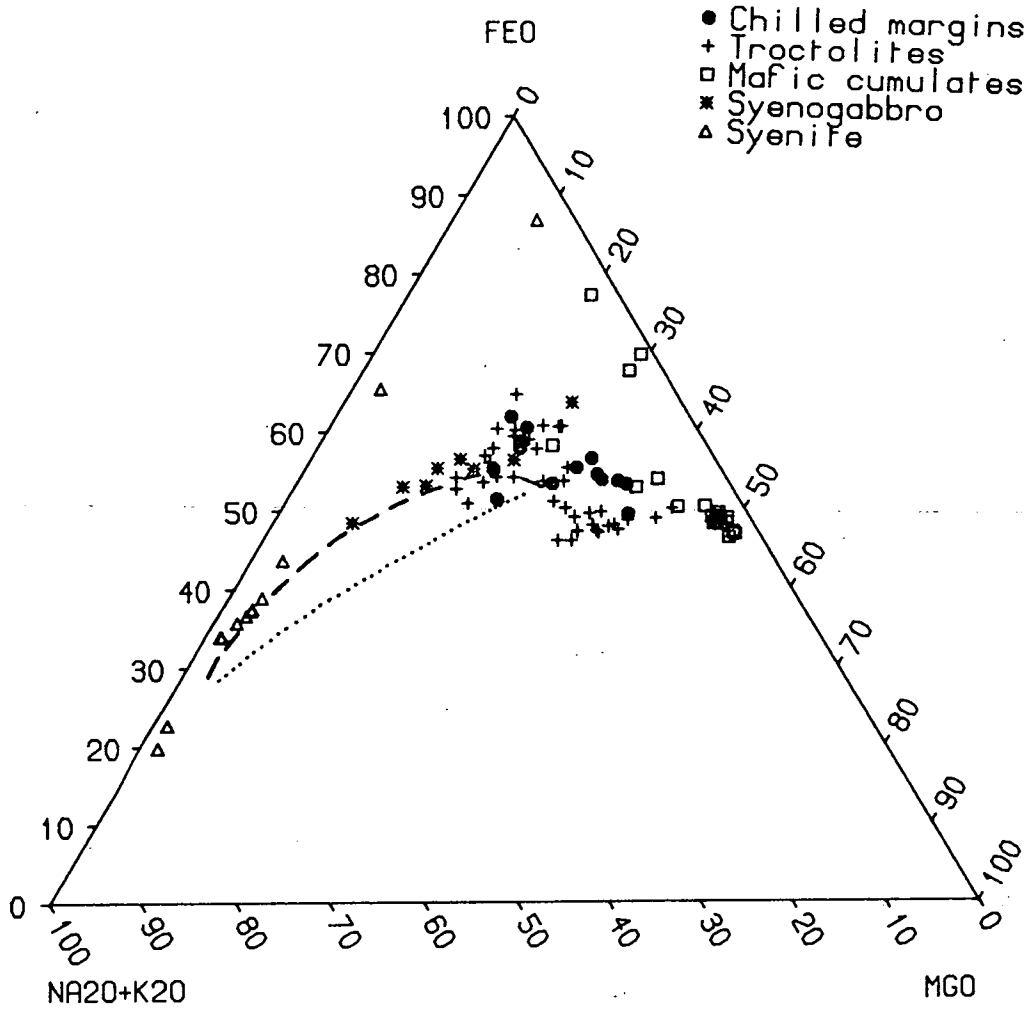


**Figure 4.30** YGDC whole-rock analyses plotted on an AFM diagram. The dashed line indicates the average Gardar trend (from Watt, 1966), and the dotted line the Klokken trend (from Parsons, 1979).

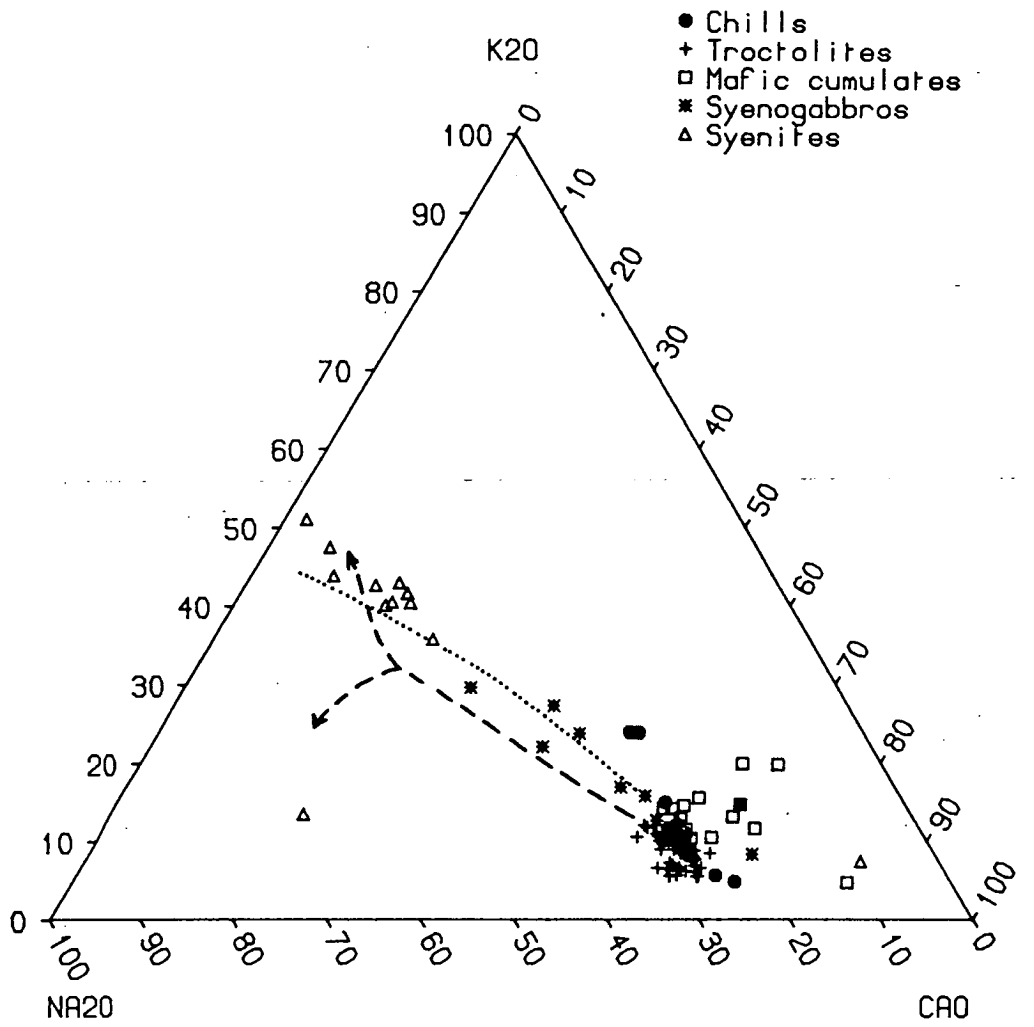


**Figure 4.31** YGDC whole-rock analyses in terms of $Na_2O$:$K_2O$:CaO. The dashed line indicates the average Gardar trend (from Watt, 1966), and the dotted line the Klokken trend (from Parsons, 1979).

normative plagioclase in Fig. 4.29a,b. Olivine ± magnetite ± apatite cumulates, whose whole-rock compositions are substantially different from liquids, have been omitted. Despite the problems of interpreting the compositions of the cumulate rocks, it can be seen that the overall trend of the YGDC rocks is that of alkali basalt differentiating to trachyte. It closely follows the trend of the smaller dykes (shown on the diagrams) which differentiate as far as rhyolite.

It appears that with the exception of the OGDC, the Tugtutôq-Narsaq dyke swarm is relatively poor in silica-undersaturated dykes compared to its ENE continuation (Upton and Fitton, 1985; Pearce, 1988). Macdonald (1970) found only seven feldspathoid-bearing dykes on Tugtutôq and Martin (1985) only two. Undersaturated derivatives of the YGDC in this region are likewise volumetrically insignificant, occurring only as rare cross-cutting veins. However, substantial volumes of undersaturated magma were emplaced to form the OGDC which has margins of alkali gabbro and a central portion ranging in composition from augite syenite in the west to sodalite foyaite in the east. In addition, the YGDC itself produced large pods of undersaturated derivatives in nunataq region, so the oversaturated trend only applies to a particular time period in a particular area.

The whole-rock differentiation trends can also be shown on diagrams of alkalis:FeO:MgO (AFM) and $Na_2O$:$K_2O$:CaO (Figs. 4.30 and 4.31).

Wager and Brown (1968) suggested that the Skaergaard intrusion experienced a trend of iron-enrichment in the residual liquids until the very last stages of crystallisation. This concept has recently been questioned by Hunter and Sparks (1987) who proposed that, in common with other tholeiitic suites, the Skaergaard intrusion would have shown a trend of increasing silica and decreasing iron after the onset of magnetite fractionation. The iron-enrichment trend was, however, vigorously defended by McBirney and Naslund (1990), Morse (1990) and Brooks and Nielsen (1990). Morse (*op. cit.*) drew parallels between Skaergaard and the Kiglapait intrusion of Labrador, which shows similar features to the YGDC (Chapter 7). However, reference to Fig. 4.2 will indicate that the YGDC liquids underwent very little iron-enrichment and that the residual liquids were silica-rich and iron-poor. There is little room for argument over the residual liquid compositions, because the YGDC is made up of orthocumulates rather than adcumulates, and in addition, the whole-rock analyses of the more evolved YGDC rocks closely match those of the compositionally similar swarm of smaller dykes in the region.

## 4.8 Summary

The magmas which were intruded to form the YGDC were alkali olivine basalts to hawaiites with about 5 wt% MgO. They were near or at the olivine-plagioclase cotectic and contained varying proportions of olivine phenocrysts of c. $Fo_{66}$, probably the cotectic composition. Upon intrusion, plagioclase began to crystallise with olivine, initially as stellate aggregates, until the level of supersaturation declined. Troctolites accumulated, probably on the magma chamber floors. Periodically, layers of olivine cumulate formed (see Chapter 7). 20-30% of the interstitial liquid in the cumulates must have been expelled, probably by compaction, such that the troctolites became lower than the chills in elements excluded from olivine and plagioclase.

At around 4 wt% MgO, magnetite and ilmenite joined the fractionating assemblage and sulphides were precipitated in slightly greater amounts than previously. At 3-3.5 wt% Mgo, when most of the dyke complex had crystallised and only a few isolated pods of magma remained, clinopyroxene began to fractionate and alkali feldspar began gradually to replace plagioclase. By this stage the magmas were trachytic in composition (giving rise to syenites); late stage veins differentiated further to alkali granite or to nepheline syenites.

# CHAPTER 5: ISOTOPE CHEMISTRY

## 5.1 General Comments

Determinations of strontium and oxygen isotope ratios were made on a series of samples to impose constraints upon the source of the magma, the possibility of magma chamber replenishment, and any hydrothermal alteration of the intrusion. This work was undertaken at SURRC, East Kilbride. In particular, adjacent pairs of mafic and felsic layers from different localities within the dyke were analysed for both strontium and oxygen isotope ratios to look for systematic differences. A suite of samples taken across the dyke and its contact was also analysed for oxygen isotopes.

## 5.2 Strontium Isotopes

Present-day $^{87}Sr/^{86}Sr$ ratios were determined on nine mafic-felsic pairs from localities B, C, D (2 pairs), F, G, L and M of Fig. 2.1 and the nunataq region of Fig. 1.1. Sample names and localities are shown in Table 5.1. The nunataq sample was taken from the layered syenite pod and was intended as an analogue of the syenite of locality K which is unlayered.

Analytical procedures are detailed in Appendix II and results, together with strontium isotope ratios corrected to 1150 Ma, are given in Table 5.2. The value of $\lambda\,^{87}Rb$ was taken as $1.42 \times 10^{-11}\ a^{-1}$, in accordance with the recommendation of Steiger and Jäger (1977). The date of 1150 Ma is the best available estimate of the age of the YGDC (bracketed by dates for the OGDC, Upton *et al.*, 1985, and the Tugtutôq Central Complex, Upton *et al.*, 1990). There is some uncertainty in the Rb-Sr dates for the Gardar Province as a whole but two U-Pb dates have recently been obtained. One of the mid-Gardar BD0 dykes has been dated at 1280Ma (L. Heaman, pers. comm., 1989). This is within the possible range of dates bracketed by Rb-Sr. On the other hand, a date of 1160Ma for the Klokken intrusion (Harper, 1988) is some 30 Ma older than the Rb-Sr date. Rb and Sr concentrations obtained from X-ray fluorescence spectrometry were used for age-correction.

Table 5.1 Location of samples used for strontium isotope analysis

| Sample Name | Troctolite (T)<br>Mafic (M)<br>Syenite (S) | Locality of Fig. 2.1 |
|---|---|---|
| YGD 306 | M | B |
| YGD 307 | T | |
| YGD 255 | M | C |
| YGD 256 | T | |
| YGD 5 | M | D |
| YGD 6 | T | |
| YGD 36A | M | D |
| YGD 36B | T | |
| YGD 312 | M | F |
| YGD 313 | T | |
| YGD 157 | T | G |
| YGD 158 | M | |
| YGD 195 | T | I |
| YGD 196 | M | |
| YGD 381 | M | M |
| YGD 382 | T | |
| 216627A | M | nunataq |
| 216627B | S | |

Table 5.2 Measured and age-corrected strontium isotope ratios

| Sample Name | $^{87}Sr/^{86}Sr_{meas}$ | Rb (ppm) | Sr (ppm) | $^{87}Sr/^{86}Sr_{1150}$ |
|---|---|---|---|---|
| YGD 306 | 0.70713±5 | 16.7 | 200.5 | 0.70316 |
| YGD 307 | 0.70361±6 | 8.2 | 716.1 | 0.70307 |
| YGD 255 | 0.70412±4 | 5.9 | 299.7 | 0.70318 |
| YGD 256 | 0.70353±3 | 6.2 | 769.6 | 0.70314 |
| YGD 5 | 0.70359±3 | 5.3 | 383.2 | 0.70293 |
| YGD 6 | 0.70337±5 | 7.7 | 1014.1 | 0.70301 |
| YGD 36A | 0.70479±4 | 8.9 | 268.3 | 0.70321 |
| YGD 36B | 0.70347±4 | 9.1 | 980.6 | 0.70303* |
| YGD 312 | 0.70407±4 | 10.4 | 538.9 | 0.70315 |
| YGD 313 | 0.70378±4 | 16.0 | 1070.1 | 0.70307 |
| YGD 157 | 0.70411±4 | 16.6 | 853.9 | 0.70318 |
| YGD 158 | 0.70401±5 | 6.2 | 344.7 | 0.70315 |
| YGD 195 | 0.70357±4 | 12.3 | 1177.0 | 0.70307 |
| YGD 196 | 0.70673±5 | 9.6 | 117.5 | 0.70284 |
| YGD 381 | 0.70774±3 | 21.9 | 210.5 | 0.70278 |
| YGD 382 | 0.70366±5 | 13.4 | 1034.1 | 0.70304 |
| 216627A | 0.71786±4 | 18.5 | 58.4 | 0.70275 |
| 216627B | 0.71081±4 | 65.2 | 418.9 | 0.70339 |

Errors quoted at the 2σ level are those actually obtained for each sample.

* Rb and Sr values averaged from six XRF analyses.

It can be seen from Table 5.2 that the majority of the samples have $^{87}Sr/^{86}Sr_{1150} = 0.70293$ to 0.70321. Three mafic samples show lower values than this: YGD196 from locality I of Fig. 2.1, YGD382 from locality M and 216627A from the nunataq region. Sample 216627B, the syenite, has a slightly higher initial $^{87}Sr/^{86}Sr$ ratio of 0.70339. There is no significant variation with geographic location or with distance from the dyke margin. The results are all within the range of mantle values; during Gardar magmatism the country rocks had a $^{87}Sr/^{86}Sr$ ratio of around 0.710 (Blaxland *et al.*, 1978) and have an average Rb/Sr ratio of about 6, much greater than that of the YGDC, so that any crustal contamination would have increased the initial strontium ratio. No marginal samples were analysed for $^{87}Sr/^{86}Sr$, but from field and petrographic evidence for wall rock melting it is probable that the outer few cm or tens of cm would show isotopic evidence of contamination by Julianehåb granite. It is possible that depleted lower crust with low $^{87}Sr/^{86}Sr$ underlies the Gardar region and could have been assimilated without affecting the strontium isotope ratios. However, in the absence of any positive evidence for the existence of such a contaminant, it is concluded that the YGDC magmas were mantle-derived and for the most part did not undergo any significant crustal assimilation.

The separation of initial $^{87}Sr/^{86}Sr$ values of adjacent pairs of samples is shown in Fig. 5.1. Owing to the uncertainties in the dating of the YGDC, age corrections have also been made to 1100 Ma and 1200 Ma and are shown on the same diagram. For the majority of the samples this uncertainty makes little difference since they possess low Rb/Sr ratios (0.1 or less, except for the nunataq syenites where Rb/Sr is up to 0.3). Both the younger and the older age bring some of the pairs closer but spread others apart. In most cases the initial strontium isotope ratios of pairs of samples are within error of one another. Of those that are not, one pair (YGD36A/36B) shows a slightly higher initial $^{87}Sr/^{86}Sr$ ratio for the mafic sample and three pairs (YGD195/196, YGD381/382 and 216627A/B) have lower initial $^{87}Sr/^{86}Sr$ ratios in the mafic samples. The greatest difference is seen in the nunataq syenite sample, 216627A/B. This may be due to an incorrect age; at 1050 Ma the initial strontium isotope ratios lie within error of one another at about 0.70405. However, the samples are very unlikely to be this young since the youngest Rb-Sr date obtained for any of the Gardar rocks is 1119±48 (Alangorssuaq Gabbro of Nunarssuit, recalculated from Blaxland *et al.*, 1978) and it is considered unlikely that magmatism continued after 1100 Ma. In addition the giant dyke complex is cut by numerous smaller dykes and on Tugtutôq by the Tugtutôq Central Complex. It was obviously not the last manifestation of magmatic activity in the area. Another explanation for the differences in the syenite pair might be that the mafic layer

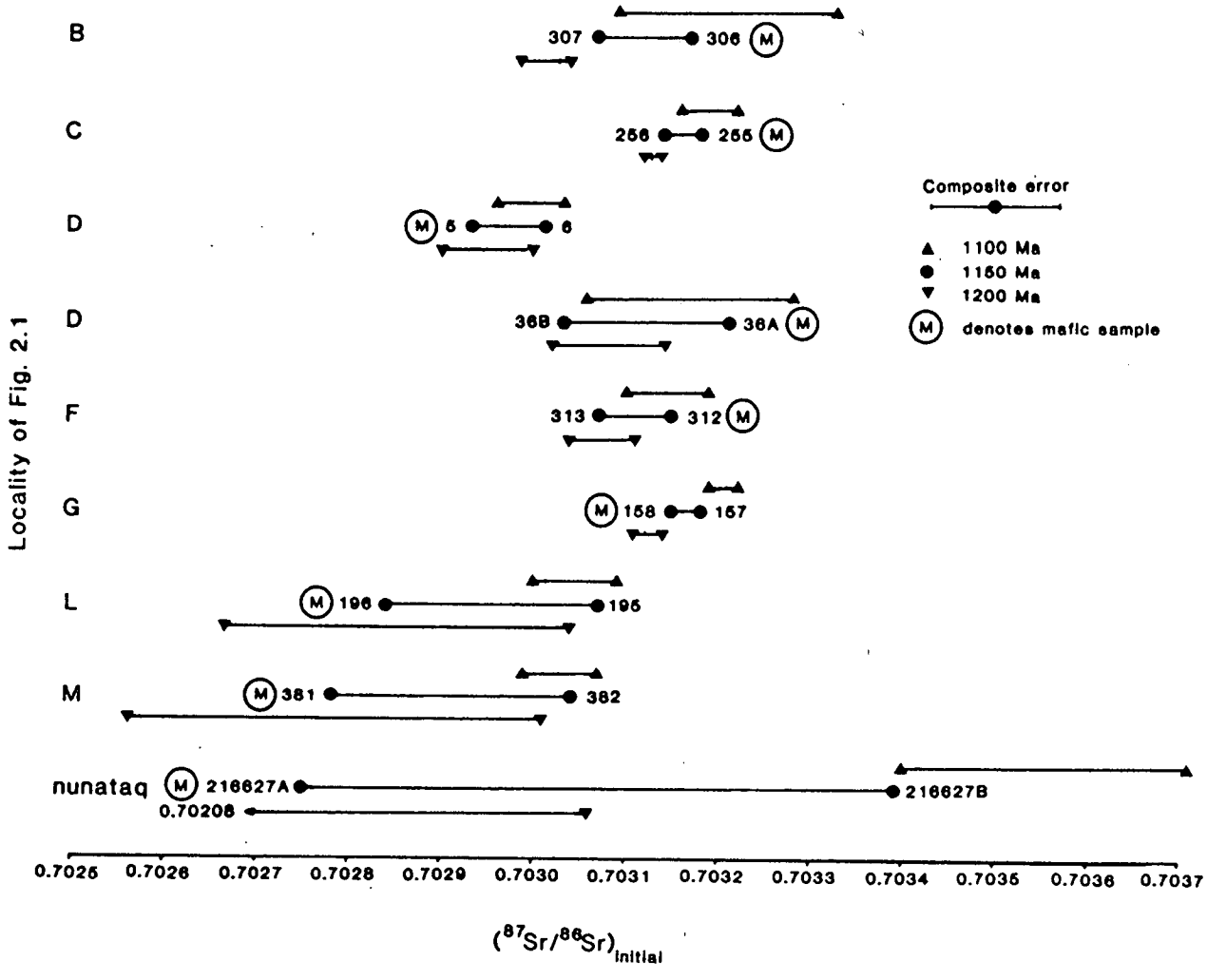


**Figure 5.1** Initial $^{87}Sr/^{86}Sr$ ratios ratios of mafic-felsic pairs from the YGDC. Age corrections have been made to 1100, 1150 and 1200 Ma owing to the uncertainty in dating the complex. The error bar takes into account the average analytical error on the measured isotope ratios and also the uncertainty in Rb and Sr determinations (see Appendix II). Samples numbers have YGD prefixes, except for 216627A/B.

became impermeable to fluids slightly earlier than the syenite and that some contamination with country rock strontium took place within the latter, raising the initial strontium isotope ratio.

Initial strontium isotope ratios for other Gardar rocks given by Blaxland *et al.* (1978) are also predominantly within the field of mantle values (0.7024±0.0010 to 0.7043±0.0002) except for the North Qôroq complex at 0.7052±0.0030 (which is within error of many of the other values), the Nunarssuit Biotite Granite (0.7068±0.0013), the Ilímaussaq complex (0.7096±0.0022) and the Ivigtut granite (0.7125±0.0048). Blaxland *et al.* explain the initial strontium isotope ratios of the Nunarssuit Biotite Granite by assimilation of Julianehåb granite, and those of Ilímaussaq and Ivigtut by selective enrichment of strontium, possibly in late-stage F-rich fluids. Initial $^{87}Sr/^{86}Sr$ ratios for the YGDC are compared with others for the Gardar province in Fig. 5.2, which is a modified version of Fig. 8 from Blaxland *et al.* (1978). Values of $\varepsilon_{Sr}$ were not calculated owing to the uncertainty in ages and in initial strontium ratios for the Gardar rocks in general, and to the fact that recent Sr and Nd isotopic data for oceanic basalts throw doubt on the uniform reservoir (UR) value for $^{87}Sr/^{86}Sr$ used in $\varepsilon_{Sr}$ calculations (White and Hofmann, 1982).

Initial strontium isotope ratios given by Patchett *et al.* (1976) and Martin (1985) for anorthosite xenoliths within the YGDC are indistinguishable from those of the dyke complex (0.70287 to 0.70303±7), suggesting that the anorthosites came from a very similar source.

## 5.3 Oxygen Isotopes

### 5.3.1 Procedure and results

Seven of the sample pairs used for strontium isotope ratio determinations were also analysed for oxygen isotope ratios. These were from localities B, D (two pairs), F, G and I of Fig. 2.1 and from the nunataq region. In addition, samples from the two evolved pods (localities J and K) were analysed together with a suite of samples taken in a traverse from the dyke centre to a few metres into the country rock at locality D. It was found that the country rock had relatively low $\delta^{18}O$ up to 11m away from the dyke, probably as a result of hydrothermal alteration by a system of circulating groundwater set up by the intrusion. Three granite samples which were located 100-1000m from any later intrusion were taken from various parts of the field

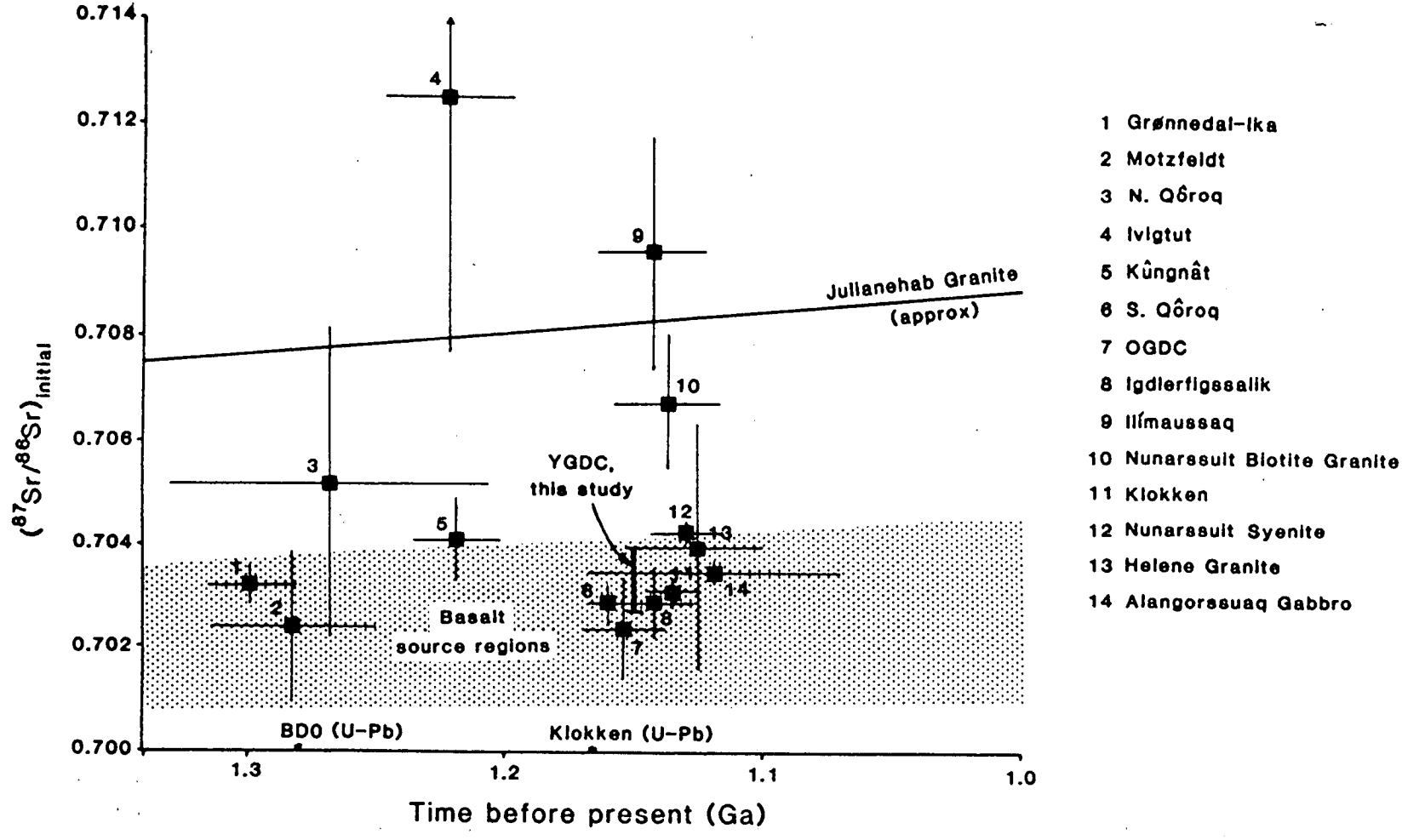


Figure 5.2 Comparison between initial $^{87}Sr/^{86}Sr$ ratios for the YGDC and other Gardar complexes, after Fig. 8 of Blaxland *et al.* (1978).

area and analysed for comparison. Feldspar was separated from all samples for analysis, and whole-rock values for all but the mafic samples were also obtained. Sample localities are given in Table 5.3 while separation techniques and analytical procedures are detailed in Appendix II.

For most of the samples multiple determinations were made for oxygen isotopes, since reproducibility was sometimes poor, especially on whole-rock samples where reaction with $ClF_3$ is less likely to be complete. The results are given in Table 5.4 and are for the most part averages of two or more results within error of one another. However, for a few samples (especially whole-rocks) it was necessary to average two or more results that differed by more than the determinative error; these are shown in brackets. Values with a question mark are single analyses for that particular sample. In selecting the values in the table, oxygen yields were taken into account; yields lower than average may indicate incomplete reaction or incomplete transfer of oxygen to the collecting tube, while unusually high yields may indicate the presence of water in the sample which will reduce the overall $\delta^{18}O$. Feldspar yields were in the range 10.9-14.0 μmoles/mg with most around 13 μmoles/mg. Whole-rock yields were more variable and, with the exception of the granitic samples, lower than those for feldspar due to the presence of ferromagnesian minerals.

The results can be summarised as follows (values are given as $\delta^{18}O_{SMOW}$ and are all positive):

| | Feldspar | Whole rock |
|---|---|---|
| Troctolites | 5.0-6.5‰ | 4.0-5.4‰ |
| Mafic cumulates | 4.4-6.9‰ | |
| Syenites | 6.1-6.8‰ | 4.2-5.9‰ |
| Granites | 7.6-8.7‰ | 7.2-8.2‰ |

Figure 5.3 is a plot of whole-rock $\delta^{18}O$ against feldspar $\delta^{18}O$. A profile of oxygen isotope ratios across the dyke segment at locality D, showing a marked depletion in $\delta^{18}O$ at the margin, is presented in Fig. 5.4.

Table 5.3 Location of samples used for oxygen analysis

| Sample Name | Troctolite (T) Syenite (S) Granite (G) | Locality of Fig. 2.1 | Distance from dyke margin (m) |
|---|---|---|---|
| (Troctolite-mafic pairs as Table 5.1; YGD225/256 and YGD381/382 not analysed for oxygen isotopes) | | | |
| YGD 51 | T | D | 300 |
| YGD 39 | T | D | 180 |
| YGD 36B | T | D | 150 |
| YGD 8 | T | D | 75 |
| YGD 6 | T | D | 20 |
| YGD 227 | Hybrid | D | 0 |
| YGD 230 | G | D | 2 |
| YGD 231 | G | D | 11 |
| JG1 | G | | |
| JG2 | G | | |
| JG3 | G | | |
| YGD 362 | S | K | |
| YGD 175 | S | L | |

Table 5.4 Oxygen isotope ratios (as $\delta^{18}O_{SMOW}$)

| Sample Name | | Feldspar | Whole Rock | $\Delta_{Fsp-wr}$ |
|---|---|---|---|---|
| YGD 306 | Layer pairs | 4.4 | | |
| YGD 307 | | 5.6? | 5.1 | 0.4 |
| YGD 5 | | 4.8 | | |
| YGD 6 | | 5.6 | (4.0) | 1.6 |
| YGD 36A | | 6.2 | | |
| YGD 36B | | 5.9 | 5.4? | 0.5 |
| YGD 312 | | (5.5) | | |
| YGD 313 | | 6.1 | (5.0) | 1.1 |
| YGD 157 | | 6.5 | 5.3? | 1.2 |
| YGD 158 | | 6.9 | | |
| YGD 195 | | 5.0 | (4.0) | 1.0 |
| YGD 196 | | 4.6 | | |
| 216627A | Syenites | 6.7 | | |
| 216627B | | 6.1 | 5.7 | 0.4 |
| YGD 362 | | 6.8 | 5.9 | 0.9 |
| YGD175 | | (6.2) | 4.2? | 2.0 |
| YGD 51 | Traverse across dyke | 5.5 | 5.0 | 0.5 |
| YGD 39 | | 5.9 | 4.9 | 1.0 |
| YGD 8 | | 6.0 | 5.0 | 1.0 |
| YGD 227 | | (5.1) | 4.4 | 0.7 |
| YGD 230 | Country-rock granites | 6.5 | 6.1 | 0.4 |
| YGD 231 | | 6.4 | 6.6 | -0.2 |
| JG 1 | | | 7.2 | |
| JG 2 | | 8.7 | 8.2 | 0.5 |
| JG 3 | | 7.6 | 7.4 | 0.2 |

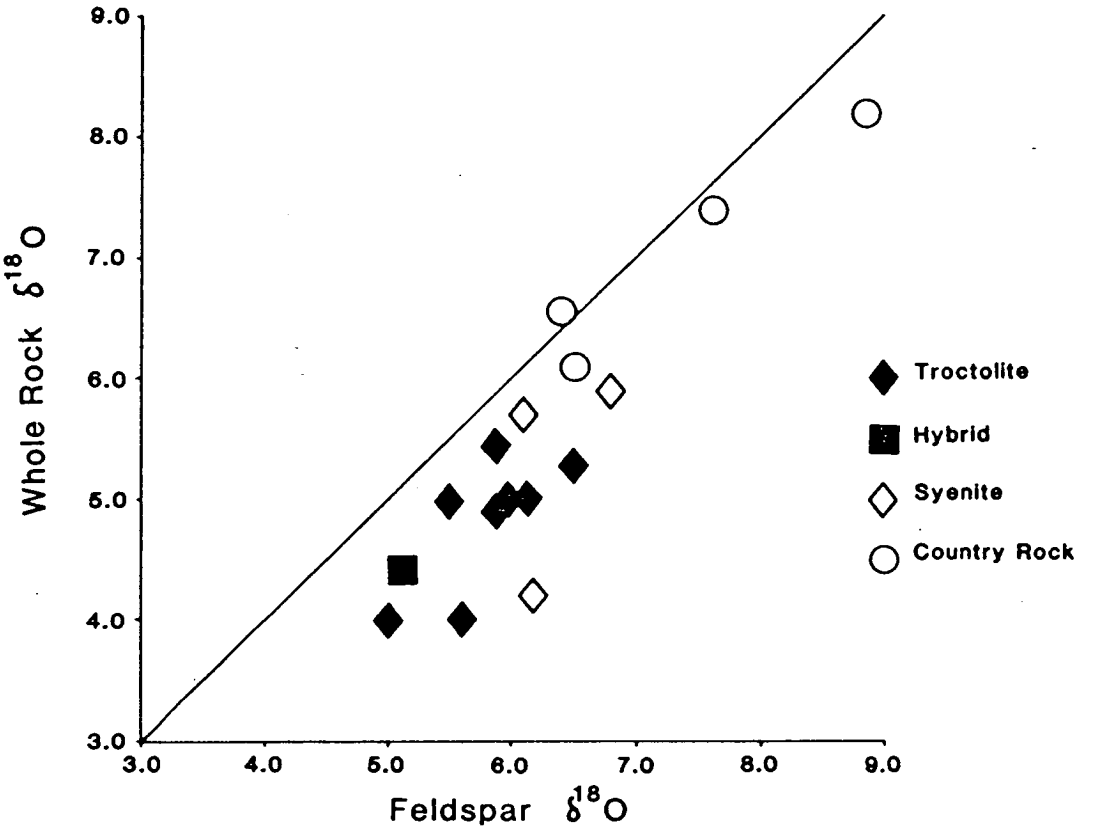


Figure 5.3 Whole-rock $\delta^{18}O$ against feldspar for YGDC samples. The line indicates a 1:1 ratio.

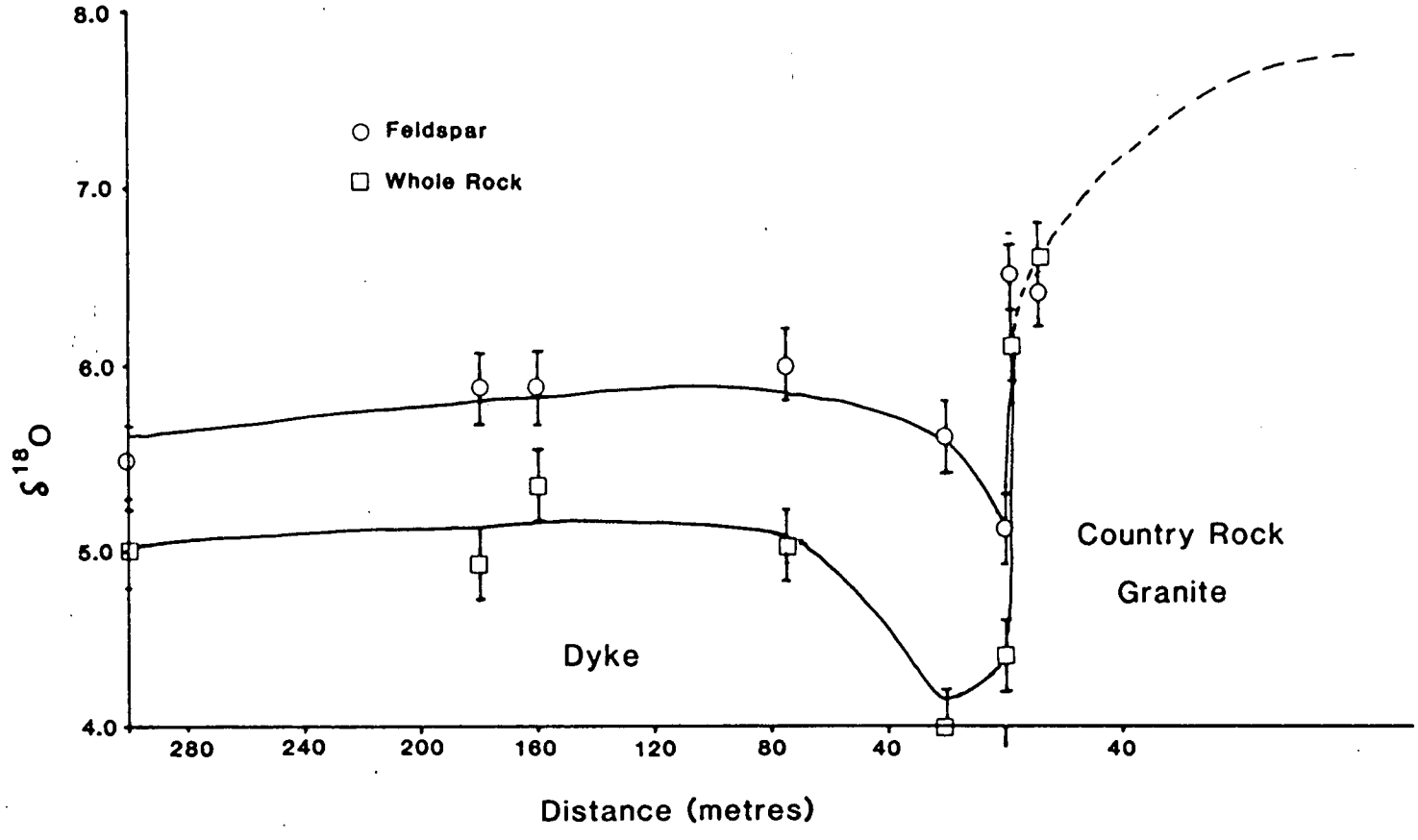


**Figure 5.4** Feldspar and whole-rock $\delta^{18}O$ for a series of samples taken in a traverse across the dyke segment at locality D. In the interior of the dyke, $\delta^{18}O$ is fairly constant, with whole-rock values lower than those of feldspar. At the margin of the dyke, a depletion of about $1^{o}/_{oo}$ is seen for both whole-rock and feldspar values. Samples of country-rock granite 2m and 11m outside the dyke give $\delta^{18}O$ of about $+6.5^{o}/_{oo}$ for both whole-rock and feldspar, but granite samples well away from any later intrusion have $\delta^{18}O$ values of $+7.2\text{-}8.2^{o}/_{oo}$ for whole-rock and $+7.6\text{-}8.7^{o}/_{oo}$ for feldspar. It is thought that at locality D $\delta^{18}O$ values in the feldspars rise to similar levels at an unspecified distance from the intrusion (shown schematically on the diagram).

### 5.3.2 Origins of isotope ratios

Primary $\delta^{18}O$ values of continental igneous rocks are thought to be in the range +5.0 to +7.0‰ (Kyser, 1986). Thus whole-rock values greater than +5.0‰ obtained in this study are probably magmatic values. In a basalt, magmatic fractionation at about 1100°C gives $\Delta^{18}O_{plag\text{-}melt}$ of about 0.5 (Kyser, 1986) and closed system $^{18}O$ exchange to lower temperatures would increase this fractionation (Taylor and Forester, 1979). In the YGDC rocks, oxygen isotope ratios in the feldspars are invariably higher, by 0.4-2.0‰, than whole-rock values for the same samples. The differences >1‰ arise from less accurate analyses and in fact the range may be nearer to 0.5-1.0‰. This strongly supports the probability of magmatic values in the YGDC. The YGDC oxygen isotope ratios are similar to, though slightly lower than, unaltered Skaergaard rocks which have plagioclase values of +6.4‰ and whole-rock values of +5.5-5.6‰ (Taylor and Forester, 1979). Some of the mafic layers in the YGDC have low values (<+5.0‰) for plagioclase (YGD306, YGD5 and YGD196).

The values of whole-rock $\delta^{18}O$ which are less than +5.0‰ are difficult to explain. Five possibilities might be:

1. Source characteristics.

2. Crystallisation

3. Assimilation of low $\delta^{18}O$ country rock.

4. Interaction of meteoric water with magma.

5. Hydrothermal alteration by meteoric water at high or low temperature.

1. Source characteristics

There is no evidence of any trend in the $\delta^{18}O$ of igneous rocks with time (Kyser, 1986; Taylor and Sheppard, 1986). Kyser *et al.* (1981) measured olivine fractionation at mantle temperatures and found that above 1200°C olivine becomes more $^{18}O$ rich than its equilibrium melt and thus melting of undepleted mantle might be expected to produce lower $\delta^{18}O$ melts than mantle that had previously undergone a

melting event. However, from rocks of the East African rift and other areas of within-plate magmatism, Sheppard (1986) concluded that enriched mantle parental to continental alkali magmatism tends to have higher $\delta^{18}O$ (+6.0 to +8.0‰) than does depleted mantle producing mid-ocean ridge basalts. Thus the literature at present appears to be inconclusive on this matter.

2. Crystallisation

Below 1200°C, mafic minerals are lower in $\delta^{18}O$ than basaltic magmas while plagioclase is slightly higher (Kyser, 1986). The whole-rock values of mafic cumulates would thus be lower than those of the troctolites due to their mineral assemblages. However, the low $\delta^{18}O$ plagioclase in some of the mafic cumulates must either have crystallised from a low $\delta^{18}O$ magma, or undergone alteration after crystallisation. Fractionation of plagioclase alone could have lowered the $\delta^{18}O$ of the magma, but the lack of negative Sr and Eu anomalies in the chilled margins of the YGDC rule out substantial plagioclase fractionation before intrusion of the magma. Fractionation of olivine could only have resulted in lowering the $\delta^{18}O$ of the magma if it occurred above 1200°C, since at high temperatures olivine is probably higher in $^{18}O$ than the magma with which it is in equilibrium. It seems unlikely that high-temperature fractionation occurring before emplacement could have caused the localised depletion in $\delta^{18}O$, because any inhomogeneities would not have survived the intrusive event.

3. Assimilation

It can be seen from the values obtained for Julianehåb granite, especially samples JG1-3 which were taken well away from any later intrusions, that the country rock had a higher $\delta^{18}O$ than the magma. Thus assimilation would raise and not lower the $\delta^{18}O$ of the YGDC. Assimilation has also been ruled out by the strontium isotope ratios obtained.

4. Water-magma interaction

South Greenland is thought to have been at about 36°N at the time of Gardar magmatic activity (Piper and Steam, 1977) and assuming that Proterozoic meteoric water had the same characteristics as it does at the present time, it would have had low $\delta^{18}O$ (perhaps -2 to -4‰, Sheppard, 1986) and thus been able to deplete the YGDC magma. If interaction between meteoric water and magma had taken place, whole-rock values would have been lowered but plagioclase-whole rock isotope fractionation due to crystallisation would have been unaffected. Water does not diffuse easily through magma (Taylor and Sheppard, 1986), since intrusions are generally under a lithostatic pressure greater than the outside hydrostatic pressure in fissures, but this process could have affected the margins of the intrusion. This might explain the marginal depletion seen in Fig. 5.4. However, even if the water were meteoric in origin, it would probably have exchanged some oxygen with the hot country rocks, raising its $\delta^{18}O$ before contact was made with the magma. In addition, there is no evidence from analyses of biotite or apatite for an increased water content at the margins of the intrusion. The water to halogens ratio appears to have been extremely low throughout the intrusion.

5. Hydrothermal alteration

High temperature hydrothermal alteration of cumulates has been shown to have occurred extensively in the Skaergaard intrusion (Taylor and Forester, 1979). However, large amounts of $^{18}O$ depletion only occurred in the upper part of the Skaergaard intrusion where the country rocks are basalts, highly fractured and with a $\delta^{18}O$ similar to that of the intrusion. The gneissose basement beneath the basalts was much less permeable and had a higher whole-rock $\delta^{18}O$. Oxygen isotope exchange was minimal in the lower part of the Skaergaard intrusion and it is thought that the similar situation of the YGDC to this lower part makes it unlikely that significant hydrothermal exchange would have taken place. It is possible that a hydrothermal alteration signature is present in the Narsaq troctolites, but these were not analysed for oxygen isotopes, since the numerous inclusions of magnetite within the feldspar (especially in sample YGD382) made it impossible to obtain a clean feldspar separate. In addition, any hydrothermal alteration affects feldspars more readily than most other minerals (Taylor and Sheppard, 1986), giving feldspar $\delta^{18}O$ values that are similar to or lower than whole-rock values, and this is not observed.

Partitioning of oxygen isotopes between minerals is greater at lower temperatures and thus low-temperature hydrothermal alteration would have had an even greater effect on the plagioclase/whole-rock partitioning. It would also have resulted in the formation of low-temperature alteration products which, although they occur, are not abundant in YGDC rocks, away from the dyke margins.

### 5.3.3 Differences between layers

Mafic layers were not analysed for whole-rock oxygen isotope ratios since the samples are very iron-rich and thus difficult to react. Whole-rock values would in any case be determined to some extent by modal variation. Feldspar analyses are used to compare adjacent layers and it can be seen that of the seven pairs of samples analysed, four show lower and three higher $\delta^{18}O$ in feldspar from the mafic layer. As with the initial strontium isotope ratios, no pattern emerges. Oxygen and strontium isotope data have been combined in Fig 5.5. The plagioclase values less than +5.0 seen in some mafic cumulates may indicate a small amount of localised high temperature hydrothermal alteration. This, however, does not fit with the field evidence from axial breccias at locality D which suggests that the mafic layers solidified, and presumably became impermeable to fluids, earlier than the troctolite and thus might be expected to be less susceptible to hydrothermal alteration.

## 5.4 Summary and Conclusions

Strontium isotope data show that the YGDC magma was mantle-derived with no discernible contamination by the Julianehåb granite, in common with many other Gardar intrusions. It is possible that depleted low $^{87}Sr/^{86}Sr$ lower crust exists beneath the Gardar province and could have been assimilated without raising the initial $^{87}Sr/^{86}Sr$ ratio of the magmas. The explanation for the close association in space and time of over- and undersaturated magmas in the whole of the Gardar province may be that crustal assimilation by some magmas caused them to move towards oversaturated residues. Replenishment of the YGDC magma chamber from a source with constant $^{87}Sr/^{86}Sr$ is not ruled out by the data. Pairs of mafic and troctolitic or syenitic layers show no systematic differences in initial $^{87}Sr/^{86}Sr$ ratio. Anorthosite inclusions in the YGDC appear to have an initial $^{87}Sr/^{86}Sr$ ratio identical to their host magma (Patchett *et al.*, 1976; Martin, 1985).

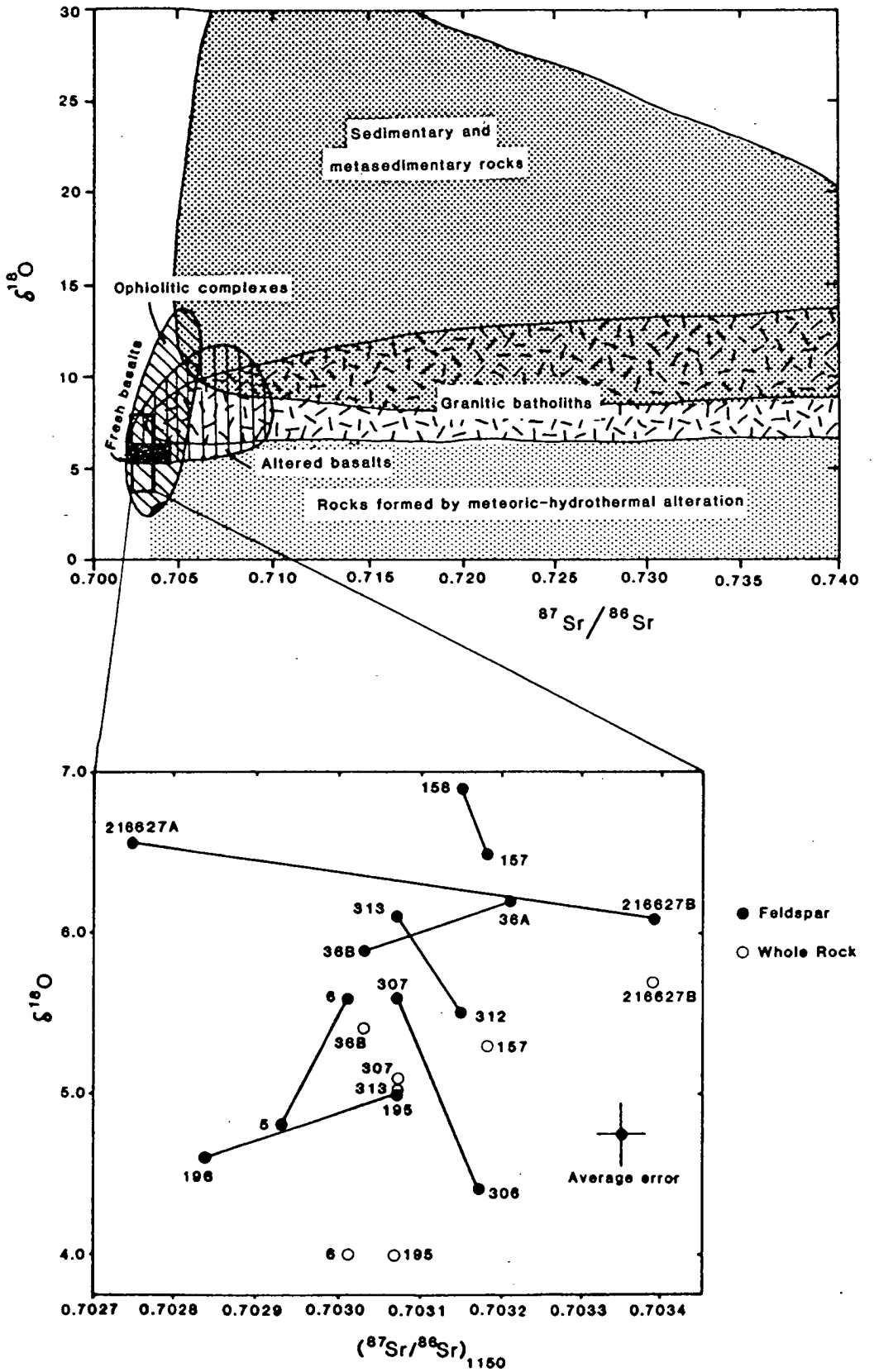


Figure 5.5 (a) $\delta^{18}O$ against $^{87}Sr/^{86}Sr$ for a range of terrestrial rocks, generalised from several literature sources. After Taylor and Sheppard (1986). (b) $\delta^{18}O$ against $(^{87}Sr/^{86}Sr)_{1150}$ for YGDC rocks. No systematic variation is seen. The strontium isotope ratio values lie within the range for fresh basalts but the $\delta^{18}O$ values cover a slightly greater range than fresh basalts.

Oxygen isotope ratios in the YGDC are probably primary for the most part, although there has been some lowering of whole-rock $\delta^{18}O$ from expected primary values of +5.0 and above. This may have been due to some low $\delta^{18}O$ meteoric water interacting with the magma, particularly at the margins. Hydrothermal alteration of cumulates is excluded, except perhaps in some of the mafic layers, by magmatic partitioning between whole-rock and plagioclase values. No systematic differences are seen between layers. In general it can be concluded that isotopic signatures in the YGDC are primary in origin; there has been some localised $\delta^{18}O$ depletion but to constrain this properly more sampling and analysis would be needed.

# CHAPTER 6: REGIONAL PERSPECTIVES, AND YGDC EMPLACEMENT

## 6.1 The Greenland-North American Proterozoic Rift

### 6.1.1 Description of rock types

The assemblage of rock types found within the Gardar Province, together with the abundant normal faulting and dyking, suggests that the magmatic activity was the result of an extended period of continental rifting. The abundance of alkaline rocks, including carbonatites, of major faults (which have exerted an influence on topography and the location of fjords) and aligned dyke swarms all resemble the features of present day and fossil rifts such as those of Kenya (Baker *et al.*, 1972; King and Chapman, 1972), Ethiopia (Mohr, 1983), the Rhine graben (Illies, 1978) and the Oslo graben (Ramberg and Spjeldnaes, 1978). A particularly good analogue is the Afar Depression of Ethiopia (Barberi *et al.*, 1975).

Many of these rifts are also characterised by axial gravity "highs" of +200 to +600 g.u., interpreted as being due to the presence of elongate mafic bodies at depth. These are sometimes flanked by gravity "lows", probably due, in the present day rifts, to the presence of a zone of partial melting (Fairhead, 1976). The Tugtutôq-Ilímaussaq dyke swarm is also underlain by a 30km wide gravity "high" with an amplitude of +300 g.u. (Blundell, 1978), which is superimposed on a coast-parallel system of contours resulting from isostatic response to loading by the ice cap (Fig. 6.1). This "high", by analogy with other rifts, is attributed to the presence of a mafic body beneath Tugtutôq, and the cross-sectional profile of the anomaly suggests that the density contrast occurs high up in the crust (Blundell, 1978). Blundell constructed two possible shapes for such an intrusive body, one sill-like and one dyke-like (Fig. 6.2). Any intermediate shape between the two would also be possible. The high becomes broader and reduced in magnitude towards the west, suggesting that the underlying structure may reach shallower levels to the east, possible outcropping as the Narsaq gabbro. Anorthosite bodies may be present at depth, giving rise to the abundant anorthosite xenoliths of the Gardar Province (Bridgwater and Harry, 1968), but the density contrast between anorthosite and the country rock is too small for such bodies to contribute to the gravity anomaly.

Figure 6.1 Bouguer anomaly map of the eastern Gardar region, contoured at 50 g.u. intervals. X-X' and Y-Y' indicate profile lines. From Blundell (1978).

Figure 6.2 Crustal models for the Tugtutôq gravity anomaly along profile X-X': (a) tabular intrusive body, in solid outline, +150 kg $m^{-3}$ density contrast, (b) dyke-like intrusive body, in dashed outline, +100 kg $m^{-3}$ density contrast. From Blundell (1978).

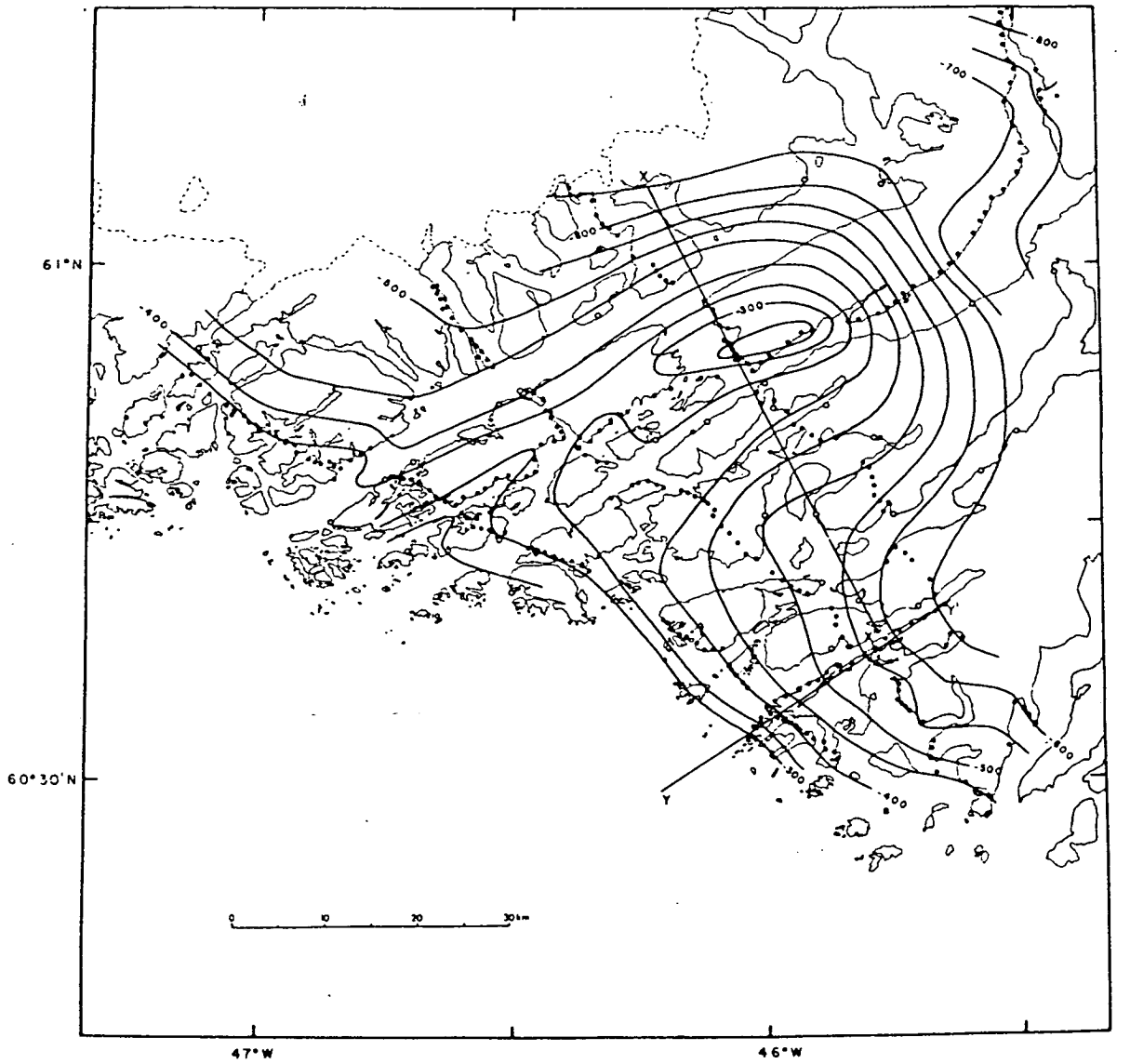
61°N
60°30'N
47°W
46°W
X
Y
800
700
600
500
400
300
0
10
20
30km

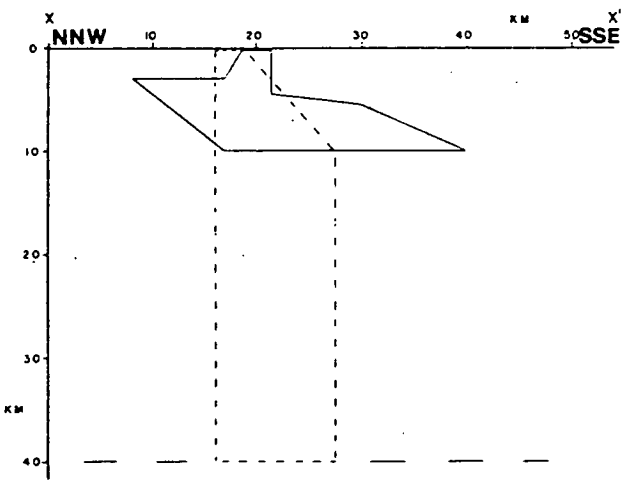
X
NNW
10
20
30
40
KM
50
SSE
X'
0
10
20
30
KM
40

There is no flanking gravity "low" to the positive anomaly, an observation attributed by Upton and Blundell (1978) to the absence of a partial melt zone. The "high" appears not to extend NE from Narsaq where the giant dykes may be present beneath the Eriksfjord Formation and there is no gravity high associated with the Nunarsuit-Isortoq dykes (Upton and Blundell, 1978), so it appears that the greatest volumes of basic magma were generated in the Tugtutôq region. The total amount of extension of the Gardar rift was probably about 10km (Blundell, 1978).

A similar gravity "high" marks a rift zone in the central United States (Ocola and Meyer, 1973; Van Schmus and Hinze, 1985; Cannon *et al.*, 1989). This is thought to be a graben structure of Keweenawan age (about 1100 Ma, similar in age to late Gardar activity), filled with basaltic lavas and sediments which outcrop in the region of Lake Superior but are buried beneath younger rocks elsewhere. It does have flanking "lows", unlike the structure in Greenland, but these are thought to be due to the presence of low density sediments. The total length of the rift is about 2000km and the amount of separation has been estimated at 60-75km (Van Schmus and Hinze, 1985). In places, the crust was thinned to a quarter of its original thickness or less (Cannon *et al.*, 1989), indicating that crustal separation was nearly achieved before rifting ceased.

This mid-continent rift is only a part of the widespread magmatism that occurred in North America at around the same time as the Gardar magmatism in Greenland. There had been some earlier Proterozoic activity, but magmatism reached a peak in the period 1300-1100 Ma (Baragar, 1977). The general similarities between the activity in Greenland and in North America have led to the idea that there may have been a continuous zone of rifting extending from Greenland to Lake Superior.

The distribution of Proterozoic magmatism in North America is shown in Fig. 6.3, and ages are tabulated in Table 6.1. The Helikian period lasted from ~1700-1100Ma with the peak period of magmatic activity between 1300 and 1100Ma (Baragar, 1977). Some authors subdivide the Helikian period, but this practice is not followed here, because the ages of some complexes are uncertain due to disagreement between different dating methods, the Sm-Nd dates of Ashwal and Wooden (1985) giving older ages than Rb-Sr or U-Pb dates. Early Helikian magmatic activity was characterised by the intrusion of numerous massif-type anorthosites, associated with troctolites, leuconorites and leucogabbros, while later activity became increasingly dominated by basaltic and less common felsic compositions. The anorthosites include the Nain (Hill, 1988), Harp Lake (Emslie, 1980), Michikamau (Emslie,

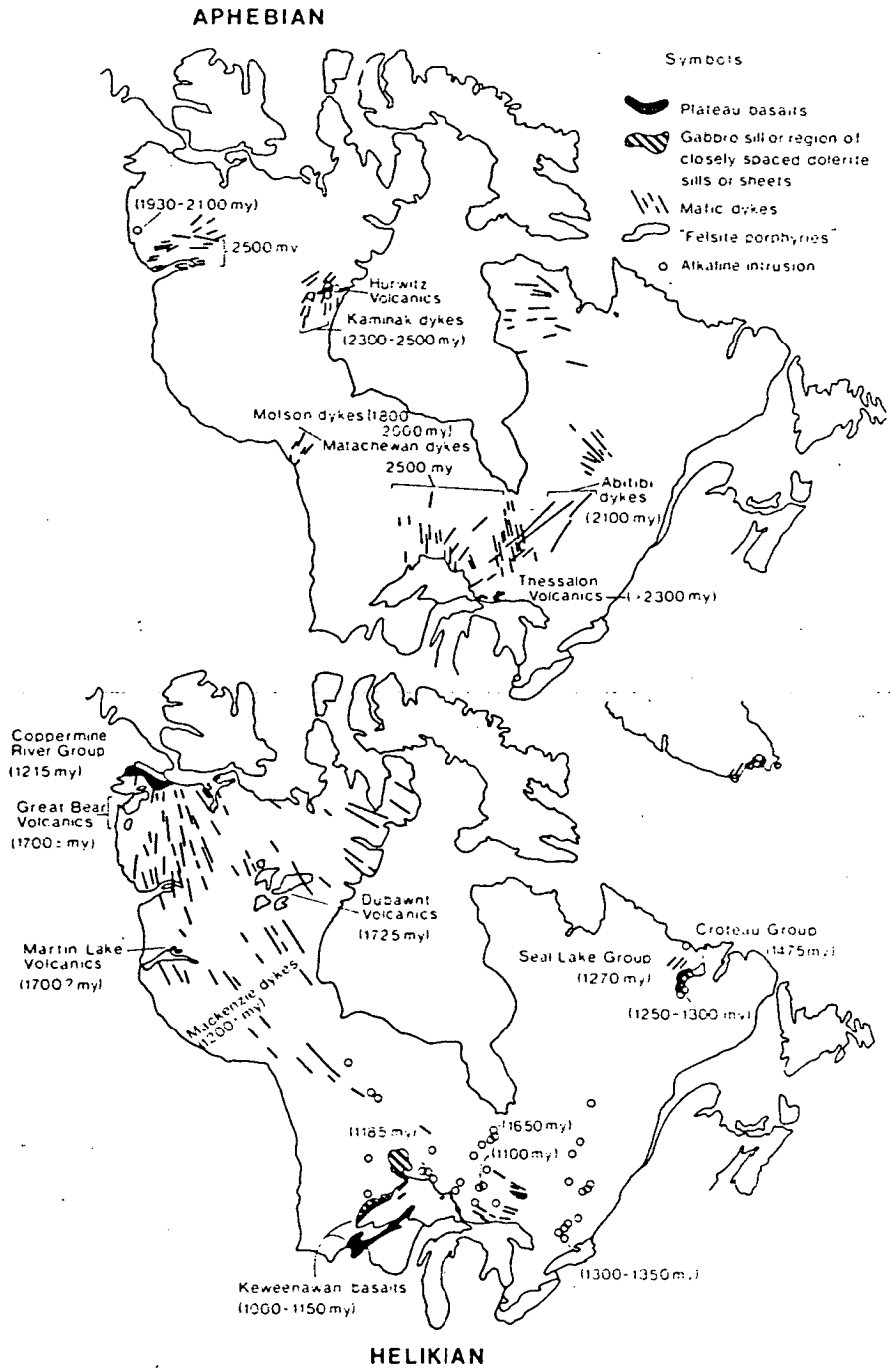


**Figure 6.3** Precambrian volcanic rocks of the stable North American crust, from Baragar (1977). Rb-Sr ages are quoted to $\lambda^{87}Rb = 1.47 \times 10^{-11}$ a$^{-1}$

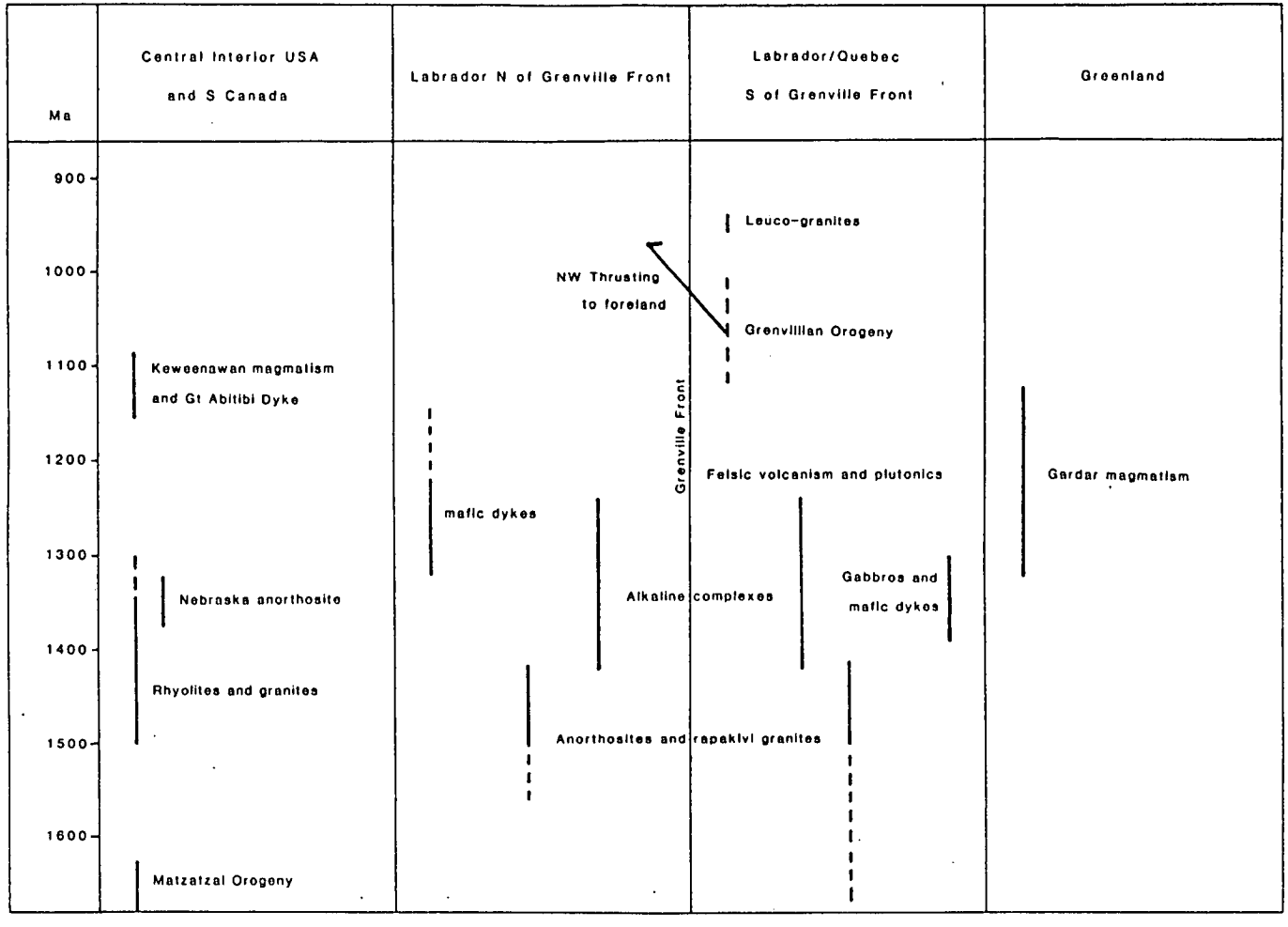


**Table 6.1** Timing of Helikian-age magmatism in North America and Greenland. Adapted from Windley (1989).

1970), Mealy Mountains (Emslie *et al.* (1983)) and Atikonak River complexes (Nunn *et al.*, 1986) (Fig. 6.4). Those within the Grenville province have been slightly affected by the 1100-1000 Ma metamorphism, but still show fairly good igneous textures. Many of the complexes have troctolitic to gabbroic marginal facies which are thought to be parental to the anorthosites. These marginal facies are usually high in Al (nearly 19 wt% $Al_2O_3$ in Michikamau, 15-18 wt% in Harp Lake, Emslie, 1980). They tend to be olivine tholeiites in composition and the most common mafic mineral of the anorthosites is orthopyroxene, followed by olivine and clinopyroxene. The plagioclase compositions are generally $An_{50\pm10}$ (Emslie, 1985).

Most of the complexes are the result of multiple intrusion. Many display feldspar lamination and/or modal layering, sometimes graded or cross-bedded (Emslie, 1980; Nunn *et al.*, 1986; Hill, 1988 Fig. 4b). Minor low-Al ferrodiorites, ferromonzonites and ferrosyenites are thought to be residual liquids. Late-stage emplacement of adamellites and alkali granites, sometimes making up nearly 50% of the exposed lithologies, is seen in many complexes. Several of the centres underwent uplift and erosion soon after solidification (for example the Harp Lake complex, upon which the slightly younger Seal Lake lavas rest unconformably).

Slightly younger magmatism produced several gabbroic or troctolitic complexes (sometimes with associated anorthosite), often closely associated with and intruding the older anorthosites. These include the Kiglapait (Morse, 1979), Hettasch (Berg, 1980), Shabogamo and Michael intrusions in Labrador (the first two being part of the Nain complex) and the Duluth and Mellen complexes of Lake Superior (Weiblen and Morey, 1980; Klewin, 1990). These intrusions, like the more anorthositic massifs, are frequently layered. The Kiglapait and Duluth intrusions are described in more detail in Chapter 7. The complexes often occur at irregular intervals along roughly linear trends (Baragar, 1977) (Fig. 6.3). Three major flood basalt provinces also date from this period: the Coppermine Bay (1215 Ma, Baragar, 1977), Keweenawan (1140-1120 Ma, Green, 1977) and Seal Lake (1350±92 Ma, Emslie, 1980) Provinces. These are similar to the Eriksfjord lavas in being associated with continental red beds, but are more tholeiitic in composition. The Seal Lake basalts could be contemporaneous with the Eriksfjord Formation, but the Coppermine and Keweenawan basalts appear to be substantially younger than those of Greenland. The North American lavas are closely associated with gabbroic plutons and may have been fed from the magma chambers represented by the intrusions. Phinney (1970) demonstrated that fractionation in the Duluth Complex had an influence on the

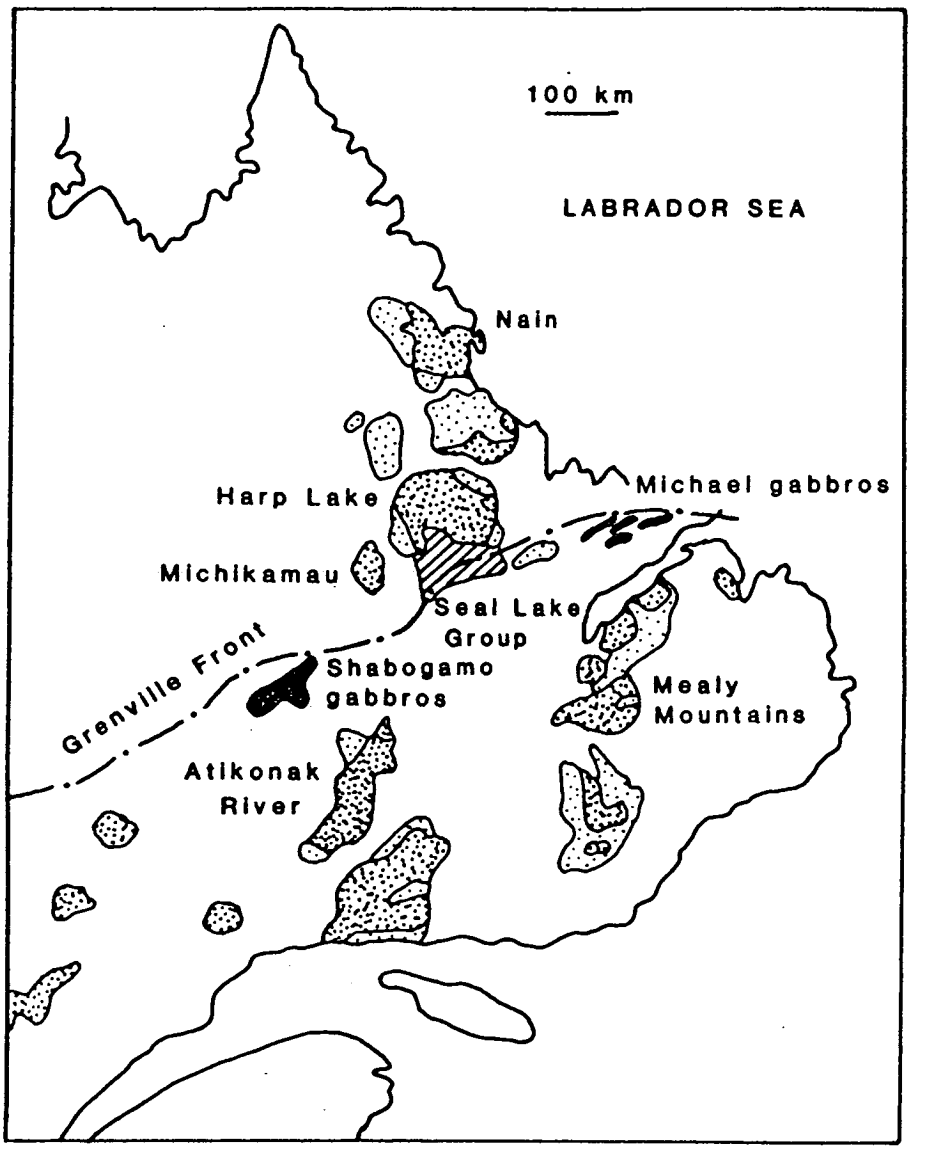


Figure 6.4 Location of Proterozoic anorthosite complexes in Labrador and eastern Quebec. Heavy stipple = anorthosite, light stipple = alkali granite, black = gabbro, striped ornament = Seal Lake lavas. Compiled from various sources in the text.

compositions of the Keweenawan lavas and Baragar (1977) suggested a connection, though not a direct correlation, between compositional variation in the Coppermine Bay lavas and in the underlying Muskox intrusion.

Several felsic igneous centres of a similar age occur, and may contain both intrusive and extrusive rocks. The intrusive rocks (for example those in the Flowers Bay, Strange Lake and Red Wine complexes of Labrador) are peralkaline granites with minor nepheline syenites and ijolites in the Red Wine complex (Collerson, 1982; Hill and Miller, in press). The occurrence of rare alkaline minerals, especially in the Red Wine complex, is reminiscent of Ilímaussaq. Extrusive rocks are generally rhyolites and pyroclastic deposits. The magmas were relatively anhydrous, rich in iron, alkalies and halogens and initial $^{87}Sr/^{86}Sr$ ratios were commonly higher than those of the Gardar intrusives.

Gabbroic dykes, striking mainly ENE, are associated with many of the anorthositic complexes and cut across all other lithologies. Three groups have been studied in detail: the Nain (Wiebe, 1985), Harp (Meyers and Emslie, 1977) and Mealy dykes (Emslie *et al.*, 1984). The Nain dykes have been dated at 1290-1042 Ma, the Harp dykes at about 1316 Ma and the Mealy dykes at 1380±54 Ma. All are slightly oversaturated to slightly undersaturated with respect to silica and the Harp dykes may have acted as feeders for the Seal Lake lavas. The Nain dykes are characterised by radiating clusters of plagioclase in the chilled margins, as are some of the Tugtutôq dykes, including the YGDC. The north American dykes appear to be direct continuations of the ENE-WSW dyke activity in Greenland. A proposed pre-Grenvillian rift running from Greenland to the Great Lakes is shown in Fig. 6.5.

In the region to the NE of Lake Superior are found the Abitibi dykes, the largest of which, the Great Abitibi Dyke, is more than 600km long and up to 250m wide (Ernst *et al.*, 1987). This was placed in an earlier phase of magmatic activity by Baragar (1977) (Fig. 6.3) but a recent U-Pb date of 1140 Ma (Krogh *et al.*, 1987) places it in the late Helikian period. It is thus almost exactly contemporaneous with the YGDC, if the Gardar dating is accurate. The Great Abitibi Dyke is composed of olivine gabbro with a central portion of more evolved rocks (gabbros and monzodiorites) thought to result from a separate magma pulse. The central part shows plagioclase lamination but the dyke is otherwise unlayered. Concentrations of Al, P and Ti are unusually high, and the composition appears to be similar to that of the YGDC but less alkaline. On the evidence of host rock metamorphic grade, Ernst *et al.* (1987) proposed that the dyke has been tilted along its axis, exposing deeper

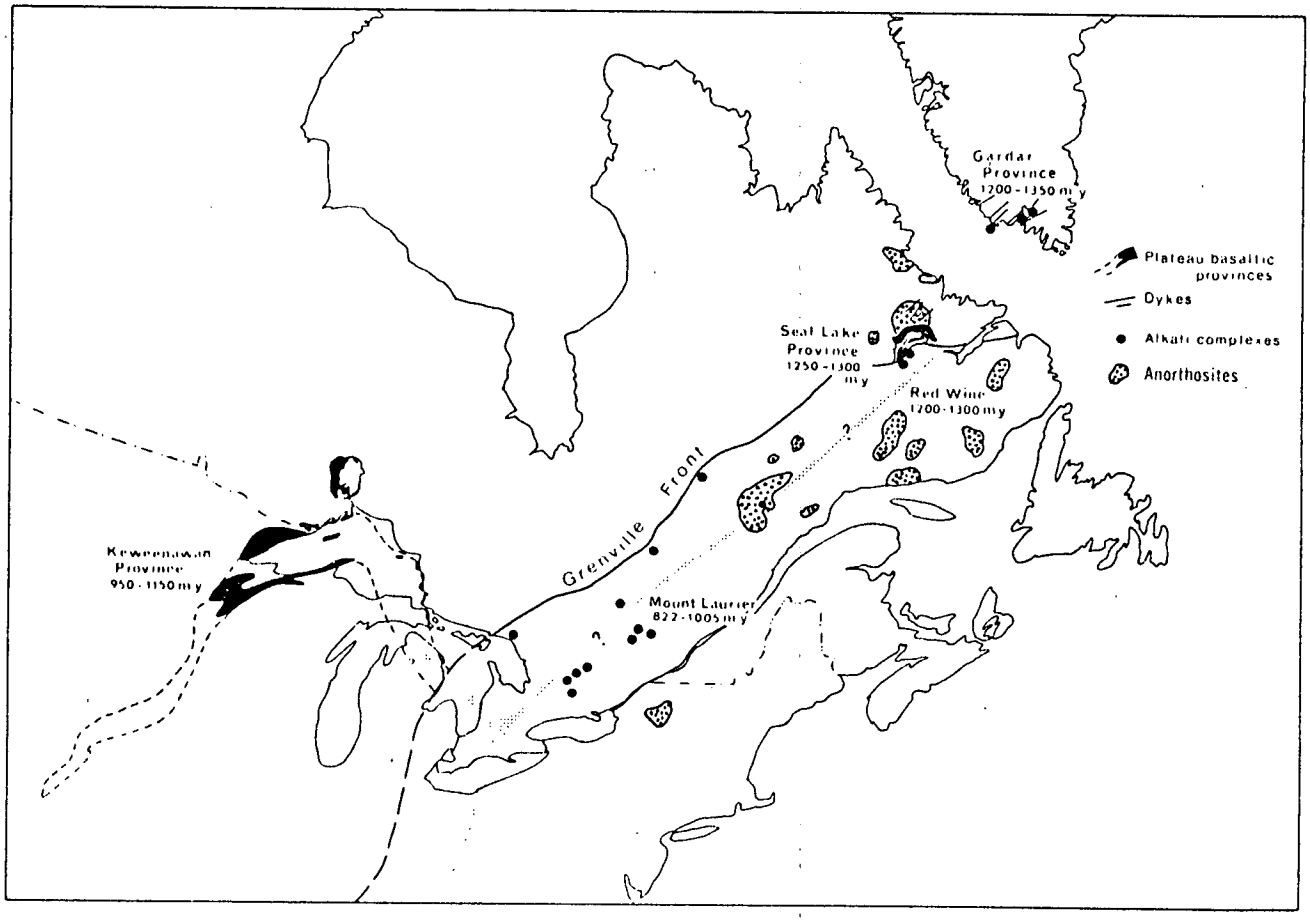


**Figure 6.5** Hypothetical pre-Grenvillian rift zone shown within the Grenville province. Greenland is restored to its pre-drift position relative to North America according to the Bullard fit (Bullard et al., 1965). The age of initial rifting is thought to be about 1250 Ma. After Baragar (1977).

levels to the SW. They also proposed that it was emplaced in response to a stress field related to Grenville orogenesis, as was postulated by Windley (1989) for the Keweenawan rift.

### 6.1.2 Origin of the magmas

The magmas parental to the anorthosite complexes have aroused much speculation. Such complexes are virtually confined to the Proterozoic (Emslie, 1985) and may result from unusual melting events in the crust or mantle which have not occurred since. Taylor *et al.* (1984) proposed a lower crustal source for massif-type anorthosites. They postulated that a large melting event in the Archaean or early Proterozoic, producing potassian granites and granodiorites, would have left the lower crust depleted in K, Rb, U, Th, REE and other elements concentrated in granitic melts, and enriched in Al, Sr and Eu. A more accepted view, however, is that anorthositic magmas originate in the mantle. They may have arisen by melting of a cpx-poor mantle source (Morse, 1982) or may have developed plagioclase supersaturation by fractionation of mafic minerals (Morse, 1982, Emslie, 1985). This may have been by high pressure fractionation at the base of the crust, or by crystallisation of both mafic minerals and plagioclase either during or after emplacement higher in the crust, with gravitational separation operating. Geophysical evidence shows that the negative gravity anomalies associated with the anorthosite complexes are often ovoid and shallow. Several complexes have small gravity "highs" within this "low" and this is attributed to the presence of mafic cumulates at depth (Morse, 1982). In addition, the Fe-rich presumed residual liquids do not show such a pronounced Eu anomaly as would be expected if they had crystallised only plagioclase, so settling of mafic minerals appears a reasonable explanation. The anorthosite complexes possess variable $^{87}Sr/^{86}Sr$ ratios (Ashwal et al., 1986) and minor contamination with crustal material is thought to have occurred. The adamellites and granites associated with the anorthosite complexes are thought to have different parent magmas, probably resulting largely from crustal anatexis (Morse, 1982; Emslie, 1985). The felsic magmas are thought to have resulted from mixing between mantle-derived melts and partially melted quartzofeldspathic crust (Collerson, 1982).

## 6.2 Genesis of the YGDC magmas

The Gardar rocks as a whole are more alkaline in nature than contemporaneous rocks in North America, and may result from lower degrees of partial melting. The basic rocks of the Gardar province, including the YGDC chilled margins, share certain characteristics, including high Fe/Mg, high Al/Ca ratios and high contents of F, Cl and $CO_2$ (Upton and Emeleus, 1987). It has been suggested that these attributes are the result of high pressure fractionation of mafic minerals, since the levels of compatible trace elements in the Gardar magmas are too low and the incompatible elements too high, for the liquids to have been primary melts (e.g. Martin, 1985). Olivine fractionation would increase the Fe/Mg ratio, while clinopyroxene would increase both the Fe/Mg and the Al/Ca ratios. Plagioclase is not on the liquidus at high pressures (Upton, 1971) and plagioclase crystallisation would not substantially affect the Ca/Al ratio. Alternatively, it is possible that the high Fe/Mg ratios may result from melting of unusually Fe-rich mantle while the high Al/Ca ratios could be due to melting from a mantle source with a low cpx:spinel ratio, as proposed for anorthositic magmas (Morse, 1982).

It is thought that melting was induced as a response to pressure release attendant upon rifting and asthenosphere upwelling, possibly aided by an influx of volatiles (Upton and Emeleus, 1987). The extensional stress field may possibly have been related to Grenvillian orogenesis to the south, as suggested for the Abitibi dykes and the Keweenawan rift. Giant dykes are restricted to late Gardar times and may be evidence for exceptionally high strain rates of the lithosphere. Incompatible element plots (section 4.5.1) show that the YGDC shares the characteristics of high P and low Nb with other Gardar rocks (Fig. 6.6). Thompson *et al.* (1983) explained low values of Nb in continental flood basalts by contamination by low-Nb crust, but this would not have led to the high P values in the Gardar rocks and would probably also have raised the $^{87}Sr/^{86}Sr$ ratio. Pearce (1988) found that Nb troughs were only observed for oversaturated dykes in the area around Narsarsuaq. He proposed that $CO_2$ was more important in the generation of the undersaturated rocks while $H_2O$ was involved in the generation of the oversaturated members of the suite, and that the presence of water may have stabilised a Nb-bearing phase in the mantle, as suggested by Saunders *et al.* (1980).

A depleted lower crustal granulite source with low $^{87}Sr/^{86}Sr$, as proposed for anorthosites by Taylor et al. (1984) could also have been a source for the Gardar magmas but this could not account for the enrichment in incompatible elements

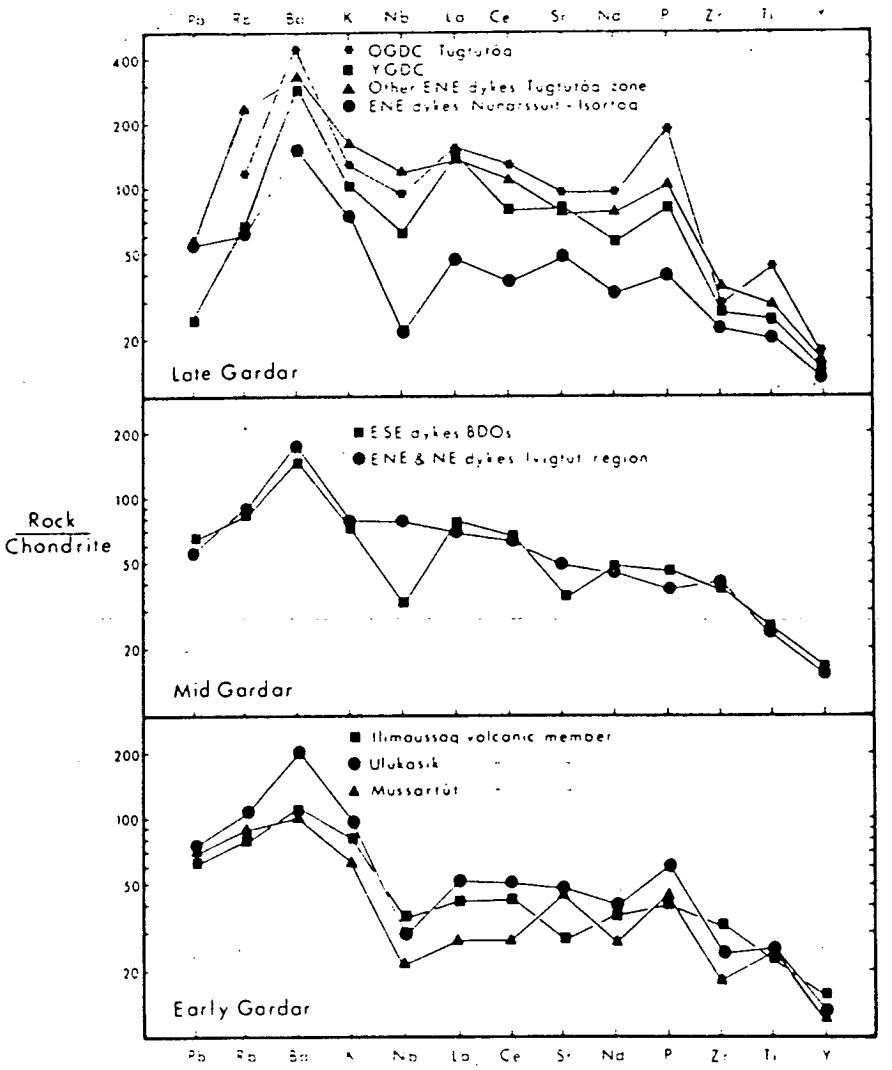


**Figure 6.6** Chondrite-normalised incompatible-element plots for averaged groups of Gardar basaltic-hawaiitic rocks. From Upton and Emeleus (1987).

(Martin, 1985). In addition, almost complete melting of such a source would have been necessary, requiring unreasonable heat fluxes (Upton and Emeleus, 1987).

The magma volume in the YGDC probably approaches 2000km$^3$, and it must be one of the largest bodies of alkali gabbro known. The magmas were already residual at the time of emplacement and so the volume of the chamber in which high pressure fractionation took place must have been considerably larger. The parental magma (high in Mg, Ni and Cr) was the result of small degree partial melting, and thus melt must have been extracted from extremely large volumes of mantle. For this process to operate efficiently, it may be necessary to postulate the existence of a mantle plume, which provided a constant source of undepleted mantle over a considerable period of time.

The Tugtutôq-nunataq dyke swarm is geochemically distinct from earlier Gardar basic rocks and from those of the Nunarssuit-Isortoq zone in having high K, P, Ba, Sr, Nb and LREE contents (Upton and Emeleus, 1987). The Zr/Nb ratio provides a useful discriminator, with most Gardar basic rocks having a Zr/Nb ratio of about 18 while that of the Tugtutôq-nunataq dykes ranges from 3 to 7. The latter can be further subdivided (Pearce, 1988) into undersaturated rocks with Zr/Nb of about 3.9 and oversaturated rocks (including the YGDC and its continuations) with Zr/Nb of about 6.4. The differences between the Tugtutôq-nunataq dykes and other Gardar basic rocks are thought to be primary and due to source characteristics, differing degrees or depths of partial melting, or wall-rock interaction. They are not thought to result from the extent of fractional crystallisation (Upton and Emeleus, 1987). The degree of partial melting probably provides the best explanation, with the undersaturated rocks representing lower degrees of melting than the oversaturated rocks. The depth of melting may also play a part. Modelling by Pearce (1988) suggests that the oversaturated rocks are products of a spinel-bearing source while the undersaturated rocks were generated from a garnet-bearing (deeper) mantle source. The small volumes of ultramafic lamprophyres and many of the carbonatites probably reflect very small partial melts (Upton and Emeleus, 1987).

The variety of rock types in the Gardar province arises from low pressure fractionation of the relatively homogeneous basic magmas which rose to higher levels in the crust. Olivine and plagioclase were the first fractionating phases, joined later by other phases, the order of fractionation depending upon the silica saturation and other factors such as the oxygen fugacity. Klewin (1989) proposed a similar model

for the evolution of the Keweenawan magmas, involving high pressure fractionation of olivine and clinopyroxene to give high-Al magmas, followed by low pressure olivine + plagioclase ± clinopyroxene fractionation.

## 6.3 Emplacement and cooling of the YGDC

### 6.3.1 YGDC emplacement

Partial melts of the Gardar upper mantle must have collected in large chambers, perhaps being halted by the density contrast at the base of the crust (Cox, 1980; Morse, 1982; Sparks and Huppert, 1984). Here they underwent extensive fractionation of olivine ± clinopyroxene, until the magma density was lowered sufficiently to rise through the crust. Some batches of hawaiitic magma were trapped higher in the crust and fractionated plagioclase, possibly with other minerals, forming large anorthosite bodies by plagioclase flotation. Other magmas ascended to higher levels or to the surface in response to buoyancy forces and extensional stresses. Some gained anorthosite xenoliths as they ascended.

The size and shape of a magma pulse ascending within the crust depends upon several parameters such as the direction of principal stress, the variation of stress with depth, the tensile strength of the crust and the rheology of the melt and its surroundings (Maaløe, 1985; Macdonald *et al.*, 1988). In homogeneous crust, a dyke will have a vertical cross-section like a highly elongated, inverted tear-drop (Weertman, 1971; Pollard and Muller, 1976). If the YGDC ascended with this shape, then it probably narrows with depth, but it is not possible to tell how rapidly it narrows, or whether it still remains connected to a reservoir within the crust.

A dyke may be driven either by excess pressure in the magma chamber or by buoyancy. Excess pressure can move the magma either horizontally or vertically but buoyancy forces only operate vertically. The rates of vertical ascent of magmas can be estimated from the settling velocities of xenoliths to be between several cm/sec and several tens of cm/sec (Spera, 1980). However, emplacement of elongate dykes (such as the 430km long Cleveland Dyke of Northern England, Macdonald *et al.* (1988)) by purely vertical movement requires an extremely small horizontal stress gradient and also a highly elongate magma chamber, so a substantial amount of lateral movement is probably involved in the emplacement of such dykes.

Macdonald *et al.* (1988) gave equations to calculate lateral flow and found that the Cleveland Dyke was probably emplaced at a rate of between 1 and 5 m/sec. Einarson and Brandsdottir (1980) also obtained a figure of around 1m/sec from seismic evidence for lateral dyke propagation in Iceland. Solution of Macdonald *et al.*'s equations requires an iterative approach since several quantities are unknown, and this has not been attempted for the YGDC.

It is thought that the YGDC also had a large component of lateral emplacement. If the YGDC magmas moved at even a tenth of the speed suggested above, then the complex would have been emplaced in a very short time, perhaps days or weeks. The centre for emplacement of the complex may have been in the Ilímaussaq area, since this obviously acted as a focus for magmatic activity during the Late Gardar period. The presence of a feeder for the YGDC in this area might explain the maximum gravity anomaly observed. The presence of widespread troctolitic xenoliths in the Dymæs-Narsaq and Ilímaussaq complexes suggests that to the east of the present-day outcrop in the Narsaq area, the complex was more extensive. Lateral movement to the west and east from this region would have produced the Tugtutôq and nunataq sections of the dyke. The presence of a zoned magma chamber within the crust could explain the compositional variation within the dyke, if successively deeper and less fractionated levels were tapped as dyke emplacement proceeded. Compositional variation within the chamber would have been produced by olivine + plagioclase fractionation. This hypothesis does not rule out later vertical tilting along the dyke axis towards the ENE, as suggested in Chapter 2. It seems likely that there was some vertical separation of the denser, more primitive melts and the less dense syenitic residual liquids. A possible reconstruction of the complex is shown in Fig. 6.7. However, the lack of structure in the basement rocks, and the fact that dips of the Eriksfjord Formation have been affected by the later Dymæs-Narsaq and Ilímaussaq complexes, make it impossible to assess the degree of tilting that might have occurred.

The halting of the YGDC at the unconformity between granitic basement and overlying lavas and sediments was probably a result of the change in density of the host rocks. The lack of crustal xenoliths within the YGDC suggests that stoping was not an important process in the emplacement of the dyke, although it does appear to have been significant in the intrusion of the Isortoq giant dykes (Bridgwater and Coe, 1970). It is possible that some transtension accompanied the dilation of the country rocks, but further fieldwork would be required to determine the exact emplacement

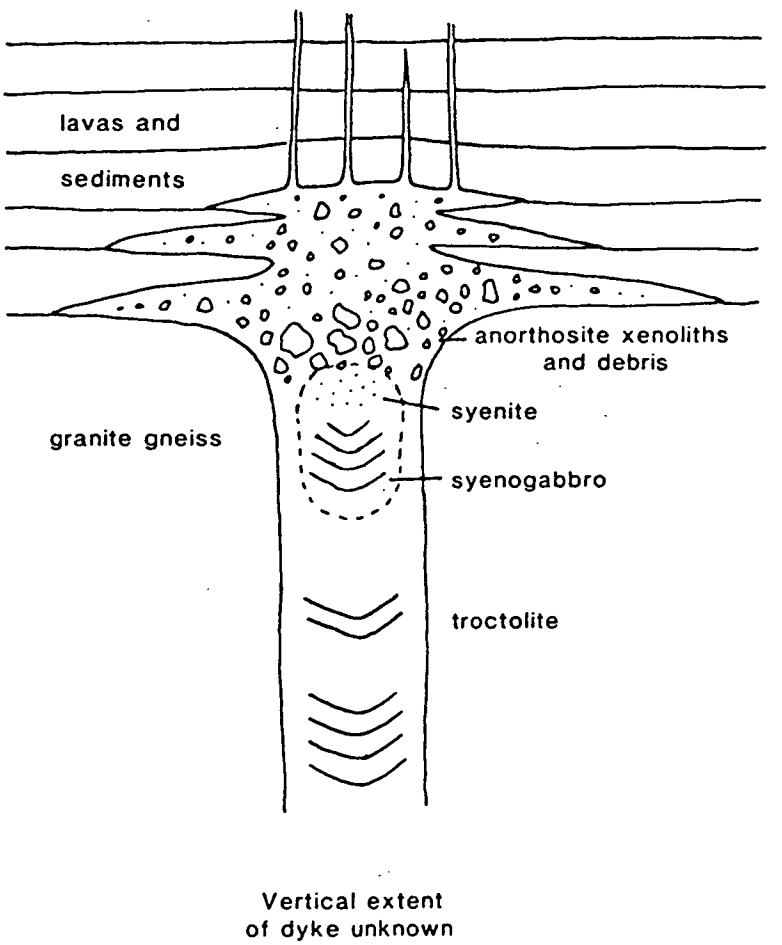


**Figure 6.7** Inferred structure of the YGDC in the Tugtutôq-Narsaq area.

mechanism. The dyke shows constrictions in places (Fig. 2.1) and it is thought that this also occurs in vertical sections, so that the sidewalls are not always vertical but undulatory.

Most of the complex was intruded as a series of closely-spaced pulses, with insufficient time between each for internal contacts to form. The layered pod at locality G (Marrait) may have been produced by a pulse of magma emplaced after the main intrusive episode. It is finer-grained than the surrounding troctolite with fairly sharp margins, and small patches of the surrounding material are found within the pod. In addition, the order of crystallisation of phases is slightly different from that seen elsewhere in the YGDC in that apatite appears earlier. Furthermore, it was noted in Chapter 4 that the incompatible element signature of troctolites from the layered pod differs from that of all other YGDC trocotlites in showing no Sr peak, and in fact resembles the patterns seen in the chilled margins. The 10m synformally layered pod 140m from the south margin at locality I may be another example of a later pulse of magma, but apart from these two examples no evidence for multiple intrusion has been found.

### 6.3.2 An estimate of solidification time for the YGDC

An estimate of the time taken for solidification of the intrusion can be obtained using Equation 4-143 of Turcotte and Schubert (1982). This equation assumes that the magma and country rock had the same thermal properties and that no convection, thermal erosion or crystal sedimentation occurred. These assumptions are obviously simplifications but enable an order-of-magnitude time to be calculated. The time for solidification, $t_s$ is given by:

$$t_s = \frac{a^2}{4\kappa\lambda^2}$$

Where: $a$ = dyke half-width

$\kappa$ = thermal diffusivity

$\lambda$ = the dimensionless position of the solidification front, dependent on L (latent heat), c (specific heat) and $\Delta T$ (initial temperature contrast)

Using Equation 4-142 and Fig. 4-36 of Turcotte and Schubert with L = 320 kJ $kg^{-1}$, c = 1.2 kJ $kg^{-1}$ $K^{-1}$ and DT = 900 K, it can be found that $\lambda$ is about 1.75. Taking a as 300m and $\kappa$ as 5 x $10^{-5}$ $m^2$ $s^{-1}$, then $t_s$ = 2540 years. The errors on the values of L, c etc. are not known, and the presence of convection would reduce the solidification time, but it is thought that the YGDC may have solidified in 1000 to 3000 years.

## 6.4 Summary

The Gardar magmatism was only part of a widespread Proterozoic rifting event across eastern North America. The Tugtutôq-Narsaq zone is characterised by an elongate gravity high, similar to those observed along modern rifts. The magmatic activity in the North American province was characterised by the extrusion of flood basalts and the intrusion of massif-type anorthosites associated with ferrodioritic and ferrosyenitic derivatives, together with alkali granites. To the NE of Lake Superior the Abitibi dyke swarm shows many similarities in age, trend and composition to the Tugtutôq-Narsaq dyke swarm, including the YGDC. Magmas in the entire rift zone were generally high in Al and Fe, and it is thought that they were generated within the upper mantle. This may have been poor in cpx, resulting in high Al/Ca ratios, or the magmas may have undergone high-pressure fractionation of ol + cpx (Upton and Emeleus, 1987). The Greenland magmas were more silica-undersaturated than their North American equivalents and probably represent a lower degree of partial melting. The genesis of the alkaline Gardar magmas required a very large volume of mantle and it is possible that a mantle plume was involved.

The YGDC magmas probably collected in a chamber higher in the crust and were then emplaced relatively rapidly. It is likely that there was a substantial component of lateral movement during intrusion. Once emplaced, heat flow calculations indicate that the YGDC may have solidified in 1000-3000 years.

# CHAPTER 7: ORIGINS OF LAYERING

## 7.1 The YGDC in comparison with other layered intrusions

Brief descriptions of various well-known layered intrusions are given below; many more layered igneous bodies are known but only key examples are described here for comparative purposes. The reader is referred to Wager and Brown (1968) for further examples.

### 7.1.1 Archaean and Proterozoic examples

Stillwater Complex, Montana, USA

This 2700 Ma complex is exposed in a 30km strip between metamorphosed rocks and tilted Palaeozoic sediments. About 5km remains of what must originally have been a thicker body. The complex shows many similarities to the lower part of the Bushveld Intrusion of South Africa. It is divided into Basal, Ultramafic and Banded Zones on the basis of phase appearance or disappearance. A stratigraphic column is shown in Fig. 7.1.

A chilled facies is occasionally developed but in many places cumulates directly overlie country rock. Different zones show lateral variations in thickness. The Basal Zone consists of norites, bronzitites and gabbros while the Ultramafic Zone contains at least 15 cyclic units of dunite (commonly with a chromite horizon near the top) followed by poikilitic harzburgite, granular harzburgite and usually orthopyroxenite (McBirney, 1984). Most units have plagioclase and clinopyroxene as intercumulus phases.

The Banded Zone (the remainder of the intrusion) consists of norites, gabbros and anorthosites. The following descriptions of layering are taken from Wager and Brown (1968) and McCallum *et al.* (1980). Modal layering is well developed in the norites and may be very fine and regular ("inch-scale" layering) or coarser (layers up to 1m thick). Mineral lamination, slump and scour features, elongate inclusions of orthopyroxenite and highly elongate orthopyroxene crystals (10-15cm) are all found. Within this zone the J-M Reef occurs. This is rich in Pt-bearing sulphides and shows many similarities to the Merensky Reef of the Bushveld Intrusion.

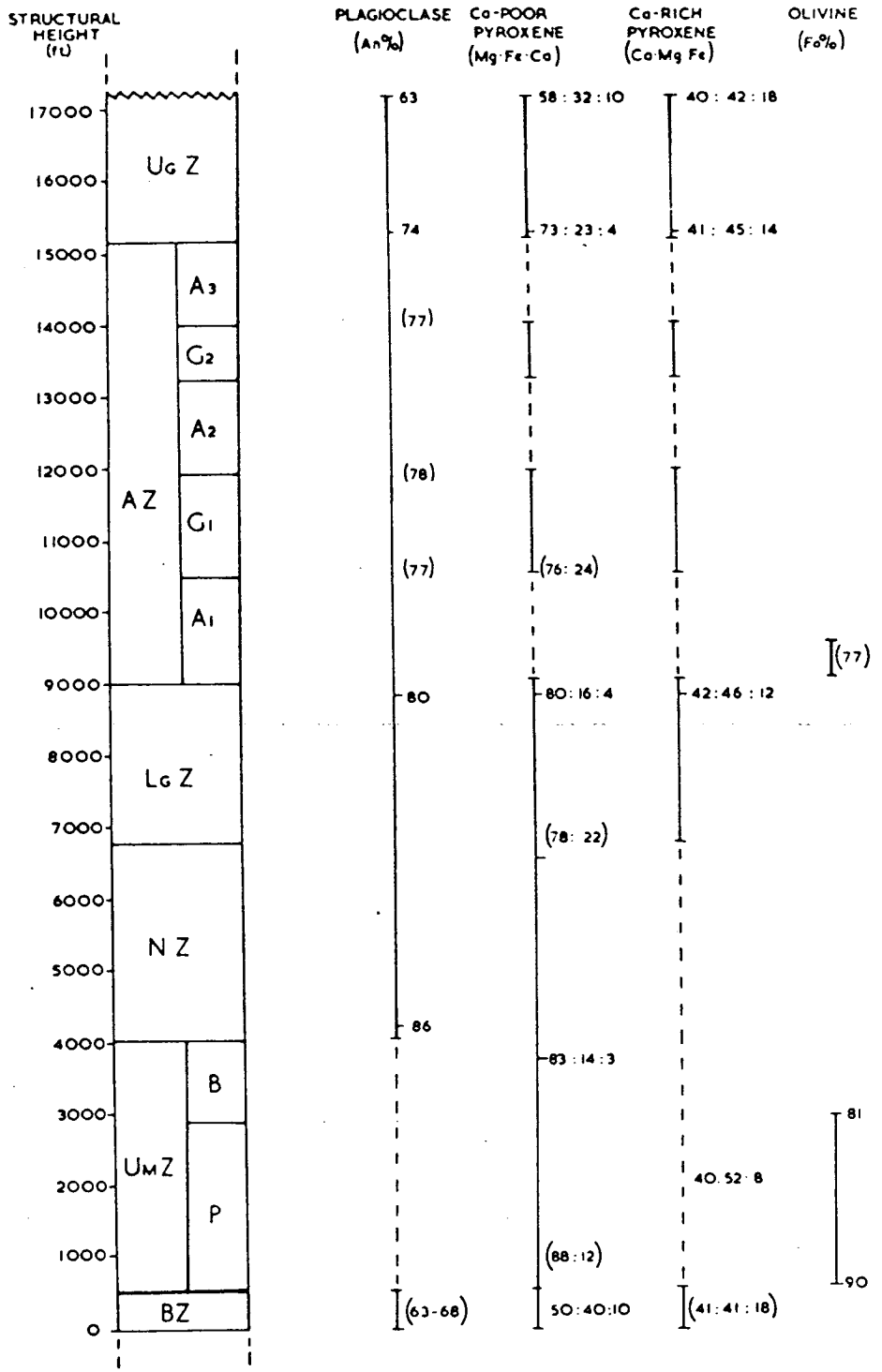


**Figure 7.1** Subdivision of the Stillwater intrusion. Broken lines indicate horizons where minerals only have intercumulus status. Compositions were determined analytically, except for those in brackets, which were determined optically. BZ = Border Zone, UmZ = Ultramafic Zone (P = Peridotite Member, B = Bronzitite Member), NZ = Norite Zone, LgZ = Lower Gabbro Zone, AZ = Anorthosite Zone (A1, G1 ... = Anorthosite and Gabbro Subzones), UgZ = Upper Gabbro Zone. From Wager and Brown (1968)

The gabbros are plagioclase-orthopyroxene-clinopyroxene cumulates. Layering is less well developed than in the ultramfic rocks but some modal variation (including reverse modal grading) and mineral lamination may be seen.

The Great "Dyke", Zimbabwe

Dated at 2500Ma (Hamilton, 1977), the Great "Dyke" extends for about 480km in a NNE-SSW direction and has an average width of 8km. It is thought to be a series of four separate complexes giving the appearance of a dyke (Worst, 1958, Wilson, 1982). Ultramafic rocks dominate the "Dyke" but at the centre of each of the four complexes an area of gabbroic rocks is found, elongated along the length of the intrusion. Layering dips inwards from the margins, flattening from about 25° to 5°, and dipping towards the centre of each complex from north and south.

The sequence of rock types differs in detail within each complex but some generalisations can be made. The ultramafic rocks are dunites, harzburgites and bronzitites and several cycles can be recognised. An idealised cycle begins with a chromite layer overlain by a dunite (or harzburgite) grading upwards through olivine bronzitite to bronzitite. Rhythmic modal variations on the scale of a few cms are seen in the olivine bronzitites and harzburgites. In all four complexes a websterite marks the top of the ultramafic succession and is overlain by gabbro. The gabbros (which all contain either primary hypersthene or inverted pigeonite in addition to plagioclase and augite) are laminated but otherwise apparently unlayered. Mineral compositions are among the most primitive seen in any layered intrusion. A summary of the mineralogy of the Hartley Complex (which has the thickest sequence of exposed rocks) is shown in Fig. 7.2.

Jimberlana Intrusion, W. Australia

A smaller analogue of the Great "Dyke", of a similar age (2420 Ma, Campbell *et al.*, 1970), the Jimberlana Intrusion is an E-W trending body, dyke-like at the surface but tapering downwards. A schematic cross-section of the intrusion is shown in Fig. 7.3. It is 180km in length and about 5.5km deep with a maximum width of 2.5km, and shows seven "boat-shaped" complexes along its length. The ultramafic and basic rocks making up the separate complexes occur as synformal layers dipping inwards from the sides and are near vertical at the margins but horizontal in the

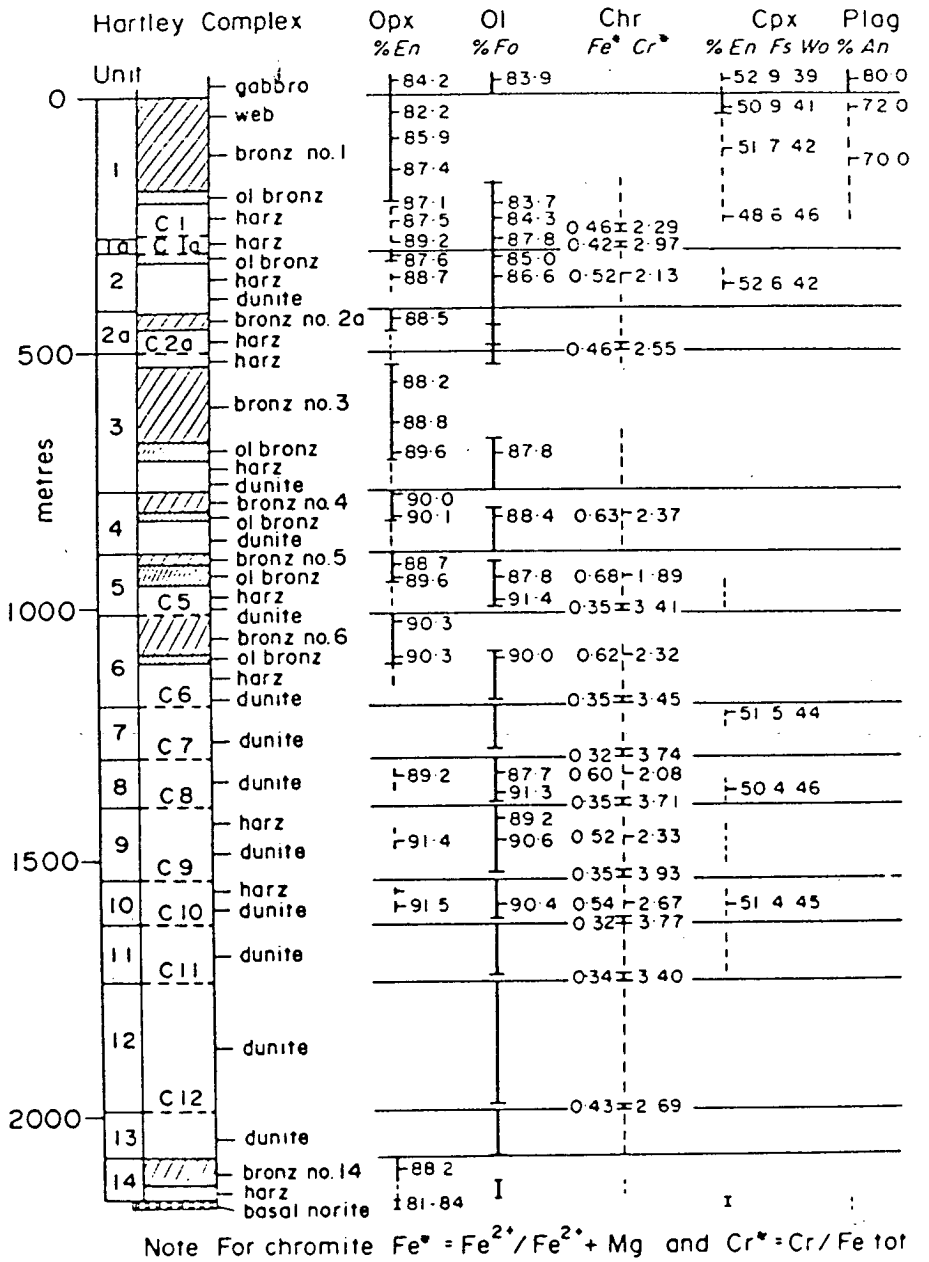


**Figure 7.2** Stratigraphic section of the ultramafic zone of the Hartley Complex of the Great Dyke. Chromite seams are numbered C1 to C12. Open hatching represents bronzites (bronz) and close hatching, olivine bronzitites (ol bronz) Unhatched areas represent poikilitic harzburgite (hartz) and dunite. Cumulus phases are shown by the solid lines and intercumulus phases by the dashed lines. For chromite, dashed lines indicate that the mineral is cumulus but constitutes a small proportion of the rock. A summary of the cryptic variation is also given. From Wilson (1982).

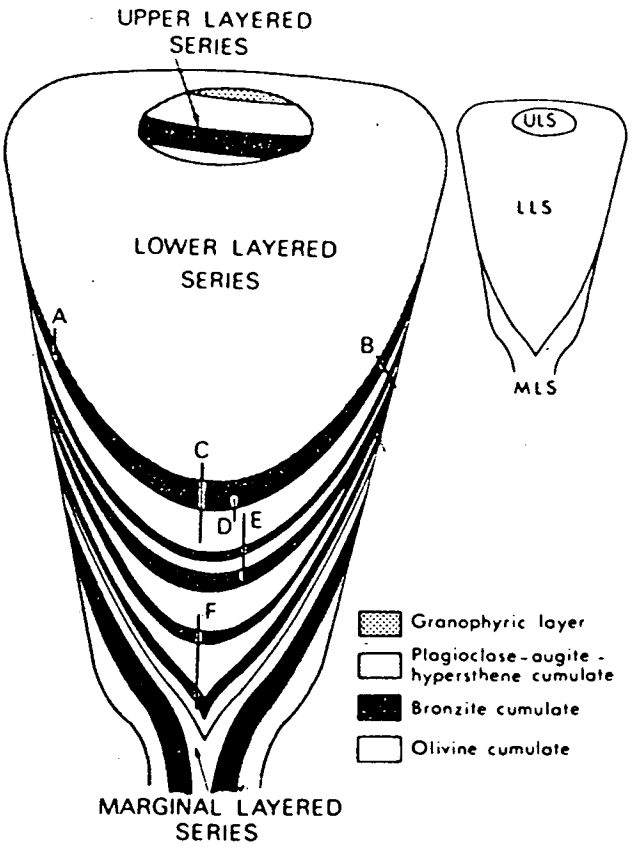


**Figure 7.3** Schematic cross-section showing the general structure of the Jimberlana intrusion. The locations of some of the drill holes used to construct the section are indicated. The diagram has been simplified by omitting the macrorhythmic layering of the upper layered series. From Campbell (1978).

centre. Two layered series have been recognised (Campbell *et al.*, 1970). The Lower Layered Series (LLS) consists of an alternating sequence of olivine cumulate and bronzite cumulate layers overlain by a thick hypersthene gabbro. The Upper Layered Series is similar to the LLS but smaller with flatter dips, and has an upper granophyric layer. The intrusion has a shallow easterly plunge causing deeper levels to be exposed to the west. The dyke connecting and surrounding the layered complexes is itself layered and is referred to as the Marginal Series (McClay and Campbell, 1976).

Within the Marginal Series, a fine-grained chilled gabbro is succeeded inwards by bronzite and then olivine cumulates. In the two layered series, layers traced from the centre to the edge of the intrusion become thinner and more orthocumulate in texture. Occasional modally-graded layers occur (usually showing reverse grading), with adcumulus textures at the base and orthocumulate textures at the top.

Bushveld Intrusion, S Africa

This large layered body of tholeiitic rock has an area of outcrop that measures about 270km N-S by 450km E-W. It is thought to consist of a lopolithic body emplaced through two to four feeders, with an original thickness in excess of 8km. The age of intrusion is about 2000 Ma. Much of the roof of the intrusion consists of metasediments and felsic volcanics only slightly younger than the gabbroic complex (McBirney, 1984).

A chilled marginal facies is only locally developed and in many places cumulates rest directly on country rock. The rocks are usually adcumulates (some are poikilitic adcumulates) and a summary of the mineralogy of the intrusion is given in Fig. 7.4. The Basal Series consists of olivine cumulate layers about 7m thick between thicker layers of bronzite cumulate. Above this comes the Critical Zone where olivine disappears, and chromite and plagioclase become modally important phases. The junction between the Basal Series and the Critical Series is marked by the Main Chromite Seam. Within the Critical Series, numerous sharply defined layers of chromite cumulate several cms in thickness occur. These tend to bifurcate laterally but the total thickness remains the same in any one section. Anorthosite xenoliths may be found within the chromite layers. Just below the base of the Main Zone is the bronzite cumulate of the Merensky Reef, which contains Pt-bearing

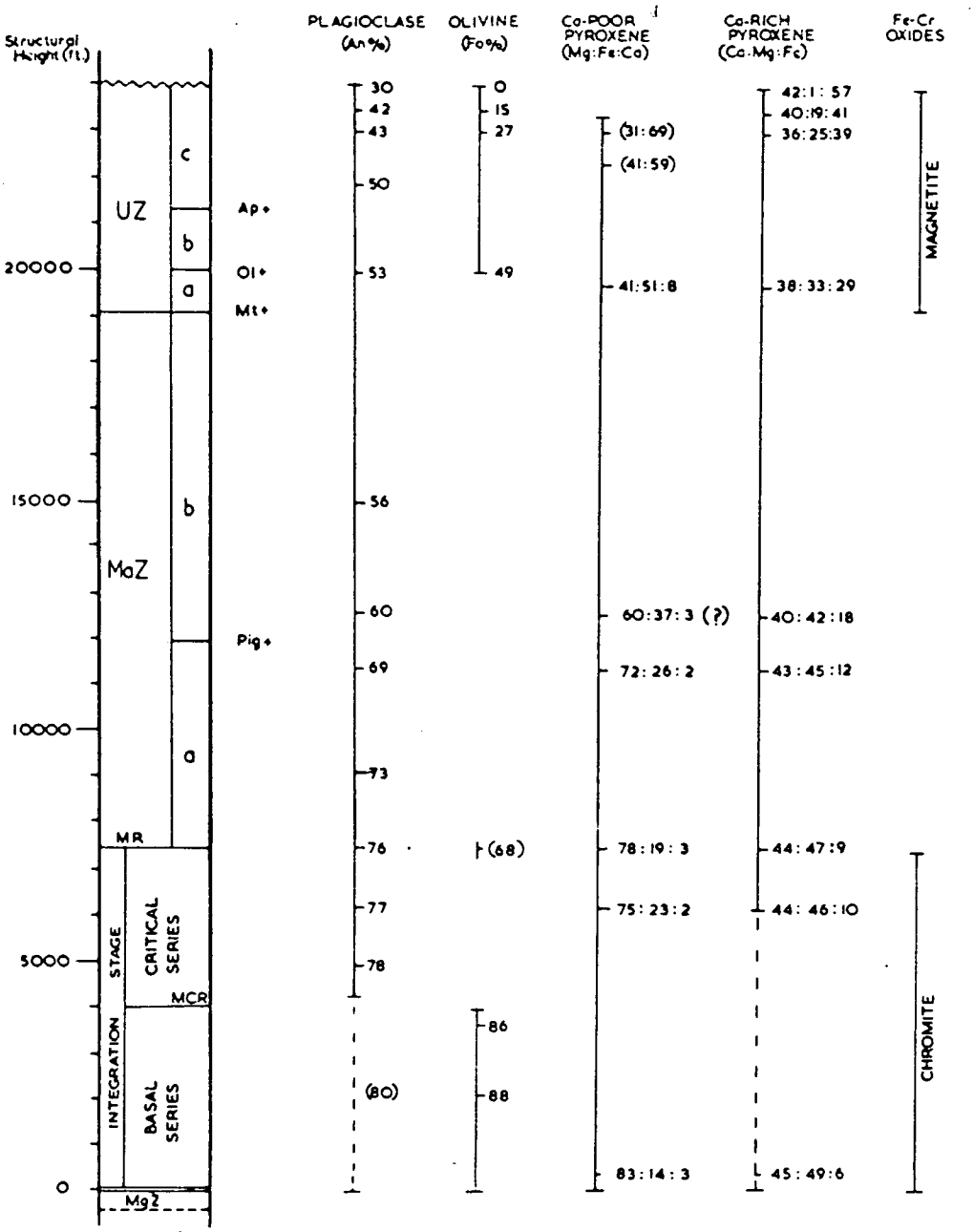


**Figure 7.4** Stratigraphy of the Bushveld intrusion Compositional determinations are predominantly optical and broken lines indicate the intercumulus status of a mineral. MgZ = Marginal Zone, MCR = Main Chromitite Layer, MR = Merensky Reef, MaZ = Main Zone, UZ = Upper Zone. From Wager & Brown (1968).

sulphides. The Reef, although only 1-5m thick, can be traced over more than 300km. The base of the Reef is irregular with "potholes" protruding down into the rocks below. Channel and scour structures also occur within the Reef.

The Main Zone is composed of intermittently layered two-pyroxene gabbros (cpx dominant) and gabbronorites (opx dominant), with layering defined by regular modal variations. Anorthosite xenoliths still occur. The layers dip at 10-15° towards the centre of the intrusion, but these are not thought to be primary; initial dips were probably only about 1° (Cawthorn, pers. comm. 1988).

The base of the Upper Zone is marked by the first appearance of cumulus magnetite and the zone is subdivided where olivine reappears and where cumulus apatite begins to crystallise. Magnetite (with some ilmenite) forms about 16 major monomineralic layers, the largest about 7m thick, often alternating with anorthositic layers. The layers are frequently graded. Anorthosite xenoliths occur within the magnetite layers and are often elongated parallel to the layer bases. The uppermost rocks of the intrusion are ferrodiorites and ferrosyenodiorites.

The Kapalagulu intrusion in Tanzania shows many similarities to the Bushveld intrusion (Wadsworth *et al.*, 1982) but is less well exposed.

Muskox Intrusion, NW Territories, Canada

This intrusion has the form of a 150-600m dyke which widens upwards into an elongated intrusion, a maximum of 11km wide and with a cross-section roughly that of an apex-down triangle (Figure 7.5). It has been tilted so that the dyke (presumably a feeder) is exposed for 55km to the south of the wider part of the intrusion. The age is approximately 1200Ma (Irvine and Smith, 1969). The wider part coincides with an unconformity between earlier Proterozoic metamorphic basement and overlying mid-Proterozoic sediments passing up into lavas.

Within the feeder dyke, bands of bronzite gabbro and picritic gabbro are found parallel to the walls. The wider part of the intrusion consists of a marginal series, a central layered series and an upper border zone. In the marginal series, pyroxene contents decrease, olivine increases and mineral compositions become more primitive inwards. In the layered series, olivine and orthopyroxene, sometimes with chromite, are cumulus phases in the lower rocks, subsequently joined by augite and finally plagioclase. Olivine compositions are fairly uniform at $Fo_{85-80}$ in the lower

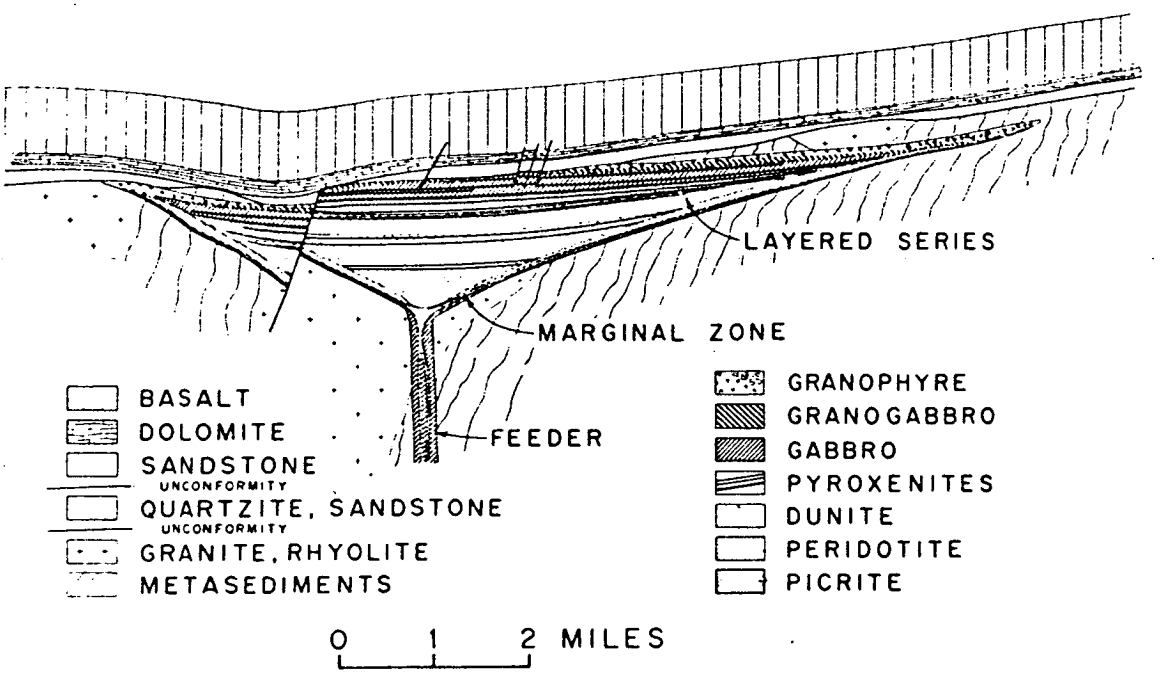


**Figure 7.5** Restored cross-section of the exposed part of the Muskox Intrusion. Granogabbro = granophyre-rich gabbroic rocks. From Irvine (1970).

part of the layered series and change from $Fo_{80-60}$ in the plagioclase-bearing portion. Chromite seems to have ceased crystallising whenever clinopyroxene appeared. Most of the layers, defined by variations in proportions of cumulus minerals, are several tens of metres thick and laterally continuous with sharp contacts. There is some cyclicity, with olivine decreasing in amount upwards through the cyclic units. Smaller-scale layering is only rarely developed.

Magnetite, and then ilmenite, only appear as cumulus phases within a few hundred metres of the roof contact. The upper border zone consists of gabbro grading up into granophyre, the latter probably being a product of melted country rock sandstones.

Kiglapait Intrusion, Labrador

One of the best-documented of the Helikian plutons of North America, the Kiglapit intrusion possesses many features which closely resemble those of the YGDC. Part of the predominantly anorthositic Nain Complex, the Kiglapait Intrusion has an age slightly younger than 1400Ma (Morse, 1979). This makes it contemporaneous with, or slightly older than the Gardar magmatism. Compositionally it is similar to the YGDC, but slightly more tholeiitic in nature. The magma was probably a basalt high in $Al_2O_3$ and FeO but low in $K_2O$, which remained critically undersaturated throughout its crystallisation (Morse, 1979). The intrusion is about 25km by 20km and roughly ovoid in plan. Unlayered Border Zone rocks make up only 6% by voume of the Kiglapait Intrusion, the remainder being the Layered Group (Morse, 1969, 1979).

The Lower Zone of the Layered Group, which forms most of the intrusion, is a plagioclase-olivine adcumulate. The Upper Zone is characterised by cumulus augite and subdivided where magnetite, sulphides and apatite appear and where plagioclase grades into perthitic alkali feldspar (Fig. 7.6). The layering is defined by modal variation and plagioclase lamination is also widely developed. A lineation formed by lenticles of olivine is found locally. Sharp millimetre-scale layering occurs but is relatively rare and most layers are on a decimetre scale. They may be uniform (often with rather diffuse contacts) or modally graded, either in a normal or reverse sense. Layers may change thickness and anastomose laterally and are sometimes affected by slumping. Localised olivine-rich troughs and channel-like features also occur. Blocks of anorthosite are found throughout the intrusion and the

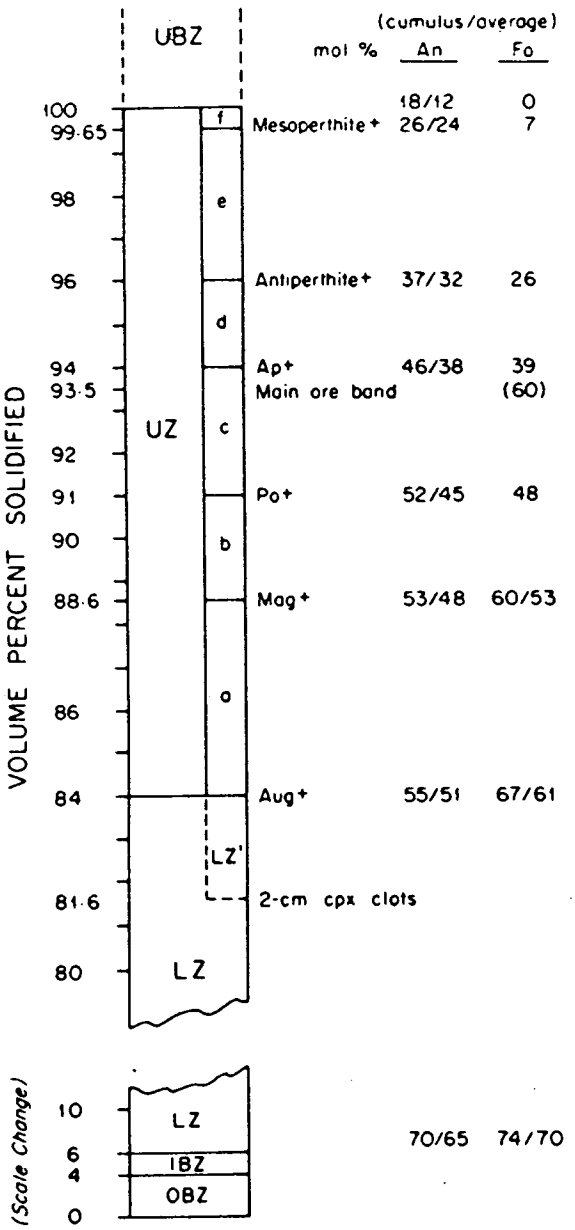


**Figure 7.6** Stratigraphy of the Kiglapait Intrusion from Morse (1979). OBZ = Outer Border Zone, IBZ = Inner Border Zone, LZ = Lower Zone, UZ = Upper Zone, UBZ = Upper Border Zone, Mag = Fe-Ti oxide minerals (chiefly titanomagnetite), Po = sulphide.

layering deflects around them. In one area layered blocks have been brecciated. In the Lower Zone, the olivine content of the dark layers is commonly about 30% but may reach 90%; similarly in the light layers it is usually 15% but may reach 50%. In the Upper Zone, olivine is subsidiary to augite and mafic layers contain 50-100% augite+magnetite.

Duluth Complex, Minnesota, USA

This complex is intimately connected with the Lake Superior Keweenawan volcanics which were associated with the opening of the American mid-continental rift. It is thus almost identical in age to activity in eastern Canada and southwest Greenland. It is compositionally similar to the Kiglapait intrusion and consists of layered troctolites overlain by laminated anorthosites (Weiblen and Morey, 1980). The anorthosites appear to have formed first and are underlain and intruded by the troctolite series. The troctolites were emplaced as several separate intrusions. They locally show layers on a millimetre to centimetre scale defined by modal variations in cumulus olivine and plagioclase, and intercumulus ortho- and clinopyroxene and Fe-Ti oxides. Some modally graded layers occur. Mineral lamination is less well-developed than in the anorthosites.

This complex, together with the Kiglapait intrusion and several others of Helikian age in North America, show many similarities to the YGDC, in terms of their cumulus assemblages, layering styles and whole-rock compositions. The magmas were predominantly Al-rich, crystallising as troctolites and anorthosites and giving rise to "dry", Fe-rich residua.

Gardar Province, SW Greenland

In addition to the YGDC, most of the other large Gardar intrusions display igneous layering features. The majority, however, are syenitic, unlike the intrusions described above. Other layered basic bodies include the Alangorssuaq and Bangs Havn gabbros of the Nunarsuit complex and several other giant dykes, including the Eqaloqarfia dyke of Isortoq (Pulvertaft, 1965). The Eqaloqarfia dyke consists of a medium-grained dolerite dyke enclosing a central layered pod of plagioclase-phyric

gabbro. Between the two, an elongate plagioclase rock is intermittently developed. The layering is characterised by sharply bounded layers of olivine cumulate between normal gabbro on a scale of centimetres to tens of centimetres.

Examples of well-layered syenitic Gardar intrusions include Nunarsuit (Harry and Pulvertaft, 1963), Kûngnât (Stephenson and Upton, 1982), Klokken (Parsons and Becker, 1987) and the highly alkaline Ilímaussaq intrusion (Larsen and Sørensen, 1987; Sørensen and Larsen, 1987). At Nunarsuit and Kûngnât, mafic layers within syenogabbroic and syenitic cumulates may be parallel or show pronounced channel and scour structures. The Klokken intrusion has an outer gabbro sheath and a central syenite portion characterised by inward-dipping (30-50°) layering. Both textural layering (alternations of granular and laminated syenite) and inverse modally-graded layering occur. The Ilímaussaq intrusion shows uniform modal layering on both centimetre and metre scale, as well as modally graded layers.

Many of the layered syenite complexes, especially those with outer gabbroic portions such as Klokken, are very similar to the evolved pods of the YGDC, although on a larger scale. The evolved pods on Tugtutôq show little well-developed layering, but the nunataq syenites are strongly layered and display erosive features similar to those of Nunarsuit and Kûngnât. The YGDC shows one of the largest ranges of lithologies of any of the Gardar complexes and encompasses most of the rock types seen in the other Gardar intrusions.

### 7.1.2 Phanerozoic examples

Duke Island, Alaska

This predominantly ultramafic complex is of early Cretaceous age and one of about 35 complexes making up a belt that runs across Alaska and into the Yukon. The Duke Island complex is the only one which appears to have developed significant layering (Irvine, 1987a). The complex is emplaced into older gabbros and consists of dunite (olivine cumulate), wehrlite (olivine-augite cumulate), olivine clinopyroxenite (augite-olivine cumulate) and magnetite-augite cumulate. Abundant hornblende is found in some lithologies but appears to be a replacement mineral.

Two major intrusive units are present, the younger one containing numerous blocks (tens of metres in size) and fragments of the older unit. The blocks are often internally layered or brecciated. Layering is well developed in both intrusions and

may consist of a poorly-defined modal variation or more commonly of grain-size graded layers. Both pyroxene and olivine are size-graded but the olivine crystals are finer and so tend to be concentrated towards the tops of layers. Each layer is commonly 10-20cm thick but they may reach over 1m. In the younger intrusion, fragmental layers resembling graded conglomerate beds occur, and the layering is commonly distorted beneath large blocks and draped over the top of them. Local angular unconformities superficially resemble cross-beds. In some parts of the complex there has been extensive metasomatic replacement of pyroxene-rich rocks by coarse-grained peridotite or dunite.

Rhum Complex, Scotland

A number of layered intrusions of Tertiary age, associated with the opening of the North Atlantic, are found in the Inner Hebrides. Those of Skye and Mull are less spectacularly layered than the Rhum complex and will not be described here. The following description of the Rhum complex closely follows that of Emeleus (1987). It is a stock-like body about 8km in diameter, composed of ultrabasic and gabbroic rocks, divided into three major components: the Eastern and Western Layered Series (ELS and WLS) and the Central Series (CS). The rocks are usually adcumulates, with the plagioclase often displaying igneous lamination, but poikilitic adcumulates and orthocumulates are also found. The ELS is made up of 15 gently dipping cyclic units composed of feldspathic peridotite (olivine cumulate) layers overlain by allivalite (plagioclase-olivine cumulate) and rare anorthosite. Clinopyroxene is a minor cumulus phase in many of the allivalites but orthopyroxene and apatite are only found as minor intercumulus phases. The units range from 10-80m in thickness with the peridotites commonly being thicker than the allivalites. In addition to this macro-scale layering there is modal variation (and sometimes textural variation) on the scale of cms to tens of cms. Modally-graded layers are occasionally found. Thin chromite layers, (up to 2cm but usually <2mm) occur where peridotite overlies allivalite or anorthosite and, very occasionally, between peridotite and overlying allivalite. The upper surfaces of the peridotites are frequently characterised by "finger structures" (Butcher *et al.*,1985). There is evidence that some of the peridotites are metasomatic in origin (Bédard et al., 1988). No overall cryptic layering is seen, although small scale variations in mineral compositions do occur within individual units.

Layering in the WLS is predominantly on a cm to m scale, again horizontal or gently dipping and defined by variations in modal mineralogy and in textures. Peridotite is the dominant rock type and cryptic variation is slight. A notable feature is the widespread development of harrisite, a rock characterised by highly elongate tabular olivine crystals which may be several cms or occasionally over a metre in length. The olivines occur in subparallel groups or radiating bunches. The ELS and WLS are separated by a prominent fault and by the chaotic CS. Rocks of the Central Series are feldspathic peridotites and peridotite breccias with dunite, allivalite and gabbro. Breccias of peridotite blocks in a feldspathic matrix are widespread and the opposite case also occurs but is less common. Layering, lamination, folding and slumping occurred before brecciation. The Central Series is interpreted as a late intrusive unit of the complex.

Skaergaard Intrusion, E. Greenland

Like Rhum, the Skaergaard Intrusion is one of a number of Tertiary complexes associated with North Atlantic rifting. It has been described by McBirney (1984) as "probably the single most intensively studied body of igneous rocks in the world". Approximately 10km long and 6km wide, geophysical surveys have shown that the intrusion narrows to two feeder pipes at about 4km depth (Blank and Gettings, 1973). It was emplaced into gneissic basement and appears to have halted and expanded at the unconformity between basement and overlying Tertiary basalts. Once emplaced, the magma evolved as a closed system.

It has been divided into three major sections: a Marginal Border Series (MBS) which crystallised against the walls, an Upper Border Series (UBS) which crystallised downwards from the roof, and a Layered Series which crystallised on the floor. The MBS and UBS were formerly known as the marginal and upper border groups (Naslund, 1984; Hoover, 1989). The Sandwich Horizon, where the most strongly differentiated rocks are found, appears to be where the UBS and the Layered Series converged. A stratigraphic column is shown in Fig. 7.7. The Layered Series is divided into three zones (Lower, Middle and Upper) and several subzones, on the appearance and disappearance of phases. Olivine and plagioclase were the first cumulus phases, joined by augite, pigeonite and then magnetite. Olivine disappears in the Middle Zone but reappears in the Upper Zone. Apatite and then an Fe-rich pyroxenoid (ferrobustamite), appear at different levels within the Upper Zone. The Sandwich Horizon contains interstitial granophyric intergrowths. There are also

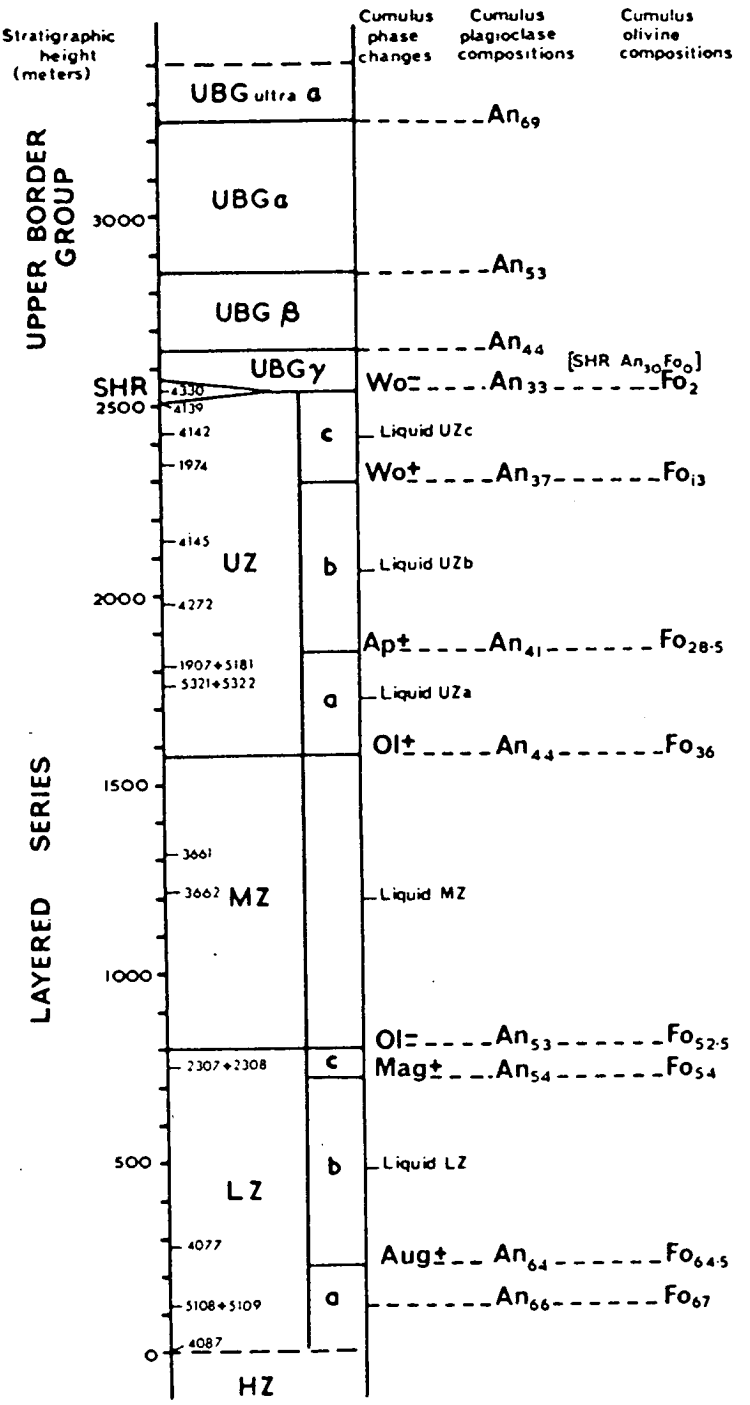


Figure 7.7 Classification and thickness of the Skaergaard Layered Series and Upper Border Group. Cumulus mineral compositions are generalised values from optically determined compositions. HZ = Hidden Zone, LZ = Lower Zone, MZ = Middle Zone, UZ = Upper Zone. After Wager & Brown (1968).

some transgressive granophyre bodies that appear to represent segregations of interstitial liquids (others, however, result from melting of the country rock gneiss). The MBS and UBS show similar phase and cryptic variation inwards from the margins but the sequences are much thinner than that of the Layered Series. Rocks of the UBS are slightly more feldspathic than their Layered Series equivalents.

The UBS shows some modal layering while the MBS has an outer unlayered portion succeeded inwards by the "banded zone" which is characterised by colloform or corrugated vertical layering produced by concentrations of particular minerals. Highly elongate feldspars are found perpendicular to the wall in the unlayered zone and sometimes grow in fans in the troughs of the vertical layering, forming the "perpendicular feldspar rock". Between the marginal series and the layered series is the "cross-bedded belt" in which local unconformities abound. Small, magmatically-healed normal faults dipping into the intrusion are also found in this zone (Irvine, 1987a; Hoover, 1989). In most parts of the intrusion, there is a marked angular mismatch between the MBS and the more gently-dipping Layered Series.

The layered series is generally saucer-shaped and several types of layers are present (Irvine, 1987a):

1. Modally-graded layers 5-50cm thick varying considerably in appearance depending upon the sharpness of the upper and lower contacts, the proportion of various minerals present and the degree of sorting. They can be traced for tens of metres. Within part of the Upper Zone, the modally-graded layers form a series of "troughs" separated laterally by unlayered ridges of ferrodiorite.

2. Relatively uniform 1-5m thick layers that are alternately slightly melanocratic and slightly leucocratic.

3. Thin layers (1-5cm) defined by rather diffuse modal variation.

Throughout the layered series, blocks of anorthosite, thought to come from the upper border zone, are abundant. Layers have frequently been distorted or even "ploughed up" by the impact of these blocks.

There is evidence for some metasomatic replacement of the cumulates by transgressive anorthosites (very different in texture from the blocks) and by gabbro pegmatite. It is thought that these bodies were caused by infiltration of water-rich fluids (perhaps of intercumulus origin) which reacted with the cumulates while the latter were still hot enough to be remelted (Irvine, 1987).

### 7.1.3 Comparison between YGDC and other layered intrusions

In common with several other layered complexes (Muskox, Skaergaard, and possibly Kiglapait and the Bushveld), the YGDC has been emplaced into crystalline basement and appears to have halted and expanded at the unconformity between the basement and overlying lavas or sediments. In form, it is apparently like the Great "Dyke" although to a certain extent the resemblance is misleading since the Great "Dyke" is thought to consist of four lopolithic complexes giving the appearance of a dyke (possibly due to later faulting). However, the complexes were probably fed through fissures in the same manner as the YGDC. The Jimberlana Intrusion is probably a closer analogue, since it appears to have been intruded as an elongate body, but it is not known whether the YGDC narrows at depth in the same manner as the Jimberlana intrusion. If the YGDC is tilted towards the east, then the westward narrowing would indicate that it does narrow at depth; if on the other hand there was a large component of lateral emplacement with only minor tilting, if any, then the westward narrowing would indicate a decline of the magmatic pressure driving the emplacement. The complexes spaced at intervals along both the Great "Dyke" and the Jimberlana intrusion could find a parallel in the differentiated pods of the YGDC (Chapter 2).

However, both the Great "Dyke" and the Jimberlana intrusion, together with several of the other intrusions described above (the Bushveld, Stillwater, Muskox and Kapalagulu intrusions), are characterised by an abundance of ultramafic rocks lacking plagioclase. This is not seen in the exposed part of the YGDC. In addition, orthopyroxene is an important phase in all of the intrusions characterised by an ultramafic series, indicating a tholeiitic character. In the Skaergaard and Rhum Intrusions orthopyroxene is less important but still present. The Duluth and Kiglapait intrusions are very similar to the YGDC in their low contents of orthopyroxene, but even here, clinopyroxene precipitation is not delayed until after magnetite as it is in the YGDC, making the latter apparently unique in terms of its crystallisation sequence.

The YGDC contains no chromite, although it is a common phase in many other layered intrusions. It can be seen, however, in the Great "Dyke" (Fig. 7.2) and the Bushveld intrusion (Fig. 7.3) that where chromite occurs, mineral compositions are more primitive than those of the YGDC. Thus the relatively evolved nature of the YGDC magmas makes it unsurprising that no chromite is observed. It seems

probable that, either directly underlying the observed cumulates or at a greater depth in the crust, a series of ultramafic rocks exists, formed from the YGDC magma. This has already been postulated in Chapters 4 and 6 to explain the whole-rock chemistry and the gravity anomaly. The cumulates probably consist of olivine, with clinopyroxene if fractionation occurred at sufficient depth (Upton, 1972; Upton and Thomas, 1980). It is probable, considering the low chromium contents of the exposed rocks, that chromite would also be found.

The overall variation in YGDC mineral compositions is: olivine, $Fo_{68}$-$Fo_{3}$, plagioclase, $An_{65}$-$An_{0}$, cumulus clinopyroxene, $Wo_{46}En_{42}Fs_{12}$ to $Wo_{48}En_{15}Fs_{37}$ (Chapter 3). These correspond approximately to mineral compositions in the Main and Upper Zone of the Bushveld and in most of the exposed layered rocks of Kiglapait and Skaergaard. The YGDC plagioclase compositional range is equivalent to that of the uppermost gabbro zone of Stillwater and the upper part of the Great "Dyke" gabbro but neither of these contain olivine, as a result of its reaction relationship with the more silicic magmas. It is difficult to propose a stratigraphic column for the YGDC since it is uncertain how much of the mineral variation is lateral and how much vertical. Even if it were all vertical, the amount of tilting of the dyke and thus the vertical distance represented are unknown. However, a comparison may be made with between Figs. 7.1-7.7 and Fig. 3.10.

Layering defined by modal variation (rather than by texture, grain size or mineral lamination) is a feature of almost all layered intrusions. The YGDC differs from many in that laterally continuous metre-scale layering is not seen and modally-graded layers are rare. Regular cm-scale layering is seen at locality J of Fig. 2.1 but is very localised. The YGDC layering shows most similarities with that seen in the Rhum, Skaergaard and Kiglapait Intrusions and the Eqaloqarfia dyke, where mafic layers occur within troctolite or gabbro. It seems to be rare, however, to find such regular and repeated variation from "average rock" to mafic cumulate. In the Skaergaard Intrusion, for example, modally-graded layers separated by uniform rock occur on roughly the same scale as the gabbro picrite layers in the western part of the YGDC but the latter normally show no trace of grading. However, the troughs and cross-bedding of the western YGDC are similar, though not identical, to those of the Skaergaard and Kiglapait Intrusions and in some syenitic Gardar intrusions, while the gabbro picrite breccias bear some resemblance to those of the Rhum Central Series. Plagioclase lamination too is a common feature of layered intrusions, although it is developed only sporadically in the YGDC and appears to be entirely absent in the western (more primitive) part of the YGDC. The elongate feldspar rock (or feldspar

*crescumulate*) of locality B is similar to the perpendicular feldspar rocks of Skaergaard, the Eqaloqarfia dyke and the Kûngnât ring dyke, while the elongate pyroxene facies (pyroxene crescumulate) of locality L finds parallels in the harrisitic olivines of Rhum and the elongate pyroxenes of Stillwater.

Anorthosite xenoliths are also common in many layered intrusions, but it is generally thought that they are detached blocks of roofing facies rather than xenoliths brought from a body at depth, as is the case in the Gardar Province.

## 7.2 Theories of Layering

### 7.2.1 Background

The idea that crystals could sink in a magma and thus produce magmatic diversity was suggested by Darwin (1844). Bowen (1915) confirmed experimentally that olivine and diopside crystals could sink, and that tridymite could float, in liquids from the system diopside-forsterite-silica. The theory of crystal settling became accepted by many workers, to account for the differentiation of igneous rocks and also for the structures of layered intrusions, although other mechanisms, such as differing ease of nucleation and variations in water pressure, were also believed to be important in the genesis of certain features (Wager, 1959; Wadsworth, 1963). Particularly influential among the proponents of crystal settling were Wager and coworkers (Wager and Deer, 1939; Wager and Brown, 1968), whose theories were formulated with special reference to Skaergaard.

In brief, the conclusions of Wager and Brown (1968) concerning the crystallisation of the Skaergaard Intrusion were as follows. The outer part of the Skaergaard border series crystallised from an essentially stationary magma - in particular, the perpendicular feldspar rock could not have formed had there been anything more than very slight movement in the magma. The feldspars were considered to have grown into a supercooled liquid until the heat diffusion eliminated the supercooling, preventing further growth. With continued cooling, another burst of nucleation would form a layer of smaller crystals. The cooling of the magma would then have set up a convection system with currents descending at the margins of the intrusion, sweeping across the floor and rising at the centre. Crystals would have formed near the roof (where the heat loss was greatest), been carried down the walls (adhering to form the vertical corrugated banding of the MBS) and across the

floor (the most compelling evidence for this being the cross-bedded belt and the trough bands). Two types of current were envisaged: one a gentle, continuous type which deposited the "uniform rock", the other intermittent and with higher velocity, depositing the modally-graded layers. The higher proportion of feldspar in the UBS gave Wager and Brown evidence for an upward-moving central convective plume, since feldspar would have been carried more easily than ferromagnesian minerals by such a current. The formation of the UBS was thought to be due to crystals kept in suspension by turbulance becoming trapped by an advancing solidification front.

A decade later, doubt began to be cast on some of these mechanisms for producing layering. Campbell (1978), with reference to the Jimberlana Intrusion, drew attention to the lack of an angular discontinuity between texturally-identical shallowly-dipping and near-vertical layers. While the former could have formed by crystal settling, it is difficult to explain how steeply-dipping layers with the same textures could have formed by the same process. In addition, "inch scale" layering and reverse modally-graded layers seemed best explained by a mechanism of *in situ* crystallisation with alternate nucleation of different minerals. Plagioclase presented a problem to Wager and Brown (1968) in that its density is very similar to that of the probable Skaergaard liquids; they concluded that it must have remained slightly denser than the liquid until a late stage. However, Campbell (1978) calculated that it would have been slightly less dense throughout the crystallisation history of the intrusion, and thus should not have been able to sink. Furthermore, Campbell questioned the assumption that nucleation of crystals occurred within the magma (i.e. homogeneous nucleation) rather than upon pre-existing crystals (heterogeneous nucleation). Heterogeneous nucleation is more likely to occur because it requires a lower degree of supercooling of the magma (Carmichael *et al*, 1974) and this would favour *in situ* crystallisation (see section 7.3.1).

McBirney and Noyes (1979) also raised the problem of plagioclase density and the fact that layers parallel to the walls of an intrusion could not have formed by settling. In addition, they considered magma rheology as known from experiments and from observations on Hawaiian lava lakes. A magma behaves as a Newtonian fluid (deforming easily by viscous flow even under small stresses) only when it is at high temperature and relatively free of crystals. With increasing concentrations of crystals, these properties change and the magma tends to deform as a visco-elastic substance at moderate stresses or an elastic substance at low stresses. This means that in order to sink (or rise), crystals would have to overcome a yield strength before

any movement was possible, and at low stresses they could not move at all. With more than 60% of the magma crystalline, only elastic deformation of the magma seems to be possible, whatever the stress applied.

### 7.2.2 Proposed origins for layering

The recognition of such problems with the theory of crystal settling has led to a wide range of proposed mechanisms for layering, including both physical and chemical processes. Many layered intrusions have been re-examined in the light of new ideas and some of the theories that have been proposed for different types of layering are summarised below.

#### Microrhythmic layering

Most workers agree that small-scale modal layers are formed by a process of *in situ* cyclic crystallisation where, in crystallising a particular assemblage, the magma becomes progressively enriched in excluded components and is driven into the stability field of another mineral which then begins to nucleate. Nucleation oscillates in this way between two or more mineral species (McBirney and Noyes, 1979). Periodic nucleation with some attendant crystal settling was proposed by Goode, (1976). Boudreau (1987) proposed a mechanism whereby segregation of phases to form fine-scale layers is a result of postcumulus textural coarsening.

#### Macrorhythmic layering

Relatively uniform layering defined by modal variation on a scale of metres, such as occurs in the Stillwater, Skaergaard, Klokken and Kiglapait Intrusions, is probably one of the least well-understood types of layering (Irvine, 1987c). It is still thought that it may be due to crystal settling, as proposed by Wager and Brown (1968), for example in the Ilímaussaq Intrusion (Larsen and Sørensen, 1987). However, most authors favour a mechanism similar to that proposed for microrhythmic layering (e.g. Parsons, 1987).

Cyclic Layering

The repeated occurrence of groups of layers (usually on a large scale) accompanied by little cryptic layering or by reversals in the trend of mineral compositions, is thought to result from periodic replenishment of the magma chamber, accompanied by fractional crystallisation. Examples of this may be found in the Stillwater (Raedecke and McCallum, 1984), Muskox (Irvine and Smith 1967), Great Dyke (Wilson, 1982) and Rhum intrusions (Tait, 1985; Renner and Palacz, 1987).

On a smaller scale, repeated layering patterns may result from periodic convective overturn or periodic fluctuations in pressure or oxygen fugacity (for example, all of these have been suggested for magnetite layers in the Bushveld. See Cawthorn and McCarthy, 1980).

Graded Layers

Grain-size graded layers are almost certainly due to deposition from currents (Irvine, 1987a). Well-developed grain-size grading appears to be confined to ultramafic intrusions (e.g. Duke Island), but modally graded layering (either normal or reverse) is common. There is still controversy over the origin of normal modally-graded layers. Some authors have proposed deposition from density currents in the manner envisaged by Wager and Brown (1968) due to their similarity (in terms of scale) to grain size graded layers, and from studies of density current deposition mechanisms (Irvine, 1980a; 1987; Conrad and Naslund, 1989). Others (e.g. McBirney and Noyes, 1979) believe that they must have formed by *in situ* crystallisation with successive nucleation of different minerals. For reverse modal grading there is less disagreement, since it is difficult to see how layers with denser minerals overlying less dense ones could have formed by current action. Mechanisms proposed usually involve variations in crystal nucleation and growth combined with varying degrees of supercooling of the magma or varying water pressure (for example in the Klokken Intrusion, Parsons, 1979).

Troughs

McBirney and Noyes (1979) followed the suggestion of Taylor and Forester (1979) that the Skaergaard Intrusion trough bands may have resulted from a change in the crystallisation behaviour caused by water penetration into the magma along radial fractures in the underlying hot but essentially consolidated cumulates. However, Irvine (1987a) maintained that they formed from density currents, as suggested by Wager and Brown (1968), but that the ridges between the troughs crystallised *in situ* from roller-type convection cells.

Unconformities and Cross-bedding

Such features are generally thought to be due to erosion by convective currents (Wager and Brown, 1968; McBirney and Noyes, 1979; Irvine, 1987) but may also result from repeated injection, for example in the Stillwater intrusion (Todd *et al.*, 1983) or from chemical-thermal erosion of underlying cumulates by the magma, for example in the Bushveld Intrusion (Irvine *et al.*, 1983).

Concentrations of chromite or Pt-bearing sulphides

Concentrations of particular minerals such as chromite or sulphide minerals are widely supposed to result from the replenishment of the magma chamber by the parental magma or its differentiates and subsequent mixing with the residual magma in the chamber (Todd *et al.*, 1983; Sharpe and Irvine, 1983). Variations in oxygen fugacity due to new influxes of magma (Wilson, 1982) or changes in pressure (Cameron, 1980) have also been suggested.

## 7.3 Magma crystallisation behaviour (and implications for the YGDC)

Before considering the crystallisation of a magma chamber it is necessary to define the nature of the walls on which crystals accumulate. The physical properties and initial temperatures of the magma and the wall-rock will determine whether a chill zone is formed or whether the magma chamber boundary will move outwards by

melting of the wall rocks (Carrigan, 1988; Day, 1989; Huppert and Sparks, 1989). Three different regimes are possible, depending upon the relative magnitudes of the heat flow in the magma ($Q_m$) and the country rocks ($Q_c$) (Day, 1989):

1. $Q_c > Q_m$. A chilled margin will form at the wall. If the accumulation is slow enough, cumulates may form by the separation of crystals and residual fluid. Heating of the wall-rocks may be sufficient to form a partial melt capable of migration, but they do not lose their rigidity (Fig. 7.8a).

2. $Q_c < Q_m$. The wall-rock or a previously-formed chill zone will melt (Fig. 7.8b). The behaviour of the melt will depend upon its density relative to the magma, and on the rate of melting (at slow melting rates wall-rock melt may be carried downward by thermal convection currents, regardless of its density).

3. $Q_c > Q_m$ but the temperature of the magma is much higher than the melting temperature of the wall-rocks. In this case, a chill zone may form on the wall but the wall-rocks may exceed their melting temperature, so a zone of anatectic melt forms outside the chilled margin. This will cause the chill to break up periodically into blocks (Fig. 7.8c,d).

The initial behaviour of a magma intruded into relatively cold country rocks will be to chill against them (Huppert and Sparks, 1989), but as the conductive profile relaxes, $Q_c$ will decrease. Meanwhile, $Q_m$ may remain approximately constant, or increase due to the onset of convection, and some erosion of the previously-formed chill and the wall-rocks may occur. At some point in time, however, provided there is no internal heat source, $Q_m$ will decrease sufficiently for solidification of the whole body to occur (Fig. 7.9).

In the YGDC there is some evidence that wall-rock melting (regime 2) did occur in certain localities (Chapters 2 and 3) but the width of hybrid zones is usually no more than a few metres, implying that this condition was transient. The sharp transition between fine- and coarse-grained troctolite at the north margin of locality D (Plate 2.1b) could indicate melting of a previously-formed chill, but equally the fine-grained material may have been intruded later, as suggested in Chapter 2. It is possible that regime 3 also occurred at times; this may explain the fine-grained xenoliths found near the dyke margins at localities D, G and I of Fig. 2.1, especially those at locality G which are slab-like in shape and orientated parallel to the margin

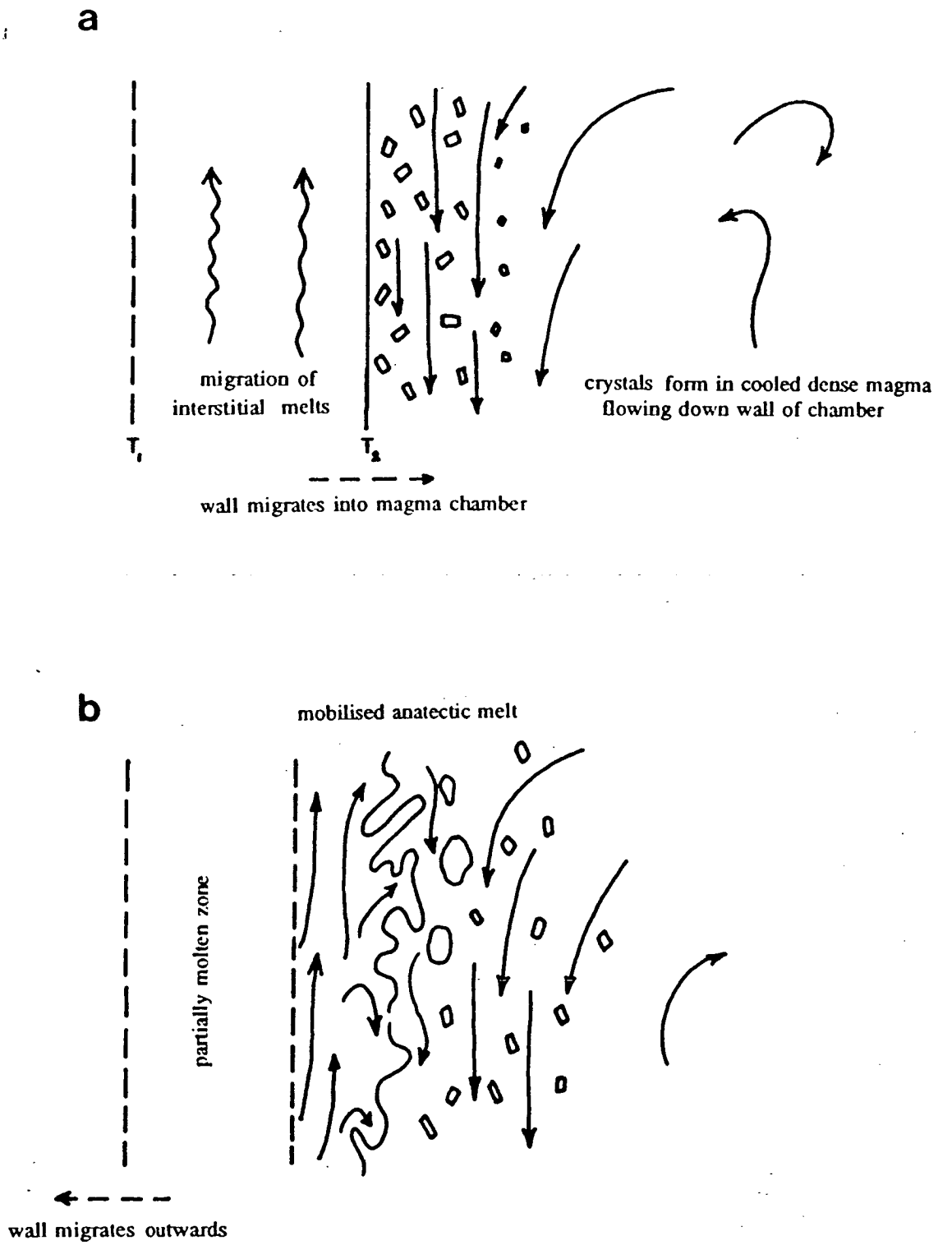


**Figure 7.8** Sketch cross-sections of the three types of magma chamber wall boundary, after Day (1989). (a) $Q_c > Q_m$ and a chill zone forms on the wall. $T_1$ = solidus temperature, $T_2$ = temperature at which a rigid crystal framework forms. (b) $Q_c < Q_m$ and wall-rock (country-rock or chill zone) melts. The case of compositionally buoyant wall-rock is shown. Continued overleaf.

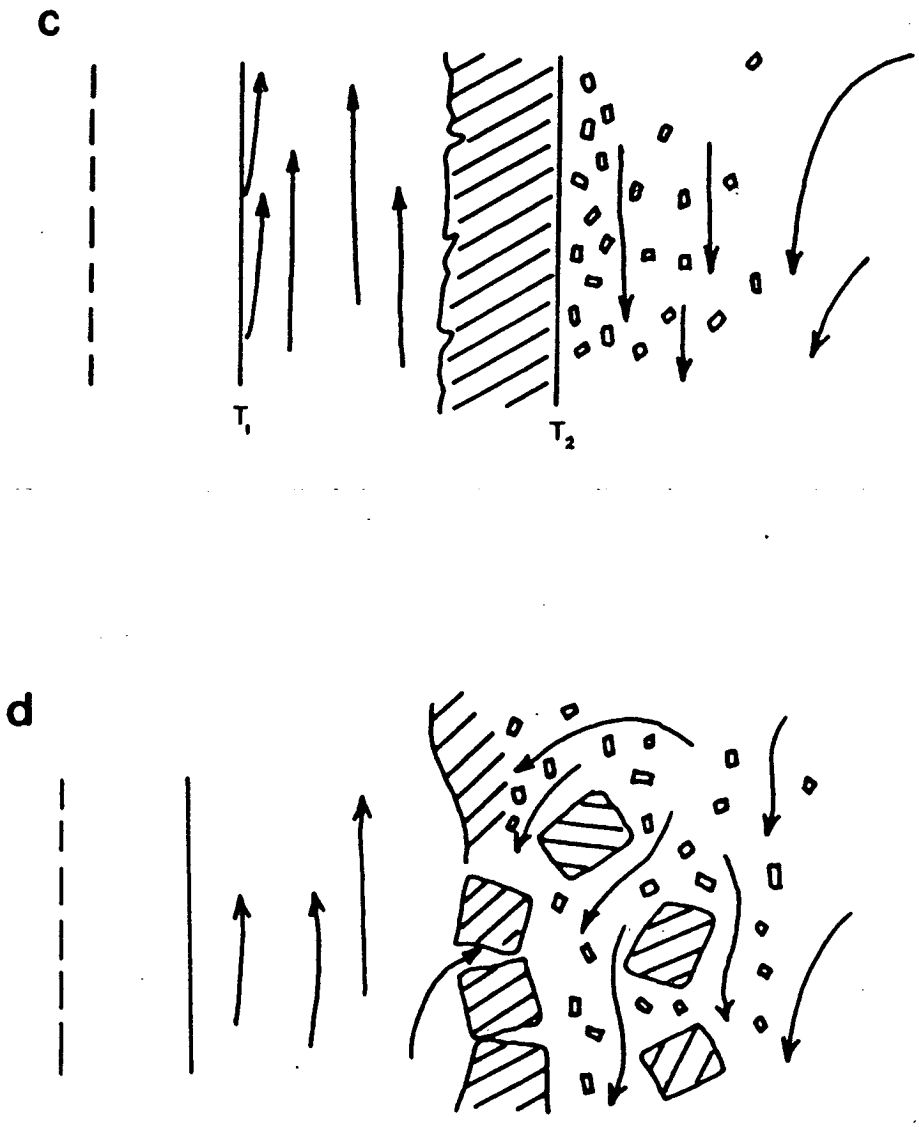


**Figure 7.8 (continued)** (c, d) $Q_c > Q_m$ but magma temperature much higher than wall-rock melting temperature. (c) chill zone forms between ascending wall-rock melt and descending cooled mafic magma. $T_1$ = temperature at which country-rocks become rigid, $T_2$ = temperature at which magma becomes rigid. (d) old chill breaks into blocks and falls away; new chill forms.

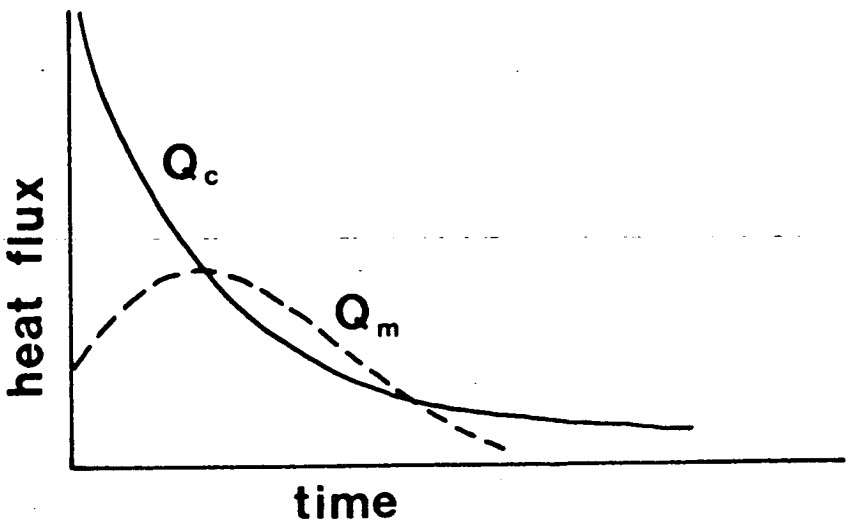


**Figure 7.9** Generalised variation of heat flux $Q_m$ in the magma (dashed line) and conductive flux $Q_c$ in the wall-rocks (solid line). After Huppert and Sparks (1989).

(section 2.5.2). However, for most of the crystallisation history of the YGDC it is inferred that $Q_m$ was greater than $Q_c$ and that solidification inwards from the wall was the dominant process.

### 7.3.1 Crystal nucleation and growth

In a crystallising solution, nucleation does not take place at the liquidus temperature but at some degree of undercooling below it. Two types of nucleation behaviour are possible: homogeneous nucleation (within the body of the liquid) and heterogeneous nucleation (on a pre-existing substrate or discontinuity, including a shear plane in the liquid (Morse, 1988)). Many experimental and theoretical studies have been made of nucleation behaviour in magmas (e.g. Donaldson, 1979; Dowty, 1980; Lofgren, 1983 and refs therein). These have shown that in general, homogeneous nucleation requires a greater degree of undercooling, or a longer time at a particular undercooling, than heterogeneous nucleation. In addition, the degree of undercooling and the cooling rate determine the crystal shape, with elongate crystals forming at high degrees of undercooling or at high cooling rates and more equant crystals forming when cooling is slow (Lofgren, 1980). It seems likely that nucleation in a magma chamber with crystalline walls, floor and roof, would be dominated by heterogeneous nucleation (producing *in situ* crystallisation) (Campbell, 1978).

Both experiments and rock textures have shown that some minerals nucleate with greater ease than others (Gibb, 1974; Kirkpatrick, 1977; Donaldson, 1979; Lofgren, 1983). Minerals with simple structures such as olivine and spinels nucleate most easily while framework silicates such as plagioclase nucleate with the most difficulty, and only on substrates with the same or a similar structure. This is shown either by greater degrees of undercooling being required for nucleation, or by longer times for nucleation at the same undercooling. For example, plagioclase may take 10 times as long as olivine to nucleate at 20°C of undercooling (Gibb, 1974; Donaldson, 1979).

Crystal growth is determined by several factors: reactions at the crystal-melt interface, diffusion of chemical components to and from the crystal, removal of latent heat and bulk flow of the melt (Kirkpatrick, 1981). The effect of bulk melt transport (convection) is usually ignored in crystal growth studies and Kirkpatrick considered

latent heat removal a minor factor. Interface processes probably dominate at small undercoolings but at larger undercoolings, diffusion becomes more important.

Several features of layered intrusions have been explained by processes involving variations in crystal nucleation and growth coupled with diffusion. It is still thought that crescumulates arise by constitutional supercooling (as suggested by Wager and Brown, 1968), where crystals grow sufficiently fast that rejected chemical components cannot diffuse away from the vicinity of a crystal. These components tend to lower the liquidus temperature near the crystal, and if chemical diffusion is temporarily faster than the diffusion of heat, a zone of supercooling will result (Fig. 7.10). Any protruberance on the crystal which intersects this zone will grow rapidly, resulting in an elongate crystal perpendicular to the cooling front. Since the diffusion of chemical components depends upon $\sqrt{\text{time}}$ whereas the temperature gradient will be a linear function of time, the heat diffusion will at some later time, "overtake" the chemical diffusion and eliminate the zone of supercooling (McBirney and Noyes, 1979).

Periodic nucleation behaviour has been observed in many chemical systems (Noyes and Field, 1977), and it has been suggested that magma chamber crystallisation is similarly periodic (Campbell, 1978; Maaløe, 1978; McBirney and Noyes, 1979). Dowty (1980) and Brandeis *et al.* (1984) suggested that latent heat does in fact play a significant role in magmatic crystallisation. The numerical experiments of Brandeis and co-workers have shown that, on emplacement of a magma, a burst of nucleation will occur when a suitable degree of undercooling is reached. The latent heat released by the nucleation and growth of these crystals suppresses further nucleation until growth declines and the temperature drops far enough for another burst of nucleation.

Brandeis *et al.* (1984) only considered a single-phase system but bands of alternating phases can be produced in the laboratory using two chemicals with different diffusivities, as first shown by Liesegang (1913). They are produced because crystallisation of one phase depletes the surrounding region in the components of that phase and causes a different phase to become stable and nucleate. A magma can probably show similar oscillatory behaviour, and this is thought to be the origin of the "centimetre scale" layering found in many intrusions. It may also account for modally-graded layers (Campbell, 1978) because the phases found at the bases of layers are those easiest to nucleate and those at the top (predominantly plagioclase) the most difficult.

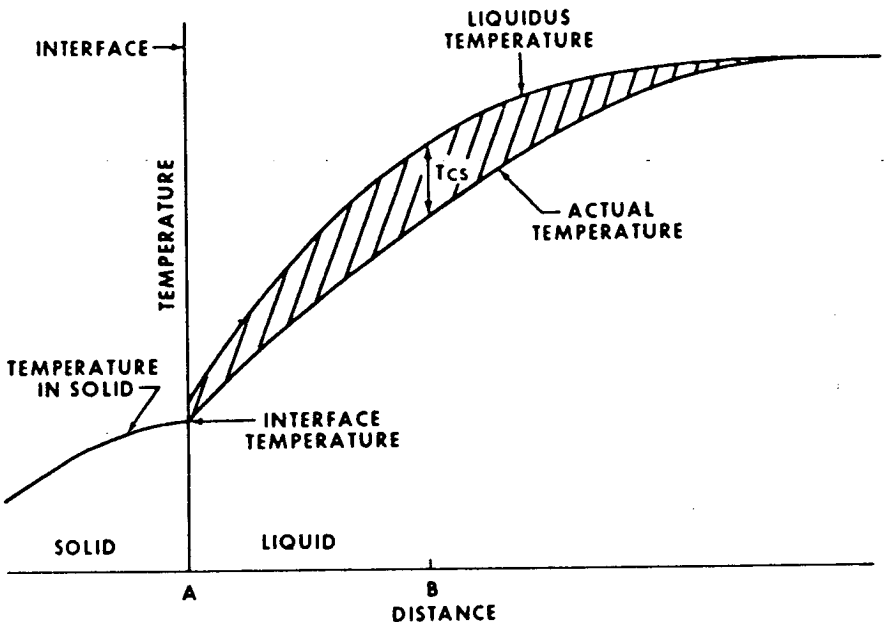


**Figure 7.10** Schematic representation of constitutional supercooling in advance of a growing crystal interface where the heat is extracted through the crystal. This supercooling exists because low temperature components rejected by the growing crystal do not diffuse away as fast as the crystal interface is advancing. From Lofgren (1980)

Fine-scale alternation between two phases is rarely seen in the YGDC but some mechanism of periodic suppression of plagioclase nucleation during *in situ* crystallisation may be able to account for the parallel layering of localities B to D, G and K (Fig. 2.1). During crystallisation, heterogeneous nucleation seems likely since previously formed crystals will provide appropriate sites, and there should have been more-or-less continuous nucleation. This being the case, the differing ease of nucleation of the different minerals should not have had much affect. However, it may be that plagioclase is more sensitive to factors tending to suppress nucleation (possibly latent heat generation) than other phases, notably olivine. But this theory does not account for features such as the gabbro-picrite filled troughs at localities B to D, so other processes will have to be considered.

It has already been proposed (Chapter 4) that the YGDC magmas were carrying olivine phenocrysts and that the stellate plagioclase + olivine glomerocrysts and the elongate feldspars indicate that the magmas were also supersaturated with respect to plagioclase. The stellate plagioclase textures are similar to those observed by Berg (1980) in the field and by Lofgren (1974, 1980) in experiments.

### 7.3.2 Movement of crystals and liquid

Crystal settling

Despite thermodynamic arguments for heterogeneous nucleation, it appears, from the presence of phenocrysts in lavas, that some crystals do nucleate within the body of a magma and that crystal settling may occur (e.g. Cox and Mitchell, 1988). For a Newtonian liquid containing spheres of a different density from the liquid, velocities of particle movement can be calculated using Stokes' equation:

$$V = \frac{2r^2g(\rho_1-\rho_2)}{9\eta}$$

Where:

V = velocity of sphere
r = radius of sphere
$\rho_1$ = density of sphere
$\rho_2$ = density of liquid
$\eta$ = viscosity of liquid

There is still debate as to whether or not Stokes' Equation is applicable to crystals in a magma, because the bulk properties of a magma containing crystals appear to be non-Newtonian (Murase and McBirney, 1973; McBirney and Noyes, 1979). However, many workers believe that, provided the crystal fraction is sufficiently small (below 20-25% (Marsh and Maxey, 1985)) that crystals do not interfere with each other, Stokes' Law does apply (Huppert and Sparks, 1980; Marsh, 1988; Morse, 1988; Martin and Nokes, 1989). At high crystal concentrations, grain dispersive forces (the Bagnold effect) will tend to act against crystal settling (Wadsworth, 1973). A magma no longer remains fluid-like, with crystals able to move relative to one another, at crystal concentrations greater than 50-60% (McBirney and Noyes, 1979; Marsh and Maxey, 1985; Day, 1989).

Magma densities and viscosities have been calculated for the YGDC chilled margins using the methods of Bottinga *et al.* (1982) and Shaw (1972) respectively. Mineral densities have been calculated using data from Clark (1966), and settling velocities obtained using Stokes' Equation. Values used in the calculations were: $\rho_{mag} = 2.8$ g cm$^{-3}$, $\eta = 150$ poise (g cm$^{-1}$ sec$^{-1}$), $\rho_{ol} = 3.49$ g cm$^{-3}$, $\rho_{mt} = 4.96$ g cm$^{-3}$, $\rho_{pl} = 2.65$ g cm$^{-3}$. The temperature used was 1150°C. The presence of olivine and plagioclase phenocrysts in the chilled margins, and the composition of the olivine phenocrysts, suggest that the magma was intruded with a temperature approximately that of the olivine-plagioclase cotectic. Experimental work by Upton (1971) and numerical modelling (Chapter 4) indicate 1150°C as a probable temperature for the appearance of plagioclase on the liquidus. The resulting settling velocities (in cm sec$^{-1}$) for primary minerals in the YGDC are shown below (positive values indicate a tendency to sink):

| Diameter (cm) | 0.2 | 0.4 | 0.6 | 1.0 |
|---|---|---|---|---|
| Olivine ($Fo_{65}$) | 0.02 | 0.07 | 0.16 | 0.44 |
| Magnetite | 0.05 | 0.19 | 0.43 | 1.20 |

| Length (cm) | 1.0 | 2.0 | 4.0 | 6.0 |
|---|---|---|---|---|
| Plagioclase ($An_{62}$) | -0.02 | -0.08 | -0.31 | -0.70 |

These values would probably increase if the effect of volatiles could be taken into account since these tend to lower the viscosity. The approximation of a spherical shape is reasonable for magnetite and squat olivine prisms, but plagioclase crystals are tabular, so the values obtained for spheres were divided by a factor of 1.4 (cf.

Maaløe, 1985). Pressure causes a density increase in both magma and crystals. However, at depths of a few km, settling velocities of dense minerals will be little affected. The tendency of plagioclase to float would be enhanced slightly, since the density of magma increases faster than that of plagioclase (Kushiro, 1980).

It can be seen from these figures that plagioclase could not sink (unless perhaps the magma density was in fact lower than that used in the calculations, due to the presence of volatiles), but both olivine and magnetite (where the latter is a cumulus phase) would tend to settle. The presence of plagioclase at the base of the intrusion therefore means either that the crystals were carried down in a convection current or that they grew *in situ*. It is possible, however, that the glomerocrysts of olivine and plagioclase would have settled since their bulk density was slightly greater than that of the liquid (2.9 g $cm^{-3}$); their large size (up to about 3cm) would have assisted this process.

Thermal convection

It is generally accepted that heat loss from a magma chamber to its wall rock will cause the magma to convect, so the interaction between moving magma and settling crystals (if there are any) must be considered. A convecting fluid may be described in terms of several dimensionless numbers, among which are the Rayleigh number, Ra and the Prandtl number, Pr. These are given by:

$$Ra = \frac{g \alpha \Delta T L^3}{\nu \kappa}$$

$$Pr = \frac{\nu}{\kappa}$$

Where:

g = gravitational acceleration

$\alpha$ = coefficient of thermal expansion

$\Delta T$ = temperature contrast

L = thickness of convecting layer

$\nu$ = kinematic viscosity

$\kappa$ = thermal diffusivity

The Rayleigh number indicates the likelihood and the nature of the thermal convection, and the Prandtl number gives the rate at which the temperature contrast is reduced by heat diffusion to the surrounding rocks. The Rayleigh number assumes a fixed temperature at the wall. This may be difficult to define (Carrigan, 1988) since it could be taken as the magma liquidus temperature, a temperature between the liquidus and the solidus at which the magma becomes rigid, or the initial wall-rock temperature. Here, the initial wall-rock temperature is used, since this implies some coupling between the thermal regime of the magma and that of its host, which the other quantities do not. The wall-rock temperature is estimated at about 200-400°C. This is partly from an average continental geotherm (e.g. Oxburgh, 1980), with the temperature slightly raised by the intrusion of the OGDC 5-30Ma earlier, and partly because the rocks must have been considerably below their liquidus temperature, since only minor amounts of wall-rock melting occurred. The wall-rock liquidus temperature would be 750-1000°C, depending on water content (McBirney, 1984, p. 357). This definition means that the Rayleigh number will decrease with time as heat is conducted to the wall-rocks (raising their temperature) and as the magma chamber decreases in size.

The Ra and Pr together define the nature of the convection, which may be laminar (ordered, steady and cellular) or turbulent (unstable and time-dependent). When temperature gradients are vertical, Rayleigh numbers of about $10^3$ or above indicate that convection will take place (Bhattacharji, 1974; Cox *et al.*, 1979; Maaløe, 1985), but any horizontal temperature gradient will cause movement of magma. Turbulent convection occurs when $Ra>10^6$, although at high Prandtl numbers this value may rise to about $10^9$ (Jarvis, 1984). There is some disagreement over whether Ra or Pr is more important. Krishnamurthi (1970) considered that the transition to turbulent flow depends only weakly on Pr at high Pr. However, Marsh and Maxey (1985) suggest that flow is always laminar when $Pr>10^5$. Heiber and Gebhart (1971) give a relationship between the critical Rayleigh number and the Prandtl number:

$$Ra_{crit} = A\ Pr^{2.5}$$

where A is a constant equal to about $10^{10}$.

Basaltic magma chambers typically have $Ra = 10^{12}$ to $10^{16}$ and $Pr = 10^4$ to $10^7$ (McBirney, 1984; Nilson *et al.*, 1985; Martin and Nokes, 1989). If the relationship of Heiber and Gebhart is used then magmas with $Pr>10^4$ will show laminar convection, but many authors believe that all magma chambers undergo turbulent convection.

The YGDC magma chamber is considered to have had a large height to width ratio in the stages immediately after emplacement. Partial crystallisation of the complex may have led to the existance of several isolated chambers. The vertical extent of these chambers is unknown, but an estimated figure of 1-2km gives a height:width ratio of between 2:1 and 4:1. Calculations using a figure of 1-2km and values of $\alpha$ and $\kappa$ from Nilson *et al.* (1985) give a Rayleigh number of around $10^{16}$ and a Prandtl number of $10^4$. The high Ra and the low Pr are due to the low viscosity of the YGDC magma and indicate that convection within the magma chamber would have been turbulent. In the YGDC, thermal convection would have been dominated by sidewall cooling causing thermal contraction and an increase in density, and creating descending plumes. The return upward flow was probably more diffuse due to lack of a localised driving force (Brandeis and Jaupart, 1986; Marsh and Maxey, 1985).

In a crystallising magma chamber, there is a zone of decoupling, or boundary layer, between the well-mixed and approximately homogeneous interior of the magma and the zone of crystallisation (McBirney and Noyes, 1979; Brandeis and Jaupart, 1986). Within the boundary layer there will be gradients of heat, chemical components and momentum. The different rates of diffusion of these quantities mean that the compositional boundary layer will be thinner than the thermal boundary layer and that both will be thinner than the viscous or mechanical boundary layer (Fig. 7.11).

Nilson *et al.* (1985) suggested that in a turbulently convecting magma chamber there will be a laminar sublayer at the margins and that the thermal and compositional boundary layers (but not the mechanical one) probably lie within this sublayer. However, motion in the boundary layer itself may be laminar or turbulent, depending on the local Rayleigh number of the layer; for a horizontal boundary, convection will only occur if $Ra>10^3$. If the flow in the boundary layer is turbulent, mechanical mixing will govern rates of transfer and the mechanical and compositional boundary layers will be the same width (McBirney, 1984). The laminar/turbulent transition within a boundary layer may be gradual with some areas still laminar while others show varying degrees of turbulence (Nilson *et al.*, 1985). However, some workers (Turner and Campbell, 1986) consider that the steady-state heat flux across a vertical boundary layer will always result in laminar rather than turbulent convection.

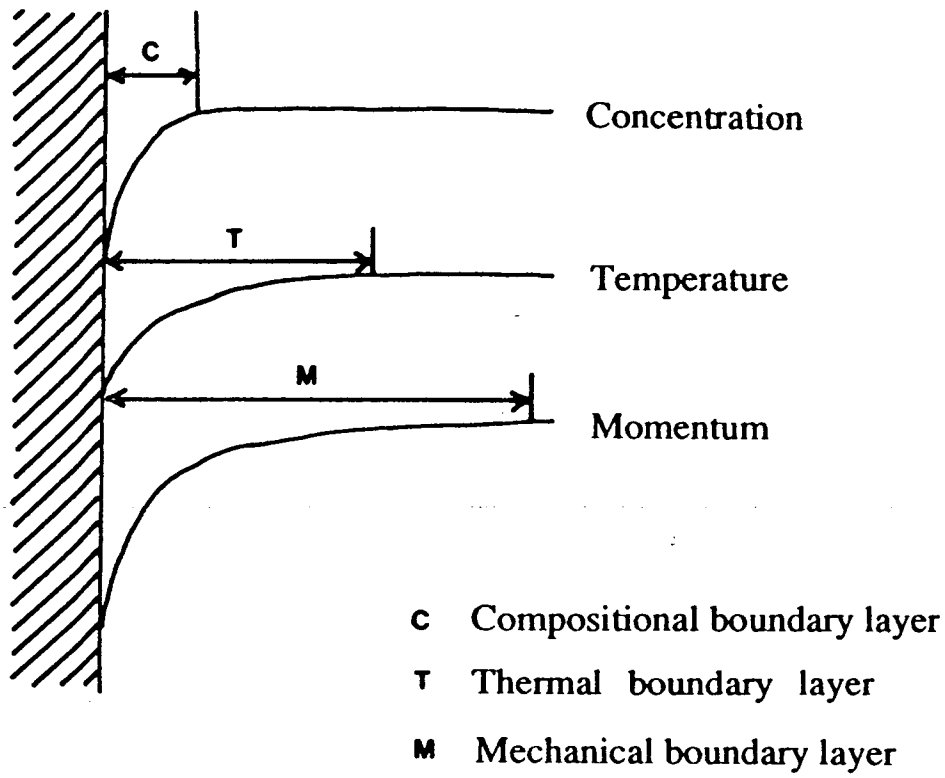


**Figure 7.11** Relative thicknesses of different boundary layers, after McBirney (1984).

The width of the boundary is a function of Pr (McBirney and Noyes, 1979 and references therein). Estimates of mechanical boundary layer thickness range from about a metre in a basaltic magma chamber (Martin *et al.*, 1987) to several hundred metres in rhyolitic magmas (Spera *et al.*, 1982). Mechanical boundary layers in the YGDC are thought to have been of the order of 1-10m, probably near the lower end of this range due to its high cooling rate. Within the thermal boundary layer, the lowering of temperature will result in crystallisation. The crystal distribution in the thermal boundary layer depends upon the type of nucleation occurring but is generally assumed to increase towards the magma chamber wall, as a response to the temperature decrease. However, this assumption may not be correct as the liquidus temperature will be lowered in the compositional boundary layer as a result of the increase in the concentration of residual components, and this effect may reduce or even reverse this trend (Nilson *et al.*, 1985).

The Reynolds number (another measure of whether the flow is laminar or turbulent) uses the boundary layer thickness in the equation:

$$Re = \frac{U\,d}{\nu}$$

Where: $U$ = peak convective velocity in boundary layer
$d$ = thickness of boundary layer
$\nu$ = kinematic viscosity

This measure has been used by several authors (turbulence occurs when Re>500) but it relies on estimates of the convective velocity and boundary layer thickness which are difficult to obtain. McBirney and Noyes (1979) used values given by Wager and Brown (1968) for the Skaergaard Intrusion to calculate the Reynolds number of the intrusion and concluded that the flow must have been laminar, but the quantities that they used were at best only rough estimates and the viscosity was probably too large by a factor of 10. Most equations used to calculate the convective velocity (e.g. Marsh and Maxey, 1985; Shirley, 1987) include assumptions such as constant viscosity or laminar convection which make them inaccurate. It was found that estimates of convective velocity for the YGDC varied by several orders of magnitude depending upon the equation used. It is considered that the quantities required to calculate the Reynolds number are too poorly constrained for it to be of use and it has not been calculated for the YGDC.

Interaction between convection and crystal settling

Several authors (Marsh and Maxey, 1985; Weinstein *et al.*, 1988; Brophy, 1989) have developed models of crystal settling in steady, laminar convection and concluded that there will be a region or regions where a certain proportion of the crystals would be retained indefinitely. However, a more widely accepted opinion is that magma chamber convection is unsteady or turbulent. Huppert and Sparks (1980), Spera *et al.* (1982) and Sparks *et al.* (1984) modelled the transport of crystals by turbulent convection. They also predicted that since the mid-depth root mean square (rms) vertical component of the convective velocity would be several times greater than the settling velocity of typical crystals, and thus crystal settling would be ineffective. However, the approach of Martin and Nokes (1989) differed from that of Huppert and Sparks (1980) and Sparks *et al.* (1984) in that they included the depth dependence of the convective velocities, which must be zero at the margins of the magma chamber. Their predictions, backed up by experimental work, showed that crystal settling can be a very effective process. Although their treatment relies upon certain assumptions and also deals with a magma chamber cooled from the top rather than the sides, it is considered that Martin and Nokes' conclusions have general implications for the YGDC. These conclusions only apply, however, if there are crystals within the main body of convecting magma due to homogeneous nucleation, or to nucleation of crystals at the roof which then become detached.

One way in which efficient crystal movement may be achieved is by two-phase convection (Morse, 1986a, 1988; Brandeis and Jaupart, 1986, Marsh, 1988) where packets of liquid with suspended crystals have a bulk density higher than that of the surrounding liquid and can settle faster than individual crystals under the influence of gravity. Such packets may also be dense due to cooling and/or crystallisation, the latter condition depending upon the crystallising assemblage (see below). The authors cited above only consider horizontal boundary layers at the roof of an intrusion where instabilities of a certain size have to develop before descending plumes can form. In the YGDC, roof cooling must have occurred, but since the height:width ratio was probably large it is uncertain whether processes occurring at the roof would have had any effect on floor crystallisation. If the roof zone present above the developing layers in the western YGDC (localities B to D of Fig. 2.1) was similar to that seen in the Narsaq area (locality M) today then there cannot have been interaction between the two, because the cumulus assemblages differ. It is assumed, for the purposes of this study, that there was no interaction between the roof and the floor of the crystallising YGDC. The vertical sidewall boundary layers would have

responded rapidly to any density difference and thus distinct plumes of magma containing suspended crystals would probably have formed only if there was a burst of nucleation or if a volume of crystals accreted onto the wall became detached. Such plumes would become density currents when they reached the less steeply dipping base of the chamber.

There is evidence for current action in several layered intrusions, notably Skaergaard (Irvine, 1987a). The YGDC also shows numerous features which are indicative of magmatic currents, such as channelling, cross-bedding and unconformities. Irvine (1977, 1980a, 1983) studied the structure of density currents and suggested that much of the crystal accumulation in layered intrusions could be due to deposition of crystals by density currents. In a magma with a viscosity of 100 poise, Irvine (1980a) calculated that a current carrying 45% suspended crystals would be 1-1.5m thick and move at 2-3km $hr^{-1}$. Such currents provide a possible explanation for the occurrence of plagioclase on the floor of intrusions when it is less dense than the magma. Irvine explained the modally-graded layers of Skaergaard as being due to such currents, with dense minerals being deposited by the head of the current and plagioclase being carried over the back of the current to be deposited by a trailing layer above the mafic minerals. Conrad and Naslund (1989) also considered such layers to be due to periodic deposition by convection or density currents, but believed the uniform rock between to be due to *in situ* crystallisation. However, the mafic layers in the troctolitic parts of the YGDC are rarely graded and do not show concentrations of plagioclase at the top. It seems that if rapidly-moving plumes or currents were responsible for the formation of these layers, the suspended crystals could not have included much, if any, plagioclase. Graded layers are more common in the evolved pods. There are poorly defined graded layers at locality K and well-defined ones in the nunataq region, similar to those seen in some of the Gardar syenitic central complexes. The troctolite or syenite between mafic layers could have been deposited by currents but shows no small-scale layering or feldspar lamination that might suggest such a process.

Compositional convection

In addition to the thermal convection described above, compositional convection may result from density differences between depleted liquid next to growing crystals and the main magma body. The idea that basaltic magmas change in density during fractional crystallisation is well established but has been developed

by Sparks *et al.* (1980), Stolper and Walker (1980) and many authors since. Changes in density are only of the order of 1-2% but have an important effect on magma behaviour. The effects of compositional convection may even be greater than those of thermal convection (Sparks and Huppert, 1984, Turner and Campbell, 1986). A measure of the relative rates of chemical and thermal diffusion is given by the Lewis number, Le, which is of the order of $10^2$-$10^5$ in magmas (Nilson *et al.*, 1985).

$$Le = \frac{\kappa}{D}$$

Where: $\kappa$ = thermal diffusivity

D = chemical diffusivity (e.g. Mg in basalt)

Compositional convection of light residual fluid provides the mechanism of fractional crystallisation if all crystallisation occurs in situ; it is sometimes termed *convective fractionation* (Sparks and Huppert, 1984) or *liquid fractionation* (McBirney *et al.*, 1985). Sparks and Huppert (1984) introduced the concept of *fractionation density*, which is the bulk density of those components in the fluid being removed by crystallisation. This concept has been found useful in the present study although it could perhaps be better named. Residual fluid will be denser than the main magma if plagioclase forms a large proportion of the fractionating assemblage but if mafic minerals (especially Fe oxides) are crystallising the residual fluid will be less dense. For a basalt, the magma density decreases with decreasing Mg content while only olivine (± pyroxene) is crystallising, begins to increase from the time that plagioclase appears on the liquidus and then decreases again while Fe oxides fractionate (Fig. 7.12).

During crystallisation at the margins of a magma chamber, a compositional boundary layer forms, usually narrower than the thermal boundary layer since chemical diffusivity in magmas is lower than thermal diffusivity (Figure 7.11). Martin *et al.* (1987) estimated the compositional boundary layer thickness in a basaltic magma chamber as being of the order of 1cm. In the same way as for thermal convection, gravitationally unstable magma in horizontal compositional boundary layers has to develop instabilities of a certain size before any movement can occur. At sloping or vertical compositional boundary layers flow will occur for any size of instability, either in the same or in the opposite direction to the thermal boundary layer.

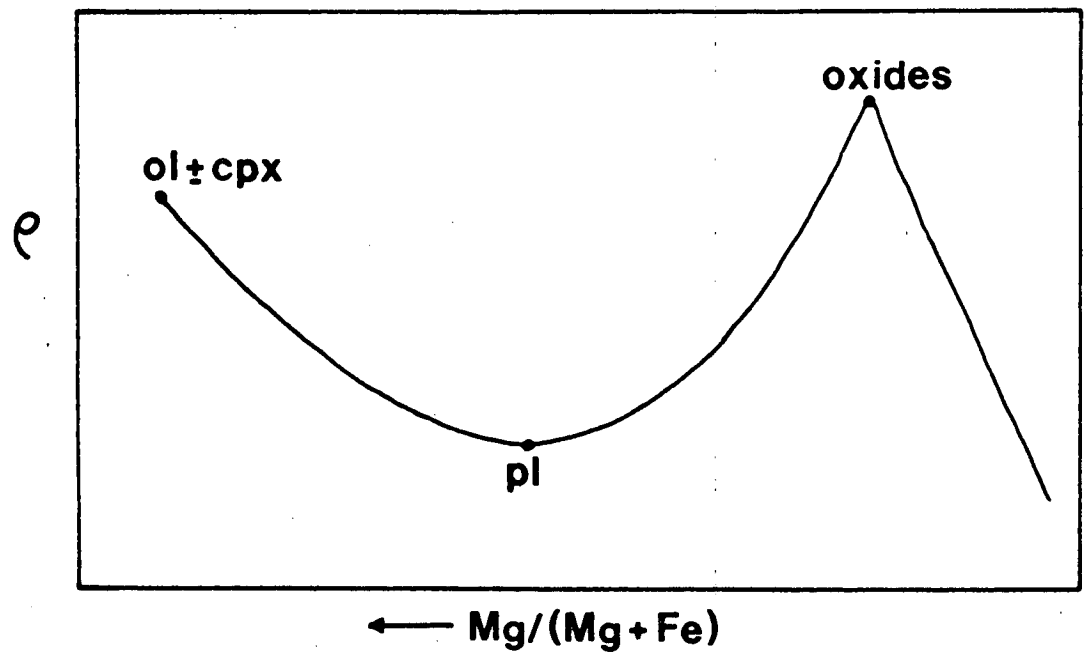


Figure 7.12 Schematic relationship between magma density and Mg/(Mg+Fe) for basaltic melts related to one another by fractional crystallisation. After Huppert and Sparks (1980).

Magma densities for the YGDC chilled margins, calculated by the method of Bottinga *et al.* (1982) at 1150°C, range from 2.75 to 2.85 g $cm^{-3}$. Fractionation densities have also been calculated for mineral species from microprobe analyses using the same method and are shown in Fig. 7.13. Where more than one mineral is crystallising, fractionation densities are calculated as a weighted mean (Sparks and Huppert, 1984).

Fractionation densities have been calculated for different cumulus assemblages in the YGDC. The mineral proportions were determined by point counting and the volume percentages thus obtained converted to weight percentages using room-temperature mineral density data from Clark (1966). In the western part of the YGDC only olivine and plagioclase are cumulus phases, occurring in the volume proportions 25% olivine and 75% plagioclase (± 5%). Compositions of $Fo_{65}$ and $An_{62}$ were used, giving a fractionation density of between 2.66 and 2.75 g $cm^{-3}$ at 1150°C. The value given by Sparks and Huppert (1984) for a troctolite of roughly this composition is 2.68 g $cm^{-3}$. Thus the residual fluid resulting from crystallisation of this assemblage would be slightly denser than the initial magma. Compositional convection at the dyke margins would have tended to reinforce the thermal convection and the fluid released from crystallisation at the base of the magma would have ponded there.

Where Fe-Ti oxides are also fractionating phases, phase proportions are roughly 14:73:13 ol:pl:oxides. Apatite is ignored for the purposes of this calculation. The fractionation density ranges from 3.03 to 3.16 g $cm^{-3}$. The residual liquid was thus lighter than the bulk magma and would have formed a buoyant compositional boundary layer at the walls and floor of the chamber. The residual liquid may have accumulated to form the differentiated pods of syenogabbro and syenite.

Liquid stratification can develop from compositional gradients in a magma chamber. If the least dense liquid is at the top, the stratification is stable but if heavy liquid is released at the top (by cooling or by crystallisation of light phases) or light liquid is released at the base, a system of double-diffusive convecting layers may develop (McBirney and Noyes, 1979; Huppert and Sparks, 1984). Horizontal temperature or density gradients, produced by cooling or crystallisation at sloping or vertical walls, can also result in double-diffusive convection (Turner and Campbell, 1986) and this may have occurred during the crystallisation of the YGDC.

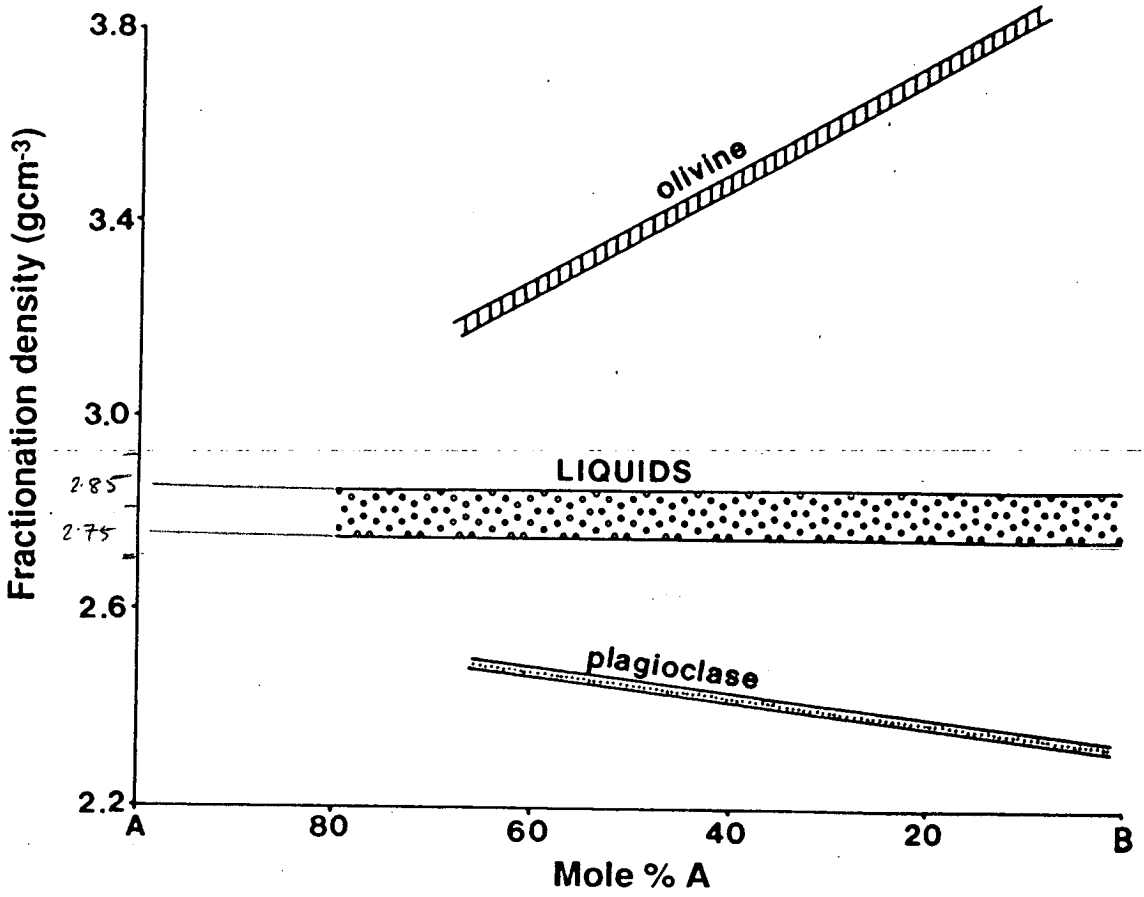


**Figure 7.13** Fractionation densities at 1150°C for olivines and plagioclases from the YGDC, plotted against composition. For olivine, A = $Mg_2SiO_4$ and B = $Fe_2SiO_4$; for plagioclase, A = $CaAl_2Si_2O_8$ and B = $NaAlSi_3O_8$. The density range of the chills at 1150°C is also shown. Adapted from Huppert and Sparks (1984).

### 7.3.3 Postcumulus processes

Once the crystals have formed a touching framework (when the liquid is 50-60% crystalline), a variety of postcumulus processes may operate. The cumulus crystals continue to grow and other phases usually nucleate. In order to have crystal growth there must be a supply of the required chemical components. Wager and Brown (1968) and Morse (1986b) envisaged crystals near the surface of the crystal pile maintaining communication with the main magma body by diffusion. This would be aided by convective currents flowing across the surface of the pile, replacing the residual liquid produced by crystallisation with undepleted magma and helping to disperse the latent heat of crystallisation.

Crystal growth would also be aided by light residual fluid at the floor or dense residual fluid at the roof causing compositional convection through the porous network of the crystals (Tait *et al.*, 1984, Sparks et al., 1985). Convection is a more efficient method than diffusion for maintaining a constant melt composition next to the growing crystals. However, the efficiency of convection decreases dramatically as the porosity decreases (Campbell, 1987) so crystal growth alone cannot produce the extreme adcumulates (with <1% intercumulus material) seen in some intrusions. Sparks *et al.* (1985) proposed that compaction, resulting from density differences between the matrix (the interlocking crystal framework) and the interstitial melt, would be capable of producing such rocks. Several of the quantities required are poorly known, but they calculated that for olivine cumulates, significant compaction can occur on a time scale of a few hundred to a few thousand years. This time scale is an order of magnitude larger than the time required to develop an interconnected melt network (Shirley, 1986). Shirley found that theoretically, in a system undergoing rapid deposition, compaction occurs in a single zone extending throughout the crystal pile and the velocity of the interstitial fluid approaches the fluidisation velocity of the system. When deposition is slow, there are two compaction zones at the top and base of the crystal pile, separated by a region of almost constant porosity. The effects of compaction are small in intrusions with a minimum dimension of less than 1km (Sparks *et al.*, 1985). However, it was calculated in Chapter 4 that 20-30% of the interstitial melt must have been lost from the troctolites to produce the incompatible element signatures seen, so it appears that some compaction did occur.

The processes of compositional convection and compaction require the migration of interstitial fluid. The removal of melt by compaction is also known as

"filter pressing". Such movement may lead to the process which Irvine (1980b) termed "magmatic infiltration metasomatism", where a change in mineral composition due to reequilibration with infiltrating interstitial fluid is offset from a phase layer boundary. If the fluid is rich in water and residual components, it may result in partial remelting of the cumulus crystals, by lowering the liquidus and solidus temperatures of the system. This process will extract components which preferentially partition into the fluid, leading to "zone refining" as the fluid moves upwards through the cumulates (McBirney, 1987). The melt may also accumulate in certain areas due to variations in size, shape or packing of crystals, to differing extents of preferred crystal orientations or intercumulus growth, to variable porosity or the presence of xenoliths. Accumulated liquid will generally crystallise as pegmatite, due to the relatively high volatile contents (e.g. Donaldson, 1982).

Campbell (1987) argued that neither extensive convection-assisted growth nor compaction may be required to explain adcumulates, but that in-situ crystallisation may in fact result in a much lower initial porosity than crystal settling. This is seen in some aqueous crystallisation experiments.

Both Campbell (1987) and Barnes (1986) suggested, in contrast to authors cited above, that large-scale movement of interstitial fluid does not occur, since it would smooth out the observed small-scale compositional variability observed in many layered intrusions. Barnes calculated the compositional shift in ferromagnesian cumulus minerals that would result from the crystallisation of trapped interstitial liquid. This shift depends strongly on the original cumulus assemblage (the absolute iron + magnesium content) and on the proportion of trapped liquid. It depends only weakly on the composition of the liquid, provided it is kept within likely values for basaltic melts. Barnes showed that the crystallisation of trapped liquid can lead to a shift in the Mg number of olivine or pyroxene which is significant in comparison to the changes produced by fractional crystallisation.

Small-scale processes that may operate are thermal migration (Lesher and Walker, 1988) and grain coarsening (textural equilibration). Thermal migration results from the differing solubilities of minerals at different temperatures. It has been shown that in a temperature gradient, an adcumulate can form by dissolution of one or more minerals at higher temperature and reprecipitation at lower temperatures (for ferromagnesian minerals) or vice versa (for silica). This process will only operate on a small scale in layered intrusions, but unlike compositional convection or compaction, it does not require an interconnected melt network. Textural

equilibration has already been considered in section 3.3.1; grain coarsening can enhance modal variations (Boudreau, 1987) but the large variation in grain size shows that the cooling of the YGDC was too rapid for this process to proceed far.

The YGDC rocks show little or no sign of adcumulate texture, due to their rapid cooling rate. If the initial liquid constituted 50% of the rock, then incompatible element signatures show that roughly half of it was expelled, probably by compaction, leaving rocks consisting of about 70% cumulus crystals and 30% intercumulus material. This matches petrographically-estimated proportions. The presence of interstitial melt segregations as pockets trapped below xenoliths (localities B-D), pegmatitic patches (localities K and L) or veins within the troctolites, also suggests some compaction. In the western part of the YGDC, compositional convection could only have occurred once the density of the intercumulus liquid had been lowered sufficiently by crystallisation of intercumulus Fe-Ti oxides. The proportion of liquid remaining at this stage would have been small and movement difficult, even if the porosity was still interconnected. It is apparent from the late-stage turbid alkali feldspars in the troctolites that some very evolved, volatile-rich fluid did remain trapped.

Thus about half of the interstitial liquid was trapped and solidified more-or-less in place within the western troctolites. This probably led to some shift in olivine compositions, as suggested by Barnes (1986). Considering olivine, the only mineral in the YGDC troctolites and gabbro picrites likely to experience such compositional shifts, crystallisation of 30% trapped liquid in a dunite leads to a shift of 3 mol% Fo, but the same amount of liquid in a troctolite or olivine gabbro will lead to a shift of 5-8 mol% Fo.

The difference in composition between the olivines within the troctolite and the gabbro picrite layers (section 3.4.1) is attributed to this process, with the same proportion of trapped liquid causing a larger compositional shift in the troctolite olivines. The average olivine composition in a gabbro picrite is $Fo_{66}$ and in the troctolite is $Fo_{62}$, so the original composition might have been about $Fo_{68}$. However, the composition of the accumulated olivines (Chapter 4) was about $Fo_{66}$, so the gabbro picrites may not have undergone any compositional re-equilibration.

In the eastern part of the YGDC, compositional convection may have had more effect since the residual fluid was lighter than the bulk magma. Slightly more

of the interstitial liquid was probably expelled here than in the western YGDC, possibly causing the lack of clinopyroxene seen in some of the cumulates from locality I.

The feldspar lamination observed at localities G, I and M in the Tugtutôq area, and at various localities in the nunataq region, cannot be due to current alignment of crystals because it is not seen at localities B to D where the most spectacular evidence for current activity occurs. Feldspar alignment is often taken as evidence for compaction but again it would be expected at localities B to D. Even if some of the western troctolites accumulated as stellate glomerocrysts of olivine + plagioclase, compaction would have led to some rotation of the crystals. The occurrence of localised plagioclase lamination east of locality G is not fully understood. There is no evidence for lower cooling rates or geater loading, which might have led to greater compaction. However, the removal of a greater proportion of interstitial liquid due to compositional convection operating in addition to convection may have caused the plagioclase crystals to pack slightly closer and become aligned with the synformal floor of the chamber. In addition, the development of a lamination would have been facilitated if the level of plagioclase supersaturation had declined so that plagioclase nucleated as single crystals more often than as stellate aggregates.

It has already been shown that the degree of textural reequilibration (above and below the solidus) was small (section 3.3.1). It is not known to what degree thermal migration may have operated, but this too is thought to be minimal or non-existent.

## 7.4 Crystallisation experiments

In recent years several workers have performed experiments with aqueous solutions in an attempt to simulate magma chamber crystallisation (McBirney *et al.*, 1985; Sparks and Huppert, 1987 and refs therein; Kerr *et al.*, 1989; Tait and Jaupart, 1989). Many of these studies have been concerned with simulating a magma chamber cooled at the roof, but Turner and Gustafson (1981) cooled a solution by circulating coolant down a vertical rod. As part of the present project a few experiments were carried out at the Department of Applied Mathematics and Theoretical Physics at Cambridge University. Aqueous solutions in a Perspex tank were cooled by means of two vertical plates, in order to simulate a crystallising dyke.

The tank measured 20 x 20 x 20cm and was open at the top. Two moveable Perspex cooling plates with 0.25cm brass plates on the inner faces were cooled by a 1:1 mixture of ethylene glycol (antifreeze) and water, introduced through a coiled metal tube (Fig. 7.14). The coolant was circulated by two Hooke cryostatic circulators with 12 litre reservoirs. The tank was insulated on all sides by expanded polystyrene about 3cm thick. Illumination was provided from behind using a slide projector and density differences in the liquid could be observed by means of a shadow-graph. Experiments were performed with the cooling plates 7cm apart, to give a height:width ratio of roughly 3:1.

It is possible either to pre-cool the plates below the liquidus of the solution or to cool the solution from room temperature. Although pre-cooling the plates would have been geologically more accurate, in these experiments the solution was cooled from room temperature since, by this method, crystallisation occurs more slowly and is easier to observe.

The two solutions used were sodium carbonate and sodium nitrate, chosen because their phase diagrams are well-constrained, crystallisation occurs at temperatures attainable in the laboratory, the chemicals are relatively inexpensive and available in large quantities (several litres of solution were needed) and they should stay clear even at high concentrations. In fact, some problems of cloudiness were encountered when using the sodium carbonate solutions. An additional advantage is that the concentration of the solution at any one time can be constrained using refractive index measurements.

At the start of each experiment the whole tank was filled with solution, the temperature and concentration measured and the cooling plates switched on. The rate of cooling of the two plates was slightly different and varied between 20°C and 29°C per hour. Further temperature and composition measurements were made during the course of each experiment. Two experiments were performed using sodium carbonate solution, crystallising $NaCO_3.10H_2O$ and producing light residual fluid. One experiment was performed, and then repeated, using sodium nitrate solution, crystallising ice and producing dense residual fluid. A dilute solution of sodium carbonate could have been used to crystallise ice but sodium nitrate was chosen because the phase diagram has a much larger ice field (Fig. 7.15).

In the first sodium carbonate experiment, the brass faces of the cooling plates were covered with rough gauze to assist crystal nucleation and to simulate the irregular walls of a magma chamber, but in the second experiment the gauzes were

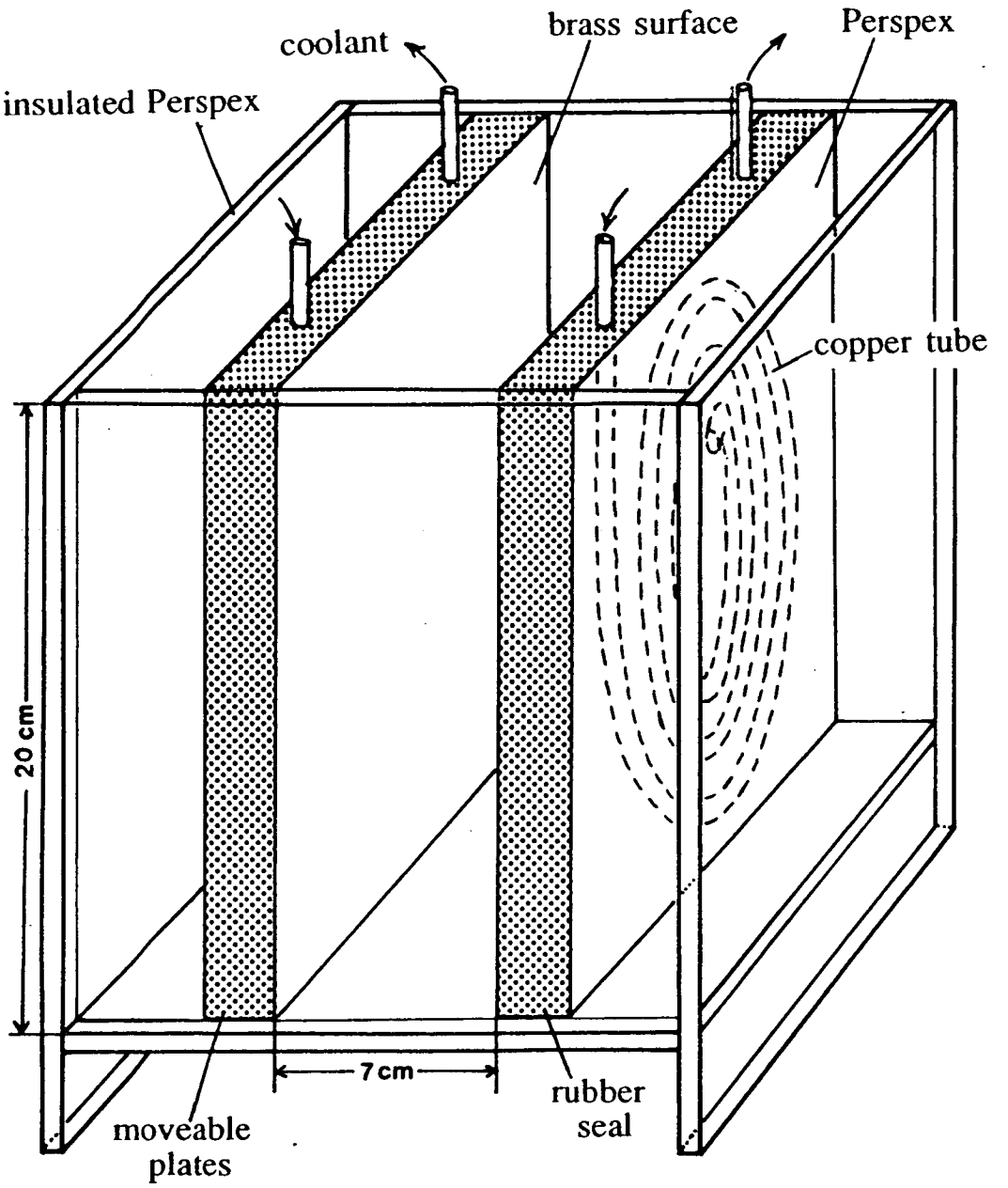


**Figure 7.14** Experimental apparatus used to simulate a crystallising dyke.

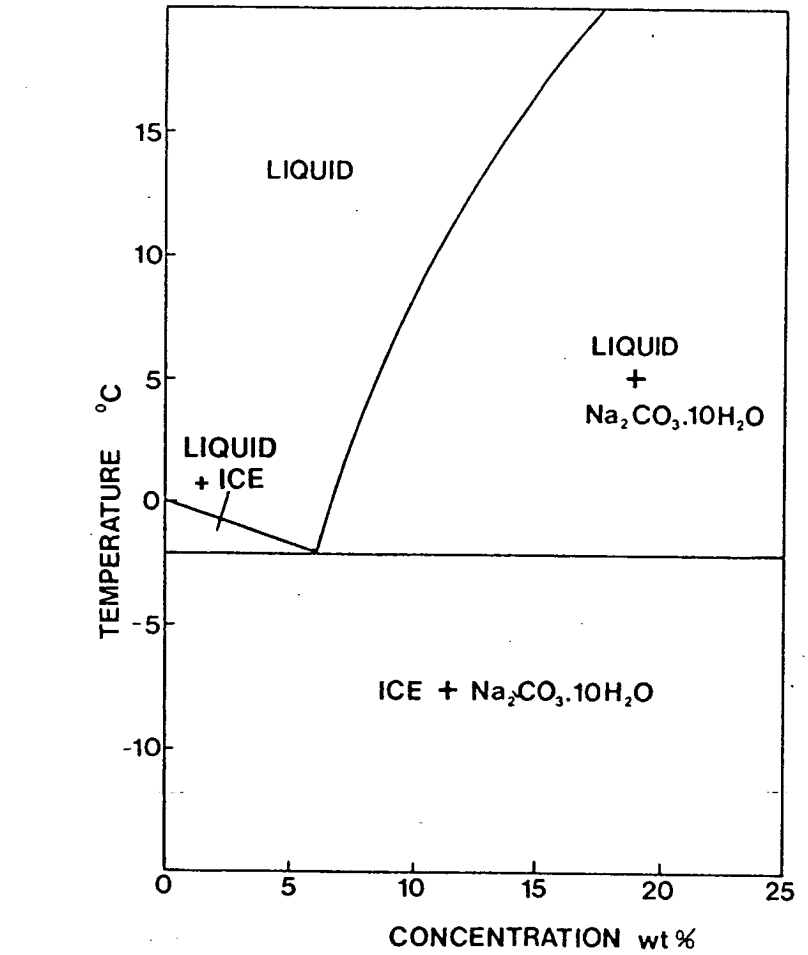


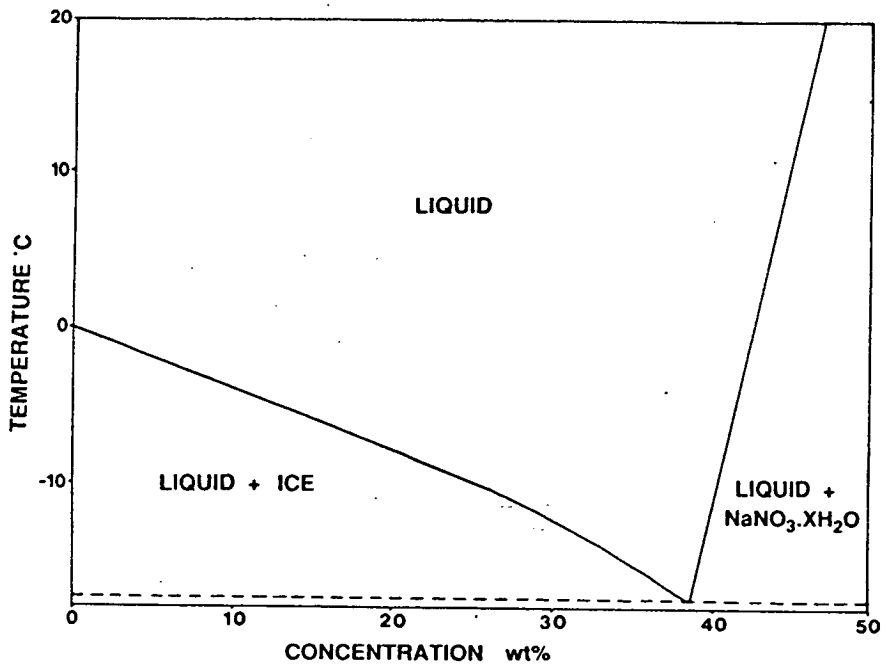


**Figure 7.15** Phase diagrams for (a) $NaCO_3$ and (b)$NaNO_3$ solutions.

removed to observe any differences in crystal behaviour that resulted. In both experiments, no thermal convection was observable in the initial stages but temperature measurements indicated that a thermal stratification had developed, with the fluid at the base of the tank becoming about 4°C colder than the top. Crystallisation began after 25 mins and the first crystals formed in the coldest layer about 1cm above the base of the tank. The lowest 1cm of the tank was gaining heat from the room. Compositional convection began and a boundary layer of buoyant residual fluid was observed rising along each cooling plate and collecting as a discrete layer at the top of the liquid. During the next 30 mins, crystals nucleated all over the plate and there was strong turbulent marginal compositional convection with a thermal downflow in the centre of the tank (Fig. 7.16). Some crystals (about 10% with the gauzes and 30-40% without the gauzes) detached themselves from the cooling plates; sometimes these were aggregates of several crystals. A few of the smaller crystals were carried upwards by the compositional convection currents and remained suspended in the compositionally light layer at the top of the tank for a time before being melted by the heat of the room. Most, however, sank to the floor of the tank, where they continued to grow. The crystals were always elongate with length: width ratios of betweeen 5:1 and 10:1 and the largest ones had grown to a length of about 4cm by the time the experiments were terminated.

Some weak double-diffusive convecting layers developed for a time in the first experiment but were not observed in the second experiment. After about 2hrs, nucleation of crystals appeared to have ceased and crystal growth was very slow. After 3hrs in the second experiment and 4hrs in the first experiment, the liquid temperature and composition had reached the eutectic and a composite eutectic solid began to form at both cooling plates. The experiments were terminated when the eutectic solid was about 1cm thick.

The evolution of the liquid compositional profile with time during the second experiment is shown in Fig. 7.17. It can be seen that about 5°C of undercooling developed before nucleation occurred and the liquid composition began to move towards the eutectic. The liquid did not come back to the liquidus curve until it reached the eutectic.

In the third experiment, using sodium nitrate, a temperature gradient again developed before crystallisation occurred. With the same shape of tank as that used in the first two experiments, crystallisation (which started from a point on one plate) happened extremely quickly. Within 30 seconds the lower half of the tank was full of

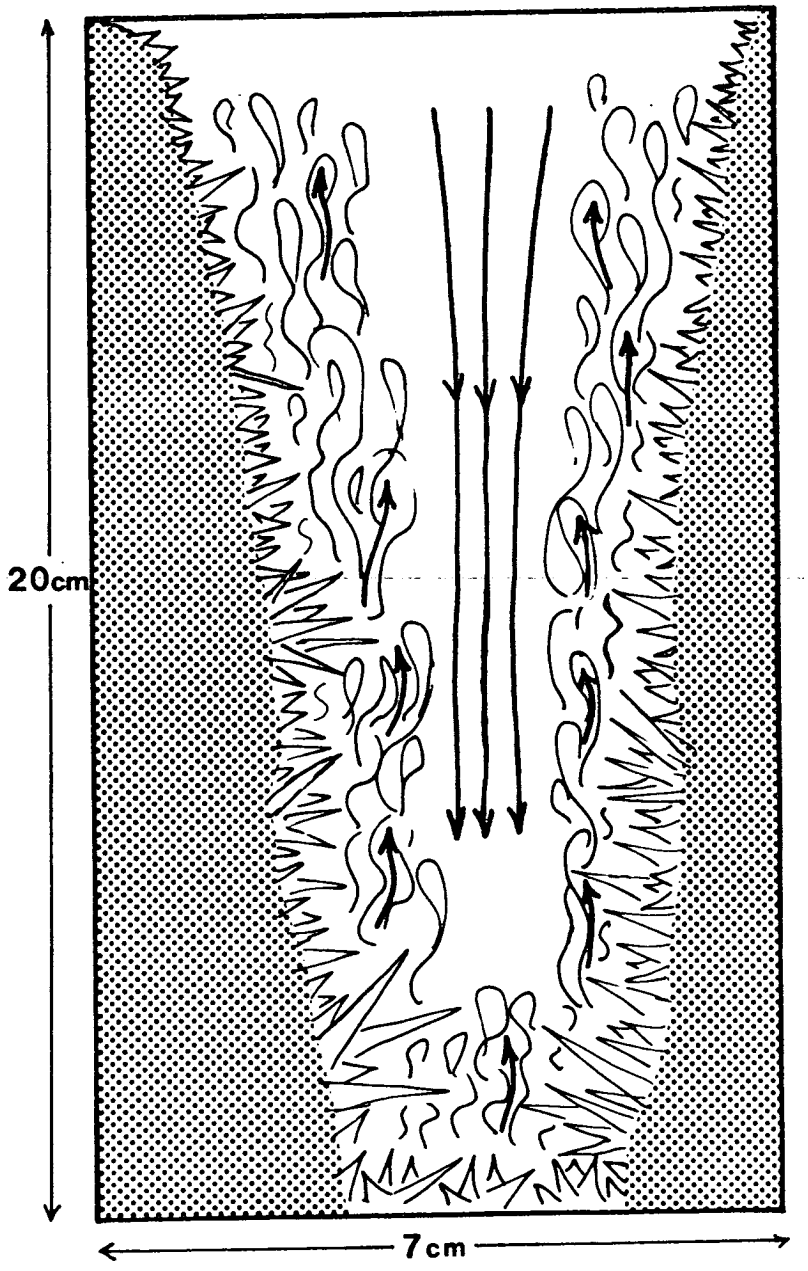


**Figure 7.16** Sketch of the second experiment after about 1.5 hours. Elongate crystals had formed on both cooling plates with larger crystals growing near the colder base of the tank. Some crystals had become detached and settled to the floor of the tank. Buoyant compositional plumes were rising from all the crystals and there was a central compensating downflow.

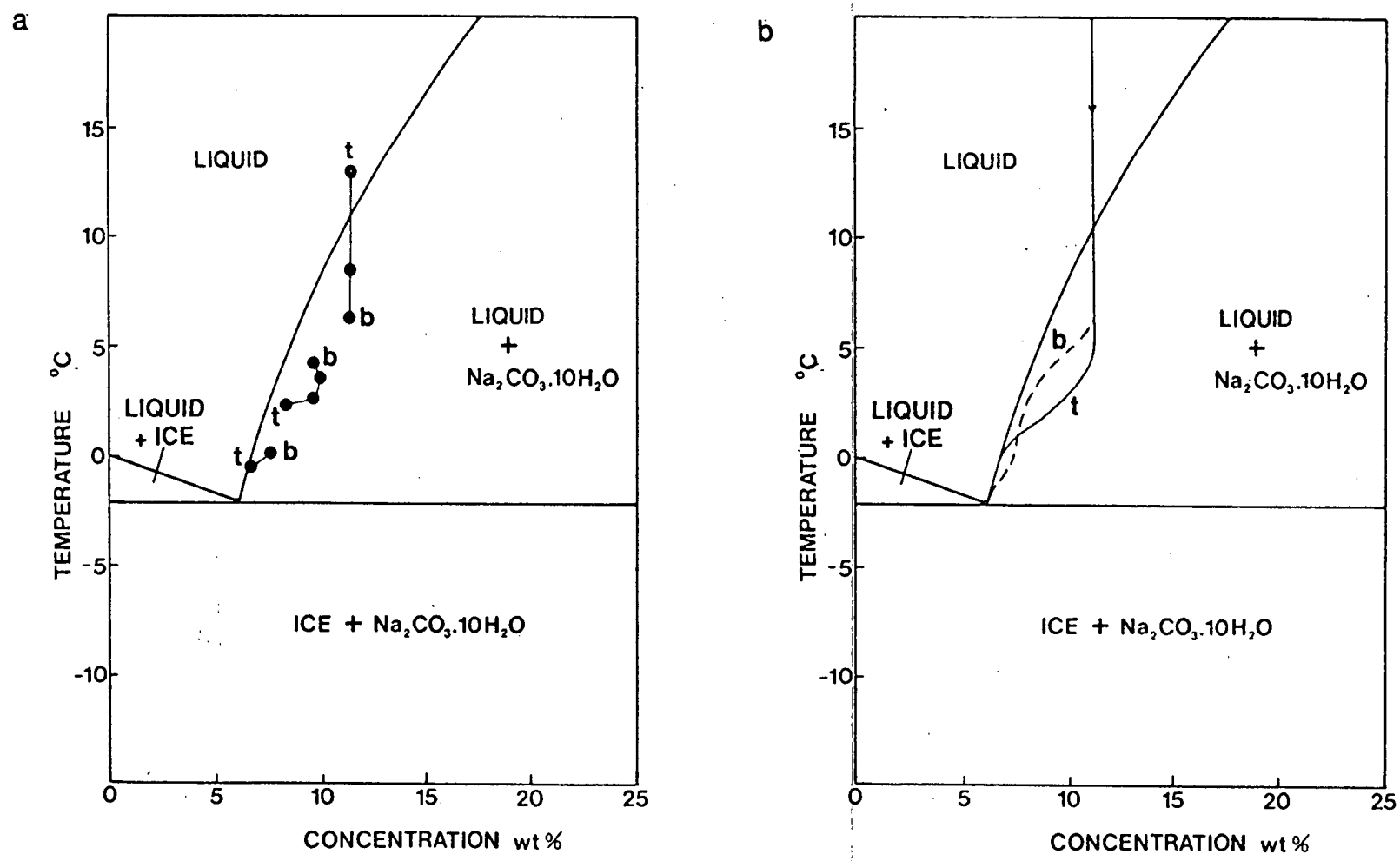


**Figure 7.17** (a) Liquid profiles at three different stages in the second experiment with $NaCO_3$ solution; (b) the T-X path followed by the solution. t = top of tank, b = base of tank.

an interlocking mass of elongate crystals up to 0.5cm long, slowly rising. Clusters of crystals detached themselves at intervals from the top of this mass and rose to the surface. Little compositional convection was seen.

The experiment was repeated with the cooling plates moved to the sides of the tank giving a height:width ratio of nearly 1:1. This time a well-developed thermal stratification could be observed, and ice crystallisation began at two discrete levels in the tank. The thermal profile gradually evened out and a layer of ice began to grow into the tank from each cooling plate. The liquid path for the experiment is shown in Fig. 7.18 and it can be seen that the system came back to the equilibrium curve much more rapidly than for the sodium carbonate experiments. The crystals were generally smaller than those formed in the first two experiments (up to 1cm long) and very few became detached from the walls, despite the absence of gauzes. Compositional convection appeared to be weak.

An aqueous solution in a square tank is obviously an imperfect analogy for a crystallising magma chamber, but since magma chambers cannot be observed, crystallisation experiments of this sort may provide insights into processes such as double-diffusive convection which may be important in magma chambers but would not otherwise have been considered. It is important to consider the degree of dynamic similarity between the two situations. The most important condition is that the flow in both cases should be in the same physical regime (Sparks and Huppert, 1987) and this can be determined by calculating dimensionless parameters for the experimental case and comparing them to those for the magma chamber. The Rayleigh number for the experiments is of the order of $10^{10}$, smaller than that for the magma chamber but above the laminar/turbulent transition. The Prandtl number for the experiments is lower than for a magma chamber, around $10^2$-$10^3$, but the Lewis numbers of both cases are comparable ($10^2$-$10^3$). The Rayleigh and Prandtl numbers are smaller for the experiments because the viscosity of the aqueous solutions is lower and this may lead to behaviour that would not characterise a molten magma. Some experiments have been performed by Tait and Jaupart (1989) using ammonium chloride solution with a hydroxymethyl cellulose compound added to increase the viscosity, but their work was concerned with horizontal boundaries and their approach was not practical for the experiments described here.

Another problem encountered when comparing aqueous experiments with magma chambers is the relative size of crystals and boundary layers (Martin and Campbell, 1988). The elongate $NaCO_3.10H_2O$ crystals (and probably the ice

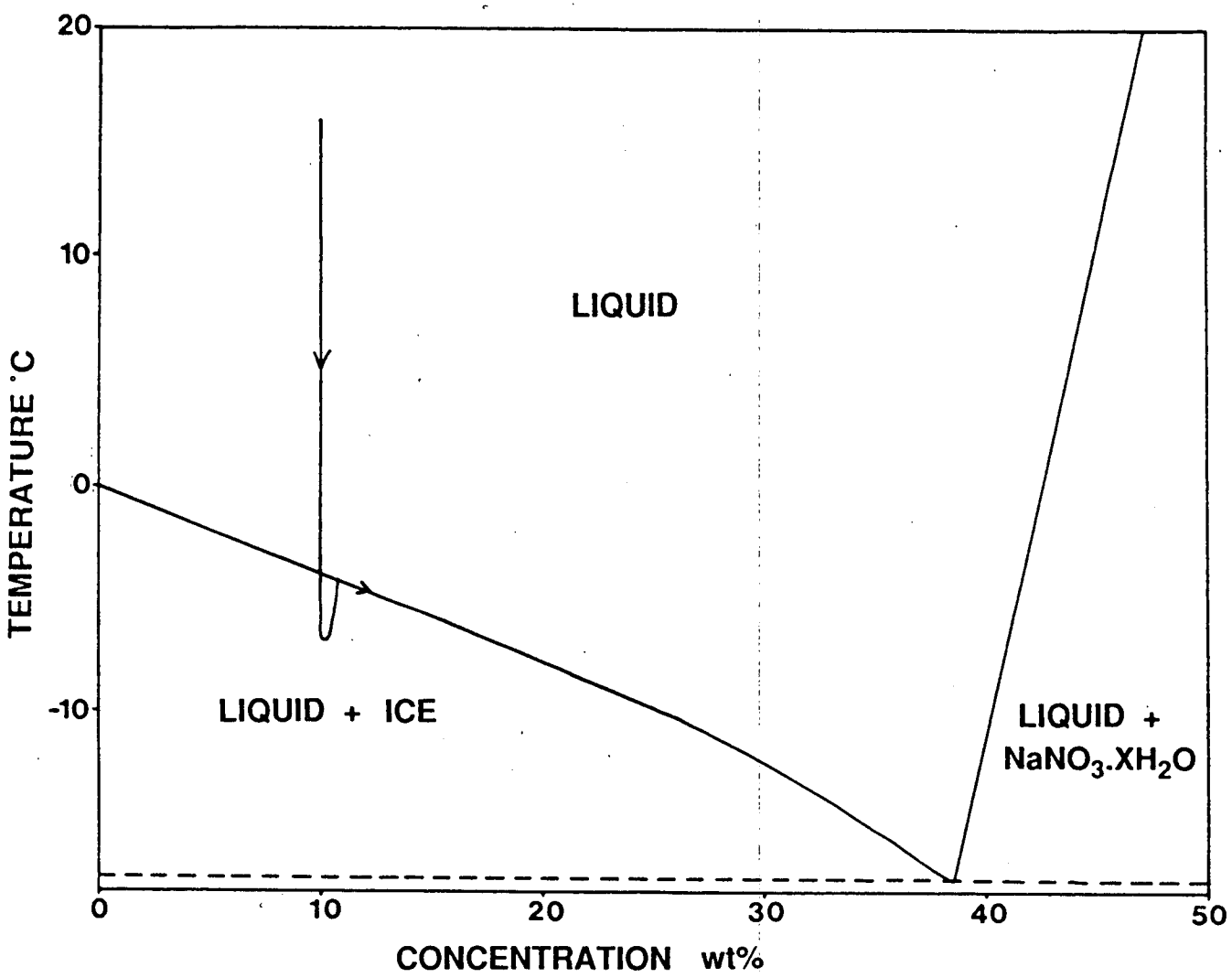


**Figure 7.18** The T-X path followed by the liquid in the experiment with $NaNO_3$. The solution returned to the liquidus curve more rapidly than in the experiments with $NaCO_3$.

crystals) produced in the experiments are longer than the compositional boundary layer, while crystals in magma chambers are probably many times smaller than the boundary layer. This means that each crystal produces a separate compositional plume, instead of a thin compositional boundary layer within the thermal boundary layer as predicted for magma chambers (Nilson *et al.*, 1985). It is concluded that while the experiments illustrated well the processes of supercooling, crystal nucleation and growth, and the existence of compositional convection as a potentially important factor in the evolution of magma chambers, they did not provide a very accurate modal of the crystallisation of the YGDC. The most interesting observation was that crystals could nucleate heterogeneusly on the walls but then detach themselves, sometimes as crystal aggregates. It is thought that this process could also occur in magma chambers, as could the collection of light residual fluid as a discrete layer at the top of the tank or chamber.

## 7.5 Origin of the YGDC Layering

The YGDC magma was probably intruded at a temperature of about 1150°C, carrying phenocrysts of olivine and stellate aggregates of plagioclase crystals with olivine. The latter may have formed in the magma conduit. Anorthosite xenoliths were also borne upwards by the magma and subsequently floated towards the roof of the intrusion. After causing localised wall-rock melting, the intrusion began to solidify. The YGDC magma chambers were tall in relation to their widths. The overall length of the complex in the Tugtutôq area must have been at least 20km, even if there has since been tilting along the axis of the complex, but during the course of solidification several separate magma chambers probably developed. The floors of the chambers formed V-shaped synforms with axes parallel to the trend of the dyke segments, but the primary dips of these synforms are not known, since they may have been steepened by compaction. Upton (1987) suggested that the double synform at locality D formed because the dyke segment had formed by the merging of two separate dykes, and the layering was draped over a thin septum of country rock which is not visible at the present level of erosion. No other explanation has so far been found for this phenomenon.

It is thought that convection occurred within the dyke segments and that it was probably turbulent, although boundary layers (perhaps a few metres thick) may have experienced laminar flow. Descending sidewall thermal convection currents probably flowed across the floor and ponded in the axes of the synforms, with the

return upward convective flow being more diffuse. Crystals formed within the boundary layer rather than in the magma interior because only at the margins of the intrusion would there have been sufficient supercooling to allow nucleation. Most of the nucleation was probably heterogeneous, although the stellate clusters of plagioclase found within the troctolite at some localities may have formed by homogeneous nucleation, as the composite phenocrysts in some of the chilled margins probably did. Crystallisation would have occurred on the vertical or steeply-dipping walls and roof due to cooling, and also on the shallowly-sloping floor if the magma reaching the floor was still sufficiently supercooled. The decrease of liquidus temperature with increasing pressure (about 3°C per km, Jackson, 1961; Wager and Brown, 1968; Martin *et al.*,1987) would make this process more likely. It is not certain to what extent processes in the roof laccolith were coupled with those occurring in the dyke-like chambers, but they probably formed two essentially independent systems. Certainly the coarser grain-size of the troctolite in the Narsaq area (locality M of Fig. 2.1) is consistent with slower cooling in a broader chamber.

Vertical layering at the sides of the dyke is uncommon and layering at dips of 30-40° may extend to within a few metres of the margin (especially at localities B to D), indicating that in the layered pods, most crystal accumulation took place on the floor. To some extent, the floor and sidewalls would have been continuous one with the other; there is no obvious change in dip angle as seen, for example, in the Skaergaard intrusion. In the unlayered parts of the dyke and in the border zones to the layered pod at locality G, it is possible that crystallisation occurred predominantly on the walls, but if this were the case, vertical modal and/or cryptic layering might be expected, and this is not observed. It is considered more likely that crystals accumulated on the chamber floors.

Thermal convection currents flowing down the walls could have carried with them any crystals within the boundary layers that either formed by homogeneous nucleation or else grew at the sidewalls but subsequently became detached, in the manner observed in experiments with aqueous solutions. Olivine crystals in these currents, or those growing within the basal boundary layer, would have been able to sink, since the convective velocity of the magma would vanish at the walls and floor. Plagioclase could only have settled in aggregates with ferromagnesian minerals.

The evidence for current activity in the western YGDC might suggest that olivine separated from plagioclase under the influence of gravity as currents carrying cumulus crystals swept across the chamber floor. However, if this were the case it

would be expected that the majority of the mafic layers would be graded, as seen in the Skaergaard intrusion (Conrad and Naslund, 1989), and they are not. Alternatively, the modal variations could have been due to a change in the crystallisation behaviour of the magma. The magma could have been moved from the olivine-plagioclase cotectic to the olivine field in one of several ways: introducing a new influx of more olivine-saturated magma, raising the temperature or raising the water vapour pressure. There is no evidence in the the form of physical disturbance of the layers, or in the form of systematic differences in the strontium isotopic signatures of adjacent layers, for new inputs of magma from any lower-level reservoir, but the possibility of repeated small influxes from an isotopically constant surce cannot be ruled out. Frequent and intermittent changes of temperature in the layer of magma immediately adjacent to the crystallisation front could have resulted from periodic nucleation with the release of latent heat, as proposed by Brandeis *et al.* (1984), but it is difficult to explain why this should only have occurred in certain areas. Similarly, the periodic delay of plagioclase crystallisation due to depletion in required components by crystal growth proceeding faster than chemical diffusion, should have occurred throughout the chamber. Changes in the vapour pressure were proposed by Upton (1964b) as a cause of modal layering in the YGDC, and by Parsons (1979) for layering in the Klokken Intrusion. Numerous sudden changes in vapour pressure would have been required to produce the layering. It is difficult to envisage how these could have arisen; gradual increases in vapour pressure, coupled with sudden decreases, could have been produced by periodic surface volcanism, but not the sudden increases required to produce such sharply bounded layers. In addition, the volatile components in the YGDC were probably predominantly $CO_2$ and halogens rather than water, and it is not certain whether they would have had the same effect on the phase diagram. It is concluded that some factor caused suppression of plagioclase nucleation, but none of the possible mechanisms seems much more plausible than the others.

A model is suggested for the western YGDC in which olivine and plagioclase were crystallising at the walls and floor, and crystals at the walls were sometimes carried down to the floor by convection currents (Fig. 7.19). For some reason, periodic suppression of plagioclase nucleation resulted in olivine nucleation in the boundary layers, probably on other crystals but not necessarily adhering to them. The olivine crystals caused a substantial increase in the density of the magma in the boundary layers, especially if nucleation occurred in bursts, and led to two-phase plumes descending from the sidewalls more rapidly than the normal convection currents. Olivine crystals were carried to the base of the chamber by these plumes,

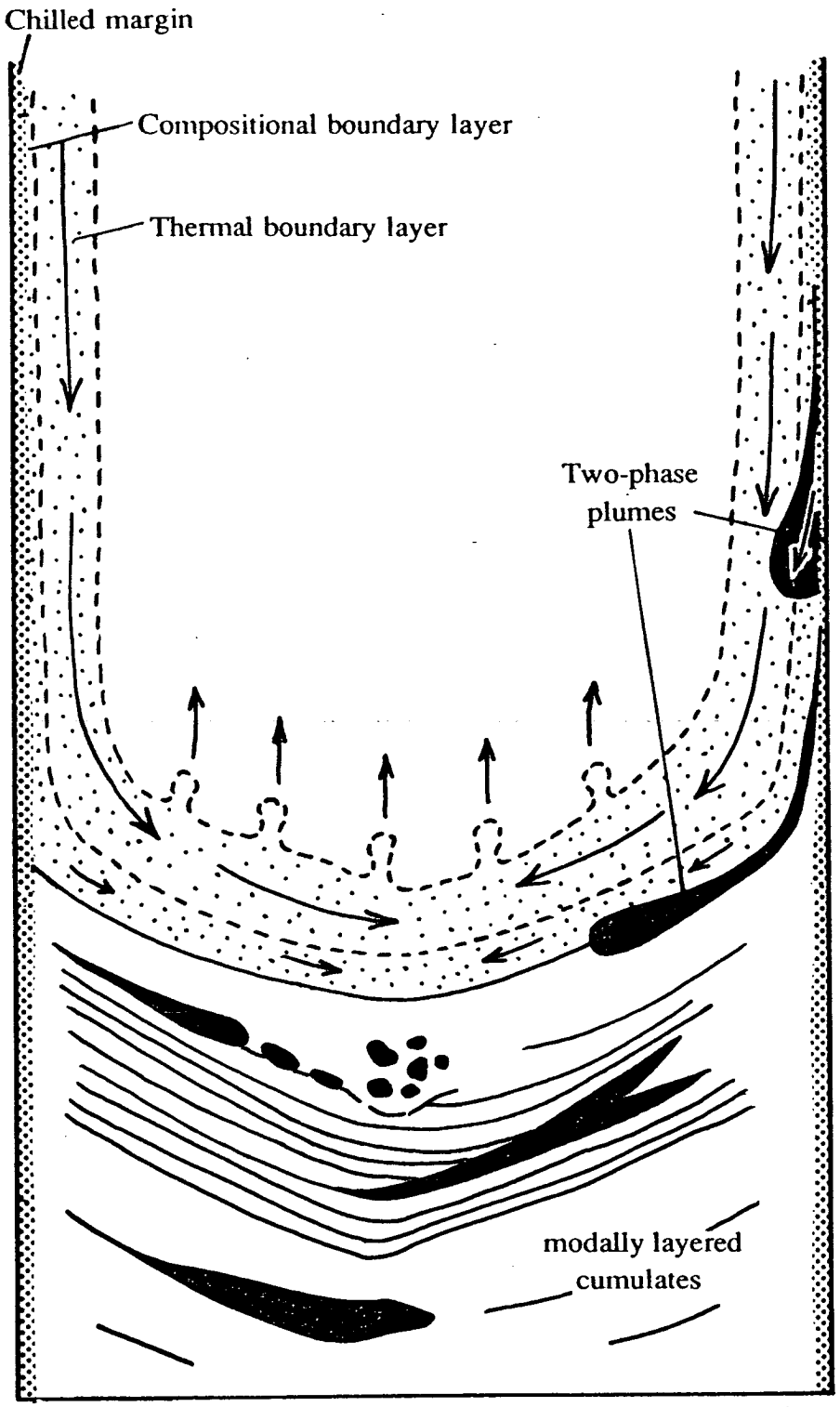


**Figure 7.19** Sketch of some of the processes occurring in the crystallising magma chambers of the western YGDC on Tugtutôq. Dots in the boundary layers represent crystals. The dyke is 200-600m wide.

which became density currents as they swept across the floor (and possibly along the central valleys). The olivine would probably have settled out as a layer before the remaining liquid attained the cotectic and resumed olivine + plagioclase crystallisation. A sharp boundary between the olivine layers and the troctolite above and below it would be expected if the olivine settling was sufficiently rapid. If the olivine crystals were to settle efficiently, the crystal content of the flows would have to be below about 25%, less than the 45% proposed by Irvine (1980a). In this part of the YGDC, crystallisation of plagioclase and olivine would have resulted in a residual liquid slightly denser than the bulk magma. This would have tended to flow down the walls together with the thermal convection currents and ponded along the axial trough, unable to rise (unless forced to by compaction of floor cumulates) until crystallisation of intercumulus Fe-Ti oxides and subsequently pyroxene lowered its density sufficiently. The general similarity of textures and mineral compositions within a large part of the western YGDC may be due to this process of ponding of residual liquid.

This hypothesis can explain several observed features at localities B-D of Fig. 2.1 such as the fact that many of the thin (few cm) picritic layers show irregular bases and smoother tops (Plate 2.7c). Some of this irregularity may be due to loading but it frequently appears that the layer is resting on an irregular floor of plagioclase crystals; the olivine grains, being smaller and more equant, would tend to form a smoother upper surface. The large olivines in the synform axis arrived there under the influence of gravity. Thicker gabbro picrite layers could form if the olivine was deposited from a particular current but the remaining liquid then swept away by a subsequent olivine-bearing current before having a chance to crystallise. In any case the currents would tend to be of irregular volume as well as having irregular temporal spacing. If a particularly strong current scoured out a channel this might have become a site of preferential deposition for a period of time, giving rise to the large troughs observed, whereas the thinner, more regular layers would have been deposited by currents flowing more evenly over the developing cumulate pile. A mechanism of deposition of thin layers by currents has been put forward by Irvine (1980a). Alternatively, the thin, parallel layers could have formed *in situ* on the surface of the crystal pile during periods of olivine-only crystallisation. An alternative theory for the origin of the large troughs is that olivine crystals may have remained attached to the walls until a mass of them became gravitationally unstable, and then slumped periodically, entraining liquid as they did so. This mechanism is similar to the one outlined above, relying on the high density of the olivine crystals to produce periodic density currents, but proposing that a mass of crystals became

detached from the wall at the same time rather than individually. It still requires that plagioclase nucleation be suppressed, allowing olivine to crystallise alone. The first theory is favoured, because although near-vertical disturbed layers are occasionally found near the margins of the dyke (locality F) they are rare and it is more common for layering to die out gradually towards the margins with no signs of disturbance. The troctolite between the layers may have formed from olivine and plagioclase nucleated at the sidewalls and carried down by convection currents in the same way as proposed for the mafic layers. Alternatively they may have crystallised *in situ* on the chamber floor. The clusters of olivine and plagioclase observed in thin section suggest that heterogeneous nucleation took place, with each mineral nucleating on its own species. At the base of the magma chambers, previously-formed cumulates would have insulated the magma adjacent to the crystal pile, hindering the dissipation of latent heat, so for *in situ* crystallisation to occur, a source of supercooled magma would have been required, possibly in the form of descending crystal-free plumes. These would have been only just supercooled, because otherwise olivine, as well as plagioclase, would be expected to show elongate crystal forms, similar to the Rhum harrisite.

The presence of feldspar crescumulates at locality B implies localised strong supersaturation with regard to plagioclase. The fact that the crystals grow from troctolite layers across gabbro picrite layers may indicate that this supersaturation event was connected to the suppression of plagioclase nucleation during the crystallisation of olivine alone, and that the crystals nucleated on the surface of the crystal pile and on xenoliths, and grew while olivine was being deposited around them. This implies that the currents must have been very gentle, although the bending of the crystals may be due to current action while they grew (as proposed for the "perpendicular feldspars" in the Skaergaard intrusion (Wager and Brown, 1968)).

The leucocratic xenoliths in the western YGDC are thought to be predominantly blocks of fine-grained marginal facies, carried down with the olivine crystals by convection currents. The reasons for their apparent concentration of plagioclase over and above that normally seen in the chilled margins are not fully understood.

In the eastern part of the YGDC, (locality G of Fig. 2.1 and eastwards) Fe-Ti oxides joined the fractionating assemblage. The layering is much less well-defined and may be graded (at locality G). It still has features which indicate current action: at locality G the layers thicken and become graded towards the axis of the synform,

and small unconformities occur. The residual fluid from crystallisation would have opposed the descending thermal convection currents and this may have had the effect of weakening the thermal currents and preventing any unattached crystals within the boundary layer from being carried to the floor (Fig. 7.20). The currents may perhaps have had more of a "winnowing" than a depositional role, assisting the flotation of plagioclase and leaving olivine, oxides and apatite, as suggested by Upton (1964b). Alternatively, the mechanism of suppression nucleation might have been less efficient at locality G than at localities I and M, where the mafic cumulates are virtually feldspar free, and in the western YGDC. It is difficult to see how the irregular masses of olivine-oxide cumulate at locality I could have arisen through any form of current deposition. Their formation is attributed either to very localised plagioclase suppression or to their derivation from elsewhere in the magma chamber (possibly the laccolith-like roof chamber?) as xenoliths.

The pyroxene crescumulate at locality L indicates that when pyroxene first became a cumulus phase the liquid was initally supersaturated in the pyroxene component. The apparently random arrangement of the bunches of pyroxene crystals suggests that the magma chamber wall or floor was poorly-defined and the crystals may have grown within a thick layer of unconsolidated crystals, nucleating wherever a slightly firmer substrate existed. The layering at locality K may be due to a nucleation-diffusion mechanism. However, this was not the case in all evolved rocks, as the erosive features in the evolved pods of the nunataq region, and in other Gardar syenites, testify to the frequent operation of currents. These features imply low viscosities in the Gardar syenites as a whole, probably due to high volatile contents.

Any theory for the origin of the YGDC layering has to take into account the intermittent nature of the layering within the dyke. This is linked to the question of why layering is only found within large intrusions, to which the answer would seem to be that the development of layering requires a slow cooling rate. However, in the YGDC there is not a simple correlation between dyke width and layering, so some other factor must be involved. It is possible that the development of layering requires a "floor" and that crystal accumulation took place on the walls in unlayered parts of the complex, but if this were the case, vertical modal and/or cryptic layering should have developed, similar to that seen in the Marginal Border Series of Skaergaard. It could be that the development of a convective system was only possible in certain areas. It could be that the suppression of plagioclase nucleation only took place in certain areas of the YGDC, in which case influxes of new magma or fluctuations in

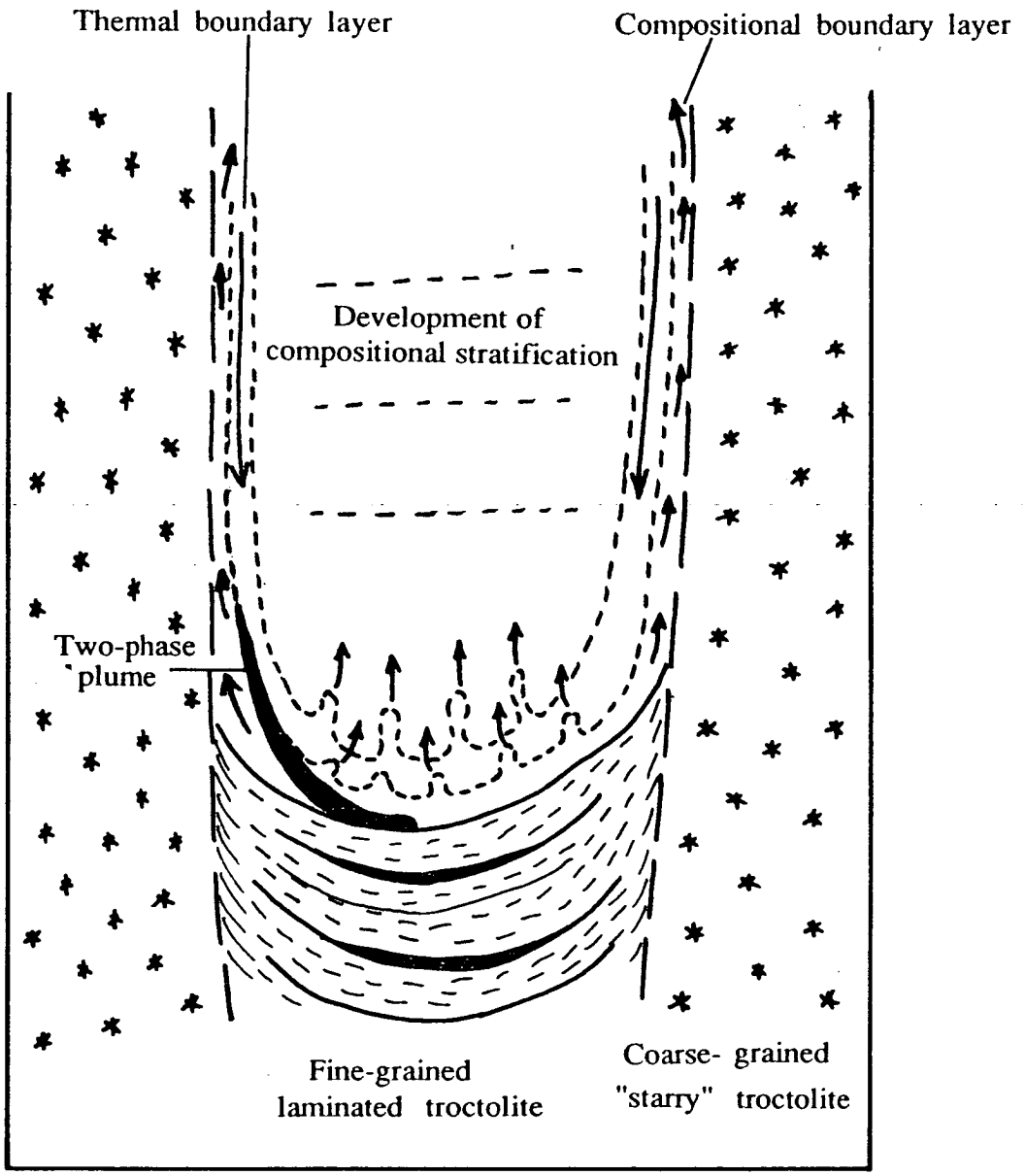


**Figure 7.20** Sketch of locality G (Marrait) during crystallisation of the central layered pod. Compositional convection was in the opposite direction to thermal convection and light residual fluid was collecting at higher levels in the chamber, creating a compositional stratification. Dashes indicate plagioclase lamination. The dyke is about 350m wide.

volatile pressure might be more likely to be localised than suppression of plagioclase nucleation by temperature or diffusion. It has proved impossible to chose between these alternatives.

### 7.5.1 Summary

The YGDC magma chambers in which layering developed had a large height to width ratio and probably underwent turbulent convection. There was probably little interaction between the roof and floor. Crystals nucleated at the walls and floor, either on pre-existing crystals or in the thermal boundary layer. Unattached crystals were carried down to the floor in descending sidewall convection currents. Mafic minerals could settle out of such currents but plagioclase could do so only as glomerocrysts with other minerals. Much of the troctolite may have crystallised *in situ* on the floor from descending crystal-free currents of supercooled liquid. Periodically, suppression of plagioclase nucleation occurred. In the western part of the YGDC, currents laden with olivine crystals could descend with enough energy to erode previously-formed cumulates. In the eastern part of the complex, buoyant compositional convection may have weakened the downward currents, preventing the formation of such well-defined layering. At locality K, modal variation may have been produced by alternating nucleation of different phases, but in other syenitic pods, considerable current action occurred.

# CHAPTER 8: SUMMARY AND CONCLUSIONS

The Younger Giant Dyke Complex (YGDC) is part of the Gardar Province of SW Greenland, and was intruded during a major period of Proterozoic continental magmatism. The Gardar Province, together with compositionally-similar intrusive rocks of Labrador and other parts of North America, was the product of an episode of continental rifting. In Greenland, the activity lasted from about 1320 to 1120 Ma and the products of the magmatism include lavas, dykes and central complexes. Compositions range from basalt (or gabbro) to trachyte, phonolite and comenditic rhyolite (silica under- or over-saturated syenite when coarse-grained).

The YGDC was emplaced early in the Late Gardar period (Upton and Emeleus, 1987) at around 1150 Ma. It is exposed on the island of Tugtutôq where it cuts the Older Giant Dyke Complex (also a product of Late Gardar magmatism) and is cut by the Tugtutôq Central Complex. Lithologically-similar giant dykes in the nunataq region NE of Narsarsuaq are thought to represent continuations of the same complex, making the total observed length about 145km. The complex was intruded into earlier Proterozoic granites and consists of a series of interconnected branching dykes from <100m to 800m wide. It is thought that the dyke halted and expanded at the unconformity between the basement and the Eriksfjord Formation, an Early Gardar series of sandstones and lavas. The YGDC magmas were alkali olivine-basalts to hawaiites, critically undersaturated with respect to silica, which differentiated to both silica-oversaturated and undersaturated derivatives. Most of the YGDC exposure is of troctolite, but mafic cumulates are also found and these may define igneous layering in isolated "pods" up to 3km long. These pods occur at irregular intervals along the dyke segments.

The margins of the dyke segments have been contaminated by melted country-rock and have undergone hydrothermal alteration, resulting in the replacement of the mafic minerals by green amphibole and biotite, and alteration of the feldspars. Low $\delta^{18}O$ values are found in the marginal rocks and also locally elsewhere in the intrusion, probably indicating some interaction between the magma and meteoric water. About 1m into the dyke the rocks are relatively fresh with a grain size of 0.2-2mm. These "chilled margins" are made up of plagioclase and olivine with interstitial Fe-Ti oxides, clinopyroxene, biotite and minor alkali feldspar. Olivine and

plagioclase phenocrysts are found in the chilled margins, sometimes as roughly spherical glomerocrysts up to 3cm across, in which the plagioclase has a stellate arrangement.

In the western part of the YGDC, the troctolites are plagioclase-olivine cumulates with discrete intercumulus phases being magnetite, ilmenite, clinopyroxene, apatite, biotite and alkali feldspar. In eastern Tugtutôq, Narsaq and the nunataq region they are plagioclase-olivine-magnetite-ilmenite(-apatite) cumulates with intercumulus clinopyroxene, biotite and alkali feldspar. The rocks are all orthocumulates, according to the definition of Irvine (1982). Olivine compositions range from $Fo_{68}$-$Fo_{49}$ and are more forsteritic in the plagioclase-olivine than in the plagioclase-olivine-magnetite-ilmenite cumulates. Feldspars are labradorites and andesines, normally zoned by up to $An_{20}$. The pyroxene is salitic in composition while apatites and biotites are relatively F-rich. Associated mafic cumulates lack plagioclase. In the western YGDC they are olivine cumulates (gabbro picrites) and the eastern part of the complex they are olivine-magnetite-ilmenite or olivine-magnetite-ilmenite-apatite cumulates.

In eastern Tugtutôq two pods of more evolved rocks enclosed by troctolite occur. These pods are ovoid in shape, elongated along the dyke and up to 3km long. The syenogabbros and syenites making up the pods have clinopyroxene (salite to ferrosalite) as a cumulus phase. Alkali feldspar, as cryptoperthite rimming plagioclase, becomes modally important in the syenogabbros. In the syenites plagioclase disappears and the feldspars are cryptoperthites to fairly coarse antiperthites. Olivine ($Fo_{55}$-$Fo_3$), Fe-Ti oxides and hastingsitic amphibole are also present. The syenogabbros have higher modal contents of apatite and biotite than the troctolites or the syenites, and at one locality are characterised by the development of a pyroxene crescumulate. Interstitial quartz and calcite are found in the syenites and also in many of the late-stage veins of alkali feldspar and arfvedsonite which cut the YGDC. Some of the veins lack quartz and contain pseudomorphs after nepheline. In the nunataq region two similar evolved pods are found, but these are silica-undersaturated in character.

Layering in the YGDC is synformal and may be defined by modal variation or plagioclase lamination, or both. Modal layering is best developed in the western YGDC, where plagioclase lamination is absent. Layers of gabbro picrite are commonly 1-5cm thick with intervening troctolite of 2-50cm. These are frequently parallel but may show unconformities or be highly irregular. Gabbro picrite also fills channels which have eroded underlying parallel layers or which occur isolated from

any other form of layering. The channels can be up to 8m broad and 4m deep and invariably plunge towards the synform axis. At two localities, breccias of gabbro picrite blocks within a troctolite matrix occupy the axial zone of the synform. It is inferred that these resulted from the breakup of thick gabbro picrite layers and the subsequent transport of the blocks downslope or along the axis as a debris flow. The breccias and channels provide evidence that the synform was a primary feature, but the original dips are not known, as they may have been steepened by compaction of the less well-consolidated central cumulates. The double synform at locality D is thought to be due to layers draping over an underlying septum of country-rock which separates two dyke branches at depth.

In the eastern YGDC, where Fe-Ti oxides and apatite joined the fractionating assemblage, modal layering is less well-developed but plagioclase lamination is common. Mafic layers are usually parallel to the lamination but are often poorly defined and indistinct. At one locality they may be up to 15cm thick and show normal modal grading. At another, olivine-magnetite-ilmenite cumulates form highly irregular patches up to 50cm in size within the troctolite, frequently cutting across the feldspar lamination.

One of the evolved pods on Tugtutôq and both of those in the nunataq region show layering. In one pod in the nunataq region, layers of olivine-magnetite-ilmenite-apatite-clinopyroxene cumulate show unconformities and channelling structures similar to those formed by the gabbro picrites in western Tugtutôq. The other two pods (involving syenite) contain intermittent parallel mafic and felsic layers which range from sharply defined to indistinct.

Fine-grained leucocratic xenoliths are common in the western YGDC but less so in the eastern part of the complex. They are often found within mafic layers, aligned parallel to the layers, and are thought to be blocks of fine-grained marginal facies carried to the chamber floor by convection currents. Some of the xenoliths appear to have trapped migrating liquids beneath them, which crystallised to give syenogabbroic pegmatites. At one locality such xenoliths are often associated with the development of elongated feldspar crystals (feldspar crescumulates) growing perpendicular to the layering. In eastern Tugtutôq and the Narsaq area, xenoliths (up to 100m in size) of anorthosite and xenocrysts of plagioclase are common, as they are in a large number of basic and intermediate Gardar rocks.

Petrographic examination of mineral textures indicates that partial textural equilibration has occurred. Thus cooling was relatively rapid compared to many other

layered intrusions where equilibration has proceeded to a greater degree, but not sufficiently rapid to prevent some degree of equilibration. Olivine zoning of up to 9 mol% Fo in the chilled margins also indicates rapid cooling. However, in the western troctolites and gabbro picrites, and in a layered syenite from the nunataq region, olivines in the mafic layers are slightly more forsteritic than those from adjacent felsic layers. This indicates some compositional re-equilibration with interstitial liquid, although the compositional change involved was probably only about 3 mol% Fo.

It is thought that the evolved rocks of the YGDC differentiated *in situ*. There is no direct evidence for the compositions of the evolved liquids which gave rise to the syenogabbros and syenites. However, a slightly younger swarm of smaller dykes on Tugtutôq is composed of dykes ranging in composition from basalt to rhyolite and phonolite, which are thought to be products of a similar magma source to that which produced the YGDC (Martin, 1985). They provide an indication of an analogous "liquid line of descent" to which the YGDC rocks may be compared. Comparison of whole-rock analyses shows that the compositions of YGDC rocks with MgO<5 wt% correspond fairly closely to the presumed liquid compositions. These rocks show a fractionation trend from hawaiite to trachyte. Whole-rock variation diagrams combined with mineral analyses show that fractionation of olivine + plagioclase began when MgO = c. 5 wt%, Fe-Ti oxides at MgO = c. 4 wt%, clinopyroxene at MgO = c. 3.5 wt% and alkali feldspar at MgO = 3 wt% or less. The late entry of clinopyroxene into the fractionation scheme is unusual among basaltic magmas and may result in part from high Al/Ca ratios and in part from low oxygen fugacities in the magma (Upton and Thomas, 1980).

At MgO>6 wt%, whole-rock compositions of chills, troctolites and gabbro picrites follow an olivine accumulation trend. The composition of the accumulated olivine was about $Fo_{66}$, that of the most magnesian olivines in the rocks. Computer prediction of liquidus olivine compositions in the chilled marginal samples shows that only samples with whole-rock MgO = 4.5-5.5 wt%, which are near or at the olivine-plagioclase cotectic, contain olivine of near this composition ($Fo_{72}$-$Fo_{68}$). Chill samples with MgO>6 wt% are predicted to be in equilibrium with more forsteritic olivines. It is concluded that the more magnesian chills are not true liquids but have accumulated varying amounts of olivine as phenocrysts, prior to emplacement. Decompression may have resulted in the resorption of some of these phenocrysts. The troctolites with MgO>6 wt% are offset from most of the chills and probably resulted from accumulation of 20-30% olivine + plagioclase into the liquid, which itself contained variable proportions of olivine phenocrysts. This might have been achieved

by the removal of an interstitial liquid phase, rich in components excluded from olivine and plagioclase. Two chills are similar to the troctolites in their major and trace element chemistry and are inferred to haye resulted from the accumulation of about 60% plagioclase into the liquid, possibly by melting of plagioclase phenocrysts or xenocrysts.

The YGDC magmas, in common with other Gardar basic rocks, had high Fe/Mg and Al/Ca ratios and low Ni and Cr (<200 and <40ppm respectively). The Fe/Mg ratios and low concentrations of compatible trace elements imply that they were derivative magmas after olivine fractionation. The Al/Ca ratios may result from fractionation of clinopyroxene or may be a source characteristic. It is thought that the magmas underwent high pressure olivine $\pm$ clinopyroxene fractionation, possibly at the base of the crust, before intrusion. $^{87}Sr/^{86}Sr$ ratios for the YGDC rocks, corrected to 1150Ma, give mantle values, as do the majority of oxygen isotope ratios. Assimilation of crust has thus been minimal, unless the lower crust was sufficiently low in $^{87}Sr/^{86}Sr$ and in $\delta^{18}O$ to be assimilated without affecting the isotope ratios. However, crustal assimilation may have been just sufficient to cause the magmas to follow a silica-oversaturated rather than an undersaturated trend.

Partial melting of the upper mantle resulted from pressure release caused by crustal extension and asthenospheric upwelling. High volatile contents (of halogens, mainly F, and $CO_2$) in many rocks of the Gardar province suggest that mantle melting was aided by an influx of volatiles. North American equivalents of the Gardar province are more silica-saturated and probably reflect a greater degree of partial melting. The anorthosite inclusions in Gardar rocks are thought to be fragments of a large body or bodies of anorthosite at depth, analogous to the massif anorthosites of Labrador. $^{87}Sr/^{86}Sr$ ratios of anorthositic inclusions in the YGDC are identical to those of the host troctolites. Although the lack of negative Eu and Sr anomalies in the giant dyke chills shows that the anorthosites could not have crystallised from the same batch of magma, they probably came from similar magmas which failed to reach the surface.

The YGDC shows few internal contacts (the layered pod at Marrait may have been intruded after the surrounding troctolite) and thus must have been emplaced relatively rapidly. Before emplacement, the magma existed in a reservoir, possibly at the base of the crust but probably within in the crust. The dyke segments probably narrow with depth.

Heat flow calculations show that the YGDC took between 1000 and 3000 years to crystallise and cool. During this time, the processes occurring within the magma chambers produced the range of rock types observed and also the layering. Crystal nucleation probably occurred predominantly in the thermal boundary layers at the sidewalls and roof, since the heat loss was greatest there. Crystallisation could also have taken place on the gently-sloping floor from descending crystal-free supercooled liquid. Heterogeneous nucleation (on a pre-existing substrate) is more energetically favourable than homogeneous nucleation, and was probably dominant. However, crystals nucleating heterogeneously could have become detached from their place of nucleation.

Convection was probably turbulent in the main parts of the magma chambers, although mechanical boundary layers could have experienced laminar flow. Cooling at the sidewalls would have produced descending currents with a more diffuse return flow. Shallowly-dipping synformal layers sometimes extend to within a few metres of the dyke margins, suggesting that most crystal accumulation took place on the floor. Thus crystals forming at the sidewalls either nucleated within the boundary layer but unattached from the wall, or they became detached from the walls, and were carried to the base of the chambers by descending convection currents. It is thought that the tall thin shape of the magma chambers prevented significant interaction between processes occurring at the roof and at the floor.

In the western YGDC, residual liquid after crystallisation of olivine + plagioclase would have been more dense than the magma in the bulk of the chambers. This liquid would have flowed down the sidewalls, reinforcing the thermal convection, and ponded in the synform axes. To explain the whole-rock chemistry, it has been postulated that some of this interstitial liquid must have been removed; if the liquid was dense it could not convect away and thus must have been expelled by compaction.

In the eastern part of the YGDC, the crystallisation of magnetite and ilmenite and increasingly dense olivines as cumulus phases would have resulted in light residual fluid. At the sidewalls this formed thin buoyant layers between the crystallising zone and the downward-flowing thermal convection currents. On the floor, compositional plumes would have risen from the crystal pile. This would also have occurred in the western YGDC after the onset of postcumulus crystallisation of Fe-Ti oxides. The observation that plagioclase lamination in the YGDC only occurs where oxides are cumulus phases may be linked to the phenomenon of compositional

convection. The convection may have led to the expulsion of a greater proportion of interstitial liquid, allowing the plagioclase crystals to rotate and become aligned with the topography of the magma chamber floor; in effect, causing a greater amount of compaction. In addition the declining plagioclase supersaturation may have led to the crystallisation of plagioclase as single crystals rather than aggregates, making rotation of the crystals on the magma chamber floor easier.

The modal layering seems to have resulted from the periodic suppression of plagioclase crystallisation, possibly due to volatile fluctuations or to the repeated injection of small quantities of magma after the major intrusive episode. This only occurred in certain portions of the complex and led to the crystallisation of olivine ± oxides in the thermal boundary layers. The presence of these minerals increased the density of the magma and may have led to the formation of intermittent fast-moving two-phase plumes. The plumes carried the crystals to the base of the chambers and become density currents, possibly eroding previously-formed cumulates if they had sufficient energy. The dense minerals would have been able to settle out from the slowing currents relatively rapidly, provided the crystal content was not too great, and the remaining liquid would subsequently have crystallised olivine + plagioclase or olivine + plagioclase + oxides. The fact that modal layering is less well-developed in the eastern YGDC could be due to the buoyant compositional convection reducing the efficiency of these descending plumes. However, evidence for strong current activity in some of the syenites shows that this was not always the case.

Although crystals do not seem to have adhered efficiently to the walls of the magma chambers, much of the crystallisation at the bases of the chambers may have taken place *in situ*. The thin parallel mafic layers, instead of forming from low-energy plumes, could have formed *in situ* during periods of plagioclase suppression.

Localised plagioclase supersaturation gave rise to the feldspar crescumulate and at one locality, the magma became supersaturated with respect to clinopyroxene at the onset of cumulus pyroxene crystallisation. This produced the syenogabbroic pyroxene crescumulate rock surrounding one of the syenitic pods. Within the syenites, some of the parallel mafic or felsic layering may have formed *in situ* by a nucleation-diffusion mechanism, where nucleation and growth of one phase depletes the surrounding liquid in the components required for the growth of that phase and eventually moves the liquid composition into the stability field of another phase. However, other syenites evidently experienced current activity.

This study has shown that layering in the YGDC cannot have been formed solely by *in situ* crystallisation but that current activity played an important role in determining the layering characterisitics. This conclusion may be of significance in other intrusions where evidence for the origins of layering is sometimes obscured by later re-equilibration and the movement of residual fluids. However, the style of layering, involving troctolites and mafic cumulates but rarely more feldspathic cumulates, is unusual and conclusions regarding its origin may not be widely applicable. The fractionation sequence also implies unusual crystallisation conditions, possibly very low $fO_2$, coupled with the high Al/Ca ratio of the magma.

Further work on the YGDC should include a detailed investigation of the giant dykes of the nunataq region. Comparison between these and the dykes of Tugtutôq, especially of the evolved pods, would yield much useful information regarding the conditions and the path of crystallisation, and the mechanisms of layer formation. In addition, a study of the various types of anorthosite xenoliths and their layering should prove fruitful. More isotope work, using Sr, O and Pb would help to constrain processes occurring before, during and after crystallisation. Some Pb work has already been undertaken by P.N. Taylor at Oxford and further studies are underway at SURRC, East Kilbride, under G. Rogers. In addition, a more rigorous theoretical study of the physical processes likely to occur during magma chamber crystallisation would shed further light on the processes of layering formation.

The YGDC is of major importance to the understanding of the entire Gardar region, since it encompasses one of the widest ranges of rock types and gives insights into the processes affecting the magmas before and after emplacement. It was the major precursor to the intrusion of more evolved magmas in the same area, including the Ilímaussaq intrusion, which may be unique in its concentrations of elements such as Zr, Be, U, Th and Nb. It is hoped that this study will further the understanding of the Gardar province as a whole.

# REFERENCES


Abbey, S (1980) Studies in "standard samples" for use in the general analysis of silicate rocks and minerals. Part 6: 1979 edition of "usable" values. Geol. Surv. Canada. Paper 80-14

Abbott, MJ (1969) Petrology of the Nandewar volcano, N.S.W. Australia. Contr Miner Petrol 20 115-134

Aoki, K (1964) Clinopyroxenes from alkaline rocks of Japan. Am Miner 49 1199-1223

Aoki, K and Kushiro, I (1968) Some clinopyroxenes from ultramafic inclusions in Dreiser Weiher, Eifel. Contr Miner Petrol 18 326-337

Ashwal, LD and Wooden, JL (1985) Sm-Nd isotopic studies of Proterozoic anorthosites: Systematics and implications. *In* The Deep Proterozoic Crust of the North Atlantic Provinces, Tobi, AC and Touret, JL (eds.) Proceedings of NATO Advanced Study Institute. Reidel, Boston 61-73

Ashwal, LD, Wooden, JL, Emslie, RF (1986) Sr, Nd and Pb isotopes in Proterozoic intrusives astride the Grenville Front in Labrador: Implications for crustal contamination and basement mapping. Geochim cosmochim Acta 50 2571-2585

Baker, BH, Mohr, PA, Williams, LAJ (1972) Geology of the eastern rift system of Africa. Geol Soc Am Sp Paper 136 67pp

Baragar, WRA (1977) Volcanism of the stable crust. *In* Volcanic Regimes in Canada, Baragar, WRA, Coleman, LC and Hall, JM. (eds.) Geol Ass Canada Sp Paper 16 377-405

Barberi, F, Ferrara, G, Santacroce, R, Treuil, M, Varet, J (1975) A transitional basalt-pantellerite sequence of fractional crystallisation, the Boina Centre (Afar Rift, Ethiopia). J Petrology 16 22-56

Barnes, SJ (1986) The effect of trapped liquid crystallisation on cumulus mineral compositions in layered intrusions. Contr Miner Petrol 93 524-531

Becker, SM (1984) Petrology of the giant dykes of Isortoq and feldspar variation in the Klokken complex, South Greenland. Unpubl. PhD thesis, University of Aberdeen.

Bédard, JH, Sparks, RSJ, Renner, R, Cheadle, MJ, Hallworth, MA (1988) Peridotite sills and metasomatic gabbros in the Eastern Layered Series of the Rhum complex. J geol Soc Lond 145 207-224

Berg, JH (1980) Snowflake troctolite in the Hettasch Intrusion, Labrador: evidence for magma-mixing and supercooling in a plutonic environment. Contr Miner Petrol 72 339-351

Bhattacharji, S (1974) Scale models for natural thermal convection in magmatic systems. Indian J Earth Sci 1 73-83

**Blank, HR and Gettings, ME (1973)** Subsurface form and extent of the Skaergaard intrusion, East Greenland. Trans Am Geophys Union 54 507

**Blaxland, AB and Upton, BGJ (1978)** Rare-earth distribution in the Tugtutôq Younger Giant Dyke Complex: evidence bearing on alkaline magma genesis in S Greenland. Lithos 11 291-299

**Blaxland, AB, van Breemen, O, Emeleus, CH, Anderson, JG (1978)** Age and origin of the major syenite centres in the Gardar province of S Greenland. Geol Soc Am Bull 89 231-244

**Blundell, DJ (1978)** A gravity survey across the Gardar Igneous Province, SW Greenland. J geol Soc Lond 135 545-554

**Borthwick, J and Harmon, RS (1982)** A note regarding $ClF_3$ as an alternative to $BrF_5$ for oxygen isotope analysis. Geochim cosmochim Acta 46 1665-1668

**Bottinga, Y, Weill, DF, Richet, P (1982)** Density calculations for silicate liquids 1. Revised method for aluminosilicate compositions. Geochim cosmochim Acta 46 (6) 909-919

**Boudreau, AE (1987)** Pattern formation during crystallisation and the formation of fine-scale layering. *In* Origins of Igneous Layering, Parsons, I (ed.) Reidel 453-471

**Bowen, NL (1915)** Crystallisation differentiation in silicate rocks. Am J Sci 4th Ser 39 175-191

**Brandeis, G and Jaupart, C (1986)** On the interaction between convection and crystallisation in cooling magma chambers. Earth planet Sci Lett 77 345-361

**Brandeis, G, Jaupart, C, Allègre, CJ (1984)** Nucleation, crystal growth and the thermal regime of cooling magmas. J geophys Res 89 B10 10161-10177

**Bridgwater, D (1967)** Feldspathic inclusions in the Gardar igneous rocks and their relevance to the formation of major anorthosites in the Canadian Shield. Canadian J Earth Sciences 4 995-1014

**Bridgwater, D and Coe, K (1970)** The role of stoping in the emplacement of the giant dykes of Isortoq, S. Greenland. *In* Mechanism of Igneous Intrusion (Symposium) Newall, G and Rast, N. (eds.) Geol Jour Sp Issue 2 67-78

**Bridgwater, D and Harry, WT (1968)** Anorthosite xenoliths and plagioclase megacrysts in Precambrian intrusions of South Greenland. Meddr om Grønland 185 243pp.

**Brooks, CK and Neilsen, TFD (1990)** The differentiation of the Skaergaard Intrusion: A discussion of Hunter and Sparks (Contrib Mineral Petrol 95: 451-461). Contr Miner Petrol 104 235-247

**Brophy, JG (1989)** Basalt convection and plagioclase retention: a model for the generation of high-alumina arc basalt. J Geol 97 319-329

**Brown, GM and Vincent, EA (1963)** Pyroxenes from the late stages of fractionation of the Skaergaard intrusion, East Greenland. J Petrology 4 175-197

**Buddington, AF and Lindsley, DH (1964)** Iron-titanium oxide minerals and synthetic equivalents. J Petrology 5 310-357

**Bullard, EC, Everett, JE, Smith, AG (1965)** The fit of the continents around the Atlantic. Phil Trans R Soc Lond A-258 41-75

**Bussen, IV and Sakharov AS (1972)** Petrology of the Lovozero alkaline massif (in Russian). Nauka 1-296 Leningrad

**Butcher, AR, Young, IM, Faithfull, JW (1985)** Finger structures in the Rhum complex. Geol Mag 122 491-502

**Butterfield, AW (1980)** Geology of the western part of the Nunarssuit alkaline complex, S. Greenland. Unpubl. PhD thesis, University of Aberdeen

**Cameron, EN (1980)** Evolution of the Lower Critical Zone, central sector, eastern Bushveld Complex, and its chromite deposits. Econ Geol 75 845-871

**Campbell, IH (1978)** Some problems with the cumulus theory. Lithos 11 311-323

**Campbell, IH (1987)** Distribution of orthocumulate textures in the Jimberlana Intrusion. J Geol 95 35-53

**Campbell, IH, McCall, GJH, Tyrwhitt, DS (1970)** The Jimberlana Norite, W. Australia - a smaller analogue of the Great Dyke of Rhodesia. Geol Mag 107 1-12

**Cannon, WF, Green, AG, Hutchison, DR, Lee, M, Milkereit, B, Behrendt, JC, Halls, HC, Green, JC, Dickas, AB, Morey, GB, Sutcliffe, R, Spencer, C (1989)** The North American Midcontinent Rift beneath Lake Superior from GLIMPCE seismic reflection profiling. Tectonics 8 305-332

**Carmichael, ISE, Turner, FJ, Verhoogen, J, (1974)** Igneous Petrology. McGraw-Hill New York 739pp

**Carrigan, CR (1988)** Biot number and the thermos bottle effect: implications for magma-chamber convection. Geology 16 771-771

**Cashman, KV (1986)** Crystal size distribution in igneous and metamorphic rocks. Unpubl. PhD thesis, John Hopkins University, USA.

**Cashman, KV and Marsh, BD (1988)** Crystal size distribution (CSD) in rocks and the kinetics and dynamics of crystallization II. Igneous crystallization. Contr Miner Petrol 99 292-305.

**Cawthorn, RG and McCarthy, TS (1980)** Variations in Cr content of magnetite from the Upper Zone of the Bushveld Complex - Evidence for heterogeneity and convection currents in magma chambers. Earth planet Sci Lett 46 335-343

**Chambers, AD (1976)** The petrology of the N Qôroq centre, Igaliko Complex, S Greenland. Unpubl. PhD thesis, University of Durham

**Chalokwu, CI and Grant, NK (1987)** Reequilibration of olivine with trapped liquid in the Duluth complex, Minnesota. Geology 15 71-74

Clark, SP Jr (1966) Handbook of physical constants. Geol Soc Am Memoir 97

Collerson, KD (1982) Geochemistry and Rb-Sr geochronology of associated Proterozoic peralkaline and subalkaline orogenic granites from Labrador. Contr Miner Petrol 81 126-147

Conrad, ME and Naslund, HR (1989) Modally graded rhythmic layering in the Skaergaard Intrusion. J Petrology 30(2) 251-269

Coombs, DS and Wilkinson, JFG (1969) Lineages and fractionation trends in undersaturated volcanic rocks from the East Otago Volcanic Province (New Zealand) and related rocks. J Petrology 10 440-501

Cooper, RF and Kohlstedt, DL (1986) Rheology and structure of olivine-basalt partial melts. J geophys Res 91 9315-9323

Cox, KG (1980) A model for flood basalt volcanism. J Petrology 21 629-650

Cox, KG, Bell, JD, Pankhurst, RJ (1979) The Interpretation of Igneous Rocks. Allen & Unwin, London

Cox, KG and Mitchell, C (1988) Importance of crystal settling in the differentiation of Deccan Trap basaltic magmas. Nature 333 447-449

Day, SJ (1989) The geology of the Hypersthene Gabbro of Ardnamurchan Point and implications for its evolution as an upper crustal basic magma chamber. Unpubl. PhD thesis, Univ of Durham

Darwin, C (1844) Geological observations on the Volcanic islands, visited during the voyage of H.M.S. Beagle, together with some brief notices on the geology of Australia and the Cape of Good Hope. Being the second part of the geology of the Beagle, under the command of Capt. Fitzroy, R.N., during the years 1832 to 1836. Smith, Elder, London 175pp

Deer, WA, Howie, RA, Zussman, J (1966) An Introduction to the Rock Forming Minerals. Longman Group, London

Donaldson, CH (1979) An experimental investigation of the delay in nucleation in mafic magmas. Contr Miner Petrol 69 21-32

Donaldson, CH (1982) Origin of some of the Rhum harrisite by segregation of intercumulus liquid. Miner Mag 45 201-9

Dowty, E (1980) Crystal growth and nucleation theory and the numerical simulation of igneous crystallisation. *In* The physics of magmatic processes, Hargraves, RB (ed.). Princeton Univ Press 419-485

Droop, GTR (1987) A general equation for estimating $Fe^{3+}$ concentrations in ferromagnesian silicates and oxides from microprobe analyses, using stoichiometric criteria. Miner Mag 51 431-435

Einarsson, P and Brandsdottir, B (1980) Seismological evidence for lateral magma intrusion during the July 1978 deflation of the Krafla volcano in NE-Iceland. J Geophys 47 160-165

Emeleus, CH (1987) The Rhum layered complex, Inner Hebrides, Scotland. *In* Origins of Igneous Layering, Parsons, I (ed.) Reidel. 263-286

Emeleus, CH and Upton, BGJ (1976) The Gardar Period in southern Greenland. *In* The Geology of Greenland, Escher, A and Watt, WS (eds.) Grønl. Geol Unders., Copenhagen 153-181

Emslie, RF (1970) The geology of the Michikamau intrusion, Labrador. Geol Surv Canada Paper 68-57 85pp.

Emslie, RF (1980) Geology and petrology of the Harp Lake complex, central Labrador: an example of Elsonian magmatism. Geol Survey Can Bull 293

Emslie, RF (1985) Proterozoic anorthosite massifs. *In* The Deep Proterozoic Crust of the North Atlantic Provinces, Tobi, AC and Touret, JL (eds.) Proceedings of NATO Advanced Study Institute. Reidel, Boston 39-59

Emslie, RF, Loveridge, WD, Stevens, RD (1984) The Mealy dykes, Labrador: petrology, age and tectonic significance. Canadian J Earth Sci 21 437-446

Emslie, RF, Loveridge, WD, Stevens, RD, Sullivan, RW (1983) Igneous and tectonothermal evolution, Mealy Mountains, Labrador (abstr.) Geol Assoc Canada Ann Mtg 8 A-20

Ernst, RE, Bell, K, Ranalli, G, Hall, HC (1987) The Great Abitibi Dyke, Southeastern Province, Canada. *In* Mafic Dyke Swarms, Halls, HC and Fahrig, WF (eds.) Geol Assoc Canada Sp Paper 34 123-135

Fairhead, JD (1976) The structure of the lithosphere beneath the Eastern Rift, East Africa, deduced from gravity studies. Tectonophysics 30 269-298

Finch, AA (1990) The chemical and isotopic nature of fluids associated with alkaline magmatism, S Greenland. Unpubl. PhD thesis, University of Edinburgh

Fitton, JG and Dunlop, HM (1985) The Cameroon Line, W Africa, and its bearing on the origin of oceanic and continental alkali basalts. Earth Planet Sci Lett 72 23-38

Fitton, JG James, DE, Thirlwall, MF, (1984) A user's guide to the X-ray fluorescence analysis of rock samples. 2nd edition. Unpubl report Univ of Edinburgh

Flink, G (1898) Berättelse om en mineralogiske Resa i Syd-Grönland 1897. Meddr om Grønland 14 (2) 221-262

Ford, CE (1981) Parental liquids of the Skaergaard intrusion cumulates. Nature 291 2125

Gibb, FGF (1974) Supercooling and the crystallisation of plagioclase from a basaltic magma. Miner Mag 39 641-653

Giesecke, KL (1910) Karl Ludwig Gieseckes mineralogisches Rejsejournal über Grönland 1806-13. Meddr om Grønland 35 532 pp.

Giret, A, Bonin, B, Leger, J-M (1980) Amphibole compositional trends in oversaturated and undersaturated alkaline plutonic ring-complexes. Canadian Mineralogist 18 481-495

Gomes, C DE B, Moro, SL, Dutra, CV (1970) Pyroxenes from the alkaline rocks Itipirapua, Sao Paolo, Brazil. Am Miner 55 224-230

Goode, ADT (1976) Small scale primary cumulus layering in the Kalka layered intrusion, Giles Complex, Central Australia. J Petrology 17 379-397

Green, JC (1977) Keweenawan plateau volcanism in the Lake Superior region. In Volcanic Regimes in Canada, Baragar, WRA, Coleman, LC, Hall, JM (eds.) Geol Assoc Canada Sp Paper 16

Haggerty, SE (1976) Opaque mineral oxides in terrestrial igneous rocks. *In* Oxide Minerals, Rumble, D (ed.) Min Soc Am Short Course Notes 3 Hg101-Hg300

Halliday, AN, Dickin, AP, Fallick, AE and Fitton, JG (1988) Mantle dynamics: A Nd, Sr, Pb and O isotope study of the Cameroon Line Volcanic Chain. J Petrology 29(1) 181-211

Hamilton, J (1977) Sr isotope and trace element studies of the Great Dyke and Bushveld mafic phase and their relation to early Proterozoic magma genesis in southern Africa. J Petrology 18 24-52

Harper, CL (1988) On the nature of time in cosmological perspective. Unpubl. DPhil Thesis, University of Oxford

Harry, WT and Pulvertaft, TCR (1963) The Nunarssuit intrusive Complex, South Greenland. Bull Grønl. Geol Unders. 36 (also Meddr om Grønland 169 (1))

Heiber, CA and Gebhart, B (1971) Stability of vertical natural convection boundary layers: expansions at large Prandtl number. J Fluid Mech 49 577-91

Henderson, P (1982) Inorganic Geochemistry. Pergamon Press, Oxford.

Hill, JD (1988) Alkalic to transitional ferrobasaltic magma associated with Paleohelikian anorthositic plutons in the Flowers River area, southeastern Nain igneous complex, Labrador. Contr Miner Petrol 99 113-125

Hill, JD and Miller, RR (in press) A review of early Neohelikian epigenic felsic magmatism in Labrador.

Hoover, JD (1978) Petrologic features of the Skaergaard Marginal Border Group. Carnegie Inst Wash Yb 77 732-739

Hoover, JD (1989) Petrology of the Marginal Border Series of the Skaergaard Intrusion. J Petrology 30(2) 399-439

Hunter, RH (1987) Textural equilibrium in layered igneous rocks. *In* Origins of Igneous Layering, Parsons, I (ed.) Reidel 473-503

Hunter, RH and Sparks, RSJ (1987) The differentiation of the Skaergaard Intrusion. Contr Miner Petrol 95 451-461

**Huppert, HE and Sparks, RSJ (1980)** The fluid dynamics of a magma chamber replenished by an influx of hot dense ultrabasic magma. Contr Miner Petrol 75 279-289

**Huppert, HE and Sparks, RSJ (1984)** Double-diffusive convection due to crystallization in magmas. Ann Rev Earth planet Sci 12 11-37

**Huppert, HE and Sparks, RSJ (1989)** Chilled margins in igneous rocks. Earth planet Sci Lett 92 397-405

**Illies, JH (1978)** Two stages of Rhinegraben rifting. *In* Tectonics and Geophysics of Continental Rifts, Ramberg, IB and Neumann, E-R (eds.) Reidel, Dordrecht, Holland. 63-71

**Irvine, TN (1977)** Density current structure and magmatic sedimentation. Carnegie Inst Wash Yb 77 717-725

**Irvine, TN (1980a)** Magmatic density currents and cumulus processes. Am Jour Sci 280A 1-58

**Irvine, TN (1980b)** Magmatic infiltration metasomatism, double-diffusive fractional crystallization, and adcumulus growth in the Muskox intrusion and other layered intrusions. *In* The Physics of Magmatic Proceses, Hargraves, RB (ed.) Princeton Univ Press 325-383

**Irvine, TN (1982)** Terminology for layered intrusions. J Petrology 23 127-162

**Irvine, TN (1983)** Observations on the origin of Skaergaard layering. Carnegie Inst Wash Yb 82 284-295

**Irvine, TN (1987a)** Layering and related structures in the Duke Island and Skaergaard Intrusion: similarities, differences and origins. *In* Origins of Igneous Layering, Parsons, I (ed.) Reidel 185-245

**Irvine, TN (1987b)** Glossary of terms for layered intrusions. Appendix I *In* Origins of Igneous Layering, Parsons, I (ed.) Reidel 641-648

**Irvine, TN (1987c)** Processes involved in the formation and development of layered igneous rocks. Appendix II *In* Origins of Igneous Layering, Parsons, I (ed.) Reidel 649-656

**Irvine, TN and Baragar, WRA (1971)** A guide to the classification of common volcanic rocks. Can J Earth Sci 8 523-548

**Irvine, TN and Smith, CH (1967)** The ultramafic rocks of the Muskox Intrusion, NW Territories, Canada. *In* Ultramafic and Related Rocks, Wyllie, PJ (ed.) Wiley 38-49

**Irvine, TN and Smith, CH (1969)** Primary oxide minerals in the Layered Series of the Muskox Intrusion. Econ Geol Monograph 4 76-94

**Irvine, TN, Keith, DW, Todd, SG (1983)** The J-M platinum-palladium reef of the Stillwater Complex, Montana: II. Origin by double-diffusive convective magma mixing and implications for the Bushveld Complex. Econ Geol 78 1287-1334

**Jackson, ED (1961)** Primary textures and mineral associations in th ultramafic zone of the Stillwater Complex, Montana. US Geol Surv Prof Paper 358

**Jarvis, GT (1984)** Time-dependent convection in the Earth's mantle. Phys Earth Planet Inter 36 305-327

**Jessen, A (1896)** Geologiske Iattagelser. Meddr om Grønland 16 123-169

**Jones, AP (1980)** The petrology and structure of the Motzfeldt Centre, Igaliko, South Greenland. Unpubl. PhD Thesis, University of Durham

**Jurewicz, AJG and Watson, EB (1988)** Cations in olivine. Part I: Calcium partitioning between olivines and co-existing melts, with petrologic applications. Contr Miner Petrol 99 176-185

**Kalsbeek, F and Taylor, PN (1985)** Isotopic and chemical variation in granites across a Proterozoic continental margin - the Ketilidian mobile belt of South Greenland. Earth planet Sci Lett 73 65-80

**Kays, MA and McBirney, AR (1982)** Origins of the picrite blocks in the Marginal Border Group of the Skaergaard Intrusion, East Greenland. Geochim cosmochim Acta 46 23-40

**Kellerhals, R, Shaw, J and Arora, VK (1975)** On grain size from thin sections. J Geol 83 79-96

**Kerr, RC, Woods, AW, Worster, MG, Huppert, HE (1989)** Disequilibrium and macrosegregation during solidification of a binary melt. Nature 340 357-362

**King, BC and Chapman, GR (1972)** Volcanism of the Kenya Rift Valley. Phil Trans R Soc Lon A271 185-208

**Kirkpatrick, RJ (1977)** Nucleation and growth of plagioclase, Makaopuhi and Alae lava lakes, Kilauea Volcano, Hawaii. Geol Soc Am Bull 88 78-84

**Kirkpatrick, RJ (1981)** Kinetics of crystallisation from igneous rocks. *In* Kinetics of Igneous Processes, Lasaga, AC and Kirkpatrick, RJ (eds.) Revs in Min 8, Min Soc Am. 321-398

**Klewin, KW (1989)** Polybaric fractionation in an evolving continental rift: evidence from the Keweenawan Mid-Continent Rift. J Geol 97 65-76

**Klewin, KW (1990)** Petrology of the Proterozoic Potato River layered intrusion, Northern Wisconsin, USA. J Petrology 31, in press

**Kohn, SC, Henderson, CMB, Mason, RA (1989)** Element zoning trends in olivine phenocrysts from a supposed primary high-magnesian andesite: an electron and ion microprobe study. Contr Miner Petrol 103 242-252

**Krishnamurthi, R (1970)** On the transition to turbulent convection. Pt 2. The transition to time-dependent flow. J Fluid Mech 42 309-320

Krogh, TE, Corfu, F, Davis, DW, Dunning, GR, Heaman, LM, Kamo, SL, Machado, N, Greenough, JD, Nakamura, E (1987) Precise U-Pb isotopic ages of diabase dykes and mafic to ultramafic rocks using trace amounts of baddeleyite and zircon. *In* Mafic Dyke Swarms, Halls, HC and Fahrig, WF (eds.) Geol Assoc Canada Sp Paper 34 147-152

Kushiro, I (1980) Viscosity, density, and structure of silicate melts at high pressures, and their petrological applications. *In* The Physics of Magmatic Processes, Hargraves, RB (ed.) Princeton Univ Press 93-120

Kyser, TK (1986) Stable isotope variations in the mantle. *In* Stable Isotopes in High Temperature Geological Processes, Valley, JW, Taylor, HP Jr and O'Neil, JR (eds.) Min Soc Am: Revs in Min 16 141-164

Kyser, TK, O'Neil, JR and Carmichael, ISE (1978) Oxygen isotope thermometry of basic lavas and mantle nodules. Contr Miner Petrol 77 11-23

Larsen, JG (1977) Petrology of the late lavas of the Eriksfjord Formation, Gardar Province, South Greenland. Bull Grønl. Geol Unders. 125 31pp.

Larsen, LM (1976) Clinopyroxenes and co-existing mafic minerals from the alkaline Ilímaussaq Intrusion, South Greenland. J Petrology 17 258-290

Larsen, LM and Sørensen, H (1987) The Ilímaussaq intrusion - progressive crystallisation and formation of layering in an agpaitic magma. In Alkaline Igneous Rocks, Fitton, JG and Upton, BGJ (eds.) Geol Soc Sp Pub 30 473-488

Langmuir, CH (1989) Geochemical consequences of in situ crystallisation. Nature 340 199-205

Leake, BE (1978) Nomenclature of amphiboles. Canadian Mineralogist 16 501-520

Le Bas, MJ, Le Maitre, RW, Streckeisen, A and Zanettin, B (1986) A chemical classification of volcanic rocks based on the total alkali-silica diagram. J Petrology 27 745-750

Lesher, CE and Walker, D (1988) Cumulate maturation and melt migration in a temperature gradient. J geophys Res 93 B9 10295-10311

Liesegang, RE (1913) Geologische Diffusionen. Dresden and Leipzig: T Steinkopff

Lofgren, GE (1974) An experimental study of plagioclase crystal morphology: isothermal crystallisation. Am Jour Sci 274 243-273

Lofgren, GE (1980) Experimental studies on the dynamic crystallisation of silicate melts. *In* The Physics of Magmatic Processes, Hargraves, RB (ed.) Princeton Univ Press 487-551

Lofgren, GE (1983) Effect of heterogeneous nucleation on basaltic textures: a dynamic crystallisation study. J Petrology 24 229-255

Maaløe, S (1978) The origin of rhythmic layering. Miner Mag 42 337-45

Maaløe, S (1985) Principles of Igneous Petrology. Springer-Verlag, Berlin

Macdonald, R (1969) The petrology of alkaline dykes from the Tugtutôq area, South Greenland. Bull Geol Soc Denmark 19 257-282

Macdonald, R (1970) Mid-Gardar feldspathoidal dykes in the Tugtutôq region, South Greenland. Bull Geol Soc Denmark 20 64-66

Macdonald, R and Edge, RA (1970) Trace element distribution in alkaline dykes from the Tugtutoq region, S Greenland. Bull Geol Soc Denmark 20 38-50

Macdonald, R, Wilson, L, Thorpe, RS, Martin, A (1988) Emplacement of the Cleveland Dyke: Evidence from geochemistry, mineralogy and physical modelling. J Petrology 29 559-583

Marsh, BD (1988) Crystal capture, sorting and retention in convecting magma. Geol Soc Am Bull 100 1720-1737

Marsh, BD and Maxey, MR (1985) On the distribution and separation of crystals in a convecting magma. J Volc Geoth Res 24 95-150

Marshall, DJ (1988) The cathodoluminescence of geologic materials. Unwin Hyman

Martin, AR (1985) The evolution of the Tugtutôq-Ilímaussaq dyke swarm, SW Greenland. Unpubl. PhD thesis, University of Edinburgh

Martin, D and Campbell, IH (1988) Laboratory modeling of convection in magma chambers: crystallisation against sloping floors. J geophys Res 93 B7 7974-7988

Martin, D, Griffiths, RW and Campbell, IH (1987) Compositional and thermal convection in magma chambers. Contr Miner Petrol 96 465-475

Martin, D and Nokes, R (1989) A fluid dynamical study of crystal settling in convecting magmas. J Petrology 30(6) 1471-1500

McBirney, AR (1984) Igneous Petrology. Oxford University Press

McBirney, AR (1987) Constitutional Zone Refining of Layered Intrusions. *In* Origins of igneous layering, Parsons, I, (ed.) Reidel 437-452

McBirney, AR, Baker, BH, Nilson, RH (1985) Liquid factionation. Part I: Basic principles and experimental simulations. J Volc Geoth Res 24 1-24

McBirney, AR and Naslund, HR (1990) The differentiation of the Skaergaard Intrusion: A discussion of Hunter and Sparks (Contrib Mineral Petrol 95: 451-461). Contr Miner Petrol 104 235-247

McBirney, AR and Noyes, RM (1979) Crystallisation and layering of the Skaergaard Intrusion. J Petrology 20(3) 487-554

McCallum, IS, Raedecke, LD, Mathez, EA (1980) Investigations of the Stillwater Complex: Part I. Stratigraphy and Structure of the Banded Zone. Am Jour Sci 280-A 59-87

McClay, KR and Campbell, IH (1976) The structure and shape of the Jimberlana Intrusion, W Australia, as indicated by an investigation of the Bronzite Complex. Geol Mag 113 129-139

Meyers, RE and Emslie, RF (1977) The Harp dykes and their relationship to the Helikian geological record in central Labrador. Canadian J Earth Sci 14 2683-2696

Mohr, PA (1983) The Ethiopian flood basalt province. Nature 303 577-584

Morse, SA (1969) Geology of the Kiglapait layered intrusion, Labrador. Mem Geol Soc Am 112

Morse, SA (1979) Kiglapait geochemistry I: Systematics, sampling and density. J Petrology 20 555-590

Morse, SA (1982) A partisan review of Proterozoic anorthosites. Am Mineral 67 1087-1100

Morse, SA (1986a) Thermal structure of crystallising magma with two-phase convection. Geol Mag 123(3) 205-214

Morse, SA (1986b) Convection in aid of adcumulus growth. J Petrology 27 1183-1214

Morse, SA (1988) Motion of crystals, solute and heat in layered intrusions. Canadian Mineral 26 209-224

Morse, SA (1990) The differentiation of the Skaergaard Intrusion: A discussion of Hunter and Sparks (Contrib Mineral Petrol 95: 451-461). Contr Miner Petrol 104 235-247

Munoz, JL (1984) F-OH and Cl-OH exchange in micas with applications to hydrothermal ore deposits. *In* Micas, Bailey, SW (ed.) Min Soc Am, Revs in Min 13 469-494

Murase, T and McBirney, AR (1973) Properties of some common igneous and their melts at high temperature. Bull Geol Soc Am 84 3563-3592

Naslund, HR (1984) Petrology of the Upper Border Series of the Skaergaard Intrusion. J Petrology 25 185-212

Naslund, HR, Conrad, ME, Urquhart, J and Turner, PA (1986) Computer simulations of apparent grain size in thin section - applications to grain size variation in the Skaergaard Intrusion. (abstract) EOS 67 384

Nathan, HD and Van Kirk, CK (1978) A model of magmatic crystallization. J Petrology 19 66-94

Nicholls, J and Carmichael, ISE (1969) Peralkaline acid liquids: A petrological study. Contr Miner Petrol 20 268-294

Nilson, RH, McBirney, AR, Baker, BH (1985) Liquid fractionation. Part II: Fluid dynamics and quantitative implications for magmatic systems. J Volc Geoth Res 24 25-54

Noyes, RM and Field, RJ (1977) Mechanisms of chemical oscillators: experimental examples. Accounts Chem Res 10 273-280

Nunn, GAG, Emslie, RF, Lefebvre, CE, Noel, N, Wells, S (1986) The Atikonak River massif and surrounding area, Western Labrador and Québec. Newfoundland Dept Mines & Energy Mineral Development Division, Report 86-1 125-145

Ocola, LC and Meyer, PR (1973) The central North American Rift, 1. Structure of the Midcontinent gravity high from seismic and gravimetric data. J geophys Res 78 5173-5194

O'Hara, MJ (1968) The bearing of phase equilibria studies in synthetic and natural systems on the origin and evolution of basic and ultrabasic rocks. Earth-Science Reviews 4 69-133

Oxburgh, ER (1980) Heat flow and magma genesis. *In* The Physics of Magmatic Processes, Hargraves, RB (ed.) Princeton Univ Press 161-199

Parsons, I (1979) The Klokken gabbro-syenite complex, South Greenland: cryptic variation and the origin of inversely-graded layering. J Petrology 20 653-694

Parsons, I (1981) The Klokken gabbro-syenite complex, South Greenland: quantitative interpretation of mineral chemistry. J Petrology 22 233-260

Parsons, I and Becker, SM (1987) Layering, compaction and post-magmatic processes in the Klokken Intrusion. *In* Origins of Igneous Layering, Parsons, I (ed.) Reidel 29-92

Parsons, I, Becker, SM, Mason, RA, Finch, AA (1990) Biotite equilibria and fluid circulation in the Klokken stock, South Greenland. J Petrology, in press

Patchett, PJ, Hutchinson, J, Blaxland, AB, Upton, BGJ (1976) Origin of anorthosites, gabbros and potassic ultramafic rocks from the Gardar Province, S. Greenland: Sr isotopic ratio studies. Bull Geol Soc Denmark 25 79-84

Pearce, NJG (1988) Petrology and geochemistry of the Igaliko dyke swarm. Unpubl. PhD thesis, University of Durham

Phinney, WC (1970) Chemical relations between Keweenawan lavas and the Duluth complex, Minnesota. Bull Geol Surv Am 81 2487-2496

Piper, JDA (1982) The Precambrian palaeomagnetic record: the case for the Proterozoic Supercontinent. Earth planet Sci Lett 59 61-89

Piper, JDA and Stearn, JEF (1977) Palaeomagnetism of the dyke swarms of the Gardar Igneous Province, S. Greenland. *In* Physics of the Earth and Planetary Interiors 14, Elsevier, Amsterdam. 345-358

Pollard, DD and Muller, OH (1976) The effects of gradients in regional stress fields and magma pressure on the form of sheet intrusions in cross-section. J geophys Res 81 975-984

Poulsen, V (1964) The sandstones of the Precambrian Eriksfjord in South Greenland. Rapp. Grønlands Geol. Unders. 2

**Powell, M (1978)** The crystallisation history of the Igdlerfigssalik nepheline syenite intrusion, Greenland. Lithos **11** 99-120

**Powell, R and Powell, M (1977)** Geothermometry and oxygen barometry using coexisting Fe-Ti oxides: a reappraisal. Miner Mag **41** 257-263

**Pulvertaft, TCR (1965)** The Eqaloqarfia Layered Dyke, Nunarssuit, South Greenland. Meddr om Grønland **169**(10) 1-39

**Rae, DA (1988)** Metasomatism associated with the North Qôroq Centre, Igaliko Complex, South Greenland. Unpubl. PhD thesis, Aston University

**Raedecke, LD and McCallum, IS (1984)** Investigations of the Stillwater Complex: Part II. Petrology and petrogenesis of the Ultramafic Series. J Petrology 25 395-420

**Ramberg, IB and Spjeldnaes, N (1978)** The tectonic history of the Oslo Region. *In* Tectonics and Geophysics of Continental Rifts, Ramberg, IB and Neumann, E-R (eds.) Reidel, Dordrecht, Holland 167-194

**Renner, R (1989)** Cooling and crystallisation of komatiite flows from Zimbabwe. Unpubl. PhD thesis, Univ. of Cambridge

**Renner, R and Palacz, Z (1987)** Basaltic replenishment of the Rhum magma chamber: evidence from Unit 14. J geol Soc Lond **144** 961-970

**Saunders, AD, Tarney, J, Weaver, SD (1980)** Transverse geochemical variations across the Antarctic Peninsula: Implications for the genesis of calc-alkaline magmas. Earth planet Sci Lett **46** 344-360

**Sharpe, MR and Irvine, TN (1983)** Melting relations of two Bushveld chilled margin rocks and implications for the origin of chromitite. Carnegie Inst Wash Yb **82** 295-300

**Shaw, HR (1972)** Viscosities of magmatic silicate liquids: an empirical method of prediction. Am Jour Sci 272 870-893

**Sheppard, SMF (1986)** Characterization and isotope variations in natural waters. *In* Stable Isotopes in High Temperature Geological Processes, Valley, JW, Taylor, HP Jr and O'Neil, JR (eds.) Min Soc Am: Revs in Min **16** 165-183

**Shirley, DN (1986)** Compaction of igneous cumulates. J Geol 94 795-809

**Shirley, DN (1987)** Differentiation and compaction in the Palisades Sill, New Jersey. J Petrology 28 835-865

**Simkin, T and Smith, JV (1970)** Minor element distribution in olivine. J Geol **78** 304-325

**Smith, JV (1974)** Feldspar minerals. I. Crystal Structure and Physical Properties. Springer-Verlag Heidelberg 627pp

**Sørensen, H and Larsen, LM (1987)** Layering in the Ilímaussaq Intrusion, South Greenland. *In* Origins of Igneous Layering. Parsons, I (ed.). Reidel 1-28

**Sparks, RSJ and Huppert, HE (1984)** Density changes during the fractional crystallisation of basaltic magmas: fluid dynamical implications. Contr Miner Petrol 85 300-309

**Sparks, RSJ and Huppert, HE (1987)** Laboratory experiments with aqueous solutions modelling magma chamber processes. I. Discussion of their validity and geological application. *In* Origins of Igneous Layering, Parsons, I (ed.) Reidel 527-538

**Sparks, RSJ, Huppert, HE, Kerr, RC, McKenzie, DP and Tait, SR (1985)** Postcumulus processes in layered intrusions. Geol Mag 122(5) 558-568

**Sparks, RSJ, Huppert, HE, Turner, JS (1984)** The fluid dynamics of evolving magma chambers. Phil Trans R Soc Lond Ser A 310 511-534

**Sparks, RSJ, Meyer, P, Sigurdson, H (1980)** Density variation amongst mid-ocean ridge basalts: implications for magma mixing and the scarcity of primitive lavas. Earth planet Sci Lett 46 419-430

**Spera, FJ (1980)** Aspects of magma transport. *In* The Physics of Magmatic Processes, Hargraves, RB (ed.) Princeton Unversity Press. 265-323

**Spera, FJ, Yuen, DA, Kirschvink, SJ (1982)** Thermal boundary layer convection in silicic magma chambers: effects of temperature-dependent rheology and implications for thermogravitational chemical fractionation. J geophys Res 87 B10 8755-8767

**Steenstrup, KJV (1881)** Bemärkninger til et geognostisk Oversigtskaart over en Del af Julianehaabs Distrikt i 1876. Meddr om Gronland 2 27-41

**Steiger, RH and Jäger, E (1977)** Subcommission on geochronology: Convention on the use of decay constants in geo- and cosmochronology. Earth planet Sci Lett 36 359

**Stephenson, D (1972)** Alkali clinopyroxenes from nepheline syenites of the South Qôroq Centre, South Greenland. Lithos 5 187-201

**Stephenson, D (1974)** Mn and Ca enriched olivines from nepheline syenites of the South Qôroq centre, south Greenland. Lithos 7 35-41

**Stephenson, D and Upton, BGJ (1982)** Ferromagnesian silicates in a differentiated alkaline complex: Kûngnât Fjeld, South Greenland. Miner Mag 46 283-300

**Stolper, E, and Walker, D (1980)** Melt density and the average composition of basalt. Contr Miner Petrol 74 1-12

**Streckeisen, A (1976)** To each plutonic rock its proper name. Earth-Science Reviews 12 1-33

**Sun, S-S (1980)** Lead isotopic study of young volcanic rocks from mid-ocean ridges, ocean islands and island arcs. Phil Trans R Soc Lond Ser A 297 409-445

**Sweatman, TR and Long, JVP (1969)** Quantitative electron probe microanalysis of rock-forming minerals. J Petrology 10 332-379

**Tait, SR (1985)** Fluid dynamical and geochemical evolution of Unit 10, Rhum, Eastern Layered Series. Geol Mag 122 469-484

**Tait, SR, Huppert, HE, Sparks, RSJ (1984)** The role of compositional convection in the formation of adcumulate rocks. Lithos 17 139-146

**Tait, SR and Jaupart, C (1989)** Compositional convection in viscous melts. Nature 338 571-574

**Taylor, HP and Forester, RW (1979)** An oxygen and hydrogen isotope study of the Skaergaard Intrusion and its country rocks: a description of a 55-M.Y. old fossil hydrothermal system. J Petrology 20(3) 355-419

**Taylor, HP and Sheppard, SMF (1986)** Igneous rocks: I Processes of isotope fractionation and isotope systematics. *In* Stable Isotopes in High Temperature Geological Processes, Valley, JW, Taylor, HP Jr and O'Neil, JR (eds) Min Soc Am: Revs in Min 16 227-271

**Taylor, SR, Campbell, IH, McCulloch, MT, McLennan, SM (1984)** A lower crustal origin for massif-type anorthosites. Nature 311 372-374

**Thompson, RN (1973)** One atmosphere melting behaviour and nomenclature of terrestrial lavas. Contrib Min and Pet 41 197-204.

**Thompson, RN (1982)** Magmatism of the British Tertiary Province. Scott J Geol 18 49-107

**Thompson, RN, Morrison, MA, Dickin, AP, Hendry, GL (1983)** Continental Flood Basalts . . . Arachnids Rule OK? *In* Continental Basalts and Mantle Xenoliths, Hawksworth, CJ and Norrey, MJ (eds.) Shiva Publishing Ltd., Nantwich, Cheshire. 158-185

**Todd, SG, Keith, DW, Scissel, DJ, LeRoy, LL, Mann, EL, Irvine, TN (1983)** The J-M platinum-palladium reef of the Stillwater Complex, Montana: I. Stratigraphy and petrology. Econ Geol 77 1454-1480

**Turcotte, DL and Schubert, G (1982)** Geodynamics Applications of Continuum Physics to Geological Problems. John Wiley and Sons, New York

**Turner, JS and Campbell, IH (1986)** Convection and mixing in magma chambers. Earth-Science Reviews 23 255-352

**Turner, JS and Gustafson, LB (1981)** Fluid motions and compositional gradients produced by crystallisation or melting at vertical boundaries. J Volc Geoth Res 11 93-125

**Tyler, RC and King, BC (1967)** The pyroxenes of the alkaline igneous complexes of Eastern Uganda. Miner Mag 280 5-22

**Upton, BGJ (1962)** The geology of Tugtutoq and neighbouring islands, South Greenland. Part I. Bull Grønl. Geol Unders. 34 (also Meddr om Grønland 169(8)) 60pp

**Upton, BGJ (1964a)** The geology of Tugtutoq and neighbouring islands, South Greenland. Part II: Nordmarkitic syenites and related alkaline rocks. Bull Grønl. Geol Unders. 44 (also Meddr om Grønland 169(2)) 62pp

**Upton, BGJ (1964b)** The geology of Tugtutoq and neighbouring islands, South Greenland. Part III: Olivine gabbros, syeno-gabbros and anorthosites. Part IV: The nepheline syenites of the Hviddal composite dyke. Meddr om Grønland 169(3) 80pp

**Upton, BGJ (1971)** Melting experiments on chilled gabbros and syenogabbros. Camegie Inst Wash Yb 70 112-118

**Upton, BGJ (1974)** The alkaline province of SW Greenland. *In* The Alkaline Rocks, Sørensen, H (ed.) Wiley, New York 221-238

**Upton, BGJ (1987)** Gabbroic, syenogabbroic and syenitic cumulates of the Tugtutoq Younger Giant Dyke Complex, South Greenland. *In* Origins of Igneous Layering, Parsons, I (ed.) Reidel 93-123

**Upton, BGJ and Blundell, DJ (1978)** The Gardar Igneous Province: evidence for Proterozoic continental rifting. *In* Petrology and Geochemistry of Continental Rifts, Neumann, E-R and Ramburg, IB, (eds.) Reidel 163-172

**Upton, BGJ and Emeleus, CH (1987)** Mid-Proterozoic alkaline magmatism in S. Greenland: The Gardar Province. *In* Alkaline Igneous Rocks. Fitton, JG and Upton, BGJ (eds.) Geol Soc Spec Pub 30 449-471

**Upton, BGJ and Fitton, JG (1985)** Gardar dykes north of the Igaliko Syenite Complex, S. Greenland. Geol Survey Greenland Report No. 127: 24 pp.

**Upton, BGJ, Martin, AR and Stephenson, D (1990)** Evolution of the Tugtutôq Central Complex, South Greenland: a high-level, rift axial, late-Gardar centre. J Volc Geoth Res, in press

**Upton, BGJ, Stephenson, D and Martin, AR (1985)** The Tugtutôq Older Giant Dyke Complex: Mineralogy and geochemistry of an alkali-gabbro - augite-syenite - foyaite association in the Gardar Province of S. Greenland. Miner Mag 49 623-642

**Upton, BGJ and Thomas, JE (1980)** The Tugtutoq Younger Giant Dyke Complex, S. Greenland: Fractional crystallisation of a transitional olivine basalt magma. Jour Pet 21(1) 167-198

**Ussing, NV (1912)** Geology of the country around Julianehåb, Greenland. Meddr om Gronland 38 376 pp.

**van Breemen, O, Aftalion, M and Allaart, JH (1974)** Isotopic and geochronologic studies on granites from the Ketilidian Mobile Belt of S. Greenland. Geol Soc Am Bull 85 403-412

**Van Schmus, WR and Hinze, WJ (1985)** The Midcontinent rift system. Ann Rev E planet Sci 13 345-383

**Varet, J (1969)** Les pyroxènes des phonolites du Cantal (Auvergne, France). Neues Jb Miner Mh 4 174-184

**Wadsworth, WJ (1963)** The Kapalagulu layered intrusion of Western Tanganyika. Sp Paper Min Soc Am 1 108-115

Wadsworth, WJ (1973) Magmatic sediments. Minerals Sci Eng 5(1) 25-35

Wadsworth, WJ (1985) Terminology of postcumulus processes and products in the Rhum layered intrusion. Geol Mag 122(5) 549-554

Wadsworth, WJ, Dunham, AC, Almohandis, AA (1982) Cryptic variation in the Kapalagulu intrusion, W Tanzania. Miner Mag 45 227-36

Wager, LR (1959) Differing powers of crystal nucleation as a factor producing diversity in layered igneous intrusions. Geol Mag 96 75-80

Wager, LR and Brown, GM (1968) Layered Igneous Rocks. Oliver and Boyd, Edinburgh

Wager, LR, Brown, GM and Wadsworth, WJ (1960) Types of igneous cumulates. J Petrology 1(1) 73-85

Wager, LR and Deer, WA (1939) Geological investigations in East Greenland, Part III. The petrology of the Skaergaard Intrusion, Kangerdlugssuak, E. Greenland. Meddr om Grønland 105 1-352

Walton, BJ (1965) Sanerutian appinitic rocks and Gardar dykes and diatremes north of Narssarssuaq, South Greenland. Bull Grønlands Geol Surv 57 (also Meddr om Grønland 179(9)) 66pp

Watt, WS (1966) Chemical analyses from the Gardar igneous province, south Greenland. Grønl. Geol Unders. Rapport 6

Weertman, J (1971) Theory of water-filled crevasses in glaciers applied to vertical magma transport beneath ocean ridges. J Geophys Res 76 1171-1183

Wegmann, CE (1938) Geological investigations in South Greenland. Part I. On the structural divisions of South Greenland. Meddr om Grønland 113 (2) 149pp.

Weibe, RA (1985) Proterozoic basalt dykes in the Nain anorthosite complex, Labrador. Can J Earth Sci 22 1149-1157

Weiblen, PW, and Morey, GB (1980) A summary of the stratigraphy, petrology and structure of the Duluth Complex. Am Jour Sci 280-A 88-133

Weinstein, SA, Yuen, DA, Olsen, PL (1988) Evolution of crystal settling in magma-chamber convection. Earth planet Sci Lett 87 237-248

White, WM and Hofmann, AW (1982) Sr and Nd isotope geochemistry of oceanic basalts and mantle evolution. Nature 296 821-825

Wilson, AH (1982) The geology of the Great "Dyke", Zimbabwe: The ultramafic rocks. J Petrology 23(2) 240-292

Wilson, JR, Menuge, JF, Pedersen, S and Engell-Sørensen, O (1987) The southern part of the Fongen-Hyllingen Layered Complex, Norway: Emplacement and crystallisation of a compositionally stratified magma. *In* Origins of Igneous Layering, Parsons, I (ed.) Reidel 145-184

Windley, BF (1989) Anorogenic magmatism and the Grenvillian Orogeny. Canadian J Earth Sci 26 479-489

Worst, BG (1958) The Differentiation and Structure of the Great Dyke of S. Rhodesia. Trans Geol Soc S. Africa LXI 283-354

Wright, TL (1974) Presentation and interpretation of chemical data for igneous rocks. Contr Miner Petrol 48 233-248

Yagi, K (1966) The system acmite-diopside and its bearing on the stability relations of natural pyroxenes of the acmite-hedenbergite-diopside series. Am Miner 51 976-1000

# APPENDIX I: SAMPLE LOCALITIES

Abbreviations:
T = examined in thin section
P = probed
X = analysed by XRF

Lettered localities are indicated on Fig. 2.1

| Sample | Locality | Description | |
|---|---|---|---|
| YGD1 | D | "Coarse" chill, 1m in from N margin | T,P,X |
| YGD2 | D | Mafic xenolith near N margin | T |
| YGD3 | D | Felsic xenolith near N margin | T |
| YGD4 | D | Troctolite 5cm below 20cm picrite layer, 20m from N margin | |
| YGD5 | D | Within 20cm picrite layer | X |
| YGD6 | D | Troctolite at top of 20cm picrite layer | X |
| YGD7 | D | Troctolite 50m from N margin | X |
| YGD8 | D | Troctolite 75m from N margin | X |
| YGD9 | D | Picrite 100m from N margin | |
| YGD10 | D | Troctolite 120m from N margin | X |
| YGD11 | D | Troctolite 140m from N margin | X |
| YGD12-38 | D | Vertical layered sequence of several metres, 150m from N margin | |
| (YGD23 | D | Troctolite | X) |
| (YGD36 | D | Picrite layer (36A) overlain by troctolite(36B) | P,XX) |
| YGD39 | D | Troctolite 180m from N margin | X |
| YGD40-47 | D | Samples taken along a single troctolite layer, 250m from N margin | |
| (YGD41 | D | Troctolite | X) |
| YGD48 | D | Picrite block, axis of N synform | |
| YGD49 | D | Picrite block, axis of N synform | P |
| YGD50 | D | Picrite block, axis of N synform | |
| YGD51 | D | Troctolite, 300m from N margin | X |
| YGD52 | D | Troctolite, 340m from N margin | X |
| YGD53 | D | Troctolite, 370m from N margin | |
| YGD54 | D | Diffuse mafic layer, 380m from N margin | P |
| YGD55 | D | Troctolite, 380m from N margin | |
| YGD56 | D | Picrite layer 5m E of YGD54/55 | |
| YGD57 | D | Picrite layer passing up into troctolite, 450m from N margin | |
| YGD58 | D | Troctolite 500m from N margin | |

| | | | |
|---|---|---|---|
| YGD59 | D | Picrite layer, 520m from N margin | |
| YGD60 | D | Layered sample, 520m from N margin | |
| YGD61 | D | Fine-grained felsic xenolith, 520m from N margin | |
| YGD62 | D | 2cm later dyke at synform contact (550m from N margin, 100m from S margin) | |
| YGD63 | D | Troctolite a few m N of synform contact | |
| YGD64 | D | Troctolite a few m S of synform contact | P |
| YGD65 | D | Mafic layer, a few m S of synform contact | |
| YGD66 | D | Fine-grained felsic xenolith, 50m S of synform contact | |
| YGD67 | D | Picrite, as above | T |
| YGD68 | D | Picrite, 80m from S margin | |
| YGD69 | D | Picrite, 80m from S margin | |
| YGD70 | D | Troctolite, 80m from S margin | |
| YGD71 | D | Troctolite/picrite contact, 80m from S margin | |
| YGD72 | D | Picrite, 80m from S margin | P |
| YGD73 | D | Vein within felsic xenolith, 80m from S margin | |
| YGD74 | D | Base of thick picrite layer, 80m from S margin | T |
| YGD75 | D | Near top of thick picrite layer, 80m from S margin | |
| YGD76 | D | Troctolite from just above set of five faulted picrite layers, 80m from S margin | |
| YGD77 | B | Loose block, probably chilled margin | |
| YGD78 | B | Chilled margin 1m from probable position of N margin | X,P |
| YGD79 | B | Troctolite 2m from N margin | |
| YGD80 | B | Troctolite 3.5m from N margin | T,P |
| YGD81 | B | Troctolite 5.5m from N margin | |
| YGD82 | B | Troctolite just west of tarn | |
| YGD83 | B | ?BD0 | |
| YGD84, 84a | G | Coarse- and fine-grained facies 50cm from S margin, W side of bay | T |
| YGD85 | G | Troctolite 1m from S margin | |
| YGD86 | G | Fine-grained vein, 30m from S margin | T |
| YGD87 | G | Edge of same vein, 30m from S margin | |
| YGD88 | G | Coarse-grained vein, 30m from S margin | T |
| YGD89 | G | Troctolite, 30m from S margin | |
| YGD90 | G | Troctolite, 30m from S margin | |
| YGD91 | G | Troctolite, 80m from S margin | |
| YGD92 | G | Troctolite, 70m from S margin | |
| YGD93 | G | Troctolite, 20m east from YGD92 | |

| | | | |
|---|---|---|---|
| YGD94 | G | Troctolite 100m from S margin | |
| YGD95 | G | 2 vein samples, 30m from S margin | |
| YGD96 | G | Vein, 30m from S margin | |
| YGD97 | G | Troctolite 40m from S margin | |
| YGD98 | G | Troctolite 70m from S margin | |
| YGD99 | G | Epidote and feldspar vein, 150m from S margin | T |
| YGD100 | G | Miarolitic cavity, 150m from S margin | |
| YGD101 | G | Troctolite 200m from S margin | |
| YGD102 | G | Troctolite 300m from S margin | |
| YGD103 | G | Troctolite 400m from S margin | T |
| YGD104 | G | Vein 450m from S margin | |
| YGD105 | G | Troctolite 450m from S margin | |
| YGD106 | G | Vein 450m from S margin | |
| YGD107 | G | Massive troctolite 550m from S margin | |
| YGD108 | G | Crumbly troctolite 550m from S margin | |
| YGD109 | G | Troctolite 550m from S margin | |
| YGD110 | G | Altered marginal sample, N margin | |
| YGD111 | G | Fine-grained troctolite 4m from N margin | |
| YGD112 | G | Troctolite 40m from N margin, E side of bay | |
| YGD113 | G | Troctolite 80m from N margin | |
| YGD114 | G | Troctolite 120m from N margin | |
| YGD115 | G | Troctolite 150m from N margin | |
| YGD116 | G | Coarse troctolite from island in bay | |
| YGD117 | G | Finer-grained troctolite from E side of island | |
| YGD118 | F | Chilled margin with stellate plag phenocrysts | |
| YGD119-122 | F | Suite of samples across contact with country rock, S margin | Tx4 |
| (YGD122,122W | | Chilled margin, 122W = with phenocrysts | XX) |
| YGD123 | F | Fine-grained troctolite, 10m from S margin | P |
| YGD124 | F | Coarse-grained troctolite, 10m from S margin | |
| YGD125 | F | Troctolite, 30m from S margin | X,T |
| YGD126 | F | Fine-grained troctolite, 50m from S margin | T |
| YGD127 | F | Troctolite, 70m from S margin | |
| YGD128 | F | Troctolite, 100m from S margin | |
| YGD129 | F | Vein, 120m from S margin | |
| YGD130 | F | Troctolite 20m from N margin | |
| YGD131 | F | Fine-grained dark pod in troctolite | T |
| YGD132 | F | Troctolite near N margin | |

| | | | |
|---|---|---|---|
| YGD133 | F | Fine-grained pod in troctolite, 20m from N margin | |
| YGD134-136 | F | Loose block of breccia | T |
| YGD137 | G | Fine-grained troctolite, E side of island in bay | |
| YGD138 | G | Large block with faint mafic layer, E side of island in bay | |
| YGD139 | G | A few metres along same mafic layer as YGD138 | |
| YGD140 | G | Near S margin of dyke, E side of bay | X,T |
| YGD141 | G | Troctolite, 50m from S margin | X |
| YGD142 | G | Troctolite, 100m from S margin | X |
| YGD143-145 (YGD145 | G | Edge of fine-grained pod, 200m from S margin | X) |
| YGD146 | G | Fine-grained troctolite, 220m from S margin | |
| YGD147-156 | G | Samples of a layered section, 300m from S margin | |
| YGD157 | G | Troctolite, synform axis, 350m from S margin | X |
| YGD158 | G | 15cm Mafic layer, synform axis | X,P |
| YGD159 | G | Troctolite, 370m from S margin | X |
| YGD160 | G | N edge of layered pod, 390m from S margin | |
| YGD161 | L | Granite near S contact | |
| YGD162 | L | Chill, 1m from S margin | X,T |
| YGD163 | L | Troctolite, 10m from S margin | |
| YGD164 | L | Pegmatite in troctolite, 10m from S margin | T |
| YGD165 | L | Vein, 50m from S margin | |
| YGD166 | L | Propylitised trctolite, 70m from S margin | |
| YGD167 | L | Troctolite, 100m from S margin | |
| YGD168 | L | Vein, 100m from S margin | |
| YGD169 | L | Troctolite, 100m from S margin | |
| YGD170 | L | Vein, 120m from S margin | X,P,T |
| YGD171 | L | Syenogabbro, 140m from S margin | |
| YGD172 | L | Vein, 140m from S margin | |
| YGD173 | L | Vein 200m from S margin | |
| YGD174 | L | Granular syenogabbro, 240m from S margin | |
| YGD175 | L | Syenite, 280m from S margin | |
| YGD176 | L | Syenite, 300m from S margin | X,T |
| YGD177 | L | Syenite, 50m W of YGD176 | |
| YGD178 | L | Aplite, 360m from S margin | |
| YGD179 | L | Syenite, 360m from S margin | X |
| YGD180 | L | Syenite 500m from S margin | X |
| YGD181 | L | Syenite on peninsula in bay, 460m from S margin | |

| | | | |
|---|---|---|---|
| YGD182-183 | L | Pegmatites in syenite, 540m from S margin | |
| (YGD183 | | | X) |
| YGD184 | L | Elongate pyroxenes in syenogabbro, 660m from S margin (160m from N margin) | |
| YGD185 | L | Syenite, 580m from S margin | |
| YGD186 | L | Troctolite, 70m from N margin (N coast Assorutit peninsula) | |
| YGD187 | L | Troctolite, 300m W from YGD186 | |
| YGD188 | L | Syenite, 380m from S margin | |
| YGD189 | I | Fine-grained troctolite a few m from S margin | |
| YGD190 | I | Troctolite, 40m from S margin | |
| YGD191 | I | Troctolite, 100m from S margin | T |
| YGD192 | I | Layered troctolite, 100m from S margin | T |
| YGD193 | I | Troctolite 140m from S margin, 500m E of YGD192 | T |
| YGD194 | I | Laminated troctolite, 300m from S margin | |
| YGD195 | I | Laminated troctolite, 500m from S margin, on coast | X,P |
| YGD196 | I | Ol-oxide cumulate from irregular pod, 500m from S margin, on coast | X,P,T |
| YGD197 | I | Laminated troctolite, 350m NE of YGD195/196, on coast | X |
| YGD198 | I | Laminated troctolite between YGD196 and 197 | |
| YGD199 | K | Syenogabbro, E end of evolved pod | |
| YGD200 | I | Laminated troctolite, 430m from S margin, 200m W of YGD195/196 | |
| YGD201 | I | Laminated troctolite, 430m from S margin | |
| YGD202 | I | Laminated troctolite, 540m from S margin, 140m from N margin | |
| YGD203 | I | Laminated troctolite 40m from N margin | X |
| YGD204 | L | Epidotised troctolite, N coast Assorutit peninsula | |
| YGD205 | L | Small anorthosite xenolith, N coast Assorutit peninsula | |
| YGD206 | L | a = edge of anorthosite xenolith, b = troctolite c = xenolith, 50m E of YGD205 | |
| YGD207-213 | L | Samples of N side of largest anorthosite xenolith, Assorutit peninsula | |
| YGD218-224 | L | Samples of S side of largest anorthosite xenolith, Assorutit peninsula | |
| (YGD218 | | | P) |
| (YGD221 | | | T) |
| (YGD223 | | | P) |
| YGD225 | M | Laminated troctolite, Nugarmiut peninsula | |
| YGD226,227 | D | Hybrid facies, N margin | X,T |

| | | | |
|---|---|---|---|
| YGD228 | D | Fine grained chill, 1m from N margin | X,P |
| YGD229 | D | Coarser grained chill, 1m from N margin | X,P |
| YGD230 | D | Country-rock granite, 2m from N margin | X |
| YGD231 | D | Country-rock granite, 11m from N margin | X |
| YGD232 | D | Faint mafic layer, 11m from N margin | |
| YGD233 | D | Fine grained felsic xenolith, near N margin | |
| YGD234 | D | Syenogabbroic pegmatite associated with YGD233 | T |
| YGD235 | D | 20cm Picrite layer, 20m from N margin | |
| YGD236 | D | Felsic xenolith, 60m from N margin | |
| YGD237 | D | Gabbro picrite in small channel, 60m from N margin | X |
| YGD238 | D | Troctolite, 80m from N margin | T |
| YGD239 | D | Troctolite, 90m from N margin | |
| YGD240 | D | Layered troctolite, 150m from N margin | |
| YGD241 | D | Small felsic xenolith in mafic layer, 160m from N margin | |
| YGD242-244 | D | Base, middle and top of 80cm picrite layer, 160m from N margin | X x3 |
| YGD245 | D | Top of 20cm picrite layer YGD242-244 X | |
| YGD246 | D | Base of 20cm picrite layer of sample YGD245 | |
| YGD247 | D | Troctolite, 260m from N margin | |
| YGD248 | D | Troctolite, 260m from N margin | T |
| YGD249,250 | D | Large gabbro picrite block, 270m from N margin | |
| YGD251 | B | 30cm picrite layer 3m from N margin | |
| YGD252 | B | Troctolite 30m from N margin | |
| YGD253 | C | 30cm vein | T |
| YGD254 | C | Poorly defined 30-40cm picrite | P |
| YGD255 | C | Picrite, 2m thick trough | X,P |
| YGD256 | C | Troctolite, just about YGD255 | X,P |
| YGD257 | B | Coarse-grained layer 6m from S contact | |
| YGD258 | B | Finer-grained troctolite just beneath YGD257 | |
| YGD259 | B | Chill, 2m from S margin | X,P |
| YGD260,261 | B | Picrite layer 75m from S margin | |
| YGD262 | B | Elongate feldspars 100 from S margin | P |
| YGD263 | B | Troctolite just above YGD262 | |
| YGD264 | B | Picrite just above YGD262 | |
| YGD265 | C | Picrite trough | X,P |
| YGD266 | D | Picrite, 100m from N margin | |
| YGD267-269 | D | Troctolite 100m from N margin | |
| YGD270 | C | Fine-grained felsic xenolith within picrite channel | |

| | | | |
|---|---|---|---|
| YGD271 | C | Troctolite inclusion within picrite channel | |
| YGD272 | C | Troctolite same location | |
| YGD273 | C | Fine-grained felsic xenolith same location | |
| YGD274 | C | Picrite same location | X,P |
| YGD275 | C | 2m thick picrite channel | X,P |
| YGD276 | C | Top of channel, above YGD276 | X |
| YGD277 | C | Fine-grained felsic xenolith, locality 5 of Fig. 2.2 | X |
| YGD278 | C | Troctolite, locality 5 of Fig. 2.2 | |
| YGD279a,b | C | a=Picrite, b=fine-grained felsic inclusion, locality 5 of Fig. 2.2 | |
| YGD280 | C | Picrite locality 5 of Fig. 2.2 | |
| YGD281-283 | D | Picrite blocks in breccia, 270m from N margin | XX |
| YGD284,285 | D | Troctolite, 270m from N margin | X |
| YGD286 | D | Elongate feldspars in later dyke | |
| YGD287 | D | Picrite, 450m from N margin | |
| YGD288 | D | Troctolite, 450m from N margin | |
| YGD289 | D | Fine-grained felsic xenolith, 520m from N margin | X,P |
| YGD290 | D | Picrite, 520m from N margin | |
| YGD291 | D | Fine-grained felsic xenolith, 520m from N margin | |
| YGD292 | D | Chill, ~1m from N margin, E of fault | X,P |
| YGD293 | D | Troctolite with plag xenocryst, 200m from N margin, E of fault | X,P |
| YGD294 | D | Troctolite, 500m from N margin, E of fault | |
| YGD295 | D | Troctolite, 350m from N margin, E of fault | |
| YGD296 | D | Troctolite, 600m from N margin, E of fault | |
| YGD297 | D | Near S margin of dyke, E of fault | |
| YGD298 | B | Chill, 1m from N contact | X,P |
| YGD299 | B | Country-rock granite 1m from dyke | |
| YGD300 | B | Troctolite between large and small tarns | |
| YGD301 | B | Poorly-defined picritic layer, 10m from N margin | |
| YGD302 | B | Fine-grained felsic xenolith with elongate feldspars, 10m from N margin | X |
| YGD303 | B | Poorly-defined picritic layer, 10m from N margin | X |
| YGD304 | B | Mafic block? containing elongate feldspars, 20m from N margin | |
| YGD305 | B | Troctolite, 100m from N margin | |
| YGD306 | B | Picrite, thickest channel, 100m from S margin | X,P |
| YGD307 | B | Troctolite just above YGD306 | X,P |
| YGD308,309 | D | Troctolite, 450m from N margin | |
| YGD310 | F | Country-rock granite | |

| | | | |
|---|---|---|---|
| YGD311 | F | Later sill, near S margin of dyke | |
| YGD312 | F | Picrite channel, near N margin | X,P |
| YGD313 | F | Troctolite near YGD312 | X |
| YGD314 | F | Picrite, 40m from N margin | |
| YGD315 | F | Massive picrite, without feldspar tablets, 80m from S margin | |
| YGD316 | F | Massive picrite with feldspar tablets, 80m from S margin | X,P |
| YGD317 | G | Chill, 1m from S contact, W side of bay | X,P |
| YGD318 | G | Hybrid zone, S contact | |
| YGD319 | G | Dark fine-grained xenolith? within dyke margin | T |
| YGD320 | G | Hybrid rock, S contact | |
| YGD321 | G | Country-rock granite 2m from S contact | |
| YGD322 | G | Country-rock granite 20m from S contact | |
| YGD323 | L | Country-rock granite 6m from S contact | |
| YGD324 | L | Country-rock granite 1m from S contact | |
| YGD325 | L | Chill, 1m from S contact | X,P |
| YGD326 | L | Fine-grained aplite, 400m from S contact | X,P |
| YGD327 | L | Troctolite, 350m from S margin, 200m inland | |
| YGD328 | L | Chill, 1m from N margin | X,P |
| YGD329 | L | Country-rock granite 2m from N contact | |
| YGD330 | L | Country-rock granite 8m from N contact | |
| YGD331 | L | Pegmatite in troctolite, 60m from N margin | |
| YGD332 | L | Dyke margin to anorthosite xenolith, location 1 of Fig. 2.4 | |
| YGD333 | L | Anorthosite xenolith, location 1 of Fig. 2.4 | |
| YGD334 | L | Troctolite, location 1 of Fig. 2.4 | X,P,T |
| YGD335 | L | Grey plagioclase xenocryst, N side of Assorutit peninsula | |
| YGD336-338 | L | Anorthosite xenoliths, N side of Assorutit peninsula | |
| YGD339 | L | Troctolite, N side of Assorutit peninsula | |
| YGD340-349 (YGD340,343 | L | Different types of xenoliths, N side of Assorutit peninsula | P) |
| YGD350 | L | Syenite aplite, 550m from S margin | |
| YGD351 | L | Syenite aplite, 450m from S margin | |
| YGD352 | K | Syenogabbro, 120m from S margin | |
| YGD353 | K | Syenogabbro, 200m from S margin, lake shore | |
| YGD354 | K | Mafic syenogabbro, 250m from S margin, lake shore | X,T |
| YGD355,356 | K | Syenogabbro, just above YGD354 | X |
| YGD357 | K | Mafic syenogabbro, 200m from S margin, rigde crest | |
| YGD358 | K | Syenogabbro, just above YGD357 | |

| | | | |
|---|---|---|---|
| YGD359 | K | Vein, 370m from S margin | |
| YGD360 | K | Syenogabbro, 250m from S margin, ridge crest | |
| YGD361 | K | Syenogabbro, 350m from S margin, ridge crest | |
| YGD362 | K | Fresh syenogabbro, 250m from S margin, ridge crest | X,P |
| YGD363 | K | Syenogabbro, 350m from S margin, lake shore | |
| YGD364 | K | Chill, 1m from N margin | X,P |
| YGD365 | K | Troctolite, 20m from N margin | X,P |
| YGD366 | K | Troctolite, 50m from N margin | X |
| YGD367 | K | Fine-grained syenitic vein/dyke, 100m from N margin | T |
| YGD368 | K | Syenogabbro, 100m from N margin | |
| YGD369 | K | Syenogabbro, 250m from N margin | |
| YGD370 | I | Weathered chill, 1m from S margin | |
| YGD371 | I | Country-rock granite, 50cm from S margin of dyke | |
| YGD372 | I | Country-rock granite, 10m from S margin of dyke | |
| YGD373 | I | Mafic layer from small pod 140m from S margin | X,T |
| YGD374 | I | Troctolite with mafic layer, 140m from S margin | |
| YGD375 | I | Troctolite, 300m from S margin | |
| YGD376 | I | Troctolite + picrite, 450m from S margin, on coast | |
| YGD377 | I | Troctolite with feldspathic patch, 450m from S margin on coast | T |
| YGD378,379 | I | Base and top of 4m mafic block, 350m from S margin, on coast | X,P |
| YGD380 | M | Syenite pegmatite, E coast Nugarmiut | T |
| YGD381 | M | Ol-oxide cumulate lens, NE tip Nugarmiut | X,P |
| YGD382 | M | Grey troctolite near YGD381 | X,T |
| YGD383,384 | M | Troctolite, NW of Nugarmiut peninsula | |
| YGD385 | M | Dark, fine-grained xenolith in altered troctolite, Narsaq | |
| YGD386 | M | Anorthosite xenolith, same locality as YGD385 | |
| YGD387 | M | Troctolite with aligned plagioclase xenocrysts, E Narsaq | T |
| YGD388 | M | Contact between troctolite and Eriksfjord sandstone | T |
| YGD389 | M | Troctolite, centre of Narsaq | |
| YGD390 | M | Troctolite, centre of Narsaq | |
| YGD391 | M | Troctolite, SW of Narsaq | |
| YGD392 | M | Troctolite, quarry, SW Narsaq | X,P,T |

## Drill Cores

| | | | |
|---|---|---|---|
| YGD393-399 | D | Start of regular layering, 80m from N margin | |
| YGD400-409 | D | 50cm layered section, 100m from N margin | T x10 |
| YGD410,411 | D | 450m from N margin | |
| YGD412-421 | G | Start of regular layering, S side of layered pod, E side of bay | |
| YGD422-433 | L | Traverse from S margin to syenite | |
| 422 | | Troctolite, 15m from S margin | X |
| 423 | | Troctolite, 30m from S margin | X,P |
| 424 | | Troctolite, 45m from S margin | X |
| 425 | | Troctolite, 92m from S margin | X |
| 426 | | Troctolite, 106m from S margin | X,P |
| 427 | | Troctolite, 121m from S margin | X |
| 428 | | Syeno-gabbro, 158m from S margin | X,P |
| 429 | | Syeno-gabbro, 173m from S margin | X |
| 430 | | Syeno-gabbro, 185m from S margin | X |
| 431 | | Syeno-gabbro, 188m from S margin | X |
| 432 | | Syeno-gabbro, 198m from S margin | X |
| 433 | | Syenite, 248m from S margin | X |

## GGU Samples

(X indicates analysed as part of this project; XRF analyses of other samples may have been done by other workers)

| | | | |
|---|---|---|---|
| 30659 | G | Mafic cumulate from syenite axis | T |
| 30766 | M | Well-laminated feldspathic troctolite | T |
| 40425 | | West coast of Sejlfjord | P |
| 40454 | | Very sharp contact between dyke and country rock, dyke branch to S of loc B | T |
| 40548 | L | Syenogabbro, S of syenite | P |
| 50217 | L | Syenite | T,X |
| 50218 | L | Mafic syenite | P,X |
| 86055 | I | Laminated troctolite, N side of dyke | T |
| 101211 | M | Chill, Narsaq Island | T,P |
| 186221 | K | Syenite just S of small lake E of Kryssø | P |
| 186224 | K | Mafic syenogabbro near W end Krydssø peninsula | P |
| 186377 | | Nepheline syenite sheet cutting YGDC near loc B | T |
| 186400 | D | Layered sequence, N limb of N synform | T |
| 216627 | | Layered syenite, W of Syenitknold, nunataqs (A=mafic cumulate, B=syenite) | P,X |

# APPENDIX II: ANALYTICAL TECHNIQUES

## II.1 Electron Microprobe

Mineral analyses were for the most part made on a Cambridge Instruments Microscan Mk V with automated WDS crystal spectrometers. The accelerating voltage was 20kV and the beam current 30nA. Count times used were 40 seconds on the peak and 20 seconds on the background. ZAF corrections were applied according to the method of Sweatman and Long (1969). Standards and crystals used for analysis are given in Table II.1.

All apatite analyses, and traverses across zoned olivine grains, were made on a Cameca Camebax Microbeam. WDS analysis used an accelerating voltage of 20kV and a beam current of 20nA. Standards and crystals used are also given in Table II.1.

Analytical precision and detection limits can be calculated from a single analysis using the equations:

$$2\sigma = \frac{2W}{\sqrt{T_p}\ (\sqrt{R_p} - \sqrt{R_b})} \qquad \text{det. lim.} = \frac{3W\ \sqrt{R_b}}{R_p\ \sqrt{T_b}}$$

Where:

$T_p$ = peak count time
$T_b$ = background count time
$R_p$ = peak count rate
$R_b$ = background count rate
$W$ = wt% element or oxide

These have been calculated for a representative analysis for each phase analysed and results are presented below.

Table II.1 Operating conditions of the electron microprobes

| Element | Standard | Crystal | | |
|---|---|---|---|---|
| | | Microscan | Camebax (silicates) | Camebax (apatites) |
| K | Orthoclase | QTZ | PET | - |
| Ca | Wollastonite | QTZ | PET | PET |
| Ti | Rutile | QTZ | PET | - |
| Ba | Barytes | QTZ | - | - |
| Cr | Metal | QTZ | LIF | - |
| Mn | Metal | QTZ | LIF | - |
| Fe | Metal | QTZ | LIF | - |
| Ni | Metal | - | LIF | - |
| F | Mag. Fluoride | RAP | - | TAP |
| Na | Jadeite | RAP | TAP | TAP |
| Mg | Periclase | RAP | TAP | - |
| Al | Corundum | RAP | TAP | - |
| Si | Wollastonite | RAP | TAP | TAP |
| P | Apatite | - | - | PET |
| Cl | Halite | - | - | PET |
| La | Glass * | - | - | PET |
| Ce | Glass | - | - | PET |

QTZ = Quartz

PET = Penta eurythritol

LIF = Lithium fluoride

RAP = Rubidium acid phthalate

TAP = Thallium acid phthalate

* Calcium silicate glasses with 12-13% rare earth elements

Olivine (Microscan)

| | Wt% Oxide | 2σ | det. lim. |
|---|---|---|---|
| $SiO_2$ | 37.15 | 0.25 | 0.04 |
| $Al_2O_3$ | 0.04 | 0.02 | 0.01 |
| FeO | 30.77 | 0.22 | 0.04 |
| MnO | 0.41 | 0.04 | 0.02 |
| MgO | 31.62 | 0.19 | 0.02 |
| CaO | 0.34 | 0.03 | 0.02 |
| Total | 100.33 | | |

Plagioclase (Microscan)

| | Wt% Oxide | 2σ | det.lim. |
|---|---|---|---|
| $SiO_2$ | 53.90 | 0.29 | 0.03 |
| $Al_2O_3$ | 28.53 | 0.16 | 0.02 |
| FeO | 0.15 | 0.04 | 0.01 |
| MgO | 0.03 | 0.02 | 0.005 |
| CaO | 12.15 | 0.13 | 0.02 |
| BaO | 0.05 | 0.06 | 0.01 |
| $Na_2O$ | 4.61 | 0.09 | 0.02 |
| $K_2O$ | 0.25 | 0.03 | 0.01 |
| Total | 99.68 | | |

Pyroxene (Microscan)

| | Wt% Oxide | 2σ | det. lim. |
|---|---|---|---|
| $SiO_2$ | 48.53 | 0.27 | 0.04 |
| $TiO_2$ | 2.37 | 0.07 | 0.03 |
| $Al_2O_3$ | 3.95 | 0.07 | 0.002 |
| FeO | 9.96 | 0.13 | 0.04 |
| MnO | 0.19 | 0.04 | 0.02 |
| MgO | 12.09 | 0.12 | 0.02 |
| CaO | 21.64 | 0.17 | 0.02 |
| $Na_2O$ | 0.62 | 0.04 | 0.02 |
| Total | 99.34 | | |

Magnetite (Microscan)

| | Wt% Oxide | 2σ | det.lim. |
|---|---|---|---|
| $SiO_2$ | 0.07 | 0.04 | 0.01 |
| $TiO_2$ | 22.98 | 0.17 | 0.03 |
| $Al_2O_3$ | 2.05 | 0.06 | 0.03 |
| $Cr_2O_3$ | 0.07 | 0.29 | 0.01 |
| FeO | 69.28 | 0.31 | 0.04 |
| MnO | 0.70 | 0.05 | 0.03 |
| MgO | 1.77 | 0.06 | 0.03 |
| Total | 96.93 | | |

Biotite (Microscan)

| | Wt% Oxide | 2σ | det. lim. |
|---|---|---|---|
| F | 0.33 | 0.13 | 0.07 |
| K2O | 8.75 | 0.11 | 0.02 |
| Na2O | 0.51 | 0.04 | 0.02 |
| CaO | 0.05 | 0.02 | 0.01 |
| MgO | 7.81 | 0.10 | 0.02 |
| MnO | 0.17 | 0.04 | 0.01 |
| FeO | 24.53 | 0.20 | 0.04 |
| Al2O3 | 12.90 | 0.12 | 0.02 |
| TiO2 | 6.71 | 0.11 | 0.03 |
| SiO2 | 34.49 | 0.24 | 0.04 |
| Total | 96.25 | | |

Amphibole (Microscan)

| | Wt% Oxide | 2σ | det.lim. |
|---|---|---|---|
| $SiO_2$ | 44.73 | 0.26 | 0.04 |
| $TiO_2$ | 2.67 | 0.07 | 0.03 |
| $Al_2O_3$ | 4.32 | 0.08 | 0.02 |
| FeO | 29.05 | 0.21 | 0.04 |
| MnO | 0.53 | 0.04 | 0.02 |
| MgO | 3.40 | 0.07 | 0.02 |
| CaO | 8.26 | 0.11 | 0.02 |
| $Na_2O$ | 4.06 | 0.10 | 0.03 |
| $K_2O$ | 1.40 | 0.05 | 0.02 |
| Total | 94.42 | | |

Olivine(Camebax)

| | Wt% Oxide | 2σ | det. lim. |
|---|---|---|---|
| $SiO_2$ | 31.67 | 0.17 | 0.01 |
| $Al_2O_3$ | 0.05 | 0.02 | 0.01 |
| FeO | 36.26 | 0.23 | 0.03 |
| MnO | 0.35 | 0.04 | 0.02 |
| MgO | 31.70 | 0.18 | 0.02 |
| CaO | 0.45 | 0.03 | 0.01 |
| Total | 100.50 | | |

Apatite (Camebax)

| | Wt% Oxide | 2σ | det.lim. |
|---|---|---|---|
| $Na_2O$ | 0.06 | 0.29 | 0.03 |
| $SiO_2$ | 0.16 | 0.16 | 0.02 |
| $P_2O_5$ | 41.61 | 0.04 | 0.01 |
| CaO | 55.46 | 0.02 | 0.005 |
| $La_2O_3$ | 0.09 | 0.13 | 0.02 |
| $Ce_2O_3$ | 0.16 | 0.06 | 0.01 |
| F | 5.91 | 0.09 | 0.02 |
| Cl | 0.04 | 0.03 | 0.01 |
| Total | 103.49 | | |

## II.2 Sample preparation for whole-rock and mineral analysis

### II.2.1 Whole-rock samples

Whole-rock samples of the freshest rocks available were crushed for XRF an for isotope analysis. Between 100 and 400 g of cumulates were crushed to a size c 0.5-1.0 cm in a jaw crusher and noticeably weathered fragments picked out an discarded. These chips were then crushed in a Tema tungsten carbide swing-mill fo 1-3 minutes to a grain size of <200μm. For the more homogeneous chilled margina samples 50 - 100 g were used and 0.5cm thick slices cut to 1-3 cm in size to plac directly in the tungsten carbide mill.

### II.2.2 Mineral separation

Feldspar was separated for all the samples used for oxygen isotop determination. Samples were crushed and seived and the 60-100 mesh (150-250 μm fraction used for separation, after being washed to remove fines. A Franz electromagnetic separator was used to separate feldspar from mafic minerals; for this a side slope of ~13° and a magnet strength of ~0.75 were found appropriate. To remove any remaining mafic minerals from the feldspar separate a side slope of abou 5° and a magnet setting of 1.0 were used. For the granite samples, feldspar was separated from quartz using a side slope of ~3° and a magnet strength of ~1.25; this was the only case where the feldspar was the more magnetic mineral.

A certain amount of sample bias may have been introduced during these procedures. Most samples contain some cloudy altered feldspar as well as clear fresh feldspar and there may be differences in the ease of crushing or the electromagnetic properties of the two types. Such differences were not rigorously investigated as part of this project but are being studied in more detail by A.A. Finch and F.D.L. Walker of Edinburgh University. However, one sample, YGD 6, was coarsely crushed and clear fragments of feldspar picked out by hand. Analysis of this clear feldspar gave an oxygen isotope ratio indistinguishable from that obtained for the mixed cloudy and clear feldspar of the rock, so differences are not thought to be large enough seriously to affect the results.

In the samples where apatite was present in any quantity (samples from locality G of Fig. 2.1 and eastwards), heavy liquids had to be used to separate apatite from feldspar. Tetrabromoethane (specific gravity 2.96 g/cm$^3$) was found to be suitable as feldspar floated easily and apatite sank. The samples were centrifuged twice at 1500 rpm for 2-3 minutes and the separates filtered, washed with acetone and dried.

## II.3 X-Ray fluorescence spectrometry

Samples were analysed for 10 major and 17 trace elements using a rhodium tube on Philips PW1450 and 1480 automatic X-Ray fluorescence spectrometers. Major elements were analysed on fused glass discs prepared using Johnson Matthey Spectroflux 105$^R$ and trace elements were analysed on pressed powder pellets. Details of preparation procedure are given in Fitton *et al.* (1984) and Fitton and Dunlop (1985).

Matrix corrections for trace elements were made using mass absorption coefficients based on the major element analyses. USGS and CRPG rock standards (Abbey, 1980) were used to calibrate each element. Six separate glass discs and powder pellets were made for the troctolite sample YGD 36B to measure analytical precision. Mean and standard deviation ($2\sigma$) of the results are given in Table II.2, together with a crude estimate of the accuracy given by the root mean squared deviations of the standard calibration points about the regression line.

## II.4 Isotopic determination

### II.4.1 Strontium Isotopes

Between 0.03 and 0.2 g of whole-rock powder was weighed into PFA (Savillex) Teflon capsules which had been thoroughly cleaned in $HNO_3$, HCl and distilled $H_2O$ before use. Strontium was separated by dissolution using 1 part 16M $HNO_3$ with 8 parts HF, then 16M $HNO_3$ and finally 6M HCl. Samples were left to react overnight at 150°C with each acid and then evaporated to dryness before the next was added. Cation exchange was then carried out using 2.5M HCl, as detailed in Blaxland *et al.* (1978). Sr blanks were less than 1 ng. Samples were heated to dryness and then treated with one drop of $HNO_3$.

Table II.2 Precision and accuracy of whole-rock analyses

| Sample YGD 36B | Mean (n=6) | 2σ | RMSD |
|---|---|---|---|
| $SiO_2$ | 46.28 | 0.14 | 0.22 |
| $Al_2O_3$ | 17.45 | 0.13 | 0.12 |
| $Fe_2O_3$ | 13.19 | 0.07 | 0.05 |
| MgO | 9.02 | 0.06 | 0.08 |
| CaO | 7.59 | 0.04 | 0.05 |
| $Na_2O$ | 3.45 | 0.06 | 0.06 |
| $K_2O$ | 0.77 | 0.003 | 0.02 |
| $TiO_2$ | 1.43 | 0.01 | 0.01 |
| MnO | 0.16 | 0.002 | 0.01 |
| $P_2O_5$ | 0.58 | 0.004 | 0.01 |
| | | | |
| Ni | 108.9 | 0.3 | 4.3 |
| Cr | 12.7 | 0.8 | 11.0 |
| V | 77.6 | 1.1 | 11.5 |
| Sc | 13.0 | 1.9 | 2.4 |
| Cu | 32.1 | 1.0 | 5.3 |
| Zn | 75.0 | 0.6 | 5.0 |
| Sr | 980.6 | 2.0 | 9.6 |
| Rb | 9.1 | 0.2 | 3.5 |
| Zr | 75.3 | 6.7 | 14.8 |
| Nb | 12.4 | 0.2 | 2.4 |
| Ba | 798.3 | 3.3 | 39.0 |
| Pb | * | | 4.0 |
| Th | * | | 2.8 |
| La | 18.0 | 0.5 | 5.6 |
| Ce | 45.1 | 1.5 | 13.5 |
| Nd | 23.6 | 0.9 | 3.6 |
| Y | 16.5 | 0.8 | 3.4 |

* Below detection limits

Strontium was loaded onto a single tantalum filament using $H_3PO_4$ and isotope ratios were measured on a semi-automatic VG Micromass 30B thermal ionisation mass spectrometer. At least four sets of ten scans were measured for each sample, both up- and down-mass. Isotopic data were corrected for mass fractionation using $^{88}Sr/^{86}Sr=8.37521$. A value of 0.75(up-mass value) + 0.25(down-mass value) was used for subsequent calculations. The NBS 987 standard gave $^{87}Sr/^{86}Sr=0.71028\pm4$ during the course of the work. All data have been normalised to NBS 987=0.71022 (equivalent to Eimer and Amend $^{87}Sr/^{86}Sr=0.70800$). Measured mass spectrometer run errors ($2\sigma$) are given for each sample in Table 5.2; the mean error is 0.000042. Uncertainties in the XRF determination for Rb and Sr (section II.3) give additional errors of about 0.00002 in the age-corrected ratios.

### II.4.2 Oxygen isotopes

Oxygen was extracted from whole-rock powders and from feldspar separates following the method of Borthwick and Harmon (1982). Sample sizes were 10-15 mg and reaction with $ClF_3$ was carried out at 670°C, overnight for feldspar and over at least 36 hours for whole-rock samples.

$\delta^{18}O$ data relative to SMOW were determined by gas source mass spectrometry on the $CO_2$ produced after oxygen extraction. The mass spectrometer was a VG SIRA10 with a reference gas calibrated against international carbonate and silicate standards (NBS 19 and NBS 28). During the course of this work analyses of the NBS 28 quartz standard gave $\delta^{18}O=9.6‰$ relative to SMOW. Machine errors were about 0.2‰ and reproducability was usually also within 0.2‰, but occasionally poorer than this. Values in brackets in Table 5.4 are those averaged from two or more results with reproducability less good than 0.2‰. Very high or low values were discarded.

# APPENDIX III: REPRESENTATIVE MINERAL ANALYSES

**(nd-not detectable)**

## Olivines in chilled margins

| | 1 | 2 | 3 | 4 | 5 | 6 | 7 | 8 |
|---|---|---|---|---|---|---|---|---|
| SiO2 | 36.36 | 35.29 | 37.38 | 34.12 | 34.12 | 36.10 | 35.41 | 35.06 |
| Al2O3 | 0.03 | 0.04 | 0.05 | 0.05 | 0.07 | 0.03 | 0.05 | 0.05 |
| FeO | 32.52 | 36.38 | 29.58 | 43.79 | 45.88 | 35.76 | 38.53 | 38.69 |
| MnO | 0.44 | 0.59 | 0.34 | 0.82 | 0.87 | 0.54 | 0.68 | 0.67 |
| MgO | 30.43 | 27.19 | 32.66 | 20.86 | 19.33 | 28.60 | 25.64 | 25.60 |
| CaO | 0.33 | 0.38 | 0.29 | 0.45 | 0.20 | 0.28 | 0.35 | 0.37 |
| total= | 100.11 | 99.87 | 100.30 | 100.09 | 100.47 | 101.31 | 100.66 | 100.44 |
| Si | 1.00 | 0.99 | 1.00 | 0.99 | 1.00 | 0.99 | 1.00 | 0.99 |
| Fe2 | 0.74 | 0.85 | 0.66 | 1.07 | 1.12 | 0.82 | 0.91 | 0.91 |
| Mn | 0.01 | 0.01 | - | 0.02 | 0.02 | 0.01 | 0.02 | 0.02 |
| Mg | 1.24 | 1.14 | 1.31 | 0.91 | 0.84 | 1.17 | 1.07 | 1.08 |
| Ca | - | 0.01 | - | 0.01 | - | - | 0.01 | 0.01 |
| total= | 3.00 | 3.01 | 2.99 | 3.00 | 3.00 | 3.01 | 3.00 | 3.01 |
| oxygens= | [4] | [4] | [4] | [4] | [4] | [4] | [4] | [4] |
| FO | 62.2 | 56.7 | 66.0 | 45.5 | 42.4 | 58.4 | 53.8 | 53.7 |
| FA | 37.3 | 42.6 | 33.6 | 53.5 | 56.5 | 41.0 | 45.4 | 45.5 |

1 2, 40488
2 2 rim, 40488
3 5, 40488
4 10, 40488
5 11, 40488
6 3, YGD78
7 6, YGD364
8 2, YGD325

| | 9 | 10 | 11 | 12 | 13 | 14 | 15 | 16 |
|---|---|---|---|---|---|---|---|---|
| SiO2 | 34.61 | 35.80 | 34.83 | 35.87 | 35.23 | 34.47 | 33.38 | 35.75 |
| Al2O3 | 0.05 | 0.05 | 0.04 | 0.04 | 0.05 | 0.04 | 0.02 | 0.03 |
| FeO | 40.10 | 34.61 | 40.69 | 37.84 | 39.03 | 41.10 | 41.49 | 38.56 |
| MnO | 0.69 | 0.50 | 0.67 | 0.59 | 0.69 | 0.74 | 0.72 | 0.64 |
| MgO | 24.35 | 29.04 | 23.43 | 26.11 | 25.30 | 23.88 | 23.08 | 25.92 |
| CaO | 0.29 | 0.31 | 0.41 | 0.36 | 0.33 | 0.40 | 0.45 | 0.36 |
| total= | 100.09 | 100.31 | 100.07 | 100.81 | 100.63 | 100.63 | 99.14 | 101.26 |
| Si | 0.99 | 0.99 | 1.00 | 1.00 | 0.99 | 0.98 | 0.97 | 1.00 |
| Fe2 | 0.96 | 0.80 | 0.97 | 0.88 | 0.92 | 0.98 | 1.01 | 0.90 |
| Mn | 0.02 | 0.01 | 0.02 | 0.01 | 0.02 | 0.02 | 0.02 | 0.02 |
| Mg | 1.04 | 1.20 | 1.00 | 1.09 | 1.06 | 1.02 | 1.00 | 1.08 |
| Ca | - | - | 0.01 | 0.01 | - | 0.01 | 0.01 | 0.01 |
| total= | 3.01 | 3.01 | 3.00 | 3.00 | 3.01 | 3.01 | 3.02 | 3.00 |
| oxygens= | [4] | [4] | [4] | [4] | [4] | [4] | [4] | [4] |
| FO | 51.5 | 59.6 | 50.2 | 54.8 | 53.2 | 50.4 | 49.3 | 54.1 |
| FA | 47.6 | 39.8 | 48.9 | 44.5 | 46.0 | 48.7 | 49.8 | 45.1 |

9 2, YGD325
10 3, YGD325
11 3, YGD228
12 5, YGD228
13 2, YGD328
14 4, YGD328
15 1, YGD1
16 2, YGD1

| | 17 | 18 | 19 | 20 | 21 | 22 | 23 | 24 |
|---|---|---|---|---|---|---|---|---|
| SiO2 | 37.14 | 36.23 | 37.22 | 35.59 | 37.32 | 35.91 | 36.54 | 36.10 |
| Al2O3 | 0.03 | 0.05 | 0.05 | 0.04 | 0.06 | 0.05 | 0.05 | 0.04 |
| FeO | 29.56 | 33.01 | 29.94 | 36.43 | 29.21 | 35.16 | 28.71 | 32.90 |
| MnO | 0.35 | 0.47 | 0.37 | 0.58 | 0.34 | 0.52 | 0.35 | 0.46 |
| MgO | 33.52 | 30.41 | 33.20 | 27.50 | 33.52 | 28.46 | 34.41 | 30.25 |
| CaO | 0.25 | 0.32 | 0.26 | 0.37 | 0.27 | 0.30 | 0.25 | 0.28 |
| total= | 100.85 | 100.49 | 101.05 | 100.50 | 100.71 | 100.41 | 100.31 | 100.03 |
| Si | 0.99 | 0.99 | 0.99 | 0.99 | 1.00 | 0.99 | 0.98 | 0.99 |
| Fe2 | 0.66 | 0.76 | 0.67 | 0.85 | 0.65 | 0.81 | 0.64 | 0.76 |
| Mn | - | 0.01 | - | 0.01 | - | 0.01 | - | 0.01 |
| Mg | 1.34 | 1.24 | 1.32 | 1.14 | 1.33 | 1.17 | 1.38 | 1.24 |
| Ca | - | - | - | 0.01 | - | - | - | - |
| total= | 3.01 | 3.01 | 3.00 | 3.01 | 3.00 | 3.01 | 3.02 | 3.01 |
| oxygens= | [4] | [4] | [4] | [4] | [4] | [4] | [4] | [4] |
| FO | 66.6 | 61.8 | 66.1 | 57.0 | 66.9 | 58.7 | 67.8 | 61.8 |
| FA | 33.0 | 37.6 | 33.5 | 42.3 | 32.7 | 40.7 | 31.8 | 37.7 |

17 5, YGD1
18 5 rim, YGD1
19 1, YGD229
20 1 rim, YGD229
21 3, YGD229
22 3 rim, YGD229
23 2, YGD259
24 2 rim, YGD259

## Olivines in chilled margins

| | 25 | 26 | 27 | 28 | 29 | 30 | 31 | 32 |
|---|---|---|---|---|---|---|---|---|
| SiO2 | 35.93 | 35.63 | 34.90 | 34.25 | 36.25 | 36.11 | 35.00 | 34.69 |
| Al2O3 | 0.06 | 0.03 | 0.02 | 0.03 | 0.05 | 0.05 | 0.02 | 0.04 |
| FeO | 34.16 | 33.13 | 36.38 | 37.10 | 32.93 | 34.55 | 38.73 | 41.93 |
| MnO | 0.47 | 0.45 | 0.55 | 0.60 | 0.51 | 0.56 | 0.67 | 0.79 |
| MgO | 29.43 | 31.17 | 27.84 | 27.07 | 30.48 | 28.81 | 24.67 | 22.54 |
| CaO | 0.27 | 0.29 | 0.23 | 0.35 | 0.38 | 0.39 | 0.21 | 0.25 |
| total= | 100.32 | 100.70 | 99.92 | 99.40 | 100.60 | 100.47 | 99.30 | 100.24 |
| Si | 0.99 | 0.98 | 0.98 | 0.97 | 0.99 | 1.00 | 1.00 | 1.00 |
| Fe2 | 0.79 | 0.76 | 0.85 | 0.88 | 0.75 | 0.80 | 0.93 | 1.01 |
| Mn | 0.01 | 0.01 | 0.01 | 0.01 | 0.01 | 0.01 | 0.02 | 0.02 |
| Mg | 1.21 | 1.27 | 1.17 | 1.15 | 1.24 | 1.18 | 1.05 | 0.97 |
| Ca | - | - | - | 0.01 | 0.01 | 0.01 | - | - |
| total= | 3.01 | 3.02 | 3.02 | 3.03 | 3.01 | 3.00 | 3.00 | 3.00 |
| oxygens= | [4] | [4] | [4] | [4] | [4] | [4] | [4] | [4] |
| FO | 60.2 | 62.3 | 57.3 | 56.1 | 61.9 | 59.4 | 52.7 | 48.5 |
| FA | 39.2 | 37.2 | 42.0 | 43.2 | 37.5 | 40.0 | 46.5 | 50.6 |

25 3, YGD259
26 3, YGD292
27 3 rim, YGD292
28 5, YGD292
29 1, 30736
30 2, 30736
31 2, 101211
32 3, 101211

## Olivines in troctolites

| | 33 | 34 | 35 | 36 | 37 | 38 | 39 | 40 |
|---|---|---|---|---|---|---|---|---|
| SiO2 | 33.78 | 34.24 | 34.14 | 35.21 | 36.40 | 36.72 | 35.81 | 36.30 |
| Al2O3 | 0.04 | 0.04 | 0.02 | 0.06 | 0.05 | 0.05 | 0.04 | 0.05 |
| FeO | 45.73 | 45.18 | 43.62 | 33.82 | 32.64 | 31.67 | 35.13 | 33.27 |
| MnO | 0.92 | 0.92 | 0.86 | 0.48 | 0.44 | 0.40 | 0.53 | 0.46 |
| MgO | 19.65 | 19.74 | 21.25 | 30.32 | 30.92 | 31.58 | 28.93 | 30.66 |
| CaO | 0.44 | 0.48 | 0.49 | 0.36 | 0.37 | 0.40 | 0.37 | 0.38 |
| total= | 100.56 | 100.60 | 100.38 | 100.25 | 100.82 | 100.82 | 100.81 | 101.12 |
| Si | 0.99 | 1.00 | 0.99 | 0.97 | 0.99 | 0.99 | 0.99 | 0.99 |
| Fe2 | 1.12 | 1.10 | 1.06 | 0.78 | 0.74 | 0.72 | 0.81 | 0.76 |
| Mn | 0.02 | 0.02 | 0.02 | 0.01 | 0.01 | - | 0.01 | 0.01 |
| Mg | 0.86 | 0.86 | 0.92 | 1.25 | 1.25 | 1.27 | 1.19 | 1.24 |
| Ca | 0.01 | 0.02 | 0.02 | 0.01 | 0.01 | 0.01 | 0.01 | 0.01 |
| total= | 3.01 | 3.00 | 3.01 | 3.03 | 3.01 | 3.01 | 3.01 | 3.01 |
| oxygens= | [4] | [4] | [4] | [4] | [4] | [4] | [4] | [4] |
| FO | 42.9 | 43.3 | 46.0 | 61.2 | 62.5 | 63.7 | 59.1 | 61.8 |
| FA | 56.0 | 55.6 | 53.0 | 38.3 | 37.0 | 35.8 | 40.3 | 37.6 |

33 2 nearer rim, 30638
34 2 rim, 30638
35 5, 30638
36 14, YGD36
37 4, YGD54
38 6 rim, YGD54
39 3, YGD12
40 2, YGD34

| | 41 | 42 | 43 | 44 | 45 | 46 | 47 | 48 |
|---|---|---|---|---|---|---|---|---|
| SiO2 | 35.15 | 35.00 | 35.20 | 35.03 | 35.18 | 35.24 | 35.29 | 35.80 |
| Al2O3 | 0.07 | 0.06 | 0.05 | 0.04 | nd | 0.01 | 0.03 | 0.03 |
| FeO | 40.41 | 42.00 | 39.73 | 39.58 | 37.55 | 37.46 | 37.19 | 34.92 |
| MnO | 0.68 | 0.76 | 0.68 | 0.72 | 0.62 | 0.68 | 0.59 | 0.50 |
| MgO | 24.52 | 22.70 | 25.38 | 25.06 | 27.00 | 26.37 | 27.16 | 29.10 |
| CaO | 0.49 | 0.38 | 0.46 | 0.44 | 0.45 | 0.47 | 0.43 | 0.42 |
| total= | 101.32 | 100.90 | 101.50 | 100.87 | 100.80 | 100.23 | 100.69 | 100.77 |
| Si | 0.99 | 1.00 | 0.99 | 0.99 | 0.98 | 0.99 | 0.99 | 0.99 |
| Fe2 | 0.95 | 1.00 | 0.93 | 0.93 | 0.88 | 0.88 | 0.87 | 0.81 |
| Mn | 0.02 | 0.02 | 0.02 | 0.02 | 0.01 | 0.02 | 0.01 | 0.01 |
| Mg | 1.03 | 0.97 | 1.06 | 1.05 | 1.13 | 1.11 | 1.13 | 1.20 |
| Ca | 0.01 | 0.01 | 0.01 | 0.01 | 0.01 | 0.01 | 0.01 | 0.01 |
| total= | 3.01 | 3.00 | 3.01 | 3.01 | 3.02 | 3.01 | 3.01 | 3.01 |
| oxygens= | [4] | [4] | [4] | [4] | [4] | [4] | [4] | [4] |
| FO | 51.5 | 48.6 | 52.8 | 52.6 | 55.8 | 55.2 | 56.2 | 59.4 |
| FA | 47.7 | 50.5 | 46.4 | 46.6 | 43.5 | 44.0 | 43.1 | 40.0 |

41 1, YGD293
42 1, YGD293
43 3, YGD293
44 4, YGD293
45 8, YGD138
46 10, YGD138
47 1, YGD423
48 2, YGD423

# Olivines in troctolites

| | 49 | 50 | 51 | 52 | 53 | 54 | 55 | 56 |
|---|---|---|---|---|---|---|---|---|
| SiO2 | 34.02 | 33.61 | 35.24 | 34.04 | 35.21 | 36.32 | 35.01 | 34.10 |
| Al2O3 | 0.06 | 0.04 | 0.04 | 0.05 | 0.05 | 0.03 | 0.05 | 0.05 |
| FeO | 44.63 | 46.91 | 39.02 | 41.21 | 37.07 | 34.75 | 38.74 | 44.12 |
| MnO | 0.92 | 1.02 | 0.64 | 0.72 | 0.70 | 0.58 | 0.68 | 0.84 |
| MgO | 20.76 | 18.95 | 25.62 | 23.54 | 26.69 | 28.69 | 25.81 | 21.09 |
| CaO | 0.47 | 0.30 | 0.43 | 0.43 | 0.21 | 0.31 | 0.42 | 0.47 |
| total= | 100.86 | 100.83 | 100.99 | 99.99 | 99.93 | 100.68 | 100.71 | 100.67 |
| Si | 0.99 | 0.99 | 0.99 | 0.98 | 0.99 | 1.00 | 0.99 | 0.99 |
| Fe2 | 1.08 | 1.15 | 0.92 | 0.99 | 0.87 | 0.80 | 0.91 | 1.07 |
| Mn | 0.02 | 0.03 | 0.02 | 0.02 | 0.02 | 0.01 | 0.02 | 0.02 |
| Mg | 0.90 | 0.83 | 1.07 | 1.01 | 1.12 | 1.18 | 1.08 | 0.91 |
| Ca | 0.01 | - | 0.01 | 0.01 | - | - | 0.01 | 0.01 |
| total= | 3.01 | 3.01 | 3.01 | 3.02 | 3.01 | 3.00 | 3.01 | 3.01 |
| oxygens= | [4] | [4] | [4] | [4] | [4] | [4] | [4] | [4] |
| FO | 44.8 | 41.3 | 53.5 | 50.0 | 55.7 | 59.1 | 53.8 | 45.5 |
| FA | 54.1 | 57.4 | 45.7 | 49.1 | 43.4 | 40.2 | 45.3 | 53.4 |

49 2, YGD426
50 2 rim, YGD426
51 1, YGD365
52 4 rim, YGD365
53 1 rim, YGD80
54 4, YGD80
55 3, YGD392
56 3 rim, YGD392

| | 57 | 58 | 59 | 60 | 61 | 62 | 63 | 64 |
|---|---|---|---|---|---|---|---|---|
| SiO2 | 34.40 | 35.86 | 36.08 | 35.76 | 35.42 | 34.21 | 34.54 | 35.93 |
| Al2O3 | 0.06 | 0.04 | 0.04 | 0.04 | 0.04 | 0.04 | 0.04 | 0.05 |
| FeO | 41.55 | 35.66 | 33.95 | 33.66 | 35.32 | 42.66 | 41.62 | 34.39 |
| MnO | 0.72 | 0.56 | 0.51 | 0.48 | 0.56 | 0.85 | 0.82 | 0.51 |
| MgO | 23.21 | 28.33 | 29.56 | 30.16 | 28.42 | 22.12 | 22.42 | 29.13 |
| CaO | 0.30 | 0.45 | 0.35 | 0.30 | 0.40 | 0.40 | 0.39 | 0.42 |
| total= | 100.24 | 100.90 | 100.49 | 100.40 | 100.16 | 100.28 | 99.83 | 100.43 |
| Si | 0.99 | 0.99 | 0.99 | 0.98 | 0.99 | 0.99 | 1.00 | 0.99 |
| Fe2 | 1.00 | 0.82 | 0.78 | 0.77 | 0.82 | 1.03 | 1.01 | 0.79 |
| Mn | 0.02 | 0.01 | 0.01 | 0.01 | 0.01 | 0.02 | 0.02 | 0.01 |
| Mg | 0.99 | 1.17 | 1.21 | 1.24 | 1.18 | 0.95 | 0.97 | 1.20 |
| Ca | - | 0.01 | 0.01 | - | 0.01 | 0.01 | 0.01 | 0.01 |
| total= | 3.01 | 3.01 | 3.01 | 3.02 | 3.01 | 3.01 | 3.00 | 3.01 |
| oxygens= | [4] | [4] | [4] | [4] | [4] | [4] | [4] | [4] |
| FO | 49.5 | 58.2 | 60.5 | 61.2 | 58.5 | 47.5 | 48.5 | 59.8 |
| FA | 49.7 | 41.1 | 39.0 | 38.3 | 40.8 | 51.4 | 50.5 | 39.6 |

57 5, YGD392
58 2, YGD334
59 3, YGD334
60 1, YGD64
61 2, YGD64
62 3, YGD426
63 3 rim, YGD426
64 3, YGD195

| | 65 | 66 | 67 |
|---|---|---|---|
| SiO2 | 35.97 | 36.36 | 36.19 |
| Al2O3 | 0.04 | 0.05 | 0.04 |
| FeO | 34.37 | 32.42 | 33.39 |
| MnO | 0.52 | 0.42 | 0.44 |
| MgO | 28.98 | 30.48 | 29.74 |
| CaO | 0.32 | 0.34 | 0.30 |
| total= | 100.20 | 100.07 | 100.10 |
| Si | 0.99 | 1.00 | 1.00 |
| Fe2 | 0.79 | 0.74 | 0.77 |
| Mn | 0.01 | - | 0.01 |
| Mg | 1.19 | 1.24 | 1.22 |
| total= | 3.01 | 3.00 | 3.00 |
| oxygens= | [4] | [4] | [4] |
| FO | 59.7 | 62.3 | 61.0 |
| FA | 39.7 | 37.2 | 38.4 |

65 3 rim, YGD195
66 1, YGD307
67 2, YGD307

# Olivines in mafic cumulates

| | 68 | 69 | 70 | 71 | 72 | 73 | 74 | 75 |
|---|---|---|---|---|---|---|---|---|
| SiO2 | 36.73 | 36.79 | 36.79 | 36.19 | 35.79 | 34.93 | 35.66 | 36.03 |
| Al2O3 | 0.02 | 0.04 | 0.07 | 0.05 | 0.03 | 0.03 | 0.05 | 0.05 |
| FeO | 31.21 | 30.64 | 31.05 | 34.39 | 36.21 | 37.69 | 33.16 | 33.90 |
| MnO | 0.45 | 0.43 | 0.42 | 0.47 | 0.57 | 0.62 | 0.46 | 0.47 |
| MgO | 32.13 | 31.80 | 32.35 | 29.41 | 28.38 | 27.07 | 30.67 | 29.87 |
| CaO | 0.32 | 0.31 | 0.28 | 0.35 | 0.02 | 0.04 | 0.40 | 0.31 |
| total= | 100.86 | 100.01 | 100.96 | 100.86 | 101.00 | 100.38 | 100.40 | 100.63 |
| Si | 0.99 | 1.00 | 0.99 | 0.99 | 0.99 | 0.98 | 0.98 | 0.99 |
| Fe2 | 0.70 | 0.70 | 0.70 | 0.79 | 0.84 | 0.89 | 0.76 | 0.78 |
| Mn | 0.01 | - | - | 0.01 | 0.01 | 0.01 | 0.01 | 0.01 |
| Mg | 1.29 | 1.29 | 1.30 | 1.20 | 1.17 | 1.13 | 1.26 | 1.22 |
| Ca | - | - | - | 0.01 | - | - | 0.01 | - |
| total= | 3.01 | 3.00 | 3.01 | 3.01 | 3.01 | 3.02 | 3.02 | 3.01 |
| oxygens= | [4] | [4] | [4] | [4] | [4] | [4] | [4] | [4] |
| FO | 64.4 | 64.6 | 64.7 | 60.1 | 57.9 | 55.7 | 61.9 | 60.8 |
| FA | 35.1 | 34.9 | 34.8 | 39.4 | 41.4 | 43.5 | 37.6 | 38.7 |

68 13, 186375
69 18, 186375
70 7, YGD72
71 8, YGD72
72 2 rim, YGD381
73 3, YGD381
74 3, YGD312
75 3 rim, YGD312

| | 76 | 77 | 78 | 79 | 80 | 81 | 82 | 83 |
|---|---|---|---|---|---|---|---|---|
| SiO2 | 36.12 | 36.47 | 36.42 | 36.38 | 34.89 | 34.64 | 36.99 | 36.86 |
| Al2O3 | 0.04 | 0.02 | 0.02 | 0.05 | 0.02 | 0.03 | 0.05 | 0.05 |
| FeO | 32.71 | 31.85 | 32.00 | 29.71 | 40.43 | 40.95 | 29.09 | 29.66 |
| MnO | 0.44 | 0.42 | 0.44 | 0.41 | 0.70 | 0.74 | 0.35 | 0.39 |
| MgO | 31.09 | 31.03 | 30.25 | 34.06 | 24.73 | 24.06 | 33.54 | 32.76 |
| CaO | 0.36 | 0.39 | 0.30 | 0.23 | 0.06 | 0.06 | 0.29 | 0.35 |
| total= | 100.76 | 100.18 | 99.43 | 100.84 | 100.83 | 100.48 | 100.31 | 100.07 |
| Si | 0.98 | 0.99 | 1.00 | 0.98 | 0.99 | 0.99 | 0.99 | 1.00 |
| Fe2 | 0.75 | 0.73 | 0.74 | 0.67 | 0.96 | 0.98 | 0.65 | 0.67 |
| Mn | 0.01 | - | 0.01 | - | 0.02 | 0.02 | - | - |
| Mg | 1.26 | 1.26 | 1.24 | 1.36 | 1.04 | 1.02 | 1.34 | 1.32 |
| Ca | 0.01 | 0.01 | - | - | - | - | - | - |
| total= | 3.01 | 3.00 | 3.00 | 3.02 | 3.01 | 3.01 | 3.01 | 3.00 |
| oxygens= | [4] | [4] | [4] | [4] | [4] | [4] | [4] | [4] |
| FO | 62.6 | 63.1 | 62.4 | 66.8 | 51.7 | 50.7 | 67.0 | 66.0 |
| FA | 36.9 | 36.4 | 37.1 | 32.7 | 47.4 | 48.4 | 32.6 | 33.5 |

76 5, YGD312
77 3, YGD49
78 4 rim, YGD49
79 2 rim, YGD306
80 3, 40411
81 5, 40411
82 3, YGD316
83 4, YGD316

| | 84 | 85 | 86 | 87 | 88 |
|---|---|---|---|---|---|
| SiO2 | 35.73 | 35.61 | 35.97 | 36.14 | 36.03 |
| Al2O3 | 0.04 | 0.03 | 0.04 | 0.06 | 0.04 |
| FeO | 37.76 | 37.40 | 37.76 | 33.49 | 34.49 |
| MnO | 0.59 | 0.60 | 0.59 | 0.48 | 0.46 |
| MgO | 26.44 | 26.74 | 25.80 | 30.04 | 29.40 |
| CaO | 0.41 | 0.40 | 0.42 | 0.38 | 0.38 |
| total= | 100.98 | 100.78 | 100.58 | 100.59 | 100.81 |
| Si | 1.00 | 0.99 | 1.01 | 0.99 | 0.99 |
| Fe2 | 0.88 | 0.87 | 0.88 | 0.77 | 0.79 |
| Mn | 0.01 | 0.01 | 0.01 | 0.01 | 0.01 |
| Mg | 1.10 | 1.11 | 1.08 | 1.23 | 1.20 |
| Ca | 0.01 | 0.01 | 0.01 | 0.01 | 0.01 |
| total= | 3.00 | 3.01 | 2.99 | 3.01 | 3.01 |
| oxygens= | [4] | [4] | [4] | [4] | [4] |
| FO | 55.1 | 55.6 | 54.5 | 61.2 | 60.0 |
| FA | 44.2 | 43.7 | 44.8 | 38.3 | 39.5 |

84 3, YGD158
85 3 rim, YGD158
86 5, YGD158
87 1, YGD196
88 1 rim, YGD196

## Olivines in syenogabbros

| | 89 | 90 | 91 | 92 | 93 | 94 |
|---|---|---|---|---|---|---|
| SiO2 | 32.27 | 32.27 | 31.87 | 31.51 | 34.97 | 34.96 |
| Al2O3 | 0.01 | 0.02 | nd | 0.02 | 0.04 | 0.02 |
| FeO | 53.76 | 51.60 | 54.65 | 55.70 | 37.63 | 37.92 |
| MnO | 1.37 | 1.32 | 1.51 | 1.54 | 0.76 | 0.76 |
| MgO | 12.52 | 14.13 | 11.31 | 10.68 | 27.15 | 26.83 |
| CaO | 0.29 | 0.22 | 0.33 | 0.24 | 0.19 | 0.22 |
| total= | 100.22 | 99.56 | 99.67 | 99.69 | 100.74 | 100.71 |
| Si | 1.00 | 0.99 | 1.00 | 0.99 | 0.98 | 0.98 |
| Fe2 | 1.39 | 1.33 | 1.43 | 1.47 | 0.88 | 0.89 |
| Mn | 0.04 | 0.03 | 0.04 | 0.04 | 0.02 | 0.02 |
| Mg | 0.58 | 0.65 | 0.53 | 0.50 | 1.13 | 1.12 |
| Ca | - | - | 0.01 | - | - | - |
| total= | 3.00 | 3.01 | 3.00 | 3.01 | 3.02 | 3.02 |
| oxygens= | [4] | [4] | [4] | [4] | [4] | [4] |
| FO | 28.8 | 32.2 | 26.4 | 24.9 | 55.8 | 55.3 |
| FA | 69.4 | 66.1 | 71.6 | 73.0 | 43.4 | 43.8 |

89 1, YGD362
90 3 rim, YGD362
91 5, YGD362
92 5 rim, YGD362
93 4, 186224
94 5, 186224

## Olivines in syenites

| | 95 | 96 | 97 | 98 | 99 | 100 | 101 | 102 |
|---|---|---|---|---|---|---|---|---|
| SiO2 | 30.46 | 29.50 | 30.38 | 29.83 | 30.14 | 29.84 | 29.77 | 30.24 |
| Al2O3 | 0.01 | 0.03 | 0.02 | 0.02 | 0.06 | 0.03 | 0.05 | 0.04 |
| FeO | 62.23 | 62.93 | 61.33 | 62.01 | 64.72 | 65.57 | 65.72 | 63.88 |
| MnO | 1.94 | 2.00 | 1.78 | 2.14 | 2.23 | 2.22 | 2.36 | 2.12 |
| MgO | 4.42 | 3.68 | 5.57 | 4.10 | 2.04 | 1.73 | 1.37 | 2.43 |
| CaO | 0.98 | 0.92 | 0.86 | 0.73 | 0.23 | 0.39 | 0.44 | 0.45 |
| total= | 100.04 | 99.06 | 99.94 | 98.83 | 99.42 | 99.78 | 99.71 | 99.16 |
| Si | 1.00 | 0.98 | 0.99 | 0.99 | 1.01 | 1.00 | 1.00 | 1.01 |
| Fe2 | 1.70 | 1.76 | 1.67 | 1.72 | 1.81 | 1.84 | 1.85 | 1.78 |
| Mn | 0.05 | 0.06 | 0.05 | 0.06 | 0.06 | 0.06 | 0.07 | 0.06 |
| Mg | 0.22 | 0.18 | 0.27 | 0.20 | 0.10 | 0.09 | 0.07 | 0.12 |
| Ca | 0.03 | 0.03 | 0.03 | 0.03 | - | 0.01 | 0.02 | 0.02 |
| total= | 3.00 | 3.01 | 3.01 | 3.01 | 2.99 | 3.00 | 3.00 | 2.99 |
| oxygens= | [4] | [4] | [4] | [4] | [4] | [4] | [4] | [4] |
| FO | 10.9 | 9.2 | 13.6 | 10.2 | 5.1 | 4.4 | 3.5 | 6.2 |
| FA | 86.3 | 88.0 | 83.9 | 86.7 | 91.7 | 92.5 | 93.2 | 90.8 |

95 3, 216627
96 5, 216627
97 8, 216627
98 1, 40549
99 1 rim, 50218
100 2, 50218
101 3, 50218
102 6, 50218

## Olivines in anorthosite xenoliths

| | 103 | 104 | 105 | 106 | 107 | 108 | 109 | 110 |
|---|---|---|---|---|---|---|---|---|
| SiO2 | 37.67 | 37.72 | 37.86 | 37.36 | 36.97 | 33.04 | 36.27 | 36.66 |
| Al2O3 | 0.04 | 0.03 | 0.05 | 0.05 | 0.05 | 0.02 | 0.04 | 0.05 |
| FeO | 26.03 | 25.91 | 25.47 | 27.63 | 27.02 | 43.74 | 28.75 | 28.58 |
| MnO | 0.35 | 0.35 | 0.30 | 0.35 | 0.33 | 0.82 | 0.41 | 0.42 |
| MgO | 36.28 | 36.28 | 36.74 | 34.06 | 34.65 | 21.11 | 33.57 | 33.85 |
| CaO | 0.18 | 0.12 | 0.25 | 0.30 | 0.29 | 0.54 | 0.45 | 0.27 |
| total= | 100.55 | 100.41 | 100.67 | 99.75 | 99.31 | 99.27 | 99.49 | 99.83 |
| Si | 0.99 | 0.99 | 0.99 | 1.00 | 0.99 | 0.98 | 0.98 | 0.99 |
| Fe2 | 0.57 | 0.57 | 0.56 | 0.62 | 0.61 | 1.08 | 0.65 | 0.64 |
| Mn | - | - | - | - | - | 0.02 | - | - |
| Mg | 1.43 | 1.43 | 1.44 | 1.36 | 1.39 | 0.93 | 1.36 | 1.36 |
| Ca | - | - | - | - | - | 0.02 | 0.01 | - |
| total= | 3.01 | 3.00 | 3.01 | 3.00 | 3.01 | 3.02 | 3.02 | 3.01 |
| oxygens= | [4] | [4] | [4] | [4] | [4] | [4] | [4] | [4] |
| FO | 71.0 | 71.1 | 71.8 | 68.4 | 69.3 | 45.8 | 67.2 | 67.5 |
| FA | 28.6 | 28.5 | 27.9 | 31.2 | 30.3 | 53.2 | 32.3 | 32.0 |

103 1, 50220
104 1 rim, 50220
105 6, 50220
106 1, YGD218
107 4, YGD218
108 1, YGD340
109 1, YGD343
110 4, YGD343

## Zoned olivines (analysed on Camebax)

| | 1 | 2 | 3 | 4 | 5 | 6 | 7 | 8 |
|---|---|---|---|---|---|---|---|---|
| SiO2 | 36.49 | 36.37 | 36.50 | 36.49 | 36.66 | 36.63 | 36.59 | 36.29 |
| TiO2 | 0.04 | 0.05 | 0.06 | 0.06 | 0.05 | 0.06 | 0.07 | 0.03 |
| Al2O3 | 0.04 | 0.06 | 0.05 | 0.07 | 0.05 | 0.04 | 0.03 | 0.06 |
| Cr2O3 | 0.50 | 0.50 | 0.50 | 0.54 | 0.50 | 0.50 | 0.54 | 0.53 |
| FeO | 31.41 | 31.59 | 31.19 | 31.63 | 31.78 | 32.03 | 32.48 | 32.58 |
| MnO | 0.03 | nd | nd | 0.02 | 0.00 | 0.02 | 0.01 | 0.04 |
| NiO | 0.00 | 0.02 | 0.03 | nd | 0.01 | 0.02 | 0.05 | 0.00 |
| MgO | 31.56 | 31.89 | 31.80 | 31.66 | 31.44 | 31.14 | 30.80 | 30.52 |
| CaO | 0.27 | 0.26 | 0.27 | 0.28 | 0.28 | 0.27 | 0.28 | 0.31 |
| Na2O | 0.00 | nd | 0.02 | 0.03 | 0.04 | nd | 0.02 | 0.02 |
| K2O | nd | 0.01 | 0.01 | 0.00 | nd | 0.02 | 0.00 | 0.01 |
| total= | 100.35 | 100.74 | 100.41 | 100.79 | 100.80 | 100.72 | 100.88 | 100.40 |
| Si | 0.99 | 0.98 | 0.99 | 0.99 | 0.99 | 0.99 | 0.99 | 0.99 |
| Cr | 0.01 | 0.01 | 0.01 | 0.01 | 0.01 | 0.01 | 0.01 | 0.01 |
| Fe2 | 0.71 | 0.72 | 0.71 | 0.72 | 0.72 | 0.73 | 0.74 | 0.74 |
| Mg | 1.28 | 1.29 | 1.28 | 1.28 | 1.27 | 1.26 | 1.25 | 1.24 |
| total= | 3.00 | 3.01 | 3.00 | 3.01 | 3.00 | 3.00 | 3.00 | 3.00 |
| oxygens= | [4] | [4] | [4] | [4] | [4] | [4] | [4] | [4] |
| FO | 64.14 | 64.28 | 64.50 | 64.06 | 63.80 | 63.40 | 62.82 | 62.52 |
| FA | 35.82 | 35.72 | 35.50 | 35.91 | 36.19 | 36.58 | 37.17 | 37.44 |

1 LG OL, 40559, centre
2 LG OL, 40559
3 LG OL, 40559
4 LG OL, 40559
5 LG OL, 40559
6 LG OL, 40559
7 LG OL, 40559
8 LG OL, 40559

| | 9 | 10 | 11 | 12 | 13 | 14 | 15 | 16 |
|---|---|---|---|---|---|---|---|---|
| SiO2 | 36.09 | 35.87 | 36.26 | 35.97 | 35.95 | 37.28 | 37.23 | 36.88 |
| TiO2 | 0.08 | 0.02 | 0.05 | 0.06 | 0.06 | 0.05 | 0.05 | 0.03 |
| Al2O3 | 0.05 | 0.05 | 0.03 | 0.03 | 0.04 | 0.05 | 0.06 | 0.06 |
| Cr2O3 | 0.51 | 0.53 | 0.52 | 0.57 | 0.59 | 0.41 | 0.42 | 0.49 |
| FeO | 32.80 | 33.56 | 33.35 | 33.85 | 34.07 | 28.47 | 29.27 | 30.51 |
| MnO | 0.01 | 0.01 | 0.01 | 0.01 | nd | 0.01 | 0.03 | nd |
| NiO | 0.03 | 0.03 | 0.00 | 0.00 | 0.05 | 0.04 | 0.03 | 0.02 |
| MgO | 30.02 | 30.33 | 30.04 | 29.85 | 29.16 | 34.22 | 33.40 | 32.28 |
| CaO | 0.37 | 0.31 | 0.34 | 0.35 | 0.36 | 0.28 | 0.30 | 0.30 |
| Na2O | 0.01 | 0.02 | 0.01 | 0.02 | 0.01 | 0.00 | 0.02 | 0.02 |
| K2O | 0.00 | 0.00 | nd | 0.00 | 0.01 | 0.01 | 0.01 | nd |
| total= | 99.96 | 100.73 | 100.62 | 100.73 | 100.30 | 100.82 | 100.79 | 100.60 |
| Si | 0.99 | 0.98 | 0.99 | 0.99 | 0.99 | 0.99 | 0.99 | 0.99 |
| Cr | 0.01 | 0.01 | 0.01 | 0.01 | 0.01 | - | - | 0.01 |
| Fe2 | 0.75 | 0.77 | 0.76 | 0.78 | 0.79 | 0.63 | 0.65 | 0.69 |
| Mg | 1.23 | 1.24 | 1.22 | 1.22 | 1.20 | 1.36 | 1.33 | 1.30 |
| Ca | 0.01 | - | 0.01 | 0.01 | 0.01 | - | - | - |
| total= | 3.00 | 3.01 | 3.00 | 3.01 | 3.00 | 3.00 | 3.00 | 3.00 |
| oxygens= | [4] | [4] | [4] | [4] | [4] | [4] | [4] | [4] |
| FO | 61.99 | 61.69 | 61.61 | 61.11 | 60.41 | 68.17 | 67.02 | 65.35 |
| FA | 38.00 | 38.29 | 38.38 | 38.87 | 39.59 | 31.82 | 32.95 | 34.65 |

9 LG OL, 40559
10 LG OL, 40559
11 LG OL, 40559
12 LG OL, 40559
13 LG OL, 40559, edge
14 1, YGD229, centre
15 1, YGD229
16 1, YGD229

# Zoned olivines (analysed on Camebax)

| | 17 | 18 | 19 | 20 | 21 | 22 | 23 | 24 |
|---|---|---|---|---|---|---|---|---|
| SiO2 | 36.60 | 36.41 | 36.40 | 36.40 | 36.16 | 36.01 | 35.99 | 37.04 |
| TiO2 | 0.06 | 0.07 | 0.04 | 0.06 | 0.08 | 0.09 | 0.06 | 0.03 |
| Al2O3 | 0.06 | 0.07 | 0.07 | 0.06 | 0.06 | 0.06 | 0.03 | 0.06 |
| Cr2O3 | 0.53 | 0.54 | 0.52 | 0.51 | 0.55 | 0.61 | 0.60 | 0.43 |
| FeO | 32.05 | 33.28 | 32.52 | 32.06 | 32.90 | 34.93 | 35.39 | 28.73 |
| MnO | 0.02 | 0.01 | 0.02 | 0.02 | 0.01 | nd | 0.02 | 0.01 |
| NiO | 0.01 | nd | 0.05 | 0.02 | 0.03 | 0.04 | nd | 0.01 |
| MgO | 30.87 | 29.66 | 30.08 | 30.55 | 30.20 | 28.31 | 27.84 | 34.32 |
| CaO | 0.32 | 0.35 | 0.33 | 0.34 | 0.31 | 0.37 | 0.29 | 0.27 |
| Na2O | 0.02 | 0.02 | 0.01 | 0.03 | 0.01 | 0.01 | 0.00 | 0.04 |
| K2O | nd | nd | nd | 0.01 | nd | 0.01 | 0.01 | nd |
| total= | 100.55 | 100.40 | 100.03 | 100.06 | 100.32 | 100.42 | 100.23 | 100.95 |
| Si | 0.99 | 1.00 | 1.00 | 0.99 | 0.99 | 0.99 | 1.00 | 0.99 |
| Cr | 0.01 | 0.01 | 0.01 | 0.01 | 0.01 | 0.01 | 0.01 | - |
| Fe2 | 0.73 | 0.76 | 0.74 | 0.73 | 0.75 | 0.81 | 0.82 | 0.64 |
| Mg | 1.25 | 1.21 | 1.23 | 1.24 | 1.23 | 1.17 | 1.15 | 1.36 |
| Ca | - | 0.01 | - | - | - | 0.01 | - | - |
| total= | 3.00 | 3.00 | 3.00 | 3.00 | 3.00 | 3.00 | 2.99 | 3.01 |
| oxygens= | [4] | [4] | [4] | [4] | [4] | [4] | [4] | [4] |
| FO | 63.17 | 61.36 | 62.23 | 62.93 | 62.05 | 59.09 | 58.36 | 68.04 |
| FA | 36.81 | 38.63 | 37.75 | 37.05 | 37.93 | 40.91 | 41.62 | 31.95 |

17 1, YGD229
18 1, YGD229
19 1, YGD229
20 1, YGD229
21 1, YGD229
22 1, YGD229
23 1, YGD229, edge
24 1, YGD229, centre

| | 25 | 26 | 27 | 28 | 29 | 30 | 31 | 32 |
|---|---|---|---|---|---|---|---|---|
| SiO2 | 36.80 | 36.72 | 36.76 | 36.71 | 36.59 | 35.80 | 35.96 | 35.06 |
| TiO2 | 0.06 | 0.06 | 0.05 | 0.02 | 0.04 | 0.05 | 0.06 | 0.07 |
| Al2O3 | 0.07 | 0.06 | 0.07 | 0.08 | 0.05 | 0.05 | 0.03 | 0.05 |
| Cr2O3 | 0.45 | 0.45 | 0.52 | 0.52 | 0.45 | 0.56 | 0.65 | 0.55 |
| FeO | 29.84 | 30.58 | 31.12 | 31.08 | 31.15 | 33.89 | 34.86 | 34.15 |
| MnO | 0.02 | 0.00 | 0.01 | 0.01 | 0.03 | 0.01 | 0.01 | 0.01 |
| NiO | 0.05 | 0.03 | 0.04 | 0.06 | 0.03 | 0.06 | 0.02 | 0.02 |
| MgO | 33.05 | 32.50 | 32.16 | 31.96 | 32.09 | 29.27 | 28.32 | 29.22 |
| CaO | 0.27 | 0.28 | 0.27 | 0.28 | 0.27 | 0.34 | 0.31 | 0.40 |
| Na2O | nd | nd | 0.02 | nd | 0.02 | 0.02 | 0.01 | 0.01 |
| K2O | 0.00 | nd | 0.01 | 0.00 | nd | 0.01 | 0.00 | 0.00 |
| total= | 100.60 | 100.69 | 101.01 | 100.72 | 100.73 | 100.08 | 100.24 | 99.56 |
| Si | 0.99 | 0.99 | 0.99 | 0.99 | 0.99 | 0.99 | 0.99 | 0.98 |
| Cr | - | - | 0.01 | 0.01 | - | 0.01 | 0.01 | 0.01 |
| Fe2 | 0.67 | 0.69 | 0.70 | 0.70 | 0.70 | 0.78 | 0.81 | 0.80 |
| Mg | 1.32 | 1.30 | 1.29 | 1.29 | 1.29 | 1.20 | 1.17 | 1.21 |
| Ca | - | - | - | - | - | 0.01 | - | 0.01 |
| total= | 3.00 | 3.00 | 3.00 | 3.00 | 3.01 | 3.00 | 3.00 | 3.02 |
| oxygens= | [4] | [4] | [4] | [4] | [4] | [4] | [4] | [4] |
| FO | 66.37 | 65.45 | 64.80 | 64.69 | 64.72 | 60.61 | 59.14 | 60.39 |
| FA | 33.61 | 34.55 | 35.19 | 35.30 | 35.25 | 39.38 | 40.85 | 39.59 |

25 1, YGD229
26 1, YGD229
27 1, YGD229
28 1, YGD229
29 1, YGD229
30 1, YGD229
31 1, YGD229, edge
32 3, YGD229, edge

# Zoned olivines (analysed on Camebax)

| | 33 | 34 | 35 | 36 | 37 | 38 |
|---|---|---|---|---|---|---|
| SiO2 | 35.42 | 35.39 | 35.29 | 35.18 | 34.93 | 35.30 |
| TiO2 | 0.05 | 0.05 | 0.02 | 0.05 | 0.04 | 0.04 |
| Al2O3 | 0.07 | 0.07 | 0.07 | 0.05 | 0.06 | 0.05 |
| Cr2O3 | 0.53 | 0.49 | 0.50 | 0.43 | 0.35 | 0.40 |
| FeO | 33.13 | 32.22 | 30.92 | 29.95 | 29.30 | 28.76 |
| MnO | nd | 0.02 | 0.02 | 0.02 | 0.02 | 0.02 |
| NiO | 0.01 | 0.02 | 0.04 | 0.05 | 0.06 | 0.05 |
| MgO | 30.11 | 31.08 | 31.89 | 33.11 | 34.07 | 34.57 |
| CaO | 0.36 | 0.32 | 0.29 | 0.25 | 0.28 | 0.25 |
| Na2O | 0.02 | 0.03 | nd | 0.02 | 0.01 | 0.02 |
| K2O | 0.00 | 0.01 | 0.01 | nd | 0.01 | 0.01 |
| total= | 99.70 | 99.69 | 99.04 | 99.11 | 99.13 | 99.47 |
| Si | 0.98 | 0.97 | 0.97 | 0.97 | 0.96 | 0.96 |
| Cr | 0.01 | 0.01 | 0.01 | - | - | - |
| Fe2 | 0.77 | 0.74 | 0.71 | 0.69 | 0.67 | 0.65 |
| Mg | 1.24 | 1.28 | 1.31 | 1.35 | 1.39 | 1.40 |
| Ca | 0.01 | - | - | - | - | - |
| total= | 3.01 | 3.02 | 3.02 | 3.03 | 3.04 | 3.04 |
| oxygens= | [4] | [4] | [4] | [4] | [4] | [4] |
| FO | 61.83 | 63.21 | 64.75 | 66.32 | 67.43 | 68.16 |
| FA | 38.17 | 36.77 | 35.23 | 33.67 | 32.54 | 31.82 |

33 3, YGD229
34 3, YGD229
35 3, YGD229
36 3, YGD229
37 3, YGD229
38 3, YGD229, centre

# Feldspars in chilled margins

| | 1 | 2 | 3 | 4 | 5 | 6 | 7 | 8 |
|---|---|---|---|---|---|---|---|---|
| SiO2 | 55.01 | 61.69 | 54.61 | 54.39 | 63.15 | 53.70 | 51.83 | 53.52 |
| Al2O3 | 27.98 | 23.24 | 28.15 | 28.08 | 21.73 | 27.78 | 29.60 | 28.51 |
| FeO | 0.31 | 0.23 | 0.43 | 0.23 | 0.16 | 0.26 | 0.14 | 0.11 |
| MgO | 0.07 | 0.03 | 0.04 | 0.05 | 0.01 | 0.04 | 0.02 | 0.03 |
| CaO | 10.67 | 4.81 | 10.85 | 10.64 | 3.23 | 10.94 | 13.36 | 11.92 |
| Na2O | 5.42 | 7.82 | 5.42 | 5.54 | 8.97 | 5.34 | 4.05 | 4.89 |
| K2O | 0.37 | 1.37 | 0.26 | 0.27 | 1.52 | 0.22 | 0.26 | 0.26 |
| BaO | 0.11 | 0.65 | 0.09 | 0.14 | 0.36 | 0.11 | 0.05 | 0.07 |
| total= | 99.94 | 99.84 | 99.85 | 99.34 | 99.13 | 98.39 | 99.31 | 99.31 |
| Si | 9.96 | 11.06 | 9.90 | 9.91 | 11.34 | 9.88 | 9.50 | 9.77 |
| Al | 5.97 | 4.91 | 6.02 | 6.03 | 4.60 | 6.03 | 6.40 | 6.13 |
| Fe2 | 0.05 | 0.03 | 0.07 | 0.04 | 0.02 | 0.04 | 0.02 | 0.02 |
| Mg | 0.02 | - | 0.01 | 0.01 | - | 0.01 | - | - |
| Ca | 2.07 | 0.92 | 2.11 | 2.08 | 0.62 | 2.16 | 2.62 | 2.33 |
| Na | 1.90 | 2.72 | 1.91 | 1.96 | 3.12 | 1.91 | 1.44 | 1.73 |
| K | 0.09 | 0.31 | 0.06 | 0.06 | 0.35 | 0.05 | 0.06 | 0.06 |
| Ba | - | 0.05 | - | - | 0.03 | - | - | - |
| total= | 20.05 | 20.01 | 20.07 | 20.09 | 20.09 | 20.08 | 20.05 | 20.06 |
| oxygens= | [32] | [32] | [32] | [32] | [32] | [32] | [32] | [32] |
| AN | 51.0 | 23.4 | 51.7 | 50.7 | 15.2 | 52.4 | 63.6 | 56.6 |
| AB | 46.9 | 68.7 | 46.8 | 47.8 | 76.3 | 46.3 | 34.9 | 42.0 |
| OR | 2.1 | 7.9 | 1.5 | 1.5 | 8.5 | 1.3 | 1.5 | 1.5 |

1 5, 40488 (phenocryst)
2 5 rim, 40488
3 9, 40488
4 10, 40488
5 15, 40488
6 16, 40488
7 5, YGD78
8 6, YGD364

| | 9 | 10 | 11 | 12 | 13 | 14 | 15 | 16 |
|---|---|---|---|---|---|---|---|---|
| SiO2 | 57.29 | 52.64 | 52.18 | 53.97 | 58.64 | 54.19 | 51.63 | 51.11 |
| Al2O3 | 26.01 | 29.26 | 29.36 | 29.03 | 25.28 | 28.25 | 29.33 | 29.93 |
| FeO | 0.17 | 0.10 | 0.16 | 0.22 | 0.14 | 0.12 | 0.13 | 0.18 |
| MgO | 0.01 | 0.02 | 0.03 | 0.03 | 0.03 | 0.02 | 0.02 | 0.02 |
| CaO | 8.60 | 12.26 | 12.50 | 11.42 | 6.92 | 10.79 | 12.10 | 13.31 |
| Na2O | 6.45 | 4.46 | 4.44 | 5.02 | 6.84 | 5.34 | 4.57 | 4.23 |
| K2O | 0.58 | 0.28 | 0.23 | 0.28 | 0.96 | 0.40 | 0.27 | 0.19 |
| BaO | 0.20 | 0.06 | 0.04 | 0.09 | 0.42 | 0.08 | 0.06 | 0.03 |
| total= | 99.31 | 99.08 | 98.94 | 100.06 | 99.23 | 99.19 | 98.11 | 99.00 |
| Si | 10.38 | 9.64 | 9.58 | 9.77 | 10.60 | 9.88 | 9.56 | 9.41 |
| Al | 5.55 | 6.31 | 6.35 | 6.19 | 5.39 | 6.07 | 6.40 | 6.49 |
| Fe2 | 0.03 | 0.02 | 0.02 | 0.03 | 0.02 | 0.02 | 0.02 | 0.03 |
| Ca | 1.67 | 2.40 | 2.46 | 2.21 | 1.34 | 2.11 | 2.40 | 2.63 |
| Na | 2.27 | 1.58 | 1.58 | 1.76 | 2.40 | 1.89 | 1.64 | 1.51 |
| K | 0.13 | 0.07 | 0.05 | 0.06 | 0.22 | 0.09 | 0.06 | 0.04 |
| Ba | 0.01 | - | - | - | 0.03 | - | - | - |
| total= | 20.04 | 20.03 | 20.06 | 20.05 | 20.01 | 20.07 | 20.09 | 20.12 |
| oxygens= | [32] | [32] | [32] | [32] | [32] | [32] | [32] | [32] |
| AN | 41.0 | 59.3 | 60.1 | 54.8 | 33.9 | 51.6 | 58.5 | 62.8 |
| AB | 55.7 | 39.1 | 38.6 | 43.6 | 60.6 | 46.2 | 40.0 | 36.1 |
| OR | 3.3 | 1.6 | 1.3 | 1.6 | 5.6 | 2.3 | 1.6 | 1.1 |

9 6 rim, YGD364
10 8, YGD364
11 8 rim, YGD364
12 1, YGD317
13 4, YGD317
14 1, YGD325
15 2, YGD325
16 1, YGD228

# Feldspars in chilled margins

| | 17 | 18 | 19 | 20 | 21 | 22 | 23 | 24 |
|---|---|---|---|---|---|---|---|---|
| SiO2 | 52.44 | 54.50 | 53.30 | 53.67 | 57.43 | 53.80 | 57.89 | 55.10 |
| Al2O3 | 29.47 | 28.21 | 29.07 | 28.28 | 25.59 | 29.01 | 26.84 | 28.01 |
| FeO | 0.15 | 0.32 | 0.13 | 0.15 | 0.38 | 0.25 | 0.28 | 0.27 |
| MgO | 0.03 | 0.04 | 0.02 | 0.02 | 0.07 | 0.01 | nd | 0.03 |
| CaO | 12.72 | 11.11 | 12.30 | 11.57 | 8.46 | 11.62 | 8.98 | 10.63 |
| Na2O | 4.48 | 5.33 | 4.75 | 5.24 | 6.70 | 4.75 | 6.19 | 5.30 |
| K2O | 0.19 | 0.35 | 0.32 | 0.38 | 0.69 | 0.29 | 0.43 | 0.41 |
| BaO | 0.07 | 0.09 | 0.04 | 0.05 | 0.12 | 0.09 | 0.15 | 0.09 |
| total= | 99.55 | 99.95 | 99.93 | 99.36 | 99.44 | 99.82 | 100.76 | 99.84 |
| Si | 9.57 | 9.88 | 9.68 | 9.80 | 10.41 | 9.76 | 10.32 | 9.97 |
| Al | 6.34 | 6.03 | 6.22 | 6.09 | 5.47 | 6.20 | 5.64 | 5.97 |
| Fe2 | 0.02 | 0.05 | 0.02 | 0.02 | 0.06 | 0.04 | 0.04 | 0.04 |
| Mg | - | 0.01 | - | - | 0.02 | - | - | - |
| Ca | 2.49 | 2.16 | 2.39 | 2.26 | 1.64 | 2.26 | 1.72 | 2.06 |
| Na | 1.59 | 1.87 | 1.67 | 1.86 | 2.35 | 1.67 | 2.14 | 1.86 |
| K | 0.04 | 0.08 | 0.07 | 0.09 | 0.16 | 0.07 | 0.10 | 0.09 |
| Ba | - | - | - | - | - | - | 0.01 | - |
| total= | 20.07 | 20.08 | 20.08 | 20.13 | 20.12 | 20.01 | 19.97 | 20.02 |
| oxygens= | [32] | [32] | [32] | [32] | [32] | [32] | [32] | [32] |
| AN | 60.4 | 52.5 | 57.8 | 53.8 | 39.5 | 56.5 | 43.4 | 51.3 |
| AB | 38.5 | 45.6 | 40.4 | 44.1 | 56.6 | 41.8 | 54.1 | 46.3 |
| OR | 1.1 | 2.0 | 1.8 | 2.1 | 3.8 | 1.7 | 2.5 | 2.4 |

17 3, YGD228
18 5, YGD228
19 2, YGD328
20 3, YGD328
21 3 rim, YGD328
22 2, YGD1
23 2 rim, YGD1
24 5, YGD1 (phenocryst)

| | 25 | 26 | 27 | 28 | 29 | 30 | 31 | 32 |
|---|---|---|---|---|---|---|---|---|
| SiO2 | 53.65 | 54.68 | 53.72 | 53.84 | 52.09 | 55.55 | 61.87 | 53.58 |
| Al2O3 | 28.78 | 28.21 | 29.27 | 28.76 | 29.78 | 27.38 | 22.39 | 28.44 |
| FeO | 0.15 | 0.27 | 0.19 | 0.16 | 0.12 | 0.40 | 0.25 | 0.16 |
| MgO | 0.01 | 0.04 | 0.02 | 0.03 | 0.02 | 0.06 | 0.03 | 0.02 |
| CaO | 11.83 | 10.94 | 11.68 | 11.71 | 12.52 | 9.75 | 3.93 | 11.49 |
| Na2O | 4.67 | 5.11 | 4.70 | 4.85 | 4.30 | 5.86 | 7.73 | 4.98 |
| K2O | 0.27 | 0.43 | 0.30 | 0.24 | 0.19 | 0.27 | 1.85 | 0.30 |
| BaO | 0.09 | 0.06 | 0.09 | 0.14 | 0.08 | 0.10 | 1.34 | 0.06 |
| total= | 99.45 | 99.74 | 99.97 | 99.73 | 99.10 | 99.37 | 99.39 | 99.03 |
| Si | 9.77 | 9.91 | 9.73 | 9.78 | 9.54 | 10.08 | 11.19 | 9.80 |
| Al | 6.18 | 6.03 | 6.25 | 6.16 | 6.43 | 5.86 | 4.77 | 6.13 |
| Fe2 | 0.02 | 0.04 | 0.03 | 0.02 | 0.02 | 0.06 | 0.04 | 0.02 |
| Mg | - | 0.01 | - | - | - | 0.02 | - | - |
| Ca | 2.31 | 2.13 | 2.27 | 2.28 | 2.46 | 1.90 | 0.76 | 2.25 |
| Na | 1.65 | 1.80 | 1.65 | 1.71 | 1.53 | 2.06 | 2.71 | 1.77 |
| K | 0.06 | 0.10 | 0.07 | 0.06 | 0.04 | 0.06 | 0.43 | 0.07 |
| Ba | - | - | - | - | - | - | 0.09 | - |
| total= | 20.00 | 20.02 | 20.01 | 20.02 | 20.03 | 20.05 | 20.00 | 20.05 |
| oxygens= | [32] | [32] | [32] | [32] | [32] | [32] | [32] | [32] |
| AN | 57.4 | 52.9 | 56.9 | 56.4 | 61.0 | 47.2 | 19.5 | 55.1 |
| AB | 41.0 | 44.7 | 41.4 | 42.3 | 37.9 | 51.3 | 69.5 | 43.2 |
| OR | 1.6 | 2.5 | 1.7 | 1.4 | 1.1 | 1.6 | 10.9 | 1.7 |

25 5 rim, YGD1
26 6, YGD1 (phenocryst)
27 6 rim, YGD1
28 8, YGD1
29 2, YGD259
30 2 rim, YGD259
31 7, YGD259
32 1, YGD292

## Feldspars in chilled margins

| | 33 | 34 | 35 | 36 | 37 | 38 | 39 | 40 |
|---|---|---|---|---|---|---|---|---|
| SiO2 | 53.01 | 53.30 | 62.78 | 53.27 | 52.12 | 52.91 | 53.52 | 60.16 |
| Al2O3 | 28.98 | 28.18 | 21.99 | 28.72 | 28.93 | 29.29 | 28.16 | 24.13 |
| FeO | 0.17 | 0.15 | 0.22 | 0.44 | 0.24 | 0.25 | 0.24 | 0.21 |
| MgO | 0.02 | 0.03 | 0.02 | 0.16 | 0.03 | 0.03 | 0.03 | 0.02 |
| CaO | 12.31 | 12.04 | 3.73 | 12.16 | 12.18 | 11.77 | 11.08 | 5.94 |
| Na2O | 4.70 | 4.78 | 7.60 | 4.59 | 4.41 | 4.59 | 5.09 | 7.25 |
| K2O | 0.21 | 0.31 | 2.84 | 0.24 | 0.36 | 0.37 | 0.37 | 1.40 |
| BaO | 0.05 | 0.12 | 1.23 | 0.07 | 0.02 | 0.09 | 0.06 | 0.42 |
| total= | 99.45 | 98.91 | 100.41 | 99.65 | 98.29 | 99.30 | 98.55 | 99.53 |
| Si | 9.68 | 9.78 | 11.27 | 9.71 | 9.63 | 9.66 | 9.84 | 10.84 |
| Al | 6.23 | 6.10 | 4.65 | 6.17 | 6.30 | 6.31 | 6.10 | 5.12 |
| Fe2 | 0.03 | 0.02 | 0.03 | 0.07 | 0.04 | 0.04 | 0.04 | 0.03 |
| Mg | - | - | - | 0.04 | - | - | - | - |
| Ca | 2.41 | 2.37 | 0.72 | 2.37 | 2.41 | 2.30 | 2.18 | 1.15 |
| Na | 1.66 | 1.70 | 2.64 | 1.62 | 1.58 | 1.63 | 1.81 | 2.53 |
| K | 0.05 | 0.07 | 0.65 | 0.06 | 0.08 | 0.09 | 0.09 | 0.32 |
| Ba | - | - | 0.09 | - | - | - | - | 0.03 |
| total= | 20.06 | 20.06 | 20.05 | 20.05 | 20.05 | 20.04 | 20.07 | 20.03 |
| oxygens= | [32] | [32] | [32] | [32] | [32] | [32] | [32] | [32] |
| AN | 58.4 | 57.2 | 17.9 | 58.6 | 59.2 | 57.4 | 53.4 | 28.7 |
| AB | 40.4 | 41.1 | 65.9 | 40.0 | 38.8 | 40.5 | 44.4 | 63.3 |
| OR | 1.2 | 1.8 | 16.2 | 1.4 | 2.1 | 2.1 | 2.1 | 8.0 |

33 1 rim, YGD292
34 4, YGD292
35 4 rim, YGD292
36 7, YGD292
37 2, 30736
38 2, 101211
39 3, 101211
40 3 rim, 101211

## Feldspars in troctolites

| | 41 | 42 | 43 | 44 | 45 | 46 | 47 | 48 |
|---|---|---|---|---|---|---|---|---|
| SiO2 | 56.40 | 57.77 | 53.94 | 51.80 | 55.35 | 51.20 | 52.57 | 54.12 |
| Al2O3 | 27.65 | 26.65 | 28.51 | 30.03 | 27.81 | 29.69 | 29.81 | 28.18 |
| FeO | 0.13 | 0.13 | 0.12 | 0.16 | 0.17 | 0.16 | 0.18 | 0.15 |
| MgO | 0.04 | 0.03 | 0.03 | 0.02 | 0.02 | 0.02 | 0.03 | 0.02 |
| CaO | 9.74 | 8.64 | 10.92 | 12.42 | 9.81 | 12.86 | 12.47 | 10.67 |
| Na2O | 5.76 | 6.46 | 5.11 | 4.40 | 5.82 | 4.00 | 4.40 | 5.26 |
| K2O | 0.51 | 0.60 | 0.39 | 0.27 | 0.46 | 0.27 | 0.26 | 0.38 |
| BaO | 0.11 | 0.16 | 0.10 | 0.07 | 0.11 | 0.08 | 0.06 | 0.08 |
| total= | 100.34 | 100.44 | 99.12 | 99.17 | 99.55 | 98.28 | 99.78 | 98.86 |
| Si | 10.13 | 10.34 | 9.84 | 9.49 | 10.03 | 9.48 | 9.57 | 9.90 |
| Al | 5.85 | 5.62 | 6.13 | 6.49 | 5.94 | 6.48 | 6.39 | 6.07 |
| Fe2 | 0.02 | 0.02 | 0.02 | 0.02 | 0.03 | 0.02 | 0.03 | 0.02 |
| Mg | 0.01 | - | - | - | - | - | - | - |
| Ca | 1.87 | 1.66 | 2.13 | 2.44 | 1.91 | 2.55 | 2.43 | 2.09 |
| Na | 2.01 | 2.24 | 1.81 | 1.56 | 2.05 | 1.44 | 1.55 | 1.86 |
| K | 0.12 | 0.14 | 0.09 | 0.06 | 0.11 | 0.06 | 0.06 | 0.09 |
| Ba | - | 0.01 | - | - | - | - | - | - |
| total= | 20.01 | 20.04 | 20.04 | 20.08 | 20.07 | 20.04 | 20.04 | 20.05 |
| oxygens= | [32] | [32] | [32] | [32] | [32] | [32] | [32] | [32] |
| AN | 46.9 | 41.1 | 52.9 | 60.0 | 47.0 | 63.0 | 60.1 | 51.7 |
| AB | 50.2 | 55.6 | 44.8 | 38.5 | 50.4 | 35.4 | 38.4 | 46.1 |
| OR | 2.9 | 3.4 | 2.3 | 1.6 | 2.6 | 1.6 | 1.5 | 2.2 |

41 6, 30638
42 6 rim, 30638
43 8, 30638
44 9, YGD36
45 10, YGD36
46 2, YGD54
47 3, YGD54
48 3 rim, YGD54

# Feldspars in troctolites

| | 49 | 50 | 51 | 52 | 53 | 54 | 55 | 56 |
|---|---|---|---|---|---|---|---|---|
| SiO2 | 54.91 | 53.02 | 55.66 | 53.03 | 54.58 | 57.64 | 66.87 | 51.92 |
| TiO2 | nd | nd | nd | nd | nd | nd | 0.02 | nd |
| Al2O3 | 28.04 | 29.00 | 27.48 | 29.51 | 28.14 | 26.35 | 19.94 | 29.93 |
| FeO | 0.22 | 0.18 | 0.21 | 0.28 | 0.29 | 0.27 | 0.47 | 0.15 |
| MnO | nd | nd | nd | nd | nd | nd | 0.02 | nd |
| MgO | 0.04 | 0.04 | 0.03 | 0.04 | 0.03 | 0.02 | 0.02 | 0.02 |
| CaO | 10.40 | 12.08 | 10.18 | 12.29 | 10.86 | 8.49 | 0.72 | 12.80 |
| Na2O | 5.44 | 4.60 | 5.47 | 4.53 | 5.28 | 6.48 | 11.28 | 4.23 |
| K2O | 0.41 | 0.35 | 0.50 | 0.30 | 0.54 | 0.68 | 0.12 | 0.31 |
| BaO | 0.10 | 0.07 | 0.13 | 0.12 | 0.07 | 0.21 | nd | 0.05 |
| total= | 99.56 | 99.34 | 99.66 | 100.10 | 99.79 | 100.14 | 99.46 | 99.41 |
| Si | 9.96 | 9.69 | 10.08 | 9.62 | 9.91 | 10.36 | 11.81 | 9.50 |
| Al | 6.00 | 6.24 | 5.87 | 6.31 | 6.02 | 5.58 | 4.15 | 6.45 |
| Fe2 | 0.03 | 0.03 | 0.03 | 0.04 | 0.04 | 0.04 | 0.07 | 0.02 |
| Mg | 0.01 | 0.01 | - | 0.01 | - | - | - | - |
| Ca | 2.02 | 2.36 | 1.98 | 2.39 | 2.11 | 1.64 | 0.14 | 2.51 |
| Na | 1.91 | 1.63 | 1.92 | 1.59 | 1.86 | 2.26 | 3.86 | 1.50 |
| K | 0.09 | 0.08 | 0.12 | 0.07 | 0.13 | 0.16 | 0.03 | 0.07 |
| Ba | - | - | - | - | - | 0.01 | - | - |
| total= | 20.04 | 20.05 | 20.01 | 20.05 | 20.08 | 20.05 | 20.06 | 20.06 |
| oxygens= | [32] | [32] | [32] | [32] | [32] | [32] | [32] | [32] |
| AN | 50.2 | 58.0 | 49.2 | 59.0 | 51.6 | 40.4 | 3.4 | 61.5 |
| AB | 47.5 | 40.0 | 47.9 | 39.3 | 45.4 | 55.8 | 95.9 | 36.8 |
| OR | 2.4 | 2.0 | 2.9 | 1.7 | 3.1 | 3.8 | 0.7 | 1.8 |

49 6, YGD54
50 2, YGD12
51 3, YGD12
52 1, YGD34
53 2, YGD34
54 3, YGD34
55 Turbid interstitial feldspar, YGD34
56 2, YGD293

| | 57 | 58 | 59 | 60 | 61 | 62 | 63 | 64 |
|---|---|---|---|---|---|---|---|---|
| SiO2 | 54.62 | 53.57 | 59.60 | 51.80 | 60.03 | 55.24 | 55.20 | 53.60 |
| Al2O3 | 28.34 | 28.43 | 24.49 | 29.35 | 23.26 | 27.58 | 27.52 | 28.82 |
| FeO | 0.14 | 0.10 | 0.14 | 0.22 | 0.25 | 0.34 | 0.20 | 0.22 |
| MgO | 0.01 | nd | nd | 0.02 | 0.02 | 0.04 | 0.03 | 0.03 |
| CaO | 10.84 | 11.28 | 6.37 | 12.65 | 4.81 | 9.86 | 9.37 | 11.33 |
| Na2O | 5.37 | 4.96 | 7.42 | 4.24 | 7.35 | 5.36 | 5.69 | 4.68 |
| K2O | 0.22 | 0.36 | 0.78 | 0.22 | 1.93 | 0.79 | 0.64 | 0.48 |
| BaO | 0.08 | 0.03 | 0.34 | 0.08 | 0.91 | 0.12 | 0.12 | 0.11 |
| total= | 99.62 | 98.73 | 99.14 | 98.58 | 98.56 | 99.33 | 98.77 | 99.27 |
| Si | 9.90 | 9.82 | 10.76 | 9.55 | 10.96 | 10.05 | 10.08 | 9.78 |
| Al | 6.06 | 6.14 | 5.21 | 6.38 | 5.00 | 5.91 | 5.92 | 6.20 |
| Fe2 | 0.02 | 0.02 | 0.02 | 0.03 | 0.04 | 0.05 | 0.03 | 0.03 |
| Mg | - | - | - | - | - | 0.01 | - | - |
| Ca | 2.11 | 2.21 | 1.23 | 2.50 | 0.94 | 1.92 | 1.83 | 2.21 |
| Na | 1.89 | 1.76 | 2.60 | 1.52 | 2.60 | 1.89 | 2.01 | 1.66 |
| K | 0.05 | 0.08 | 0.18 | 0.05 | 0.45 | 0.18 | 0.15 | 0.11 |
| Ba | - | - | 0.02 | - | 0.07 | - | - | - |
| total= | 20.04 | 20.04 | 20.02 | 20.04 | 20.06 | 20.03 | 20.04 | 20.01 |
| oxygens= | [32] | [32] | [32] | [32] | [32] | [32] | [32] | [32] |
| AN | 52.1 | 54.5 | 30.7 | 61.5 | 23.6 | 48.1 | 45.9 | 55.6 |
| AB | 46.7 | 43.4 | 64.8 | 37.3 | 65.2 | 47.3 | 50.4 | 41.6 |
| OR | 1.3 | 2.1 | 4.5 | 1.3 | 11.3 | 4.6 | 3.7 | 2.8 |

57 2 rim, YGD293
58 3, YGD293
59 3 rim, YGD293
60 2, YGD289
61 2 rim, YGD289
62 3, YGD138
63 3 rim, YGD138
64 6, YGD138

# Feldspars in troctolites

| | 65 | 66 | 67 | 68 | 69 | 70 | 71 | 72 |
|---|---|---|---|---|---|---|---|---|
| SiO2 | 54.11 | 56.68 | 52.27 | 53.79 | 59.21 | 52.13 | 52.24 | 54.04 |
| Al2O3 | 28.27 | 26.30 | 30.16 | 28.71 | 24.53 | 29.80 | 30.06 | 28.58 |
| FeO | 0.21 | 0.20 | 0.15 | 0.11 | 0.20 | 0.14 | 0.10 | 0.13 |
| MgO | 0.04 | 0.03 | 0.03 | 0.04 | 0.03 | 0.05 | 0.04 | 0.03 |
| CaO | 10.60 | 8.43 | 12.43 | 10.89 | 6.42 | 12.52 | 12.54 | 10.76 |
| Na2O | 5.05 | 6.08 | 4.47 | 5.34 | 7.16 | 4.39 | 4.59 | 5.49 |
| K2O | 0.50 | 0.96 | 0.32 | 0.45 | 1.51 | 0.27 | 0.26 | 0.36 |
| BaO | 0.10 | 0.18 | 0.07 | 0.10 | 0.36 | 0.06 | 0.05 | 0.13 |
| total= | 98.88 | 98.86 | 99.90 | 99.43 | 99.42 | 99.36 | 99.88 | 99.52 |
| Si | 9.89 | 10.32 | 9.51 | 9.80 | 10.71 | 9.53 | 9.51 | 9.83 |
| Al | 6.09 | 5.65 | 6.47 | 6.16 | 5.23 | 6.42 | 6.45 | 6.13 |
| Fe2 | 0.03 | 0.03 | 0.02 | 0.02 | 0.03 | 0.02 | 0.02 | 0.02 |
| Mg | 0.01 | - | - | 0.01 | - | 0.01 | 0.01 | - |
| Ca | 2.08 | 1.65 | 2.42 | 2.13 | 1.24 | 2.45 | 2.45 | 2.10 |
| Na | 1.79 | 2.15 | 1.58 | 1.89 | 2.51 | 1.56 | 1.62 | 1.94 |
| K | 0.12 | 0.22 | 0.07 | 0.10 | 0.35 | 0.06 | 0.06 | 0.08 |
| Ba | - | 0.01 | - | - | 0.03 | - | - | - |
| total= | 20.02 | 20.04 | 20.08 | 20.11 | 20.11 | 20.07 | 20.11 | 20.11 |
| oxygens= | [32] | [32] | [32] | [32] | [32] | [32] | [32] | [32] |
| AN | 52.1 | 41.0 | 59.5 | 51.6 | 30.3 | 60.2 | 59.3 | 50.9 |
| AB | 44.9 | 53.5 | 38.7 | 45.8 | 61.2 | 38.2 | 39.3 | 47.0 |
| OR | 2.9 | 5.6 | 1.8 | 2.5 | 8.5 | 1.5 | 1.5 | 2.0 |

65 6 rim, YGD138
66 7, YGD138
67 1, YGD423
68 1 nearer rim, YGD423
69 1 rim, YGD423
70 3, YGD423
71 3, YGD426
72 3 rim, YGD426

| | 73 | 74 | 75 | 76 | 77 | 78 | 79 | 80 |
|---|---|---|---|---|---|---|---|---|
| SiO2 | 54.15 | 55.95 | 60.56 | 51.40 | 54.16 | 60.08 | 54.47 | 56.46 |
| Al2O3 | 28.87 | 27.16 | 22.33 | 29.29 | 28.75 | 24.76 | 28.72 | 27.53 |
| FeO | 0.14 | 0.31 | 0.12 | 0.21 | 0.15 | 0.20 | 0.12 | 0.17 |
| MgO | 0.04 | 0.04 | 0.03 | 0.03 | 0.02 | 0.03 | 0.02 | 0.01 |
| CaO | 11.08 | 9.13 | 3.88 | 12.48 | 11.51 | 6.38 | 10.88 | 9.31 |
| Na2O | 5.31 | 6.33 | 5.57 | 4.33 | 4.92 | 7.42 | 5.18 | 6.02 |
| K2O | 0.31 | 0.37 | 5.76 | 0.43 | 0.36 | 0.80 | 0.47 | 0.62 |
| BaO | 0.11 | 0.16 | 0.78 | 0.05 | 0.07 | 0.29 | 0.09 | 0.11 |
| total= | 100.01 | 99.45 | 99.03 | 98.22 | 99.94 | 99.96 | 99.95 | 100.23 |
| Si | 9.80 | 10.15 | 11.12 | 9.53 | 9.81 | 10.75 | 9.86 | 10.15 |
| Al | 6.16 | 5.81 | 4.83 | 6.40 | 6.14 | 5.22 | 6.12 | 5.83 |
| Fe2 | 0.02 | 0.05 | 0.02 | 0.03 | 0.02 | 0.03 | 0.02 | 0.03 |
| Mg | 0.01 | 0.01 | - | - | - | - | - | - |
| Ca | 2.15 | 1.77 | 0.76 | 2.48 | 2.23 | 1.22 | 2.11 | 1.79 |
| Na | 1.86 | 2.23 | 1.98 | 1.56 | 1.73 | 2.57 | 1.82 | 2.10 |
| K | 0.07 | 0.09 | 1.35 | 0.10 | 0.08 | 0.18 | 0.11 | 0.14 |
| Ba | - | 0.01 | 0.06 | - | - | 0.02 | - | - |
| total= | 20.09 | 20.11 | 20.13 | 20.10 | 20.03 | 20.01 | 20.04 | 20.05 |
| oxygens= | [32] | [32] | [32] | [32] | [32] | [32] | [32] | [32] |
| AN | 52.6 | 43.4 | 18.6 | 59.9 | 55.2 | 30.7 | 52.3 | 44.5 |
| AB | 45.6 | 54.5 | 48.4 | 37.6 | 42.7 | 64.7 | 45.0 | 52.0 |
| OR | 1.8 | 2.1 | 32.9 | 2.5 | 2.1 | 4.6 | 2.7 | 3.5 |

73 4, YGD426
74 4 rim, YGD426
75 5, YGD426
76 4, YGD365
77 7, YGD365
78 7 rim, YGD365
79 2, YGD80
80 2 rim, YGD80

# Feldspars in troctolites

| | 81 | 82 | 83 | 84 | 85 | 86 | 87 | 88 |
|---|---|---|---|---|---|---|---|---|
| SiO2 | 54.37 | 53.25 | 51.98 | 51.30 | 51.69 | 57.91 | 51.27 | 63.55 |
| Al2O3 | 29.14 | 29.92 | 29.60 | 30.18 | 29.68 | 25.54 | 30.33 | 19.38 |
| FeO | 0.12 | 0.13 | 0.12 | 0.14 | 0.13 | 0.36 | 0.21 | 0.02 |
| MgO | 0.02 | 0.01 | 0.01 | 0.02 | 0.02 | 0.05 | 0.02 | 0.02 |
| CaO | 10.91 | 12.31 | 12.64 | 13.05 | 12.59 | 7.51 | 13.10 | 0.10 |
| Na2O | 5.20 | 4.70 | 4.26 | 4.09 | 4.27 | 6.80 | 3.89 | 0.91 |
| K2O | 0.35 | 0.20 | 0.33 | 0.31 | 0.31 | 0.75 | 0.29 | 15.44 |
| BaO | 0.09 | 0.06 | 0.05 | 0.05 | 0.08 | 0.23 | 0.03 | 0.44 |
| total= | 100.20 | 100.58 | 98.99 | 99.14 | 98.77 | 99.15 | 99.14 | 99.86 |
| Si | 9.81 | 9.60 | 9.54 | 9.42 | 9.51 | 10.50 | 9.41 | 11.79 |
| Al | 6.20 | 6.36 | 6.40 | 6.53 | 6.44 | 5.46 | 6.56 | 4.24 |
| Fe2 | 0.02 | 0.02 | 0.02 | 0.02 | 0.02 | 0.05 | 0.03 | - |
| Mg | - | - | - | - | - | 0.01 | - | - |
| Ca | 2.11 | 2.38 | 2.49 | 2.57 | 2.48 | 1.46 | 2.58 | 0.02 |
| Na | 1.82 | 1.64 | 1.52 | 1.46 | 1.52 | 2.39 | 1.38 | 0.33 |
| K | 0.08 | 0.05 | 0.08 | 0.07 | 0.07 | 0.17 | 0.07 | 3.66 |
| Ba | - | - | - | - | - | 0.02 | - | 0.03 |
| total= | 20.04 | 20.06 | 20.05 | 20.08 | 20.06 | 20.06 | 20.04 | 20.08 |
| oxygens= | [32] | [32] | [32] | [32] | [32] | [32] | [32] | [32] |
| AN | 52.6 | 58.5 | 60.9 | 62.7 | 60.9 | 36.3 | 64.0 | 0.5 |
| AB | 45.4 | 40.4 | 37.2 | 35.5 | 37.4 | 59.4 | 34.4 | 8.2 |
| OR | 2.0 | 1.1 | 1.9 | 1.8 | 1.8 | 4.3 | 1.7 | 91.3 |

81 4, YGD80
82 4 rim, YGD80
83 1, YGD392
84 1 rim, YGD392
85 2, YGD392
86 2 rim, YGD392
87 3, YGD392
88 Turbid interstitial feldspar, YGD392

| | 89 | 90 | 91 | 92 | 93 | 94 |
|---|---|---|---|---|---|---|
| SiO2 | 52.24 | 54.95 | 57.89 | 52.38 | 53.55 | 57.00 |
| Al2O3 | 29.18 | 28.05 | 25.44 | 29.57 | 29.13 | 26.33 |
| FeO | 0.20 | 0.19 | 0.36 | 0.42 | 0.22 | 0.34 |
| MgO | 0.03 | 0.02 | 0.03 | 0.06 | 0.03 | 0.04 |
| CaO | 12.02 | 10.25 | 7.62 | 12.25 | 11.50 | 8.38 |
| Na2O | 4.47 | 5.47 | 6.54 | 4.20 | 4.78 | 6.60 |
| K2O | 0.41 | 0.68 | 1.26 | 0.37 | 0.38 | 0.61 |
| BaO | 0.06 | 0.10 | 0.27 | 0.08 | 0.10 | 0.12 |
| total= | 98.61 | 99.71 | 99.41 | 99.33 | 99.69 | 99.42 |
| Si | 9.62 | 9.97 | 10.49 | 9.58 | 9.73 | 10.32 |
| Al | 6.33 | 6.00 | 5.44 | 6.37 | 6.24 | 5.62 |
| Fe2 | 0.03 | 0.03 | 0.05 | 0.06 | 0.03 | 0.05 |
| Mg | - | - | - | 0.02 | - | 0.01 |
| Ca | 2.37 | 1.99 | 1.48 | 2.40 | 2.24 | 1.63 |
| Na | 1.60 | 1.92 | 2.30 | 1.49 | 1.68 | 2.32 |
| K | 0.10 | 0.16 | 0.29 | 0.09 | 0.09 | 0.14 |
| Ba | - | - | 0.02 | - | - | - |
| total= | 20.06 | 20.08 | 20.08 | 20.02 | 20.03 | 20.10 |
| oxygens= | [32] | [32] | [32] | [32] | [32] | [32] |
| AN | 58.4 | 48.9 | 36.4 | 60.4 | 55.8 | 39.8 |
| AB | 39.3 | 47.2 | 56.5 | 37.5 | 42.0 | 56.7 |
| OR | 2.4 | 3.9 | 7.2 | 2.2 | 2.2 | 3.4 |

89 3, YGD334
90 5, YGD334
91 5 rim, YGD334
92 3, YGD195
93 3, YGD307
94 3 rim, YGD307

# Feldspars in mafic cumulates

| | 95 | 96 | 97 | 98 | 99 | 100 | 101 | 102 |
|---|---|---|---|---|---|---|---|---|
| SiO2 | 56.16 | 52.19 | 53.02 | 57.23 | 53.57 | 53.51 | 51.98 | 56.51 |
| Al2O3 | 25.95 | 28.83 | 28.51 | 26.97 | 29.20 | 28.61 | 30.24 | 27.46 |
| FeO | 0.32 | 0.16 | 0.19 | 0.33 | 0.17 | 0.42 | 0.30 | 0.25 |
| MgO | 0.03 | 0.02 | 0.03 | 0.03 | 0.03 | 0.04 | 0.03 | 0.04 |
| CaO | 8.96 | 12.47 | 12.10 | 8.81 | 11.58 | 11.66 | 12.99 | 9.50 |
| Na2O | 6.28 | 4.36 | 4.49 | 6.18 | 4.87 | 4.93 | 4.20 | 6.13 |
| K2O | 0.43 | 0.22 | 0.31 | 0.52 | 0.25 | 0.22 | 0.14 | 0.42 |
| BaO | 0.14 | 0.06 | 0.08 | 0.12 | 0.07 | 0.12 | 0.08 | 0.11 |
| total= | 98.27 | 98.31 | 98.73 | 100.19 | 99.74 | 99.51 | 99.96 | 100.42 |
| Si | 10.30 | 9.64 | 9.74 | 10.27 | 9.73 | 9.76 | 9.46 | 10.14 |
| Al | 5.61 | 6.28 | 6.17 | 5.71 | 6.25 | 6.15 | 6.49 | 5.81 |
| Fe2 | 0.05 | 0.02 | 0.03 | 0.05 | 0.03 | 0.06 | 0.05 | 0.04 |
| Mg | - | - | - | - | - | 0.01 | - | 0.01 |
| Ca | 1.76 | 2.47 | 2.38 | 1.69 | 2.25 | 2.28 | 2.53 | 1.83 |
| Na | 2.23 | 1.56 | 1.60 | 2.15 | 1.71 | 1.74 | 1.48 | 2.13 |
| K | 0.10 | 0.05 | 0.07 | 0.12 | 0.06 | 0.05 | 0.03 | 0.10 |
| Ba | 0.01 | - | - | - | - | - | - | - |
| total= | 20.07 | 20.03 | 20.01 | 20.01 | 20.04 | 20.06 | 20.05 | 20.07 |
| oxygens= | [32] | [32] | [32] | [32] | [32] | [32] | [32] | [32] |
| AN | 43.0 | 60.5 | 58.8 | 42.7 | 56.0 | 55.9 | 62.6 | 45.0 |
| AB | 54.5 | 38.3 | 39.5 | 54.3 | 42.6 | 42.8 | 36.6 | 52.6 |
| OR | 2.5 | 1.3 | 1.8 | 3.0 | 1.4 | 1.3 | 0.8 | 2.4 |

95 3, 186375
96 5, 186375
97 6, 186375
98 2, YGD36
99 4, YGD36
100 2, YGD72
101 4, YGD72
102 6, YGD72

| | 103 | 104 | 105 | 106 | 107 | 108 | 109 | 110 |
|---|---|---|---|---|---|---|---|---|
| SiO2 | 62.22 | 55.04 | 55.61 | 51.65 | 53.71 | 52.13 | 52.78 | 55.02 |
| Al2O3 | 22.64 | 28.25 | 26.87 | 30.12 | 29.07 | 29.96 | 30.43 | 28.50 |
| FeO | 0.36 | 0.13 | 0.25 | 0.14 | 0.27 | 0.15 | 0.21 | 0.28 |
| MgO | 0.02 | 0.02 | 0.04 | 0.02 | 0.02 | 0.01 | 0.01 | 0.03 |
| CaO | 4.10 | 10.99 | 9.41 | 12.90 | 11.70 | 13.03 | 12.88 | 10.92 |
| Na2O | 8.17 | 5.20 | 6.16 | 4.40 | 5.17 | 4.23 | 4.19 | 5.34 |
| K2O | 1.71 | 0.12 | 0.07 | 0.20 | 0.18 | 0.22 | 0.20 | 0.32 |
| BaO | 0.76 | 0.12 | 0.13 | 0.05 | 0.09 | 0.07 | 0.04 | 0.06 |
| total= | 99.98 | 99.87 | 98.54 | 99.48 | 100.21 | 99.80 | 100.74 | 100.47 |
| Si | 11.15 | 9.95 | 10.16 | 9.45 | 9.72 | 9.50 | 9.51 | 9.90 |
| Al | 4.78 | 6.02 | 5.79 | 6.49 | 6.20 | 6.43 | 6.46 | 6.05 |
| Fe2 | 0.05 | 0.02 | 0.04 | 0.02 | 0.04 | 0.02 | 0.03 | 0.04 |
| Mg | - | - | 0.01 | - | - | - | - | - |
| Ca | 0.79 | 2.13 | 1.84 | 2.53 | 2.27 | 2.54 | 2.49 | 2.11 |
| Na | 2.84 | 1.82 | 2.18 | 1.56 | 1.81 | 1.49 | 1.46 | 1.86 |
| K | 0.39 | 0.03 | 0.02 | 0.05 | 0.04 | 0.05 | 0.05 | 0.07 |
| Ba | 0.05 | - | - | - | - | - | - | - |
| total= | 20.07 | 19.97 | 20.05 | 20.11 | 20.10 | 20.06 | 20.01 | 20.04 |
| oxygens= | [32] | [32] | [32] | [32] | [32] | [32] | [32] | [32] |
| AN | 19.6 | 53.5 | 45.6 | 61.1 | 55.0 | 62.2 | 62.2 | 52.1 |
| AB | 70.7 | 45.8 | 54.0 | 37.7 | 44.0 | 36.5 | 36.6 | 46.1 |
| OR | 9.7 | 0.7 | 0.4 | 1.1 | 1.0 | 1.2 | 1.2 | 1.8 |

103 9, YGD72
104 2, YGD381
105 2 rim, YGD381
106 3, YGD312
107 3 rim, YGD312
108 5, YGD312
109 2, YGD49
110 6, YGD49

## Feldspars in mafic cumulates

| | 111 | 112 | 113 | 114 | 115 | 116 | 117 |
|---|---|---|---|---|---|---|---|
| SiO2 | 52.36 | 53.28 | 51.55 | 51.83 | 56.02 | 57.72 | 54.24 |
| Al2O3 | 29.79 | 28.81 | 30.18 | 30.01 | 27.50 | 26.75 | 28.83 |
| FeO | 0.20 | 0.23 | 0.15 | 0.15 | 0.07 | 0.21 | 0.14 |
| MgO | nd | 0.02 | nd | 0.01 | 0.02 | 0.04 | 0.02 |
| CaO | 12.56 | 11.43 | 13.06 | 12.84 | 9.45 | 8.54 | 10.84 |
| Na2O | 4.29 | 4.95 | 4.01 | 4.18 | 6.16 | 6.80 | 5.38 |
| K2O | 0.17 | 0.25 | 0.21 | 0.23 | 0.13 | 0.07 | 0.13 |
| BaO | 0.07 | 0.10 | 0.05 | 0.05 | 0.09 | 0.09 | 0.03 |
| total= | 99.44 | 99.07 | 99.21 | 99.30 | 99.44 | 100.22 | 99.61 |
| Si | 9.56 | 9.74 | 9.45 | 9.49 | 10.13 | 10.33 | 9.83 |
| Al | 6.41 | 6.21 | 6.52 | 6.47 | 5.86 | 5.64 | 6.16 |
| Fe2 | 0.03 | 0.04 | 0.02 | 0.02 | 0.01 | 0.03 | 0.02 |
| Mg | - | - | - | - | - | 0.01 | - |
| Ca | 2.46 | 2.24 | 2.56 | 2.52 | 1.83 | 1.64 | 2.11 |
| Na | 1.52 | 1.76 | 1.42 | 1.48 | 2.16 | 2.36 | 1.89 |
| K | 0.04 | 0.06 | 0.05 | 0.05 | 0.03 | 0.02 | 0.03 |
| total= | 20.02 | 20.06 | 20.03 | 20.04 | 20.03 | 20.04 | 20.05 |
| oxygens= | [32] | [32] | [32] | [32] | [32] | [32] | [32] |
| AN | 61.2 | 55.3 | 63.5 | 62.1 | 45.5 | 40.8 | 52.3 |
| AB | 37.8 | 43.3 | 35.3 | 36.6 | 53.7 | 58.8 | 47.0 |
| OR | 1.0 | 1.4 | 1.2 | 1.3 | 0.7 | 0.4 | 0.7 |

111 1, YGD306
112 1 rim, YGD306
113 3, YGD306
114 7, YGD255
115 3, 40411
116 3 rim, 40411
117 4, 40411

## Feldspars in syenogabbros

| | 118 | 119 | 120 | 121 | 122 | 123 | 124 | 125 |
|---|---|---|---|---|---|---|---|---|
| SiO2 | 63.00 | 62.40 | 63.30 | 66.08 | 64.56 | 62.58 | 61.49 | 64.43 |
| Al2O3 | 22.03 | 18.37 | 22.23 | 19.83 | 20.86 | 22.33 | 22.93 | 20.95 |
| FeO | 0.13 | 0.02 | 0.14 | 0.10 | 0.20 | 0.16 | 0.15 | 0.13 |
| MgO | nd | 0.02 | nd | nd | nd | 0.01 | 0.01 | 0.02 |
| CaO | 3.26 | 0.02 | 3.34 | 1.00 | 1.92 | 3.62 | 4.24 | 2.31 |
| Na2O | 8.73 | 0.86 | 8.88 | 7.07 | 7.46 | 8.38 | 7.97 | 7.99 |
| K2O | 0.90 | 15.00 | 1.07 | 5.73 | 4.28 | 1.47 | 1.55 | 3.40 |
| BaO | 1.23 | 2.41 | 1.06 | 0.90 | 1.24 | 0.51 | 0.75 | 0.34 |
| total= | 99.28 | 99.10 | 100.02 | 100.71 | 100.52 | 99.06 | 99.09 | 99.57 |
| Si | 11.32 | 11.84 | 11.30 | 11.80 | 11.56 | 11.26 | 11.10 | 11.55 |
| Al | 4.67 | 4.11 | 4.68 | 4.17 | 4.40 | 4.73 | 4.88 | 4.43 |
| Fe2 | 0.02 | - | 0.02 | 0.01 | 0.03 | 0.02 | 0.02 | 0.02 |
| Ca | 0.63 | - | 0.64 | 0.19 | 0.37 | 0.70 | 0.82 | 0.44 |
| Na | 3.04 | 0.32 | 3.07 | 2.45 | 2.59 | 2.92 | 2.79 | 2.78 |
| K | 0.21 | 3.63 | 0.24 | 1.31 | 0.98 | 0.34 | 0.36 | 0.78 |
| Ba | 0.09 | 0.18 | 0.07 | 0.06 | 0.09 | 0.04 | 0.05 | 0.02 |
| total= | 19.97 | 20.08 | 20.02 | 19.99 | 20.02 | 20.01 | 20.03 | 20.02 |
| oxygens= | [32] | [32] | [32] | [32] | [32] | [32] | [32] | [32] |
| AN | 16.2 | 0.1 | 16.1 | 4.9 | 9.4 | 17.6 | 20.7 | 11.1 |
| AB | 78.5 | 8.0 | 77.7 | 62.1 | 65.8 | 73.8 | 70.3 | 69.5 |
| OR | 5.3 | 91.9 | 6.2 | 33.1 | 24.8 | 8.5 | 9.0 | 19.4 |

118 1, 40548
119 2, 40548
120 6, 186227
121 6 rim, 186227
122 7, 186227
123 2, YGD362
124 3, YGD362
125 3 rim, YGD362

## Feldspars in syenogabbros

| | 126 | 127 | 128 | 129 | 130 | 131 | 132 | 133 |
|---|---|---|---|---|---|---|---|---|
| SiO2 | 61.11 | 64.29 | 56.10 | 59.25 | 57.48 | 61.08 | 56.68 | 63.94 |
| Al2O3 | 23.33 | 21.13 | 26.93 | 24.35 | 25.34 | 22.40 | 25.68 | 20.33 |
| FeO | 0.18 | 0.21 | 0.24 | 0.24 | 0.18 | 0.17 | 0.17 | 0.16 |
| MgO | 0.01 | 0.04 | 0.04 | 0.04 | 0.02 | 0.01 | 0.02 | 0.02 |
| CaO | 4.58 | 2.95 | 9.48 | 6.33 | 7.57 | 4.06 | 8.32 | 1.98 |
| Na2O | 7.70 | 8.51 | 5.84 | 7.57 | 6.64 | 7.72 | 6.47 | 6.59 |
| K2O | 1.41 | 2.28 | 0.51 | 0.79 | 0.72 | 1.82 | 0.48 | 5.58 |
| BaO | 0.73 | 0.22 | 0.16 | 0.39 | 0.31 | 1.22 | 0.23 | 0.38 |
| total= | 99.05 | 99.63 | 99.30 | 98.96 | 98.26 | 98.48 | 98.05 | 98.98 |
| Si | 11.04 | 11.49 | 10.18 | 10.74 | 10.51 | 11.14 | 10.39 | 11.61 |
| Al | 4.97 | 4.45 | 5.76 | 5.20 | 5.46 | 4.82 | 5.55 | 4.35 |
| Fe2 | 0.03 | 0.03 | 0.04 | 0.04 | 0.03 | 0.03 | 0.03 | 0.02 |
| Mg | - | 0.01 | 0.01 | 0.01 | - | - | - | - |
| Ca | 0.89 | 0.56 | 1.84 | 1.23 | 1.48 | 0.79 | 1.63 | 0.39 |
| Na | 2.70 | 2.95 | 2.06 | 2.66 | 2.35 | 2.73 | 2.30 | 2.32 |
| K | 0.32 | 0.52 | 0.12 | 0.18 | 0.17 | 0.42 | 0.11 | 1.29 |
| Ba | 0.05 | 0.02 | 0.01 | 0.03 | 0.02 | 0.09 | 0.02 | 0.03 |
| total= | 19.99 | 20.02 | 20.02 | 20.08 | 20.02 | 20.02 | 20.04 | 20.02 |
| oxygens= | [32] | [32] | [32] | [32] | [32] | [32] | [32] | [32] |
| AN | 22.7 | 14.0 | 45.9 | 30.2 | 37.0 | 20.1 | 40.4 | 9.6 |
| AB | 69.0 | 73.1 | 51.2 | 65.3 | 58.8 | 69.2 | 56.8 | 58.0 |
| OR | 8.3 | 12.9 | 2.9 | 4.5 | 4.2 | 10.7 | 2.8 | 32.3 |

126 5, YGD362
127 5, 186224
128 6, 186224
129 6 rim, 186224
130 4, YGD428
131 4 rim, YGD428
132 5, YGD428
133 5 rim, YGD428

## Feldspars in syenites

| | 134 | 135 | 136 | 137 | 138 | 139 | 140 | 141 |
|---|---|---|---|---|---|---|---|---|
| SiO2 | 69.34 | 68.22 | 67.47 | 66.03 | 65.48 | 64.84 | 65.59 | 65.61 |
| Al2O3 | 19.26 | 19.06 | 18.51 | 18.53 | 20.25 | 19.64 | 20.17 | 19.63 |
| FeO | 0.02 | 0.05 | 0.39 | 0.36 | 0.10 | 0.10 | nd | 0.10 |
| MgO | 0.01 | 0.01 | 0.01 | nd | 0.02 | 0.02 | 0.02 | 0.02 |
| CaO | nd | nd | nd | nd | 0.93 | 0.70 | 0.66 | 0.28 |
| Na2O | 11.70 | 11.60 | 6.51 | 4.59 | 7.88 | 7.51 | 9.54 | 6.42 |
| K2O | 0.04 | 0.07 | 7.68 | 10.35 | 4.57 | 5.42 | 2.72 | 7.33 |
| BaO | nd | nd | 0.09 | 0.06 | 0.44 | 0.49 | 0.43 | 0.50 |
| total= | 100.37 | 99.01 | 100.66 | 99.92 | 99.67 | 98.72 | 99.13 | 99.89 |
| Si | 12.05 | 12.03 | 12.04 | 11.99 | 11.73 | 11.78 | 11.74 | 11.83 |
| Al | 3.94 | 3.96 | 3.89 | 3.97 | 4.28 | 4.20 | 4.26 | 4.17 |
| Fe2 | - | - | 0.06 | 0.05 | 0.01 | 0.02 | - | 0.02 |
| Ca | - | - | - | - | 0.18 | 0.14 | 0.13 | 0.05 |
| Na | 3.94 | 3.97 | 2.25 | 1.62 | 2.74 | 2.64 | 3.31 | 2.24 |
| K | - | 0.02 | 1.75 | 2.40 | 1.04 | 1.26 | 0.62 | 1.69 |
| Ba | - | - | - | - | 0.03 | 0.03 | 0.03 | 0.04 |
| total= | 19.95 | 19.98 | 20.01 | 20.03 | 20.02 | 20.07 | 20.09 | 20.05 |
| oxygens= | [32] | [32] | [32] | [32] | [32] | [32] | [32] | [32] |
| AN | - | - | - | - | 4.5 | 3.4 | 3.1 | 1.4 |
| AB | 99.8 | 99.6 | 56.3 | 40.3 | 69.1 | 65.5 | 81.6 | 56.3 |
| OR | 0.2 | 0.4 | 43.7 | 59.7 | 26.4 | 31.1 | 15.3 | 42.3 |

134 6, YGD170
135 7, YGD170
136 2, YGD326
137 7, YGD326
138 8, YGD326
139 2, 216627
140 4, 216627 (turbid)
141 6, 216627

## Feldspars in syenites

| | 142 | 143 | 144 | 145 | 146 | 147 |
|---|---|---|---|---|---|---|
| SiO2 | 64.76 | 69.15 | 64.61 | 66.08 | 65.95 | 67.67 |
| Al2O3 | 19.91 | 18.73 | 18.02 | 18.69 | 19.16 | 19.33 |
| FeO | 0.08 | 0.47 | 0.09 | 0.21 | 0.14 | 0.40 |
| MgO | 0.02 | 0.01 | 0.03 | nd | nd | nd |
| CaO | 0.59 | nd | 0.02 | 0.20 | 0.31 | nd |
| Na2O | 7.22 | 11.89 | 0.19 | 6.75 | 6.89 | 11.95 |
| K2O | 6.07 | 0.07 | 16.61 | 7.23 | 7.03 | 0.04 |
| BaO | 0.53 | nd | 0.06 | nd | 0.04 | nd |
| total= | 99.18 | 100.32 | 99.63 | 99.16 | 99.52 | 99.39 |
| Si | 11.74 | 12.07 | 12.02 | 11.96 | 11.90 | 11.93 |
| Al | 4.25 | 3.85 | 3.95 | 3.99 | 4.07 | 4.02 |
| Fe2 | 0.01 | 0.07 | 0.01 | 0.03 | 0.02 | 0.06 |
| Ca | 0.11 | - | - | 0.04 | 0.06 | - |
| Na | 2.54 | 4.02 | 0.07 | 2.37 | 2.41 | 4.09 |
| K | 1.40 | 0.02 | 3.94 | 1.67 | 1.62 | - |
| Ba | 0.04 | - | - | - | - | - |
| total= | 20.10 | 20.03 | 20.01 | 20.06 | 20.08 | 20.11 |
| oxygens= | [32] | [32] | [32] | [32] | [32] | [32] |
| AN | 2.8 | - | 0.1 | 1.0 | 1.5 | - |
| AB | 62.6 | 99.6 | 1.7 | 58.1 | 59.0 | 99.8 |
| OR | 34.6 | 0.4 | 98.2 | 40.9 | 39.6 | 0.2 |

142 7, 216627
143 1, 40517
144 3, 40517
145 1, 50218
146 3, 50218
147 3 rim, 50218

## Feldspars in anorthosite xenoliths

| | 148 | 149 | 150 | 151 | 152 | 153 | 154 | 155 |
|---|---|---|---|---|---|---|---|---|
| SiO2 | 54.04 | 54.87 | 54.89 | 52.82 | 55.45 | 55.47 | 53.59 | 52.14 |
| Al2O3 | 28.28 | 26.69 | 27.17 | 28.60 | 27.90 | 26.80 | 28.53 | 29.29 |
| FeO | 0.36 | 0.36 | 0.39 | 0.39 | 0.31 | 0.29 | 0.23 | 0.21 |
| MgO | 0.11 | 0.10 | 0.10 | 0.07 | 0.07 | 0.07 | 0.07 | 0.02 |
| CaO | 11.36 | 10.40 | 10.66 | 12.29 | 11.10 | 9.99 | 12.05 | 12.33 |
| Na2O | 4.83 | 5.12 | 5.03 | 4.23 | 5.04 | 5.76 | 4.67 | 4.35 |
| K2O | 0.45 | 0.59 | 0.58 | 0.39 | 0.53 | 0.41 | 0.34 | 0.36 |
| BaO | 0.06 | 0.02 | 0.04 | 0.01 | 0.08 | 0.12 | 0.10 | 0.07 |
| total= | 99.49 | 98.15 | 98.86 | 98.80 | 100.48 | 98.91 | 99.58 | 98.77 |
| Si | 9.84 | 10.10 | 10.04 | 9.71 | 9.98 | 10.13 | 9.77 | 9.59 |
| Al | 6.07 | 5.79 | 5.86 | 6.19 | 5.92 | 5.77 | 6.13 | 6.35 |
| Fe2 | 0.05 | 0.06 | 0.06 | 0.06 | 0.05 | 0.04 | 0.04 | 0.03 |
| Mg | 0.03 | 0.03 | 0.03 | 0.02 | 0.02 | 0.02 | 0.02 | - |
| Ca | 2.22 | 2.05 | 2.09 | 2.42 | 2.14 | 1.95 | 2.35 | 2.43 |
| Na | 1.71 | 1.83 | 1.78 | 1.51 | 1.76 | 2.04 | 1.65 | 1.55 |
| K | 0.10 | 0.14 | 0.14 | 0.09 | 0.12 | 0.10 | 0.08 | 0.08 |
| total= | 20.03 | 19.99 | 19.99 | 20.00 | 20.00 | 20.06 | 20.04 | 20.05 |
| oxygens= | [32] | [32] | [32] | [32] | [32] | [32] | [32] | [32] |
| AN | 55.1 | 51.1 | 52.1 | 60.2 | 53.2 | 47.8 | 57.6 | 59.8 |
| AB | 42.4 | 45.5 | 44.5 | 37.5 | 43.7 | 49.9 | 40.4 | 38.2 |
| OR | 2.6 | 3.4 | 3.4 | 2.3 | 3.0 | 2.3 | 1.9 | 2.1 |

148 2, 50220
149 2 rim, 50220
150 4, 50220
151 4 rim, 50220
152 1, YGD218
153 1 rim, YGD218
154 2, YGD218
155 4, YGD340

# Feldspars in anorthosite xenoliths

| | 156 | 157 | 158 | 159 | 160 | 161 | 162 |
|---|---|---|---|---|---|---|---|
| SiO2 | 53.71 | 51.62 | 52.84 | 54.35 | 54.30 | 53.09 | 51.29 |
| Al2O3 | 28.00 | 29.87 | 28.76 | 28.01 | 27.86 | 28.67 | 30.00 |
| FeO | 0.09 | 0.20 | 0.15 | 0.27 | 0.26 | 0.25 | 0.17 |
| MgO | 0.03 | 0.03 | 0.02 | 0.03 | 0.02 | 0.03 | 0.01 |
| CaO | 10.68 | 13.24 | 11.93 | 10.84 | 10.77 | 11.68 | 13.50 |
| Na2O | 5.26 | 4.11 | 4.76 | 5.19 | 5.13 | 4.69 | 3.96 |
| K2O | 0.48 | 0.28 | 0.43 | 0.57 | 0.55 | 0.50 | 0.25 |
| BaO | 0.07 | 0.04 | 0.06 | 0.12 | 0.11 | 0.10 | 0.06 |
| total= | 98.32 | 99.39 | 98.95 | 99.38 | 99.00 | 99.01 | 99.24 |
| Si | 9.88 | 9.46 | 9.70 | 9.91 | 9.93 | 9.73 | 9.42 |
| Al | 6.07 | 6.45 | 6.22 | 6.02 | 6.00 | 6.20 | 6.49 |
| Fe2 | 0.01 | 0.03 | 0.02 | 0.04 | 0.04 | 0.04 | 0.03 |
| Ca | 2.11 | 2.60 | 2.35 | 2.12 | 2.11 | 2.29 | 2.66 |
| Na | 1.88 | 1.46 | 1.69 | 1.83 | 1.82 | 1.67 | 1.41 |
| K | 0.11 | 0.07 | 0.10 | 0.13 | 0.13 | 0.12 | 0.06 |
| total= | 20.08 | 20.08 | 20.09 | 20.07 | 20.04 | 20.06 | 20.07 |
| oxygens= | [32] | [32] | [32] | [32] | [32] | [32] | [32] |
| AN | 51.4 | 63.0 | 56.7 | 51.8 | 52.0 | 56.3 | 64.4 |
| AB | 45.8 | 35.4 | 40.9 | 44.9 | 44.8 | 40.9 | 34.2 |
| OR | 2.8 | 1.6 | 2.4 | 3.2 | 3.2 | 2.9 | 1.4 |

156 7, YGD340
157 1 rim, YGD293 (xenocryst)
158 1 between core and rim, YGD293
159 1 core, YGD293
160 1 core, YGD293
161 1 between core and rim, YGD293
162 1 rim, YGD293

## Intercumulus pyroxenes

| | 1 | 2 | 3 | 4 | 5 | 6 | 7 | 8 |
|---|---|---|---|---|---|---|---|---|
| SiO2 | 49.68 | 49.19 | 50.59 | 50.05 | 47.28 | 48.05 | 50.61 | 49.41 |
| TiO2 | 2.15 | 2.51 | 1.44 | 1.25 | 3.10 | 2.85 | 1.58 | 2.26 |
| Al2O3 | 3.01 | 3.96 | 2.21 | 1.77 | 4.98 | 4.54 | 2.54 | 3.56 |
| Cr2O3 | nd | nd | nd | nd | nd | nd | 0.03 | nd |
| FeO | 11.26 | 10.23 | 10.30 | 11.23 | 8.97 | 8.91 | 8.53 | 9.34 |
| MnO | 0.25 | 0.25 | 0.24 | 0.27 | 0.17 | 0.14 | 0.17 | 0.18 |
| MgO | 11.26 | 11.88 | 12.81 | 12.22 | 12.36 | 12.64 | 14.04 | 13.11 |
| CaO | 21.53 | 21.53 | 21.50 | 21.94 | 21.66 | 21.62 | 21.67 | 21.65 |
| Na2O | 0.72 | 0.66 | 0.56 | 0.47 | 0.70 | 0.69 | 0.68 | 0.69 |
| total= | 99.86 | 100.21 | 99.65 | 99.20 | 99.22 | 99.44 | 99.85 | 100.20 |
| Si | 1.88 | 1.85 | 1.90 | 1.90 | 1.78 | 1.81 | 1.88 | 1.84 |
| Ti | 0.06 | 0.07 | 0.04 | 0.04 | 0.09 | 0.08 | 0.04 | 0.06 |
| Al | 0.13 | 0.18 | 0.10 | 0.08 | 0.22 | 0.20 | 0.11 | 0.16 |
| Fe3 | 0.04 | 0.04 | 0.05 | 0.08 | 0.09 | 0.08 | 0.08 | 0.08 |
| Fe2 | 0.32 | 0.28 | 0.27 | 0.27 | 0.19 | 0.20 | 0.18 | 0.21 |
| Mg | 0.64 | 0.66 | 0.72 | 0.69 | 0.69 | 0.71 | 0.78 | 0.73 |
| Ca | 0.87 | 0.87 | 0.87 | 0.89 | 0.87 | 0.87 | 0.86 | 0.86 |
| Na | 0.05 | 0.05 | 0.04 | 0.03 | 0.05 | 0.05 | 0.05 | 0.05 |
| total= | 4.00 | 4.00 | 4.00 | 4.00 | 4.00 | 4.00 | 4.00 | 4.00 |
| oxygens= | [6] | [6] | [6] | [6] | [6] | [6] | [6] | [6] |
| WO | 47.8 | 47.8 | 46.7 | 48.0 | 49.6 | 48.9 | 47.4 | 48.0 |
| EN | 34.8 | 36.7 | 38.7 | 37.2 | 39.4 | 39.7 | 42.7 | 40.5 |
| FS | 17.5 | 15.6 | 14.5 | 14.7 | 11.0 | 11.4 | 9.9 | 11.5 |

1 3, 40488
2 6, 40488
3 1, 30638
4 2 rim, 30638
5 1, 186375
6 2, 186375
7 1, YGD36
8 5, YGD36

| | 9 | 10 | 11 | 12 | 13 | 14 | 15 | 16 |
|---|---|---|---|---|---|---|---|---|
| SiO2 | 49.04 | 49.73 | 49.73 | 49.14 | 50.94 | 49.84 | 47.62 | 48.43 |
| TiO2 | 2.34 | 2.01 | 1.98 | 2.41 | 1.62 | 1.93 | 2.92 | 2.46 |
| Al2O3 | 3.94 | 3.54 | 3.24 | 3.87 | 2.47 | 3.30 | 4.48 | 3.81 |
| Cr2O3 | 0.01 | 0.01 | nd | nd | nd | nd | nd | 0.01 |
| FeO | 9.36 | 8.83 | 8.26 | 8.97 | 9.07 | 8.87 | 10.12 | 9.60 |
| MnO | 0.20 | 0.17 | 0.11 | 0.14 | 0.14 | 0.20 | 0.18 | 0.15 |
| MgO | 13.10 | 13.41 | 13.26 | 13.10 | 13.83 | 13.09 | 12.14 | 12.51 |
| CaO | 21.37 | 21.38 | 21.82 | 21.48 | 21.55 | 21.65 | 21.93 | 22.20 |
| Na2O | 0.63 | 0.62 | 0.85 | 0.67 | 0.59 | 0.74 | 0.72 | 0.64 |
| K2O | nd | nd | nd | nd | nd | 0.02 | nd | nd |
| total= | 99.99 | 99.70 | 99.25 | 99.78 | 100.21 | 99.64 | 100.11 | 99.81 |
| Si | 1.83 | 1.86 | 1.86 | 1.84 | 1.89 | 1.86 | 1.79 | 1.82 |
| Ti | 0.07 | 0.06 | 0.06 | 0.07 | 0.05 | 0.05 | 0.08 | 0.07 |
| Al | 0.17 | 0.16 | 0.14 | 0.17 | 0.11 | 0.15 | 0.20 | 0.17 |
| Fe3 | 0.08 | 0.06 | 0.08 | 0.07 | 0.06 | 0.07 | 0.12 | 0.10 |
| Fe2 | 0.22 | 0.22 | 0.18 | 0.21 | 0.22 | 0.21 | 0.20 | 0.20 |
| Mg | 0.73 | 0.75 | 0.74 | 0.73 | 0.77 | 0.73 | 0.68 | 0.70 |
| Ca | 0.86 | 0.86 | 0.88 | 0.86 | 0.86 | 0.87 | 0.88 | 0.89 |
| Na | 0.05 | 0.04 | 0.06 | 0.05 | 0.04 | 0.05 | 0.05 | 0.05 |
| total= | 4.00 | 4.00 | 4.00 | 4.00 | 4.00 | 4.00 | 4.00 | 4.00 |
| oxygens= | [6] | [6] | [6] | [6] | [6] | [6] | [6] | [6] |
| WO | 47.5 | 47.0 | 48.9 | 47.7 | 46.4 | 48.1 | 50.1 | 49.9 |
| EN | 40.5 | 41.0 | 41.3 | 40.5 | 41.4 | 40.5 | 38.6 | 39.1 |
| FS | 12.0 | 11.9 | 9.8 | 11.8 | 12.2 | 11.4 | 11.3 | 11.0 |

9 4, YGD72
10 6, YGD72
11 2, YGD54
12 5, YGD54
13 1, YGD12
14 3, YGD34
15 2, YGD78
16 5, YGD78

# Intercumulus pyroxenes

| | 17 | 18 | 19 | 20 | 21 | 22 | 23 | 24 |
|---|---|---|---|---|---|---|---|---|
| SiO2 | 49.11 | 49.20 | 49.45 | 49.23 | 49.35 | 49.15 | 48.96 | 50.85 |
| TiO2 | 2.28 | 2.08 | 2.16 | 2.22 | 2.04 | 2.03 | 2.13 | 1.77 |
| Al2O3 | 3.58 | 5.31 | 3.60 | 4.10 | 3.33 | 4.00 | 3.46 | 3.11 |
| Cr2O3 | 0.02 | nd | nd | nd | nd | 0.01 | 0.03 | nd |
| FeO | 10.34 | 9.51 | 9.19 | 8.51 | 10.12 | 8.34 | 8.88 | 8.12 |
| MnO | 0.19 | 0.18 | 0.15 | 0.13 | 0.20 | 0.17 | 0.14 | 0.13 |
| MgO | 12.36 | 11.46 | 13.02 | 12.46 | 13.07 | 12.78 | 12.79 | 13.10 |
| CaO | 21.86 | 21.01 | 21.56 | 21.89 | 21.68 | 22.81 | 21.65 | 22.06 |
| Na2O | 0.62 | 0.90 | 0.68 | 1.03 | 0.51 | 0.61 | 0.59 | 0.79 |
| total= | 100.36 | 99.65 | 99.81 | 99.57 | 100.30 | 99.90 | 98.63 | 99.93 |
| Si | 1.84 | 1.85 | 1.85 | 1.84 | 1.84 | 1.83 | 1.85 | 1.89 |
| Ti | 0.06 | 0.06 | 0.06 | 0.06 | 0.06 | 0.06 | 0.06 | 0.05 |
| Al | 0.16 | 0.24 | 0.16 | 0.18 | 0.15 | 0.18 | 0.15 | 0.14 |
| Fe3 | 0.08 | 0.02 | 0.07 | 0.09 | 0.09 | 0.09 | 0.06 | 0.04 |
| Fe2 | 0.24 | 0.28 | 0.22 | 0.18 | 0.23 | 0.17 | 0.22 | 0.22 |
| Mg | 0.69 | 0.64 | 0.73 | 0.69 | 0.73 | 0.71 | 0.72 | 0.73 |
| Ca | 0.88 | 0.85 | 0.86 | 0.88 | 0.87 | 0.91 | 0.88 | 0.88 |
| Na | 0.04 | 0.07 | 0.05 | 0.07 | 0.04 | 0.04 | 0.04 | 0.06 |
| total= | 4.00 | 4.00 | 4.00 | 4.00 | 4.00 | 4.00 | 4.00 | 4.00 |
| oxygens= | [6] | [6] | [6] | [6] | [6] | [6] | [6] | [6] |
| WO | 48.5 | 47.8 | 47.8 | 50.1 | 47.7 | 50.7 | 48.2 | 48.2 |
| EN | 38.2 | 36.3 | 40.2 | 39.7 | 40.0 | 39.5 | 39.6 | 39.8 |
| FS | 13.3 | 16.0 | 12.0 | 10.2 | 12.4 | 9.7 | 12.2 | 11.9 |

17 1, YGD293 19 2, YGD289 21 3, YGD138 23 2, YGD312
18 3, YGD293 20 3, YGD289 22 4, YGD138 24 5, YGD312

| | 25 | 26 | 27 | 28 | 29 | 30 | 31 | 32 |
|---|---|---|---|---|---|---|---|---|
| SiO2 | 48.92 | 49.96 | 51.13 | 50.01 | 50.16 | 50.71 | 49.41 | 51.16 |
| TiO2 | 2.09 | 1.60 | 1.10 | 1.42 | 1.53 | 1.45 | 1.76 | 1.36 |
| Al2O3 | 3.11 | 2.61 | 1.79 | 2.14 | 2.26 | 2.34 | 2.81 | 1.94 |
| Cr2O3 | 0.03 | 0.03 | 0.02 | 0.03 | nd | nd | nd | nd |
| FeO | 10.09 | 9.57 | 11.08 | 11.51 | 10.25 | 9.16 | 10.76 | 10.48 |
| MnO | 0.23 | 0.21 | 0.32 | 0.33 | 0.24 | 0.19 | 0.22 | 0.23 |
| MgO | 12.28 | 12.58 | 12.14 | 11.81 | 12.41 | 13.02 | 12.53 | 12.87 |
| CaO | 21.77 | 22.09 | 21.83 | 21.74 | 21.72 | 22.25 | 21.64 | 22.12 |
| Na2O | 0.68 | 0.67 | 0.66 | 0.61 | 0.59 | 0.68 | 0.57 | 0.48 |
| total= | 99.20 | 99.32 | 100.07 | 99.60 | 99.16 | 99.80 | 99.70 | 100.64 |
| Si | 1.85 | 1.88 | 1.92 | 1.89 | 1.90 | 1.90 | 1.86 | 1.91 |
| Ti | 0.06 | 0.05 | 0.03 | 0.04 | 0.04 | 0.04 | 0.05 | 0.04 |
| Al | 0.14 | 0.12 | 0.08 | 0.10 | 0.10 | 0.10 | 0.12 | 0.09 |
| Fe3 | 0.09 | 0.08 | 0.06 | 0.08 | 0.06 | 0.07 | 0.10 | 0.06 |
| Fe2 | 0.23 | 0.22 | 0.29 | 0.29 | 0.27 | 0.22 | 0.24 | 0.27 |
| Mn | - | - | 0.01 | 0.01 | - | - | - | - |
| Mg | 0.69 | 0.71 | 0.68 | 0.67 | 0.70 | 0.73 | 0.70 | 0.72 |
| Ca | 0.88 | 0.89 | 0.88 | 0.88 | 0.88 | 0.89 | 0.87 | 0.88 |
| Na | 0.05 | 0.05 | 0.05 | 0.04 | 0.04 | 0.05 | 0.04 | 0.03 |
| total= | 4.00 | 4.00 | 4.00 | 4.00 | 4.00 | 4.00 | 4.00 | 4.00 |
| oxygens= | [6] | [6] | [6] | [6] | [6] | [6] | [6] | [6] |
| WO | 48.9 | 48.9 | 47.6 | 48.1 | 47.7 | 48.6 | 48.0 | 47.3 |
| EN | 38.4 | 38.8 | 36.8 | 36.3 | 37.9 | 39.6 | 38.6 | 38.3 |
| FS | 12.7 | 12.3 | 15.6 | 15.6 | 14.4 | 11.7 | 13.4 | 14.5 |

25 1, YGD423 28 2, YGD426 31 4, YGD365
26 2, YGD423 29 2, YGD364 32 4 rim, YGD365
27 1 rim, YGD426 30 5, YGD364

## Intercumulus pyroxenes

| | 33 | 34 | 35 | 36 | 37 | 38 | 39 | 40 |
|---|---|---|---|---|---|---|---|---|
| SiO2 | 49.25 | 50.59 | 50.83 | 49.55 | 47.67 | 49.33 | 50.27 | 49.39 |
| TiO2 | 1.99 | 1.64 | 1.54 | 2.23 | 2.77 | 1.55 | 1.45 | 1.88 |
| Al2O3 | 3.31 | 2.65 | 2.64 | 3.84 | 4.35 | 2.46 | 2.44 | 2.87 |
| Cr2O3 | nd | nd | 0.01 | nd | 0.01 | 0.02 | 0.01 | 0.01 |
| FeO | 9.94 | 9.17 | 8.16 | 8.74 | 11.18 | 10.57 | 9.69 | 10.48 |
| MnO | 0.20 | 0.18 | 0.12 | 0.13 | 0.24 | 0.21 | 0.17 | 0.21 |
| MgO | 11.99 | 13.16 | 13.13 | 12.69 | 11.21 | 11.89 | 12.09 | 11.92 |
| CaO | 21.97 | 21.98 | 22.53 | 21.94 | 21.16 | 21.95 | 22.33 | 21.70 |
| Na2O | 0.64 | 0.48 | 0.66 | 0.64 | 0.63 | 0.70 | 0.74 | 0.57 |
| total= | 99.29 | 99.85 | 99.62 | 99.76 | 99.22 | 98.68 | 99.19 | 99.03 |
| Si | 1.86 | 1.89 | 1.90 | 1.86 | 1.82 | 1.88 | 1.90 | 1.88 |
| Ti | 0.06 | 0.05 | 0.04 | 0.06 | 0.08 | 0.04 | 0.04 | 0.05 |
| Al | 0.15 | 0.12 | 0.12 | 0.17 | 0.20 | 0.11 | 0.11 | 0.13 |
| Fe3 | 0.06 | 0.04 | 0.05 | 0.04 | 0.06 | 0.09 | 0.06 | 0.05 |
| Fe2 | 0.25 | 0.25 | 0.21 | 0.23 | 0.29 | 0.24 | 0.24 | 0.28 |
| Mg | 0.68 | 0.73 | 0.73 | 0.71 | 0.64 | 0.67 | 0.68 | 0.68 |
| Ca | 0.89 | 0.88 | 0.90 | 0.88 | 0.86 | 0.90 | 0.90 | 0.88 |
| Na | 0.05 | 0.03 | 0.05 | 0.05 | 0.05 | 0.05 | 0.05 | 0.04 |
| total= | 4.00 | 4.00 | 4.00 | 4.00 | 4.00 | 4.00 | 4.00 | 4.00 |
| oxygens= | [6] | [6] | [6] | [6] | [6] | [6] | [6] | [6] |
| WO | 48.9 | 47.3 | 48.9 | 48.3 | 48.1 | 49.4 | 49.5 | 48.0 |
| EN | 37.2 | 39.4 | 39.7 | 38.9 | 35.5 | 37.2 | 37.3 | 36.7 |
| FS | 13.9 | 13.3 | 11.4 | 12.8 | 16.4 | 13.4 | 13.2 | 15.3 |

33 1, YGD80
34 3 rim, YGD80
35 2, YGD49
36 4, YGD49
37 1, YGD317
38 2, YGD325
39 4, YGD325
40 1, YGD392

| | 41 | 42 | 43 | 44 | 45 | 46 | 47 | 48 |
|---|---|---|---|---|---|---|---|---|
| SiO2 | 48.73 | 47.00 | 49.39 | 49.66 | 50.34 | 48.12 | 50.03 | 49.59 |
| TiO2 | 2.37 | 3.41 | 2.22 | 1.69 | 1.34 | 2.87 | 2.08 | 2.15 |
| Al2O3 | 3.66 | 5.00 | 3.61 | 2.47 | 2.23 | 4.07 | 3.10 | 3.51 |
| Cr2O3 | 0.01 | nd | nd | nd | nd | nd | nd | 0.01 |
| FeO | 10.87 | 11.15 | 10.32 | 11.68 | 11.00 | 12.01 | 11.87 | 9.85 |
| MnO | 0.21 | 0.23 | 0.21 | 0.24 | 0.21 | 0.24 | 0.29 | 0.23 |
| MgO | 11.51 | 11.09 | 12.12 | 11.16 | 11.53 | 10.62 | 11.08 | 12.20 |
| CaO | 21.51 | 21.71 | 22.07 | 22.21 | 22.86 | 21.34 | 21.42 | 21.29 |
| Na2O | 0.59 | 0.73 | 0.68 | 0.65 | 0.70 | 0.68 | 0.65 | 0.58 |
| total= | 99.46 | 100.32 | 100.62 | 99.76 | 100.21 | 99.95 | 100.52 | 99.41 |
| Si | 1.85 | 1.77 | 1.84 | 1.88 | 1.89 | 1.83 | 1.89 | 1.87 |
| Ti | 0.07 | 0.10 | 0.06 | 0.05 | 0.04 | 0.08 | 0.06 | 0.06 |
| Al | 0.16 | 0.22 | 0.16 | 0.11 | 0.10 | 0.18 | 0.14 | 0.16 |
| Fe3 | 0.05 | 0.10 | 0.08 | 0.08 | 0.09 | 0.05 | 0.02 | 0.02 |
| Fe2 | 0.30 | 0.25 | 0.24 | 0.29 | 0.25 | 0.33 | 0.35 | 0.29 |
| Mg | 0.65 | 0.62 | 0.67 | 0.63 | 0.65 | 0.60 | 0.62 | 0.69 |
| Ca | 0.87 | 0.88 | 0.88 | 0.90 | 0.92 | 0.87 | 0.86 | 0.86 |
| Na | 0.04 | 0.05 | 0.05 | 0.05 | 0.05 | 0.05 | 0.05 | 0.04 |
| total= | 4.00 | 4.00 | 4.00 | 4.00 | 4.00 | 4.00 | 4.00 | 4.00 |
| oxygens= | [6] | [6] | [6] | [6] | [6] | [6] | [6] | [6] |
| WO | 48.0 | 50.0 | 49.0 | 49.4 | 50.5 | 48.2 | 47.0 | 46.8 |
| EN | 35.7 | 35.5 | 37.4 | 34.5 | 35.5 | 33.4 | 33.8 | 37.3 |
| FS | 16.3 | 14.5 | 13.5 | 16.1 | 14.0 | 18.4 | 19.2 | 15.9 |

41 6, YGD392
42 1, YGD228
43 2, YGD228
44 2, YGD328
45 4, YGD328
46 1, YGD1
47 3, YGD1
48 1, YGD378

# Intercumulus pyroxenes

| | 49 | 50 | 51 | 52 | 53 | 54 | 55 | 56 |
|---|---|---|---|---|---|---|---|---|
| SiO2 | 47.41 | 49.29 | 50.28 | 49.59 | 46.24 | 50.27 | 47.83 | 48.78 |
| TiO2 | 3.18 | 2.05 | 1.73 | 1.85 | 3.76 | 1.49 | 2.54 | 2.56 |
| Al2O3 | 4.54 | 3.36 | 3.09 | 3.38 | 5.42 | 2.13 | 4.10 | 4.08 |
| Cr2O3 | 0.01 | 0.01 | nd | nd | 0.01 | nd | nd | 0.04 |
| FeO | 10.35 | 10.28 | 9.40 | 9.04 | 10.86 | 9.54 | 9.72 | 8.62 |
| MnO | 0.24 | 0.19 | 0.20 | 0.18 | 0.19 | 0.18 | 0.16 | 0.14 |
| MgO | 11.41 | 11.99 | 12.60 | 12.59 | 10.89 | 13.37 | 12.13 | 13.33 |
| CaO | 21.24 | 22.07 | 22.06 | 22.24 | 21.16 | 21.70 | 21.77 | 21.49 |
| Na2O | 0.67 | 0.64 | 0.60 | 0.61 | 0.72 | 0.57 | 0.64 | 0.73 |
| total= | 99.05 | 99.88 | 99.96 | 99.48 | 99.25 | 99.25 | 98.89 | 99.77 |
| Si | 1.80 | 1.85 | 1.88 | 1.86 | 1.76 | 1.89 | 1.81 | 1.82 |
| Ti | 0.09 | 0.06 | 0.05 | 0.05 | 0.11 | 0.04 | 0.07 | 0.07 |
| Al | 0.20 | 0.15 | 0.14 | 0.15 | 0.24 | 0.09 | 0.18 | 0.18 |
| Fe3 | 0.05 | 0.07 | 0.04 | 0.06 | 0.07 | 0.08 | 0.09 | 0.09 |
| Fe2 | 0.28 | 0.25 | 0.25 | 0.22 | 0.27 | 0.22 | 0.22 | 0.18 |
| Mg | 0.65 | 0.67 | 0.70 | 0.71 | 0.62 | 0.75 | 0.69 | 0.74 |
| Ca | 0.87 | 0.89 | 0.88 | 0.90 | 0.86 | 0.87 | 0.88 | 0.86 |
| Na | 0.05 | 0.05 | 0.04 | 0.04 | 0.05 | 0.04 | 0.05 | 0.05 |
| total= oxygens= | 4.00 [6] | 4.00 [6] | 4.00 [6] | 4.00 [6] | 4.00 [6] | 4.00 [6] | 4.00 [6] | 4.00 [6] |
| WO | 48.4 | 49.1 | 48.2 | 49.2 | 49.2 | 47.4 | 49.5 | 48.2 |
| EN | 36.2 | 37.1 | 38.3 | 38.7 | 35.2 | 40.6 | 38.4 | 41.6 |
| FS | 15.4 | 13.8 | 13.6 | 12.1 | 15.6 | 11.9 | 12.1 | 10.2 |

49 2, YGD378
50 2, YGD334
51 3, YGD334
52 4, YGD334
53 3, YGD259
54 1, YGD292
55 4, YGD292
56 1, YGD306

| | 57 | 58 | 59 | 60 | 61 | 62 | 63 | 64 |
|---|---|---|---|---|---|---|---|---|
| SiO2 | 50.19 | 49.63 | 48.92 | 49.45 | 49.07 | 50.45 | 49.42 | 50.89 |
| TiO2 | 1.96 | 1.37 | 2.27 | 1.98 | 2.52 | 1.57 | 1.61 | 1.06 |
| Al2O3 | 3.31 | 2.44 | 3.68 | 3.23 | 4.23 | 2.56 | 2.48 | 1.73 |
| Cr2O3 | 0.01 | nd | nd | nd | 0.02 | 0.02 | 0.03 | nd |
| FeO | 7.86 | 11.10 | 9.04 | 8.78 | 9.41 | 8.74 | 10.93 | 11.75 |
| MnO | 0.12 | 0.24 | 0.15 | 0.15 | 0.14 | 0.14 | 0.22 | 0.33 |
| MgO | 13.53 | 11.78 | 12.57 | 12.77 | 12.20 | 13.03 | 11.92 | 12.25 |
| CaO | 22.01 | 21.82 | 21.95 | 22.32 | 21.39 | 21.90 | 21.49 | 21.12 |
| Na2O | 0.92 | 0.59 | 0.59 | 0.57 | 0.70 | 0.73 | 0.58 | 0.48 |
| total= | 99.91 | 98.97 | 99.17 | 99.25 | 99.68 | 99.14 | 98.68 | 99.61 |
| Si | 1.86 | 1.89 | 1.85 | 1.86 | 1.84 | 1.90 | 1.89 | 1.93 |
| Ti | 0.05 | 0.04 | 0.06 | 0.06 | 0.07 | 0.04 | 0.05 | 0.03 |
| Al | 0.14 | 0.11 | 0.16 | 0.14 | 0.19 | 0.11 | 0.11 | 0.08 |
| Fe3 | 0.09 | 0.08 | 0.06 | 0.06 | 0.03 | 0.06 | 0.07 | 0.04 |
| Fe2 | 0.16 | 0.28 | 0.22 | 0.21 | 0.26 | 0.22 | 0.28 | 0.33 |
| Mn | - | - | - | - | - | - | - | 0.01 |
| Mg | 0.75 | 0.67 | 0.71 | 0.72 | 0.68 | 0.73 | 0.68 | 0.69 |
| Ca | 0.88 | 0.89 | 0.89 | 0.90 | 0.86 | 0.88 | 0.88 | 0.86 |
| Na | 0.07 | 0.04 | 0.04 | 0.04 | 0.05 | 0.05 | 0.04 | 0.04 |
| total= oxygens= | 4.00 [6] | 4.00 [6] | 4.00 [6] | 4.00 [6] | 4.00 [6] | 4.00 [6] | 4.00 [6] | 4.00 [6] |
| WO | 49.1 | 48.5 | 48.8 | 49.2 | 47.6 | 48.2 | 47.8 | 45.7 |
| EN | 42.0 | 36.4 | 38.9 | 39.2 | 37.8 | 39.9 | 36.9 | 36.9 |
| FS | 8.8 | 15.0 | 12.4 | 11.6 | 14.6 | 11.9 | 15.4 | 17.5 |

57 2, YGD306
58 4, YGD426
59 1, YGD195
60 2, YGD195
61 1, YGD307
62 3, YGD307
63 2, 101211
64 1, 85955

## Cumulus pyroxenes

| | 65 | 66 | 67 | 68 | 69 | 70 | 71 | 72 |
|---|---|---|---|---|---|---|---|---|
| SiO2 | 50.78 | 50.15 | 50.63 | 50.17 | 49.85 | 50.47 | 50.33 | 50.72 |
| TiO2 | 1.40 | 1.15 | 0.58 | 1.08 | 0.80 | 1.23 | 0.76 | 0.90 |
| Al2O3 | 2.26 | 1.88 | 0.85 | 1.66 | 1.16 | 1.92 | 1.06 | 1.15 |
| Cr2O3 | 0.01 | nd | 0.01 | 0.01 | 0.01 | 0.01 | 0.01 | nd |
| FeO | 10.77 | 10.88 | 14.49 | 12.10 | 13.74 | 11.49 | 13.89 | 15.54 |
| MnO | 0.31 | 0.33 | 0.46 | 0.38 | 0.46 | 0.33 | 0.46 | 0.48 |
| MgO | 13.58 | 13.49 | 10.52 | 12.41 | 11.37 | 12.71 | 11.15 | 9.95 |
| CaO | 20.82 | 20.82 | 21.26 | 21.10 | 21.03 | 21.13 | 21.26 | 21.37 |
| Na2O | 0.44 | 0.40 | 0.57 | 0.43 | 0.50 | 0.44 | 0.48 | 0.20 |
| total= | 100.37 | 99.10 | 99.37 | 99.34 | 98.92 | 99.73 | 99.40 | 100.31 |
| Si | 1.90 | 1.90 | 1.94 | 1.91 | 1.91 | 1.90 | 1.93 | 1.95 |
| Ti | 0.04 | 0.03 | 0.02 | 0.03 | 0.02 | 0.03 | 0.02 | 0.03 |
| Al | 0.10 | 0.08 | 0.04 | 0.07 | 0.05 | 0.09 | 0.05 | 0.05 |
| Fe3 | 0.06 | 0.09 | 0.08 | 0.08 | 0.11 | 0.07 | 0.09 | 0.02 |
| Fe2 | 0.27 | 0.26 | 0.38 | 0.30 | 0.33 | 0.30 | 0.35 | 0.48 |
| Mn | - | 0.01 | 0.01 | 0.01 | 0.01 | 0.01 | 0.01 | 0.02 |
| Mg | 0.76 | 0.76 | 0.60 | 0.70 | 0.65 | 0.71 | 0.64 | 0.57 |
| Ca | 0.83 | 0.84 | 0.87 | 0.86 | 0.87 | 0.85 | 0.87 | 0.88 |
| Na | 0.03 | 0.03 | 0.04 | 0.03 | 0.04 | 0.03 | 0.04 | 0.01 |
| total= | 4.00 | 4.00 | 4.00 | 4.00 | 4.00 | 4.00 | 4.00 | 4.00 |
| oxygens= | [6] | [6] | [6] | [6] | [6] | [6] | [6] | [6] |
| WO | 44.7 | 45.4 | 47.0 | 46.1 | 46.8 | 45.8 | 46.8 | 45.6 |
| EN | 40.6 | 40.9 | 32.4 | 37.8 | 35.2 | 38.3 | 34.2 | 29.5 |
| FS | 14.7 | 13.8 | 20.7 | 16.1 | 18.0 | 15.8 | 19.0 | 24.9 |

65 2, 40548
66 3, 40548
67 3 rim, 40548
68 4, 40548
69 4 rim, 40548
70 5, 40548
71 5 rim, 40548
72 1, 186227

| | 73 | 74 | 75 | 76 | 77 | 78 | 79 | 80 |
|---|---|---|---|---|---|---|---|---|
| SiO2 | 49.15 | 50.53 | 50.48 | 51.17 | 49.93 | 49.84 | 49.61 | 49.55 |
| TiO2 | 1.04 | 1.08 | 0.59 | 1.14 | 0.87 | 0.73 | 0.88 | 0.67 |
| Al2O3 | 1.34 | 1.53 | 0.93 | 1.52 | 1.06 | 1.05 | 1.03 | 1.07 |
| FeO | 14.83 | 13.68 | 17.90 | 14.35 | 19.13 | 19.50 | 19.64 | 19.55 |
| MnO | 0.45 | 0.44 | 0.51 | 0.43 | 0.49 | 0.45 | 0.52 | 0.42 |
| MgO | 10.38 | 10.97 | 7.68 | 10.58 | 6.72 | 6.03 | 6.48 | 5.98 |
| CaO | 21.16 | 21.22 | 21.94 | 21.17 | 21.61 | 22.07 | 21.67 | 22.06 |
| Na2O | 0.23 | 0.22 | 0.26 | 0.62 | 0.54 | 0.63 | 0.52 | 0.63 |
| total= | 98.58 | 99.67 | 100.29 | 100.98 | 100.35 | 100.30 | 100.35 | 99.93 |
| Si | 1.91 | 1.93 | 1.96 | 1.93 | 1.95 | 1.95 | 1.94 | 1.95 |
| Ti | 0.03 | 0.03 | 0.02 | 0.03 | 0.03 | 0.02 | 0.03 | 0.02 |
| Al | 0.06 | 0.07 | 0.04 | 0.07 | 0.05 | 0.05 | 0.05 | 0.05 |
| Fe3 | 0.07 | 0.02 | 0.02 | 0.05 | 0.04 | 0.05 | 0.06 | 0.06 |
| Fe2 | 0.41 | 0.42 | 0.56 | 0.41 | 0.58 | 0.58 | 0.58 | 0.58 |
| Mn | 0.01 | 0.01 | 0.02 | 0.01 | 0.02 | 0.01 | 0.02 | 0.01 |
| Mg | 0.60 | 0.63 | 0.45 | 0.60 | 0.39 | 0.35 | 0.38 | 0.35 |
| Ca | 0.88 | 0.87 | 0.91 | 0.86 | 0.90 | 0.93 | 0.91 | 0.93 |
| Na | 0.02 | 0.02 | 0.02 | 0.05 | 0.04 | 0.05 | 0.04 | 0.05 |
| total= | 4.00 | 4.00 | 4.00 | 4.00 | 4.00 | 4.00 | 4.00 | 4.00 |
| oxygens= | [6] | [6] | [6] | [6] | [6] | [6] | [6] | [6] |
| WO | 46.6 | 45.4 | 47.5 | 46.0 | 48.2 | 49.7 | 48.6 | 50.0 |
| EN | 31.8 | 32.6 | 23.1 | 32.0 | 20.8 | 18.9 | 20.2 | 18.9 |
| FS | 21.6 | 22.0 | 29.4 | 21.9 | 31.0 | 31.4 | 31.2 | 31.1 |

73 2, 186227
74 3, 186227
75 5, 186227
76 6, 186227
77 1, 216627
78 1 rim, 216627
79 3, 216627
80 4, 216627

## Cumulus pyroxenes

| | 81 | 82 | 83 | 84 | 85 | 86 | 87 | 88 |
|---|---|---|---|---|---|---|---|---|
| SiO2 | 49.71 | 49.92 | 49.52 | 49.00 | 51.11 | 51.53 | 50.73 | 51.28 |
| TiO2 | 0.93 | 0.67 | 0.87 | 0.90 | 0.92 | 0.58 | 0.86 | 0.83 |
| Al2O3 | 1.08 | 0.99 | 1.04 | 1.16 | 1.47 | 1.17 | 1.51 | 1.42 |
| Cr2O3 | nd | 0.01 | nd | nd | 0.02 | nd | 0.01 | nd |
| FeO | 18.59 | 18.85 | 19.31 | 19.68 | 12.44 | 13.86 | 12.18 | 12.41 |
| MnO | 0.48 | 0.43 | 0.48 | 0.53 | 0.34 | 0.39 | 0.33 | 0.36 |
| MgO | 7.41 | 6.48 | 6.29 | 6.42 | 11.69 | 10.12 | 11.49 | 11.33 |
| CaO | 21.32 | 22.27 | 22.03 | 21.77 | 21.46 | 21.93 | 21.55 | 21.45 |
| Na2O | 0.53 | 0.62 | 0.62 | 0.51 | 0.49 | 0.52 | 0.49 | 0.47 |
| total= | 100.05 | 100.24 | 100.16 | 99.97 | 99.94 | 100.10 | 99.15 | 99.55 |
| Si | 1.94 | 1.95 | 1.94 | 1.92 | 1.94 | 1.97 | 1.94 | 1.95 |
| Ti | 0.03 | 0.02 | 0.03 | 0.03 | 0.03 | 0.02 | 0.02 | 0.02 |
| Al | 0.05 | 0.05 | 0.05 | 0.05 | 0.07 | 0.05 | 0.07 | 0.06 |
| Fe3 | 0.06 | 0.06 | 0.07 | 0.08 | 0.05 | 0.02 | 0.05 | 0.02 |
| Fe2 | 0.55 | 0.55 | 0.56 | 0.56 | 0.35 | 0.42 | 0.34 | 0.38 |
| Mn | 0.02 | 0.01 | 0.02 | 0.02 | 0.01 | 0.01 | 0.01 | 0.01 |
| Mg | 0.43 | 0.38 | 0.37 | 0.38 | 0.66 | 0.58 | 0.65 | 0.64 |
| Ca | 0.89 | 0.93 | 0.92 | 0.92 | 0.87 | 0.90 | 0.88 | 0.88 |
| Na | 0.04 | 0.05 | 0.05 | 0.04 | 0.04 | 0.04 | 0.04 | 0.03 |
| total= | 4.00 | 4.00 | 4.00 | 4.00 | 4.00 | 4.00 | 4.00 | 4.00 |
| oxygens= | [6] | [6] | [6] | [6] | [6] | [6] | [6] | [6] |
| WO | 47.6 | 50.1 | 49.8 | 49.4 | 46.3 | 47.4 | 46.9 | 46.2 |
| EN | 23.0 | 20.3 | 19.8 | 20.3 | 35.1 | 30.4 | 34.8 | 33.9 |
| FS | 29.3 | 29.7 | 30.4 | 30.4 | 18.5 | 22.2 | 18.3 | 19.9 |

81 5, 216627
82 7, 216627
83 8, 216627
84 9, 216627
85 1, YGD362
86 1 rim, YGD362
87 2, YGD362
88 2 rim, YGD362

| | 89 | 90 | 91 | 92 | 93 | 94 | 95 | 96 |
|---|---|---|---|---|---|---|---|---|
| SiO2 | 51.77 | 51.08 | 50.97 | 50.98 | 51.10 | 51.17 | 51.61 | 50.93 |
| TiO2 | 0.49 | 0.97 | 0.62 | 0.80 | 0.50 | 1.11 | 1.18 | 0.94 |
| Al2O3 | 0.95 | 1.52 | 1.23 | 1.42 | 1.01 | 1.73 | 2.01 | 1.90 |
| Cr2O3 | nd | nd | 0.02 | 0.01 | nd | nd | nd | nd |
| FeO | 12.08 | 12.31 | 12.77 | 12.41 | 13.99 | 9.67 | 9.09 | 8.85 |
| MnO | 0.36 | 0.35 | 0.33 | 0.34 | 0.38 | 0.28 | 0.29 | 0.26 |
| MgO | 11.40 | 11.50 | 10.82 | 11.41 | 9.91 | 14.05 | 13.96 | 13.89 |
| CaO | 22.34 | 21.16 | 21.80 | 21.53 | 21.78 | 21.18 | 21.52 | 21.74 |
| Na2O | 0.53 | 0.48 | 0.52 | 0.47 | 0.50 | 0.54 | 0.61 | 0.60 |
| total= | 99.92 | 99.37 | 99.08 | 99.37 | 99.17 | 99.73 | 100.27 | 99.11 |
| Si | 1.96 | 1.95 | 1.95 | 1.94 | 1.97 | 1.91 | 1.92 | 1.91 |
| Ti | 0.01 | 0.03 | 0.02 | 0.02 | 0.01 | 0.03 | 0.03 | 0.03 |
| Al | 0.04 | 0.07 | 0.06 | 0.06 | 0.05 | 0.08 | 0.09 | 0.08 |
| Fe3 | 0.05 | 0.02 | 0.04 | 0.04 | 0.02 | 0.08 | 0.06 | 0.09 |
| Fe2 | 0.34 | 0.38 | 0.37 | 0.36 | 0.43 | 0.23 | 0.22 | 0.19 |
| Mn | 0.01 | 0.01 | 0.01 | 0.01 | 0.01 | - | - | - |
| Mg | 0.64 | 0.65 | 0.62 | 0.65 | 0.57 | 0.78 | 0.77 | 0.78 |
| Ca | 0.91 | 0.86 | 0.90 | 0.88 | 0.90 | 0.85 | 0.86 | 0.87 |
| Na | 0.04 | 0.04 | 0.04 | 0.03 | 0.04 | 0.04 | 0.04 | 0.04 |
| total= | 4.00 | 4.00 | 4.00 | 4.00 | 4.00 | 4.00 | 4.00 | 4.00 |
| oxygens= | [6] | [6] | [6] | [6] | [6] | [6] | [6] | [6] |
| WO | 48.1 | 45.7 | 47.5 | 46.6 | 47.4 | 45.7 | 46.2 | 47.4 |
| EN | 34.1 | 34.5 | 32.8 | 34.4 | 30.0 | 42.2 | 41.7 | 42.2 |
| FS | 17.8 | 19.8 | 19.6 | 19.0 | 22.6 | 12.2 | 12.1 | 10.4 |

89 3, YGD362
90 5, YGD362
91 5 rim, YGD362
92 6, YGD362
93 6 rim, YGD362
94 2, 186224
95 3, 186224
96 3 rim, 186224

## Cumulus pyroxenes

| | 97 | 98 | 99 | 100 | 101 | 102 | 103 | 104 |
|---|---|---|---|---|---|---|---|---|
| SiO2 | 51.31 | 52.00 | 51.10 | 50.10 | 51.31 | 50.86 | 50.64 | 51.43 |
| TiO2 | 0.97 | 0.99 | 1.21 | 0.54 | 0.67 | 0.57 | 1.17 | 0.77 |
| Al2O3 | 1.95 | 2.01 | 1.92 | 1.23 | 1.34 | 1.10 | 1.97 | 1.32 |
| Cr2O3 | nd | nd | 0.02 | 0.02 | nd | 0.01 | nd | nd |
| FeO | 9.13 | 9.03 | 10.10 | 13.80 | 12.19 | 12.90 | 10.72 | 11.01 |
| MnO | 0.26 | 0.28 | 0.28 | 0.34 | 0.36 | 0.41 | 0.28 | 0.28 |
| MgO | 13.94 | 13.85 | 14.08 | 9.79 | 11.70 | 11.10 | 12.75 | 12.07 |
| CaO | 21.73 | 21.87 | 20.41 | 22.63 | 21.91 | 21.85 | 21.29 | 21.71 |
| Na2O | 0.56 | 0.59 | 0.42 | 0.60 | 0.53 | 0.52 | 0.51 | 0.60 |
| total= | 99.85 | 100.62 | 99.54 | 99.05 | 100.01 | 99.32 | 99.33 | 99.19 |
| Si | 1.91 | 1.92 | 1.92 | 1.93 | 1.94 | 1.94 | 1.91 | 1.95 |
| Ti | 0.03 | 0.03 | 0.03 | 0.02 | 0.02 | 0.02 | 0.03 | 0.02 |
| Al | 0.09 | 0.09 | 0.08 | 0.06 | 0.06 | 0.05 | 0.09 | 0.06 |
| Fe3 | 0.08 | 0.05 | 0.04 | 0.10 | 0.06 | 0.07 | 0.06 | 0.04 |
| Fe2 | 0.21 | 0.23 | 0.27 | 0.35 | 0.32 | 0.34 | 0.28 | 0.31 |
| Mn | - | - | - | 0.01 | 0.01 | 0.01 | - | - |
| Mg | 0.77 | 0.76 | 0.79 | 0.56 | 0.66 | 0.63 | 0.72 | 0.68 |
| Ca | 0.87 | 0.87 | 0.82 | 0.93 | 0.89 | 0.89 | 0.86 | 0.88 |
| Na | 0.04 | 0.04 | 0.03 | 0.04 | 0.04 | 0.04 | 0.04 | 0.04 |
| total= | 4.00 | 4.00 | 4.00 | 4.00 | 4.00 | 4.00 | 4.00 | 4.00 |
| oxygens= | [6] | [6] | [6] | [6] | [6] | [6] | [6] | [6] |
| WO | 46.9 | 46.7 | 43.6 | 50.6 | 47.5 | 47.9 | 46.3 | 47.0 |
| EN | 41.9 | 41.1 | 41.9 | 30.5 | 35.3 | 33.8 | 38.5 | 36.4 |
| FS | 11.3 | 12.2 | 14.5 | 18.9 | 17.3 | 18.3 | 15.2 | 16.6 |

97 4, 186224
98 5, 186224
99 1, 40551
100 1 rim, 40551
101 2, 40551
102 2 rim, 40551
103 5 rim, YGD428
104 5 core, YGD428

| | 105 | 106 |
|---|---|---|
| SiO2 | 49.43 | 49.34 |
| TiO2 | 0.55 | 0.58 |
| Al2O3 | 0.56 | 0.55 |
| Cr2O3 | 0.01 | nd |
| FeO | 21.53 | 21.70 |
| MnO | 0.69 | 0.62 |
| MgO | 5.20 | 4.93 |
| CaO | 20.58 | 20.84 |
| Na2O | 0.81 | 0.57 |
| total= | 99.36 | 99.13 |
| Si | 1.97 | 1.98 |
| Ti | 0.02 | 0.02 |
| Al | 0.03 | 0.03 |
| Fe3 | 0.07 | 0.03 |
| Fe2 | 0.65 | 0.70 |
| Mn | 0.02 | 0.02 |
| Mg | 0.31 | 0.29 |
| Ca | 0.88 | 0.89 |
| Na | 0.06 | 0.04 |
| total= | 4.00 | 4.00 |
| oxygens= | [6] | [6] |
| WO | 47.8 | 47.5 |
| EN | 16.8 | 15.6 |
| FS | 35.4 | 36.9 |

105 1, 50218
106 2, 50218

## Magnetites

| | 1 | 2 | 3 | 4 | 5 | 6 | 7 | 8 |
|---|---|---|---|---|---|---|---|---|
| SiO2 | 0.07 | 0.05 | 0.04 | 0.08 | 0.01 | 0.01 | 0.05 | 0.03 |
| TiO2 | 24.24 | 25.30 | 28.03 | 22.91 | 19.64 | 12.48 | 22.48 | 23.30 |
| Al2O3 | 2.20 | 2.63 | 2.08 | 2.46 | 2.77 | 2.99 | 2.73 | 2.91 |
| Fe2O3 | 18.86 | 17.93 | 13.34 | 21.64 | 27.67 | 41.42 | 22.89 | 20.60 |
| Cr2O3 | 0.08 | 0.04 | 0.03 | 0.64 | 0.35 | 0.05 | 0.30 | 0.18 |
| FeO | 51.56 | 52.91 | 54.68 | 48.00 | 45.98 | 41.21 | 48.80 | 49.68 |
| MnO | 0.65 | 0.73 | 0.80 | 0.40 | 0.43 | 0.33 | 0.49 | 0.47 |
| MgO | 0.91 | 1.07 | 1.40 | 2.67 | 1.96 | 0.95 | 2.03 | 1.81 |
| total= | 98.57 | 100.67 | 100.41 | 98.80 | 98.81 | 99.44 | 99.77 | 98.97 |
| Si | 0.02 | 0.01 | 0.01 | 0.02 | - | - | 0.01 | - |
| Ti | 5.46 | 5.56 | 6.16 | 5.08 | 4.38 | 2.81 | 4.95 | 5.17 |
| Al | 0.78 | 0.91 | 0.72 | 0.85 | 0.97 | 1.05 | 0.94 | 1.01 |
| Fe3 | 4.25 | 3.94 | 2.93 | 4.80 | 6.18 | 9.32 | 5.05 | 4.58 |
| Cr | 0.02 | - | - | 0.15 | 0.08 | 0.01 | 0.07 | 0.04 |
| Fe2 | 12.91 | 12.93 | 13.36 | 11.83 | 11.41 | 10.30 | 11.96 | 12.27 |
| Mn | 0.16 | 0.18 | 0.20 | 0.10 | 0.11 | 0.08 | 0.12 | 0.12 |
| Mg | 0.41 | 0.47 | 0.61 | 1.17 | 0.87 | 0.42 | 0.89 | 0.80 |
| total= | 24.00 | 24.00 | 24.00 | 24.00 | 24.00 | 24.00 | 24.00 | 24.00 |
| oxygens= | [32] | [32] | [32] | [32] | [32] | [32] | [32] | [32] |

1 2, 40488
2 3, 30638
3 4, 30638
4 3, 186375
5 1, YGD36
6 4, YGD36
7 3, YGD72
8 4, YGD72

| | 9 | 10 | 11 | 12 | 13 | 14 | 15 | 16 |
|---|---|---|---|---|---|---|---|---|
| SiO2 | 0.06 | 0.06 | 0.05 | 0.13 | nd | nd | 0.02 | 0.04 |
| TiO2 | 18.62 | 19.02 | 17.56 | 19.79 | 24.51 | 23.18 | 24.94 | 19.99 |
| Al2O3 | 3.25 | 3.92 | 2.97 | 2.46 | 3.51 | 4.20 | 2.85 | 2.82 |
| Fe2O3 | 28.44 | 27.29 | 31.74 | 27.20 | 17.77 | 19.27 | 18.10 | 27.29 |
| Cr2O3 | 0.97 | 0.26 | 0.03 | 0.04 | 0.15 | 0.19 | 0.08 | 0.09 |
| FeO | 45.09 | 46.21 | 44.54 | 48.09 | 49.50 | 49.58 | 51.68 | 46.60 |
| MnO | 0.44 | 0.41 | 0.36 | 0.64 | 0.60 | 0.53 | 0.76 | 0.50 |
| MgO | 2.04 | 1.62 | 1.79 | 0.65 | 2.53 | 1.85 | 1.32 | 1.66 |
| Na2O | nd | nd | nd | nd | nd | nd | 0.05 | 0.05 |
| total= | 98.91 | 98.79 | 99.04 | 98.99 | 98.57 | 98.80 | 99.79 | 99.04 |
| Si | 0.02 | 0.02 | 0.01 | 0.04 | - | - | - | 0.01 |
| Ti | 4.14 | 4.23 | 3.92 | 4.46 | 5.41 | 5.12 | 5.51 | 4.46 |
| Al | 1.13 | 1.37 | 1.04 | 0.87 | 1.21 | 1.45 | 0.99 | 0.99 |
| Fe3 | 6.33 | 6.08 | 7.09 | 6.13 | 3.93 | 4.26 | 4.00 | 6.09 |
| Cr | 0.23 | 0.06 | - | - | 0.03 | 0.04 | 0.02 | 0.02 |
| Fe2 | 11.15 | 11.43 | 11.05 | 12.04 | 12.16 | 12.18 | 12.69 | 11.55 |
| Mn | 0.11 | 0.10 | 0.09 | 0.16 | 0.15 | 0.13 | 0.19 | 0.13 |
| Mg | 0.90 | 0.71 | 0.79 | 0.29 | 1.11 | 0.81 | 0.58 | 0.73 |
| Na | - | - | - | - | - | - | 0.03 | 0.03 |
| total= | 24.00 | 24.00 | 24.00 | 24.00 | 24.00 | 24.00 | 24.00 | 24.00 |
| oxygens= | [32] | [32] | [32] | [32] | [32] | [32] | [32] | [32] |

9 4, YGD54
10 3, YGD12
11 6, YGD12
12 3, YGD34
13 2, YGD78
14 3, YGD78
15 2, YGD293
16 2, YGD289

## Magnetites

| | 17 | 18 | 19 | 20 | 21 | 22 | 23 | 24 |
|---|---|---|---|---|---|---|---|---|
| SiO2 | 0.02 | 0.06 | 0.02 | 0.05 | 0.06 | 0.11 | 0.08 | 0.07 |
| TiO2 | 21.93 | 17.81 | 16.89 | 25.40 | 24.38 | 23.39 | 24.59 | 23.53 |
| Al2O3 | 2.74 | 0.46 | 0.69 | 3.03 | 2.80 | 2.59 | 2.55 | 2.07 |
| Fe2O3 | 24.73 | 33.57 | 35.71 | 17.24 | 19.29 | 21.15 | 17.89 | 21.26 |
| Cr2O3 | 0.13 | 0.01 | nd | 0.30 | 0.23 | 0.03 | 0.02 | 0.03 |
| FeO | 47.22 | 46.88 | 46.13 | 50.47 | 50.55 | 50.98 | 52.51 | 50.68 |
| MnO | 0.57 | 0.66 | 0.59 | 0.48 | 0.52 | 0.71 | 0.68 | 0.72 |
| MgO | 2.57 | 0.03 | 0.04 | 2.67 | 2.03 | 1.05 | 0.57 | 1.09 |
| Na2O | 0.04 | nd | 0.03 | 0.02 | 0.01 | 0.02 | 0.01 | 0.03 |
| total= | 99.95 | 99.48 | 100.10 | 99.67 | 99.86 | 100.03 | 98.90 | 99.48 |
| Si | - | 0.02 | - | 0.01 | 0.02 | 0.03 | 0.02 | 0.02 |
| Ti | 4.81 | 4.06 | 3.83 | 5.55 | 5.36 | 5.18 | 5.52 | 5.25 |
| Al | 0.94 | 0.16 | 0.25 | 1.04 | 0.96 | 0.90 | 0.90 | 0.72 |
| Fe3 | 5.42 | 7.67 | 8.10 | 3.77 | 4.24 | 4.69 | 4.02 | 4.75 |
| Cr | 0.03 | - | - | 0.07 | 0.05 | - | - | - |
| Fe2 | 11.51 | 11.90 | 11.63 | 12.27 | 12.35 | 12.55 | 13.11 | 12.57 |
| Mn | 0.14 | 0.17 | 0.15 | 0.12 | 0.13 | 0.18 | 0.17 | 0.18 |
| Mg | 1.12 | 0.01 | 0.02 | 1.16 | 0.88 | 0.46 | 0.25 | 0.48 |
| Na | 0.02 | - | 0.02 | 0.01 | - | 0.01 | - | 0.02 |
| total= | 24.00 | 24.00 | 24.00 | 24.00 | 24.00 | 24.00 | 24.00 | 24.00 |
| oxygens= | [32] | [32] | [32] | [32] | [32] | [32] | [32] | [32] |

17 4, YGD289 19 5, 40548 21 3, YGD423 23 3, YGD426
18 1, 40548 20 2, YGD423 22 5, YGD423 24 4, YGD364

| | 25 | 26 | 27 | 28 | 29 | 30 | 31 | 32 |
|---|---|---|---|---|---|---|---|---|
| SiO2 | 0.03 | 0.06 | 0.06 | 0.06 | 0.26 | 0.81 | 0.11 | 0.02 |
| TiO2 | 25.48 | 22.41 | 26.73 | 26.93 | 17.20 | 17.96 | 19.96 | 22.75 |
| Al2O3 | 2.20 | 2.45 | 2.62 | 2.80 | 0.15 | 0.96 | 2.69 | 2.62 |
| Fe2O3 | 17.47 | 22.99 | 14.26 | 13.91 | 34.04 | 30.44 | 27.43 | 22.57 |
| Cr2O3 | 0.03 | 0.05 | 0.04 | 0.05 | 0.04 | 0.03 | 0.05 | 0.04 |
| FeO | 51.49 | 49.24 | 53.03 | 53.25 | 46.24 | 47.48 | 46.92 | 49.14 |
| MnO | 0.64 | 0.66 | 0.69 | 0.67 | 0.75 | 1.02 | 0.66 | 0.61 |
| MgO | 1.69 | 1.41 | 1.49 | 1.53 | nd | 0.06 | 1.59 | 1.81 |
| Na2O | 0.03 | 0.02 | 0.02 | 0.03 | nd | nd | nd | nd |
| total= | 99.06 | 99.29 | 98.94 | 99.23 | 98.68 | 98.76 | 99.41 | 99.56 |
| Si | - | 0.02 | 0.02 | 0.02 | 0.08 | 0.25 | 0.03 | - |
| Ti | 5.67 | 4.99 | 5.94 | 5.96 | 3.96 | 4.10 | 4.44 | 5.04 |
| Al | 0.77 | 0.86 | 0.91 | 0.97 | 0.05 | 0.34 | 0.94 | 0.91 |
| Fe3 | 3.89 | 5.12 | 3.17 | 3.08 | 7.85 | 6.95 | 6.11 | 5.00 |
| Cr | - | 0.01 | - | 0.01 | - | - | 0.01 | - |
| Fe2 | 12.74 | 12.20 | 13.11 | 13.10 | 11.85 | 12.06 | 11.61 | 12.10 |
| Mn | 0.16 | 0.17 | 0.17 | 0.17 | 0.19 | 0.26 | 0.17 | 0.15 |
| Mg | 0.75 | 0.62 | 0.66 | 0.67 | - | 0.03 | 0.70 | 0.79 |
| Na | 0.02 | 0.01 | 0.01 | 0.02 | - | - | - | - |
| total= | 24.00 | 24.00 | 24.00 | 24.00 | 24.00 | 24.00 | 24.00 | 24.00 |
| oxygens= | [32] | [32] | [32] | [32] | [32] | [32] | [32] | [32] |

25 5, YGD364 27 3, YGD365 29 3, 216627 31 1, YGD80
26 6, YGD364 28 4, YGD365 30 5, 216627 32 3, YGD80

# Magnetites

| | 33 | 34 | 35 | 36 | 37 | 38 | 39 | 40 |
|---|---|---|---|---|---|---|---|---|
| SiO2 | 0.02 | 0.04 | 0.07 | 0.06 | 0.06 | 0.05 | 0.05 | 0.08 |
| TiO2 | 22.20 | 30.94 | 19.19 | 25.67 | 26.32 | 22.42 | 24.48 | 27.20 |
| Al2O3 | 2.62 | 2.11 | 3.56 | 3.33 | 2.24 | 2.17 | 2.68 | 2.51 |
| Fe2O3 | 23.41 | 6.67 | 27.33 | 15.90 | 16.41 | 23.89 | 17.72 | 12.93 |
| Cr2O3 | 0.07 | 0.07 | 0.09 | 0.11 | 0.14 | 0.21 | 0.13 | 0.15 |
| FeO | 48.77 | 58.15 | 48.19 | 51.60 | 52.94 | 49.74 | 52.03 | 53.66 |
| MnO | 0.70 | 0.99 | 0.60 | 0.54 | 0.70 | 0.80 | 0.64 | 0.67 |
| MgO | 1.63 | 0.43 | 0.25 | 1.89 | 1.44 | 1.14 | 0.78 | 1.33 |
| Na2O | nd | 0.06 | 0.05 | 0.06 | 0.05 | 0.04 | nd | 0.01 |
| total= | 99.43 | 99.46 | 99.33 | 99.16 | 100.30 | 100.46 | 98.52 | 98.54 |
| Si | - | 0.01 | 0.02 | 0.02 | 0.02 | 0.01 | 0.01 | 0.02 |
| Ti | 4.93 | 6.89 | 4.30 | 5.66 | 5.79 | 4.95 | 5.50 | 6.08 |
| Al | 0.91 | 0.74 | 1.25 | 1.15 | 0.77 | 0.75 | 0.94 | 0.88 |
| Fe3 | 5.20 | 1.49 | 6.12 | 3.51 | 3.61 | 5.28 | 3.99 | 2.89 |
| Cr | 0.02 | 0.02 | 0.02 | 0.03 | 0.03 | 0.05 | 0.03 | 0.04 |
| Fe2 | 12.04 | 14.39 | 12.00 | 12.65 | 12.95 | 12.23 | 13.01 | 13.33 |
| Mn | 0.18 | 0.25 | 0.15 | 0.13 | 0.17 | 0.20 | 0.16 | 0.17 |
| Mg | 0.72 | 0.19 | 0.11 | 0.83 | 0.63 | 0.50 | 0.35 | 0.59 |
| Na | - | 0.03 | 0.03 | 0.03 | 0.03 | 0.02 | - | - |
| total= | 24.00 | 24.00 | 24.00 | 24.00 | 24.00 | 24.00 | 24.00 | 24.00 |
| oxygens= | [32] | [32] | [32] | [32] | [32] | [32] | [32] | [32] |

33 5, YGD80 35 5, YGD317 37 2, YGD392 39 1, YGD328
34 3, YGD317 36 2, YGD325 38 3, YGD392 40 5, YGD1

| | 41 | 42 | 43 | 44 | 45 | 46 | 47 | 48 |
|---|---|---|---|---|---|---|---|---|
| SiO2 | 0.13 | 0.06 | 0.04 | 0.04 | 0.02 | 0.03 | 0.04 | 0.06 |
| TiO2 | 26.22 | 23.01 | 26.17 | 23.54 | 19.50 | 22.31 | 20.56 | 14.75 |
| Al2O3 | 3.06 | 1.61 | 2.21 | 2.60 | 2.61 | 2.72 | 2.26 | 1.04 |
| Fe2O3 | 13.96 | 21.89 | 15.99 | 20.53 | 27.87 | 22.52 | 26.82 | 38.02 |
| Cr2O3 | 0.08 | 0.02 | 0.17 | 0.12 | 0.09 | 0.15 | nd | 0.03 |
| FeO | 54.09 | 50.84 | 52.80 | 49.82 | 46.29 | 48.70 | 47.33 | 43.81 |
| MnO | 0.55 | 0.70 | 0.71 | 0.59 | 0.71 | 0.54 | 0.68 | 0.58 |
| MgO | 0.66 | 0.38 | 1.39 | 1.76 | 1.42 | 1.72 | 1.52 | 0.07 |
| Na2O | 0.02 | 0.05 | nd | nd | nd | nd | nd | nd |
| total= | 98.77 | 98.56 | 99.48 | 99.00 | 98.51 | 98.69 | 99.21 | 98.36 |
| Si | 0.04 | 0.02 | 0.01 | 0.01 | - | - | 0.01 | 0.02 |
| Ti | 5.86 | 5.22 | 5.81 | 5.24 | 4.39 | 4.98 | 4.59 | 3.40 |
| Al | 1.07 | 0.57 | 0.77 | 0.91 | 0.92 | 0.95 | 0.79 | 0.38 |
| Fe3 | 3.12 | 4.97 | 3.55 | 4.57 | 6.27 | 5.03 | 6.00 | 8.78 |
| Cr | 0.02 | - | 0.04 | 0.03 | 0.02 | 0.04 | - | - |
| Fe2 | 13.45 | 12.83 | 13.03 | 12.32 | 11.58 | 12.09 | 11.76 | 11.24 |
| Mn | 0.14 | 0.18 | 0.18 | 0.15 | 0.18 | 0.14 | 0.17 | 0.15 |
| Mg | 0.29 | 0.17 | 0.61 | 0.78 | 0.63 | 0.76 | 0.67 | 0.03 |
| Na | 0.01 | 0.03 | - | - | - | - | - | - |
| total= | 24.00 | 24.00 | 24.00 | 24.00 | 24.00 | 24.00 | 24.00 | 24.00 |
| oxygens= | [32] | [32] | [32] | [32] | [32] | [32] | [32] | [32] |

41 3, YGD378 43 1, YGD259 45 5, YGD292 47 1, 186224
42 4, YGD362 44 1, YGD292 46 6, YGD292 48 2, YGD428

# Magnetites

| | 49 | 50 | 51 | 52 |
|---|---|---|---|---|
| SiO2 | 0.08 | 0.07 | 0.07 | 0.05 |
| TiO2 | 20.68 | 22.98 | 13.60 | 31.19 |
| Al2O3 | 3.38 | 2.05 | 2.47 | 0.59 |
| Fe2O3 | 25.18 | 22.35 | 38.96 | 6.83 |
| Cr2O3 | 0.31 | 0.07 | 0.06 | 0.05 |
| FeO | 46.57 | 49.17 | 43.26 | 58.08 |
| MnO | 0.51 | 0.70 | 0.42 | 0.57 |
| MgO | 2.33 | 1.77 | 0.13 | 0.60 |
| total= | 99.04 | 99.16 | 98.97 | 97.96 |
| Si | 0.02 | 0.02 | 0.02 | 0.02 |
| Ti | 4.57 | 5.12 | 3.10 | 7.10 |
| Al | 1.17 | 0.72 | 0.88 | 0.21 |
| Fe3 | 5.57 | 4.98 | 8.87 | 1.56 |
| Cr | 0.07 | 0.02 | 0.01 | 0.01 |
| Fe2 | 11.45 | 12.18 | 10.95 | 14.69 |
| Mn | 0.13 | 0.18 | 0.11 | 0.15 |
| Mg | 1.02 | 0.78 | 0.06 | 0.27 |
| total= | 24.00 | 24.00 | 24.00 | 24.00 |
| oxygens= | [32] | [32] | [32] | [32] |

49 2, YGD307
50 3, YGD307
51 1, 101211
52 2, 40411

# Ilmenites

| | 1 | 2 | 3 | 4 | 5 | 6 | 7 | 8 |
|---|---|---|---|---|---|---|---|---|
| SiO2 | 0.03 | nd | nd | 0.04 | nd | 0.02 | 0.04 | 0.09 |
| TiO2 | 53.82 | 53.53 | 54.02 | 52.77 | 53.19 | 52.60 | 52.91 | 52.66 |
| Al2O3 | 0.04 | 0.07 | 0.03 | 0.08 | 0.10 | 0.07 | 0.04 | 0.11 |
| Cr2O3 | 0.01 | nd | nd | 0.07 | 0.01 | nd | 0.05 | nd |
| FeO | 44.08 | 44.12 | 44.14 | 43.45 | 43.35 | 43.05 | 43.30 | 46.00 |
| MnO | 1.21 | 0.73 | 0.72 | 0.48 | 0.51 | 0.49 | 0.53 | 0.52 |
| MgO | 1.18 | 1.82 | 2.00 | 3.50 | 3.40 | 3.82 | 3.47 | 1.52 |
| total= | 100.37 | 100.27 | 100.91 | 100.39 | 100.56 | 100.05 | 100.34 | 100.90 |
| Ti | 2.01 | 2.00 | 2.00 | 1.96 | 1.97 | 1.96 | 1.96 | 1.97 |
| Fe2 | 1.83 | 1.83 | 1.82 | 1.79 | 1.78 | 1.78 | 1.79 | 1.91 |
| Mn | 0.05 | 0.03 | 0.03 | 0.02 | 0.02 | 0.02 | 0.02 | 0.02 |
| Mg | 0.09 | 0.13 | 0.15 | 0.26 | 0.25 | 0.28 | 0.26 | 0.11 |
| total= | 3.99 | 4.00 | 4.00 | 4.04 | 4.03 | 4.04 | 4.03 | 4.02 |
| oxygens= | [6] | [6] | [6] | [6] | [6] | [6] | [6] | [6] |

1 1, 40488 3 6, 30638 5 2, YGD36 7 2, YGD54
2 8, 40488 4 1, 186375 6 8, YGD36 8 1, YGD12

| | 9 | 10 | 11 | 12 | 13 | 14 | 15 | 16 |
|---|---|---|---|---|---|---|---|---|
| SiO2 | nd | 0.05 | 0.07 | 0.06 | 0.07 | 0.27 | 0.03 | 0.03 |
| TiO2 | 53.55 | 53.08 | 54.86 | 51.18 | 45.45 | 54.06 | 54.52 | 53.20 |
| Al2O3 | 0.08 | 0.05 | 0.15 | 0.06 | 1.01 | 0.09 | 0.09 | 0.06 |
| Cr2O3 | nd | nd | nd | 0.03 | 0.05 | nd | nd | nd |
| FeO | 42.94 | 45.35 | 42.01 | 45.99 | 51.54 | 43.15 | 42.06 | 45.93 |
| MnO | 0.48 | 2.29 | 0.59 | 0.53 | 0.87 | 0.58 | 0.68 | 1.02 |
| MgO | 3.56 | 0.02 | 2.85 | 2.32 | 1.08 | 2.59 | 3.18 | 0.55 |
| Na2O | nd | 0.04 | 0.02 | 0.02 | 0.04 | 0.04 | 0.01 | 0.03 |
| total= | 100.61 | 100.88 | 100.55 | 100.19 | 100.11 | 100.78 | 100.57 | 100.82 |
| Si | - | - | - | - | - | 0.01 | - | - |
| Ti | 1.98 | 2.00 | 2.02 | 1.93 | 1.77 | 1.99 | 2.00 | 2.00 |
| Al | - | - | - | - | 0.06 | - | - | - |
| Fe2 | 1.76 | 1.90 | 1.72 | 1.93 | 2.23 | 1.77 | 1.72 | 1.92 |
| Mn | 0.02 | 0.10 | 0.02 | 0.02 | 0.04 | 0.02 | 0.03 | 0.04 |
| Mg | 0.26 | - | 0.21 | 0.17 | 0.08 | 0.19 | 0.23 | 0.04 |
| total= | 4.02 | 4.00 | 3.98 | 4.07 | 4.20 | 3.99 | 3.99 | 4.00 |
| oxygens= | [6] | [6] | [6] | [6] | [6] | [6] | [6] | [6] |

9 5, YGD34 11 6, YGD138 13 1, YGD426 15 2, YGD334
10 4, 186227 12 3, YGD381 14 2, YGD328 16 3, YGD362

| | 17 | 18 | 19 | 20 | 21 | 22 |
|---|---|---|---|---|---|---|
| SiO2 | 0.04 | 0.02 | 0.05 | 0.02 | 0.04 | 0.04 |
| TiO2 | 53.34 | 53.22 | 53.00 | 52.14 | 52.37 | 51.34 |
| Al2O3 | 0.06 | 0.09 | 0.04 | 0.02 | 0.07 | 0.04 |
| Cr2O3 | nd | 0.06 | nd | nd | nd | nd |
| FeO | 43.72 | 42.15 | 45.10 | 43.37 | 45.98 | 46.63 |
| MnO | 0.55 | 0.45 | 1.67 | 3.94 | 1.06 | 0.61 |
| MgO | 2.22 | 4.31 | 0.09 | 0.04 | 0.81 | 1.18 |
| total= | 99.93 | 100.30 | 99.95 | 99.53 | 100.33 | 99.84 |
| Ti | 1.99 | 1.96 | 2.01 | 1.99 | 1.98 | 1.95 |
| Fe2 | 1.82 | 1.73 | 1.90 | 1.84 | 1.93 | 1.97 |
| Mn | 0.02 | 0.02 | 0.07 | 0.17 | 0.05 | 0.03 |
| Mg | 0.16 | 0.31 | - | - | 0.06 | 0.09 |
| total= | 4.00 | 4.03 | 3.99 | 4.01 | 4.02 | 4.04 |
| oxygens= | [6] | [6] | [6] | [6] | [6] | [6] |

17 6, YGD259 19 3, YGD428 21 3, 101211
18 3, YGD306 20 1, 50218 22 1, 40411

# Apatites

| | 1 | 2 | 3 | 4 | 5 | 6 | 7 | 8 |
|---|---|---|---|---|---|---|---|---|
| SiO2 | 0.12 | 0.16 | 0.19 | 0.17 | 0.16 | 0.13 | 0.25 | 0.17 |
| CaO | 55.19 | 54.73 | 55.45 | 55.11 | 55.25 | 55.18 | 54.82 | 54.18 |
| Na2O | nd | nd | nd | 0.01 | 0.03 | 0.01 | 0.05 | 0.01 |
| P2O5 | 42.05 | 42.38 | 41.91 | 42.00 | 42.33 | 42.30 | 41.48 | 41.95 |
| La2O3 | 0.08 | 0.08 | 0.13 | 0.09 | 0.05 | 0.05 | 0.14 | 0.09 |
| Ce2O3 | 0.12 | 0.17 | 0.17 | 0.13 | 0.14 | 0.11 | 0.21 | 0.11 |
| total= | 97.57 | 97.52 | 97.85 | 97.50 | 97.95 | 97.79 | 96.95 | 96.51 |
| F | 4.87 | 5.46 | 3.94 | 4.71 | 3.69 | 5.40 | 4.67 | 5.13 |
| Cl | 0.16 | 0.16 | 0.09 | 0.12 | 0.13 | 0.08 | 0.30 | 0.15 |
| Si | 0.02 | 0.02 | 0.03 | 0.02 | 0.02 | 0.02 | 0.04 | 0.03 |
| Ca | 8.82 | 8.72 | 8.85 | 8.81 | 8.78 | 8.78 | 8.84 | 8.72 |
| Na | - | - | - | - | - | - | 0.01 | - |
| P | 6.85 | 6.89 | 6.83 | 6.85 | 6.86 | 6.87 | 6.82 | 6.88 |
| Ce | - | - | - | - | - | - | 0.01 | - |
| total= | 15.70 | 15.64 | 15.72 | 15.70 | 15.68 | 15.68 | 15.73 | 15.64 |
| oxygens= | [26] | [26] | [26] | [26] | [26] | [26] | [26] | [26] |

1 4, 30638 3 6, 30638 5 5, 40402 7 1, 40559
2 5, 30638 4 3, 40402 6 6, 40402 8 4, 40559

| | 9 | 10 | 11 | 12 | 13 | 14 | 15 | 16 |
|---|---|---|---|---|---|---|---|---|
| SiO2 | 0.23 | 0.22 | 0.45 | 0.18 | 0.16 | 0.50 | 0.44 | 0.25 |
| CaO | 55.10 | 55.32 | 54.85 | 55.73 | 55.45 | 54.63 | 54.80 | 54.21 |
| Na2O | nd | 0.14 | 0.15 | 0.08 | 0.06 | 0.19 | 0.14 | 0.16 |
| P2O5 | 42.15 | 41.60 | 41.17 | 41.36 | 41.60 | 40.90 | 41.00 | 41.50 |
| La2O3 | 0.07 | 0.18 | 0.26 | 0.10 | 0.09 | 0.26 | 0.22 | 0.16 |
| Ce2O3 | 0.09 | 0.31 | 0.54 | 0.17 | 0.16 | 0.51 | 0.44 | 0.35 |
| total= | 97.63 | 97.77 | 97.42 | 97.61 | 97.52 | 96.98 | 97.04 | 96.62 |
| F | 4.15 | 5.37 | 5.03 | 4.90 | 5.91 | 4.35 | 6.31 | 6.80 |
| Cl | 0.11 | 0.01 | 0.02 | 0.01 | 0.04 | nd | 0.03 | 0.08 |
| Si | 0.03 | 0.03 | 0.07 | 0.03 | 0.02 | 0.08 | 0.07 | 0.04 |
| Ca | 8.78 | 8.87 | 8.84 | 8.96 | 8.90 | 8.85 | 8.87 | 8.76 |
| Na | - | 0.04 | 0.05 | 0.02 | 0.02 | 0.05 | 0.04 | 0.05 |
| P | 6.85 | 6.80 | 6.77 | 6.78 | 6.81 | 6.76 | 6.77 | 6.84 |
| La | - | 0.01 | 0.01 | - | - | 0.01 | 0.01 | - |
| Ce | - | 0.02 | 0.03 | - | - | 0.03 | 0.02 | 0.02 |
| total= | 15.68 | 15.77 | 15.77 | 15.80 | 15.76 | 15.79 | 15.78 | 15.71 |
| oxygens= | [26] | [26] | [26] | [26] | [26] | [26] | [26] | [26] |

9 5, 40559 11 2, 40548 13 7, 40548 15 8, 40549
10 1, 40548 12 5, 40548 14 3, 40549 16 2, 186227

# Apatites

| | 17 | 18 | 19 | 20 | 21 | 22 | 23 | 24 |
|---|---|---|---|---|---|---|---|---|
| SiO2 | 0.68 | 0.39 | 0.24 | 0.19 | 0.30 | 0.35 | 0.26 | 0.15 |
| CaO | 54.05 | 54.61 | 54.92 | 53.46 | 54.82 | 53.73 | 54.96 | 54.80 |
| Na2O | 0.07 | 0.11 | 0.05 | 0.07 | 0.06 | 0.10 | 0.01 | 0.04 |
| P2O5 | 40.98 | 41.35 | 40.79 | 41.35 | 41.38 | 41.24 | 41.98 | 41.37 |
| La2O3 | 0.17 | 0.20 | 0.17 | 0.13 | 0.08 | 0.17 | 0.04 | 0.08 |
| Ce2O3 | 0.29 | 0.38 | 0.26 | 0.20 | 0.25 | 0.34 | 0.11 | 0.15 |
| total= | 96.25 | 97.04 | 96.43 | 95.39 | 96.89 | 95.92 | 97.36 | 96.60 |
| F | 6.38 | 5.80 | 5.51 | 5.46 | 5.16 | 4.56 | 3.18 | 6.20 |
| Cl | 0.07 | 0.06 | 1.27 | 1.00 | 0.53 | 1.09 | 0.09 | 0.17 |
| Si | 0.10 | 0.06 | 0.04 | 0.03 | 0.04 | 0.05 | 0.04 | 0.02 |
| Ca | 8.77 | 8.81 | 8.94 | 8.72 | 8.85 | 8.74 | 8.79 | 8.86 |
| Na | 0.02 | 0.03 | 0.01 | 0.02 | 0.02 | 0.03 | - | 0.01 |
| P | 6.79 | 6.80 | 6.78 | 6.88 | 6.81 | 6.84 | 6.85 | 6.83 |
| La | - | 0.01 | - | - | - | - | - | - |
| Ce | 0.02 | 0.02 | 0.01 | 0.01 | 0.01 | 0.02 | - | - |
| total= | 15.71 | 15.73 | 15.79 | 15.66 | 15.74 | 15.69 | 15.69 | 15.74 |
| oxygens= | [26] | [26] | [26] | [26] | [26] | [26] | [26] | [26] |

17 4, 186227 19 1, 85954 21 4, 85954 23 1, YGD72
18 6, 186227 20 3, 85954 22 7, 85954 24 2, YGD72

| | 25 | 26 | 27 | 28 |
|---|---|---|---|---|
| SiO2 | 0.36 | 0.30 | 0.26 | 0.24 |
| CaO | 55.21 | 55.06 | 55.49 | 55.81 |
| Na2O | 0.01 | 0.00 | nd | 0.01 |
| P2O5 | 41.59 | 41.88 | 41.78 | 41.70 |
| La2O3 | 0.04 | 0.07 | 0.03 | 0.05 |
| Ce2O3 | 0.05 | 0.08 | 0.06 | 0.05 |
| total= | 97.25 | 97.39 | 97.63 | 97.86 |
| F | 4.22 | 3.68 | 4.82 | 3.79 |
| Cl | 0.09 | 0.11 | 0.08 | 0.20 |
| Si | 0.05 | 0.05 | 0.04 | 0.04 |
| Ca | 8.86 | 8.81 | 8.87 | 8.92 |
| P | 6.81 | 6.84 | 6.82 | 6.80 |
| total= | 15.73 | 15.70 | 15.73 | 15.76 |
| oxygens= | [26] | [26] | [26] | [26] |

25 4, YGD72 27 2, YGD229
26 6, YGD72 28 4, YGD229

## Biotites

| | 1 | 2 | 3 | 4 | 5 | 6 | 7 | 8 |
|---|---|---|---|---|---|---|---|---|
| SiO2 | 35.78 | 35.94 | 36.55 | 37.10 | 36.91 | 35.53 | 36.46 | 33.52 |
| TiO2 | 10.63 | 8.74 | 8.27 | 5.15 | 5.66 | 5.84 | 6.36 | 5.23 |
| Al2O3 | 14.06 | 14.00 | 14.02 | 15.13 | 14.44 | 11.84 | 12.00 | 13.34 |
| FeO | 14.69 | 13.34 | 14.37 | 11.90 | 12.34 | 28.94 | 24.78 | 32.83 |
| MnO | 0.03 | 0.05 | 0.03 | 0.02 | 0.03 | 0.15 | 0.27 | 0.20 |
| MgO | 12.07 | 13.83 | 13.56 | 16.47 | 15.73 | 5.59 | 8.07 | 2.96 |
| CaO | nd | 0.04 | nd | nd | nd | 0.09 | nd | nd |
| Na2O | 0.22 | 0.19 | 0.69 | 0.45 | 0.48 | 0.20 | 0.47 | 0.25 |
| K2O | 9.68 | 9.60 | 9.42 | 9.72 | 9.32 | 9.09 | 9.30 | 9.08 |
| total= | 97.16 | 95.73 | 96.91 | 95.94 | 94.91 | 97.27 | 97.71 | 97.41 |
| F | 0.51 | 0.23 | 0.82 | 1.22 | 0.78 | 0.26 | 0.50 | 0.09 |
| Si | 5.28 | 5.34 | 5.39 | 5.45 | 5.48 | 5.60 | 5.61 | 5.40 |
| Ti | 1.18 | 0.98 | 0.92 | 0.57 | 0.63 | 0.69 | 0.74 | 0.63 |
| Al | 2.45 | 2.45 | 2.44 | 2.62 | 2.53 | 2.20 | 2.17 | 2.53 |
| Fe2 | 1.81 | 1.66 | 1.77 | 1.46 | 1.53 | 3.82 | 3.19 | 4.42 |
| Mn | - | - | - | - | - | 0.02 | 0.04 | 0.03 |
| Mg | 2.65 | 3.07 | 2.98 | 3.60 | 3.48 | 1.31 | 1.85 | 0.71 |
| Ca | - | - | - | - | - | 0.02 | - | - |
| Na | 0.06 | 0.05 | 0.20 | 0.13 | 0.14 | 0.06 | 0.14 | 0.08 |
| K | 1.82 | 1.82 | 1.77 | 1.82 | 1.77 | 1.83 | 1.82 | 1.87 |
| total= | 15.26 | 15.39 | 15.46 | 15.65 | 15.57 | 15.55 | 15.55 | 15.67 |
| oxygens= | [22] | [22] | [22] | [22] | [22] | [22] | [22] | [22] |

1 1, YGD78
2 2, YGD78
3 1, YGD293
4 2, YGD293
5 3, YGD293
6 1, 40548
7 2, 40548
8 3, 40548

| | 9 | 10 | 11 | 12 | 13 | 14 | 15 | 16 |
|---|---|---|---|---|---|---|---|---|
| SiO2 | 37.95 | 37.98 | 33.22 | 34.48 | 35.30 | 37.40 | 37.37 | 35.96 |
| TiO2 | 5.78 | 5.73 | 6.18 | 2.95 | 6.01 | 7.55 | 8.56 | 8.54 |
| Al2O3 | 13.28 | 13.43 | 12.16 | 11.27 | 12.58 | 13.37 | 13.25 | 13.31 |
| FeO | 11.26 | 13.07 | 33.60 | 37.21 | 28.88 | 11.45 | 12.60 | 14.97 |
| MnO | 0.02 | 0.05 | 0.18 | 0.24 | 0.23 | 0.04 | 0.06 | 0.08 |
| MgO | 16.92 | 15.89 | 2.42 | 2.16 | 5.39 | 16.48 | 15.55 | 13.04 |
| CaO | nd | nd | 0.02 | 0.01 | nd | 0.03 | 0.28 | 0.01 |
| Na2O | 0.45 | 0.47 | 0.28 | 0.05 | 0.44 | 0.65 | 0.49 | 0.40 |
| K2O | 9.64 | 9.79 | 8.79 | 8.40 | 8.84 | 9.63 | 9.52 | 9.44 |
| total= | 95.30 | 96.41 | 96.85 | 96.77 | 97.67 | 96.60 | 97.68 | 95.75 |
| F | 1.05 | 1.19 | 0.12 | 0.10 | 0.48 | 1.30 | 0.79 | 0.67 |
| Si | 5.59 | 5.58 | 5.41 | 5.69 | 5.53 | 5.46 | 5.42 | 5.39 |
| Ti | 0.64 | 0.63 | 0.76 | 0.37 | 0.71 | 0.83 | 0.93 | 0.96 |
| Al | 2.31 | 2.33 | 2.34 | 2.19 | 2.32 | 2.30 | 2.27 | 2.35 |
| Fe2 | 1.39 | 1.61 | 4.58 | 5.14 | 3.79 | 1.40 | 1.53 | 1.88 |
| Mn | - | - | 0.02 | 0.03 | 0.03 | - | - | 0.01 |
| Mg | 3.72 | 3.48 | 0.59 | 0.53 | 1.26 | 3.58 | 3.36 | 2.91 |
| Ca | - | - | - | - | - | - | 0.04 | - |
| Na | 0.13 | 0.13 | 0.09 | 0.02 | 0.13 | 0.18 | 0.14 | 0.12 |
| K | 1.81 | 1.84 | 1.83 | 1.77 | 1.77 | 1.79 | 1.76 | 1.81 |
| total= | 15.58 | 15.61 | 15.62 | 15.74 | 15.55 | 15.55 | 15.46 | 15.43 |
| oxygens= | [22] | [22] | [22] | [22] | [22] | [22] | [22] | [22] |

9 2, YGD289
10 3, YGD289
11 3, 40548
12 2, 186227
13 3, 186227
14 1, YGD138
15 3, YGD138
16 2, YGD364

# Biotites

| | 17 | 18 | 19 | 20 | 21 | 22 | 23 | 24 |
|---|---|---|---|---|---|---|---|---|
| SiO2 | 35.98 | 34.77 | 35.81 | 36.82 | 33.82 | 34.83 | 34.27 | 36.80 |
| TiO2 | 9.18 | 6.79 | 5.50 | 8.31 | 5.93 | 6.78 | 6.35 | 8.61 |
| Al2O3 | 12.98 | 13.63 | 14.53 | 13.97 | 12.48 | 12.67 | 12.40 | 13.75 |
| FeO | 16.16 | 21.08 | 18.08 | 14.90 | 30.81 | 28.12 | 28.78 | 16.19 |
| MnO | 0.09 | 0.21 | 0.11 | 0.06 | 0.30 | 0.20 | 0.21 | 0.12 |
| MgO | 12.09 | 9.66 | 12.61 | 13.37 | 3.50 | 5.61 | 5.23 | 11.74 |
| CaO | nd | nd | 0.05 | 0.02 | nd | 0.01 | nd | nd |
| Na2O | 0.57 | 0.28 | 0.24 | 0.80 | 0.42 | 0.61 | 0.64 | 0.55 |
| K2O | 9.37 | 9.69 | 9.51 | 9.10 | 8.90 | 8.81 | 8.60 | 9.36 |
| total= | 96.42 | 96.11 | 96.44 | 97.35 | 96.16 | 97.64 | 96.48 | 97.12 |
| F | 0.47 | 0.58 | 0.57 | 0.73 | 0.14 | 0.53 | 0.66 | 0.85 |
| Si | 5.39 | 5.37 | 5.40 | 5.40 | 5.47 | 5.45 | 5.46 | 5.45 |
| Ti | 1.03 | 0.79 | 0.62 | 0.92 | 0.72 | 0.80 | 0.76 | 0.96 |
| Al | 2.29 | 2.48 | 2.58 | 2.42 | 2.38 | 2.34 | 2.33 | 2.40 |
| Fe2 | 2.02 | 2.72 | 2.28 | 1.83 | 4.17 | 3.68 | 3.83 | 2.01 |
| Mn | 0.01 | 0.03 | 0.01 | - | 0.04 | 0.03 | 0.03 | 0.02 |
| Mg | 2.70 | 2.22 | 2.83 | 2.93 | 0.84 | 1.31 | 1.24 | 2.59 |
| Na | 0.17 | 0.08 | 0.07 | 0.23 | 0.13 | 0.19 | 0.20 | 0.16 |
| K | 1.79 | 1.91 | 1.83 | 1.70 | 1.84 | 1.76 | 1.75 | 1.77 |
| total= | 15.41 | 15.60 | 15.64 | 15.44 | 15.60 | 15.55 | 15.59 | 15.35 |
| oxygens= | [22] | [22] | [22] | [22] | [22] | [22] | [22] | [22] |

17 3, YGD364
18 1, YGD365
19 2, YGD365
20 3, YGD365
21 2, 216627
22 3, 216627
23 4, 216627
24 1, YGD80

| | 25 | 26 | 27 | 28 | 29 | 30 | 31 | 32 |
|---|---|---|---|---|---|---|---|---|
| SiO2 | 35.05 | 37.24 | 36.59 | 36.21 | 36.23 | 36.24 | 36.69 | 37.07 |
| TiO2 | 5.50 | 4.35 | 8.29 | 8.59 | 7.95 | 6.20 | 7.13 | 7.26 |
| Al2O3 | 14.88 | 13.98 | 13.83 | 13.50 | 14.15 | 13.42 | 13.42 | 12.88 |
| FeO | 19.82 | 13.91 | 13.65 | 14.87 | 16.33 | 16.61 | 15.21 | 14.41 |
| MnO | 0.18 | 0.07 | 0.08 | 0.10 | 0.10 | 0.08 | 0.07 | 0.07 |
| MgO | 10.42 | 15.46 | 13.65 | 12.82 | 11.98 | 12.58 | 13.14 | 13.62 |
| CaO | 0.05 | 0.03 | nd | nd | nd | nd | nd | 0.01 |
| Na2O | 0.35 | 0.38 | 0.35 | 0.34 | 0.28 | 0.34 | 0.50 | 0.41 |
| K2O | 9.56 | 9.53 | 9.69 | 9.48 | 9.54 | 9.57 | 9.57 | 9.45 |
| total= | 95.81 | 94.95 | 96.13 | 95.91 | 96.56 | 95.04 | 95.73 | 95.18 |
| Si | 5.38 | 5.58 | 5.42 | 5.41 | 5.41 | 5.51 | 5.50 | 5.56 |
| Ti | 0.63 | 0.49 | 0.92 | 0.97 | 0.89 | 0.71 | 0.80 | 0.82 |
| Al | 2.69 | 2.47 | 2.42 | 2.38 | 2.49 | 2.41 | 2.37 | 2.28 |
| Fe2 | 2.54 | 1.74 | 1.69 | 1.86 | 2.04 | 2.11 | 1.91 | 1.81 |
| Mn | 0.02 | - | 0.01 | 0.01 | 0.01 | 0.01 | - | - |
| Mg | 2.38 | 3.45 | 3.02 | 2.86 | 2.67 | 2.85 | 2.94 | 3.04 |
| Na | 0.10 | 0.11 | 0.10 | 0.10 | 0.08 | 0.10 | 0.15 | 0.12 |
| K | 1.87 | 1.82 | 1.83 | 1.81 | 1.82 | 1.86 | 1.83 | 1.81 |
| total= | 15.63 | 15.67 | 15.41 | 15.39 | 15.40 | 15.56 | 15.50 | 15.45 |
| oxygens= | [22] | [22] | [22] | [22] | [22] | [22] | [22] | [22] |

25 2, YGD392
26 3, YGD392
27 1, YGD325
28 2, YGD325
29 1, YGD317
30 1, YGD228
31 2, YGD228
32 1, YGD328

## Biotites ( ■ -not determined)

| | 33 | 34 | 35 | 36 | 37 | 38 | 39 | 40 |
|---|---|---|---|---|---|---|---|---|
| SiO2 | 35.80 | 35.50 | 34.96 | 35.67 | 35.16 | 36.84 | 35.51 | 34.62 |
| TiO2 | 8.37 | 7.42 | 6.42 | 6.65 | 6.09 | 8.21 | 7.58 | 6.51 |
| Al2O3 | 13.18 | 13.62 | 12.85 | 12.98 | 12.69 | 13.22 | 12.03 | 13.00 |
| FeO | 18.43 | 14.28 | 24.72 | 22.25 | 21.32 | 13.60 | 23.18 | 24.36 |
| MnO | 0.12 | 0.06 | 0.17 | 0.16 | 0.12 | 0.05 | 0.18 | 0.22 |
| MgO | 10.75 | 13.87 | 7.58 | 9.25 | 9.58 | 14.68 | 8.20 | 7.83 |
| CaO | nd | nd | 0.06 | nd | nd | nd | nd | nd |
| Na2O | 0.42 | 0.32 | 0.40 | 0.51 | 0.46 | 0.67 | 0.61 | 0.57 |
| K2O | 9.33 | 9.42 | 9.00 | 9.14 | 8.89 | 9.05 | 8.81 | 8.88 |
| total= | 96.40 | 94.49 | 96.16 | 96.61 | 94.31 | 96.32 | 96.10 | 95.99 |
| F | ■ | 0.25 | 0.53 | 0.45 | 0.54 | ■ | ■ | ■ |
| Si | 5.42 | 5.38 | 5.47 | 5.48 | 5.52 | 5.44 | 5.51 | 5.42 |
| Ti | 0.95 | 0.85 | 0.76 | 0.77 | 0.72 | 0.91 | 0.89 | 0.77 |
| Al | 2.35 | 2.43 | 2.37 | 2.35 | 2.35 | 2.30 | 2.20 | 2.40 |
| Fe2 | 2.33 | 1.81 | 3.23 | 2.86 | 2.80 | 1.68 | 3.01 | 3.19 |
| Mn | 0.02 | - | 0.02 | 0.02 | 0.02 | - | 0.02 | 0.03 |
| Mg | 2.42 | 3.13 | 1.77 | 2.12 | 2.24 | 3.23 | 1.90 | 1.83 |
| Ca | - | - | 0.01 | - | - | - | - | - |
| Na | 0.12 | 0.09 | 0.12 | 0.15 | 0.14 | 0.19 | 0.18 | 0.17 |
| K | 1.80 | 1.82 | 1.80 | 1.79 | 1.78 | 1.70 | 1.75 | 1.77 |
| total= | 15.42 | 15.52 | 15.55 | 15.55 | 15.55 | 15.45 | 15.46 | 15.58 |
| oxygens= | [22] | [22] | [22] | [22] | [22] | [22] | [22] | [22] |

33 3, YGD328
34 1, YGD334
35 1, YGD362
36 2, YGD362
37 3, YGD362
38 3, 186224
39 1, YGD428
40 2, YGD428

| | 41 | 42 |
|---|---|---|
| SiO2 | 37.13 | 36.32 |
| TiO2 | 5.07 | 5.18 |
| Al2O3 | 13.22 | 11.63 |
| FeO | 14.94 | 25.26 |
| MnO | 0.06 | 0.16 |
| MgO | 15.29 | 8.84 |
| CaO | 0.02 | 0.01 |
| Na2O | 0.69 | 0.44 |
| K2O | 8.71 | 8.97 |
| total= | 95.13 | 96.81 |
| Si | 5.56 | 5.64 |
| Ti | 0.57 | 0.61 |
| Al | 2.33 | 2.13 |
| Fe2 | 1.87 | 3.28 |
| Mn | - | 0.02 |
| Mg | 3.41 | 2.05 |
| Na | 0.20 | 0.13 |
| K | 1.66 | 1.78 |
| total= | 15.63 | 15.64 |
| oxygens= | [22] | [22] |

41 1, 40411
42 1, 85955

# Amphiboles

| | 1 | 2 | 3 | 4 | 5 | 6 | 7 | 8 |
|---|---|---|---|---|---|---|---|---|
| SiO2 | 37.28 | 37.27 | 39.51 | 41.35 | 41.60 | 41.19 | 41.52 | 40.65 |
| TiO2 | 3.97 | 3.68 | 4.13 | 3.70 | 3.68 | 3.45 | 1.96 | 2.58 |
| Al2O3 | 10.53 | 10.32 | 9.22 | 8.30 | 8.33 | 8.30 | 7.44 | 7.83 |
| FeO | 28.14 | 28.83 | 23.49 | 24.04 | 23.91 | 25.06 | 29.24 | 28.72 |
| MnO | 0.42 | 0.47 | 0.35 | 0.43 | 0.41 | 0.43 | 0.39 | 0.41 |
| MgO | 2.33 | 1.95 | 5.60 | 5.92 | 6.03 | 5.42 | 3.40 | 3.67 |
| CaO | 10.78 | 10.42 | 11.06 | 10.72 | 10.77 | 10.79 | 10.61 | 10.54 |
| Na2O | 2.77 | 2.91 | 2.90 | 2.70 | 2.66 | 2.63 | 2.31 | 2.53 |
| K2O | 1.59 | 1.63 | 1.48 | 1.50 | 1.47 | 1.46 | 1.31 | 1.40 |
| total= | 97.81 | 97.48 | 97.74 | 98.66 | 98.86 | 98.73 | 98.18 | 98.33 |
| Si | 6.05 | 6.09 | 6.25 | 6.46 | 6.47 | 6.46 | 6.66 | 6.52 |
| Ti | 0.48 | 0.45 | 0.49 | 0.43 | 0.43 | 0.41 | 0.24 | 0.31 |
| Al | 2.01 | 1.99 | 1.72 | 1.53 | 1.53 | 1.53 | 1.41 | 1.48 |
| Fe2 | 3.82 | 3.94 | 3.11 | 3.14 | 3.11 | 3.29 | 3.92 | 3.85 |
| Mn | 0.06 | 0.07 | 0.05 | 0.06 | 0.05 | 0.06 | 0.05 | 0.06 |
| Mg | 0.56 | 0.47 | 1.32 | 1.38 | 1.40 | 1.27 | 0.81 | 0.88 |
| Ca | 1.87 | 1.82 | 1.87 | 1.79 | 1.80 | 1.81 | 1.82 | 1.81 |
| Na | 0.87 | 0.92 | 0.89 | 0.82 | 0.80 | 0.80 | 0.72 | 0.79 |
| K | 0.33 | 0.34 | 0.30 | 0.30 | 0.29 | 0.29 | 0.27 | 0.29 |
| total= | 16.06 | 16.10 | 15.99 | 15.90 | 15.88 | 15.91 | 15.90 | 15.97 |
| oxygens= | [23] | [23] | [23] | [23] | [23] | [23] | [23] | [23] |

1 2, 40548 3 5, 40548 5 2, 186227 7 5, 186227
2 3, 40548 4 1, 186227 6 4, 186227 8 6, 186227

| | 9 | 10 | 11 | 12 | 13 | 14 | 15 | 16 |
|---|---|---|---|---|---|---|---|---|
| SiO2 | 48.07 | 48.63 | 40.57 | 39.54 | 51.85 | 51.42 | 50.21 | 52.42 |
| TiO2 | 1.55 | 1.15 | 3.71 | 3.69 | 0.17 | 0.23 | 0.41 | 0.73 |
| Al2O3 | 2.20 | 1.72 | 8.92 | 9.36 | 0.45 | 0.32 | 0.35 | 0.30 |
| FeO | 31.05 | 32.81 | 24.97 | 25.40 | 29.76 | 36.01 | 31.24 | 28.52 |
| MnO | 0.82 | 0.74 | 0.38 | 0.36 | 0.32 | 0.19 | 0.59 | 0.13 |
| MgO | 2.47 | 1.35 | 4.32 | 4.00 | 0.02 | 0.88 | 2.12 | 3.53 |
| CaO | 6.54 | 6.15 | 10.69 | 10.72 | 1.41 | 0.69 | 2.41 | 0.18 |
| Na2O | 5.02 | 4.65 | 2.90 | 2.84 | 13.53 | 6.87 | 6.59 | 7.52 |
| K2O | 1.13 | 0.90 | 1.49 | 1.55 | nd | 0.13 | 1.23 | 1.86 |
| total= | 98.85 | 98.10 | 97.95 | 97.46 | 97.51 | 96.74 | 95.15 | 95.19 |
| Si | 7.61 | 7.78 | 6.42 | 6.32 | 8.25 | 8.28 | 8.18 | 8.35 |
| Ti | 0.18 | 0.14 | 0.44 | 0.44 | 0.02 | 0.03 | 0.05 | 0.09 |
| Al | 0.41 | 0.32 | 1.66 | 1.76 | 0.08 | 0.06 | 0.07 | 0.06 |
| Fe2 | 4.11 | 4.39 | 3.30 | 3.39 | 3.96 | 4.85 | 4.26 | 3.80 |
| Mn | 0.11 | 0.10 | 0.05 | 0.05 | 0.04 | 0.03 | 0.08 | 0.02 |
| Mg | 0.58 | 0.32 | 1.02 | 0.95 | - | 0.21 | 0.51 | 0.84 |
| Ca | 1.11 | 1.05 | 1.81 | 1.84 | 0.24 | 0.12 | 0.42 | 0.03 |
| Na | 1.54 | 1.44 | 0.89 | 0.88 | 4.17 | 2.15 | 2.08 | 2.32 |
| K | 0.23 | 0.18 | 0.30 | 0.32 | - | 0.03 | 0.26 | 0.38 |
| total= | 15.89 | 15.73 | 15.90 | 15.95 | 16.78 | 15.75 | 15.91 | 15.88 |
| oxygens= | [23] | [23] | [23] | [23] | [23] | [23] | [23] | [23] |

9 1, YGD326 11 2, 216627 13 1, 40517 15 3, 40517
10 2, YGD326 12 3, 216627 14 2, 40517 16 4, 40517

## Amphiboles

| | 17 | 18 | 19 | 20 |
|---|---|---|---|---|
| SiO2 | 43.85 | 43.81 | 47.28 | 44.13 |
| TiO2 | 2.65 | 2.68 | 2.44 | 2.67 |
| Al2O3 | 4.44 | 4.60 | 2.35 | 4.32 |
| FeO | 29.39 | 29.05 | 30.83 | 29.05 |
| MnO | 0.52 | 0.51 | 0.61 | 0.53 |
| MgO | 3.32 | 3.52 | 2.56 | 3.40 |
| CaO | 8.33 | 8.40 | 5.90 | 8.26 |
| Na2O | 3.95 | 3.97 | 5.03 | 4.06 |
| K2O | 1.45 | 1.38 | 1.36 | 1.40 |
| total= | 97.90 | 97.92 | 98.36 | 97.82 |
| Si | 7.04 | 7.02 | 7.52 | 7.08 |
| Ti | 0.32 | 0.32 | 0.29 | 0.32 |
| Al | 0.84 | 0.87 | 0.44 | 0.82 |
| Fe2 | 3.95 | 3.89 | 4.10 | 3.90 |
| Mn | 0.07 | 0.07 | 0.08 | 0.07 |
| Mg | 0.79 | 0.84 | 0.61 | 0.81 |
| Ca | 1.43 | 1.44 | 1.01 | 1.42 |
| Na | 1.23 | 1.23 | 1.55 | 1.26 |
| K | 0.30 | 0.28 | 0.28 | 0.29 |
| total= | 15.98 | 15.98 | 15.88 | 15.97 |
| oxygens= | [23] | [23] | [23] | [23] |

17 1, 50218
18 3, 50218
19 3 rim, 50218
20 4, 50218

## XRF mineral analyses

| | 1 | 2 | 3 | 4 | 5 | 6 |
|---|---|---|---|---|---|---|
| SiO2 | 36.30 | 52.78 | 52.95 | 55.10 | 61.34 | 65.94 |
| TiO2 | 0.28 | 0.17 | 0.15 | 0.18 | 0.10 | 0.05 |
| Al2O3 | 0.40 | 26.43 | 27.21 | 26.46 | 21.79 | 18.81 |
| Fe2O3 | 35.87 | 1.33 | 0.48 | 0.67 | 0.65 | 0.46 |
| MnO | 0.47 | 0.02 | nd | 0.00 | 0.01 | 0.01 |
| MgO | 28.00 | 0.51 | 0.10 | 0.21 | 0.07 | nd |
| CaO | 1.00 | 10.31 | 10.16 | 8.82 | 3.55 | 0.46 |
| Na2O | -0.01 | 4.89 | 5.05 | 5.46 | 7.60 | 7.05 |
| K2O | 0.07 | 1.18 | 1.05 | 1.34 | 2.52 | 6.37 |
| P2O5 | 0.10 | 0.67 | 0.40 | 0.08 | 0.21 | 0.02 |
| total= | 102.48 | 98.29 | 97.55 | 98.31 | 97.84 | 99.17 |
| LOI | -2.68 | 1.23 | 1.57 | 0.74 | 0.28 | 0.64 |
| Ni | 281 | 9 | 9 | 7 | 5 | 5 |
| Cr | 6 | -2 | -1 | -2 | -2 | -2 |
| V | 24 | 5 | 5 | 2 | -2 | - |
| Sc | 6 | 4 | 7 | 6 | 3 | - |
| Cu | 12 | 4 | -2 | 9 | -6 | -3 |
| Zn | 185 | 38 | 3 | 5 | 4 | 8 |
| Sr | 6 | 1459 | 1567 | 1371 | 1728 | 54 |
| Rb | - | 9 | 3 | 13 | 7 | 89 |
| Zr | 8 | 47 | 9 | 25 | 43 | 69 |
| Nb | -1 | 4 | 2 | 2 | 1 | 7 |
| Ba | 16 | 1234 | 1017 | 1267 | 4549 | 389 |
| Pb | - | -2 | -2 | - | 5 | 10 |
| Th | - | - | - | - | - | 2 |
| La | 8 | 12 | 8 | 2 | 14 | 10 |
| Ce | -4 | 39 | 20 | 15 | 35 | 18 |
| Nd | -5 | 21 | 13 | 9 | 21 | 9 |
| Y | 4 | 12 | 6 | 3 | 6 | 8 |

1 Olivine, 30677
2 Feldspar, 40452
3 Feldspar, YGD6
4 Feldspar, YGD138
5 Feldspar, YGD362
6 Feldspar, YGD175

# APPENDIX IV: WHOLE-ROCK ANALYSES

## Chilled margins

| | 1 | 2 | 3 | 4 | 5 | 6 | 7 | 8 |
|---|---|---|---|---|---|---|---|---|
| $SiO_2$ | 43.65 | 44.35 | 43.98 | 45.67 | 45.56 | 43.99 | 42.45 | 43.43 |
| $TiO_2$ | 3.85 | 1.95 | 3.32 | 3.11 | 2.32 | 2.80 | 2.58 | 2.24 |
| $Al_2O_3$ | 15.84 | 18.03 | 15.33 | 16.05 | 17.17 | 14.98 | 11.94 | 13.63 |
| $Fe_2O_3$ | 17.08 | 15.24 | 15.41 | 15.65 | 14.25 | 17.46 | 19.73 | 18.92 |
| MnO | 0.20 | 0.17 | 0.20 | 0.19 | 0.17 | 0.21 | 0.24 | 0.23 |
| MgO | 5.36 | 8.32 | 5.06 | 5.26 | 6.59 | 8.23 | 11.88 | 10.93 |
| CaO | 8.12 | 7.79 | 6.61 | 7.82 | 8.07 | 7.08 | 6.24 | 6.43 |
| $Na_2O$ | 3.52 | 2.87 | 3.17 | 3.58 | 3.47 | 3.30 | 2.64 | 2.83 |
| $K_2O$ | 1.20 | 0.64 | 3.08 | 1.43 | 1.20 | 1.17 | 1.13 | 1.01 |
| $P_2O_5$ | 1.08 | 0.35 | 1.31 | 1.07 | 0.82 | 0.85 | 0.86 | 0.76 |
| total | 99.89 | 99.70 | 97.49 | 99.84 | 99.62 | 100.08 | 99.69 | 100.41 |
| LOI | | | 1.28 | | | | | |
| Ni | 45 | 100 | 40 | 40 | 70 | 92 | 146 | 125 |
| Cr | 25 | 35 | 18 | 16 | 13 | 24 | 18 | 17 |
| V | 316 | 245 | 174 | 172 | 136 | 208 | 134 | 127 |
| Sc | 24 | 12 | 17 | 18 | 14 | 18 | 17 | 13 |
| Cu | 61 | 27 | 46 | 59 | 48 | 49 | 55 | 52 |
| Zn | 119 | 85 | 104 | 103 | 94 | 111 | 123 | 115 |
| Sr | 795 | 949 | 722 | 812 | 916 | 759 | 595 | 726 |
| Rb | 15 | 8 | 119 | 27 | 16 | 16 | 15 | 14 |
| Zr | 157 | 66 | 191 | 158 | 147 | 141 | 142 | 130 |
| Nb | 23 | 9 | 30 | 25 | 21 | 21 | 21 | 19 |
| Ba | 1151 | 636 | 1351 | 1242 | 1023 | 1013 | 980 | 949 |
| Pb | 3 | - | 5 | 4 | 3 | 1 | 2 | 2 |
| La | 33 | 11 | 36 | 40 | 29 | 29 | 23 | 23 |
| Ce | 68 | 23 | 91 | 79 | 66 | 71 | 58 | 70 |
| Nd | 35 | 12 | 48 | 42 | 36 | 37 | 37 | 31 |
| Y | 31 | 12 | 36 | 33 | 27 | 27 | 28 | 25 |
| ne | 2.17 | 0.18 | 2.99 | 0.35 | 1.52 | 1.90 | 0.79 | 0.60 |
| cen | 1.36 | 0.27 | 0.62 | 1.17 | 1.13 | 1.15 | 1.46 | 0.89 |
| cfs | 1.67 | 0.22 | 0.74 | 1.41 | 1.05 | 1.05 | 1.09 | 0.71 |
| cwo | 3.04 | 0.51 | 1.37 | 2.60 | 2.23 | 2.26 | 2.65 | 1.66 |
| fo | 8.40 | 14.33 | 8.39 | 8.36 | 10.70 | 13.56 | 19.71 | 18.45 |
| fa | 11.41 | 13.04 | 11.11 | 11.08 | 10.92 | 13.62 | 16.22 | 16.11 |
| or | 7.08 | 3.77 | 18.19 | 8.46 | 7.08 | 6.91 | 6.70 | 5.94 |
| an | 23.88 | 34.43 | 18.50 | 23.52 | 27.74 | 22.60 | 17.40 | 21.53 |
| ab | 25.79 | 23.95 | 21.33 | 29.62 | 26.55 | 24.44 | 20.85 | 22.82 |
| mag | 3.39 | 3.03 | 3.06 | 3.11 | 2.83 | 3.47 | 3.92 | 3.76 |
| ilm | 7.30 | 3.70 | 6.31 | 5.91 | 4.41 | 5.32 | 4.90 | 4.26 |
| ap | 3.23 | 1.06 | 3.91 | 3.21 | 2.47 | 2.53 | 2.56 | 2.26 |
| D.I. | 35.0 | 27.9 | 42.5 | 38.4 | 35.2 | 33.3 | 28.3 | 29.4 |

$[Fe_2O_3/(FeO+Fe_2O_3) = 0.15]$

1 YGD1
2 YGD78
3 YGD122
4 YGD162
5 YGD228
6 YGD229
7 YGD259
8 YGD292

| | 9 | 10 | 11 | 12 | 13 | 14 |
|---|---|---|---|---|---|---|
| $SiO_2$ | 45.03 | 45.58 | 42.77 | 43.68 | 45.07 | 43.85 |
| $TiO_2$ | 1.27 | 2.72 | 4.03 | 2.80 | 3.19 | 2.65 |
| $Al_2O_3$ | 18.32 | 16.83 | 16.20 | 13.63 | 16.68 | 13.31 |
| $Fe_2O_3$ | 13.76 | 13.50 | 17.38 | 18.89 | 15.66 | 18.60 |
| MnO | 0.16 | 0.17 | 0.20 | 0.23 | 0.19 | 0.23 |
| MgO | 9.43 | 5.29 | 4.73 | 9.06 | 5.14 | 9.74 |
| CaO | 8.15 | 6.34 | 7.03 | 6.63 | 7.55 | 6.78 |
| $Na_2O$ | 2.71 | 3.22 | 3.13 | 2.92 | 3.35 | 3.07 |
| $K_2O$ | 0.56 | 3.02 | 1.80 | 1.14 | 1.44 | 1.21 |
| $P_2O_5$ | 0.32 | 1.07 | 0.90 | 0.93 | 0.92 | 0.91 |
| total | 99.71 | 97.74 | 98.16 | 99.92 | 99.18 | 100.35 |
| LOI | | 1.33 | 1.17 | | | |
| Ni | 119 | 55 | 49 | 97 | 43 | 110 |
| Cr | 37 | 16 | 30 | 15 | 28 | 14 |
| V | 128 | 144 | 264 | 168 | 197 | 145 |
| Sc | 9 | 17 | 19 | 17 | 16 | 15 |
| Cu | 32 | 32 | 47 | 52 | 53 | 54 |
| Zn | 76 | 73 | 124 | 121 | 90 | 117 |
| Sr | 1030 | 866 | 789 | 677 | 938 | 710 |
| Rb | 5 | 114 | 61 | 18 | 26 | 18 |
| Zr | 63 | 153 | 162 | 153 | 131 | 142 |
| Nb | 8 | 24 | 25 | 24 | 20 | 21 |
| Ba | 564 | 1311 | 1241 | 1034 | 1210 | 1106 |
| Pb | -1 | 4 | 2 | - | 1 | - |
| La | 7 | 35 | 30 | 30 | 27 | 28 |
| Ce | 23 | 70 | 65 | 71 | 62 | 67 |
| Nd | 16 | 38 | 37 | 37 | 35 | 36 |
| Y | 11 | 29 | 27 | 28 | 27 | 28 |
| ne | - | 1.67 | 1.34 | - | - | 1.23 |
| en | 0.59 | - | - | 1.04 | 0.40 | - |
| fs | 0.41 | - | - | 0.95 | 0.49 | - |
| cen | 0.37 | - | 0.43 | 0.92 | 0.65 | 1.55 |
| cfs | 0.26 | - | 0.60 | 0.84 | 0.80 | 1.30 |
| cwo | 0.66 | - | 1.03 | 1.81 | 1.46 | 2.94 |
| fo | 15.78 | 9.23 | 7.95 | 14.44 | 8.23 | 15.92 |
| fa | 12.04 | 10.46 | 12.30 | 14.53 | 11.08 | 14.80 |
| or | 3.30 | 17.83 | 10.62 | 6.76 | 8.49 | 7.17 |
| an | 36.17 | 22.42 | 24.84 | 20.70 | 26.23 | 18.95 |
| ab | 22.93 | 24.17 | 24.01 | 24.71 | 28.35 | 23.71 |
| mag | 2.73 | 2.68 | 3.45 | 3.75 | 3.11 | 3.70 |
| ilm | 2.42 | 5.17 | 7.66 | 5.33 | 6.06 | 5.03 |
| crn | - | 0.05 | - | - | - | - |
| ap | 0.95 | 3.20 | 2.68 | 2.78 | 2.74 | 2.71 |
| [$Fe_2O_3/(FeO+Fe_2O_3) = 0.15$] | | | | | | |
| D.I. | 26.2 | 43.7 | 36.0 | 31.5 | 36.8 | 32.1 |

9 YGD298 11 YGD317 13 YGD328
10 YGD122W 12 YGD325 14 YGD364

Troctolites

| | 1 | 2 | 3 | 4 | 5 | 6 | 7 | 8 |
|---|---|---|---|---|---|---|---|---|
| $SiO_2$ | 47.31 | 46.20 | 46.43 | 46.18 | 46.03 | 47.15 | 46.34 | 46.47 |
| $TiO_2$ | 1.19 | 1.61 | 1.82 | 1.45 | 1.48 | 1.68 | 1.54 | 1.41 |
| $Al_2O_3$ | 19.27 | 17.83 | 17.85 | 17.90 | 17.17 | 18.40 | 17.87 | 17.48 |
| $Fe_2O_3$ | 11.00 | 13.71 | 13.34 | 12.79 | 14.08 | 13.07 | 12.39 | 13.06 |
| MnO | 0.13 | 0.16 | 0.16 | 0.15 | 0.17 | 0.15 | 0.15 | 0.16 |
| MgO | 6.76 | 8.29 | 7.23 | 8.24 | 8.78 | 7.63 | 7.82 | 8.87 |
| CaO | 8.15 | 7.51 | 7.67 | 7.80 | 7.33 | 7.86 | 7.52 | 7.51 |
| $Na_2O$ | 3.58 | 3.48 | 3.86 | 3.48 | 3.11 | 3.69 | 3.34 | 3.60 |
| $K_2O$ | 1.25 | 0.81 | 0.81 | 0.76 | 0.94 | 0.91 | 1.35 | 0.77 |
| $P_2O_5$ | 0.54 | 0.47 | 0.71 | 0.62 | 0.40 | 0.58 | 0.46 | 0.57 |
| total | 99.19 | 100.07 | 99.90 | 99.37 | 99.50 | 101.12 | 98.78 | 99.90 |
| LOI | | | | | | -0.63 | 0.42 | |
| Ni | 83 | 97 | 77 | 101 | 105 | 83 | 93 | 108 |
| Cr | 8 | 19 | 9 | 10 | 10 | 8 | 11 | 15 |
| V | 79 | 117 | 100 | 78 | 84 | 87 | 103 | 80 |
| Sc | 10 | 10 | 10 | 8 | 9 | 7 | 11 | 11 |
| Cu | 25 | 33 | 36 | 30 | 35 | 40 | 31 | 35 |
| Zn | 64 | 75 | 83 | 76 | 81 | 71 | 73 | 73 |
| Sr | 1104 | 1014 | 981 | 1001 | 982 | 1053 | 993 | 983 |
| Rb | 13 | 8 | 10 | 8 | 13 | 10 | 21 | 9 |
| Zr | 84 | 86 | 101 | 87 | 92 | 101 | 102 | 93 |
| Nb | 11 | 12 | 15 | 12 | 13 | 14 | 14 | 13 |
| Ba | 773 | 765 | 843 | 785 | 757 | 885 | 854 | 791 |
| Pb | - | - | 2 | 2 | 2 | - | - | - |
| La | 12 | 7 | 15 | 21 | 17 | 16 | 17 | 18 |
| Ce | 31 | 35 | 41 | 41 | 36 | 38 | 42 | 44 |
| Nd | 24 | 16 | 29 | 25 | 23 | 17 | 20 | 25 |
| Y | 16 | 16 | 20 | 17 | 17 | 19 | 16 | 19 |
| ne | 1.67 | 1.18 | 1.65 | 0.75 | - | 1.41 | 1.54 | 1.38 |
| en | - | - | - | - | 0.32 | - | - | - |
| fs | - | - | - | - | 0.24 | - | - | - |
| cen | 0.69 | 0.61 | 0.68 | 0.58 | 0.65 | 0.72 | 0.84 | 0.76 |
| cfs | 0.52 | 0.47 | 0.56 | 0.41 | 0.49 | 0.56 | 0.60 | 0.52 |
| cwo | 1.26 | 1.12 | 1.28 | 1.03 | 1.18 | 1.32 | 1.51 | 1.34 |
| fo | 11.31 | 14.03 | 12.14 | 13.98 | 14.65 | 12.82 | 13.05 | 14.95 |
| fa | 9.42 | 11.72 | 11.01 | 11.02 | 12.07 | 10.91 | 10.34 | 11.27 |
| or | 7.40 | 4.80 | 4.81 | 4.47 | 5.57 | 5.36 | 7.97 | 4.56 |
| an | 32.81 | 30.61 | 28.99 | 31.00 | 30.12 | 30.97 | 29.78 | 29.24 |
| ab | 27.24 | 27.29 | 29.59 | 28.06 | 26.29 | 28.59 | 25.44 | 27.95 |
| mag | 2.19 | 2.72 | 2.65 | 2.54 | 2.80 | 2.60 | 2.46 | 2.59 |
| ilm | 2.26 | 3.07 | 3.46 | 2.75 | 2.81 | 3.18 | 2.92 | 2.67 |
| ap | 1.63 | 1.40 | 2.13 | 1.85 | 1.20 | 1.73 | 1.38 | 1.72 |
| D.I. | 36.3 | 33.3 | 36.1 | 33.3 | 31.9 | 35.4 | 34.9 | 33.9 |

$[Fe_2O_3/(FeO+Fe_2O_3) = 0.15]$

1 YGD4
2 YGD6
3 YGD7
4 YGD8
5 YGD10
6 YGD11
7 YGD23
8 YGD36B

| | 9 | 10 | 11 | 12 | 13 | 14 | 15 | 16 |
|---|---|---|---|---|---|---|---|---|
| $SiO_2$ | 45.90 | 45.74 | 45.13 | 45.34 | 48.05 | 44.43 | 43.90 | 41.61 |
| $TiO_2$ | 1.51 | 1.24 | 1.53 | 1.49 | 2.52 | 3.64 | 3.83 | 4.40 |
| $Al_2O_3$ | 16.81 | 17.26 | 17.24 | 17.54 | 19.55 | 16.38 | 17.26 | 16.04 |
| $Fe_2O_3$ | 13.95 | 13.48 | 13.06 | 13.27 | 11.62 | 16.66 | 13.86 | 15.64 |
| MnO | 0.17 | 0.16 | 0.15 | 0.16 | 0.15 | 0.20 | 0.17 | 0.19 |
| MgO | 9.92 | 9.59 | 8.71 | 9.04 | 3.20 | 4.47 | 4.05 | 4.79 |
| CaO | 7.50 | 7.68 | 7.53 | 7.77 | 7.79 | 7.44 | 8.85 | 9.04 |
| $Na_2O$ | 3.17 | 3.17 | 3.06 | 3.18 | 4.24 | 3.85 | 3.74 | 3.62 |
| $K_2O$ | 0.99 | 0.70 | 1.32 | 0.81 | 1.42 | 1.55 | 1.32 | 1.23 |
| $P_2O_5$ | 0.61 | 0.66 | 0.61 | 0.49 | 0.48 | 0.76 | 1.83 | 2.47 |
| total | 100.53 | 99.68 | 98.35 | 99.10 | 99.03 | 99.39 | 98.81 | 99.01 |
| LOI | 0.36 | | 0.78 | | | | 0.50 | |
| Ni | 117 | 124 | 116 | 111 | 14 | 24 | 18 | 23 |
| Cr | 14 | 12 | 13 | 12 | - | - | -2 | 4 |
| V | 87 | 68 | 93 | 88 | 89 | 164 | 121 | 161 |
| Sc | 9 | 9 | 10 | 9 | 10 | 16 | 11 | 13 |
| Cu | 32 | 29 | 32 | 31 | 22 | 58 | 62 | 201 |
| Zn | 79 | 76 | 79 | 78 | 89 | 118 | 98 | 105 |
| Sr | 918 | 988 | 983 | 991 | 1004 | 833 | 907 | 854 |
| Rb | 11 | 7 | 22 | 9 | 17 | 25 | 19 | 17 |
| Zr | 86 | 83 | 98 | 90 | 152 | 180 | 144 | 126 |
| Nb | 12 | 11 | 14 | 13 | 25 | 26 | 24 | 20 |
| Ba | 790 | 743 | 789 | 735 | 1259 | 1239 | 1125 | 1075 |
| Pb | - | - | 1 | - | - | 4 | 3 | 2 |
| La | 16 | 15 | 18 | 20 | 20 | 35 | 34 | 35 |
| Ce | 40 | 44 | 42 | 32 | 60 | 78 | 86 | 103 |
| Nd | 22 | 24 | 23 | 19 | 31 | 41 | 49 | 62 |
| Y | 17 | 18 | 18 | 17 | 23 | 30 | 33 | 35 |
| ne | 0.75 | 0.06 | 1.44 | 1.19 | 1.78 | 3.83 | 0.93 | 1.38 |
| cen | 0.80 | 0.42 | 0.66 | 0.77 | 0.78 | 1.30 | 0.39 | 0.03 |
| cfs | 0.55 | 0.28 | 0.45 | 0.52 | 1.11 | 1.89 | 0.47 | 0.03 |
| cwo | 1.41 | 0.74 | 1.17 | 1.36 | 1.88 | 3.17 | 0.86 | 0.06 |
| fo | 15.72 | 16.4 | 14.74 | 15.24 | 5.05 | 6.89 | 6.79 | 8.34 |
| fa | 11.82 | 12.10 | 11.15 | 11.38 | 7.93 | 11.08 | 9.05 | 10.48 |
| or | 5.81 | 4.14 | 7.79 | 4.80 | 8.41 | 9.18 | 7.81 | 7.24 |
| an | 27.89 | 30.76 | 29.42 | 31.17 | 30.09 | 22.85 | 26.41 | 23.91 |
| ab | 25.21 | 26.75 | 23.24 | 24.73 | 32.60 | 25.48 | 29.95 | 28.06 |
| mag | 2.72 | 2.68 | 2.59 | 2.64 | 2.31 | 3.31 | 2.75 | 3.11 |
| ilm | 2.80 | 2.35 | 2.92 | 2.82 | 4.78 | 6.91 | 7.28 | 8.35 |
| ap | 1.76 | 1.97 | 1.82 | 1.47 | 1.44 | 2.29 | 5.47 | 7.38 |
| D.I. | 31.8 | 31.0 | 32.5 | 30.7 | 42.8 | 38.5 | 38.7 | 36.7 |

[$Fe_2O_3/(FeO+Fe_2O_3) = 0.15$]

9 YGD39 11 YGD51 13 YGD141 15 YGD145
10 YGD41 12 YGD52 14 YGD142 16 YGD157

| | 17 | 18 | 19 | 20 | 21 | 22 | 23 | 24 |
|---|---|---|---|---|---|---|---|---|
| $SiO_2$ | 42.11 | 45.53 | 44.79 | 44.03 | 46.94 | 46.12 | 42.96 | 45.68 |
| $TiO_2$ | 4.32 | 1.45 | 1.56 | 1.36 | 1.00 | 2.39 | 1.21 | 1.99 |
| $Al_2O_3$ | 16.27 | 16.54 | 15.57 | 13.86 | 19.15 | 19.44 | 12.60 | 18.61 |
| $Fe_2O_3$ | 15.52 | 14.15 | 15.32 | 17.70 | 11.67 | 12.16 | 19.84 | 13.35 |
| MnO | 0.19 | 0.17 | 0.18 | 0.21 | 0.15 | 0.15 | 0.23 | 0.16 |
| MgO | 4.64 | 9.74 | 10.76 | 13.35 | 7.33 | 4.60 | 15.01 | 5.86 |
| CaO | 9.37 | 7.16 | 6.91 | 6.10 | 8.09 | 8.99 | 5.70 | 7.94 |
| $Na_2O$ | 3.44 | 3.42 | 3.09 | 2.80 | 3.28 | 3.63 | 2.32 | 3.47 |
| $K_2O$ | 1.19 | 0.63 | 0.72 | 0.54 | 1.11 | 1.06 | 0.47 | 1.06 |
| $P_2O_5$ | 2.45 | 0.56 | 0.55 | 0.46 | 0.43 | 0.96 | 0.30 | 0.64 |
| total | 99.47 | 99.34 | 99.46 | 100.43 | 99.17 | 99.50 | 100.67 | 98.78 |
| Ni | 21 | 125 | 134 | 173 | 84 | 48 | 198 | 51 |
| Cr | -1 | 12 | 9 | 16 | - | 12 | 12 | 18 |
| V | 150 | 90 | 93 | 99 | 41 | 125 | 79 | 131 |
| Sc | 12 | 10 | 11 | 7 | 5 | 12 | 9 | 8 |
| Cu | 155 | 31 | 33 | 31 | 22 | 50 | 32 | 39 |
| Zn | 104 | 85 | 87 | 100 | 70 | 74 | 114 | 84 |
| Sr | 872 | 907 | 870 | 770 | 1106 | 1119 | 716 | 1007 |
| Rb | 16 | 7 | 10 | 6 | 14 | 13 | 8 | 12 |
| Zr | 131 | 90 | 94 | 83 | 95 | 131 | 69 | 120 |
| Nb | 23 | 12 | 13 | 11 | 12 | 19 | 10 | 18 |
| Ba | 1069 | 761 | 734 | 706 | 848 | 993 | 560 | 925 |
| Pb | 2 | 2 | - | 1 | -1 | - | 2 | - |
| La | 35 | 12 | 12 | 15 | 15 | 20 | 6 | 16 |
| Ce | 103 | 45 | 40 | 37 | 37 | 56 | 32 | 50 |
| Nd | 62 | 20 | 19 | 17 | 18 | 39 | 16 | 26 |
| Y | 37 | 17 | 18 | 15 | 17 | 26 | 12 | 21 |
| ne | 0.14 | 0.92 | 0.59 | 0.30 | 0.66 | 0.83 | - | 0.90 |
| en | - | - | - | - | - | - | 0.27 | - |
| fs | - | - | - | - | - | - | 0.18 | - |
| cen | 0.08 | 0.70 | 0.75 | 0.66 | 0.51 | 0.57 | 0.76 | 0.40 |
| cfs | 0.09 | 0.47 | 0.50 | 0.42 | 0.39 | 0.61 | 0.50 | 0.40 |
| cwo | 0.17 | 1.22 | 1.31 | 1.13 | 0.94 | 1.20 | 1.32 | 0.81 |
| fo | 8.04 | 16.51 | 18.26 | 22.84 | 12.44 | 7.63 | 25.48 | 9.95 |
| fa | 10.42 | 12.37 | 13.42 | 16.19 | 10.47 | q9.03 | 18.38 | 10.93 |
| or | 7.01 | 3.70 | 4.24 | 3.19 | 6.57 | 6.25 | 2.80 | 6.29 |
| an | 25.43 | 27.93 | 26.48 | 23.65 | 34.26 | 33.63 | 22.58 | 32.05 |
| ab | 28.87 | 27.22 | 25.09 | 23.17 | 26.53 | 29.15 | 19.63 | 27.74 |
| mag | 3.08 | 2.81 | 3.04 | 3.52 | 2.32 | 2.42 | 3.94 | 2.65 |
| ilm | 8.20 | 2.76 | 2.96 | 2.58 | 1.90 | 4.54 | 2.30 | 3.78 |
| ap | 7.32 | 1.66 | 1.66 | 1.39 | 1.29 | 2.87 | 0.91 | 1.92 |
| D.I. | 36.0 | 31.8 | 29.9 | 26.7 | 33.8 | 36.2 | 22.4 | 34.9 |

$[Fe_2O_3/(FeO+Fe_2O_3) = 0.15]$

17 YGD159
18 YGD244
19 YGD245B
20 YGD256
21 YGD285
22 YGD293
23 YGD307
24 YGD422

| | 25 | 26 | 27 | 28 | 29 | 30 | 31 | 32 |
|---|---|---|---|---|---|---|---|---|
| $SiO_2$ | 45.38 | 48.39 | 44.41 | 47.24 | 47.47 | 46.50 | 43.53 | 41.59 |
| $TiO_2$ | 2.12 | 2.14 | 2.43 | 2.33 | 2.56 | 2.02 | 3.33 | 4.03 |
| $Al_2O_3$ | 18.51 | 19.64 | 19.19 | 17.91 | 19.88 | 17.69 | 17.79 | 16.90 |
| $Fe_2O_3$ | 13.85 | 9.95 | 14.50 | 13.80 | 10.60 | 13.15 | 15.91 | 17.89 |
| MnO | 0.16 | 0.14 | 0.15 | 0.19 | 0.14 | 0.16 | 0.15 | 0.18 |
| MgO | 6.61 | 3.44 | 6.60 | 3.99 | 3.14 | 6.64 | 5.82 | 6.51 |
| CaO | 8.44 | 9.33 | 7.98 | 7.61 | 8.40 | 7.96 | 6.96 | 7.50 |
| $Na_2O$ | 3.35 | 4.01 | 3.28 | 3.89 | 4.06 | 3.59 | 3.39 | 3.06 |
| $K_2O$ | 0.84 | 1.23 | 0.66 | 1.54 | 1.39 | 1.14 | 1.28 | 0.93 |
| $P_2O_5$ | 0.58 | 0.89 | 0.36 | 0.72 | 1.03 | 0.81 | 0.28 | 0.87 |
| total | 99.82 | 99.15 | 99.56 | 99.22 | 98.67 | 99.66 | 98.44 | 99.46 |
| LOI | | | | | 0.36 | | 0.83 | |
| Ni | 70 | 23 | 96 | 24 | 19 | 74 | 79 | 74 |
| Cr | 39 | 5 | 32 | 15 | 4 | 10 | 21 | 17 |
| V | 189 | 97 | 343 | 125 | 71 | 89 | 377 | 374 |
| Sc | 13 | 21 | 9 | 14 | 11 | 12 | 13 | 13 |
| Cu | 39 | 57 | 30 | 66 | 50 | 36 | 20 | 38 |
| Zn | 86 | 68 | 81 | 107 | 71 | 77 | 88 | 91 |
| Sr | 1046 | 1098 | 1116 | 1049 | 1142 | 1087 | 1125 | 1099 |
| Rb | 8 | 12 | 7 | 20 | 18 | 13 | 21 | 11 |
| Zr | 98 | 134 | 73 | 175 | 155 | 111 | 123 | 89 |
| Nb | 14 | 19 | 9 | 24 | 24 | 18 | 18 | 14 |
| Ba | 817 | 1277 | 721 | 1366 | 1197 | 1119 | 1062 | 904 |
| Pb | - | - | - | 3 | 1 | -1 | - | -2 |
| La | 13 | 21 | 5 | 26 | 29 | 24 | 20 | 20 |
| Ce | 35 | 58 | 26 | 68 | 73 | 53 | 50 | 55 |
| Nd | 20 | 39 | 15 | 34 | 38 | 26 | 22 | 29 |
| Y | 19 | 27 | 13 | 27 | 27 | 22 | 16 | 19 |
| ne | 1.39 | 0.55 | 1.56 | 0.85 | 0.22 | 0.71 | 3.06 | 1.66 |
| cen | 0.85 | 1.32 | 0.18 | 0.81 | 0.19 | 0.84 | 0.52 | 0.04 |
| cfs | 0.77 | 1.51 | 0.17 | 1.19 | 0.24 | 0.72 | 0.56 | 0.04 |
| cwo | 1.67 | 2.86 | 0.36 | 1.99 | 0.43 | 1.60 | 1.09 | 0.09 |
| fo | 10.94 | 5.07 | 11.39 | 6.40 | 5.35 | 11.00 | 9.80 | 11.33 |
| fa | 10.97 | 6.39 | 11.68 | 10.38 | 7.49 | 10.43 | 11.67 | 13.22 |
| or | 4.94 | 7.27 | 3.89 | 9.10 | 8.23 | 6.72 | 7.56 | 5.51 |
| an | 33.02 | 31.96 | 35.68 | 26.89 | 31.94 | 28.79 | 29.55 | 29.62 |
| ab | 25.75 | 32.93 | 24.93 | 31.31 | 33.91 | 29.06 | 23.03 | 22.84 |
| mag | 2.75 | 1.98 | 2.88 | 2.74 | 2.11 | 2.61 | 3.16 | 3.55 |
| ilm | 4.02 | 4.06 | 4.62 | 4.42 | 4.87 | 3.83 | 6.32 | 7.65 |
| ap | 1.73 | 2.65 | 1.08 | 2.16 | 3.08 | 2.43 | 0.84 | 2.62 |
| D.I. | 32.1 | 40.8 | 30.4 | 41.3 | 42.4 | 36.5 | 33.7 | 30.0 |

$[Fe_2O_3/(FeO+Fe_2O_3) = 0.15]$

25 YGD423 27 YGD425 29 YGD427 31 YGD197
26 YGD424 28 YGD426 30 YGD125 32 YGD203

| | 33 | 34 | 35 | 36 | 37 | 38 | 39 | 40 |
|---|---|---|---|---|---|---|---|---|
| $SiO_2$ | 44.39 | 46.74 | 46.75 | 42.53 | 47.30 | 42.21 | 40.37 | 46.77 |
| $TiO_2$ | 3.04 | 2.45 | 2.31 | 3.58 | 1.90 | 3.56 | 4.77 | 2.24 |
| $Al_2O_3$ | 20.25 | 20.33 | 21.16 | 18.66 | 18.27 | 18.00 | 13.90 | 20.49 |
| $Fe_2O_3$ | 14.33 | 12.33 | 11.08 | 16.27 | 11.98 | 18.01 | 19.06 | 10.95 |
| MnO | 0.13 | 0.14 | 0.12 | 0.16 | 0.14 | 0.19 | 0.24 | 0.14 |
| MgO | 4.81 | 3.81 | 3.85 | 5.48 | 7.72 | 6.65 | 4.72 | 3.64 |
| CaO | 7.89 | 8.59 | 8.71 | 7.58 | 7.77 | 7.07 | 7.35 | 9.31 |
| $Na_2O$ | 3.43 | 3.97 | 3.58 | 3.14 | 3.77 | 2.98 | 3.12 | 3.84 |
| $K_2O$ | 0.75 | 0.94 | 1.02 | 0.87 | 1.14 | 0.91 | 1.52 | 1.09 |
| $P_2O_5$ | 0.26 | 0.67 | 0.37 | 0.45 | 0.92 | 0.31 | 1.33 | 0.93 |
| total | 99.28 | 99.97 | 98.95 | 98.71 | 100.91 | 99.90 | 96.38 | 99.40 |
| LOI | | | 0.35 | | | -0.40 | | |
| Ni | 38 | 37 | 38 | 54 | 97 | 48 | 21 | 23 |
| Cr | 1 | 7 | 11 | - | 11 | 5 | 11 | 15 |
| V | 362 | 190 | 216 | 401 | 92 | 378 | 222 | 101 |
| Sc | 2 | 10 | 10 | 11 | 11 | 8 | 25 | 9 |
| Cu | 27 | 45 | 32 | 28 | 28 | 25 | 48 | 16 |
| Zn | 69 | 68 | 62 | 91 | 66 | 97 | 154 | 48 |
| Sr | 1270 | 1214 | 1317 | 1177 | 1070 | 1034 | 624 | 1099 |
| Rb | 7 | 11 | 14 | 12 | 16 | 13 | 31 | 11 |
| Zr | 48 | 93 | 85 | 72 | 120 | 64 | 207 | 89 |
| Nb | 7 | 14 | 13 | 12 | 19 | 12 | 36 | 15 |
| Ba | 711 | 938 | 916 | 897 | 1120 | 693 | 1171 | 897 |
| Pb | -1 | -2 | -4 | - | -1 | 1 | 5 | - |
| La | 10 | 24 | 13 | 24 | 35 | 24 | 39 | 22 |
| Ce | 22 | 51 | 36 | 42 | 59 | 32 | 89 | 54 |
| Nd | 12 | 26 | 22 | 21 | 30 | 12 | 49 | 30 |
| Y | 9 | 19 | 14 | 15 | 23 | 10 | 37 | 19 |
| ne | 1.38 | 1.63 | 0.60 | 1.55 | 1.02 | 2.59 | 1.63 | 1.40 |
| cen | - | 0.39 | 0.28 | - | 0.30 | 0.13 | 0.97 | 0.54 |
| cfs | - | 0.50 | 0.32 | - | 0.20 | 0.15 | 1.46 | 0.65 |
| cwo | - | 0.89 | 0.60 | - | 0.53 | 0.28 | 2.41 | 1.20 |
| fo | 8.39 | 6.38 | 6.52 | 9.56 | 13.27 | 10.98 | 7.55 | 5.98 |
| fa | 10.84 | 9.19 | 8.22 | 12.15 | 9.77 | 13.43 | 12.45 | 7.94 |
| or | 4.43 | 5.57 | 6.03 | 5.14 | 6.74 | 5.24 | 8.99 | 6.45 |
| an | 36.93 | 34.87 | 38.65 | 33.76 | 29.55 | 31.08 | 19.44 | 35.45 |
| ab | 26.48 | 30.59 | 29.18 | 23.70 | 30.04 | 19.55 | 23.37 | 29.91 |
| mag | 2.85 | 2.45 | 2.20 | 3.23 | 2.38 | 3.43 | 3.79 | 2.18 |
| ilm | 5.78 | 4.65 | 4.38 | 6.80 | 3.60 | 6.30 | 9.07 | 4.25 |
| cm | 0.26 | - | - | 0.18 | - | - | - | - |
| ap | 0.78 | 1.99 | 1.10 | 1.36 | 2.75 | 0.85 | 3.98 | 2.79 |
| D.I. | 32.3 | 37.8 | 35.8 | 30.4 | 37.8 | 27.4 | 34.0 | 37.8 |

[$Fe_2O_3/(FeO+Fe_2O_3) = 0.15$]

33 YGD334 35 YGD366 37 YGD313 39 YGD140
34 YGD365 36 YGD195 38 YGD382 40 YGD392

## Mafic Cumulates

| | 1 | 2 | 3 | 4 | 5 | 6 | 7 | 8 |
|---|---|---|---|---|---|---|---|---|
| $SiO_2$ | 39.83 | 39.00 | 20.48 | 23.05 | 39.20 | 40.29 | 39.97 | 38.46 |
| $TiO_2$ | 1.10 | 1.11 | 13.78 | 10.13 | 1.07 | 1.14 | 1.10 | 1.07 |
| $Al_2O_3$ | 7.07 | 5.12 | 5.86 | 3.96 | 5.17 | 6.68 | 6.57 | 4.59 |
| $Fe_2O_3$ | 26.00 | 26.72 | 37.60 | 43.17 | 25.12 | 24.67 | 24.91 | 27.60 |
| MnO | 0.30 | 0.31 | 0.36 | 0.39 | 0.28 | 0.28 | 0.29 | 0.32 |
| MgO | 21.19 | 23.54 | 8.62 | 16.20 | 24.47 | 21.93 | 22.14 | 23.82 |
| CaO | 3.30 | 2.77 | 7.00 | 1.38 | 2.66 | 3.33 | 2.96 | 2.49 |
| $Na_2O$ | 1.39 | 1.12 | 0.95 | 0.33 | 1.06 | 1.36 | 1.23 | 0.89 |
| $K_2O$ | 0.51 | 0.45 | 0.39 | 0.43 | 0.63 | 0.61 | 0.62 | 0.62 |
| $P_2O_5$ | 0.34 | 0.44 | 3.63 | 0.35 | 0.41 | 0.33 | 0.37 | 0.40 |
| total | 101.02 | 100.58 | 98.67 | 99.39 | 100.09 | 100.63 | 100.17 | 100.26 |
| LOI | -1.52 | | -1.80 | | | | | |
| Ni | 274 | 331 | 45 | 190 | 356 | 305 | 310 | 336 |
| Cr | 17 | 25 | 10 | 41 | 19 | 21 | 21 | 13 |
| V | 80 | 75 | 687 | 1211 | 78 | 85 | 71 | 65 |
| Sc | 10 | 9 | 23 | 13 | 9 | 9 | 9 | 8 |
| Cu | 32 | 36 | 1040 | 50 | 28 | 31 | 30 | 32 |
| Zn | 144 | 151 | 244 | 246 | 144 | 138 | 138 | 159 |
| Sr | 383 | 268 | 345 | 118 | 252 | 335 | 337 | 227 |
| Rb | 5 | 9 | 6 | 10 | 9 | 9 | 15 | 17 |
| Zr | 47 | 58 | 106 | 59 | 56 | 64 | 62 | 62 |
| Nb | 7 | 10 | 32 | 13 | 9 | 9 | 10 | 10 |
| Ba | 453 | 438 | 440 | 351 | 449 | 474 | 525 | 373 |
| Pb | 2 | 1 | 3 | 2 | 3 | 2 | 1 | 2 |
| La | 6 | 16 | 49 | 18 | 15 | 12 | 12 | 10 |
| Ce | 19 | 34 | 115 | 19 | 20 | 18 | 31 | 22 |
| Nd | 6 | 15 | 73 | 2 | 6 | 7 | 12 | 7 |
| Y | 11 | 15 | 42 | 11 | 12 | 13 | 13 | 14 |
| ne | - | - | 1.10 | 1.50 | - | - | - | - |
| en | 2.06 | 3.39 | - | - | 2.76 | 2.42 | 4.40 | 3.55 |
| fs | 1.28 | 1.96 | - | - | 1.43 | 1.37 | 2.51 | 2.10 |
| cen | 0.48 | 0.60 | - | -1.59 | 0.59 | 0.87 | 0.24 | 0.56 |
| cfs | 0.30 | 0.35 | - | -1.60 | 0.31 | 0.50 | 0.14 | 0.33 |
| cwo | 0.82 | 1.00 | - | -3.24 | 0.96 | 1.44 | 0.39 | 0.94 |
| fo | 35.20 | 38.28 | 15.05 | 30.49 | 40.36 | 35.97 | 35.39 | 38.70 |
| fa | 24.17 | 24.35 | 21.04 | 33.88 | 23.16 | 22.52 | 22.24 | 25.20 |
| lct | - | - | - | 1.97 | - | - | - | - |
| or | 2.99 | 2.67 | 2.33 | - | 3.75 | 3.63 | 3.69 | 3.69 |
| an | 11.55 | 7.64 | 4.09 | 3.89 | 7.46 | 10.28 | 10.57 | 6.70 |
| ab | 11.76 | 9.44 | 5.97 | - | 9.01 | 11.54 | 10.41 | 7.51 |
| mag | 5.17 | 5.31 | 7.47 | 8.58 | 4.99 | 4.90 | 4.95 | 5.48 |
| ilm | 2.09 | 2.10 | 26.18 | 19.24 | 2.04 | 2.17 | 2.08 | 2.03 |
| crn | - | - | 2.37 | 1.53 | - | - | - | - |
| ap | 1.01 | 1.31 | 10.86 | 1.05 | 1.21 | 0.98 | 1.12 | 1.20 |
| D.I. | 14.8 | 12.1 | 9.4 | 1.5 | 12.8 | 15.2 | 14.1 | 11.2 |

$[Fe_2O_3/(FeO+Fe_2O_3) = 0.15]$

1 YGD5
2 YGD36A
3 YGD158
4 YGD196
5 YGD237
6 YGD242
7 YGD243
8 YGD245A

| | 9 | 10 | 11 | 12 | 13 | 14 | 15 | 16 |
|---|---|---|---|---|---|---|---|---|
| $SiO_2$ | 39.45 | 39.38 | 39.04 | 39.26 | 39.31 | 39.06 | 38.09 | 38.74 |
| $TiO_2$ | 1.00 | 0.93 | 1.37 | 1.01 | 1.02 | 1.07 | 0.96 | 0.87 |
| $Al_2O_3$ | 5.66 | 5.73 | 5.87 | 4.92 | 5.64 | 5.31 | 4.28 | 4.89 |
| $Fe_2O_3$ | 25.82 | 26.29 | 26.17 | 26.49 | 26.61 | 26.61 | 27.65 | 26.59 |
| MnO | 0.30 | 0.30 | 0.30 | 0.30 | 0.31 | 0.31 | 0.32 | 0.31 |
| MgO | 23.43 | 23.07 | 22.56 | 23.99 | 23.10 | 23.51 | 24.83 | 24.22 |
| CaO | 2.78 | 2.73 | 3.03 | 2.58 | 2.92 | 2.68 | 2.52 | 2.70 |
| $Na_2O$ | 1.21 | 1.23 | 1.36 | 1.17 | 1.25 | 1.23 | 0.68 | 0.96 |
| K2O | 0.50 | 0.51 | 0.58 | 0.62 | 0.48 | 0.49 | 0.56 | 0.43 |
| $P_2O_5$ | 0.38 | 0.36 | 0.51 | 0.35 | 0.39 | 0.36 | 0.37 | 0.40 |
| total | 100.52 | 100.55 | 100.79 | 100.70 | 101.03 | 100.61 | 100.25 | 100.10 |
| LOI | | | | | -1.87 | | | |
| Ni | 327 | 326 | 311 | 338 | 326 | 335 | 378 | 356 |
| Cr | 22 | 20 | 28 | 25 | 17 | 20 | 21 | 29 |
| V | 64 | 64 | 78 | 72 | 51 | 85 | 50 | 46 |
| Sc | 9 | 6 | 10 | 9 | 8 | 7 | 8 | 9 |
| Cu | 31 | 32 | 37 | 31 | 32 | 31 | 34 | 29 |
| Zn | 142 | 148 | 150 | 150 | 153 | 149 | 156 | 145 |
| Sr | 300 | 297 | 312 | 246 | 310 | 272 | 224 | 278 |
| Rb | 6 | 7 | 7 | 9 | 7 | 9 | 10 | 8 |
| Zr | 57 | 55 | 67 | 60 | 57 | 55 | 50 | 58 |
| Nb | 9 | 8 | 11 | 9 | 10 | 9 | 8 | 9 |
| Ba | 480 | 438 | 539 | 462 | 441 | 433 | 321 | 394 |
| Pb | 2 | - | 2 | - | 2 | 3 | 1 | 1 |
| La | 11 | 13 | 14 | 12 | 12 | 11 | 15 | 9 |
| Ce | 24 | 21 | 26 | 25 | 23 | 16 | 10 | 22 |
| Nd | 13 | 9 | 11 | 12 | 12 | 9 | 7 | 10 |
| Y | 13 | 13 | 14 | 13 | 13 | 12 | 12 | 13 |
| en | 2.77 | 2.54 | 0.73 | 1.50 | 1.77 | 1.63 | 3.89 | 3.74 |
| fs | 1.56 | 1.48 | 0.42 | 0.85 | 1.04 | 0.94 | 2.22 | 2.11 |
| cen | 0.53 | 0.47 | 0.62 | 0.88 | 0.70 | 0.69 | 0.60 | 0.59 |
| cfs | 0.30 | 0.28 | 0.36 | 0.50 | 0.41 | 0.40 | 0.34 | 0.33 |
| cwo | 0.87 | 0.79 | 1.04 | 1.46 | 1.17 | 1.15 | 1.00 | 0.97 |
| fo | 38.57 | 38.16 | 38.42 | 40.19 | 38.58 | 39.40 | 40.18 | 39.23 |
| fa | 23.89 | 24.54 | 24.60 | 24.96 | 25.01 | 25.02 | 25.28 | 24.42 |
| or | 2.97 | 3.01 | 3.45 | 3.68 | 2.81 | 2.91 | 3.28 | 2.55 |
| an | 8.50 | 8.60 | 8.21 | 6.33 | 8.37 | 7.52 | 6.97 | 7.74 |
| ab | 10.27 | 10.43 | 11.47 | 9.93 | 10.59 | 10.37 | 5.77 | 8.12 |
| mag | 5.13 | 5.22 | 5.20 | 5.26 | 5.29 | 5.29 | 5.49 | 5.28 |
| ilm | 1.90 | 1.77 | 2.60 | 1.92 | 1.93 | 2.03 | 1.82 | 1.64 |
| ap | 1.13 | 1.09 | 1.53 | 1.06 | 1.17 | 1.06 | 1.12 | 1.19 |
| D.I. | 13.2 | 13.4 | 14.9 | 13.6 | 13.4 | 13.3 | 9.1 | 10.7 |

$[Fe_2O_3/(FeO+Fe_2O_3) = 0.15]$

9 YGD255 11 YGD274 13 YGD276 15 YGD281
10 YGD265 12 YGD275 14 YGD280 16 YGD282

| | 17 | 18 | 19 | 20 | 21 | 22 | 23 |
|---|---|---|---|---|---|---|---|
| $SiO_2$ | 42.21 | 38.25 | 38.53 | 41.68 | 27.55 | 40.78 | 43.87 |
| $TiO_2$ | 2.36 | 0.85 | 0.99 | 1.71 | 9.97 | 1.76 | 3.16 |
| $Al_2O_3$ | 11.62 | 3.97 | 5.26 | 9.46 | 4.64 | 13.42 | 15.72 |
| $Fe_2O_3$ | 20.73 | 27.29 | 25.39 | 22.40 | 36.42 | 19.87 | 17.21 |
| MnO | 0.25 | 0.31 | 0.28 | 0.26 | 0.38 | 0.22 | 0.18 |
| MgO | 13.00 | 26.59 | 24.39 | 17.09 | 13.92 | 12.85 | 6.64 |
| CaO | 5.71 | 2.07 | 2.69 | 4.78 | 3.93 | 5.89 | 6.73 |
| $Na_2O$ | 2.69 | 0.89 | 0.79 | 2.02 | 0.65 | 1.52 | 3.22 |
| $K_2O$ | 0.98 | 0.49 | 0.53 | 0.81 | 1.13 | 0.98 | 1.28 |
| $P_2O_5$ | 0.80 | 0.27 | 0.39 | 0.69 | 1.57 | 0.25 | 0.76 |
| total | 100.35 | 100.98 | 99.24 | 100.90 | 100.16 | 97.53 | 98.78 |
| LOI | | | | | | 1.90 | 0.32 |
| Ni | 167 | 389 | 394 | 242 | 101 | 208 | 69 |
| Cr | 21 | 23 | 22 | 15 | 33 | 210 | 23 |
| V | 164 | 67 | 67 | 65 | 716 | 164 | 294 |
| Sc | 16 | 7 | 8 | 11 | 26 | 3 | 11 |
| Cu | 50 | 26 | 23 | 39 | 60 | 20 | 46 |
| Zn | 124 | 148 | 138 | 132 | 212 | 115 | 89 |
| Sr | 586 | 201 | 292 | 539 | 211 | 674 | 1086 |
| Rb | 14 | 17 | 7 | 10 | 22 | 12 | 17 |
| Zr | 129 | 45 | 52 | 93 | 129 | 45 | 108 |
| Nb | 19 | 7 | 9 | 16 | 29 | 7 | 18 |
| Ba | 933 | 363 | 432 | 745 | 449 | 449 | 1235 |
| Pb | 1 | - | - | 2 | 1 | -1 | 2 |
| La | 23 | 7 | 10 | 35 | 50 | 11 | 28 |
| Ce | 55 | 15 | 19 | 52 | 48 | 16 | 60 |
| Nd | 33 | 2 | 6 | 25 | 27 | 7 | 32 |
| Y | 25 | 10 | 12 | 21 | 24 | 9 | 20 |
| ne | 1.26 | - | - | - | 1.12 | - | 0.18 |
| en | - | 0.59 | 5.07 | 1.26 | - | 3.30 | - |
| fs | - | 0.31 | 2.69 | 0.80 | - | 2.44 | - |
| cen | 1.12 | 0.67 | 0.22 | 0.87 | - | 0.06 | 0.46 |
| cfs | 0.82 | 0.35 | 0.12 | 0.55 | - | 0.04 | 0.49 |
| cwo | 2.01 | 1.08 | 0.36 | 1.49 | - | 0.10 | 0.97 |
| fo | 21.90 | 45.52 | 38.86 | 28.33 | 24.29 | 20.07 | 11.27 |
| fa | 17.73 | 26.52 | 22.71 | 19.86 | 24.76 | 16.30 | 13.30 |
| or | 5.80 | 2.91 | 3.12 | 4.80 | 6.70 | 5.79 | 7.58 |
| an | 16.74 | 5.38 | 9.24 | 14.31 | 6.24 | 26.90 | 24.65 |
| ab | 20.41 | 7.53 | 6.70 | 17.13 | 3.45 | 12.86 | 26.92 |
| mag | 4.12 | 5.42 | 5.04 | 4.45 | 7.24 | 3.95 | 3.42 |
| ilm | 4.48 | 1.61 | 1.89 | 3.24 | 18.93 | 3.34 | 6.00 |
| crn | - | - | - | - | 0.05 | - | - |
| ap | 2.40 | 0.82 | 1.15 | 2.07 | 4.70 | 0.73 | 2.28 |
| D.I. | 27.5 | 10.4 | 9.8 | 21.9 | 11.3 | 18.6 | 34.7 |

$[Fe_2O_3/(FeO+Fe_2O_3) = 0.15]$

17 YGD303 19 YGD316 21 YGD381 23 YGD378
18 YGD306 20 YGD312 22 YGD373

Syenogabbros

| | 1 | 2 | 3 | 4 | 5 | 6 | 7 | 8 |
|---|---|---|---|---|---|---|---|---|
| $SiO_2$ | 46.15 | 49.03 | 50.54 | 48.15 | 52.38 | 39.54 | 43.52 | 48.89 |
| $TiO_2$ | 4.03 | 3.15 | 3.11 | 3.42 | 2.36 | 6.08 | 3.70 | 3.19 |
| $Al_2O_3$ | 13.35 | 14.41 | 13.59 | 13.39 | 15.40 | 10.58 | 14.71 | 13.45 |
| $Fe_2O_3$ | 14.35 | 13.65 | 13.67 | 14.94 | 11.43 | 21.35 | 15.59 | 14.77 |
| MnO | 0.23 | 0.20 | 0.19 | 0.21 | 0.18 | 0.26 | 0.21 | 0.24 |
| MgO | 4.21 | 3.22 | 2.69 | 3.42 | 1.80 | 7.37 | 5.41 | 3.75 |
| CaO | 8.07 | 5.53 | 5.64 | 6.13 | 4.03 | 9.15 | 7.89 | 7.33 |
| $Na_2O$ | 4.02 | 4.74 | 4.47 | 4.22 | 5.28 | 2.56 | 3.79 | 4.17 |
| $K_2O$ | 2.27 | 2.91 | 3.80 | 3.23 | 3.92 | 1.07 | 1.69 | 2.34 |
| $P_2O_5$ | 1.77 | 1.44 | 0.92 | 1.13 | 0.89 | 1.98 | 2.86 | 1.14 |
| total | 98.44 | 98.27 | 98.62 | 98.24 | 97.67 | 99.94 | 99.37 | 99.28 |
| LOI | 0.50 | 0.47 | 0.48 | 0.81 | 1.52 | | | |
| Ni | 5 | 4 | 4 | 3 | 3 | 6 | 5 | 5 |
| Cr | 2 | -1 | - | 4 | 1 | 1 | - | - |
| V | 138 | 78 | 81 | 89 | 27 | 234 | 109 | 36 |
| Sc | 34 | 18 | 20 | 27 | 8 | 34 | 4 | 28 |
| Cu | 32 | 27 | 28 | 31 | 18 | 53 | 33 | 20 |
| Zn | 124 | 134 | 148 | 148 | 135 | 128 | 97 | 116 |
| Sr | 822 | 720 | 419 | 633 | 677 | 870 | 1174 | 1034 |
| Rb | 40 | 57 | 67 | 91 | 89 | 16 | 26 | 34 |
| Zr | 202 | 214 | 335 | 240 | 245 | 128 | 140 | 196 |
| Nb | 39 | 45 | 53 | 36 | 47 | 27 | 25 | 34 |
| Ba | 2541 | 2727 | 2115 | 2807 | 3493 | 1423 | 1799 | 3178 |
| Pb | 6 | 10 | 9 | 8 | 11 | 2 | 1 | 4 |
| Th | -1 | - | 3 | -1 | - | -4 | -4 | -2 |
| La | 60 | 67 | 59 | 56 | 58 | 50 | 54 | 62 |
| Ce | 146 | 142 | 142 | 125 | 134 | 127 | 140 | 148 |
| Nd | 84 | 76 | 76 | 69 | 71 | 71 | 79 | 78 |
| Y | 46 | 43 | 47 | 40 | 38 | 36 | 39 | 42 |
| ne | 1.59 | 1.22 | 2.53 | 2.60 | 2.40 | - | - | 0.37 |
| en | - | - | - | - | - | 0.07 | 2.03 | - |
| fs | - | - | - | - | - | 0.07 | 2.22 | - |
| cen | 2.54 | 0.94 | 2.08 | 2.03 | 0.70 | 2.96 | - | 2.59 |
| cfs | 3.06 | 1.54 | 4.10 | 3.42 | 1.80 | 2.98 | - | 4.04 |
| cwo | 5.63 | 2.45 | 6.02 | 5.37 | 2.39 | 6.04 | - | 6.55 |
| fo | 5.56 | 4.96 | 3.23 | 4.55 | 2.64 | 10.74 | 8.02 | 4.73 |
| fa | 7.38 | 8.92 | 7.00 | 8.45 | 7.45 | 11.92 | 9.67 | 8.13 |
| or | 13.42 | 17.20 | 22.45 | 19.06 | 23.17 | 6.30 | 10.02 | 13.85 |
| an | 11.66 | 9.45 | 5.81 | 8.06 | 6.76 | 14.23 | 15.02 | 11.06 |
| ab | 31.09 | 37.84 | 33.11 | 30.90 | 40.20 | 21.66 | 32.07 | 34.61 |
| mag | 2.85 | 2.71 | 2.72 | 2.97 | 2.27 | 4.24 | 3.10 | 2.93 |
| ilm | 7.65 | 5.99 | 5.92 | 6.50 | 4.49 | 11.55 | 7.02 | 6.07 |
| cm | - | - | - | - | - | - | 1.14 | - |
| ap | 5.28 | 4.30 | 2.75 | 3.37 | 2.67 | 5.92 | 8.55 | 3.41 |
| D.I. | 46.1 | 56.3 | 58.1 | 52.6 | 65.8 | 28.0 | 42.1 | 48.8 |

[$Fe_2O_3/(FeO+Fe_2O_3) = 0.15$]

1 YGD428 3 YGD430 5 YGD432 7 YGD356
2 YGD429 4 YGD431 6 YGD354 8 YGD362

## Syenites

| | 1 | 2 | 3 | 4 | 5 | 6 | 7 | 8 |
|---|---|---|---|---|---|---|---|---|
| SiO2 | 59.15 | 58.74 | 61.66 | 60.05 | 59.86 | 30.38 | 56.70 | 61.99 |
| TiO2 | 0.97 | 1.15 | 0.86 | 0.93 | 0.93 | 6.87 | 1.76 | 0.21 |
| Al2O3 | 15.57 | 15.49 | 16.12 | 15.38 | 15.78 | 3.18 | 16.27 | 16.91 |
| Fe2O3 | 7.81 | 8.31 | 6.73 | 7.85 | 7.80 | 41.78 | 9.57 | 2.98 |
| MnO | 0.16 | 0.17 | 0.15 | 0.18 | 0.17 | 0.77 | 0.16 | 0.08 |
| MgO | 0.61 | 0.69 | 0.32 | 0.58 | 0.62 | 3.92 | 0.68 | 0.27 |
| CaO | 2.17 | 2.41 | 0.81 | 2.26 | 2.26 | 9.48 | 3.20 | 2.80 |
| Na2O | 5.45 | 5.50 | 5.68 | 6.10 | 5.77 | 0.96 | 5.59 | 8.84 |
| K2O | 5.72 | 5.61 | 5.86 | 5.58 | 5.45 | 0.84 | 4.90 | 1.81 |
| P2O5 | 0.19 | 0.22 | 0.17 | 0.18 | 0.18 | 2.21 | 0.45 | 0.04 |
| total= | 97.82 | 98.31 | 98.36 | 99.10 | 98.82 | 100.38 | 99.29 | 95.93 |
| LOI | 2.00 | 1.39 | 1.33 | | 0.54 | | 3.45 | |
| Ni | 3 | 4 | 3 | 3 | 4 | 2 | 3 | 3 |
| Cr | -1 | - | -3 | -1 | -1 | 6 | -2 | -2 |
| V | - | -2 | -1 | -2 | -1 | 25 | 3 | 2 |
| Sc | 9 | 8 | 8 | 7 | 9 | 48 | 9 | 5 |
| Cu | 9 | 9 | 6 | 8 | 19 | 95 | 23 | - |
| Zn | 121 | 130 | 119 | 127 | 125 | 341 | 82 | 19 |
| Sr | 56 | 66 | 57 | 61 | 45 | 58 | 419 | 245 |
| Rb | 119 | 104 | 127 | 119 | 92 | 19 | 65 | 34 |
| Zr | 235 | 280 | 339 | 403 | 434 | 270 | 285 | 97 |
| Nb | 46 | 54 | 52 | 64 | 55 | 70 | 43 | 29 |
| Ba | 344 | 522 | 475 | 465 | 318 | 302 | 3707 | 166 |
| Pb | 13 | 14 | 19 | 21 | 12 | 2 | 8 | 13 |
| Th | 4 | 5 | 9 | 10 | 6 | -2 | 2 | 4 |
| La | 61 | 50 | 67 | 70 | 65 | 152 | 51 | 54 |
| Ce | 118 | 116 | 128 | 148 | 138 | 326 | 102 | 105 |
| Nd | 54 | 54 | 55 | 59 | 60 | 180 | 55 | 39 |
| Y | 29 | 32 | 35 | 41 | 44 | 100 | 38 | 18 |
| qtz | - | - | 1.41 | - | - | - | - | - |
| ne | 0.01 | 0.88 | - | 2.16 | 0.42 | 1.14 | 2.11 | 1.89 |
| en | - | - | 0.75 | - | - | - | - | - |
| fs | - | - | 7.11 | - | - | - | - | - |
| wo | - | - | - | - | - | - | - | 1.14 |
| cen | 0.53 | 0.64 | 0.06 | 0.56 | 0.57 | 2.13 | 0.48 | 0.67 |
| cfs | 3.11 | 3.47 | 0.59 | 3.87 | 3.34 | 9.78 | 2.82 | 3.71 |
| cwo | 3.35 | 3.80 | 0.59 | 4.06 | 3.60 | 11.07 | 3.03 | 4.04 |
| fo | 0.70 | 0.76 | - | 0.62 | 0.68 | 5.35 | 0.85 | - |
| fa | 4.52 | 4.53 | - | 4.73 | 4.40 | 27.14 | 5.51 | - |
| or | 33.81 | 33.17 | 34.62 | 32.97 | 32.21 | 4.95 | 28.97 | 10.68 |
| an | 1.12 | 1.02 | 1.18 | - | 1.04 | 1.89 | 4.80 | 1.12 |
| ab | 46.08 | 44.89 | 48.05 | 44.08 | 48.10 | 6.02 | 43.42 | 71.31 |
| mag | 1.55 | 1.65 | 1.34 | - | 1.55 | 8.30 | 1.90 | 0.59 |
| ilm | 1.85 | 2.19 | 1.63 | 1.77 | 1.76 | 13.06 | 3.35 | 0.40 |
| hl | - | - | - | 0.01 | - | - | - | - |
| ap | 0.58 | 0.66 | 0.51 | 0.54 | 0.55 | 6.60 | 1.35 | 0.13 |
| acm | - | - | - | 3.11 | - | - | - | - |
| [Fe2O3/(FeO+Fe2O3) = 0.15] | | | | | | | | |
| D.I. | 79.9 | 78.9 | 84.1 | 79.2 | 80.7 | 12.1 | 74.5 | 83.9 |

1 YGD176 3 YGD179 5 YGD433 7 216627B
2 YGD177 4 YGD180 6 216627A 8 YGD170

| | 9 | 10 | 11 | 12 |
|---|---|---|---|---|
| $SiO_2$ | 64.41 | 65.77 | 53.79 | 61.12 |
| $TiO_2$ | 0.24 | 0.53 | 1.00 | 0.84 |
| $Al_2O_3$ | 16.46 | 14.04 | 11.79 | 16.12 |
| $Fe_2O_3$ | 4.22 | 6.20 | 20.37 | 7.36 |
| MnO | 0.10 | 0.15 | 0.48 | 0.16 |
| MgO | 0.25 | 0.26 | 0.84 | 0.45 |
| CaO | 0.30 | 1.02 | 2.04 | 1.85 |
| $Na_2O$ | 6.06 | 5.51 | 4.45 | 5.81 |
| $K_2O$ | 6.64 | 5.10 | 4.39 | 5.70 |
| $P_2O_5$ | 0.08 | 0.06 | 0.21 | 0.16 |
| total | 98.76 | 98.64 | 99.36 | 99.57 |
| LOI | 0.33 | 0.56 | | |
| Ni | 5 | 5 | 4 | 4 |
| Cr | -1 | 1 | 3 | - |
| V | -2 | 2 | 1 | - |
| Sc | 3 | - | - | 6 |
| Cu | -7 | 3 | 22 | 5 |
| Zn | 89 | 176 | 238 | 103 |
| Sr | 18 | 43 | 49 | 75 |
| Rb | 157 | 238 | 133 | 110 |
| Zr | 2057 | 1092 | 267 | 355 |
| Nb | 130 | 165 | 69 | 63 |
| Ba | 244 | 310 | 231 | 580 |
| Pb | 51 | 38 | 13 | 19 |
| Th | 21 | 40 | 5 | 9 |
| La | 180 | 140 | 85 | 65 |
| Ce | 396 | 300 | 175 | 150 |
| Nd | 135 | 111 | 78 | 59 |
| Y | 163 | 93 | 41 | 36 |
| qtz | 1.96 | 9.73 | - | - |
| en | 0.59 | 0.49 | 0.66 | 0.29 |
| fs | 5.47 | 6.29 | 8.37 | 2.22 |
| cen | 0.04 | 0.15 | 0.28 | 0.36 |
| cfs | 0.34 | 1.94 | 3.58 | 2.72 |
| cwo | 0.34 | 1.89 | 3.48 | 2.81 |
| fo | - | - | 0.80 | 0.33 |
| fa | - | - | 11.12 | 2.79 |
| or | 39.24 | 30.14 | 25.95 | 33.66 |
| an | - | - | - | 1.08 |
| ab | 47.70 | 43.82 | 36.20 | 49.16 |
| mag | - | - | 3.40 | 1.46 |
| ilm | 0.45 | 1.01 | 1.89 | 1.60 |
| hl | 0.39 | 0.00 | - | - |
| ap | 0.24 | 0.19 | 0.63 | 0.49 |
| acm | 1.67 | 2.46 | 1.28 | - |
| [$Fe_2O_3$/($FeO$+$Fe_2O_3$) = 0.15] | | | | |
| D.I. | 88.9 | 83.7 | 62.1 | 82.8 |

9 YGD183 10 YGD326 11 50218 12 50219

## Fine-grained felsic xenoliths

| | 1 | 2 | 3 |
|---|---|---|---|
| $SiO_2$ | 46.47 | 43.48 | 43.78 |
| $TiO_2$ | 1.45 | 1.11 | 1.56 |
| $Al_2O_3$ | 16.37 | 12.68 | 13.64 |
| $Fe_2O_3$ | 14.20 | 18.39 | 18.24 |
| MnO | 0.17 | 0.20 | 0.23 |
| MgO | 9.49 | 15.27 | 12.71 |
| CaO | 6.15 | 5.70 | 6.47 |
| $Na_2O$ | 4.03 | 2.45 | 2.57 |
| $K_2O$ | 0.87 | 0.47 | 0.72 |
| $P_2O_5$ | 0.48 | 0.38 | 0.55 |
| total | 99.67 | 100.14 | 100.47 |
| Ni | 113 | 208 | 161 |
| Cr | 12 | 18 | 11 |
| V | 105 | 69 | 84 |
| Sc | 9 | 9 | 12 |
| Cu | 30 | 28 | 39 |
| Zn | 83 | 102 | 100 |
| Sr | 818 | 695 | 807 |
| Rb | 15 | 5 | 9 |
| Zr | 126 | 62 | 90 |
| Nb | 16 | 9 | 13 |
| Ba | 1181 | 588 | 750 |
| Pb | 1 | - | - |
| La | 17 | 15 | 19 |
| Ce | 48 | 25 | 38 |
| Nd | 27 | 12 | 21 |
| Y | 18 | 11 | 17 |
| ne | 2.72 | - | - |
| en | - | 0.80 | 0.46 |
| fs | - | 0.48 | 0.32 |
| cen | 0.59 | 0.72 | 0.92 |
| cfs | 0.41 | 0.43 | 0.63 |
| cwo | 1.04 | 1.21 | 1.62 |
| fo | 16.15 | 25.58 | 21.22 |
| fa | 12.47 | 16.82 | 16.10 |
| or | 5.11 | 2.78 | 4.26 |
| an | 24.02 | 22.21 | 23.55 |
| ab | 29.07 | 20.73 | 21.75 |
| mag | 2.82 | 3.65 | 3.62 |
| ilm | 2.76 | 2.12 | 2.96 |
| ap | 1.42 | 1.12 | 1.66 |
| [$Fe_2O_3/(FeO+Fe_2O_3) = 0.15$] | | | |
| D.I. | 36.9 | 23.5 | 26.0 |

1 YGD289 3 YGD302
2 YGD277

Country-rock granites

| | 1 | 2 | 3 | 4 | 5 |
|---|---|---|---|---|---|
| $SiO_2$ | 67.19 | 66.47 | 67.05 | 65.28 | 67.26 |
| $TiO_2$ | 0.39 | 0.43 | 0.42 | 0.37 | 0.39 |
| $Al_2O_3$ | 15.08 | 15.58 | 15.36 | 16.16 | 15.11 |
| $Fe_2O_3$ | 3.45 | 4.27 | 3.84 | 3.67 | 3.57 |
| MnO | 0.06 | 0.05 | 0.06 | 0.07 | 0.06 |
| MgO | 1.20 | 2.65 | 1.52 | 1.36 | 1.31 |
| CaO | 2.99 | 0.95 | 2.63 | 3.11 | 2.73 |
| $Na_2O$ | 4.09 | 4.96 | 4.11 | 5.08 | 4.11 |
| $K_2O$ | 3.24 | 2.32 | 2.82 | 2.89 | 3.51 |
| $P_2O_5$ | 0.16 | 0.18 | 0.18 | 0.18 | 0.17 |
| total | 97.85 | 97.86 | 97.99 | 98.16 | 98.22 |
| LOI | 0.66 | 1.95 | 0.95 | 1.29 | 0.72 |
| Ni | 9 | 10 | 9 | 9 | 9 |
| Cr | 3 | 4 | 3 | 5 | 3 |
| V | 46 | 63 | 52 | 54 | 49 |
| Sc | 3 | 5 | 4 | 9 | 10 |
| Cu | 12 | 7 | 10 | 5 | 5 |
| Zn | 49 | 60 | 58 | 56 | 49 |
| Sr | 574 | 460 | 565 | 677 | 603 |
| Rb | 105 | 68 | 86 | 62 | 97 |
| Zr | 152 | 169 | 168 | 133 | 135 |
| Nb | 11 | 12 | 11 | 9 | 10 |
| Ba | 665 | 598 | 620 | 785 | 898 |
| Pb | 17 | 10 | 13 | 15 | 15 |
| Th | 15 | 14 | 18 | 11 | 11 |
| La | 33 | 34 | 30 | 48 | 26 |
| Ce | 72 | 81 | 69 | 95 | 60 |
| Nd | 28 | 34 | 29 | 35 | 27 |
| Y | 16 | 18 | 18 | 15 | 15 |
| qtz | 21.61 | 21.15 | 23.04 | 14.91 | 20.86 |
| en | 2.94 | 6.60 | 3.79 | 3.17 | 3.26 |
| fs | 3.94 | 4.99 | 4.47 | 4.05 | 4.16 |
| cen | 0.05 | - | - | 0.22 | - |
| cfs | 0.07 | - | - | 0.28 | - |
| cwo | 0.11 | - | - | 0.50 | - |
| or | 19.16 | 13.71 | 16.69 | 17.07 | 20.71 |
| an | 13.21 | 3.17 | 11.56 | 12.76 | 12.12 |
| ab | 34.61 | 41.97 | 34.78 | 42.99 | 34.78 |
| mag | 0.69 | 0.85 | 0.76 | 0.73 | 0.71 |
| ilm | 0.74 | 0.81 | 0.79 | 0.70 | 0.74 |
| crn | - | 3.75 | 1.30 | - | 0.11 |
| ap | 0.48 | 0.55 | 0.53 | 0.52 | 0.51 |

[$Fe_2O_3/(FeO+Fe_2O_3) = 0.15$]

1 JG1
2 JG2
3 JG3
4 YGD230
5 YGD231